



HAL
open science

Engineering the surface of bubbles for microalgae harvesting by flotation using a biophysical approach

Irem Demir-Yilmaz

► **To cite this version:**

Irem Demir-Yilmaz. Engineering the surface of bubbles for microalgae harvesting by flotation using a biophysical approach. Chemical and Process Engineering. INSA de Toulouse, 2022. English. NNT : 2022ISAT0040 . tel-04416397

HAL Id: tel-04416397

<https://theses.hal.science/tel-04416397>

Submitted on 25 Jan 2024

HAL is a multi-disciplinary open access archive for the deposit and dissemination of scientific research documents, whether they are published or not. The documents may come from teaching and research institutions in France or abroad, or from public or private research centers.

L'archive ouverte pluridisciplinaire **HAL**, est destinée au dépôt et à la diffusion de documents scientifiques de niveau recherche, publiés ou non, émanant des établissements d'enseignement et de recherche français ou étrangers, des laboratoires publics ou privés.



THÈSE

**En vue de l'obtention du
DOCTORAT DE L'UNIVERSITÉ DE TOULOUSE**
Délivré par l'Institut National des Sciences Appliquées de
Toulouse

**Présentée et soutenue par
Irem DEMIR-YILMAZ**

Le 26 septembre 2022

**Ingénierie de la surface des bulles pour la récolte des
microalgues par flottation à l'aide d'une approche biophysique**

Ecole doctorale : **MEGEP - Mécanique, Energétique, Génie civil, Procédés**

Spécialité : **Génie des Procédés et de l'Environnement**

Unité de recherche :

TBI - Toulouse Biotechnology Institute, Bio & Chemical Engineering

Thèse dirigée par

Pascal GUIRAUD et Cécile FORMOSA

Jury

Mme Rita Kay HENDERSON, Rapporteur

M. Georg FANTNER, Rapporteur

M. Dries VANDAMME, Examineur

M. Pascal GUIRAUD, Directeur de thèse

Mme Cécile FORMOSA-DAGUE, Co-directrice de thèse

Mme Martine MEIRELES, Présidente

Mr. Etienne DAGUE, Membre invité

Mr. Dominique LEGENDRE, Membre invité



A DISSERTATION

In order to obtain the title of
DOCTOR OF THE UNIVERSITY OF TOULOUSE
Issued by Institut National des Sciences Appliquées de Toulouse

Defended by
Irem DEMIR-YILMAZ

On 26 September 2022

**Engineering the surface of bubbles for microalgae harvesting by
flotation using a biophysical approach**

PhD School: **MEGEP - Mécanique, Energétique, Génie civil, Procédés**

Department: **Génie des Procédés et de l'Environnement**

Research Laboratory:

TBI - Toulouse Biotechnology Institute, Bio & Chemical Engineering

Supervised by
Pascal GUIRAUD and Cécile FORMOSA

The jury members

Mrs. Rita Kay HENDERSON, Referee

Mr. Georg FANTNER, Referee

Mr. Dries VANDAMME, Examiner

Mrs. Martine MEIRELES, Examiner, President of the jury

Mr. Pascal GUIRAUD, PhD Supervisor

Mrs. Cécile FORMOSA-DAGUE, PhD Co-supervisor

Mr. Etienne DAGUE, Invited member

Mr. Dominique LEGENDRE, Invited member

To my beloved family

and

My husband RBY

ACKNOWLEDGMENTS

Foremost, I would like to state my sincere gratitude to my supervisors Dr. Cecile Formosa-Dague and Prof. Dr. Pascal Guiraud for their invaluable guidance, continuous support, and interest throughout my Ph.D. study and research program. I would like to express my special thanks to Dr. Cecile Formosa Dague for her kindness, never-ending support, respect, and understanding. I am extremely grateful for her invaluable advice and critics.

I would like to thank the Agence Nationale pour la Recherche (ANR) for funding this Ph.D.

I would like to extend my deepest gratitude to the people with whom I collaborated. Because without their technical support and help, this work could not be achieved. My research would have been impossible without the help and support of Etienne Dague. I am very grateful to Etienne for his encouragement, for being closely involved in each part of my Ph.D., and for allowing me to use their AFM frequently without any complaints. I would like to express my warmest thanks to Christophe Coudret thanks to whom I had the opportunity to experience hardcore chemistry. I would like to thank Tomaso Zambelli, Koenraad Muylaert, Jonas Blockx, and Ines Luchtefeld for their collaboration, discussion, new ideas, and all the support they put in during my Ph.D. Special thanks go to Marion Schiavone for her positive energy and help with cell wall analysis and HPLC measurements as well as Jerome Esvan for his help on XPS measurements. I am grateful to all of you, and to have a chance to work with you as a team.

I am thankful to Nadica Ivosevic DeNardis, Nives Novosel, Tea Misic Radic and Maja Levak Zorinc for their great hospitality during my visits to Croatia and their collaboration on CC cells and ghost vesicles.

I am also grateful to our new collaborators from Belgium; Dries Vandamme, Michaela Pappa and Sanjaya Lama. Thanks to them I had the chance to use our new molecule (PO-chitosan) to harvest their microalgae species and analyze AOM with AFM.

I wish to thank interns; Malak Souad Ftouhi and Emma Regourd, for being the best interns. I have chance to work closely with Malak and I am sure you will have a perfect Ph.D. and succeed in the future :)

This thesis would not have been accomplished without my kindhearted friends and coworkers in TBI and LAAS. I want to thank Vincent NGU for being my first friend here in France and being the best officemate ever I could imagine. Maïke Petermann you have been very nice and patient with me. Thank you very much for listening to all of my complaints and for your very brilliant advice. Nadiia Yakovenkova is not only a collaborator for me but also a very close friend. Thank you Nadiia for all of your support and listening to all of my problems and being there for me whenever I need. To Ophélie Thomas-Chemin for sharing with me, the same technical problem on AFM and you are the best company for a conference! My followers are missing you two (Ophelie and Nadiia)!!. Thank you Gozde Eke for your friendship and all the help you offered when I try to settle in Toulouse. When you left, I really missed our coffee breaks. To Ryma Lyfa, I have a chance to get to know you a bit late but I am grateful for all the memories that I have shared with you. Once again, thank you all for being my friends.

Of course, special thanks go to Refik Baris Yilmaz (RBY) to my lovely husband. He is not only my husband but also the best coworker ever I could imagine. I could not achieve any of this without his kind hard, support, and warm smile. He is the best thing that ever happens to me. Thank you very much for moving with me to France, for your patience, and for listening to all of my problems over and over again. I know I am the chaos in your life!!! But you are managing great. My dear RBY, thank you very much again for what you have brought into my life; joy happiness, and full of success. With all my heart, I wish the same for you.

Big thank goes to my family who always found everthing I do great and perfect. Thank you very much for your support under any circumstances and for being proud of me at every step. Thank you to the most incredible family I could ask for. You all are the most important people in the world to me.

Engineering the surface of bubbles for microalgae harvesting by flotation **using a biophysical approach**

Abstract

Assisted flotation is a promising harvesting technique that consists in air dispersed into microbubbles rising through a microalgae suspension. As a result, microalgae cells get attached to bubbles and are carried out and accumulated on the surface, without being damaged. Flotation is thus a relatively rapid operation that needs low space, has moderate operational costs, and that could thus overcome the bottleneck of feasible microalgae biofuel production. To make this technique more efficient, the original strategy proposed in this work relies on functionalizing the bubbles produced during the flotation process with adhesive compounds, allowing bubbles to effectively capture cells during their ascent. This requires in a first step (i) to develop a method to produce microsized bubbles and probe their interactions with individual cells using atomic force microscopy (AFM) combined with microfluidics (FluidFM). Then in a second step, (ii) it was required to determine which molecules are present on the surface of microalgae cells to identify a molecule that could adhere to them. For that, we first analyzed the composition of their cell wall using a combination of techniques such as liquid chromatography and X-ray photoelectron spectroscopy (XPS). The information obtained from these analyses revealed the presence of chitin-like molecules on the cell surface, similar to chitosan to which they could adhere through homotypic interactions. Then, in a third step (iii) we determined whether the identified molecule, chitosan, could effectively bind to cells by measuring their interactions at the molecular level using AFM. After understanding the molecular basis of these interactions, we then (iv) chemically modified chitosan to make it amphiphilic to functionalize the bubble surface. For that, we added hydrophobic groups to the hydrophilic chitosan backbone through N-alkylation by reductive amination. Finally, we evaluated the possibility of this new molecule, polyoctyl-chitosan, to functionalize bubble surfaces and modulate their interactions with cells. For this purpose, in a fifth step (v), we evaluated the interaction between the functionalized bubbles and cells using FluidFM, and optimized an efficient functionalized bubble flotation process efficient to separate populations of microalgae cells. The results of this project, by proposing a new efficient harvesting technique based on flotation, represent an important step towards the industrial use of microalgae biomass for the production of third generation biofuels.

Résumé

La flottation assistée est une technique de récolte prometteuse qui consiste à faire monter de l'air dispersé en microbulles à travers une suspension de microalgues. En conséquence, les cellules se fixent aux bulles et sont transportées et accumulées à la surface, sans être endommagées. La flottation est donc une opération relativement rapide qui nécessite peu d'espace, a des coûts opérationnels modérés, et qui pourrait ainsi surmonter les verrous de la production réalisable de biocarburants issus de microalgues. Pour rendre cette technique plus efficace, la stratégie originale proposée dans ce travail repose sur la fonctionnalisation des bulles produites pendant le procédé de flottation avec des composés adhésifs, permettant aux bulles de capturer efficacement les cellules pendant leur ascension. Cela nécessite dans un premier temps (i) de développer une méthode pour produire des bulles micrométriques et mesurer leurs interactions avec des cellules individuelles en utilisant la microscopie à force atomique (AFM) combinée à la microfluidique (FluidFM). Puis dans une seconde étape, (ii) nous avons déterminé quelles molécules sont présentes à la surface des cellules de microalgues afin d'identifier une molécule qui pourrait y adhérer, grâce à une combinaison de techniques telles que la chromatographie liquide et la spectroscopie photoélectronique à rayons X (XPS). Les informations obtenues ont révélé la présence de molécules de type chitine à la surface des cellules, similaires au chitosan auquel elles pouvaient adhérer *via* des interactions homotypiques. Puis, lors d'une troisième étape (iii), nous avons déterminé si le chitosan pouvait effectivement se lier aux cellules en mesurant leurs interactions à l'échelle moléculaire par AFM. Après avoir compris les bases moléculaires de ces interactions, nous avons ensuite (iv) modifié chimiquement le chitosan pour le rendre amphiphile afin de le fonctionnaliser la surface des bulles. Pour cela, nous avons ajouté des groupes hydrophobes au squelette hydrophile du chitosan par N-alkylation. Enfin, nous avons évalué la possibilité pour cette nouvelle molécule, le polyoctyl-chitosan, de s'assembler à la surface des bulles et de moduler leurs interactions avec les cellules. Pour cela, dans une dernière étape v), nous avons évalué l'interaction entre les bulles fonctionnalisées et les cellules par FluidFM, et optimisé un procédé de flottation de bulles fonctionnalisées efficace pour séparer des populations de microalgues. Les résultats de ce projet, en proposant une nouvelle technique de récolte par flottation, représentent une étape importante vers l'utilisation industrielle de la biomasse microalgale pour la production de biocarburants de troisième génération.

Table of Contents

List of Publications.....	1
List of Communications.....	3
List of Abbreviations.....	5
List of Figures.....	6
List of Tables.....	7
General Introduction.....	9
Chapter 1. General Overview.....	15
1.1. General context.....	15
1.1.1. Microalgae for biofuels and value-added molecules production.....	15
1.1.2. Classic techniques used to harvest microalgae.....	18
1.1.3. Flotation is an alternative harvesting technique with great potential.....	19
1.1.4. Techniques to study microalgae; Atomic Force Microscopy (AFM).....	23
1.1.5. Conclusion.....	26
1.2. Review of the PhD work.....	28
1.2.1. Development of a method to measure the interaction between bubbles, functionalized or not, and cells at the molecular scale.....	28
1.2.2. Cell wall composition analysis to find a natural flocculant.....	35
1.2.3. Chitosan as a bioflocculant to harvest the microalgae cells.....	43
1.2.4. Synthesis, characterization and functionalization of bubbles with polyoctylchitosan (PO-chitosan), an amphiphilic chitosan-based molecule.....	50
1.2.5. Optimizing the one-step flotation process.....	58
1.3. Discussions and conclusions of the PhD work.....	62
1.3.1. Contribution of the work to other fields of research and applications.....	64
1.3.2. Future perspectives on the work performed in this PhD.....	70
Chapter 2: Bibliographic analysis.....	97
2.1. Towards a better understanding of microalgae natural flocculation mechanisms to enhance flotation harvesting efficiency.....	99
2.2. The contribution of Atomic Force Microscopy (AFM) in microalgae studies: A review	117
Chapter 3: Probing the interactions between air bubbles and (bio)-interfaces at the nanoscale using FluidFM technology.....	129
Chapter 4: Combining AFM, XPS and chemical hydrolysis to understand the complexity and dynamics of <i>C. vulgaris</i> cell wall composition and architecture.....	145

Chapter 5: Nanoscale Evidence Unravels Microalgae Flocculation Mechanism Induced by Chitosan.....	171
Chapter 6: Bubble functionalization in flotation process improve microalgae harvesting ...	187
Chapter 7 : French summary / Résumé Français	203
Appendices	223
Appendix 1: The role of microplastics in microalgae cells aggregation: a study at the molecular scale using AFM	225
Appendix 2: Investigation of the role of cell hydrophobicity and EPS production in the aggregation of the marine diatom <i>Cylindrotheca closterium</i> under salinity stress	241
Appendix 3: Reconstructed membrane vesicles from the microalga <i>Dunaliella</i> as a potential drug delivery system	295

List of Publications

- P13** Burato Rosales A., Druban-Benizio N., Nguyen X. L., Bouvier V., Lamo C., **Demir-Yilmaz I.**, Causserand C., Formosa-Dague C., Coetsier C., 2022. Minimizing bacterial adhesion on membrane: multiscale characterization of surface modifications. *Journal of membrane science (Under revision)*
- P12** **Demir-Yilmaz I.,*** Novosel N.,* Zorinc M.L., Radić T.M., Ftouhi M.S., Guiraud P., DeNardis N.I., Formosa-Dague C., 2022. Investigation of the role of cell hydrophobicity and EPS production in the aggregation of the marine diatom *Cylindrotheca closterium* under salinity stress. *Marine environmental research (Under Review)*
- P11** Zorinc M.L., **Demir-Yilmaz I.**, Formosa-Dague C., Vrana I., Gašparović B., Horvat L., Butorac A., Frkanec R., DeNardis N.I., 2022. Algal reconstructed vesicles as a potential delivery system. *Bioelectrochemistry (Under Revision)*.
- P10** **Demir-Yilmaz I.**, Schiavone M., Esvan J., Guiraud P., Formosa-Dague C., 2022. Combining AFM, XPS and chemical hydrolysis to understand the complexity and dynamics of *C. vulgaris* cell wall composition and architecture. *Algal Research (Under revision)*
- P9** **Demir-Yilmaz I.**, Ftouhi M., Coudret C., Guiraud, P., Formosa-Dague C., 2023. Bubble functionalization in flotation process improve microalgae harvesting. *Chemical Engineering Journal 452, 139349 (IF = 16.744)*.
- P8** **Demir-Yilmaz I.**, Yakovenko N., Roux C., Guiraud P., Collin F., Coudret C., ter Halle A., Formosa-Dague, C., 2022. The role of microplastics in microalgae cells aggregation: a study at the molecular scale using AFM. *Science of the total environment, 832, 155036 (IF = 10.753, Citation = 6)*
- P7** **Demir-Yilmaz I.**, Guiraud P., Formosa-Dague C., 2021. The contribution of Atomic Force Microscopy (AFM) in microalgae studies: A review. *Algal Research, 60, 102506 (IF = 5.276, Citation = 5)*
- P6** **Demir I.**, Lüchtfeld I., Lemen C., Dague E., Guiraud P., Zambelli T., Formosa-Dague C., 2021. Probing the interactions between air bubbles and (bio)-interfaces at the nanoscale using FluidFM technology. *Journal of Colloid and Interface Science, 604, 785-797 (IF = 9.965, Citation = 4)*
- P5** **Demir I.***, Blockx J.*, Dague E., Guiraud P., Thielemans W., Muylaert K., Formosa-Dague C., 2020. Nanoscale evidence unravels microalgae flocculation mechanism induced by chitosan. *ACS Applied Bio Materials, 3 (12), 8446-8459 (IF = 3.250, Citation = 15)*

P4 Demir I., Besson A., Guiraud P., Formosa-Dague C., 2020. Towards a better understanding of microalgae natural flocculation mechanisms to enhance flotation harvesting efficiency. *Water Science and Technology*, 82 (6), 1009-1024 (IF = 2.260, Citation = 12)

P1-P3 are from Master of Science studies

P3 Demir I., Çalık P., 2020. Hybrid-architected double-promoter expression systems enhance and upregulate-deregulated gene expressions in *Pichia pastoris* in methanol-free media. *Applied Microbiology and Biotechnology*, 104 (19), 8381-8397 (IF = 4.813, Citation = 7)

P2 Ergün B.G., Demir I., Özdamar T.H., Gasser B., Mattanovich D., Çalık, P., 2020. Engineered deregulation of expression in yeast with designed hybrid-promoter architectures in coordination with discovered master regulator transcription factor. *Advanced Biosystems*, 4 (4), 1900172 (IF = 3.591, Citation=14)

P1 Öztürk S., Demir I., Çalık P., 2019. Isolation of high-quality RNA from *Pichia pastoris*. *Current Protocols in Protein Science*, 98 (1), e101 (IF = 3.03, Citation = 1)

* These authors equally contributed the work.

List of Communications

- C10.** 5^{èmes} journées plénières du GDR B2I (BioIngénierie des Interfaces), **Demir-Yilmaz I.**, Ftouhi M., Coudret C., Guiraud P., Formosa-Dague C. 2022. Bubble surface engineering for optimized microalgae harvesting, Dijon, France, **Oral presentation**
- C9.** 11th International Colloids Conference, **Demir-Yilmaz I.**, Yakovenko N., Roux C., Guiraud P., Collin F., Coudret C., ter Halle A., Formosa-Dague, C. 2022. Understanding the interaction between plastic microparticles and microalgae bio-interface: a study at the molecular scale using AFM, Lisbon, Portugal, **Poster presentation**
- C8.** 3rd International NanoInBio Conference, **Demir-Yilmaz I.**, Yakovenko N., Roux C., Guiraud P., Collin F., Coudret C., ter Halle A., Formosa-Dague C., 2022. Understanding the interaction between plastic microparticles and microalgae bio-interface: a study at the molecular scale using AFM, Guadeloupe, France, **Oral presentation** (*awarded best interdisciplinary work of the conference*)
- C7.** 3rd International NanoInBio Conference, **Demir-Yilmaz I.**, Lüchtfeld I., Lemen C., Dague E., Guiraud P., Zambelli T., Formosa-Dague C., 2022. Probing the interactions between air bubbles and (bio)-interfaces at the molecular scale using FluidFM technology, Guadeloupe, France, **Poster presentation**
- C6.** C’Nano: Nanoscience meeting, **Demir I.**, Lüchtfeld I., Lemen C., Dague E., Guiraud P., Zambelli T., Formosa-Dague, C., 2021. Probing the interactions between air bubbles and (bio)-interfaces at the molecular scale using FluidFM technology Toulouse, France, **Poster presentation**
- C5.** 4^{èmes} journées plénières du GDR B2I (BioIngénierie des Interfaces), **Demir I.**, Lüchtfeld I., Lemen C., Dague E., Guiraud P., Zambelli T, Formosa-Dague C., 2021. Probing the interactions between air bubbles and (bio)-interfaces at the molecular scale using FluidFM technology, Toulouse, France, **Poster presentation** (*awarded best poster presentation*)
- C4.** XVII^{ème} colloque de la Société française des Microscopies (SF μ), **Demir I.**, Lüchtfeld I., Lemen C., Dague E., Guiraud P., Zambelli T., Formosa-Dague C., 2021. Probing the interactions between air bubbles and (bio)-interfaces at the molecular scale using FluidFM technology, Online, **Oral presentation**
- C3.** 10th International Conference on Algal Biomass, Biofuels and Bioproducts (AlgalBBB) , **Demir I.**,Blockx J., Dague E., Guiraud P., Thielemans W., Muylaert K., Formosa-Dague C., 2021. Understanding chitosan-induced flocculation mechanism in *C. vulgaris* using atomic force microscopy (AFM), Online, **Oral presentation**

- C2.** AlgalEurope Conference, **Demir I.**, Blockx J., Dague E., Guiraud P., Thielemans W., Muylaert K., Formosa-Dague C., 2020. Understanding chitosan-induced flocculation mechanism in *C. vulgaris* using atomic force microscopy (AFM), Online, **Poster presentation**

C1 is from Master of Science studies

- C1.** 9th Eastern Mediterranean Chemical Engineering Conference (EMCC9), **Demir I.**, Ergun B.G., Calik P., 2018. Recombinant protein production under double promoter expression system in *Pichia pastoris*, Ankara, Turkey, **Poster presentation**

List of Abbreviations

AFM: Atomic force microscopy

AOM: Algal organic matter

CNC: Cellulose nanocrystal

CW: Cell wall

DCW: Dry cell weight

DD: Degree of deacetylation

DLS: Dynamic light scattering

DS: Degree of substitution

FS: Force spectroscopy

FV: Force volume

HS-AFM: High speed atomic force microscopy

LPS: Lipopolysaccharide

LCA: Life cycle analysis

PDMS: Polydimethylsiloxane

PEI: Polyethylenimine

PEG: Polyethylene glycol

QI: Quantitative imaging

OD: Optical density

PBS: Phosphate buffer saline

SEM: Scanning electron microscopy

WC: Wright's cryptophyte

XPS: X-ray photoelectron spectroscopy

Ym: Young modulus

HPLC: High-performance liquid chromatography

PO-Chitosan: Polyoctyl chitosan

List of Figures

Figure 1: Schematic representation of the development of a new bubble surface engineering strategy for optimized microalgae harvesting using flotation technique.....	11
Figure 2: Bubble– (bio)-particle interaction process	20
Figure 3: Schematic representation of natural flocculation mechanisms.....	21
Figure 4: Atomic force microscopy principle	25
Figure 5: Schematic representation of the method to produce bubbles using FluidFM technology.....	30
Figure 6: Force-Volume mode atomic force microscopy (FV-AFM)	31
Figure 7: Probing interactions between bubbles and <i>C. vulgaris</i> cells	32
Figure 8: Functionalizing bubbles using a (fluorescent) surfactant and modulating its interaction with model species	34
Figure 9: Roughness and nanomechanics of <i>C. vulgaris</i> cell wall.	37
Figure 10: XPS analysis of <i>C. vulgaris</i> cell wall	38
Figure 11: Monosaccharide composition of <i>C. vulgaris</i> cell wall.....	42
Figure 12: Flocculation experiments of <i>C. vulgaris</i> with chitosan	47
Figure 13: Identification of a natural flocculent, chitosan, for <i>C. vulgaris</i>	49
Figure 14: Synthesis of N-octyl-chitosan by alkylation process.....	51
Figure 15: Characterization of PO-chitosan surface at different pH	54
Figure 16: Modulation of the interactions between bubbles and <i>C. vulgaris</i> cells by PO-chitosan	56
Figure 17: Photograph of the home-built flotation device used in this study.....	58
Figure 18: Flotation experiments of <i>C. vulgaris</i> with PO-chitosan coated bubble	60
Figure 19: Schematic representation of the development of new bubble surface engineering strategy for optimized microalgae harvesting	64

List of Tables

Table 1: Relative composition of lipids, proteins and polysaccharides in microalgae cell walls	40
Table 2: Chitosan induced flocculation studies reported in the literature.....	45

General Introduction

In the face of fossil fuels shortages and increasing pollution, which is a driver of climate change related to the combustion of fossil fuels, the need for renewable and sustainable energy sources to substitute energy production based on fossil fuels namely petroleum, coal and natural gas has become urgent (Fercoq et al., 2016; Markou & Nerantzis, 2013). Different alternative energy sources are already available, including biofuels derived from biomass. Given their interest to replace non-renewable fuels, research on this field is very active. Several types of biomass can be used including crop plants, agricultural by-products or marine resources such as seaweeds and cyanobacteria. Among them, microalgae represent the most attractive biomass, which has been extensively explored in this context for its potential to produce important quantities of oil that can be used for biofuel production (Pragya et al., 2013). In addition, the potential of microalgae is even larger as they also represent an important source of biomass and of molecules of interest for the fields of food, feed or health. Moreover, microalgae cultures are an interesting solution for wastewater treatment problems because of their capacity to utilize inorganic phosphorus and nitrogen for growth (Yu et al., 2017). Microalgae are unique microorganisms which convert light energy, water and inorganic nutrients into a biomass resource rich in value-added products such as lipids, carbohydrates, proteins and pigments (Minhas et al., 2016; Pragya et al., 2013). Despite these advantages, broad commercialization of microalgae-sourced biodiesel has been restrained due to the high costs involved with production processes, which are mainly associated with the harvesting step as microalgae grow at low concentration (0.3–3 g/L) thereby generating large amounts of water to treat (Lam & Lee, 2012). Several methods have been proposed for microalgae harvesting, including centrifugation, filtration, membrane separation process and sedimentation. However, most of these methods have low efficiencies along with high operating costs and high energy consumptions. In this context, flotation is a good alternative, which consists of generating rising air-bubbles in a microalgae suspension. As a consequence, microalgae cells attach to bubbles and are transported to the surface without being damaged. However, the efficiency of this method is limited by the fact that the interaction between the bubbles and the cells is repulsive, due to the negative surface charge of both cells and bubbles in water, and to the low hydrophobicity of microalgae cells. In order to make this technique effective for harvesting microalgae, the original strategy proposed in this PhD relies on

functionalizing the bubbles used in the flotation process with adhesive compounds, which will allow them to effectively capture the cells during their rise.

For that, we need to identify a molecule that would allow attachment to cells and verify that functionalized bubbles with this molecule could indeed promote a better attachment to cells. The different steps that have allowed us to reach this objective are presented in Figure 1. In a first step, we developed a method based on atomic force microscopy combined with microfluidics (FluidFM) to produce functionalized bubbles (Demir et al., 2021), which we use to measure at the molecular scale the interactions with cells. Then, we analyzed the composition of microalgae cell wall using a combination of surface analysis techniques that are liquid chromatography and X-ray photoelectron spectroscopy (XPS). The information obtained from these analyses revealed the presence of chitin-like polymers on the cell surface, a molecule that, in theory, is able to interact with another similar and bio-based molecule, chitosan. In a third step, we analyzed at the molecular level the interactions between chitosan and the cell wall using atomic force microscopy. Through these experiments, we were able to show that chitosan could bind efficiently with cells and we were able to understand the molecular basis of these interactions. We then continued with this molecule and in a fourth step we modified it to make it amphiphilic so that it could be functionalized at the surface of the bubbles used in flotation. To evaluate whether bubbles functionalized with chitosan could adhere to cells, we use in a fifth step the method based on FluidFM to functionalize bubbles with this amphiphilic chitosan and measure their interactions with microalgae cells at the molecular scale. This step allows validating the strategy developed in this PhD project by showing that these bubbles adhere better to cells than clean bubbles, and by understanding why. This information is necessary to optimize in a last step, the flotation process to separate whole cell populations in flotation experiments, and thus to prove experimentally the efficiency of our technique.

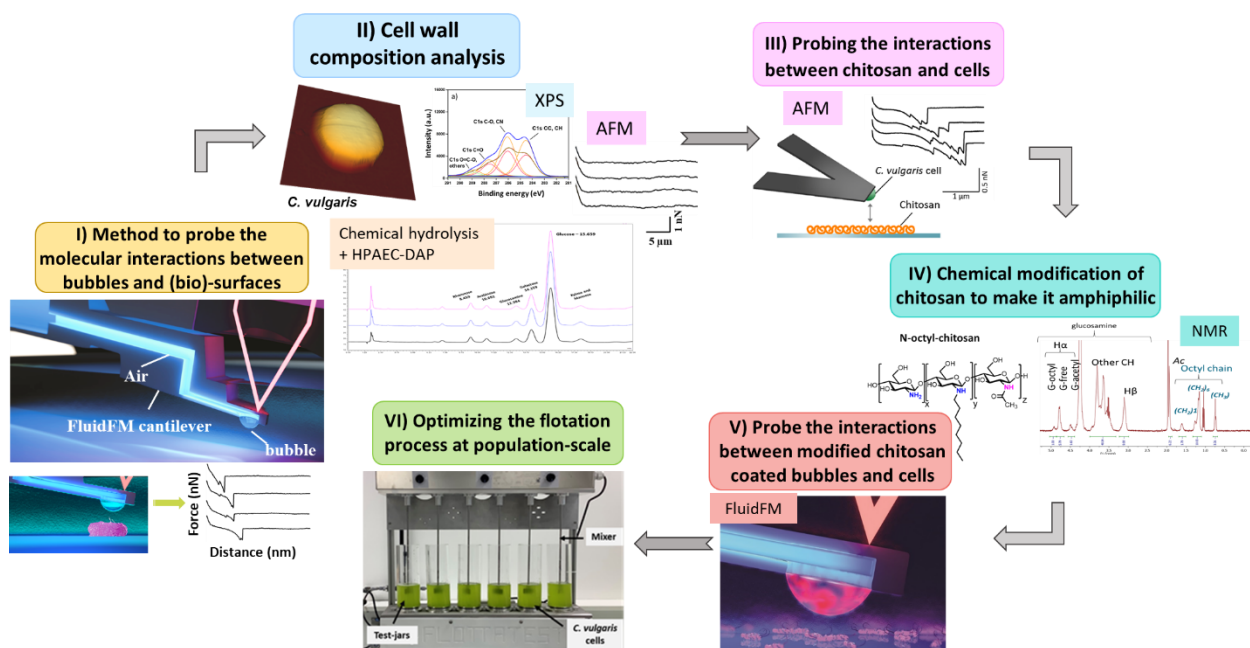


Figure 1: Schematic representation of the development of a new bubble surface engineering strategy for optimized microalgae harvesting using flotation technique. Work tasks I), II) and III) are described in chapters 3, 4 and 5 respectively whereas tasks IV), V) and VI) are described in chapter 6.

The work has been done so far with a species of green microalgae used for biofuel production in biotechnological processes, *Chlorella vulgaris*. In the future, we will be able to optimize this new separation process to harvest other species of microalgae of biotechnological interest, but also to use it for other applications than microalgae-based biomolecules production. For instance, this new separation process could be used for example to specifically separate microorganisms from complex media such as blood, which would be useful for the diagnosis of blood infections. The interest of the work carried out during this thesis thus extends well beyond the production of biofuels by microalgae, which shows its interest.

The present document is composed of 6 chapters. The **first Chapter** is a general overview of the PhD work. It will first consist of a brief literature overview about microalgae for biofuels and value-added molecules, challenges for harvesting techniques, classic harvesting techniques and their drawbacks and alternative harvesting techniques based on flotation. Then, a second part will review the work performed during the PhD and finally a discussion and conclusions on the main results obtained will be proposed. In **Chapter 2**, two reviews are presented; one focusses on natural flocculation mechanisms to separate microalgae cells from their aqueous media, and the second one treats of the use of atomic

force microscopy in microalgae studies. **Chapter 3** presents the new technique developed to produce micro-size bubbles using FluidFM, measure their interactions with (bio)-surfaces at the molecular scale and functionalize them to modulate their interactions with cells. **Chapter 4** is dedicated to the work performed on *C. vulgaris* cell wall analysis by combining AFM, XPS, and chemical hydrolysis followed by HPAEC-PAD. This part of the work has been conducted to identify the macromolecules that compose *C. vulgaris* cell wall. Then in **Chapter 5**, the interactions between chitosan, the molecule identified to adhere with *C. vulgaris* cell wall, and cells are probed at the molecular scale using AFM. Finally, in **Chapter 6**, the chemical modifications of chitosan to functionalize bubble surfaces, the interactions of functionalized bubbles with *C. vulgaris* cells, and the flotation process at the microalgae population scale are described. The appendices at the end of the document are composed of research articles in which I have participated, but that are not directly related to the subject of my PhD.

This PhD has been funded by Agence Nationale de la Recherche (ANR). It was supervised by Dr. Cécile Formosa-Dague, CNRS researcher at Toulouse Biotechnology Institute (TBI) hosted at INSA Toulouse (National Institute of Applied Sciences of Toulouse), and Prof. Dr. Pascal Guiraud, professor of Chemical engineering at INSA-Toulouse. Most of the experimental work has been performed in TBI and LAAS-CNRS (Laboratoire d'Analyse et d'Architecture des Systèmes), where my scientific responsible was Dr. Etienne Dague, CNRS research director at LAAS-CNRS. My thesis is part of national and international multidisciplinary collaborations that bring together different fields of expertise. Thus, during my thesis, I actively collaborated with Dr. Etienne Dague from LAAS for all the experiments performed with atomic force microscopy (AFM). The collaboration with Dr. Tomaso Zambelli from ETH Zurich (Switzerland) allowed the development of the method based on FluidFM to produce bubbles and measure their interactions with cells. The collaboration with Prof. Dr. Koenraad Muylaert from the Katholieke Universiteit Leuven (KU-Leuven, Belgium) helped in understanding the interactions at the molecular level between chitosan and cells. Finally, Dr. Christophe Coudret from the Laboratoire Interactions Moléculaires et Réactivités Chimiques et Photochimiques (IMRCP, Toulouse) provided valuable assistance in modifying chitosan and making it amphiphilic. Local collaborations between TBI, LAAS and IMRCP were developed within the FERMAT Research Federation. Collaborating with these experts, coming from different disciplines and complementary to mine, allowed me to evolve in a rich environment

and to work at the interface between different fields in an interdisciplinary approach. Finally, this work has been performed thanks to the technical assistance of Fabien Mesnilgrete and Sandrine Assié-Souleille from LAAS-CRNS, and of Abdlali Khalfaoui, Claude Lemen, and Nathalie Clergerie from TBI, responsible of the equipment used.

Chapter 1. General Overview

1.1. General context

The aim of this general context section is to highlight the important questions that motivated the work performed during this PhD and to give the background information about the PhD topic. It does not consist of a bibliographic analysis. Such analysis on the main general aspects of the work has been published under the form of two reviews that are presented in Chapter 2. In addition, each publication that has been written during the PhD contains more bibliographic analysis on the specific topics they treat; these publications are presented in Chapters 3, 4, 5 and 6. But because of the interdisciplinary nature of this work, this general context is important to give the information needed for all readers, coming from different fields, to understand the ins and outs of the work.

1.1.1. Microalgae for biofuels and value-added molecules production

The introduction of microalgae in the field of biofuels production could at some point allow to replace the conventional fossil fuels, and this way achieve the aim of sustainable and clean energy. The advantages that make microalgae a potential new generation of feedstock for the production of biofuel and molecules of interest are numerous. First, microalgae are capable of all year round production (Brennan & Owende, 2010), they grow on aqueous media but need less water than terrestrial crops (Dismukes et al., 2008). Besides, nutrients for their cultivation can be found in wastewater, and there is no need for herbicide or pesticide application (Rodolfi et al., 2009). They also have a rapid growth rate; to give an example, microalgae can achieve a yield 10 to 20 times higher than oil palm. Bio-lipids can be produced from different crops such as mustard, palm oil, sunflower, hemp and microalgae. But among them microalgae are the biggest oil producers (Chisti, 2008; Schenk et al., 2008). To give an example, compared to soybean, microalgae can produce up to 300 times more of oil (Ziolkowska, 2014). Moreover based on rough estimations, the yield (per acre) of oil from microalgae is over 200 times the yield of the best-performing plant/vegetable oils (Sheehan et al., 1998). Additionally, microalgae are the most effective organisms to tolerate stresses in their environment. Under stress environment, they have the ability to undergo some physiological modification that causes them to alter nutrient contents and biomass composition. For example, many species have increased their oil content up to 50-70 % dry

weight of biomass (L. Jiang et al., 2016; Pan et al., 2011) when cells are subjected to physiological stress conditions or unfavorable environment, such as nutrient limitation or photo-oxidative stress (Y. Jiang et al., 2012). For example under nitrogen deprivation condition the lipid content of the green microalgae *Chlorella emersonii* has reached up to 63% of its dry weight (Scragg et al., 2002). This property of microalgae has been utilized in many research studies, where nutrient composition or salinity have been altered in microalgae cultivation for producing biomass with high lipid yields, proteins or carbohydrates depending on the final applications (Aslam et al., 2018).

However, biofuel production is not the only application of microalgae in green biotechnology. As mentioned earlier in the introduction, they can also produce a wide range of metabolites such as proteins, lipids, carbohydrates, long-chain polyunsaturated fatty acids, carotenoids or vitamins for health, food and feed additives and cosmetics (Minhas et al., 2016). For example, dried microalgae could be used as high-protein feeds for animals such as shrimp and fish (Demirbas, 2009). Additionally, microalgae can be used in other applications, such as wastewater treatment, resources recovering systems and waste mitigation.

Although microalgae cultures have numerous interests, there are few challenges that industries need to face to scale-up their production in a cost-effective manner. For instance the use of microalgae as a feedstock for biofuel production is still in its early stages, and cost reduction at different steps of microalgae production should be carried out to make the process economically feasible, hence, competitive (Colling Klein et al., 2018). For example in 2013, industries produced only 20 kt/year of microalgae biomass at a production cost of \$20/kg (Benemann, 2013). To compete in large scale market such as energy, microalgae biomass production should be increased up to 10^4 kt/year at a production cost of \$0.50/kg (Chisti, 2008). Thus at the moment, only production of high-value compounds related to aquaculture and human consumption are being performed on an industrial scale using microalgae. An example of such compounds is astaxanthin, an anti-oxydant molecule. Astaxanthin synthetically produced at a cost of \$1000/kg has a market value of more than \$200 million per year. However, because synthetically manufactured astaxanthin is not permitted for human consumption and human related products, biologically produced astaxanthin carries a great importance in these markets (Olaizola, 2003). For example, the microalgae species *Haematococcus pluvialis* is currently used to synthesise commercial

Astaxanthin at a production cost of \$15,000/kg. In the current scenario, large-scale microalgal biomass production for biofuel production generally involves higher costs and higher technical challenges than land crops (Alam et al., 2012). Production of biolipids from microalgae is still at early stage as the use of conventional microalgae production technologies involves high investments cost and results in high biofuel production costs (Colling Klein et al., 2018). For example, algal lipids can be produced in open pond reactor with a minimum selling price of 12.33\$/gallon (Richardson & Johnson, 2014). However, the price of gasoline is 3.963 \$/gallon. Thus to compete with gasoline prices, optimization needs to be performed every stage of microalga biomass production system to produce biofuels. The first challenge that industrial meet is related to cultivation of cells. Cultivation of microalgae is nowadays possible in different types of systems; open, closed and hybrid systems (Bazaes et al., 2012). Open systems are directly exposed to harsh environmental conditions such as temperature changes and direct sun light but they provide an economic and convenient way to cultivate microalgae (Chew et al., 2018). Unstirred ponds, race track type pods and circular pods are examples of open systems. For example unstirred ponds use natural water where other microorganisms are present and can compete with microalgae growth (Converti et al., 2009). Another problem with this type of system is the poor aeration that is due to the lack of mixing. But even when mixing is introduced in open systems, other problems remain such as a lack of temperature control and a high contamination risk that can cause the culture to crash. Close systems can eliminate these disadvantages. Closed systems, also known as photobioreactors (PBR) (Tasić et al., 2016) are now widely studied. The reasons for that is that (i) growth conditions in a closed system can be controlled, and (ii) contamination of cultures by predator microorganisms can be avoided. Growth in PBRs results in a higher biomass-to-substrate conversion ratio and better economic production efficiency compared to open systems (Norsker et al., 2011). But for most of closed systems, flat panel bioreactors, airlift column bioreactors, tubular bioreactors and others, scale up can be a challenging step and often needs additional materials (Chew et al., 2018). The production efficiencies and capacities of each systems, open or closed, can vary greatly depending on the species used, the environmental conditions, the mixing mechanism and the culture medium used. Open systems have been widely used in large scale applications because of their economic aspects and simplicity. Closed systems, on the other hand, are primarily intended to cultivate microalgae in optimum conditions and overcomes most of the concerns mentioned above for open systems. But

whatever the cultivation system used, microalgae grow at low concentration (0.5-5 g/L) and thus generate liters of water to treat to harvest them. It has been estimated that microalgae biomass harvesting accounts for between 20 and 30% of the total microalgae processes costs (Molina Grima et al., 2003); more effective microalgae cell harvesting techniques should therefore be developed. This is the objective of this PhD project, which focuses on developing a cost-effective harvesting method. In the next part, microalgae harvesting techniques will be covered.

1.1.2. Classic techniques used to harvest microalgae

The problem of microalgal biomass harvesting has been extensively studied, and so far the main separation techniques used are centrifugation, sedimentation, filtration, and flocculation. However, most of these methods have a low efficiency for high operating costs and high-energy consumption. Yet, there is no single universal harvesting method for all microalgae species and/or applications that would be both technically and economically viable (Rashid et al., 2018; Tiron et al., 2017). For instance, centrifugation, the currently most used option in industrial scale production systems, is based on a mechanical gravitational force that allows an efficient harvesting of suspended cells in a short time. However, because of the high energy requirements of this technique, which may also damage cells due to the high shear forces, its use is recommended only for high-value microalgae-based products such as in foods and pharmaceuticals industries (Tiron et al., 2017; Gupta et al., 2016). In filtration processes, membranes with a pore size smaller than microalgae size are used; this way micro-sized algal cells are retained on the membrane surface when filtrated under high pressure, where they form a thick paste of algal biomass (Uduman, Qi, Danquah, Forde, et al., 2010). In this process, the membrane holds the algae whereas culture medium goes through the filters (Gerardo et al., 2015). This size-exclusion method may be useful and scalable for algae harvesting only if problems in membrane clogging can be minimized or prevented (Hwang et al., 2013). Finally for large-scale harvesting of a wide variety of microalgae species, flocculation combined with settling appears to be a promising low-cost approach (Molina Grima et al., 2003); but nevertheless, contamination remains a major concern in this technique, as synthetic flocculants that are usually used to induce flocculation end up in the harvested biomass and can interfere with its final application (Vandamme et al., 2013) (Demir, Besson, et al., 2020).

1.1.3. Flotation is an alternative harvesting technique with great potential

In this context, flotation is believed to be an effective harvesting technique based on the natural low density and self-floating tendency of microalgae cell. In air flotation, the harvesting process is based on the generation of rising air bubbles that bind to microalgal cells and bring them to the liquid surface (Laamanen et al., 2016). However, due to differences in the surface hydrophobicity and surface charge of microalgae cells, the harvesting efficiency of this technique varies greatly depending on the microalgae species used (Garg et al., 2012b) and culture conditions. The surface of the bubble being hydrophobic and negatively charged in water (Yang et al., 2001), they repel microalgae cells, thereby preventing their capture and flotation. The capture of cells by bubbles depends mainly on the probability of the bubbles to make contact with cells (Sarrot et al., 2005). This is illustrated in Figure 2. For that both the size of the cells and of the bubbles is important. Indeed, smaller cells will have a lower probability of colliding with bubbles compared to larger cells. On the other hand, more and smaller bubbles improve the probability of colliding (Coward et al., 2015). Let's detail this point. For particles smaller than 100 nm, colloidal interactions between particles and bubbles (electrical double-layer and non-DLVO hydrophobic forces), as well as Brownian diffusion of the particles are the key factors controlling particle separation. For example in the case of nanoparticles, the separation efficiency can be increased by using smaller bubbles to increase their specific surface areas for Brownian diffusion (Zhang & Guiraud, 2017). For larger particles, the efficiency of collection is mostly determined by particle interception and collision with bubbles (Miettinen et al., 2010; Mishchuk et al., 2006; Nguyen et al., 2006). In the case of the microalgae cells, working with smaller bubbles is thus very important to maximize the chances of collision of cells with bubbles. Another aspect to consider is the bubble interface contamination, which can have a significant effect on the bubble hydrodynamics and change drastically the collision efficiency, thereby the capture efficiency (Legendre et al., 2009; Sarrot et al., 2007). Contaminated bubbles rise with a decreased speed thus will have an increased residence time so enhances the change to collide with a (bio)-particles (Huang et al., 2012; Zhang & Guiraud, 2017). There are different types of flotation techniques available such as dispersed air flotation (DiAF), electro flotation and dissolved-air flotation (DAF). These techniques are different in the way bubbles are generated, which has an impact on bubble size and flow condition (Matis & Lazaridis, 2002). Among these techniques, DAF allows

producing small bubbles ($< 100 \mu\text{m}$), which take more time to rise to the surface and also offer a greater surface area per air unit volume, therefore increasing the probability of collision (Laamanen et al., 2016).

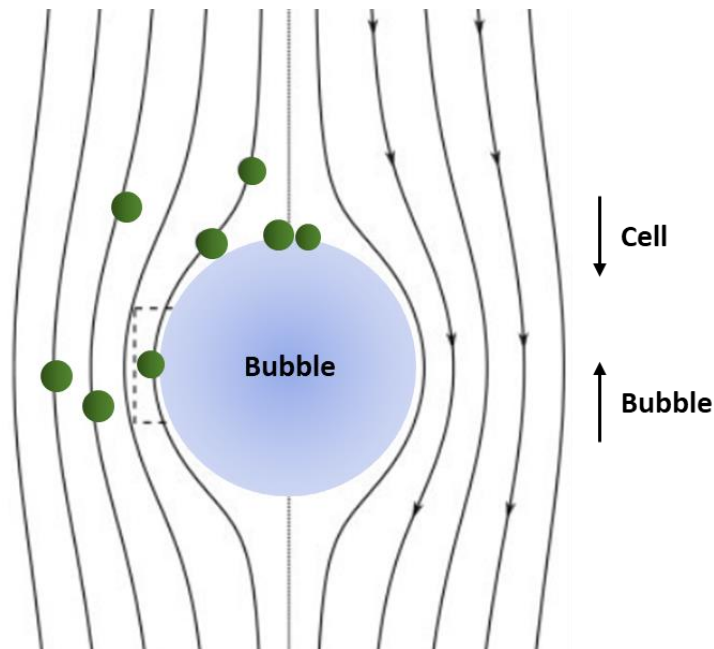


Figure 2: Bubble– (bio)-particle interaction process. Water stream line around a bubble caused by relative motion between the bubble and surrounding liquid. Adapted from (Yan et al., 2016) .

To make flotation more efficient for microalgae harvesting, one alternative is to add a flocculation step prior to the flotation process. For this, flocculants are added to the algal suspension to aggregate cells into large flocs that can be easily removed from the water (Lama et al., 2016). Usually, spontaneous aggregation of microalgal cells in suspension is prevented by the negative surface charge of most microalgae species (Molina Grima et al., 2003). To trigger floc formation, the addition of positively charged ions or polymers is thus often required. The flocculation of microalgae can be mediated through five different mechanisms acting alone or simultaneously. These mechanisms are presented in Figure 3; they are also described in detail in Chapter 2.1. Briefly, the first one is the compression of the electric double layer which consists in decreasing electrostatic repulsive forces *via* the lowering of the surface charge by pH variations in the suspension. Second, in charge neutralization, positively charged ions, polymers or colloids strongly absorb on the negatively charged surface of microalgae cells. In the bridging mechanism, polymers or positively charged colloids simultaneously bind to the surface of two different microalgae cells to form a bridge between them and bring them together. The fourth mechanism is the electrostatic patch mechanism in which a charged

polymer binds to microalgae cells with opposite charge resulting in patches of opposite charge on the microalgae surface. The last one is the sweeping mechanism where the massive precipitation of a mineral present in the cultivation media entraps microalgae cells and aggregate them (Besson & Guiraud, 2013b; Demir, Besson, et al., 2020). Depending on several parameters such as the microalgae species used, or the conditions in which they are cultured, one or another mechanism takes place. In many cases, this flocculation step is performed using synthetic flocculants, which can contaminate the harvested biomass including contamination of downstream processes and of the recycled water. For these reasons natural flocculation can be a preferred alternative. So far two types of natural flocculation mechanisms are identified: auto-flocculation, where the flocculation is triggered by a molecule or precipitate that naturally forms in the culture medium, and bio-flocculation, where a molecule produced by cells, such as biopolymers, is directly responsible for the flocculation. To mimic these natural flocculation mechanisms, bio-sourced polymers can be used as flocculants. They present different advantages; they are non-toxic, biodegradable, relatively cheap and are abundantly available in nature (Pal et al., 2005; Renault et al., 2009).

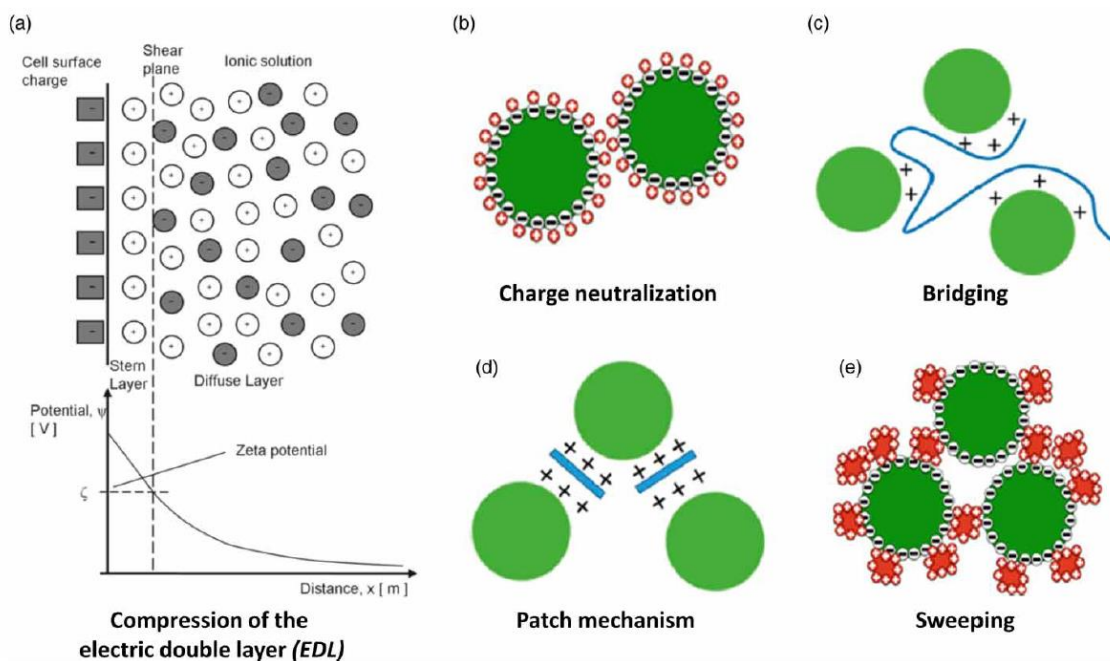


Figure 3: Schematic representation of natural flocculation mechanisms. (a) Compression of the electric double layer (EDL), (b) charge neutralization, (c) bridging, (d) sweeping, and (e) patch mechanisms. Extracted from (Demir, Besson, et al., 2020)

There is also another way to increase the flotation efficiency. Instead of working on the cells and flocculate them, an alternative is to work on the bubble surface and functionalize it with a molecule that will allow modulating their interactions with cells. The first example that shows that bubble interactions could be modulated through bubble functionalization has been performed in 1994 by Ducker and co-workers, who used sodium dodecylsulfate (SDS), a surfactant that adsorbs at the bubble surface rendering it hydrophilic. When probing the interactions with a silica sphere, their results showed the removal of the hydrophobic force that was taking place with clean bubbles (Ducker et al., 1994). These experiments were the first to demonstrate that it is possible to modify the interaction of bubbles by modifying their surface physico-chemical properties (Demir et al., 2021). It is a long time after, in 2008, that this concept was used for microalgae harvesting applications. Indeed, the team of Henderson was the first to use functionalized bubbles in flotation process to enhance harvesting efficiency (Henderson et al., 2008a, 2010). In the strategy developed by this team, bubbles are functionalized with cationic polymers that make the bubble surface positively charged. These positively charged bubble surfaces can then attract negatively charged microalgae cells without the requirement for cell flocculation. They named this technique PosiDAF as the bubbles used were generated using DAF technique. The two most promising PosiDAF cationic polymers identified were a cationic surfactant cetyltrimethylammonium bromide (CTAB), as well as a polymer polydiallyldimethylammonium chloride (polyDADMAC) (Henderson et al., 2008a, 2010). In this case, to produce the functionalized bubbles, these surfactants were directly added to the saturator containing water. This mixture was then pressurized and shaken until stabilization. The pressurized solution was then released into the microalgae suspension to let the flocculation of cells occur with the functionalized bubble. This technique has demonstrated that by functionalizing bubble surface it is possible to increase the removal efficiency of microalgae to levels comparable to those of conventional flocculation/flotation process but without the requirement for prior flocculation. A similar strategy had also been previously described in our team, where surface-functionalized microbubbles – colloidal gas aphanes (CGAs)-, were used to harvest SiO₂ nanoparticles (Zhang & Guiraud, 2017). In this case, negatively and positively charged CGAs were produced with cetyl trimethylammonium bromide (CTAB) and sodium dodecyl sulfate (SDS), leading to a separation efficiency of 90-99%. Thus, these works demonstrate that by using functionalized bubble we can perform flotation in a one-step process and this way reduce the time needed and thus its overall cost.

In the scope of this PhD, biopolymers can be interesting for instance chitosan, starch, cellulose or lignin, as our aim is to functionalize bubbles with a molecule that will stick to the cell wall without altering cells. For instance, polysaccharides like chitosan are often able to form homotypic interactions with other polysaccharides that can be present at the surface of cells (Formosa-Dague, Castelain, et al., 2018). Our idea is that if these molecules can act as a flocculent because they interact with cells, then we can functionalize them at the surface of bubbles so that the bubbles will directly interact with cells and bring them to the surface, in a one step process. But before that a required task is to first understand how flocculant and cells interact, and determine the flocculation mechanisms involved.

1.1.4. Techniques to study microalgae; Atomic Force Microscopy (AFM)

So far, there have been many attempts to understand the mechanisms involved in microalgae flocculation at the macroscopic level, yet, only a few studies confirm those mechanism at the microscopic level. Few strategies including focused beam reflectance measurement (FBRM) (Uduman, Qi, Danquah, & Hoadley, 2010), optical inverted microscopy imaging and contact angle measurements using the sessile drop method (Ozkan & Berberoglu, 2013a) have been used to understand the microalgae interaction as well as its physico-chemical surface properties. Another type of technology that can be used to study microalgae and their interactions is atomic force microscopy (AFM). AFM, first developed in 1986 (Binnig et al., 1986), relies on the control of a force acting between a sharp tip and a surface, while scanning a sample. This way nanoscale high resolution images while being operated in liquid which makes it possible to monitor and image live cells surfaces. Moreover, AFM is also a force machine able to record forces at the piconewton level thus making it possible to gain insights into the interactions of cells with their environment. This method is thus a surface probing method, making it different from other types of microscopies such as electron or optical microscopies. As the tip scans the surface of the sample, the cantilever on which it is fixed gets deflected. This deflection is recorded thanks to a laser reflected on a photodiode, thereby allowing to collect the signal (Figure 4). One of the attractive advantages of AFM over other nanoscale microscopies such as scanning electron microscopy (SEM) or transmission electron microscopy (TEM), is its ability to operate in liquid, which makes it possible to monitor live cells in real time (Demir-Yilmaz et al., 2021a). For example, in SEM, TEM and two-photon

imaging samples needs to be water-free and immobilized on surfaces which allow only static snapshot of the samples (Reifarth et al., 2018). However, AFM provides the opportunity for direct visualization of cell surface morphology in environmental conditions (adjustable pH, temperature and salt concentration) as it operates in liquid. AFM application for living cells, and more specifically for microalgae, is covered in detail in Chapter 2.2. But in short, compared to SEM or TEM, AFM can also record forces in force spectroscopy mode, thereby giving access to the nanomechanical and adhesive properties of cell surfaces. For example, nanomechanical measurements provide important information on the cell wall which is responsible for maintaining cell morphology, and which represents its interface with the surrounding environment. In addition, AFM has already been effectively used to understand adhesive behavior of microalgae cells toward flocculants and their interactions with particles or molecules present in their environment (Formosa-Dague, Gernigon, et al., 2018a; Besson et al., 2019). Finally, these recent years, new AFM developments have been made, for example FluidFM that combines AFM with microfluidics. Basically, in this system, the standard AFM cantilevers are replaced by cantilevers containing a microfluidic channel that can be filled with any liquid or air (Meister et al., 2009b). Such developments further enhance the possibilities of AFM technology to access new information and answer more fundamental questions on living systems.

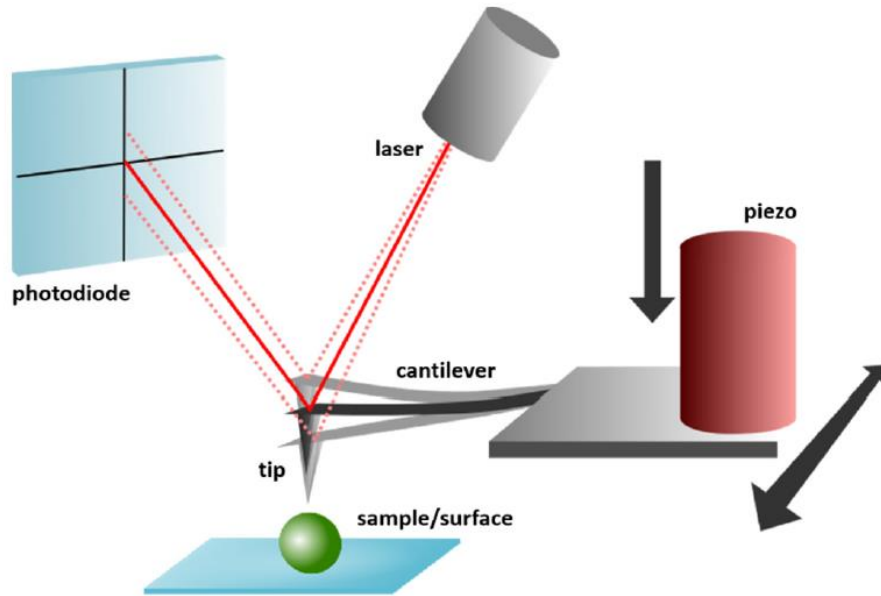


Figure 4: Atomic force microscopy principle. A sharp tip mounted on a cantilever can move in the x, y and z direction thanks to a piezo-electric ceramic. While scanning the sample, the deflection of the cantilever is recorded thanks to a laser reflected on a photodiode. Extracted from (Demir-Yilmaz et al., 2021a)

In FluidFM, a micro-sized channel is integrated into the AFM cantilever and connected to the pressure controller. Thanks to its close fluidic channels, reservoir and aperture at the end of the cantilever, liquids can be aspirated within the cantilever microfluidic channel and dispersed locally. FluidFM has already been used in various types of applications. For example in material science, it has been used for sub-micrometer etching (Meister et al., 2009b), for local functionalization of polymer layers (Hirt et al., 2015) or for electrochemical 3D printing of conductors with microscale resolution (van Nesselroy et al., 2022). For that, the microchanneled nanopipette cantilevers that are used are capable of delivering electrolyte through submicroscale openings at the edge of the cantilevers. Thus, the 3D printed constructions are built layer by layer, allowing for sophisticated geometrical shapes to be built, such as double rings, helices, and tripods (van Nesselroy et al., 2022). Moreover, FluidFM is also used in biological sciences where it provides the opportunity to overcome several single-cell spectroscopy problems. For example FluidFM enables to isolate single cells by applying an under-pressure in the microchannel; this way single cells can be tightly immobilized at the aperture of the cantilever, and can be used to probe cell-cell interactions or cell-surface interactions in a reliable way (Demir, Blockx, et al., 2020; Demir-Yilmaz, Yakovenko, et al., 2022), or to transfer cells to targeted areas to observe cell behaviors.

Moreover, a major application of FluidFM in life sciences is the extraction of molecules directly from cells' cytoplasm for molecular analysis, using the cantilevers' tips to puncture the cell outer membrane or cell wall (Guillaume-Gentil et al., 2013, 2016, 2022; Potthoff et al., 2015). Such strategy can also be used to inject cells with biomolecules or fluorescent dyes, this way by applying an overpressure (Guillaume-Gentil et al., 2016).

1.1.5. Conclusion

Microalgae really do have the potential to contribute to meet the challenges of the 21th century in terms of CO₂ emission if we can use them for biofuels production to replace fossils fuels, and this way the aim of sustainable and clean energy could be reached. Yet their industrial use is limited by different factors regarding their production, the most important one being the lack of efficient harvesting techniques. This is why microalgae harvesting is an important and active field of research, with a lot of different methods that have been developed to harvest cells. Among them, flotation is an interesting separation technique that has showed its potential in other industries such as ores (Houot, 1982; M. Ma, 2012), water treatment, and plastics separation (Pita & Castilho, 2017). However, this process is challenging in the specific case of microalgae. Being negatively charged, as the surface of air bubbles in water is also negatively charged, they repel each other preventing adhesion and thus capture and flotation. So far, flotation has already been used to separate microalgae cells but most of the time in combination with flocculation. One research group though, in Australia, worked at making this method efficient by eliminating the pretreatments like flocculation through coating the surface of bubbles with positively charged surfactants or polymers such as polydiallyldimethylammonium chloride (polyDADMAC) (Henderson et al., 2010). This process, called PosiDAF, has notably proven to be an efficient method to harvest *Melosira aeruginosa*, *C. vulgaris* and *Asterionella formosa* cells. Indeed, for these species, maximum removal efficiencies of 97% for *M. aeruginosa*, 54% for *C. vulgaris* and 89% for *A. formosa* could be reached with bubbles functionalized with cationic surfactants with different effective doses (Henderson et al., 2008a, 2008b). In this PhD we also explore this type of strategy, but instead of changing the charge of bubbles, our idea is to modify the bubble surface with a molecule that will specifically interact with the cell wall of microalgae. The next chapter will present the work performed to reach this objective. In the first part of the thesis, we developed a method to produce micro-sized, stable bubbles and measure their interactions with single microalgae

cells. Then, in the second part we analyzed the cell wall composition of *C. vulgaris*; the information obtained from these analysis and data from the literature allowed us to make strong hypothesis on the polysaccharides present in the cell wall, and select one for the rest of the project, chitosan. Then in the third part we used AFM to understand the flocculation mechanism of chitosan by measuring its interactions with cells at the molecular level. Thereafter, we modified chitosan to make it amphiphilic, and for that polyoctyl hydrophobic chains were added (N-alkylation by reductive amination) on the chitosan backbone. Finally, we took advantage of the amphiphilic characteristic of this new chitosan-based molecule to modify the bubble surface, probe the interactions between these functionalized bubbles and cells and finally perform separation of cells at the population-scale in flotation experiments.

1.2. Review of the PhD work

The aim of this review of the PhD work is to now present the experimental work that was performed to reach the objective set in this PhD, developing a new strategy to efficiently harvest microalgae cells by flotation using functionalized bubbles. The different subtitles of this section correspond to the different steps of the strategy we put in place during this PhD, exposed in the general introduction (p9). These results can also be found in the papers publications presented in Chapters 2-5. Also, in this section, elements of discussions on the results obtained are also included

1.2.1. Development of a method to measure the interaction between bubbles, functionalized or not, and cells at the molecular scale.

This part of the work is described in detail in the article entitled “Probing the interactions between air bubbles and (bio)interfaces at the nanoscale using FluidFM technology”, by Demir et al., JCIS, 2021, presented in Chapter 3.

During flotation separation process, cells are captured by rising air bubbles. While they rise, they interact with cells and bring them to the surface. Thus, for this separation technique to be the most effective with microalgae cells, during the process cells need to interact more with the air bubbles. For that the strategy that we chose to develop in this PhD is to engineer the surface of the bubble and make it adhesive for cells. But before any of that can be done, we need to find a way to understand the physico-chemical basis of these interactions at the molecular scale. While the fluid dynamics aspects of bubbles-(bio)surfaces interactions have been well studied (Walls et al., 2014), yet the molecular mechanisms involved remain largely unresolved because of the lack of techniques to probe them (Demir et al., 2021). One possibility to access these interactions is to use atomic force microscopy (AFM). It was first used to measure the interactions between air bubbles and particle(s)/surface(s) in 1994 (Ducker et al., 1994). For that, the authors used the colloidal probe method in which silica particles were attached on cantilevers; these colloidal probes were then used to measure the interactions with bubbles with diameters of several hundreds of nm, stabilized on hydrophobic surfaces (Ducker et al., 1991). Regarding the interactions between bubbles and bio-surfaces, so far in the literature, only two studies have focused on probing the interactions between bubbles and microorganisms using AFM (Ditscherlein et al., 2018; Yumiyama et al.,

2019). In the first study by Ditscherlein and coworkers, the colloidal probe method described in 1994 was further improved to analyze the interactions between air bubbles and layers of cells of the yeast species *Saccharomyces bayanus*. In this case, bubbles, generated by gas supersaturation, were picked up with hydrophobic cantilevers and yeast cells were immobilized on surfaces (Ditscherlein et al., 2018). This was the first trial to measure and characterize the interactions between an air bubble and microorganisms in liquid, using AFM. Notably, the results of this study indicate that these interactions are primarily hydrophobic, but can be affected by pH, salt concentration, ionic strength or ethanol concentration. Later, Yumiyama *et al.* measured in 2019 the interactions between single yeast cells of the species *Saccharomyces cerevisiae* instead of a layer of cells, and microbubbles using AFM (Yumiyama et al., 2019). The results showed also that hydrophobic interactions were taking place between yeast cells and microbubbles. In these two examples, even though experimental parameters such as pH or ionic strength, as well as system parameters such as applied force, approach velocity or contact time, are adjustable, a major issue remains. Indeed, the size of the bubble used to probe the surface of cells is not controlled over time because of the Laplace pressure (Eriksson & Ljunggren, 1999; Ljunggren & Eriksson, 1997). Laplace pressure is the differential pressure across inside and outside of a curved surface or interface that forms a boundary between gas and liquid region (Butt et al., 2006). Over time the gases inside the bubble dissolve in water, which modifies the size of the bubble and thus the contact area between the bubble and the sample, leading to a change in the adhesion forces recorded. To give an example, when the interactions between bubbles and a cell surface are probed, this change in the contact area modifies the number of molecules from the cell surface involved in the interaction, and results in a change in the adhesion force recorded. Moreover, uniformity of the bubble and bubble size during force measurement is another bottleneck of these studies as the different bubbles fixed on hydrophobic cantilevers do not have a controlled and homogeneous size.

To overcome this challenge, we took the advantage of the FluidFM technology that combines AFM with microfluidic AFM probes (Meister et al., 2009b). In this system, a micro-sized channel is integrated in an AFM cantilever and connected to a pressure controller system (pressure range from -800 to 1000 mbar), thus creating a continuous and closed fluidic conduit that can be filled with a solution, while the tool can be immersed in a liquid environment. An

aperture size ranging from 300 nm to 8 μm at the end of the cantilever allows liquids to be dispensed locally. Force feedback is then ensured by a standard AFM laser detection system that measures the deflection of the cantilever and thus the force applied to the sample (Meister et al., 2009b). This technology has already been used for several applications from force measurement of cell adhesion (Potthoff et al., 2012, 2015), to the nano-injection of fluids into living cells (Stiefel et al., 2012), lithography (Grüter et al., 2013) or patch-clamping (Ossola et al., 2015). But here, in the first part of this thesis, we used FluidFM in an original manner to produce micro-sized bubbles of 8 μm in diameter, directly at the aperture of the microchanneled FluidFM cantilevers. For that, instead of liquid, the cantilever is filled with air and immersed in a liquid environment. Then, by applying a positive pressure inside the cantilever, it is possible to form bubbles of controlled size directly at its aperture. A schematic representation of this system is presented in Figure 5. Because the same pressure is maintained in the cantilever during the experiment, the dissolution of the gases from the bubble is compensated, which allows keeping the size of the bubble constant over time.

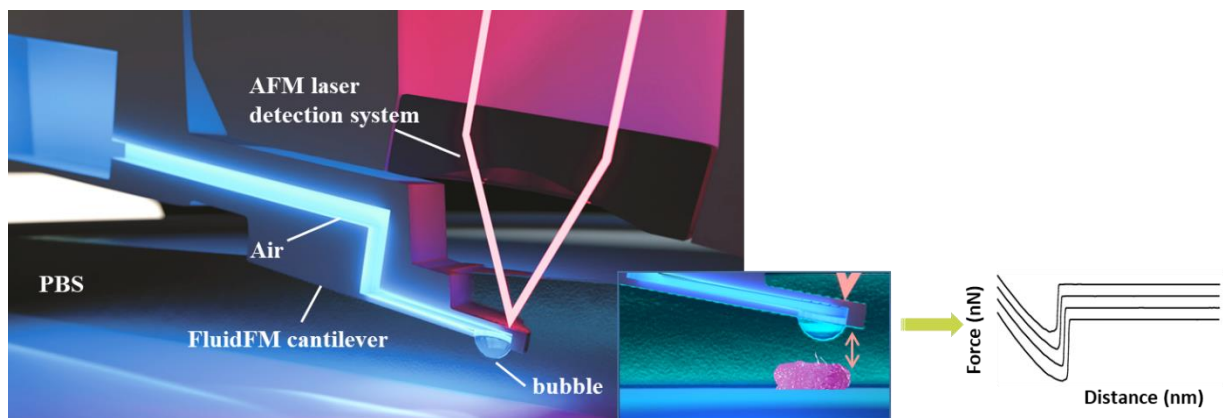


Figure 5: Schematic representation of the method to produce bubbles using FluidFM technology. A FluidFM microchanneled cantilever with a circular aperture of 8 μm diameter, connected to a pressure controller, is filled with air and immersed in liquid. By applying a positive pressure, an air bubble can be formed at the aperture of the cantilever and their interaction with the cells measured. Adapted from (Demir et al., 2021).

With this bubble, we then could probe the interactions with abiotic surfaces such as (bio)-polymers (details can be found in chapter 3) or biotic surfaces such as *C. vulgaris* cells in force spectroscopy mode. On typical force distance curves, as shown in Figure 6, the AFM tip approaches the surface, and then is retracted from it. During the approach, the tips contacts the surface at point B on the figure 6. Further, the tip indents in the surface, which gives the blue part on the curve. When it reaches the predefined applied force (C), the approach curve

ends and the retract curve, shown in red, starts. This time the tip moves away from the sample. If there is an interaction between the tip and the sample, the tip stays in contact with the sample and the cantilever starts to bend upon retraction (shown in red, D). But at some point, (point D), the retract force is higher than the adhesion force between the tip and the sample; the interaction breaks and the cantilever goes back to its initial position (E). This is reflected on the curve by a retract adhesion or retract peak. When we measure the height of this peak, we can directly access the adhesion force of the interaction. The interesting point is that depending on the shape of these retract peaks we are able to determine the physico-chemical basis of the interactions. For non-specific interaction such as hydrophobic interactions, we usually observe a sharp single peak happening right after the contact point (Dague et al., 2008). For biological interaction (*i.e.* when a polymer is unfolded from the surface of a cell by the tip), we observe multiple peaks away from the contact point reflecting the multiple and/or sequential unbinding of sub-units of the molecules. Thus, force spectroscopy experiments allow accessing the interactions between bubbles and *C. vulgaris* cells. Understanding these interactions is needed in the context of this PhD to then be able to modulate them and this way increase bubble-cell adhesion and improve the flotation process.

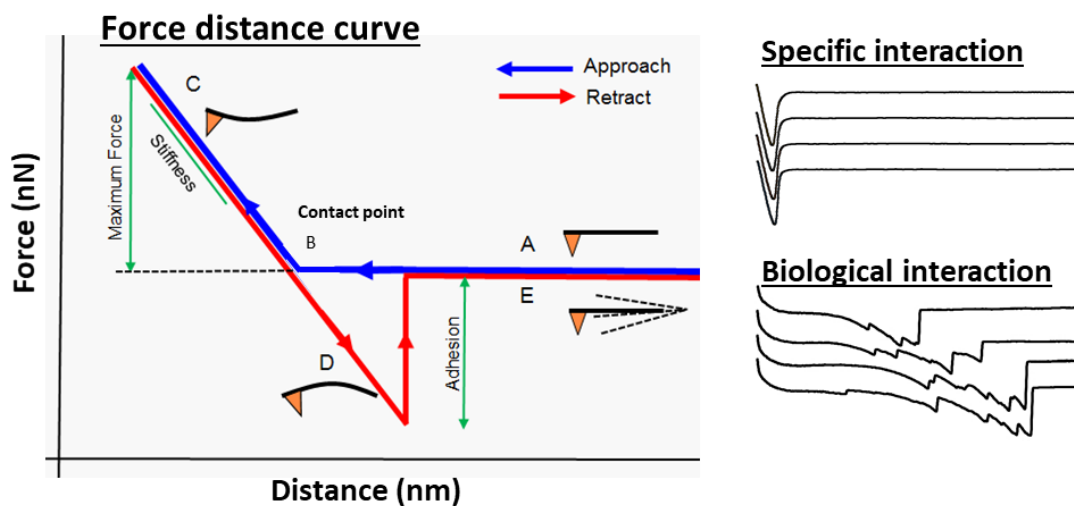


Figure 6: Force-Volume mode atomic force microscopy (FV-AFM). A typical force distance curve adapted from (Voigtländer, 2015) Approach force-distance curve (blue line) records the deflection (force) of the AFM cantilever when approaching to the sample. Retract force distance curve (red line) records the deflection of the AFM cantilever when cantilever stays away from the sample. Adapted from (Voigtländer, 2015)

The force curves obtained when probing *C. vulgaris* cells with a bubble produced by FluidFM (Figure 7a) showed a single retract peak occurring at the contact point on the force

curves, as shown in Figure 7b, with an average adhesion force of 4.2 ± 1.2 nN (Figure 7c) Giving the shape of the retract peaks obtained on the force curves, our results suggest that non-specific physico-chemical interactions are involved, most probably reflecting the hydrophobic properties of the cell surface. *C. vulgaris* cells are known as having a hydrophilic and negatively charged surface (Demir, Blockx, et al., 2020). The bubbles being also negatively charged in water (Yang et al., 2001), an electrostatic repulsion between bubbles and cells was expected. Yet the results show an interaction, that is most likely due to the hydrophobic attraction between the bubble and the cell surface, which is dominant compared to the electrostatic repulsion. To verify this, we looked at the approach curve, shown in green in Figure 7c. The approach force curves show a jump-in at the contact point that can be attributed to the hydrophobic attraction of the bubble to the cell surface, dominant over the electrostatic repulsion. Overall, the forces recorded between bubbles and microorganisms result from a balance between electrostatic repulsion and hydrophobic interaction.

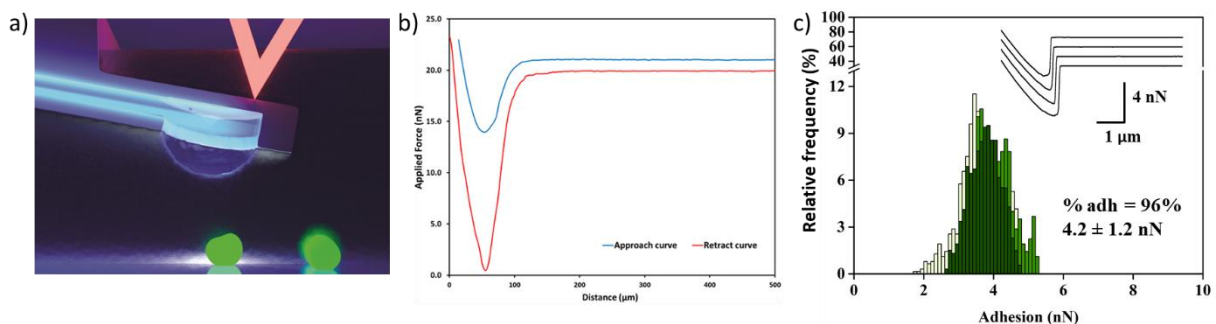


Figure 7: Probing interactions between bubbles and *C. vulgaris* cells. a) Schematic representation of bubble *C. vulgaris* interaction b) Adhesion force histograms obtained for *C. vulgaris* – bubble c) representative force curve obtained for *C. vulgaris*-bubble interaction. Adapted from (Demir et al., 2021).

But now in a next step, since we can now describe the interactions between clean bubbles and cells, we need to find a way to functionalize the surface of the bubbles produced using FluidFM and evaluate the effects of such functionalization on the interactions with cells. Ducker and co-workers demonstrated for the first time in 1994, that it was indeed possible to modify the interaction of bubbles with surfaces by modifying their surface physico-chemical properties with surfactant molecules (Ducker et al., 1994). Thus, in a next step, we developed a method to functionalize the bubble surface with a surfactant in order to modulate the interaction between bubble and cells as shown in Figure 8. For that, we worked with a model experiment, using a fluorescent surfactant that allows the direct visualization of the good

functionalization of the bubble interface. The strategy that we developed to functionalize bubbles consists in first filling the microchannel of the FluidFM probe with air and dipping it in a surfactant solution (Figure 8a), followed by aspirating the amphiphilic surfactant inside the microchannel, by applying a negative pressure (Figure 8b). The filled cantilever is then immersed in a surfactant-free petri dish where the cells are immobilized in buffer. The surfactant solution is locally released by applying a positive pressure (Figure 8c), leading to the formation of a bubble when all the surfactant solution is out (Figure 8d). Because the amphiphilic surfactant is at this moment in close proximity to the bubble, it directly assembles at the water gas interphase. The corresponding fluorescence microscopy images are presented in Figure 8e–g. Figure 8e shows a bottom-view of the cantilever filled with the fluorescent surfactant at a pressure of 0 mbar with no bubble at the aperture of the cantilever. When a pressure of 200 mbar is applied, the surfactants are ejected from the cantilever and a bubble forms at its aperture. As it can be visualized in Figure 8f the bubble produced is fluorescent, which means that the fluorescent surfactants are present at its surface. To verify the stability of the surfactant on the gas/liquid interphase, time course images were taken using fluorescence microscopy for 15 min. The resulting image (Figure. 8g) shows that the surfactant does not diffuse from the microbubble to its surroundings, proving that the functionalized bubble is stable over time and can be used in force spectroscopy.

While this model experiment demonstrates the possibility and applicability of the microbubble functionalization process, we then used this method to functionalize the bubbles with a molecule allowing to modulate the interactions of bubbles with cells. For that we chose a model microorganism, *Pseudomonas aeruginosa*. Based on our force spectroscopy experiments, the retract force curves show no retract peaks (Figure 8h) when clean bubbles are used, which means that bubbles do not interact with *P. aeruginosa* cell wall. We thus looked for an amphiphilic molecule able to bind specifically the cell wall of this bacterial species. Colistin, also known as polymyxin E, is a natural polycyclic antibacterial peptide which specifically interacts with lipopolysaccharide (LPS) (Yahav et al., 2012), the main component of *P. aeruginosa* outer cell membrane. Moreover, colistin contains both hydrophilic and hydrophobic moieties that gives it amphiphilic properties, which makes it good candidate for bubble surface functionalization. We thus used colistin to functionalize the surface of bubbles (concentration of 20 mg/L, Figure 8i) and performed force spectroscopy experiments. The

retract force curves obtained this time show multiple retract adhesions on long distances, up to 20 μm , that can be attributed to the unfolding of surface polymers, notably LPS, which interacts specifically with colistin at the surface of bubble. This experiment then proves that by functionalizing the surface of bubbles with specific molecules, we can indeed modulate their interactions with cells.

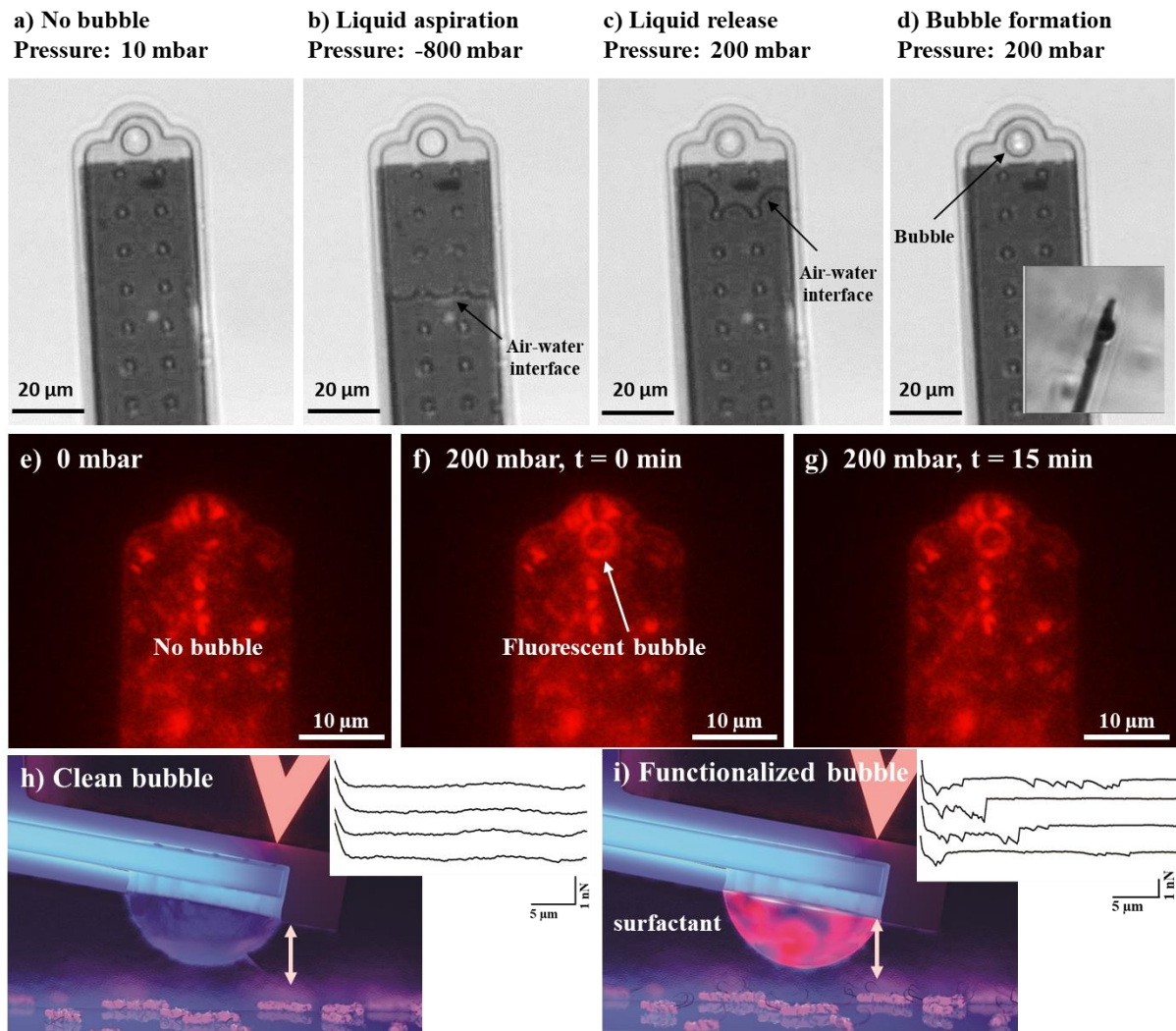


Figure 8: Functionalizing bubbles using a (fluorescent) surfactant and modulating its interaction with model species. Bottom view of a FluidFM probe at an applied pressure of (a) 10 mBar, (b) -800 mBar to aspirate the liquid, (c) 200 mBar to locally dispense the liquid outside of the cantilever and (d) 200 mBar pressure. Fluorescence images of the bottom view of a FluidFM probe containing surfactants at (e) 0 mbar, (f) 200 mbar with a bubble formed at its aperture and (g) after 15 min. Schematic representation of (h) clean bubbles – *P. aeruginosa* cell layers interactions, (i) colistin-coated bubbles – *P. aeruginosa* cell layers interactions. Adapted from (Demir et al., 2021).

This first step of this PhD is in fact a very important step as here we developed a new original strategy that provides the possibility to (i) produce microsized bubbles and measure their interactions with living cells using FluidFM, (ii) modify the surface of the bubbles

produced using FluidFM, and (iii) show in what way the modification of the bubble surface influences the nature and strength of the interaction with cells. This has many implications in the different fields where bubble-microorganisms interactions take place. For example, in water purification or membranes technologies where biofouling is an important problem, various kind of microorganisms are accumulated on the membranes, which can cause a lack of permeate flux, quality and membrane life span (Maddah & Chogle, 2017). In this case, for example, if bubbles interactions with microorganisms are stronger than the interactions between microorganisms and membranes, then bubbles could be used to clean the membranes. Now, our aim is to use this strategy to functionalize the bubble surface with a molecule that is able to interact with a molecule available at the cell surface, and probe its interactions directly with cells. For that, we need to know what type of molecules are present on *C. vulgaris* cell wall, which is why, in a second step, we analyze its cell wall composition using a combination of surface-analysis techniques, AFM, XPS and HPLC.

1.2.2. Cell wall composition analysis to find a natural flocculant

This part of the work is described in detail in the article entitled “Combining AFM, XPS and chemical hydrolysis to understand the complexity and dynamics of C. vulgaris cell wall composition and architecture”, by Demir-Yilmaz et al., under review in Algal research, presented in Chapter 4.

Microalgae have a structurally complex cell wall ensuring their protection against environmental changes and predators. This protection is ensured by cell wall rigidity, shape and mechanical strength (Demir-Yilmaz, Schiavone, et al., 2022; Demuez et al., 2015). In addition to its protective function, the cell wall is also responsible for cell's physico-chemical properties, like hydrophobicity, global charge and aggregation characteristic. In this part of the work, we investigated the cell wall composition and dynamics of *C. vulgaris* cell wall in three different conditions relevant for industrial applications such as lipid production: in exponential phase, stationary phase, and salinity stress condition (0.1 M NaCl), which induce the production of lipids in microalgae cells. The cell wall of *C. vulgaris* and other microorganisms are known to be composed of three types of molecules; lipids, proteins and polysaccharides (Gerken et al., 2013). In order to determine the relative fractions of these molecules, their dynamics depending on culture conditions and their impact on the cell wall,

the approach that we developed combined three types of analysis. First, AFM was used to image cells and probe their biophysical properties, cell wall roughness and nanomechanical properties. Then, XPS analysis was used to give a global view of the cell wall composition and determine this way the relative amounts of the three fractions, proteic, saccharidic, and lipidic. Finally, to give a more complete view of the cell wall composition, chemical hydrolysis followed by high performance liquid chromatography (HPLC) was performed to determine the saccharidic composition of the cell wall. These analyses were performed with cells grown in standard conditions in both exponential (7 days of culture) and stationary phase (21 days of culture), and with cells grown in saline stress (0.1 M of NaCl) during 21 days.

C. vulgaris cells grown in the different conditions described above were analyzed using AFM. The whole cells were imaged as showed in Figure 9a-c, and no significant morphological changes between the two different growth stages could be observed. However, under saline stress (Figure 9c), defects at the cell surface can be observed; the cell wall appears to be rougher compared to cells grown in standard conditions. To quantify this, we then recorded zoom-in high resolution images on small areas on top of cells to measure the average roughness R_a of the cell wall. This quantitative analysis, presented in Figure 9d, shows that in exponential phase, cells have an average roughness of 1.1 ± 0.4 nm that increases to 1.5 ± 0.7 nm in stationary phase and to 1.7 ± 1.2 nm in salinity stress condition. While these results are not significantly different, the distribution of the values obtained is wider for saline stressed cells, suggesting that applying a stress increases the heterogeneity of the surface roughness. Moreover, nanoindentation curves, obtained on cells in the different conditions (Figure 9e), show a different slope, meaning that the AFM probe does not indent the same way in each case. For instance, it is able to indent deeper in exponential phase cells compared to stationary phase, meaning that this change in the growth phase increases the rigidity of the cell wall. The indentation is even deeper for cells cultured in salinity stress condition (21-days of culture) compared to stationary phase cells, showing that addition of salts have a direct impact on cell wall rigidity. To verify this, young modulus values were extracted from the force curves recorded in each condition (Figure 9f), and show that there is indeed a 2-fold difference in the average Y_m value between cells in stationary phase and exponential phase. However, when cells are exposed to a salinity stress, cells become 5 times softer. These modifications of the rigidity over time could be explained by the fact that the pH of microalgae cultures changes

with time (from exponential phase to stationary phase, the pH of the culture media becomes more basic). The dramatic decrease of cell wall rigidity for cells submitted to saline stress can be explained by the direct impact of the environmental stress on the cell wall composition or architecture. To understand if the changes observed in the roughness or in the rigidity of cells can be linked to the cell wall architecture and thus composition, we need to determine the biochemical cell wall composition.

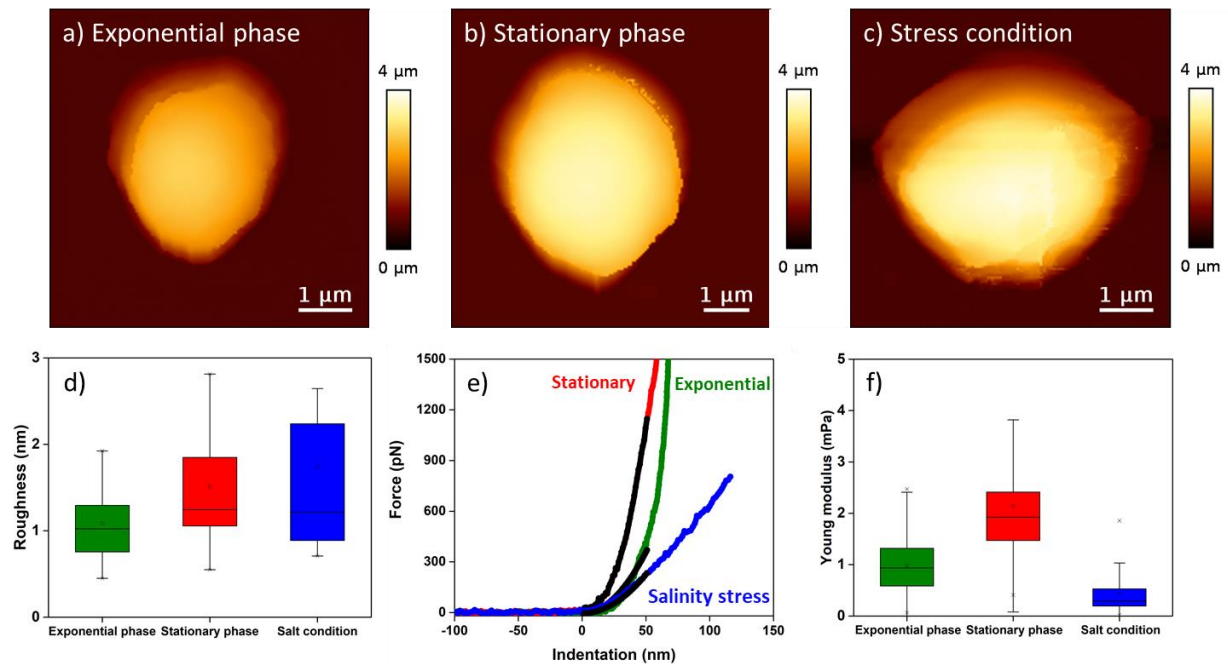


Figure 9: Roughness and nanomechanics of *C. vulgaris* cell wall. AFM images of single *C. vulgaris* cell in a) exponential phase b) stationary phase and c) salinity stress condition. d) is a box plot showing the distribution of *C. vulgaris* surface roughness. e) Indentation curves (green, red and blue lines) fitted with the Hertz model (black lines) recorded on top of *C. vulgaris* cells. f) Boxplot showing the distribution of Young's modulus values measured on top of *C. vulgaris* cells. Adapted from (Demir-Yilmaz, Schiavone, et al., 2022).

To this end we used XPS to reveal the biochemical composition of *C. vulgaris* cells, the results are presented in Figure 10. The carbon spectrum presented in Figure 10a shows different peaks that represent the different carbon configurations. Out of this spectrum, we can obtain the elemental percentages of these different carbon configurations. Then, these elemental composition can be used to calculate the relative fractions of the three model compounds of the cell wall, proteins, polysaccharides and lipids, using a model developed by Rouxhet and coworkers (Rouxhet & Genet, 2011). The results of these analyses showed that in exponential phase for *C. vulgaris* species the dominant constituents are proteins and polysaccharides (shown in Figure 10b), that are present in similar proportions (approximately

40%). Lipids represent approximately 20% of the cell wall. These proportions change with the growth phase as the cell wall evolves during growth and its composition changes. Notably the lipid amount increases significantly from the exponential to the stationary phase and then further increases in salinity stress condition at the expense of the proteic fraction which decreases. The polysaccharidic fraction stays relatively constant between the different conditions. In stress conditions or with aging, cells accumulate lipids and those lipids are known to be storage lipids, accumulated within the cells, different from lipids that have a structural role located on the cell wall. Therefore, to understand the increase in the lipid content of the cell wall that we observe using XPS, we next measured the cell wall hydrophobicity of *C. vulgaris* cells in exponential phase, stationary phase and salinity stress condition, by measuring their interaction with bubbles. As lipids are the only hydrophobic components present in the cell wall, measuring cell surface hydrophobicity will indicate if their quantity is indeed increased in stationary phase and saline stress condition. The results obtained showed that the adhesion force between bubbles and cells is higher for cells in stationary phase and saline conditions compared to cells in exponential phase, suggesting that indeed the cell wall hydrophobicity increases, which is in line with the XPS results (Figure 10b). Thus, we can conclude that in addition to storage lipid cell also accumulate lipids in their cell wall with aging or in saline stress condition.

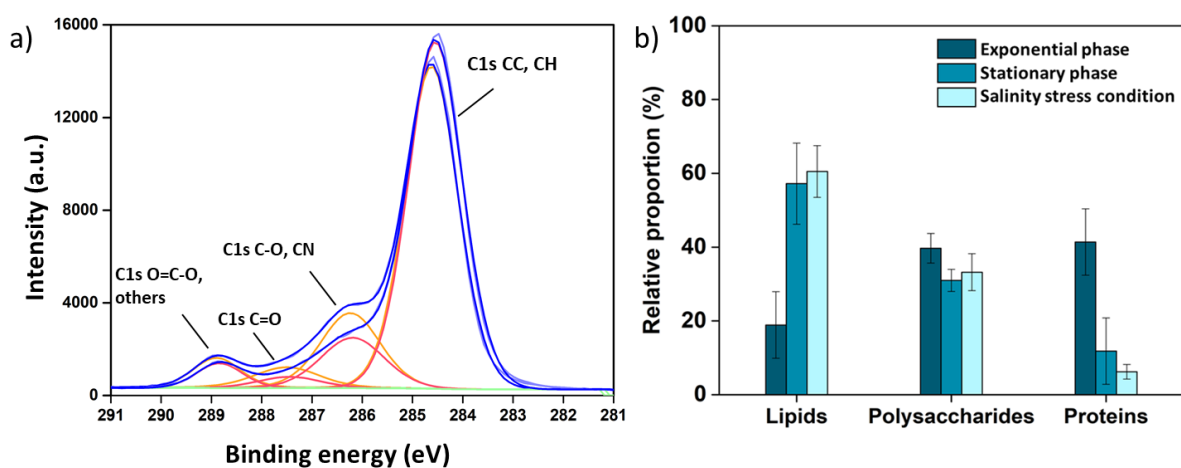


Figure 10: XPS analysis of *C. vulgaris* cell wall. a) Representative carbon 1s peaks recorded on *C. vulgaris* cell walls isolated from cells b) relative biochemical composition of *C. vulgaris* cell wall. This histogram shows the relative proportions of lipids, polysaccharides and proteins present in the cell wall. The error bars indicate the deviation from the average of the triplicates (n=3). Adapted from (Demir-Yilmaz, Schiavone, et al., 2022)

Table 1 summarizes the results on the cell wall composition of microalgae cell walls from the literature obtained for different microalgae species in different growth phases. Canelli *et al.* reported that polysaccharides are the major component on the cell wall of *C. vulgaris* both in exponential phase (around day 1.5) and stationary phase (around day 6) (Canelli *et al.*, 2021). The authors also found that the lipid content increases from 11% to 23% from exponential phase to stationary phase, which is in line with our results. Furthermore, Canelli *et al.* also highlighted that the proteic content of *C. vulgaris* cell wall in stationary phase is higher than in exponential phase, in opposition this time to our data that show a decrease of the proteic fraction in stationary phase compared to exponential phase. In the study by Shchukarev, the surface composition of *C. vulgaris* cell wall is dominated by polysaccharides in stationary phase (at day 9). On the contrary, *Coelastrella sp* cells have a higher content of both proteins and lipids. *S. obliquus* contains the highest level of proteins and lipids, that are compensated by a small amount of polysaccharides compared to the other two species in stationary phase (at day 9) (Shchukarev *et al.*, 2020). Globally, the results obtained in these three different studies including ours could be explained by the fact that in these studies different *C. vulgaris* strains were used. Moreover, culture conditions and growth medium have important effect on the cell wall composition. Lastly, in each case, cells were grown to stationary phase but durations are very different for example, it is around 6 days for Canelli *et al.*, 9 days for Shchukarev *et al.* and 21 days for our study. Thus, it is complicated to compare these data, but it highlights the species-dependence, complexity and dynamics of microalgae cell wall composition. Yet, in all these species and conditions, polysaccharides are still the dominant constituents, with high polysaccharidic contents reported for *C. vulgaris* cells wall (approximately 50 %, Table 1). Also, polysaccharides present at the surface of microorganisms have been shown to be key factors in many cell interactions with other cells or with their environment (Formosa-Dague, Castelain, *et al.*, 2018). In this PhD, the aim is to functionalize bubbles with molecules that can specifically interact with *C. vulgaris* cell wall; thus, in this context, polysaccharides represent a pertinent choice to promote the interactions between bubbles and cells. In a next step we took a closer look into the polysaccharidic content of *C. vulgaris* cell wall.

Table 1: Relative composition of lipids, proteins and polysaccharides in microalgae cell walls. The errors indicate the deviation from the average.

Species	Phases	Lipids	Proteins	Polysaccharides	References
<i>C. vulgaris</i>	exponential	19 ± 9 %	41 ± 9 %	40 ± 4 %	(Demir-Yilmaz, Schiavone, et al., 2022)
<i>C. vulgaris</i>	stationary	57 ± 11 %	12 ± 9 %	31 ± 2 %	(Demir-Yilmaz, Schiavone, et al., 2022)
<i>C. vulgaris</i>	stationary + stress	60 ± 7 %	6 ± 2 %	34 ± 5 %	(Demir-Yilmaz, Schiavone, et al., 2022)
<i>C. vulgaris</i>	exponential	11 %	19 %	70 %	(Canelli et al., 2021)
<i>C. vulgaris</i>	stationary	23 %	25 %	52 %	(Canelli et al., 2021)
<i>C. vulgaris</i>	stationary	3 ± 5 %	40 ± 9 %	57 ± 7 %	(Shchukarev et al., 2020)
<i>Coelastrella</i> <i>sp</i>	stationary	11 ± 2 %	47 ± 1 %	42 ± 2 %	(Shchukarev et al., 2020)
<i>S. obliquus</i>	stationary	16 ± 4 %	63 ± 4 %	21 ± 1 %	(Shchukarev et al., 2020)

The cell wall of *C. vulgaris* is known to be composed of rigid wall components embedded within a more plastic polymeric matrix. While this matrix contains uronic acids and saccharides (rhamnose, arabinose, fucose, xylose, mannose, galactose and glucose), the rigid cell wall is either composed of glucosamine or of a glucose-mannose polymer (Gerken et al., 2013). To determine the polysaccharidic composition of the cell wall of our species, *C. vulgaris*, in the different selected conditions, we performed acid hydrolysis to hydrolyze all the polysaccharides present in the cell wall into monosaccharides, which can then be analyzed using HPAEC-PAD. The monosaccharide composition of microalgae cell walls is reported in Figure 11. In our case, while the predominant amino sugar found in the rigid cell wall is glucose followed by galactose in all three conditions, rhamnose, arabinose, xylose, mannose and glucosamine are also present. Different studies in the literature have analyzed the monosaccharidic composition of microalgae cell walls using similar experimental approaches.

For example, in line with our findings, high glucose and galactose concentrations have also been reported by Canelli *et al.* and Kim *et al.* in the case of *C. vulgaris* (Canelli et al., 2021; K. H. Kim et al., 2014). While HPLC experiments allow to identify the monosaccharides released by the acid hydrolysis, it is not possible to identify the polysaccharides they come from, which could be an interesting information to obtain to further use these polysaccharides as cell-adhesive compounds. One way to identify the polysaccharides that could be present in the cell wall is to hydrolyze them with specific enzymes; if the substrate of the enzyme is present, the enzyme will release monosaccharides that can be detected by further HPLC analysis. So far the efficiency of such strategy has been shown in the case of yeast cells, (Schiavone et al., 2014) but has never been performed on microalgae cells walls. However, one study by Gerken *et al.* in 2013 consisted in treating cells on agar plates with specific enzymes; in this case an inhibition of cell growth was linked to the presence or not of their substrates in the cell wall (Gerken et al., 2013). Moreover, using a fluorescent DNA stain, they developed a rapid methodology to quantify changes in permeability in response to enzyme digestion. One of the conclusions from their work is that *Chlorella* is typically most sensitive to chitinases and lysozymes, enzymes that degrade polymers containing N-acetylglucosamine, a monomer of chitin-like glycans (Gerken et al., 2013) which is also present in our species, *C. vulgaris*. This means that a glucosamine-based polymer is present in the cell wall of our species: for instance, Canelli *et al.* stated that in stationary phase, a microfibrillar chitosan-like layer composed of glucosamine is present in *C. vulgaris* cell wall (Canelli et al., 2021). As for other polysaccharides that could be present in the cell wall, only hypothesis can be made at this stage, more work using specific enzymes is now needed to verify this hypothesis.

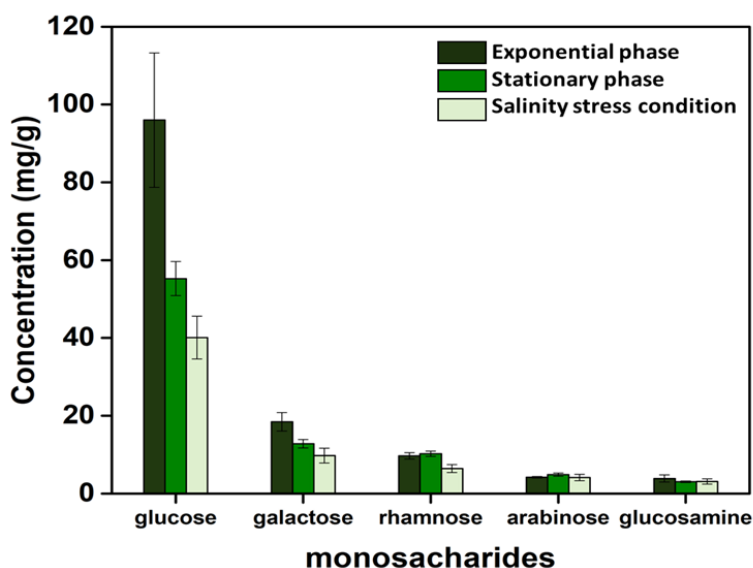


Figure 11: Monosaccharide composition of *C. vulgaris* cell wall. In exponential phase, stationary phase and salinity stress condition (0.1M NaCl). The composition is expressed as milligram of monomer per gram of dry cell wall. The error bars indicate the deviation of the triplicates (n=3) from the average.

In the end, the combination of these three techniques allowed to get a better understanding of the effects of culture condition on the cell wall composition and dynamics of *C. vulgaris* cell wall, but also to understand the link between composition and architecture and the effects of composition changes on cell surface biophysical properties. The large fraction of polysaccharides and their stable relative proportions over the different conditions confirmed our initial assumption that they are good candidates to functionalize bubble surfaces. But at this stage, it was difficult to select a specific polysaccharide given the small information we had. We thus looked at the literature, and after review, we found that chitosan, a bio-sourced polysaccharide, is widely used in microalgae flocculation as it has the ability to interact with microalgae cells at low pH. Because our results showed that a chitin-like polymer was present in the cell wall in all conditions, thus chitosan appeared as a good candidate that could interact with cells through homotypic binding (Formosa-Dague, Castelain, et al., 2018), and thus be efficient to capture cells when functionalized at the surface of bubbles. We thus focused on this molecule for the rest of the project, and first used AFM to get a better understanding of its interactions with the surface of *C. vulgaris*.

1.2.3. Chitosan as a bioflocculant to harvest the microalgae cells

This part of the work is described in detail in the article entitled “Nanoscale Evidence Unravels Microalgae Flocculation Mechanism Induced by Chitosan”, by Demir et al., ACS Applied Bio Materials, 2020, presented in Chapter 5.

Chitosan is a polyelectrolyte which is cationic at pH lower than its pKa (6.5). It is obtained by deacetylation of chitin from shrimp, crab and crawfish, and after cellulose, it is the second most abundant natural polymer on earth. Moreover, in the field of microalgae biomass harvesting, chitosan has been shown to induce more than 90% of flocculation in various species such as *Chlorella* sp. (Ahmad et al., 2011; Erdawati et al., 2020), *Nannochloropsis* sp. (Chua et al., 2019; Farid et al., 2013) , or *Scenedesmus* sp (Lama et al., 2016). To that aspect chitosan could be good candidate to coat the bubble surface to promote the interactions between bubbles and cells and their further separation from water. While in the literature flocculation mechanism is reported to rely on electrostatic interaction between chitosan and negatively charged *C. vulgaris* cells, no molecular evidence has yet confirmed this hypothesis. Thus, we decided in this part of the work to use AFM in force spectroscopy mode to probe the interactions between *C. vulgaris* cells and chitosan at the molecular scale and this way to decipher its flocculation mechanism.

Chitosan-induced flocculation has so far been used to harvest successfully both fresh-water and marine microalgae species. Studies that report on chitosan induced flocculation in the literature are summarized in table 2. It is believed that for fresh water species, the high cationic charge density of chitosan interacts with negative regions on the microalgae cell wall through electrostatic interaction. As shown in Table 2, the study by Ahmad *et al.* 2011 demonstrate the effect of different chitosan dosages on flocculation efficiency of *Chlorella* species at pH 6. Only low concentration of chitosan is needed to achieve a high flocculation efficiency. For small concentrations (up to 10 ppm) flocculation efficiencies increases with increasing chitosan concentrations whereas for higher chitosan concentrations (greater than 20 ppm) flocculation efficiency declines drastically. In the literature, these results are interpreted as follows: chitosan has a high cationic charge density whereas cells are negatively charged. When a dosage higher than the optimal concentration is used, the excess cationic charge on the chitosan leads to a restabilization of cells, reducing the efficiency of the process and hindering the formation of flocs (Ahmad et al., 2011). Besides, the other important

parameter for chitosan-induced flocculation is pH. Once the pH is increased from 6 to 7, which modifies the charge of chitosan (as the pKa of chitosan is 6.5), the required dose for maximum efficiency is increased for fresh water species like *Chlorella sorokiniana*, where the chitosan dosage has to be increased from 5 to 10 ppm with increasing pH (Xu et al., 2013). When the pH is lower than 6.5 the amino groups present on the chitosan are mostly protonated and provide a positive charge to chitosan, which then electrostatically interacts with negatively charged microalgae species. Yet, at higher pH (at pH 7) the flocculation with chitosan is still effective meaning that most probably, a different interaction mechanism is at play since at this pH chitosan does not bear its positive charge anymore. Moreover, the same authors also showed that a gradual increase in the initial cell concentration requires higher chitosan concentration to achieve the same efficiencies (Xu et al., 2013). This result is further confirmed by a study by Zhu *et al.*, where the authors found for fresh water *C. vulgaris* species that a 2-fold increase in initial cell concentration requires a 4-times higher chitosan concentration to achieve the same efficiency (Zhu et al., 2018). If we consider scale-up or industrial applications where cell concentrations can be higher, this would result in a very large quantity of chitosan to use. Furthermore, an interesting paper from 2011 focused on the influence of the cell wall carbohydrate composition of *C. vulgaris* on the efficiency of chitosan-induced flocculation (Cheng et al., 2011). The results obtained in this study showed that a higher polysaccharide content (including neutral sugars, uronic acids, and amino sugars) in the cell wall is associated with a better efficiency of flocculation with chitosan at pH 8.5 suggesting that non-electrostatic absorption of chitosan on cells may be more important than electrostatic neutralization in *C. vulgaris*.

In the case of marine microalgae species, mixed results on chitosan efficiency have been reported. It is believed that in marine waters, the high ionic strength of salts screen all the charges present on the chitosan thereby suppressing the electrostatic interaction between chitosan and cells, preventing further flocculation through charge neutralization (Matho et al., 2019; Rashid et al., 2013). Yet, flocculation still takes place. For example, for marine *Nannochloropsis* sp. species, chitosan is able to flocculate cells at pH 7 and 9, using high concentrations of chitosan (100 mg/L) (Farid et al., 2013). Moreover, in this same study by Farid *et al.*, when 6-fold higher initial cell concentration is used, only 71% of separation efficiency is reached, similar to results reported for fresh water species. An explanation for

these efficiencies in salty waters can be found in a study by Blockx *et al.*, where the authors found that chitosan is able to flocculate *N. oculata* species by sweeping mechanism at pH higher than 7.5 (Blockx *et al.*, 2018). Overall, for both fresh water and marine species, mixed results on chitosan efficiency have been reported depending on pH and initial cell concentrations, which suggest that different types of interactions between chitosan and cells are taking place. To highlight the complexity of chitosan induced flocculation mechanism and actually understand it, we performed flocculation experiments with chitosan at different pH and then used AFM to understand the mechanism of interaction at two different pH.

Table 2: Chitosan induced flocculation studies reported in the literature

Microalgae species	Habitat	pH	Dose (ppm)	Efficiency	References
<i>Chlorella</i> sp.	Freshwater	6	5	50	(Ahmad <i>et al.</i> , 2011)
<i>Chlorella</i> sp.	Freshwater	6	10	99	(Ahmad <i>et al.</i> , 2011)
<i>Chlorella</i> sp.	Freshwater	6	20	99	(Ahmad <i>et al.</i> , 2011)
<i>Chlorella</i> sp.	Freshwater	6	60	80	(Ahmad <i>et al.</i> , 2011)
<i>Chlorella</i> sp.	Freshwater	6	100	50	(Ahmad <i>et al.</i> , 2011)
<i>Chlorella sorokiniana</i>	Freshwater	6	20 ^a 5 ^b	99 99	(Xu <i>et al.</i> , 2013)
<i>Chlorella sorokiniana</i>	Freshwater	7	10 ^b	90	(Xu <i>et al.</i> , 2013)
<i>Chlorella vulgaris</i>	Freshwater	6.8	250 ^a 50 ^b	92 92	(Zhu <i>et al.</i> , 2018)
<i>Chlorella vulgaris</i>	Freshwater	6	10	99	(Demir, Blockx, <i>et al.</i> , 2020)
<i>Nannochloropsis</i> sp.	Marine	9	100	92	(Farid <i>et al.</i> , 2013)
<i>Nannochloropsis</i> sp.	Marine	7	100	84	(Farid <i>et al.</i> , 2013)
<i>Nannochloropsis</i> sp	Marine	6	22	97-99	(Chua <i>et al.</i> , 2018)
<i>Nannochloropsis oculata</i>	Marine	≥7.5	75	100	(Blockx <i>et al.</i> , 2018)
<i>Chlorella</i> sp.	Marine	6.8	2000	98	(Erdawati <i>et al.</i> , 2020)

a higher algal biomass concentration

b lower algal biomass concentration

Figure 12 shows the charge of chitosan and effects of different chitosan dosages on *C. vulgaris* flocculation at pH 6 and pH 8 (Demir, Blockx, et al., 2020). Figure 12a shows that chitosan has a positive charge at low pH and it is neutral at higher pH (pH over than 8), as expected. The flocculation efficiencies presented in Figure 12b and c showed that only a low concentration of chitosan is needed to achieve a high flocculation efficiency, the deacetylation degree of the molecule does not affect flocculation efficiency. These results are in line with the study by Ahmad *et al.* where they observed similar flocculation trends with different chitosan dosage for *Chlorella* species (Ahmad et al., 2011). Then we conducted the same experiments using a higher pH (8) where chitosan does not bear positive charges and observed a similar trend (Figure 12c). This time, for small concentrations (up to 10 mg/L) flocculation efficiencies increases with increasing chitosan concentrations. When the highest efficiency is reached at 10 mg/L, it stays in plateau until 80 mg/L; then for higher chitosan concentrations (greater than 80 mg/L) flocculation efficiency declines. These flocculation results indicate that chitosan is able to flocculate cells at pH 6 and as well as at pH 8 where there are no positive charges present on the molecule. This means that there might be a different mechanism involved in chitosan-induced *C. vulgaris* flocculation, not perhaps only relying on electrostatic interactions. To understand this, we conducted macroscopic observations using optical microscopy. The resulting images presented in Figure 12d showed that cells are randomly distributed and does not form aggregates when there is no flocculent. However, when chitosan is added at pH 6, we can observe small aggregation of cells around chitosan particles (Figure 12e). Once we increase the pH to 8, this is not the case anymore and we go back to our initial case where there is no aggregation (Figure 12f). Thus even though cells flocculate at pH 8 they do not interact with chitosan anymore. This strengthens our hypothesis that there might be a different mechanism involved.

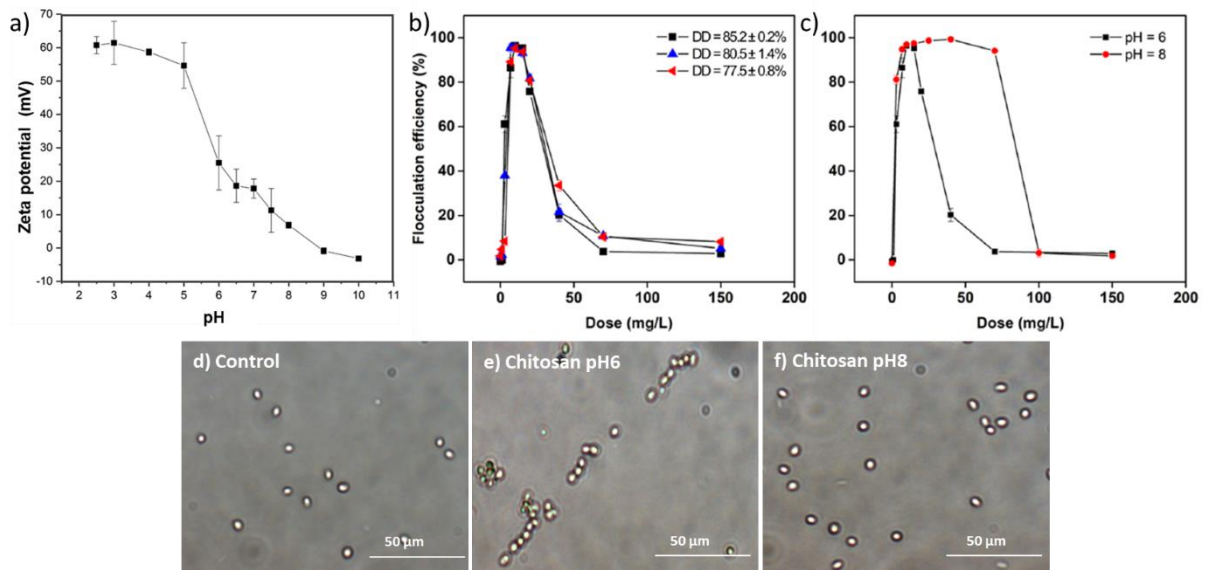


Figure 12: Flocculation experiments of *C. vulgaris* with chitosan. a) Graph showing the charge of the chitosan at different pH (adapted from (Blockx et al., 2018)). Flocculation efficiency of *C. vulgaris* with b) chitosan with different deacetylation degree (DD) at pH 6 c) chitosan molecules with DD = 77.5 ± 0.8% at pH 6 and 8. Optical image of *C. vulgaris* cells after resuspension in PBS containing d) noting e) 10 mg/L chitosan at pH 6 and f) 10 mg/L chitosan at pH 8. Adapted from (Demir, Blockx, et al., 2020).

To understand what is actually going on, we used an AFM based nanoscale approach and performed force spectroscopy experiments to understand the nature of the interaction between *C. vulgaris* cells and chitosan. For that, *C. vulgaris* cells were attached on AFM tipless cantilevers and chitosan was immobilized on glass surfaces as shown in the Figure 13a. Representative force curves obtained during the interaction at pH 6 are presented in Figure 13b. They show multiple binding events, peaks, which are characteristic of biological interactions probably due to the unfolding of long macromolecule available on the cell wall of *C. vulgaris*. When these experiments were performed at pH 8, similar force curves were observed, yet different adhesion forces were recorded as well as unfolding distances. This is unexpected as the macroscopic observation showed no interaction between chitosan and *C. vulgaris* cells at this pH. To understand this, we conducted more experiments. First, we took a closer look at cells at different pH, by imaging their surface. We observed that increasing pH changes the cell surface topography; cells became rough at pH 8, meaning that more molecules protrude from the surface of the cell. Moreover, the nanomechanical results showed that the indentation curves obtained on cells at pH 6 and 8 are different; indeed, the AFM probe is able to indent deeper into cells at pH 6 than at pH 8, meaning that increasing the pH also increases the rigidity of the cell wall. To confirm this, we quantified the young modulus values and found an almost 3-fold increase in the Y_m at pH 8 meaning that cells are

different at pH 6 and pH 8. This may explain why cells do not interact with chitosan anymore at pH 8. However still it does not explain why we record interaction at pH 8. To understand this, we then used negatively charged bead to mimic the cells by keeping the negative charges but excluding the macromolecules on the surface, and performed force spectroscopy experiments with chitosan surfaces. At pH 6 there is no interaction between chitosan and negatively charged bead. This means that electrostatic interaction are probably not involved and cell wall macromolecules are needed to interact with chitosan. However when we repeat this experiment at pH 8, we get similar interactions to what was observed with cells. We further recorded the forces with bare uncharged AFM tips, and we still record similar interactions than between cells and chitosan at pH 8 with similar unfoldings. In this case, we can only unfold chitosan, as there is no macromolecule available. To understand why chitosan would get unfolded during experiments, we performed roughness measurements on the chitosan functionalized surfaces at pH 6 and 8. Our results showed an average roughness of chitosan of 0.6 ± 0.1 nm at pH 6, which increased dramatically, to 13 ± 5 nm at pH 8. This result indicates that at pH 6 chitosan forms a homogeneous layer on the glass surface. When the pH is increased, chitosan in fact precipitates, which creates aggregates on the surface that explain the increase in the roughness observed. This explains why interactions are recorded when chitosan surface is probed at pH 8, whatever the probe used (cell, negatively charged bead, or bare AFM tip). As it was visible in the optical microscopy experiments (Figure 12e), chitosan does not interact with cells at this pH. But because it precipitates, it gets detached from the surface resulting in unfoldings with a different adhesion force than what is obtained between cells and chitosan at pH 6.

These results are summarized in Figure 13c. Using AFM force spectroscopy experiments, we could show that chitosan interact with cells through biological interactions at low pH (Demir, Blockx, et al., 2020). However, a different mechanism is at play at higher pH (pH 8), where chitosan precipitates; cells get entrapped in this precipitate and are flocculated through a sweeping mechanism. This specific interactions at low pH and the different mechanism at higher pH then explains why the efficiency of chitosan is different depending on the microalgae species used and the working pH.

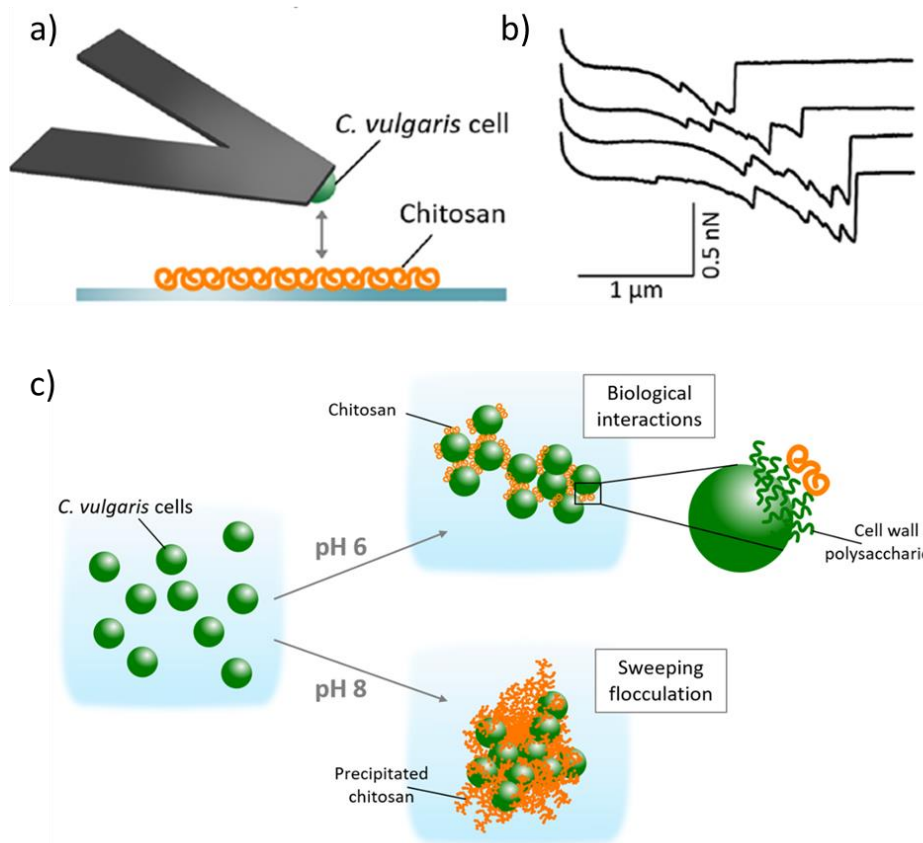


Figure 13: Identification of a natural flocculent, chitosan, for *C. vulgaris*. a) Schematic representation of *C. vulgaris* and chitosan coated surface interaction. b) representative force curves obtained during the interactions c) Schematic representation of the flocculation mechanisms induced by chitosan at pH 6 and 8 for *C. vulgaris*. Extracted from (Demir, Blockx, et al., 2020)

In this part of the work, we proved that indeed chitosan is a good candidate to coat the bubble surface as it is able to specifically interact with cells at low pH. Now that we understand these interactions, the next step is to use chitosan to functionalize the surface of bubbles. But for that, chitosan needs to be amphiphilic as bubbles are gas/liquid interfaces. To do that our approach is to add a new function to the chitosan, hydrophobicity, on its hydrophilic backbone so that the resulting molecule becomes amphiphilic and can easily be functionalized on the bubble surface. This way we will be able to measure the interactions between functionalized bubbles and cells, and optimize the flotation process with functionalized bubbles at the population scale.

1.2.4. Synthesis, characterization and functionalization of bubbles with polyoctylchitosan (PO-chitosan), an amphiphilic chitosan-based molecule.

This part of the work is described in detail in the article entitled “Bubble functionalization in flotation process improve microalgae harvesting”, by Demir-Yilmaz et al., Chemical Engineering Journal, 2023, presented in Chapter 6.

To functionalize the surface of bubbles with a molecule that specifically interact with the microalgae cell wall, in our case chitosan, we added an extra function to the molecule, hydrophobicity, by adding polyoctyl chains on the chitosan backbone through a N-alkylation reaction. The N-octyl-chitosan derivatives were obtained by reductive amination following a procedure previously described in the literature (Desbrières et al., 1996; Mati-Baouche et al., 2019) and shown in the Figure 14, where a covalent bond between aldehyde and amine functions can be formed. In our case, high molecular weight chitosan was covalently bound with a selected aldehyde; octanal, a hydrophobic molecule containing an aldehyde function. This ensures the target molecule PO-chitosan's amphiphilic property can be thus achieved without complete alkylation of all glucosamine monomers. The reaction was performed in mild conditions that did not modify the chitosan molecule itself (degree of acetylation and/or the polymerization degree) (Mati-Baouche et al., 2019). For that, basically, primary amino groups of chitosan undergo a Schiff reaction with octanal to yield the corresponding aldimines, which are then converted to an alkyl derivative by reduction with NaBH₃CN. Then ¹H-NMR spectroscopy was used to characterized both chitosan and PO-chitosan (Poly-octyl chitosan), and determine the degree of substitution of the octyl chains in D₂O/DCl (pH ~ 4). The ¹H-NMR spectra of initial chitosan and PO-chitosan are presented in Figure 14b and c respectively. PO-chitosan shows characteristic peaks in the 1.7-0.8 ppm region, linked to the protons of methyl (-CH₃) and methylene (-CH₂-) groups grafted on the initial chitosan chain. In addition to that, different H-1 signals of G-octyl were also observed, which supports the chemical modification (Desbrieres, 2004; Desbrières et al., 1996; Mati-Baouche et al., 2019)

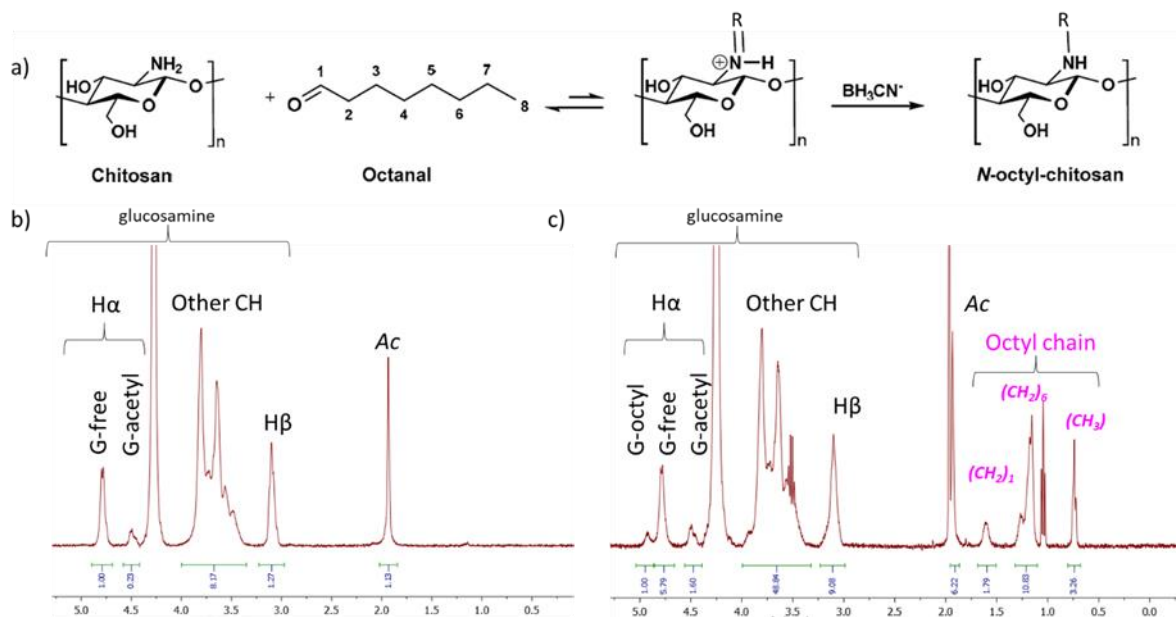


Figure 14: Synthesis of N-octyl-chitosan by alkylation process. This was performed thanks to a reaction allowing to create a covalent bond between an aldehyde (contained in octanal) and amine functions of the glucosamine units of chitosan. a) Synthesis of PO-chitosan by alkylation, b) ¹H-NMR spectra obtained for initial chitosan, c) ¹H-NMR spectra obtained for PO-chitosan. The DS obtained is of 12%.

The ¹H-NMR spectra provide information that can be used to evaluate the substitution degree (DS) of the chitosan derivatives generated. The integral of each peak allows to calculate the degree of substitution. The signals at 0.7 ppm and 1.7 ppm may be attributed to the -CH₃ and -CH₂ groups linked to the N atom, respectively. The degree of substitution was then calculated as previously described (Desbrières et al., 1996), by comparing the integral of -CH₃ signal at 0.7 ppm with the total of integrals from H 1 signals between 4.5 and 5 ppm, and was of 12%.

Further, we characterized the PO-chitosan and determined its particle size, surfactant properties, roughness and hydrophobicity. PO-chitosan has both hydrophilic (-NH₂ or -OH) and hydrophobic sites (alkyl chains, octanal) and thus possess amphiphilic properties, making it a surfactant. As for any surfactants, it should be able to decrease the surface tension of water with increasing concentration. The surface tension results that we obtained indeed showed that with increasing concentration of PO-chitosan, the surface tension of PO-Chitosan solution dissolved in water decreases from 72 mN/m to 62 mN/m for 0 to 2.5g/L PO-chitosan concentrations respectively. However, this decrease is not as important as it can be with other types of surfactant: this can be explained by the 12% alkylation level of PO-chitosan. It means

that only 12% of chitosan amine functions have been substituted by hydrophobic octanal groups, thus the hydrophobic part of the molecule may not be large enough to change in an important manner the surface tension of water. But we are limited with a low alkylation level (10-15 %) because as the alkylation level increases, water solubility of PO-chitosan decreases, and we need it to stay soluble in water to use it for the next experiments. To verify we can completely dissolve PO-chitosan in water, we measured the particle size of both initial chitosan and PO-chitosan. The size distribution graphs of chitosan and PO-chitosan obtained using zetasizer measurements (concentration of 2.5 g/L) showed similar patterns, meaning that the addition of the octanal groups on the molecule does not modify its size in a significant manner. These size measurements make sense: indeed, we are modifying a high molecular weight chitosan with octanal molecules that are relatively small compared to chitosan. Thus the size change due to octanal addition can be considered as negligible. Moreover, we also measured the turbidity of chitosan and PO-chitosan solutions at different concentrations (2.5, 1 and 0.5 g/L). The obtained turbidities are of 4.3, 3.2 and 3.5 NTU respectively. This means that solutions are clear (NTU < 5 clear water) with no aggregates present. Thus both particle size and turbidity measurements prove that PO-chitosan can be completely dissolved in water as chitosan, which is an important point for the next experiments.

Finally we measured the hydrophobicity of PO-chitosan coated surfaces in order to verify that the modification of chitosan that we realized indeed increases the hydrophobicity of the molecule. For that, we used the bubble method described in section 1.2.2., where we probe the interactions between bubbles produced by FluidFM, which behaves as hydrophobic surfaces in water, and PO-chitosan surfaces. Moreover, as pH has an influence on the hydrophilic and hydrophobic balance due to the ability of $-NH_2$ function (hydrophilic part) to be ionized in acidic conditions (Desbrières et al., 1996), we also performed these measurements at different pH (pH 6, 7.4 and 9). A schematic representation of these measurements is presented in Figure 15a. The adhesion histograms obtained for bubble PO-chitosan interactions at pH 6, 7.4 and 9 are presented in Figure 15 b, c and d respectively. At a pH of 6, the average adhesion force obtained is of 66.7 ± 13.9 nN. The force curves obtained show a single peak occurring at the contact point (inset in Figure 3b), which is characteristic of a non-specific hydrophobic interaction (Dague et al., 2007). As hydrophobic interfaces like bubbles interact with hydrophobic surfaces, then the adhesion force obtained reflects the

degree of hydrophobicity of the sample, the stronger the adhesion, the higher the hydrophobicity. Similarly, in the case of pH 7.4 and 9, single retract peaks occurring at the contact point are visible (inset of Figure 3c and d respectively), with average adhesion forces of 64.6 ± 20.3 nN for pH 7.4 (Figure 15c) and 46.5 ± 15.9 nN for pH 9 (Figure 3d). It is possible to convert these adhesion values into water contact angles (WCA), as described in Chapter 2 (Demir et al., 2021). Using the adhesion values obtained, we found that PO-chitosan surfaces have a WCA of 48.7° at pH 6, which then decreases to 48.3° at pH 7.4 and to 44.6° at pH 9, whereas surfaces covered by the initial chitosan are completely hydrophilic (WCA ~ 0). Even though the average adhesion values at pH 6 and 7.4 are close to each other, statistical analysis shows that these measurements are significantly different from each other (p-value of 0.05, unpaired student test). These results thus confirm first that the addition of octanal groups provide hydrophobic properties to chitosan, and second, they confirm the effect of the pH on the relative hydrophobicity of the molecule which decreases with increasing pH. Finally, to see if PO-chitosan also precipitates at high pH like chitosan does (Blockx et al., 2018), we used AFM in contact mode to image PO-chitosan surfaces at high resolutions at different pH. The images obtained are presented in Figure 15e (pH 6), f (pH 7.4) and g (pH 9), they show a similar homogeneous surface. At all pH considered, we do not observe aggregation of PO-chitosan meaning that it does not precipitate like chitosan did at pH 8. From these images we then quantified the surface roughness (boxplot in Figure 15h); the results show that the average roughness of PO-chitosan surfaces at pH 6, 7.4 and 9 are of 574.0 ± 105.7 pm, $528.1 \pm 144.8.1$ pm and 494.1 ± 82.2 pm respectively. Non-parametric statistical test (Mann and Whitney test) showed that these differences in all pH are not significant, thus confirming that PO-chitosan does not precipitate unlike chitosan. This is important as a potential precipitation of the molecule would interfere with its capacity to assemble at the surface of bubbles.

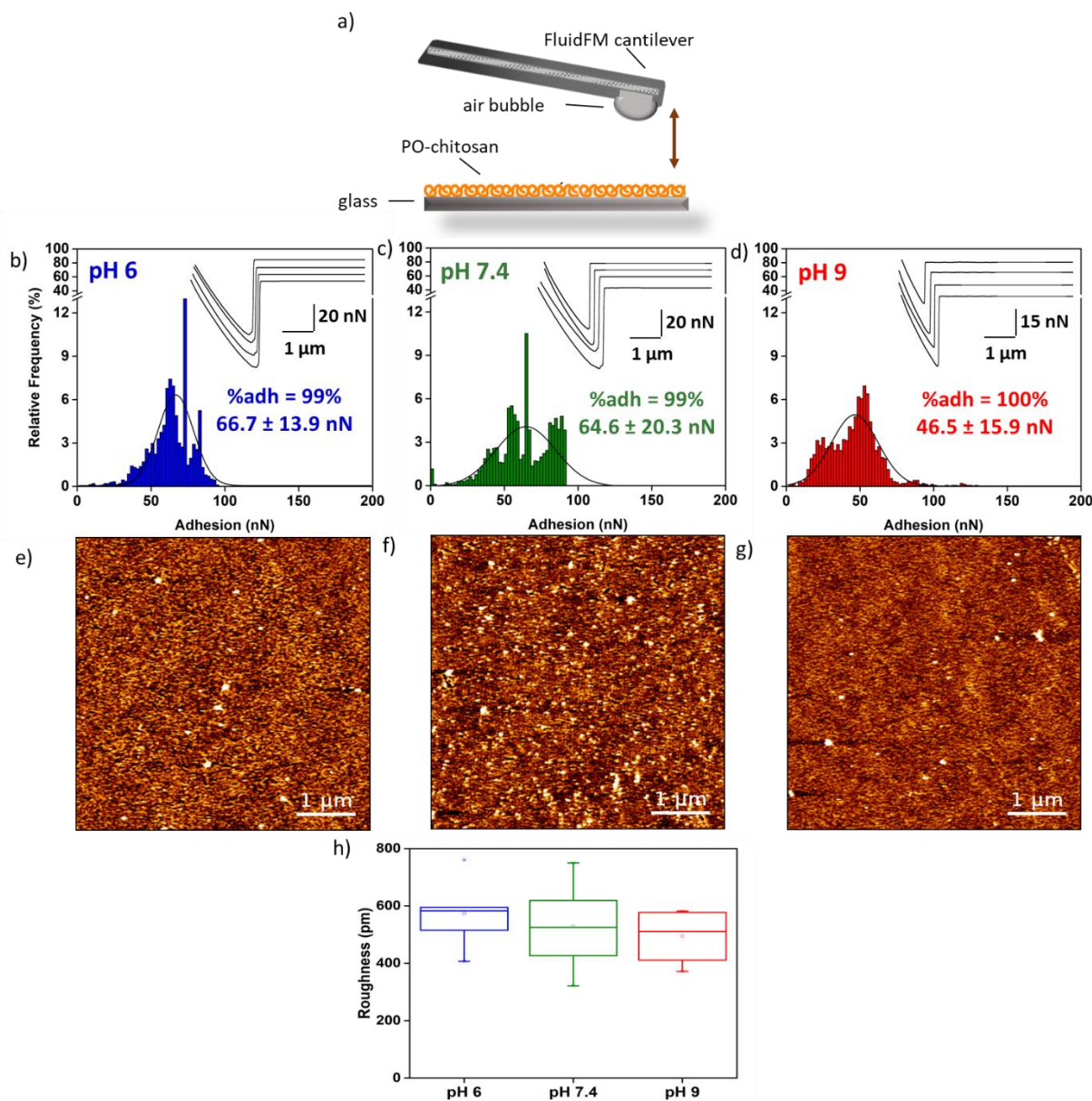


Figure 15: Characterization of PO-chitosan surface at different pH. a) Schematic representation of bubble and PO-chitosan surface interaction. Adhesion force histogram obtained between bubble and PO-chitosan surface at b) pH 6 c) pH 7.4 and d) pH 9. AFM height images of PO-Chitosan surface at e) pH 6 (color scale = 4 nm) f) pH 7.4 (color scale = 4 nm) and g) pH 9 (color scale = 4 nm). e) Quantification of PO-chitosan surface roughness at different pH.

The results presented here shows that the introduction of hydrophobic octanal groups into chitosan molecule changes its hydrophobic properties by increasing the WCA, as expected, and also its precipitation behavior. Thus PO-chitosan meets the conditions to be functionalized at the bubble surface. Thus in a next step, we used FluidFM to probe the interactions between PO-chitosan coated bubbles and *C. vulgaris* cells, and this way understand the mechanism at play in this case at the molecular level, as shown in Figure 16a. In this case the retract force curves obtained show a single retract peak at the contact point

(red curve in Figure 16b) with an average adhesion force of 12.8 ± 1.5 nN at pH 6 (Figure 16c). While this force is in the nN range as the one obtained with clean bubbles (light blue histogram in Figure 16c), it is 3.6-fold higher. This means that the functionalization of the bubble surface with PO-chitosan enhances the direct interaction with *C. vulgaris* cells, which is what was expected. But the nature itself of the interaction visible here is surprising. Indeed, our previous work on chitosan has showed that it interacts with *C. vulgaris* cells through biological interactions, with polymers unfoldings visible on the force curves obtained (Demir, Blockx, et al., 2020). In theory, PO-chitosan is absorbed on the water/gas interface with the hydrophilic chitosan monomers outside of the bubble, in the liquid part, and the hydrophobic tails with octanal molecules inside the bubble, in the gas part, as shown in Figure 16d. Thus, we should still be able to see the biological interactions that we had obtained with chitosan only. Moreover, the approach curve obtained with PO-chitosan coated bubbles (blue line in Figure 16b) also shows a “jump-in” reflecting the fact that PO-chitosan coated bubble gets suddenly attached to the *C. vulgaris* cell surface when they get into close proximity (Figure 16b, blue curve). This jump-in, as in the previous studies on bubble-hydrophobic surface interaction (Demir et al., 2021), is most likely due to a long-range hydrophobic force that causes the disruption of the water film between the bubble and the cell, and the further formation of the three point contact (TPC) line. Thus at this stage, the hypothesis that we can make is that the chitosan backbone is still able to interact with cells through biological interactions, but when the bubble probe is retracted from the cell, the hydrophobic interaction becomes dominant compared to the specific one, and this is what we see on the force curve (Figure 16b, red line). The interactions obtained in this case are higher than the ones obtained with clean bubbles (Figure 16c) because the initial interaction of bubbles with cells is stronger when bubbles are functionalized, thus the contact area between bubble and *C. vulgaris* cells increases, which increases the adhesion forces we obtained.

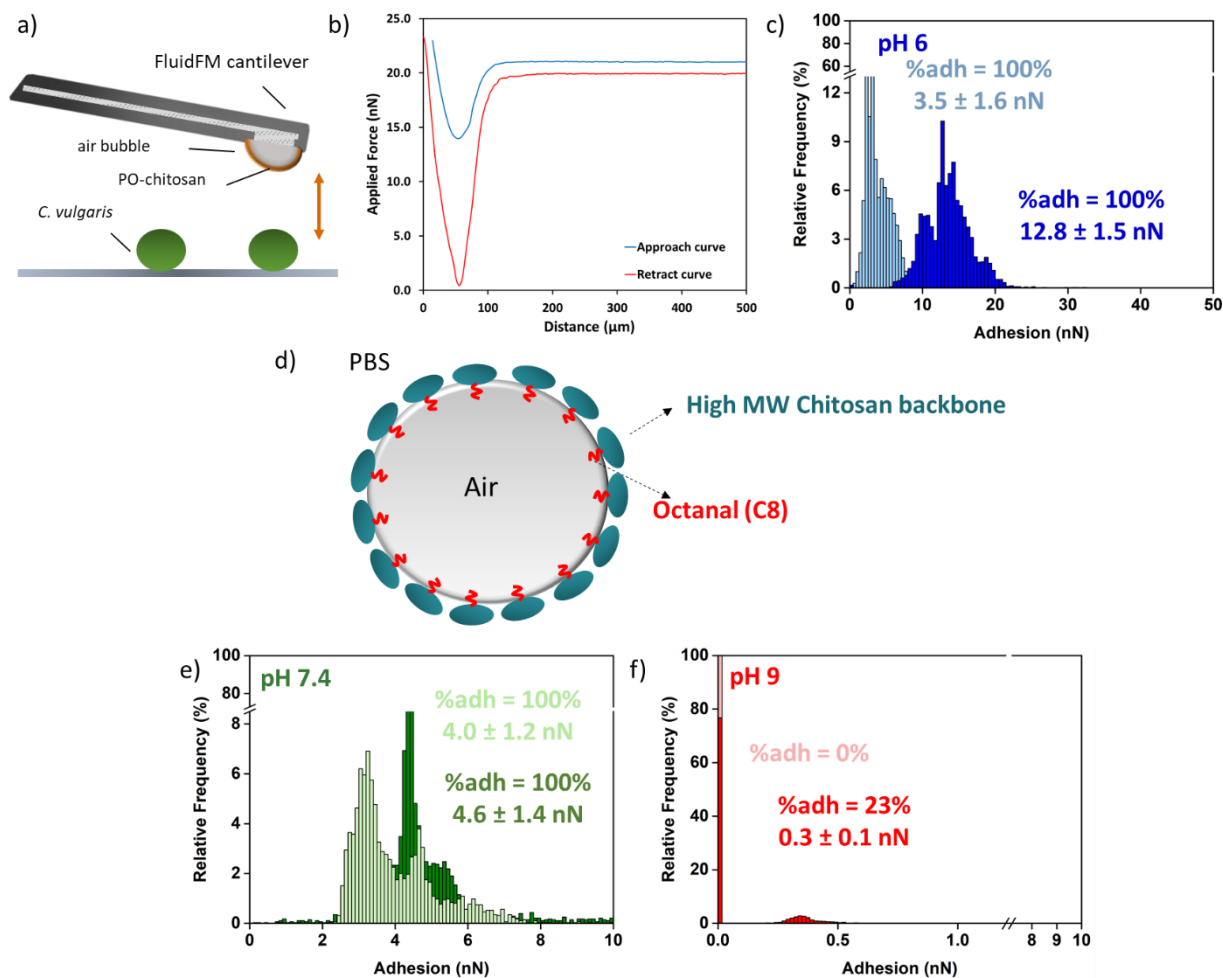


Figure 16: Modulation of the interactions between bubbles and *C. vulgaris* cells by PO-chitosan. a) Schematic representation of PO-chitosan coated bubble and single *C. vulgaris* cell interaction. b) Representative force curves obtained for PO-chitosan coated bubble and *C. vulgaris* cell at pH 6. c) Adhesion force histogram obtained for PO-chitosan coated bubble and *C. vulgaris* cell at pH 6.

We further repeated these experiments at pH 7.4 and 9 (Figure 16e and f). At pH 7.4, cells interact more with clean bubbles with an average adhesion force of $4.0 \text{ nN} \pm 1.2 \text{ nN}$ (Figure 16e, light green histogram) compared to pH 6, which can be explained by some changes perhaps in the hydrophobicity of *C. vulgaris* cells surface at this pH. When bubbles are functionalized with PO-chitosan, the average force obtained is of $4.6 \pm 1.4 \text{ nN}$ (Figure 16ed, dark green), thus almost 3 times less than at pH 6. In addition in this case, the “jump-in” peak on the approach curves is not visible anymore. This important decrease in the adhesion could be due to the decrease in the hydrophobicity of PO-chitosan molecule. Although this decrease is low, it has important consequences on the interactions with cells. At pH 9 cells do not interact with clean bubbles at all (0% of adhesion, light red bar in Figure 16f), while when

bubbles are coated with PO-chitosan, the percentage of force curves showing retract adhesions decreases to 23% compared to 100% in all other conditions, with an average force of 0.3 ± 0.1 nN (dark red histogram in Figure 16f). In the case of chitosan, there was no interaction with cells at higher pH, but this was explained by the fact that chitosan precipitated at such pH values. The roughness measurements performed in the first part of this work showed that PO-chitosan does not precipitate like chitosan does at higher pH. Therefore, this lack of interaction is probably not related to PO-chitosan, but to the cell surface itself. Indeed, in this case, clean bubbles do not interact with cells, which means that at pH 9, the cell surface is completely hydrophilic. This can be explained by a change in the cell wall composition at higher pH (Demir-Yilmaz, Schiavone, et al., 2022), or by a change in the cell surface architecture where hydrophobic molecules at the surface of cells may be masked by other components (Demir, Blockx, et al., 2020). Thus, the initial interaction between the hydrophilic chitosan backbone at the surface of bubbles still takes place, as proven by the low adhesions recorded. But then because the cell surface is hydrophilic, the liquid film between bubbles and cells cannot be ruptured, thereby resulting in a low adhesion force. These results are important because they allow understanding better the molecular mechanism underlying PO-chitosan bubbles interactions with cells. While the interaction with PO-chitosan bubbles probably starts with a specific interaction between the chitosan molecules present at the surface of bubbles and cell surface polymers, hydrophobicity remains the main factor allowing then the contact between bubbles and cells.

Thus these results show that the functionalization of bubbles with PO-chitosan enhances their interactions with cells, and allow understanding the mechanisms at the basis of these interactions. Now in the next step, we will evaluate if these enhanced interactions can influence the separation rates obtained in bench-scale flotation experiments.

1.2.5. Optimizing the one-step flotation process

This part of the work is described in detail in the article entitled “Bubble functionalization in flotation process improve microalgae harvesting”, by Demir-Yilmaz et al., Chemical engineering Journal, 2023, presented in Chapter 6.

In the last part of the work, the efficiency of flotation with PO-chitosan functionalized bubbles for freshwater microalgae harvesting was investigated. For that, we used our novel molecule, PO-chitosan, as a surfactant to functionalize the surface of the bubbles injected in microalgae suspensions in order to capture cells and bring them to the surface of the suspension. The experiments were performed on a home-built flotation device shown in detail in Figure 17.

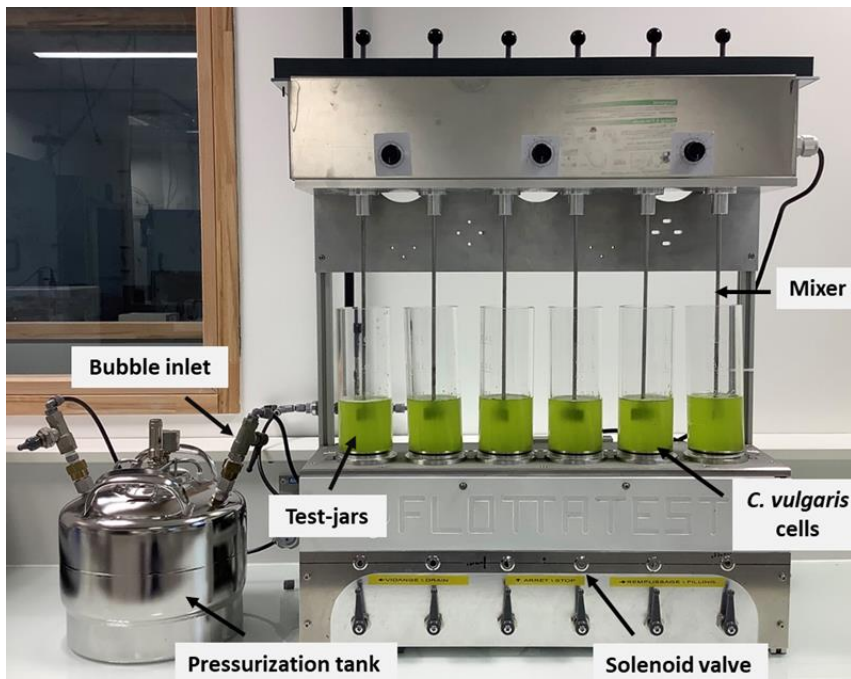


Figure 17: Photograph of the home-built flotation device used in this study. The flotation-test jars contain *C. vulgaris* cells grown. Water, air and PO-chitosan are pressurized during 30 minutes in the pressurization tank at 6 bars to produce white waters (water containing dissolved air) that is coated with PO-chitosan. The introduction of these PO-chitosan coated bubble induce the flotation of cells together with bubbles. Extracted from (Demir-Yilmaz, Yakovenko, et al., 2022)

Briefly, cell suspensions are introduced in the test-jars. To produce functionalized bubbles, air and water mixed with PO-chitosan are pressurized at 6 bar in the pressurization tank, causing the gases of air to dissolve in the water. The release of these pressurized waters (containing dissolved gases) at the bottom of the test-jars at atmospheric pressure induces the formation of bubbles forming the so called white waters. As PO-chitosan is released at the

same time, it directly assembles at the surface of bubbles. Then as the functionalized bubbles rise in the suspension, they interact with cells and bring them to the surface. The results obtained using this one-step flotation process are presented in Figure 18. Figure 18a is a schematic representation of the flotation process with bubble functionalization. Unless otherwise indicated, all the experiments were performed at pH 6. For that, in a first set of experiments, 50 mL of PO-chitosan white waters were injected from the pressurization tank to each beaker via the solenoid valves. Different PO-chitosan concentrations were tested in a range from 12.5 to 100 mg/L, and allowed to determine the best conditions, using 25 mg/L of PO-chitosan, where the highest separation efficiency was obtained. We then tested another parameter that can have an influence on the separation efficiency, the ratio of bubbles to cells. For that, we decreased or increased the volume of white waters injected in the microalgae suspensions; this results in a lower or higher number of bubbles and thus in a decreased or increased bubble surface area compared to cells. Three different injected white waters volumes were tested in addition to the control at 50 mL (20, 80 and 100 mL); the results obtained are presented in Figure 18b. On this graph, the light blue bars correspond to the control conditions (clean bubbles) and the dark blue bars correspond to PO-chitosan coated bubbles. The highest separation efficiency was of $55.1 \pm 13.1\%$, obtained with a white water volume of 50 mL, which is 2 times higher than the efficiency obtained with clean bubbles ($34.6 \pm 3.8\%$). The fact that using clean bubbles, approximately 30% of the cells could be separated from the culture medium can result from a natural flocculation of cells in these conditions. Lower separation efficiencies, close to the ones obtained in control conditions with clean bubbles, were found when using both lower volume ($33.2 \pm 2.8\%$ for 20 mL of bubbles) and higher volumes of bubbles ($14.4 \pm 1.4\%$ and $13.2 \pm 1.7\%$ respectively for 80 and 100 mL of bubbles). The results obtained using 20 mL can be explained by the fact that in this case, the surface area of the bubbles is not important enough to allow a contact with more cells. However, the low results obtained using higher volumes could be due to the fact that such large volumes injected dilute the solution too much, resulting in a low collision rate between bubbles and cells. This explanation is coherent also with the fact that for these high white waters volumes, flotation efficiency obtained with clean bubbles is reduced compared to 20 and 50 mL.

Finally, as we found that cells' interactions with PO-chitosan coated bubble are dependent on the pH, we then investigated the influence of pH variation of the separation efficiency using 25 mg/L of PO-chitosan with an injected volume of white waters of 50 mL. The results presented in Figure 18c show that the highest separation efficiency of $55.1 \pm 13.1\%$, is obtained for pH 6, and decreases gradually to $38.6 \pm 0.8\%$ at pH 7.4 and to $27.3 \pm 5.9\%$ at pH 9. This could be explained by the relative hydrophobicity difference of both *C. vulgaris* cell wall and PO-chitosan molecule at different pH. Moreover, the AFM-based force spectroscopy experiments (Figure 16) showed that with increasing pH, cells interact less with PO-chitosan coated bubbles most likely because of changes on both the cell surface (changes in the hydrophobicity, roughness and nanomechanical properties) and on the hydrophobicity of PO-chitosan itself that changes with pH variations. For example, at higher pH hydrophobic molecules on the cell surface, most likely lipids, may be masked or in a different conformation, preventing their interaction with the surface of bubbles. These experiments then prove that flotation efficiency using functionalized bubbles is dependent on the interaction that bubbles have with cells; the higher it is, the more efficient the separation process.

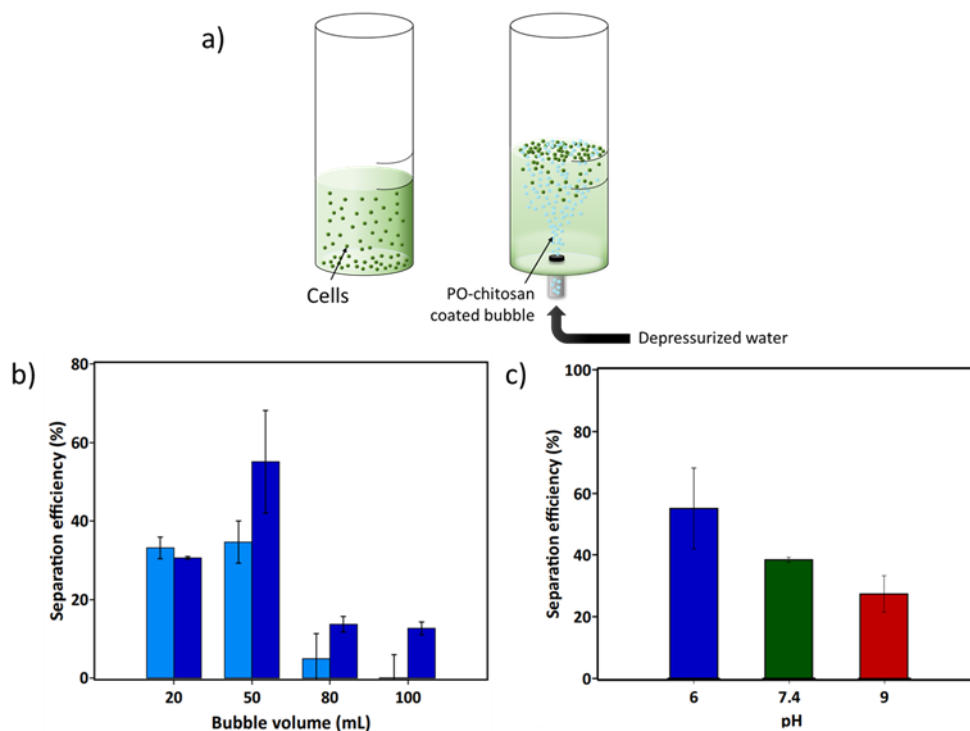


Figure 18: Flotation experiments of *C. vulgaris* with PO-chitosan coated bubble. a) Schematic representation of one-step flotation experiments. b) Flotation efficiency of *C. vulgaris* with varying PO-chitosan concentrations at pH 6. c) Flotation efficiency of *C. vulgaris* with 25 mg/L PO-chitosan coated bubble with varying bubble volume at pH 6 d) flocculation efficiency of *C. vulgaris* with 25 mg/L and 50 mL PO-chitosan coated bubble with varying pH.

Overall, these findings are promising. The first and most essential point is that using functionalized bubbles increases flotation separation efficiency by a factor of two when compared to the same procedure with clean bubbles. This finding is significant because it demonstrates that functionalization of bubble surface allows modifying the interactions between cells and bubbles, in this case, enhancing them and allowing for a more effective separation. In the case of continuous cultures, such method might be utilized to harvest the majority of the biomass while keeping the rest of the cell to continue the culture. As a result, it may be ideally suited for large-scale applications. The second important point is that using the FluidFM-based technology created by our team, we were able to identify the mechanisms by which these functionalized bubbles adhere to cells, and show that the adhesions obtained at the molecular scale directly influence the flotation separation efficiency obtained at the population scale.

1.3. Discussions and conclusions of the PhD work

The global aim of this project was to develop an original process to make flotation an efficient harvesting technique in order to better exploit the potential of the microalgal bioresource. The strategy proposed to reach this objective, summarized in Figure 19, is at the frontier between biology, physics and chemistry, and is based on the functionalization of bubbles with adhesive compounds that attach to cells and bring them to the surface. The idea was that using bio-sourced compounds existing at the surface of cells, it would be possible to avoid the toxicity and interference with downstream processes that can take place using synthetic flocculants. Thus to reach our objective, the first and challenging step of this PhD was to develop a new method to probe bubble-microorganism interactions at the molecular scale. To do so, a combination of atomic force microscopy and microfluidics was used in order to produce micro-sized bubbles at the aperture of FluidFM cantilevers (Figure 19A), and probe their interactions with individual cells. Then, to identify a molecule that could interact with cells without being toxic, we made the hypothesis that it could be a polysaccharide present in the cell wall of cells, as polysaccharides are able to form homotypic bonds. In order to identify such polysaccharide, in the next step we then determined the cell wall composition of our model microalgae species, *C. vulgaris*. For that we used a combination of methods, AFM, XPS and liquid chromatography which allowed to generate fundamental knowledge lacking in the literature about the composition and dynamics of the microalgae cell wall. Using this new data, we could apprehend the complexity of the cell wall structure and make hypothesis on the possible polysaccharides that could compose it (Figure 19B). Using these results as well as data from the literature, we identified one polysaccharide that had the potential to adhere to *C. vulgaris* cell surface, chitosan. Thereafter, it was needed to determine if indeed this molecule could interact with cells and by what type of mechanism (Figure 19C). Understanding flocculation mechanisms at the nanoscale is in fact an important point to then be able to optimize separation processes at large scales. Our results showed that chitosan interacts with *C. vulgaris* cell surface through biological interactions with an average adhesion value around of 300 pN. To compare, antigen-antibody interactions are usually in the pN range around 70-200 pN (Dammer et al., 1996; Willemsen et al., 1998). Chitosan interactions with cells is higher than that, indicating that chitosan is able to bind strongly to cells, making it a good candidate molecule to coat bubble surfaces. After that, we modified this molecule to make it amphiphilic

so that it could assemble at the surface of bubbles (Figure 19D). At this stage, it was important to understand the mechanism of adhesion to cells of bubbles functionalized with this new molecule, PO-chitosan, and see if the modification made on chitosan did not change its binding efficiency. To verify that, we used the developed method in the first step, to probe the interaction between PO-chitosan coated bubble and *C. vulgaris* cells (Figure 19E). We found that PO-chitosan interacts with *C. vulgaris* cells mainly through a dominant hydrophobic interaction with an average adhesion force around of 3 nN. This first means that PO-chitosan is able to bind to cells with a strength 10-times higher than the one obtained with chitosan. But in this case, the interactions between cells and PO-chitosan coated bubbles are more complex than with chitosan only. Indeed, PO-chitosan adsorb at the bubble surface in a way that the hydrophilic chitosan units stays outside of the bubble in the liquid part, whereas the hydrophobic tails (octanal groups) added to the molecule stay inside the bubble, in the gas part (see Figure 17d). Thus we should be able to see the biological interaction between *C. vulgaris* cells and chitosan backbone, yet, we observe hydrophobic interactions. This phenomena can be explained as follows: the specific interaction between *C. vulgaris* cell surface and the chitosan monomers probably still exists, and because it is efficient, the water film between the bubble and the cell get ruptured and causes the formation of a three phase contact line (TPC), which results in a hydrophobic interaction that becomes dominant and masks the specific one. These modifications of the bubble surface show that indeed, using such surface engineering strategies, it is possible to control and modulate the direct interactions between bubbles and cells. Finally, the efficiency of the functionalized bubbles to capture populations of cells was experimentally evaluated using a bench-scale flotation device (Figure 19F). The idea is that using this strategy, the pretreatment steps needed in cell harvesting by flotation such as flocculation could be eliminated, resulting in a gain of time and money. Using this one-step harvesting method, we were able to separate approximately 55% of cells from their aqueous culture medium. This number may not reach 100%, but is in fact very interesting when considering continuous mode processes (mainly used industrial applications), as separating only part of the cells allow the remaining ones to resume culture.

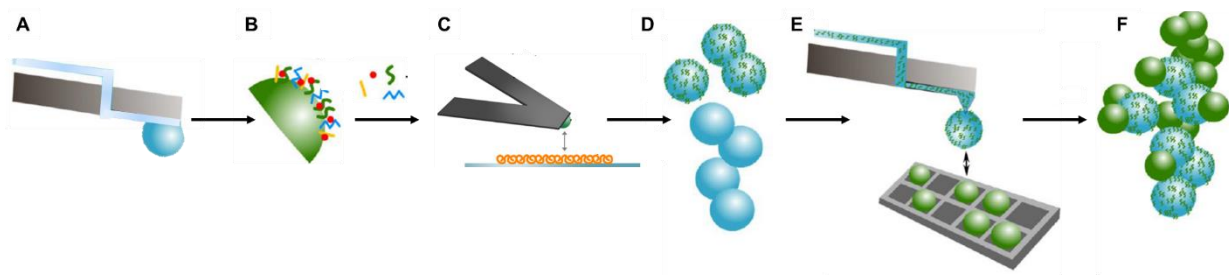


Figure 19: Schematic representation of the development of new bubble surface engineering strategy for optimized microalgae harvesting.

1.3.1. Contribution of the work to other fields of research and applications

The results of all the work produced during this PhD have so far been presented from the point of view of their interest for the objective set in this PhD, functionalizing the bubble surface to improve flotation. However, each step in this PhD led to the generation of knowledge that also can contribute to other fields of research or for other applications than flotation: this is what we are going to discuss now in this section.

As mentioned in Chapter 1.1.1, in flotation separation processes, flocculation is often used as a first step to enhance flotation efficiency. But if we want to get rid of this step, then understanding the behavior of bubbles and how they interact with cells is mandatory. To understand this, here we developed a new method to produce bubble and measure their interaction with cells using fluidic force microscopy (FluidFM). As we mentioned in section 1.1.4 FluidFM has already been used in several applications. However, here in this PhD we used FluidFM in an original and different manner, which had never been described before, to produce bubble directly at the aperture of cantilevers. For that a prerequisite was to first apply on the FluidFM microchannel a hydrophobic coating using self-assembled monolayers (SAMs) of silanes *via* SAMs vapor deposition technique. This step was important to keep the produced bubbles on the cantilever's aperture, otherwise they would have risen up to the surface. Then, for the first time we filled the cantilever with an air unlike for the all the other applications of FluidFM that use filled cantilevers with liquids. The hydrophobic coating inside the cantilever make it possible to push the air outside of the microchannel to form a bubble at its aperture. This bubble probe method is a reliable method to measure the interaction between bubble and complex surfaces as this system allows controlling the size of the bubble over consecutive measurements and even during the same measurement. In fact, keeping the bubble size constant over time was the main bottleneck in existing methods using AFM to probe bubbles'

interactions, that could thus be overcome using FluidFM. This new method is not only interesting in the context of this PhD thesis, as it can be used by the scientific community to better understand the interactions between bubbles and any kind of (bio)-surfaces, which are involved in many different applications. A first example of such application is microorganism removal from surfaces where they form biofilms, which is an important problem in many industrial processes (dentistry, water filtration, water storage and piping). To solve this problem, air bubbles could be a promising means to control fouling; for instance, a recent study by Kriegel and coworkers investigated the mechanism underlying the removal of bacteria (*P. aeruginosa*) from polycarbonate (hydrophilic) and PDMS (hydrophobic) surfaces with air bubbles (Kriegel & Ducker, 2019). In this study, the authors show that most of the bacteria on the hydrophobic solid surface could be removed just after the first interaction with bubble, whereas an important amount of bacteria remains on hydrophilic surfaces. This may mean that the interaction between hydrophilic surfaces and bacteria is stronger than interaction between bubbles and bacteria. Using the bubble probe method developed in this PhD, the interactions of bubbles with bacteria could be quantified and then compared with the interaction between bacteria and different surfaces to evaluate the possibility to actually remove cells using bubbles. In addition, factors influencing these interactions could also be investigated such as environmental factors, pH, ionic strength, or other factors i.e., bubble size and wettability of the surfaces. Another example of application where the bubble probe method could bring interesting information is for microbubbles that are used as drug carriers to treat diseases. Indeed, Tinkov, Gao and Klivanov *et al.* studied the possibility to load bubbles with a drug or a gene therapy vector, and then locally deliver and release the transported substances using ultrasound (Tinkov *et al.*, 2009; Gao *et al.*, 2008; Klivanov, 2007). In these complex systems, microbubbles are coated with antibodies that allow them to interact with specific antigen present on cell membranes. This allows their binding to the targeted cells (Delalande *et al.*, 2012; Klivanov, 2007). Then, ultrasound exposure is performed; this causes a temporary membrane permeability of cells, and it makes bubbles collapse to release the encapsulated drugs. This drastically increases the intracellular drug uptake by the cells (Delalande *et al.*, 2012; Frenkel, 2008). This bubble carrier method has been successfully applied to deliver nucleic acid *in vitro* and *in vivo*, yet fundamental information on the interactions of bubbles with cells are missing, which could help to further develop this targeted drug delivery method. In this context, the bubble probe method

developed in this PhD could be used to understand the mechanism of targeted bubble attachment to the cell membranes, which could help in better controlling cell targeting. In addition, with this method, different bubble coatings and their affinity for targeted cells as well as for the bubbles could be evaluated under different environmental conditions.

Let's now talk about the microalgae cell wall, which is responsible for the complex interplay between cells and their environment. In the context of this work, better understanding this complex interplay allowed understanding its interactions with flocculants for harvesting applications. While we chose to work with chitosan, other types of molecules could also be identified as potential bio-sourced flocculants, and this by understanding the cell wall composition. This would allow optimizing new flocculation process with natural polymers directly available on the cell wall, thus non-toxic and biocompatible. This way the issues relating with the usage of synthetic polymers could be eliminated such as contamination of the final products. However, understanding the dynamic characteristic and composition of microalgae cell wall is also important for understanding and controlling other aspects than cell adhesion. For example, rupturing the cell wall is an important challenge in extraction processes, where the goal is to break cells in order to release and harvest the intracellular products they were cultivated for. Choosing appropriate methods to do this can be a complicated task and depends on the microalgae species used, the conditions considered, and the production scale. The main cell disruption methods used are mechanical and chemical methods. They are different in terms of energy consumption, efficiency and solvent usage. Because most microalgae species possess a rigid cell wall resistant to mechanical and chemical stressors, these disruption methods can be used independently but also in combination in order to achieve high yields (Lee et al., 2017). For mechanical disruption such as bead milling, homogenizer, microfluidizers, microwave treatment, etc., important energy inputs in the form of shear pressures, electrical pulses, waves, or heat are required. Mechanical processes often feature excellent product recovery yields with good controllability and scalability, but their energy consumption is very high. Mechanical disruption can sometimes be coupled with non-mechanical disruption methods or pretreatments for example chemical disruption to reduce energy consumption and improve the efficiency (Taleb et al., 2016). In chemical disruption methods, chemicals directly interact with the cell wall to allow release of intracellular products (Dong et al., 2016). However, the selectivity, compatibility, and efficiency of these chemicals are highly influenced by the composition and structure of the microalgal cell wall (Lee et al.,

2017). Moreover, the chemical and mechanical methods consume a significant energy and cannot be scaled up easily (de Boer et al., 2012). For these reasons, it is interesting to develop or optimize other type of processes for example based on the enzymatic digestion of the microalgae cell wall. The benefits of such enzymatic digestions compared to mechanical or chemical disruption methods are the biological selectivity of the enzymes used, the mild operating conditions needed and the reduced energy consumption (Günerken et al., 2015). Enzymatic digestion has been already used in some cases but not in large scale as it is the case for mechanical and chemical treatments. Despite the important costs of enzymes, because the operational conditions are not energy-consuming, in the end such techniques can be less expensive to set up than mechanical or chemical treatments (Nagappan et al., 2019). Moreover, scaling up enzymatic treatments is relatively easy compared to mechanical methods (Pragya et al., 2013; Demuez et al., 2015). However, to develop and optimize such enzymatic process, it is fundamental to understand cell wall composition and dynamics, to actually be able to choose the right enzymes for the right microalgae species and the right conditions. The work that we have done to determine the cell wall composition and architecture of *C. vulgaris* goes in that direction but is for the moment limited. Indeed, now further research needs to be performed, using enzymatic digestion or solid-state Nuclear Magnetic Resonance (NMR) to identify mainly the polysaccharides present on the cell wall but also the lipids and proteins, and this way provide the information needed to optimize cell rupturing methods based on enzymatic digestions.

After having analyzed the composition of the cell wall, we then chose chitosan to continue the work and understand how it interacts with cells. Chitosan is a widely used flocculent for microalgae harvesting, but so far mixed results have been reported on the flocculation efficiencies depending on the microalgae species used (freshwater or marine species) and on the experimental conditions (pH). Without a precise knowledge on how flocculant works, it is very difficult to use them in a reliable manner for large scale applications. This is why it is important to understand their flocculation mechanisms. However flocculation mechanisms, whether they are naturally induced or induced by added molecules, are challenging to adapt, even at lab scales, because of their uniqueness for each culture condition and each microalgae species used (Demir, Besson, et al., 2020). This is why a large number of studies in the literature are dedicated to understand these mechanisms, particularly the important parameters that influence their efficiency. Let's give concrete examples of this. For

instance, for the same flocculant, magnesium hydroxide, the flocculation mechanisms are different depending on the microalgae species. For example charge neutralization mechanism is at play for *P. tricornutum* whereas sweeping flocculation mechanism is observed for *D. salina*, at high pH (Besson et al., 2019; Besson & Guiraud, 2013b; Formosa-Dague, Gernigon, et al., 2018a). Our work on chitosan also highlighted that the flocculation mechanism can change depending on the pH of the culture medium (Demir, Blockx, et al., 2020), showing the complexity that these mechanisms can hold. It is thus critical to identify these mechanisms involved in each case in order to be able to control and employ them in larger scales (Xu et al., 2013; Zhu et al., 2018). As we have showed in the work on chitosan interactions (Demir, Blockx, et al., 2020), using AFM is actually an interesting approach for this, as it allows understanding the molecular basis of the mechanisms at play in flocculant-cell interactions, which thus enables determining the parameters important to control these interactions and further optimize large-scale flocculation processes. Such experimental strategy could become a reference tool in order to solve the mysteries of flocculation for different flocculants and different microalgae species. So far in the literature, the most commonly used method to identify flocculation mechanisms is zeta potential measurements. Zeta potential is determined by measuring the surface charge of microalgae cell surfaces. Most of the flocculants used for microalgae harvesting are cationic flocculants (chitosan, starch, ...), thus zeta potential is well suited method to verify that indeed the flocculation mechanism relies on electrostatic interactions. For example, Vandamme *et al.* identified the flocculation mechanism of the diatom *Phaeodactylum tricornutum* with alkaline salts using such method. In this case, the increase in the zeta potential measurements during the flocculation with brucite suggested that brucite precipitation caused flocculation by charge neutralization. However, zeta potential measurements stayed negative for flocculation with calcite suggesting here that flocculation occurred through a non-electrostatic-based mechanism (Vandamme et al., 2015). However, this method is limited to electrostatic interactions and does not allow evaluating biological interactions and hydrophobic interactions. For example, as we saw in the case of chitosan, even for cationic molecules, electrostatic interactions may not be the dominant in the flocculation mechanism, showing the need for techniques other than zeta potential measurements that can go beyond and measure other types of interactions. Then, also as we saw in the work developed in this PhD, other types of interactions can be efficient to promote interactions (biological specific interactions,

hydrophobic interactions). This means that other types of flocculants could be developed, and for this a tool such AFM would allow understanding the mechanisms at play and thus extend the features to look for to find efficient flocculant molecules.

In order to optimize microalgae separation using flotation process and reduce in a significant manner the cost and time of the process, bubble functionalization is an interesting alternative. In this work, bubble functionalization concept was used, but instead of changing the charge of the bubbles as it is performed by Henderson et al., 2008b, 2010, the goal was to make it specific so that it could interact in an efficient and controlled manner with cells. Moreover, the use of chitosan can be beneficial compared to the cationic polymers used by the Henderson team, as it is non-toxic and does not interfere with down-stream processes. Harvesting is definitely a key step in any microalgae-based technology, and it has been identified as a major bottleneck in achieving the sustainability and cost-efficiency of these technologies. Moreover, in order to maximize total process efficiency, a good balance between process time and energy cost must be maintained. For example, this PhD work showed that 10 mg/L chitosan is needed to achieve maximum separation efficiency (flocculation followed by flotation) with *C. vulgaris* cells. However, when we use PO-chitosan to functionalize bubbles, 25 mg/L is needed to reach the best separation efficiency, although as chitosan and PO chitosan are different molecules, a direct comparison of the concentrations used is not really suitable. But still, at least at the lab scale, it seems that more molecules are required for bubble functionalization, but then when we consider the time needed for separation, in the first scenario, we need to add the flocculant and mix it with the suspension for 15 min. Then 30 minutes are needed for the flocs to stabilize before injecting bubbles at the bottom of the jar and collect the aggregated cells on the surface. However, with functionalized bubbles, both mixing and stabilization steps are skipped (in total 45 min), the process starts directly with the bubble injection (15 min), which reduces the process time to $\frac{1}{4}$ of the initial time. These timings are for the bench-scale process that we developed, but we can imagine that these time differences would also take place at larger scale. As at industrial scale time is money, operating separation in only one step could perhaps increase significantly the overall cost-effectiveness of microalgae production systems and make them economically more viable. In fact, a reliable economic comparison and a life cycle analysis (LCA) have to be performed in order to correctly compare the two harvesting systems (Laifa et al., 2021). This comparison has to be made at the industrial scale including the energy saving

and the infrastructure saving due to the suppression of the flocculation step. Only such type of analysis will make it possible to decide if indeed one-step flotation is more cost-effective than flocculation followed by flotation.

1.3.2. Future perspectives on the work performed in this PhD

While the knowledge and the methods developed in this PhD work can have important impacts in other fields, we would like here to look towards the future and describe in this section the concrete perspectives work that can be built based on the results generated in this PhD. Basically, there are many perspective works that could be envision based on the results obtained in this PhD thesis. A first perspective is linked to the work on FluidFM, which could be used not only to produce bubbles but also to produce other types of fluid interfaces such as liquid droplets. The development of liquid droplet systems is currently advancing at a rapid rate. A variety of proof-of-concept applications in biotechnologies are described, highlighting their potential as tools for performing rapid, reliable, and energy efficient engineering tasks e. Indeed, their various advantages, such as adaptability, diversity and high surface area to volume ratio enable them to serve a wider range of applications, going from single cell analysis, cell based assays or controlled drug release (Wei et al., 2020). For example, in the growing field of droplet-based microfluidics, different approaches are being developed to control, manipulate, and most importantly functionalize droplets (Khojasteh et al., 2019). In this context, using FluidFM to produce drops could be an efficient way to increase the knowledge needed to optimize these applications, and to measure their interaction the various types of surfaces they can be brought to interact with. We can imagine that for producing such droplets, the FluidFM cantilever microchannel could be filled with liquid instead of air and by applying over pressure liquid droplets could be form in another liquid with a different density. With this form liquid droplets interaction mechanisms with bio-surfaces could be assessed.

As mentioned earlier, another perspective of this PhD work could be about the enzymatic digestion of the *C. vulgaris* cell wall. In this manuscript we analyzed the cell wall composition of *C. vulgaris* and determined the relative fractions of main components; lipids proteins and polysaccharides. Then by going a step forward, we identified the monosaccharides present in the cell wall, using acid hydrolysis followed by liquid

chromatography. However, we never identified the polysaccharides these monosaccharides come from, which, as discussed before, could bring important information to develop for example enzymatic-based cell-disruption processes. For this reason, one can envision to perform a screening of enzymes to degrade *C. vulgaris* cell wall, and then analyze the presence of monomers. If monomers are detected, then this means that the polysaccharide targeted by the enzyme was present in the cell wall. If not, another enzyme should be tested and the same process needs to be repeated. Such procedure is based on trial and error, which takes time and can be costly. However, once it is done, this information can be really useful in various applications, at the industrial scale to digest microalgae cell wall, or to identify new compounds that could be valorized. Moreover, solid state NMR spectroscopy could be also an option to identify and quantify the polysaccharides present in the cell wall. For example, Paulhazan *et al.* recently examined the composition, dynamical characteristics, and spatial organization of glycans for the microalgae species *Parachlorella beijerinckii* (Paulhazan *et al.*, 2021). Their magic-angle-spinning (MAS) solid-state NMR (ssNMR) spectroscopy-based results showed that starch is the major rigid and predominantly abundant molecule in the cell wall. So far very few studies have used such method to analyze the cell wall of microalgae (Arnold *et al.*, 2015; Ghassemi *et al.*, 2021; Separovic & Sani, 2020), but they all show the interest of solid state NMR to gain a precise and complete understanding of the polysaccharides present in the cell wall of microalgae cells.

Then another perspective could be built on the work performed on chitosan to modify it and make it amphiphilic. In this manuscript we used octanal (C8) as a hydrophobic group to make the final molecule amphiphilic. But instead of octanal, longer or shorter hydrophobic chains could also be used, such as dodecanal (C12) or hexanal (C6). Extending or reducing the hydrophobic groups of the molecule may increase or decrease the surfactant activity of modified chitosan, and thus both their interactions with *C. vulgaris* cells and their affinity towards hydrophobic bubbles. Also this could have an impact on the solubility of the modified molecules, and further on the substitution degree that could be achieved. For instance, for high molecular weight chitosan (used in this PhD), a 10-15% alkylation level is the limit to then be able to dissolve the molecule in water and further use it in harvesting experiments. We also tried using low molecular weight chitosan, and in this case, the substitution degree that could be achieved was even lower as at an alkylation level of 10%, the final product could not be

dissolved in water anymore. This shows that there needs to be a balance between the relative lengths of the hydrophilic and hydrophobic chain in the molecule, the goal being to have a molecule perhaps with a higher surfactant activity, but that could still be dissolved. For example, for longer hydrophobic chains, in order to still be able to dissolve the molecule in water the substitution degree may have to be reduced while using shorter chains, perhaps higher alkylation levels could be reached allowing to have overall a different lipophilic/hydrophilic balance within the molecule. Thus to understand this and fine-tune in fact the properties of these amphiphilic chitosan molecules, the both longer and shorter hydrophobic groups could be used, with different molecular weight chitosan molecules, using different substitution degrees.

The further and most obvious perspective could be to use PO-chitosan coated bubble to separate different microalgae species; both marine and freshwater species. Salt in the marine water screen all the charges present both on cells and the molecule on the bubble by suppressing the electrostatic interaction. PO-chitosan based hydrophobic interaction thus could still be efficient regardless of the charges. Moreover, instead of chitosan, we can add the hydrophobic properties to different (bio)-molecules even with a negatively charge to harvest negatively-charged microalgae species. In appendix 1, this theory is well explained but in short; long-range hydrophobic interaction can be dominant over electrostatic repulsion. For instance, in the study example presented in appendix 1, negative microalgae cells could still interact with negatively-charged and hydrophobic microplastic particles. This study, for the first time, proves that we are not only limited to electrostatic interaction but thus to positively charged molecules. However, we can also use the positively charged molecules which provide broader target molecular selection both for marine and freshwater microalgae species.

Finally, a perspective that can be envisioned when considering the separation of cells from water using functionalized bubbles is to perform a selective separation. Selective separation using flotation process consists in separating fine particles from particles of other components present in a disperse phase (Mathur et al., 2000). Because historically flotation has been used in the ore and mineral industries, selective flotation has already been used to selectively separate different minerals such as wolframite (Lu et al., 2021), copper (Hassanzadeh et al., 2020), fluorite (W. Jiang et al., 2018), calcite and barite (Ren et al., 2017). The basic concept behind selective separation is based on the difference in the surface

properties of minerals to be separated (Zanin et al., 2019). To separate one mineral from the other, one has to be hydrophobic while the other one is hydrophilic so that hydrophobic minerals attach to bubbles and are carried to the surface while the hydrophilic ones remain in suspension. To actually control this, different chemicals can be used to modify the surface properties of selected minerals and change their hydrophobic properties; collectors, depressants, modifiers, or frothers. (Bulatovic, 2007). Collectors (often called surfactants) are used to improve the surface hydrophobicity thus the affinity of particles towards bubbles (Laitinen et al., 2016). For example, hydroxamic acids are a ubiquitous class of collectors that can selectively adsorb on minerals, such as wolframite (Meng et al., 2015) and rare-earth minerals (Kumari et al., 2015), to enhance their surface hydrophobicity and facilitate their separation from the polymetallic ores by flotation. Whereas depressants enlarge the floatability difference between two minerals by suppressing one of the minerals hydrophobicity (X. Wang et al., 2022). Modifying reagents react either with the mineral surfaces or with collectors and other ions in the flotation pulp, resulting in a modified and controlled flotation response. Using these chemicals, selective separation of minerals can be achieved. While these strategies work very well with mineral and ore particles, it could be an interesting aspect to adapt them to cells, and this way use flotation as a cell sorting method, allowing to separate a specific population of cells from another one in a complex medium. For that, of course, one possibility could be to modify the cell surface properties using collectors or depressants like it is performed for minerals, but another alternative would be to directly modify the bubble surface so that it interacts only with one cell type and not the others. Because the work performed in this PhD has showed that it was possible to functionalize bubbles with any type of amphiphilic molecule to control their interactions with cells, then this possibility seems quite realistic. For instance, such strategy could be used for example to separate bacterial cells from human blood cells in the case of sepsis, and this way be able to provide an early diagnosis of the bacterial species involved to target an effective treatment. This example has already caught our attention, and during this PhD we explored the potential of interaction of bubbles functionalized with colistin with Gram-negative bacterial cells (Demir et al., 2021a). Colistin is a natural polycyclic antibacterial peptide derived from *Bacillus polymyxa*, which specifically interact to the surface of bacteria by binding to the lipid A part of the lipopolysaccharide (LPS) (Yahav et al., 2012), a glycolipid found in the outer membrane of Gram-negative species (Maldonado et al., 2016). Our work showed that the

functionalization of bubbles with colistin had a positive impact on the adhesion of cells to the bubbles. Because colistin is very specific and does not bind to non-bacterial cells, such as mammalian cells found in blood, it could be a potential way to separate bacteria from the other blood components and this perform a selective separation. This is one application of such process, but many other applications can be envisioned, in different fields, for different applications.

In the end, this PhD manuscript has highlighted scientific problems that current researcher has not addressed yet. Although involved in many different biological systems, bubble-microorganisms interactions have been poorly explored due to the lack of a method or tool able to probe them. These type of interactions take place during microalgae harvesting by flotation, a promising separation technique that could enable the use of microalgal biomass in large-scale industrial processes. The work performed in this PhD has allowed to answer part of these questions, to develop a tool to access bubble-microorganisms interactions, and to develop a new and original microalgae separation process using functionalized bubbles. For that we made a number of developments and generated fundamental data on different aspects of microalgae, which can serve as basis by the scientific community for new developments, in other application fields, showing in the end the wide impact of the work produced. Moreover, this work has set the basis for new projects, new improvements and new ideas that will be hopefully be developed in the next few years.

References

- Abdullahi, A. S., Underwood, G. J. C., & Gretz, M. R. (2006). Extracellular Matrix Assembly in Diatoms (bacillariophyceae). V. Environmental Effects on Polysaccharide Synthesis in the Model Diatom, *Phaeodactylum Tricornutum*1. *Journal of Phycology*, *42*(2), 363–378. <https://doi.org/10.1111/j.1529-8817.2006.00193.x>
- Acién, F. G., Molina, E., Fernández-Sevilla, J. M., Barbosa, M., Gouveia, L., Sepúlveda, C., Bazaes, J., & Arbib, Z. (2017). 20—Economics of microalgae production. In C. Gonzalez-Fernandez & R. Muñoz (Eds.), *Microalgae-Based Biofuels and Bioproducts* (pp. 485–503). Woodhead Publishing. <https://doi.org/10.1016/B978-0-08-101023-5.00020-0>
- Ahmad, A. L., Mat Yasin, N. H., Derek, C. J. C., & Lim, J. K. (2011). Optimization of microalgae coagulation process using chitosan. *Chemical Engineering Journal*, *173*(3), 879–882. <https://doi.org/10.1016/j.cej.2011.07.070>
- Alam, F., Date, A., Rasjidin, R., Mobin, S., Moria, H., & Baqui, A. (2012). Biofuel from Algae- Is It a Viable Alternative? *Procedia Engineering*, *49*, 221–227. <https://doi.org/10.1016/j.proeng.2012.10.131>
- Alcoverro, T., Conte, E., & Mazzella, L. (2000). Production of Mucilage by the Adriatic Epipellic Diatom *Cylindrotheca Closterium* (bacillariophyceae) Under Nutrient Limitation. *Journal of Phycology*, *36*(6), 1087–1095. <https://doi.org/10.1046/j.1529-8817.2000.99193.x>
- Apoya-Horton, M. D., Yin, L., Underwood, G. J. C., & Gretz, M. R. (2006). Movement Modalities and Responses to Environmental Changes of the Mudflat Diatom *Cylindrotheca Closterium* (bacillariophyceae)1. *Journal of Phycology*, *42*(2), 379–390. <https://doi.org/10.1111/j.1529-8817.2006.00194.x>
- Araújo, C. V. M., Romero-Romero, S., Lourençato, L. F., Moreno-Garrido, I., Blasco, J., Gretz, M. R., Moreira-Santos, M., & Ribeiro, R. (2013). Going with the Flow: Detection of Drift in Response to Hypo-Saline Stress by the Estuarine Benthic Diatom *Cylindrotheca closterium*. *PLOS ONE*, *8*(11), e81073. <https://doi.org/10.1371/journal.pone.0081073>
- Arnold, A. A., Genard, B., Zito, F., Tremblay, R., Warschawski, D. E., & Marcotte, I. (2015). Identification of lipid and saccharide constituents of whole microalgal cells by ¹³C solid-state NMR. *Biochimica et Biophysica Acta (BBA) - Biomembranes*, *1848*(1), 369–377. <https://doi.org/10.1016/j.bbamem.2014.07.017>

- Aslam, A., Thomas-Hall, S. R., Manzoor, M., Jabeen, F., Iqbal, M., uz Zaman, Q., Schenk, P. M., & Asif Tahir, M. (2018). Mixed microalgae consortia growth under higher concentration of CO₂ from unfiltered coal fired flue gas: Fatty acid profiling and biodiesel production. *Journal of Photochemistry and Photobiology B: Biology*, *179*, 126–133. <https://doi.org/10.1016/j.jphotobiol.2018.01.003>
- Bazaes, J., Sepulveda, C., Ación, F. G., Morales, J., Gonzales, L., Rivas, M., & Riquelme, C. (2012). Outdoor pilot-scale production of *Botryococcus braunii* in panel reactors. *Journal of Applied Phycology*, *24*(6), 1353–1360. <https://doi.org/10.1007/s10811-012-9787-3>
- Benemann, J. (2013). Microalgae for Biofuels and Animal Feeds. *Energies*, *6*(11), Article 11. <https://doi.org/10.3390/en6115869>
- Besson, A., Formosa-Dague, C., & Guiraud, P. (2019). Flocculation-flotation harvesting mechanism of *Dunaliella salina*: From nanoscale interpretation to industrial optimization. *Water Research*, *155*, 352–361. <https://doi.org/10.1016/j.watres.2019.02.043>
- Besson, A., & Guiraud, P. (2013a). High-pH-induced flocculation-flotation of the hypersaline microalga *Dunaliella salina*. *Bioresource Technology*, *147*, 464–470. <https://doi.org/10.1016/j.biortech.2013.08.053>
- Besson, A., & Guiraud, P. (2013b). High-pH-induced flocculation–flotation of the hypersaline microalga *Dunaliella salina*. *Bioresource Technology*, *147*, 464–470. <https://doi.org/10.1016/j.biortech.2013.08.053>
- Binnig, G., Quate, C. F., & Gerber, Ch. (1986). Atomic Force Microscope. *Physical Review Letters*, *56*(9), 930–933. <https://doi.org/10.1103/PhysRevLett.56.930>
- Blockx, J., Verfaillie, A., Thielemans, W., & Muylaert, K. (2018). Unravelling the Mechanism of Chitosan-Driven Flocculation of Microalgae in Seawater as a Function of pH. *ACS Sustainable Chemistry & Engineering*, *6*(9), 11273–11279. <https://doi.org/10.1021/acssuschemeng.7b04802>
- Brennan, L., & Owende, P. (2010). Biofuels from microalgae—A review of technologies for production, processing, and extractions of biofuels and co-products. *Renewable and Sustainable Energy Reviews*, *14*(2), 557–577. <https://doi.org/10.1016/j.rser.2009.10.009>

- Butt, H.-J., Farshchi-Tabrizi, M., & Kappl, M. (2006). Using capillary forces to determine the geometry of nanocontacts. *Journal of Applied Physics*, *100*(2), 024312. <https://doi.org/10.1063/1.2210188>
- Canelli, G., Murciano Martínez, P., Austin, S., Ambühl, M. E., Dionisi, F., Bolten, C. J., Carpine, R., Neutsch, L., & Mathys, A. (2021). Biochemical and Morphological Characterization of Heterotrophic *Cryptocodinium cohnii* and *Chlorella vulgaris* Cell Walls. *Journal of Agricultural and Food Chemistry*, *69*(7), 2226–2235. <https://doi.org/10.1021/acs.jafc.0c05032>
- Cheng, Y.-S., Zheng, Y., Labavitch, J. M., & VanderGheynst, J. S. (2011). The impact of cell wall carbohydrate composition on the chitosan flocculation of *Chlorella*. *Process Biochemistry*, *46*(10), 1927–1933. <https://doi.org/10.1016/j.procbio.2011.06.021>
- Chew, K. W., Chia, S. R., Show, P. L., Yap, Y. J., Ling, T. C., & Chang, J.-S. (2018). Effects of water culture medium, cultivation systems and growth modes for microalgae cultivation: A review. *Journal of the Taiwan Institute of Chemical Engineers*, *91*, 332–344. <https://doi.org/10.1016/j.jtice.2018.05.039>
- Chisti, Y. (2008). Biodiesel from microalgae beats bioethanol. *Trends in Biotechnology*, *26*(3), 126–131. <https://doi.org/10.1016/j.tibtech.2007.12.002>
- Chua, E. T., Eltanahy, E., Jung, H., Uy, M., Thomas-Hall, S. R., & Schenk, P. M. (2019). Efficient Harvesting of *Nannochloropsis* Microalgae via Optimized Chitosan-Mediated Flocculation. *Global Challenges*, *3*(1), 1800038. <https://doi.org/10.1002/gch2.201800038>
- Colling Klein, B., Bonomi, A., & Maciel Filho, R. (2018). Integration of microalgae production with industrial biofuel facilities: A critical review. *Renewable and Sustainable Energy Reviews*, *82*, 1376–1392. <https://doi.org/10.1016/j.rser.2017.04.063>
- Converti, A., Casazza, A. A., Ortiz, E. Y., Perego, P., & Del Borghi, M. (2009). Effect of temperature and nitrogen concentration on the growth and lipid content of *Nannochloropsis oculata* and *Chlorella vulgaris* for biodiesel production. *Chemical Engineering and Processing: Process Intensification*, *48*(6), 1146–1151. <https://doi.org/10.1016/j.cep.2009.03.006>
- Coward, T., Lee, J. G. M., & Caldwell, G. S. (2015). The effect of bubble size on the efficiency and economics of harvesting microalgae by foam flotation. *Journal of Applied Phycology*, *27*(2), 733–742. <https://doi.org/10.1007/s10811-014-0384-5>

- Dague, E., Alsteens, D., Latgé, J.-P., Verbelen, C., Raze, D., Baulard, A. R., & Dufrêne, Y. F. (2007). Chemical Force Microscopy of Single Live Cells. *Nano Letters*, *7*(10), 3026–3030. <https://doi.org/10.1021/nl071476k>
- Dammer, U., Hegner, M., Anselmetti, D., Wagner, P., Dreier, M., Huber, W., & Güntherodt, H. J. (1996). Specific antigen/antibody interactions measured by force microscopy. *Biophysical Journal*, *70*(5), 2437–2441. [https://doi.org/10.1016/S0006-3495\(96\)79814-4](https://doi.org/10.1016/S0006-3495(96)79814-4)
- de Boer, K., Moheimani, N. R., Borowitzka, M. A., & Bahri, P. A. (2012). Extraction and conversion pathways for microalgae to biodiesel: A review focused on energy consumption. *Journal of Applied Phycology*, *24*(6), 1681–1698. <https://doi.org/10.1007/s10811-012-9835-z>
- de Brouwer, J. F. C., Wolfstein, K., Ruddy, G. K., Jones, T. E. R., & Stal, L. J. (2005). Biogenic Stabilization of Intertidal Sediments: The Importance of Extracellular Polymeric Substances Produced by Benthic Diatoms. *Microbial Ecology*, *49*(4), 501–512. <https://doi.org/10.1007/s00248-004-0020-z>
- De Miranda, M., Gaviano, M., & Serra, E. (2005). Changes in the cell size of the diatom *Cylindrotheca closterium* in a hyperhaline pond. *Chemistry and Ecology*, *21*(1), 77–81. <https://doi.org/10.1080/02757540512331323962>
- Delalande, A., Postema, M., Mignet, N., Midoux, P., & Pichon, C. (2012). Ultrasound and microbubble-assisted gene delivery: Recent advances and ongoing challenges. *Therapeutic Delivery*, *3*(10), 1199–1215. <https://doi.org/10.4155/tde.12.100>
- Demir, I., Besson, A., Guiraud, P., & Formosa-Dague, C. (2020). Towards a better understanding of microalgae natural flocculation mechanisms to enhance flotation harvesting efficiency. *Water Science and Technology*, *82*(6), 1009–1024. <https://doi.org/10.2166/wst.2020.177>
- Demir, I., Blockx, J., Dague, E., Guiraud, P., Thielemans, W., Muylaert, K., & Formosa-Dague, C. (2020). Nanoscale Evidence Unravels Microalgae Flocculation Mechanism Induced by Chitosan. *ACS Applied Bio Materials*, *3*(12), 8446–8459. <https://doi.org/10.1021/acsabm.0c00772>
- Demir, I., Luchtefeld, I., Lemen, C., Dague, E., Guiraud, P., Zambelli, T., & Formosa-Dague, C. (2021). Probing the interactions between air bubbles and (bio)interfaces at the

- nanoscale using FluidFM technology. *Journal of Colloid and Interface Science*, 604, 785–797. <https://doi.org/10.1016/j.jcis.2021.07.036>
- Demirbas, A. (Ed.). (2009). Introduction. In *Biohydrogen: For Future Engine Fuel Demands* (pp. 1–42). Springer. https://doi.org/10.1007/978-1-84882-511-6_1
- Demir-Yilmaz, I., Guiraud, P., & Formosa-Dague, C. (2021a). The contribution of Atomic Force Microscopy (AFM) in microalgae studies: A review. *Algal Research*, 60, 102506. <https://doi.org/10.1016/j.algal.2021.102506>
- Demir-Yilmaz, I., Guiraud, P., & Formosa-Dague, C. (2021b). The contribution of Atomic Force Microscopy (AFM) in microalgae studies: A review. *Algal Research*, 60, 102506. <https://doi.org/10.1016/j.algal.2021.102506>
- Demir-Yilmaz, I., Schiavone, M., Esvan, J., Guiraud, P., & Formosa-Dague, C. (2022). *Combining AFM, XPS and chemical hydrolysis to understand the complexity and dynamics of C. vulgaris cell wall composition and architecture* (p. 2022.07.11.499560). bioRxiv. <https://doi.org/10.1101/2022.07.11.499560>
- Demir-Yilmaz, I., Yakovenko, N., Roux, C., Guiraud, P., Collin, F., Coudret, C., ter Halle, A., & Formosa-Dague, C. (2022). The role of microplastics in microalgae cells aggregation: A study at the molecular scale using atomic force microscopy. *Science of The Total Environment*, 832, 155036. <https://doi.org/10.1016/j.scitotenv.2022.155036>
- Demuez, M., Mahdy, A., Tomás-Pejó, E., González-Fernández, C., & Ballesteros, M. (2015). Enzymatic cell disruption of microalgae biomass in biorefinery processes. *Biotechnology and Bioengineering*, 112(10), 1955–1966. <https://doi.org/10.1002/bit.25644>
- Desbrieres, J. (2004). Autoassociative natural polymer derivatives: The alkylchitosans. Rheological behaviour and temperature stability. *Polymer*, 45(10), 3285–3295. <https://doi.org/10.1016/j.polymer.2004.03.032>
- Desbrières, J., Martinez, C., & Rinaudo, M. (1996). Hydrophobic derivatives of chitosan: Characterization and rheological behaviour. *International Journal of Biological Macromolecules*, 19(1), 21–28. [https://doi.org/10.1016/0141-8130\(96\)01095-1](https://doi.org/10.1016/0141-8130(96)01095-1)
- Dismukes, G. C., Carrieri, D., Bennette, N., Ananyev, G. M., & Posewitz, M. C. (2008). Aquatic phototrophs: Efficient alternatives to land-based crops for biofuels. *Current Opinion in Biotechnology*, 19(3), 235–240. <https://doi.org/10.1016/j.copbio.2008.05.007>

- Ditscherlein, L., Jolan Gulden, S., Müller, S., Baumann, R.-P., Peuker, U. A., & Nirschl, H. (2018). Measuring interactions between yeast cells and a micro-sized air bubble via atomic force microscopy. *Journal of Colloid and Interface Science*, *532*, 689–699. <https://doi.org/10.1016/j.jcis.2018.08.031>
- Dong, T., Knoshaug, E. P., Pienkos, P. T., & Laurens, L. M. L. (2016). Lipid recovery from wet oleaginous microbial biomass for biofuel production: A critical review. *Applied Energy*, *177*, 879–895. <https://doi.org/10.1016/j.apenergy.2016.06.002>
- Ducker, W. A., Senden, T. J., & Pashley, R. M. (1991). Direct measurement of colloidal forces using an atomic force microscope. *Nature*, *353*(6341), Article 6341. <https://doi.org/10.1038/353239a0>
- Ducker, W. A., Xu, Z., & Israelachvili, J. N. (1994). Measurements of Hydrophobic and DLVO Forces in Bubble-Surface Interactions in Aqueous Solutions. *Langmuir*, *10*(9), 3279–3289. <https://doi.org/10.1021/la00021a061>
- Erdawati, Kanza, M., Saefurahman, G., Hidayatuloh, S., & Kawaroe, M. (2020). Effect of pH culture and dosage of chitosan nanoemulsion on the effectiveness of bioflocculation in harvesting *Chlorella* sp. Biomass. *IOP Conference Series: Earth and Environmental Science*, *460*(1), 012005. <https://doi.org/10.1088/1755-1315/460/1/012005>
- Eriksson, J. C., & Ljunggren, S. (1999). On the mechanically unstable free energy minimum of a gas bubble which is submerged in water and adheres to a hydrophobic wall. *Colloids and Surfaces A: Physicochemical and Engineering Aspects*, *159*(1), 159–163. [https://doi.org/10.1016/S0927-7757\(99\)00171-5](https://doi.org/10.1016/S0927-7757(99)00171-5)
- Farid, M. S., Shariati, A., Badakhshan, A., & Anvaripour, B. (2013). Using nano-chitosan for harvesting microalga *Nannochloropsis* sp. *Bioresource Technology*, *131*, 555–559. <https://doi.org/10.1016/j.biortech.2013.01.058>
- Fercoq, A., Lamouri, S., & Carbone, V. (2016). Lean/Green integration focused on waste reduction techniques. *Journal of Cleaner Production*, *137*, 567–578. <https://doi.org/10.1016/j.jclepro.2016.07.107>
- Formosa-Dague, C., Castelain, M., Martin-Yken, H., Dunker, K., Dague, E., & Sletmoen, M. (2018). The Role of Glycans in Bacterial Adhesion to Mucosal Surfaces: How Can Single-Molecule Techniques Advance Our Understanding? *Microorganisms*, *6*(2), Article 2. <https://doi.org/10.3390/microorganisms6020039>

- Formosa-Dague, C., Gernigon, V., Castelain, M., Daboussi, F., & Guiraud, P. (2018a). Towards a better understanding of the flocculation/flotation mechanism of the marine microalgae *Phaeodactylum tricornutum* under increased pH using atomic force microscopy. *Algal Research*, *33*, 369–378. <https://doi.org/10.1016/j.algal.2018.06.010>
- Formosa-Dague, C., Gernigon, V., Castelain, M., Daboussi, F., & Guiraud, P. (2018b). Towards a better understanding of the flocculation/flotation mechanism of the marine microalgae *Phaeodactylum tricornutum* under increased pH using atomic force microscopy. *Algal Research*, *33*, 369–378. <https://doi.org/10.1016/j.algal.2018.06.010>
- Francius, G., Tesson, B., Dague, E., Martin-Jézéquel, V., & Dufrêne, Y. F. (2008). Nanostructure and nanomechanics of live *Phaeodactylum tricornutum* morphotypes. *Environmental Microbiology*, *10*(5), 1344–1356. <https://doi.org/10.1111/j.1462-2920.2007.01551.x>
- Frenkel, V. (2008). Ultrasound mediated delivery of drugs and genes to solid tumors. *Advanced Drug Delivery Reviews*, *60*(10), 1193–1208. <https://doi.org/10.1016/j.addr.2008.03.007>
- Gao, Z., Kennedy, A. M., Christensen, D. A., & Rapoport, N. Y. (2008). Drug-loaded nano/microbubbles for combining ultrasonography and targeted chemotherapy. *Ultrasonics*, *48*(4), 260–270. <https://doi.org/10.1016/j.ultras.2007.11.002>
- Garg, S., Li, Y., Wang, L., & Schenk, P. M. (2012a). Flotation of marine microalgae: Effect of algal hydrophobicity. *Bioresource Technology*, *121*, 471–474. <https://doi.org/10.1016/j.biortech.2012.06.111>
- Garg, S., Li, Y., Wang, L., & Schenk, P. M. (2012b). Flotation of marine microalgae: Effect of algal hydrophobicity. *Bioresource Technology*, *121*, 471–474. <https://doi.org/10.1016/j.biortech.2012.06.111>
- Gerardo, M. L., Van Den Hende, S., Vervaeren, H., Coward, T., & Skill, S. C. (2015). Harvesting of microalgae within a biorefinery approach: A review of the developments and case studies from pilot-plants. *Algal Research*, *11*, 248–262. <https://doi.org/10.1016/j.algal.2015.06.019>
- Gerken, H. G., Donohoe, B., & Knoshaug, E. P. (2013). Enzymatic cell wall degradation of *Chlorella vulgaris* and other microalgae for biofuels production. *Planta*, *237*(1), 239–253. <https://doi.org/10.1007/s00425-012-1765-0>
- Ghassemi, N., Poulhazan, A., Deligey, F., Mentink-Vigier, F., Marcotte, I., & Wang, T. (2021). Solid-State NMR Investigations of Extracellular Matrixes and Cell Walls of Algae,

<https://doi.org/10.1021/acs.chemrev.1c00669>

- Glaser, K., & Karsten, U. (2020). Salinity tolerance in biogeographically different strains of the marine benthic diatom *Cylindrotheca closterium* (Bacillariophyceae). *Journal of Applied Phycology*, 32(6), 3809–3816. <https://doi.org/10.1007/s10811-020-02238-6>
- Grüter, R. R., Vörös, J., & Zambelli, T. (2013). FluidFM as a lithography tool in liquid: Spatially controlled deposition of fluorescent nanoparticles. *Nanoscale*, 5(3), 1097–1104. <https://doi.org/10.1039/C2NR33214K>
- Guillard, R. R. L. (1975). Culture of Phytoplankton for Feeding Marine Invertebrates. In W. L. Smith & M. H. Chanley (Eds.), *Culture of Marine Invertebrate Animals: Proceedings—1st Conference on Culture of Marine Invertebrate Animals Greenport* (pp. 29–60). Springer US. https://doi.org/10.1007/978-1-4615-8714-9_3
- Guillaume-Gentil, O., Gäbelein, C. G., Schmieder, S., Martinez, V., Zambelli, T., Künzler, M., & Vorholt, J. A. (2022). Injection into and extraction from single fungal cells. *Communications Biology*, 5(1), 180. <https://doi.org/10.1038/s42003-022-03127-z>
- Guillaume-Gentil, O., Grindberg, R. V., Kooger, R., Dorwling-Carter, L., Martinez, V., Ossola, D., Pilhofer, M., Zambelli, T., & Vorholt, J. A. (2016). Tunable Single-Cell Extraction for Molecular Analyses. *Cell*, 166(2), 506–516. <https://doi.org/10.1016/j.cell.2016.06.025>
- Guillaume-Gentil, O., Zambelli, T., & Vorholt, J. A. (2013). Isolation of single mammalian cells from adherent cultures by fluidic force microscopy. *Lab on a Chip*, 14(2), 402–414. <https://doi.org/10.1039/C3LC51174J>
- Günerken, E., D’Hondt, E., Eppink, M. H. M., Garcia-Gonzalez, L., Elst, K., & Wijffels, R. H. (2015). Cell disruption for microalgae biorefineries. *Biotechnology Advances*, 33(2), 243–260. <https://doi.org/10.1016/j.biotechadv.2015.01.008>
- Gupta, P. L., Lee, S.-M., & Choi, H.-J. (2016). Integration of microalgal cultivation system for wastewater remediation and sustainable biomass production. *World Journal of Microbiology and Biotechnology*, 32(8), 139. <https://doi.org/10.1007/s11274-016-2090-8>
- Hassanzadeh, A., Sajjady, S. A., Gholami, H., Amini, S., & Özkan, S. G. (2020). An Improvement on Selective Separation by Applying Ultrasound to Rougher and Re-Cleaner Stages of Copper Flotation. *Minerals*, 10(7), Article 7. <https://doi.org/10.3390/min10070619>

- Henderson, R. K., Parsons, S. A., & Jefferson, B. (2008a). Successful Removal of Algae through the Control of Zeta Potential. *Separation Science and Technology*, 43(7), 1653–1666. <https://doi.org/10.1080/01496390801973771>
- Henderson, R. K., Parsons, S. A., & Jefferson, B. (2008b). Surfactants as Bubble Surface Modifiers in the Flotation of Algae: Dissolved Air Flotation That Utilizes a Chemically Modified Bubble Surface. *Environmental Science & Technology*, 42(13), 4883–4888. <https://doi.org/10.1021/es702649h>
- Henderson, R. K., Parsons, S. A., & Jefferson, B. (2010). Polymers as bubble surface modifiers in the flotation of algae. *Environmental Technology*, 31(7), 781–790. <https://doi.org/10.1080/09593331003663302>
- Hertz, H. (1881). Ueber die berührung fester elastischer körper. *Journal Fur Die Reine Und Angewandte Mathematik*, 156–171.
- Hirt, L., Grüter, R. R., Berthelot, T., Cornut, R., Vörös, J., & Zambelli, T. (2015). Local surface modification via confined electrochemical deposition with FluidFM. *RSC Advances*, 5(103), 84517–84522. <https://doi.org/10.1039/C5RA07239E>
- Houot, R. (1982). Beneficiation of phosphatic ores through flotation: Review of industrial applications and potential developments. *International Journal of Mineral Processing*, 9(4), 353–384. [https://doi.org/10.1016/0301-7516\(82\)90041-2](https://doi.org/10.1016/0301-7516(82)90041-2)
- Huang, Z., Legendre, D., & Guiraud, P. (2012). Effect of interface contamination on particle–bubble collision. *Chemical Engineering Science*, 68(1), 1–18. <https://doi.org/10.1016/j.ces.2011.07.045>
- Hutter, J. L., & Bechhoefer, J. (1993). Calibration of atomic-force microscope tips. *Review of Scientific Instruments*, 64(7), 1868–1873. <https://doi.org/10.1063/1.1143970>
- Hwang, T., Park, S.-J., Oh, Y.-K., Rashid, N., & Han, J.-I. (2013). Harvesting of *Chlorella* sp. KR-1 using a cross-flow membrane filtration system equipped with an anti-fouling membrane. *Bioresource Technology*, 139, 379–382. <https://doi.org/10.1016/j.biortech.2013.03.149>
- Iversen, M. H., & Ploug, H. (2013). Temperature effects on carbon-specific respiration rate and sinking velocity of diatom aggregates – potential implications for deep ocean export processes. *Biogeosciences*, 10(6), 4073–4085. <https://doi.org/10.5194/bg-10-4073-2013>

- Jiang, L., Pei, H., Hu, W., Hou, Q., Han, F., & Nie, C. (2016). Biomass production and nutrient assimilation by a novel microalga, *Monoraphidium* spp. SDEC-17, cultivated in a high-ammonia wastewater. *Energy Conversion and Management*, *123*, 423–430. <https://doi.org/10.1016/j.enconman.2016.06.060>
- Jiang, W., Gao, Z., Khoso, S. A., Gao, J., Sun, W., Pu, W., & Hu, Y. (2018). Selective adsorption of benzhydroxamic acid on fluorite rendering selective separation of fluorite/calcite. *Applied Surface Science*, *435*, 752–758. <https://doi.org/10.1016/j.apsusc.2017.11.093>
- Jiang, Y., Yoshida, T., & Quigg, A. (2012). Photosynthetic performance, lipid production and biomass composition in response to nitrogen limitation in marine microalgae. *Plant Physiology and Biochemistry*, *54*, 70–77. <https://doi.org/10.1016/j.plaphy.2012.02.012>
- Karsten, U. (2012). Seaweed Acclimation to Salinity and Desiccation Stress. In C. Wiencke & K. Bischof (Eds.), *Seaweed Biology: Novel Insights into Ecophysiology, Ecology and Utilization* (pp. 87–107). Springer. https://doi.org/10.1007/978-3-642-28451-9_5
- Khojasteh, D., Kazerooni, N. M., & Marengo, M. (2019). A review of liquid droplet impacting onto solid spherical particles: A physical pathway to encapsulation mechanisms. *Journal of Industrial and Engineering Chemistry*, *71*, 50–64. <https://doi.org/10.1016/j.jiec.2018.11.030>
- Kim, K. H., Choi, I. S., Kim, H. M., Wi, S. G., & Bae, H.-J. (2014). Bioethanol production from the nutrient stress-induced microalga *Chlorella vulgaris* by enzymatic hydrolysis and immobilized yeast fermentation. *Bioresource Technology*, *153*, 47–54. <https://doi.org/10.1016/j.biortech.2013.11.059>
- Kim, S.-K. (2015). *Handbook of Marine Microalgae: Biotechnology Advances* (Academic Press).
- Klibanov, A. L. (2007). Ultrasound molecular imaging with targeted microbubble contrast agents. *Journal of Nuclear Cardiology*, *14*(6), 876. <https://doi.org/10.1016/j.nuclcard.2007.09.008>
- Kovač, N., Mozetič, P., Trichet, J., & Défarge, C. (2005). Phytoplankton composition and organic matter organization of mucous aggregates by means of light and cryo-scanning electron microscopy. *Marine Biology*, *147*(1), 261–271. <https://doi.org/10.1007/s00227-004-1531-3>

- Kriegel, A. T., & Ducker, W. A. (2019). Removal of Bacteria from Solids by Bubbles: Effect of Solid Wettability, Interaction Geometry, and Liquid–Vapor Interface Velocity. *Langmuir*. <https://doi.org/10.1021/acs.langmuir.9b01941>
- Laamanen, C. A., Ross, G. M., & Scott, J. A. (2016). Flotation harvesting of microalgae. *Renewable and Sustainable Energy Reviews*, *58*, 75–86. <https://doi.org/10.1016/j.rser.2015.12.293>
- Laifa, R., Morchain, J., Barna, L., & Guiraud, P. (2021). A numerical framework to predict the performances of a tubular photobioreactor from operating and sunlight conditions. *Algal Research*, *60*, 102550. <https://doi.org/10.1016/j.algal.2021.102550>
- Lam, M. K., & Lee, K. T. (2012). Microalgae biofuels: A critical review of issues, problems and the way forward. *Biotechnology Advances*, *30*(3), 673–690. <https://doi.org/10.1016/j.biotechadv.2011.11.008>
- Lama, S., Muylaert, K., Karki, T. B., Foubert, I., Henderson, R. K., & Vandamme, D. (2016). Flocculation properties of several microalgae and a cyanobacterium species during ferric chloride, chitosan and alkaline flocculation. *Bioresource Technology*, *220*, 464–470. <https://doi.org/10.1016/j.biortech.2016.08.080>
- Lee, S. Y., Cho, J. M., Chang, Y. K., & Oh, Y.-K. (2017). Cell disruption and lipid extraction for microalgal biorefineries: A review. *Bioresource Technology*, *244*, 1317–1328. <https://doi.org/10.1016/j.biortech.2017.06.038>
- Legendre, D., Sarrot, V., & Guiraud, P. (2009). On the particle inertia-free collision with a partially contaminated spherical bubble. *International Journal of Multiphase Flow*, *35*(2), 163–170. <https://doi.org/10.1016/j.ijmultiphaseflow.2008.10.002>
- Ljunggren, S., & Eriksson, J. C. (1997). The lifetime of a colloid-sized gas bubble in water and the cause of the hydrophobic attraction. *Colloids and Surfaces A: Physicochemical and Engineering Aspects*, *129–130*, 151–155. [https://doi.org/10.1016/S0927-7757\(97\)00033-2](https://doi.org/10.1016/S0927-7757(97)00033-2)
- Lu, Y., Wang, S., & Zhong, H. (2021). Study on the role of a hydroxamic acid derivative in wolframite flotation: Selective separation and adsorption mechanism. *Applied Surface Science*, *550*, 149223. <https://doi.org/10.1016/j.apsusc.2021.149223>
- Ma, J., Zhou, B., Chen, F., & Pan, K. (2021). How marine diatoms cope with metal challenge: Insights from the morphotype-dependent metal tolerance in *Phaeodactylum*

- tricornutum. *Ecotoxicology and Environmental Safety*, 208, 111715.
<https://doi.org/10.1016/j.ecoenv.2020.111715>
- Ma, J., Zhou, B., Duan, D., & Pan, K. (2019). Salinity-dependent nanostructures and composition of cell surface and its relation to Cd toxicity in an estuarine diatom. *Chemosphere*, 215, 807–814. <https://doi.org/10.1016/j.chemosphere.2018.10.128>
- Ma, M. (2012). Froth Flotation of Iron Ores. *International Journal of Mining Engineering and Mineral Processing*, 1(2), 56–61. <https://doi.org/10.5923/j.mining.20120102.06>
- Maddah, H., & Chogle, A. (2017). Biofouling in reverse osmosis: Phenomena, monitoring, controlling and remediation. *Applied Water Science*, 7(6), 2637–2651. <https://doi.org/10.1007/s13201-016-0493-1>
- Maldonado, R. F., Sá-Correia, I., & Valvano, M. A. (2016). Lipopolysaccharide modification in Gram-negative bacteria during chronic infection. *FEMS Microbiology Reviews*, 40(4), 480–493. <https://doi.org/10.1093/femsre/fuw007>
- Markou, G., & Nerantzis, E. (2013). Microalgae for high-value compounds and biofuels production: A review with focus on cultivation under stress conditions. *Biotechnology Advances*, 31(8), 1532–1542. <https://doi.org/10.1016/j.biotechadv.2013.07.011>
- Matho, C., Schwarzenberger, K., Eckert, K., Keshavarzi, B., Walther, T., Steingroewer, J., & Krujatz, F. (2019). Bio-compatible flotation of *Chlorella vulgaris*: Study of zeta potential and flotation efficiency. *Algal Research*, 44, 101705. <https://doi.org/10.1016/j.algal.2019.101705>
- Mathur, S., Singh, P., & Moudgil, B. M. (2000). Advances in selective flocculation technology for solid-solid separations. *International Journal of Mineral Processing*, 58(1), 201–222. [https://doi.org/10.1016/S0301-7516\(99\)00072-1](https://doi.org/10.1016/S0301-7516(99)00072-1)
- Mati-Baouche, N., Delattre, C., de Baynast, H., Grédiac, M., Mathias, J.-D., Ursu, A. V., Desbrières, J., & Michaud, P. (2019). Alkyl-Chitosan-Based Adhesive: Water Resistance Improvement. *Molecules*, 24(10), Article 10. <https://doi.org/10.3390/molecules24101987>
- Matis, K. A., & Lazaridis, N. K. (2002). Flotation techniques in water technology for metals recovery: Dispersed-air vs. dissolved-air flotation. *Journal of Mining and Metallurgy A: Mining*, 38(1–4), 1–27.
- Meister, A., Gabi, M., Behr, P., Studer, P., Vörös, J., Niedermann, P., Bitterli, J., Polesel-Maris, J., Liley, M., Heinzelmann, H., & Zambelli, T. (2009a). FluidFM: Combining atomic force

- microscopy and nanofluidics in a universal liquid delivery system for single cell applications and beyond. *Nano Letters*, 9(6), 2501–2507. <https://doi.org/10.1021/nl901384x>
- Meister, A., Gabi, M., Behr, P., Studer, P., Vörös, J., Niedermann, P., Bitterli, J., Polesel-Maris, J., Liley, M., Heinzemann, H., & Zambelli, T. (2009b). FluidFM: Combining Atomic Force Microscopy and Nanofluidics in a Universal Liquid Delivery System for Single Cell Applications and Beyond. *Nano Letters*, 9(6), 2501–2507. <https://doi.org/10.1021/nl901384x>
- Miettinen, T., Ralston, J., & Fornasiero, D. (2010). The limits of fine particle flotation. *Minerals Engineering*, 23(5), 420–437. <https://doi.org/10.1016/j.mineng.2009.12.006>
- Minhas, A. K., Hodgson, P., Barrow, C. J., & Adholeya, A. (2016). A Review on the Assessment of Stress Conditions for Simultaneous Production of Microalgal Lipids and Carotenoids. *Frontiers in Microbiology*, 7. <https://doi.org/10.3389/fmicb.2016.00546>
- Mishchuk, N., Ralston, J., & Fornasiero, D. (2006). Influence of very small bubbles on particle/bubble heterocoagulation. *Journal of Colloid and Interface Science*, 301(1), 168–175. <https://doi.org/10.1016/j.jcis.2006.04.071>
- Mišić Radić, T., Čačković, A., Penezić, A., Dautović, J., Lončar, J., Omanović, D., Juraić, K., & Ljubešić, Z. (2021). Physiological and morphological response of marine diatom *Cylindrotheca closterium* (Bacillariophyceae) exposed to Cadmium. *European Journal of Phycology*, 56(1), 24–36. <https://doi.org/10.1080/09670262.2020.1758347>
- Molina Grima, E., Belarbi, E.-H., Ación Fernández, F. G., Robles Medina, A., & Chisti, Y. (2003). Recovery of microalgal biomass and metabolites: Process options and economics. *Biotechnology Advances*, 20(7), 491–515. [https://doi.org/10.1016/S0734-9750\(02\)00050-2](https://doi.org/10.1016/S0734-9750(02)00050-2)
- Nagappan, S., Devendran, S., Tsai, P.-C., Dinakaran, S., Dahms, H.-U., & Ponnusamy, V. K. (2019). Passive cell disruption lipid extraction methods of microalgae for biofuel production – A review. *Fuel*, 252, 699–709. <https://doi.org/10.1016/j.fuel.2019.04.092>
- Najdek, M., Blažina, M., Djakovac, T., & Kraus, R. (2005). The role of the diatom *Cylindrotheca closterium* in a mucilage event in the northern Adriatic Sea: Coupling with high salinity water intrusions. *Journal of Plankton Research*, 27(9), 851–862. <https://doi.org/10.1093/plankt/fbi057>

- Nguyen, A. V., George, P., & Jameson, G. J. (2006). Demonstration of a minimum in the recovery of nanoparticles by flotation: Theory and experiment. *Chemical Engineering Science*, *61*(8), 2494–2509. <https://doi.org/10.1016/j.ces.2005.11.025>
- Norsker, N.-H., Barbosa, M. J., Vermuë, M. H., & Wijffels, R. H. (2011). Microalgal production—A close look at the economics. *Biotechnology Advances*, *29*(1), 24–27. <https://doi.org/10.1016/j.biotechadv.2010.08.005>
- Novosel, N., Mišić Radić, T., Levak Zorinc, M., Zemla, J., Lekka, M., Vrana, I., Gašparović, B., Horvat, L., Kasum, D., Legović, T., Žutinić, P., Gligora Udovič, M., & Ivošević DeNardis, N. (2022). Salinity-induced chemical, mechanical, and behavioral changes in marine microalgae. *Journal of Applied Phycology*. <https://doi.org/10.1007/s10811-022-02734-x>
- Olaizola, M. (2003). Commercial development of microalgal biotechnology: From the test tube to the marketplace. *Biomolecular Engineering*, *20*(4), 459–466. [https://doi.org/10.1016/S1389-0344\(03\)00076-5](https://doi.org/10.1016/S1389-0344(03)00076-5)
- Ossola, D., Amarouch, M.-Y., Behr, P., Vörös, J., Abriel, H., & Zambelli, T. (2015). Force-Controlled Patch Clamp of Beating Cardiac Cells. *Nano Letters*, *15*(3), 1743–1750. <https://doi.org/10.1021/nl504438z>
- Ozkan, A., & Berberoglu, H. (2013a). Physico-chemical surface properties of microalgae. *Colloids and Surfaces B: Biointerfaces*, *112*, 287–293. <https://doi.org/10.1016/j.colsurfb.2013.08.001>
- Ozkan, A., & Berberoglu, H. (2013b). Physico-chemical surface properties of microalgae. *Colloids and Surfaces B: Biointerfaces*, *112*, 287–293. <https://doi.org/10.1016/j.colsurfb.2013.08.001>
- Pal, S., Mal, D., & Singh, R. P. (2005). Cationic starch: An effective flocculating agent. *Carbohydrate Polymers*, *59*(4), 417–423. <https://doi.org/10.1016/j.carbpol.2004.06.047>
- Pan, Y.-Y., Wang, S.-T., Chuang, L.-T., Chang, Y.-W., & Chen, C.-N. N. (2011). Isolation of thermo-tolerant and high lipid content green microalgae: Oil accumulation is predominantly controlled by photosystem efficiency during stress treatments in *Desmodesmus*. *Bioresource Technology*, *102*(22), 10510–10517. <https://doi.org/10.1016/j.biortech.2011.08.091>

- Pillet, F., Dague, E., Pečar Ilić, J., Ružić, I., Rols, M.-P., & Ivošević DeNardis, N. (2019). Changes in nanomechanical properties and adhesion dynamics of algal cells during their growth. *Bioelectrochemistry*, *127*, 154–162. <https://doi.org/voelcker>
- Piontek, J., Händel, N., Langer, G., Wohlers, J., Riebesell, U., & Engel, A. (2009). Effects of rising temperature on the formation and microbial degradation of marine diatom aggregates. *Aquatic Microbial Ecology*, *54*(3), 305–318. <https://doi.org/10.3354/ame01273>
- Pita, F., & Castilho, A. (2017). Separation of plastics by froth flotation. The role of size, shape and density of the particles. *Waste Management*, *60*, 91–99. <https://doi.org/10.1016/j.wasman.2016.07.041>
- Pletikapić, G., & Ivošević DeNardis, N. (2017). Application of surface analytical methods for hazardous situation in the Adriatic Sea: Monitoring of organic matter dynamics and oil pollution. *Natural Hazards and Earth System Sciences*, *17*(1), 31–44. <https://doi.org/10.5194/nhess-17-31-2017>
- Pletikapić, G., Radić, T. M., Zimmermann, A. H., Svetličić, V., Pfannkuchen, M., Marić, D., Godrijan, J., & Žutić, V. (2011). AFM imaging of extracellular polymer release by marine diatom *Cylindrotheca closterium* (Ehrenberg) Reiman & J.C. Lewin. *Journal of Molecular Recognition*, *24*(3), 436–445. <https://doi.org/10.1002/jmr.1114>
- Potthoff, E., Guillaume-Gentil, O., Ossola, D., Polesel-Maris, J., LeibundGut-Landmann, S., Zambelli, T., & Vorholt, J. A. (2012). Rapid and Serial Quantification of Adhesion Forces of Yeast and Mammalian Cells. *PLOS ONE*, *7*(12), e52712. <https://doi.org/10.1371/journal.pone.0052712>
- Potthoff, E., Ossola, D., Zambelli, T., & Vorholt, J. A. (2015). Bacterial adhesion force quantification by fluidic force microscopy. *Nanoscale*, *7*(9), 4070–4079. <https://doi.org/10.1039/C4NR06495J>
- Poulhazan, A., Dickwella Widanage, M. C., Muszyński, A., Arnold, A. A., Warschawski, D. E., Azadi, P., Marcotte, I., & Wang, T. (2021). Identification and Quantification of Glycans in Whole Cells: Architecture of Microalgal Polysaccharides Described by Solid-State Nuclear Magnetic Resonance. *Journal of the American Chemical Society*, *143*(46), 19374–19388. <https://doi.org/10.1021/jacs.1c07429>

- Pragya, N., Pandey, K. K., & Sahoo, P. K. (2013). A review on harvesting, oil extraction and biofuels production technologies from microalgae. *Renewable and Sustainable Energy Reviews*, 24, 159–171. <https://doi.org/10.1016/j.rser.2013.03.034>
- Radić, T. M., Svetličić, V., Žutić, V., & Boulgaropoulos, B. (2011). Seawater at the nanoscale: Marine gel imaged by atomic force microscopy. *Journal of Molecular Recognition*, 24(3), 397–405. <https://doi.org/10.1002/jmr.1072>
- Rashid, N., Park, W.-K., & Selvaratnam, T. (2018). Binary culture of microalgae as an integrated approach for enhanced biomass and metabolites productivity, wastewater treatment, and bioflocculation. *Chemosphere*, 194, 67–75. <https://doi.org/10.1016/j.chemosphere.2017.11.108>
- Rashid, N., Rehman, S. U., & Han, J.-I. (2013). Rapid harvesting of freshwater microalgae using chitosan. *Process Biochemistry*, 48(7), 1107–1110. <https://doi.org/10.1016/j.procbio.2013.04.018>
- Reifarth, M., Hoepfener, S., & Schubert, U. S. (2018). Uptake and Intracellular Fate of Engineered Nanoparticles in Mammalian Cells: Capabilities and Limitations of Transmission Electron Microscopy—Polymer-Based Nanoparticles. *Advanced Materials*, 30(9), 1703704. <https://doi.org/10.1002/adma.201703704>
- Ren, Z., Yu, F., Gao, H., Chen, Z., Peng, Y., & Liu, L. (2017). Selective Separation of Fluorite, Barite and Calcite with Valonea Extract and Sodium Fluosilicate as Depressants. *Minerals*, 7(2), Article 2. <https://doi.org/10.3390/min7020024>
- Renault, F., Sancey, B., Badot, P.-M., & Crini, G. (2009). Chitosan for coagulation/flocculation processes – An eco-friendly approach. *European Polymer Journal*, 45(5), 1337–1348. <https://doi.org/10.1016/j.eurpolymj.2008.12.027>
- Richardson, J. W., & Johnson, M. D. (2014). Economic viability of a reverse engineered algae farm (REAF). *Algal Research*, 3, 66–70. <https://doi.org/10.1016/j.algal.2013.10.002>
- Rijstenbil, J. W. (2005). UV- and salinity-induced oxidative effects in the marine diatom *Cylindrotheca closterium* during simulated emersion. *Marine Biology*, 147(5), 1063–1073. <https://doi.org/10.1007/s00227-005-0015-4>
- Rodolfi, L., Zittelli, G. C., Bassi, N., Padovani, G., Biondi, N., Bonini, G., & Tredici, M. R. (2009). Microalgae for oil: Strain selection, induction of lipid synthesis and outdoor mass cultivation in a low-cost photobioreactor. *Biotechnology and Bioengineering*, 102(1), 100–112. <https://doi.org/10.1002/bit.22033>

- Roncarati, F., Rijstenbil, J. W., & Pistocchi, R. (2008). Photosynthetic performance, oxidative damage and antioxidants in *Cylindrotheca closterium* in response to high irradiance, UVB radiation and salinity. *Marine Biology*, 153(5), 965–973. <https://doi.org/10.1007/s00227-007-0868-9>
- Rouxhet, P. G., & Genet, M. J. (2011). XPS analysis of bio-organic systems. *Surface and Interface Analysis*, 43(12), 1453–1470. <https://doi.org/10.1002/sia.3831>
- Sarrot, V., Guiraud, P., & Legendre, D. (2005). Determination of the collision frequency between bubbles and particles in flotation. *Chemical Engineering Science*, 60(22), 6107–6117. <https://doi.org/10.1016/j.ces.2005.02.018>
- Sarrot, V., Huang, Z., Legendre, D., & Guiraud, P. (2007). Experimental determination of particles capture efficiency in flotation. *Chemical Engineering Science*, 62(24), 7359–7369. <https://doi.org/10.1016/j.ces.2007.08.028>
- Scala, S., & Bowler, C. (2001). Molecular insights into the novel aspects of diatom biology. *Cellular and Molecular Life Sciences: CMLS*, 58(11), 1666–1673. <https://doi.org/10.1007/PL00000804>
- Schenk, P. M., Thomas-Hall, S. R., Stephens, E., Marx, U. C., Mussnug, J. H., Posten, C., Kruse, O., & Hankamer, B. (2008). Second Generation Biofuels: High-Efficiency Microalgae for Biodiesel Production. *BioEnergy Research*, 1(1), 20–43. <https://doi.org/10.1007/s12155-008-9008-8>
- Schiavone, M., Vax, A., Formosa, C., Martin-Yken, H., Dague, E., & François, J. M. (2014). A combined chemical and enzymatic method to determine quantitatively the polysaccharide components in the cell wall of yeasts. *FEMS Yeast Research*, 14(6), 933–947. <https://doi.org/10.1111/1567-1364.12182>
- Scragg, A. H., Illman, A. M., Carden, A., & Shales, S. W. (2002). Growth of microalgae with increased calorific values in a tubular bioreactor. *Biomass and Bioenergy*, 23(1), 67–73. [https://doi.org/10.1016/S0961-9534\(02\)00028-4](https://doi.org/10.1016/S0961-9534(02)00028-4)
- Separovic, F., & Sani, M.-A. (Eds.). (2020). *Solid-State NMR: Applications in biomembrane structure*. IOP Publishing. <https://doi.org/10.1088/978-0-7503-2532-5>
- Shchukarev, A., Gojkovic, Z., Funk, C., & Ramstedt, M. (2020). Cryo-XPS analysis reveals surface composition of microalgae. *Applied Surface Science*, 526, 146538. <https://doi.org/10.1016/j.apsusc.2020.146538>

- Sheehan, J., Dunahay, T., Benemann, J., & Roessler, P. (1998). *Look Back at the U.S. Department of Energy's Aquatic Species Program: Biodiesel from Algae; Close-Out Report*.
https://www.academia.edu/3090889/A_look_back_at_the_US_department_of_ener_gys_aquatic_species_program_biodiesel_from_algae
- Staats, N., Stal, L. J., & Mur, L. R. (2000). Exopolysaccharide production by the epipelagic diatom *Cylindrotheca closterium*: Effects of nutrient conditions. *Journal of Experimental Marine Biology and Ecology*, 249(1), 13–27. [https://doi.org/10.1016/S0022-0981\(00\)00166-0](https://doi.org/10.1016/S0022-0981(00)00166-0)
- Steele, D. J., Franklin, D. J., & Underwood, G. J. C. (2014). Protection of cells from salinity stress by extracellular polymeric substances in diatom biofilms. *Biofouling*, 30(8), 987–998. <https://doi.org/10.1080/08927014.2014.960859>
- Stiefel, P., Schmidt, F. I., Dörig, P., Behr, P., Zambelli, T., Vorholt, J. A., & Mercer, J. (2012). Cooperative Vaccinia Infection Demonstrated at the Single-Cell Level Using FluidFM. *Nano Letters*, 12(8), 4219–4227. <https://doi.org/10.1021/nl3018109>
- Svetličić, V., Balnois, E., Žutić, V., Chevalet, J., Hozić Zimmermann, A., Kovač, S., & Vdović, N. (2006). Electrochemical Detection of Gel Microparticles in Seawater. *Croatica Chemica Acta*, 79(1), 107–113.
- Svetličić, V., Žutić, V., Radić, T. M., Pletikapić, G., Zimmermann, A. H., & Urbani, R. (2011). Polymer Networks Produced by Marine Diatoms in the Northern Adriatic Sea. *Marine Drugs*, 9(4), Article 4. <https://doi.org/10.3390/md9040666>
- Taleb, A., Kandilian, R., Touchard, R., Montalescot, V., Rinaldi, T., Taha, S., Takache, H., Marchal, L., Legrand, J., & Pruvost, J. (2016). Screening of freshwater and seawater microalgae strains in fully controlled photobioreactors for biodiesel production. *Bioresource Technology*, 218, 480–490. <https://doi.org/10.1016/j.biortech.2016.06.086>
- Tasić, M. B., Pinto, L. F. R., Klein, B. C., Veljković, V. B., & Filho, R. M. (2016). *Botryococcus braunii* for biodiesel production. *Renewable and Sustainable Energy Reviews*, 64, 260–270. <https://doi.org/10.1016/j.rser.2016.06.009>
- Thornton, D. C. O. (2002). Diatom aggregation in the sea: Mechanisms and ecological implications. *European Journal of Phycology*, 37(2), 149–161. <https://doi.org/10.1017/S0967026202003657>

- Tinkov, S., Bekeredjian, R., Winter, G., & Coester, C. (2009). Microbubbles as ultrasound triggered drug carriers. *Journal of Pharmaceutical Sciences*, *98*(6), 1935–1961. <https://doi.org/10.1002/jps.21571>
- Tiron, O., Bumbac, C., Manea, E., Stefanescu, M., & Nita Lazar, M. (2017). Overcoming Microalgae Harvesting Barrier by Activated Algae Granules. *Scientific Reports*, *7*(1), Article 1. <https://doi.org/10.1038/s41598-017-05027-3>
- Tréguer, P., Bowler, C., Moriceau, B., Dutkiewicz, S., Gehlen, M., Aumont, O., Bittner, L., Dugdale, R., Finkel, Z., Iudicone, D., Jahn, O., Guidi, L., Lasbleiz, M., Leblanc, K., Levy, M., & Pondaven, P. (2018). Influence of diatom diversity on the ocean biological carbon pump. *Nature Geoscience*, *11*(1), Article 1. <https://doi.org/10.1038/s41561-017-0028-x>
- Uduman, N., Qi, Y., Danquah, M. K., Forde, G. M., & Hoadley, A. (2010). Dewatering of microalgal cultures: A major bottleneck to algae-based fuels. *Journal of Renewable and Sustainable Energy*, *2*(1), 012701. <https://doi.org/10.1063/1.3294480>
- Uduman, N., Qi, Y., Danquah, M. K., & Hoadley, A. F. A. (2010). Marine microalgae flocculation and focused beam reflectance measurement. *Chemical Engineering Journal*, *162*(3), 935–940. <https://doi.org/10.1016/j.cej.2010.06.046>
- Van Bergeijk, S. A., Van der Zee, C., & Stal, L. J. (2003). Uptake and excretion of dimethylsulphonioacetate is driven by salinity changes in the marine benthic diatom *Cylindrotheca closterium*. *European Journal of Phycology*, *38*(4), 341–349. <https://doi.org/10.1080/09670260310001612600>
- van Nesselroy, C., Shen, C., Zambelli, T., & Momotenko, D. (2022). Electrochemical 3D printing of silver and nickel microstructures with FluidFM. *Additive Manufacturing*, *53*, 102718. <https://doi.org/10.1016/j.addma.2022.102718>
- Vandamme, D., Foubert, I., & Muylaert, K. (2013). Flocculation as a low-cost method for harvesting microalgae for bulk biomass production. *Trends in Biotechnology*, *31*(4), 233–239. <https://doi.org/10.1016/j.tibtech.2012.12.005>
- Vandamme, D., Pohl, P. I., Beuckels, A., Foubert, I., Brady, P. V., Hewson, J. C., & Muylaert, K. (2015). Alkaline flocculation of *Phaeodactylum tricornerutum* induced by brucite and calcite. *Bioresource Technology*, *196*, 656–661. <https://doi.org/10.1016/j.biortech.2015.08.042>

- Vergnes, J. B., Gernigon, V., Guiraud, P., & Formosa-Dague, C. (2019). Bicarbonate Concentration Induces Production of Exopolysaccharides by *Arthrospira platensis* That Mediate Bioflocculation and Enhance Flotation Harvesting Efficiency. *ACS Sustainable Chemistry & Engineering*, 7(16), 13796–13804. <https://doi.org/10.1021/acssuschemeng.9b01591>
- Voigtländer, B. (2015). *Scanning Probe Microscopy: Atomic Force Microscopy and Scanning Tunneling Microscopy*. Springer.
- Walls, P. L. L., Bird, J. C., & Bourouiba, L. (2014). Moving with Bubbles: A Review of the Interactions between Bubbles and the Microorganisms that Surround them. *Integrative and Comparative Biology*, 54(6), 1014–1025. <https://doi.org/10.1093/icb/icu100>
- Wei, Y., Cheng, G., Ho, H.-P., Ho, Y.-P., & Yong, K.-T. (2020). Thermodynamic perspectives on liquid–liquid droplet reactors for biochemical applications. *Chemical Society Reviews*, 49(18), 6555–6567. <https://doi.org/10.1039/C9CS00541B>
- Willemsen, O. H., Snel, M. M. E., van der Werf, K. O., de Grooth, B. G., Greve, J., Hinterdorfer, P., Gruber, H. J., Schindler, H., van Kooyk, Y., & Figdor, C. G. (1998). Simultaneous Height and Adhesion Imaging of Antibody-Antigen Interactions by Atomic Force Microscopy. *Biophysical Journal*, 75(5), 2220–2228. [https://doi.org/10.1016/S0006-3495\(98\)77666-0](https://doi.org/10.1016/S0006-3495(98)77666-0)
- Xu, Y., Purton, S., & Baganz, F. (2013). Chitosan flocculation to aid the harvesting of the microalga *Chlorella sorokiniana*. *Bioresource Technology*, 129, 296–301. <https://doi.org/10.1016/j.biortech.2012.11.068>
- Yahav, D., Farbman, L., Leibovici, L., & Paul, M. (2012). Colistin: New lessons on an old antibiotic. *Clinical Microbiology and Infection: The Official Publication of the European Society of Clinical Microbiology and Infectious Diseases*, 18(1), 18–29. <https://doi.org/10.1111/j.1469-0691.2011.03734.x>
- Yan, X., Shi, R., Xu, Y., Wang, A., Liu, Y., Wang, L., & Cao, Y. (2016). Bubble behaviors in a lab-scale cyclonic-static micro-bubble flotation column. *Asia-Pacific Journal of Chemical Engineering*, 11(6), 939–948. <https://doi.org/10.1002/apj.2028>
- Yang, C., Dabros, T., Li, D., Czarnecki, J., & Masliyah, J. H. (2001). Measurement of the Zeta Potential of Gas Bubbles in Aqueous Solutions by Microelectrophoresis Method.

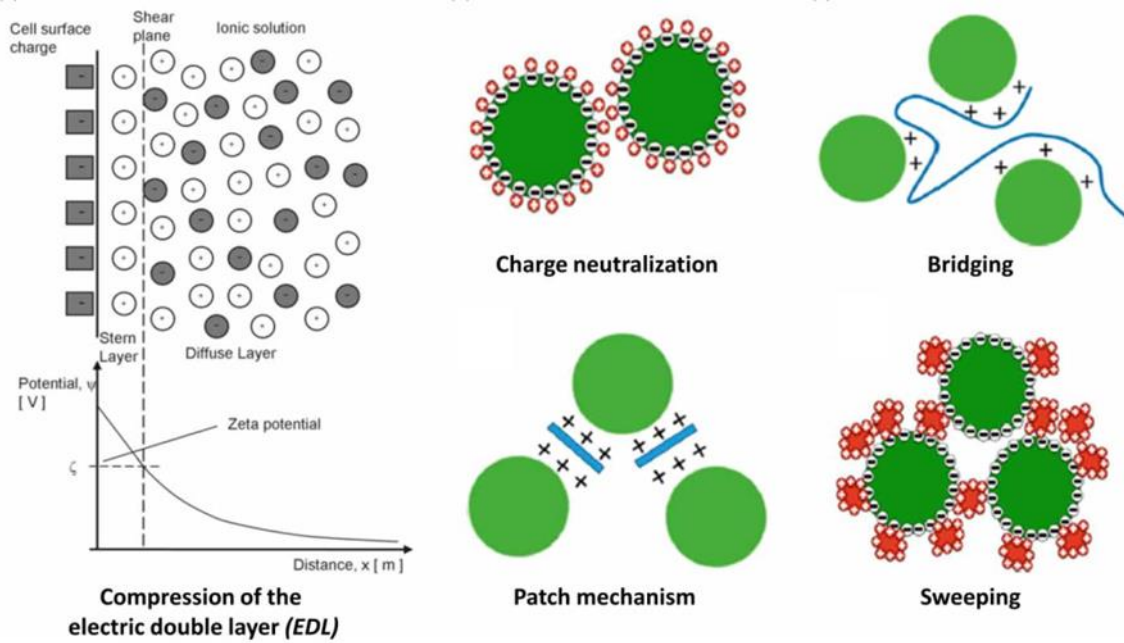
- Journal of Colloid and Interface Science*, 243(1), 128–135.
<https://doi.org/10.1006/jcis.2001.7842>
- Yu, K. L., Show, P. L., Ong, H. C., Ling, T. C., Chi-Wei Lan, J., Chen, W.-H., & Chang, J.-S. (2017). Microalgae from wastewater treatment to biochar – Feedstock preparation and conversion technologies. *Energy Conversion and Management*, 150, 1–13.
<https://doi.org/10.1016/j.enconman.2017.07.060>
- Yumiyama, S., Kato, S., Konishi, Y., & Nomura, T. (2019). Direct measurement of interaction forces between a yeast cell and a microbubble using atomic force microscopy. *Colloids and Surfaces A: Physicochemical and Engineering Aspects*, 123963.
<https://doi.org/10.1016/j.colsurfa.2019.123963>
- Zhang, M., & Guiraud, P. (2017). Surface-modified microbubbles (colloidal gas aphrons) for nanoparticle removal in a continuous bubble generation-flotation separation system. *Water Research*, 126, 399–410. <https://doi.org/10.1016/j.watres.2017.09.051>
- Zhu, L., Li, Z., & Hiltunen, E. (2018). Microalgae *Chlorella vulgaris* biomass harvesting by natural flocculant: Effects on biomass sedimentation, spent medium recycling and lipid extraction. *Biotechnology for Biofuels*, 11(1), 183. <https://doi.org/10.1186/s13068-018-1183-z>
- Ziolkowska, J. R. (2014). Prospective technologies, feedstocks and market innovations for ethanol and biodiesel production in the US. *Biotechnology Reports*, 4, 94–98.
<https://doi.org/10.1016/j.btre.2014.09.001>
- Žutić, V., & Svetličić, S. (2000). Interfacial processes. In P. Wangersky (Ed.), *The Handbook of environmental chemistry1* (pp. 149–165). Springer Verlag.

Chapter 2: Bibliographic analysis

Chapter 2.1: Towards a better understanding of microalgae natural flocculation mechanisms to enhance flotation harvesting efficiency

Chapter 2.2: The contribution of Atomic Force Microscopy (AFM) in microalgae studies: A review

2.1. Towards a better understanding of microalgae natural flocculation mechanisms to enhance flotation harvesting efficiency



Irem Demir, Alexandre Besson, Pascal Guiraud and Cécile Formosa-Dague

Water Science and Technology 82.6 (2020): 1009-1024


Abstract

Background: Flotation is believed to be a promising harvesting technique for microalgae that takes advantage of cell's natural low density and self-floating tendency. Assisted flotation consists in air or gas transformed into bubbles rising through a solid/liquid suspension. As a result, solid particles get attached to gas-liquid interfaces and are carried out and accumulated on the surface. Thus this is a fast, cheap and non-damaging technique. However, in the case of microalgae, this technique remains challenging because the interaction between the bubbles and the cells is repulsive, due to the negative surface charge of cells and bubbles in water, and to the low hydrophobicity of the microalgae cells.

Scope of the review: Among the ways to improve flotation efficiency, flocculating the cells prior to flotation is a strategy that has proven efficient. This procedure allows aggregating the cells into large flocs so that they can be easily captured by the rising air bubbles. However in order to be able to control these processes we need to identify the flocculation mechanisms. In the first part of this review we concentrate on the description of natural flocculation mechanisms. Then in the second part, we highlight detailed cases where natural flocculation mechanisms are directly induced using natural molecules, and finally we address future directions to further improve them.

Major conclusions: First, natural flocculation in microalgae species represent a sustainable and cost-effective alternative to the use of metal salts and other chemical flocculants. Second it is important to study in each case the mechanisms of flocculation involved to be able to control them and use them at larger scales. Finally, new strategies still need to be developed to improve the efficiency of flotation for microalgae harvesting.


Towards a better understanding of microalgae natural flocculation mechanisms to enhance flotation harvesting efficiency

Irem Demir, Alexandre Besson, Pascal Guiraud  and Cécile Formosa-Dague

ABSTRACT

In microalgae harvesting, flocculation is usually a compulsory preliminary step to further separation by sedimentation or flotation. For some microalgae species, and under certain growth conditions, flocculation can occur naturally. Natural flocculation presents many advantages as it does not require the addition of any flocculants to the culture medium and shows high efficiency rate. But because natural flocculation is so specific to the species and conditions, and thanks to the knowledge accumulated over the last years on flocculation mechanisms, researchers have developed strategies to induce this natural harvesting. In this review, we first decipher at the molecular scale the underlying mechanisms of natural flocculation and illustrate them by selected studies from the literature. Then we describe the developed strategies to induce natural flocculation that include the use of biopolymers, chemically modified or not, or involve mixed species cultures. But all these strategies need the addition of external compounds or microorganism which can present some issues. Thus alternative directions to completely eliminate the need for an external molecule, through genetic engineering of microalgae strains, are presented and discussed in the third part of this review.

Key words | flocculation, flotation, harvesting, microalgae

Irem Demir
Alexandre Besson
Pascal Guiraud 
Cécile Formosa-Dague (corresponding author)
TBI, Université de Toulouse, CNRS, INRAE, INSA,
Toulouse,
France
and
TBI-INSa de Toulouse,
135 avenue de Rangeuil 31077 Toulouse Cedex 4,
France
E-mail: formosa@insa-toulouse.fr

INTRODUCTION

Modern life is intimately linked to the availability of fossil fuels, which continue for the moment to meet the world's growing energy needs even though their use drives climate change (Georgianna & Mayfield 2012). But because of the increasing world population and energy demand, there is an urgent need for renewable sources to produce energy (Markou & Nerantzis 2013). In this context, microalgae are receiving increasing attention worldwide as an alternative and renewable source of energy because of their eminent oil producing capacity (Pragya *et al.* 2013). But the potential of microalgae is in fact even greater and they also represent an important source of biomass and of molecules of interest for the fields of food, feed or health. Indeed, microalgae are unique microorganisms which convert light energy, water

and inorganic nutrients into biomass resource rich in value-added products such as lipids, carbohydrates, proteins and pigments (Pragya *et al.* 2013; Minhas *et al.* 2016). Moreover, microalgae have several advantages that make them a potential new generation of feedstock for the production of biofuel and molecules of interest. First, microalgae are capable of all year round production (Brennan & Owende 2010), and they grow on aqueous media but need less water than terrestrial crops (Dismukes *et al.* 2008). Also, nutrients for their cultivation can be found in wastewater, and there is no need at the moment for herbicide or pesticide applications (Rodolfi *et al.* 2009), although this may perhaps change in the future as microalgae cultures also suffer from parasites or other unwanted algal species (Huo *et al.* 2017). They also have a rapid growth rate and many species have an oil content in the range of 50–70% dry weight of biomass. To give an example, compared to soybean, microalgae can produce up to 300 times more oil per area unit, considering ideal laboratory conditions (Ziolkowska 2014). Finally, as mentioned

This is an Open Access article distributed under the terms of the Creative Commons Attribution Licence (CC BY 4.0), which permits copying, adaptation and redistribution, provided the original work is properly cited (<http://creativecommons.org/licenses/by/4.0/>).

doi: 10.2166/wst.2020.177

above, they can also produce valuable co-products such as metabolites, long-chain polyunsaturated fatty acids and vitamins that are used in nutraceuticals industries as food additives (Minhas *et al.* 2016).

While the small-scale production of microalgae to obtain high value-added molecules is nowadays efficient, the large-scale production of molecules, substituting fossil carbon resources, from microalgae faces a number of technical challenges that have made the current growth and development of the biofuel industry economically unviable (Waltz 2009; Pragma *et al.* 2013). These include, among others, (i) the selection of algal species with specificities that meet the requirements for both biofuel production and the extraction of useful co-products (Rodolfi *et al.* 2009; Brennan & Owende 2010; Liao *et al.* 2016), (ii) the inexpensive production of large quantities of microalgae biomass (Chisti 2007) and (iii) the development of efficient harvesting methods (Molina Grima *et al.* 2003; Pragma *et al.* 2013; Kurniawati *et al.* 2014; Coward *et al.* 2015; Ndikubwimana *et al.* 2016). While recent progresses notably in synthetic biology and in culture methods provide solutions for the first two points (Jagadevan *et al.* 2018), the main limitation encountered by industry remains the harvesting of microalgae (Ndikubwimana *et al.* 2016). Harvesting consists in removing at a minimal cost the microorganisms from their aqueous culture medium where their concentration is low (Lam & Lee 2012), without destroying them so as not to lose their production in solution. This crucial step of harvesting and dewatering has been assumed to account for one third of the entire price of microalgal biomass production in industrial processes (Molina Grima *et al.* 2003). Several methods have been proposed for microalgae harvesting, including centrifugation, filtration, flocculation combined with settling or flotation (Garg *et al.* 2012). However, most of these methods are synonymous with high costs and energy consumption, often for low efficiency rates. For instance, centrifugation, the most commonly used method for harvesting, consumes a large amount of energy and can cause damage to the cells because of high shear forces (Pragma *et al.* 2013). Filtration involves using filtering media or membranes, which, in the case of microalgae separation, can get clogged because of the small size of the cells, resulting in high operating costs (Uduman *et al.* 2010). As for flocculation combined with settling, it seems to be a promising low-cost approach for large-scale harvesting of a wide variety of microalgae species (Molina Grima *et al.* 2003); however, contamination is a major issue in this technique, as the chemical flocculants used to induce flocculation end up in the harvested biomass,

and can interfere with the final application of the biomass (food or feed) (Vandamme *et al.* 2013).

In this context, flotation is believed to be a promising harvesting technique that takes advantage of algae's natural low density and self-floating tendency (Garg *et al.* 2012). Assisted flotation consists in air or gas being transformed into bubbles rising through a solid/liquid suspension. As a result, solid particles get attached to gas-liquid interfaces and are carried out and accumulate on the surface. Thus flotation allows for low-cost cell harvesting, without necessarily using flocculants that could damage them. In addition, it is a relatively rapid operation that needs little space, has moderate operational costs, and could thus overcome the bottleneck of feasible microalgal biofuel production. However, the problem with this technique is that the interaction between the bubbles and the cells is generally repulsive, due to the negative surface charge of the cells and the bubbles in water (Yang *et al.* 2001), and the low hydrophobicity of the algal cells. This results in the non-interaction of the cells with the bubbles and thus in a poor efficiency of this harvesting technique.

Among the ways to improve flotation efficiency, flocculating the cells prior to flotation is a strategy that has proven efficient. Indeed, this procedure allows aggregating the cells into large flocs that bubbles produced during the flotation process cannot avoid. This way, cells are easily removed from the water. However, in many cases, this flocculation step is performed using synthetic flocculants which, as previously stated, can contaminate the harvested biomass but also the recycled water. Therefore in many cases, natural flocculation is a preferred alternative. It is indeed possible under certain conditions to induce natural formation of algal flocs; this characteristic was first mentioned by Golueke and Oswald in 1965 who observed microalgae flocculation in cultures under optimal sunlight and heat conditions (Golueke & Oswald 1965). Among natural flocculation mechanisms, so far two types of mechanism have been identified: autoflocculation, where the flocculation is triggered by a molecule or precipitate that naturally forms in the culture medium, and bioflocculation, where a molecule produced by the cells present in the culture medium (microalgae but also other types in the case of co-cultures) is directly responsible for the flocculation. But for both auto- and bioflocculation, the mechanisms of flocculation described are the following: compression of the electric double layer, charge neutralization, bridging, patch mechanism and sweeping. Depending on several parameters such as the microalgae species used, or the conditions in which they are cultured, one or another mechanism takes place. This makes it then an important field of research to identify and understand these mechanisms for

all the different species/culturing situations, as being able to use natural flocculation, combined with flotation in harvesting processes, could be the key to reduce the costs associated with microalgae. In this review, we will focus on these natural flocculation mechanisms, and first describe and illustrate the already known mechanisms. Most studies on microalgae flocculation, and the ones that will be described in this first part of the review, propose a mechanism of flocculation. However, these studies should also be taken with caution as only a few of them also propose experiments or measurements to confirm the flocculation mechanism described or exclude alternative mechanisms. Thus in these studies, the mechanisms proposed often remain hypothetical. Then in a second part, we will detail cases where natural flocculation mechanisms are induced directly using natural molecules, and finally we will discuss what could be the future directions to further improve them.

NATURAL FLOCCULATION MECHANISMS AND KEY PARAMETERS TO CONTROL THEM

Flocculation consists in the aggregation of destabilized compounds, in our case, microalgae, to form structures of more

important apparent size, called ‘flocs’. In most cases, flocculation is often integrated into multi-stage harvesting processes and can for instance be used as a preliminary to sedimentation, centrifugation, flotation or filtration processes. But in all cases, the destabilization of algal suspensions by flocculation can be the result of one or more mechanisms, which are compression of the electric double layer, charge neutralization, bridging, patch mechanism or entrapment in a precipitate, also known as sweeping, presented in Figure 1. In this first part of the review, we will describe these mechanisms and, in each case, illustrate them with examples of microalgae auto- and bioflocculation where they have been identified.

Decreasing the electrostatic repulsion forces

The first flocculation mechanism described, screening, is due to the decrease of electrostatic repulsive forces via the lowering of the surface charge by pH variations, or via the well-known compression of the electric double layer (Figure 1(a)). Most microalgae have negatively charged surfaces (Molina Grima *et al.* 2003) and thus they can attract, through electrostatic interactions, positively charged ions available in the surrounding solution. While some of these

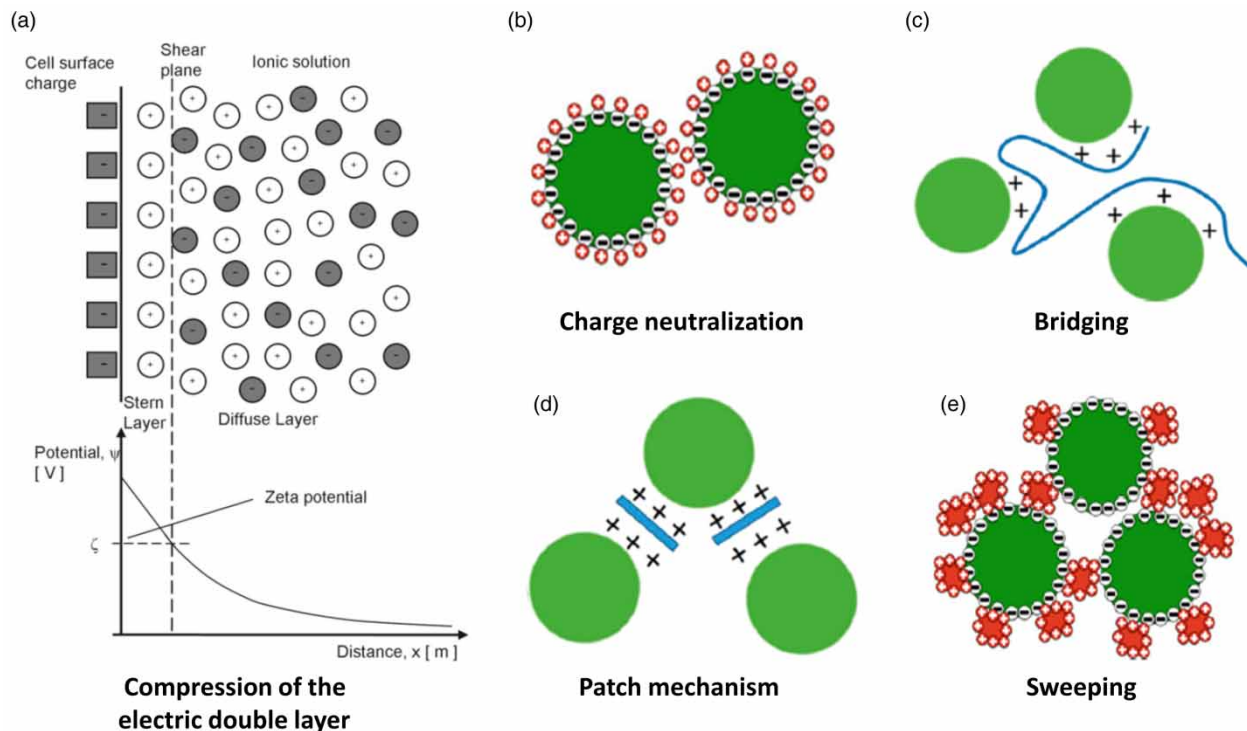


Figure 1 | Schematic representation of natural flocculation mechanisms. (a) Compression of the electric double layer, (b) charge neutralization, (c) bridging, (d) patch mechanism, and (e) sweeping. Reprinted with permission from Pahl *et al.* (2013), Muyllaert *et al.* (2015) and Blockx *et al.* (2019).

ions adsorb to the surface of the microalgae cells to form a dense layer, others remain in the solution and form what is called the diffuse layer. This two layer system is referred to as the electrical double layer, which is, according to the DLVO (Derjaguin–Landau–Verwey–Overbeek) theory, related to the ionic concentration of the solution and to the surface charge itself, the value of which depends on the pH. The interface that separates the layer bound to the cell from the unbound layer is called the shear plane, where the potential is called the zeta potential. This is depicted in Figure 1(a). The microalgae zeta potential is negative over a pH range of 4 to 10 and a point of zero charge (PZC) is regularly detected depending on the species for a pH between 3 and 4 (Phoochinda & White 2003). It is therefore possible to reduce the electrostatic repulsion forces and to promote coagulation by imposing a pH close to the PZC of microalgae. Furthermore, the more the ionic strength of a solution increases, the more the absolute value of the zeta potential of the microalgae decreases due to the compression of the unbound layer (Pahl *et al.* 2013). This decrease leads to a reduction in the electrostatic repulsion forces, which can lead to the reduction or disappearance of the energy barrier initially present and generate the agglomeration of the microalgae thanks to attractive van Der Waals' forces which in this case have become predominant. These two effects have been described in two studies. In the study by Ndikubwimana and co-workers, the authors modified the ionic strength of the culture medium of *Desmodesmus* sp. by adjusting its pH. Their results showed that this reduction of the pH induced a large decrease of the energy barrier and the further destabilization of the microalgae suspension, which flocculated with an efficiency of 78.5% (Ndikubwimana *et al.* 2015). In the study by Cui and co-authors, it was found that increasing the ionic strength of the culture medium of the microalgae species *Nannochloropsis oculata* using a higher concentration of Al^{3+} ions decreased the energy barrier of the suspension, which resulted in a higher flocculation efficiency (Cui *et al.* 2014). It must be noted that these two cases are not auto- or bioflocculation cases, as the modifications that led to the flocculation did not naturally occur.

Neutralization of negative surface charges

The second flocculation mechanism is called charge neutralization (Figure 1(b)). This mechanism also takes advantage of the negative cell surface of microalgae cells; charge neutralization then takes place when these negative charges

are decreased by a positively charged molecule that adsorbs at their surface (Levy *et al.* 1992). This charge neutralization leads to the reduction of the repulsive electrostatic forces and to the predominance of van der Waals' attractive forces, which leads to the flocculation of the microalgae. In this case, the key parameter ensuring successful flocculation is thus the flocculant concentration, as it is directly proportional to the surface area that needs to be neutralized (Muylaert *et al.* 2015). In the case where the flocculant concentration is too high, the surface charge of the cells may become positive, which results in the increase of repulsive electrostatic forces and further stabilization of the suspension. In a recent work conducted in our team, it has been shown that the flocculation of *Phaeodactylum tricornutum*, a marine diatom, induced by an increase of pH in marine water, was the result of the precipitation of magnesium ions into magnesium hydroxide presenting a positively charged surface and thus flocculating the cells through a charge neutralization mechanism (Formosa-Dague *et al.* 2018). Using atomic force microscopy, it was then possible to also show the ability of the *P. tricornutum* cell wall to adsorb magnesium hydroxide particles that formed a partial capsule around the cells, thus neutralizing their surface negative charges and destabilizing the suspension. In the case of this particular study, the pH was artificially increased for the flocculation experiments to mimic the natural pH increase over the course of the culture in *P. tricornutum* species. Indeed, a previous study conducted on *P. tricornutum* showed that the photosynthetic activity of this species could increase the pH of the culture medium up to 10.8 after discontinuing the CO_2 supply, and that at this pH, the cells were able to autoflocculate (Spilling *et al.* 2011). Although in this study, the flocculation mechanism is not described, it is most likely that it is also charge neutralization as described with the same species in Formosa-Dague *et al.* (2018).

Bridging the cells

A third flocculation mechanism is called bridging (Figure 1(c)). In the bridging mechanism, positively charged polymers interact with cells through electrostatic interactions and adsorb at their surface. At low and intermediate concentrations, the polymers can then adsorb onto other cells if the extension of the polymer from the cell surface exceeds the distance over which the cell–cell repulsion is active, thus bridging the two. In this case the efficiency of this mechanism relies on different parameters: (i) the polymer concentration: if a higher dose is used the

cells may become completely positive, which will restabilize the suspension, or the extension of the polymer in the solution may create a steric effect preventing flocculation, (ii) its length: the polymer chains should be long enough to extend from one cell to another (Pal *et al.* 2005), although it must be taken into account that the actual size of a polymer molecule in solution is smaller than its maximum length, and depends on the concentration and the chemical conditions of the solution, (iii) its molecular weight: it is reasonable to think that length and molecular weight are directly linked (to our knowledge independent study of these two parameters has never been performed), but it has been shown that high molecular weight polymers are more efficient (Muylaert *et al.* 2015), (iv) its charge: again it has been shown that low-charged polymers are more efficient, and (v) the ionic strength of the culture medium: for instance bridging by non-ionic polymers can occur only when the adsorbed layer thickness is more than two times greater than the thickness of the electrical double layer (Bolto & Gregory 2007). While for microalgae, the bridging mechanism is mostly associated with cationic polymers interacting with the cells through electrostatic interactions, polymer adsorption onto surfaces can also take place through hydrogen bonding or through ion binding in certain conditions (Bolto & Gregory 2007). A good example of the bridging mechanism can be found in Vergnes *et al.* (2019). In this study, the authors optimized culturing conditions in which *Arthrospira platensis* cells produced exopolysaccharides (EPS). Using further atomic force microscopy imaging experiments, the authors could show that these EPS formed in a culture medium a soft and adhesive gel bridging the cells together and thus bioflocculating them. Another interesting example of bridging flocculation taking place during bioflocculation can be found in Lananan *et al.* (2016). Here the authors show that *Ankistrodesmus* sp. cells could act as a cationic flocculant bridging together cells from *Chlorella vulgaris* species. Indeed, the authors showed that *Ankistrodesmus* sp. had a positive zeta potential, thus allowing it to interact electrostatically with the negative cell surface of *C. vulgaris* at a pH between 6.10 and 7.10. Moreover, *Ankistrodesmus* sp., having an elongated shape, is able to extend from one cell to the other, and thus bridge *C. vulgaris* cells together.

Patch flocculation

The fourth flocculation mechanism that has been described is known as the patch mechanism (Figure 1(d)). This mechanism involves positively charged small polymers that

adsorb at the surface of a negatively charged cell and create an irregular charge distribution at its surface, i.e. positive 'patches' or 'islands' between regions of uncoated, negatively charged surface. These positive patches can then interact with other negatively charged areas at the surface of other cells and connect them together. In this case the key parameters that will ensure successful flocculation are the length of the polymers, as only short polymers can form patches at the surface of the cells, and their charge, as highly charged polymers have been shown to be more efficient (Bolto & Gregory 2007; Muylaert *et al.* 2015). In a study by Salim *et al.* (2014), the authors identified patch mechanism as being a possible mechanism at play in a case of autoflocculation of the microalgae species *Echinocactus texensis*. Using scanning electronic microscopy (SEM) imaging, they could show that *E. texensis* cells had attached to their cell surface short EPS patches composed mainly of glycoproteins responsible for their autoflocculating behavior. Although in this study, the zeta potential measured for *E. texensis* cells was globally negative, it is not excluded that these EPS patches feature positive charges thus allowing a patch mechanism.

Sweeping flocculation

Finally, the last flocculation mechanism that we will detail here is the sweeping mechanism (Figure 1(e)). Sweeping flocculation can be described as the mechanical trapping of microalgae in the massive structure of an inorganic precipitate, resulting in their flocculation. The sweeping mechanism is often described as the result of a pH increase in the culture medium that triggers this massive precipitation; however, it should be attributed more exactly to the increase of hydroxide ions OH^- involved in the precipitation. Although this pH increase can naturally occur in microalgae cultures, as far as we know, very few examples of naturally generated sweeping flocculation have been reported (Sukenik & Shelef 1984). Natural pH variation is usually not sufficient to induce precipitation for many microalgae species, and, when flocculation is observed, often the pH was artificially increased by the addition of a base. In a first example, Besson and co-authors showed that in cultures of the hypersaline microalgae *Dunaliella salina*, the only possibility to induce flocculation was to increase the pH by addition of NaOH directly into the culture medium. The authors then showed that this increase in the pH caused the precipitation of Mg ions present in the culture medium into magnesium hydroxide, thus sweeping the cells and precipitating them (Besson & Guiraud

2013). Although magnesium hydroxide is positively charged and could also flocculate the cells through charge neutralization, this mechanism was excluded in a further work that showed using atomic force microscopy that magnesium hydroxide particles were not interacting with the surface of the cells (Besson *et al.* 2019). However, the important parameter identified to ensure the flocculation efficiency was the mixing of NaOH in the culture medium, because to achieve a high flocculation efficiency, the precipitate must be able to reach the entire volume of the suspension to entrap all the cells present. In a second example provided by Vandamme *et al.* (2015), the pH was increased in the culture medium of the diatom *P. tricornutum*, which resulted in the precipitation of both magnesium hydroxide and calcium hydroxide. Based on zeta potential analysis, the authors could conclude that while magnesium hydroxide could flocculate the cells through a charge neutralization mechanism, in the case of calcium hydroxide, the sweeping mechanism was involved. Indeed, in a culture medium lacking Mg^{2+} ions, the surface charge of the cells was not reversed to positive values at high pH, indicating that there is no adsorption of the calcium hydroxide to cells, thus excluding the charge neutralization mechanism.

Scaling-up natural flocculation for microalgae harvesting?

In natural flocculation, one or several of these flocculation mechanisms can be involved. However, as illustrated by the examples given in each case, these mechanisms are very specific to the microalgae species used and the culture conditions chosen. Indeed, for example, at high pH, magnesium hydroxide will flocculate *P. tricornutum* cells through charge neutralization, while in the case of *D. salina*, the flocculation will occur through the sweeping mechanism. It is therefore important in each case to identify these mechanisms, in order to be able to control them and use them in larger-scale processes. For instance, to our knowledge, harvesting using natural flocculation in large-scale assays has never been reported. The only case where an attempt was made was in the study by Besson and co-workers, where flocculation of *D. salina* by sweeping was achieved in a 600 L/h continuous flocculation/flotation pilot (Besson *et al.* 2019). However, in this case, the term natural flocculation cannot be used as the pH was artificially increased in the culture medium by NaOH addition. Indeed, as it is important to understand natural flocculation mechanisms to control them, it also provides the possibility to induce them artificially, by adding ions to induce

flocculation or by adjusting the ionic strength of a culture medium, as in the examples described previously, or using biomolecules to retain the sustainability aspect that is pursued in natural flocculation.

INDUCING NATURAL FLOCCULATION MECHANISMS WITH BIO-SOURCED FLOCCULANTS

As stated in the previous part of this review, natural mechanisms are difficult to implement, even at lab scales because of their specificity to each culturing situation. However, the extensive number of studies that have been dedicated to understanding these mechanisms over the last few years have allowed the research community to gain insights into these mechanisms and especially into the key parameters affecting their efficiencies. This paved the way towards new strategies where researchers started to induce these natural flocculation mechanisms, by adding biopolymers either directly extracted from other organisms, like natural polysaccharides, or modified by various means to control the functional chemical groups they present. The different bioflocculation mechanisms identified also inspired the use of mixed cultures, where one microorganism species directly flocculates the microalgae species or produces a polymer that will flocculate it. Another strategy to induce natural flocculation is to artificially increase the pH; however, this point has already been mentioned previously and described by Besson & Guiraud (2013), and will not be more detailed in this second part. The different strategies to induce natural flocculation mechanisms will be described in this second part; their advantages and drawbacks will also be discussed.

Flocculation by addition of biopolymers

Selected studies illustrating well the use of biopolymers to induce natural flocculation are compiled in Table 1. The most popular biopolymer used for microalgae flocculation is chitosan. Chitosan is a cationic polyelectrolyte obtained by deacetylation of chitin, and after cellulose, it is the second most abundant natural polymer in the world. Moreover, chitosan presents many advantages as it is non-toxic, biodegradable, biocompatible and renewable, in contrast to traditional inorganic flocculants (Renault *et al.* 2009). Finally, chitosan does not contaminate the harvested biomass as chitin-like polysaccharides are naturally present in the cell wall of many microalgae species, and thus the products extracted from the cells can then be directly used (Ahmad *et al.* 2011). So far chitosan has been successfully

Table 1 | Natural flocculation mechanisms induced by addition of biopolymers

Microalgae species	Biopolymer used	Flocculation mechanism	Harvesting efficiency	Reference
<i>Chlorella sorokiniana</i>	10 mg chitosan/g of algal dry weight	Charge neutralization + Patch	99%	Xu et al. (2013)
<i>Chlorella vulgaris</i>	10 mg/L chitosan	Bridging + Charge neutralization	96%	Blockx et al. (2018)
<i>Nannochloropsis oculata</i>	Up to 200 mg/L chitosan	Sweeping	90%	Blockx et al. (2018)
<i>C. vulgaris</i>	30 mg/L poly (γ -glutamic acid)	Bridging + Charge neutralization	91%	Zheng et al. (2012)
<i>Chlorella protothecoides</i>	30 mg/L poly (γ -glutamic acid)	Bridging + Charge neutralization	98%	Zheng et al. (2012)
<i>Chlorella</i> sp.	40 ppm cationic guar gum	Bridging	94.5%	Banerjee et al. (2013)
<i>Chlamydomonas</i> sp.	100 ppm cationic guar gum	Bridging	92.2%	Banerjee et al. (2013)
<i>Chlorella</i> sp.	35 mg/L cationic cassia	Bridging + Patch	92%	Banerjee et al. (2014)
<i>Chlamydomonas</i> sp.	80 mg/L cationic cassia	Bridging + Patch	93%	Banerjee et al. (2014)
<i>Scenedesmus dimorphus</i>	10 mg/L cationic starch	Bridging + Patch	95%	Hansel et al. (2014)
<i>S. dimorphus</i>	100 mg/L cationic starch	Bridging + Patch	70%	Hansel et al. (2014)
<i>C. vulgaris</i>	Up to 200 mg/L cationic cellulose nanocrystals	Patch	95%	Blockx et al. (2019)

used to harvest different microalgae species, both marine and fresh-water. For example in 2013, Xu and colleagues flocculated the fresh-water species *Chlorella sorokiniana* using an optimum dosage of chitosan with an efficiency of 99% at a pH of 6 (Xu et al. 2013). The pH is indeed important to control in the case of chitosan as its efficiency as a flocculant relies on the amine groups that it presents. These amino groups have a pKa value of about 6.5 (Ritthidej 2011), and thus below this pH value these groups will be protonated thus conferring a positive charge to chitosan, which allows its interaction with the negatively charged surface of microalgae cells (Bilanovic et al. 1988). Indeed, in the case of *C. sorokiniana*, the flocculation mechanism described is a combination of charge neutralization and patch mechanisms. While the bridging mechanism is often associated with chitosan, in this case the authors state that chitosan polymers are much smaller than the cells, thus excluding bridging (Xu et al. 2013). However, while chitosan is widely reported as being efficient to flocculate fresh-water microalgae species, this is not necessarily the case for marine species. Indeed, in marine water that presents high ionic strengths, it is believed that the positive charges of chitosan are screened, thus preventing the polymer to interact with the cells and further flocculate them (Bilanovic et al.

1988). However, it must be noted that studies have reported the successful use of other cationic polymers for flocculation of marine species (t Lam et al. 2014); thus there might be other parameters perhaps influencing the efficiency of chitosan in particular. In view of this, Blockx and co-authors recently investigated the conditions under which chitosan can be used as a flocculant for marine species (Blockx et al. 2018). The results the authors obtained on *N. oculata* showed that in opposition to fresh-water conditions, low pH did not trigger flocculation, while a high pH (between 7.5 and 10) was efficient. This clearly indicates that chitosan-induced flocculation in marine species occurs through another mechanism than charge neutralization or patch mechanisms, as at high pH, no or very few charges are present on the chitosan polymer. But when chitosan is uncharged, its solubility decreases, which triggers its precipitation. The authors thus suggest that in the case of *N. oculata*, chitosan flocculates the cells through a sweeping mechanisms, which can only be achieved at high pH (Blockx et al. 2018). Thus the particular case of chitosan also illustrates well the fact that a flocculation mechanism identified in one condition cannot be extrapolated to other conditions and species, as these mechanisms are specific to the species and conditions used.

But chitosan is not the only biopolymer that can be used to induce natural flocculation in microalgae. For instance, Zheng *et al.* (2012) have reported the use of poly (γ -glutamic acid) (γ -PGA) to flocculate fresh-water species. γ -PGA is a polymer of the amino acid glutamic acid produced by the bacterial species *Bacillus subtilis*. The authors showed that using this natural polymer, they could flocculate *C. vulgaris* and *Chlorella protothecoides* with efficiencies of respectively 91 and 98%. Using zeta potential measurements, they demonstrated that γ -PGA could increase the potential of the microalgae cells, thus indicating that it could interact with them through a charge neutralization mechanism. Moreover, SEM imaging also revealed that this mechanism was combined with a bridging mechanism, as microalgae cells were interlaced with γ -PGA directly within the flocs. In 2013 Banerjee and co-workers showed that guar gum, a natural polysaccharide extracted from plants and chemically cationized, was an efficient flocculant for both *Chlorella* and *Chlamydomonas* sp. cells. Indeed, flocculation efficiencies reached respectively 94.5 and 92.2%, and further imaging experiments confirmed that this flocculation was achieved through a bridging mechanism (Banerjee *et al.* 2013). In 2014, the same group also investigated the efficiency of another biopolymer extracted from plants, cassia, a polysaccharide that the authors also chemically cationized using a similar strategy as for guar gum. Their results showed that this biopolymer also was efficient at flocculating cells from the same species, through a bridging mechanism as well (Banerjee *et al.* 2014). In 2014, Hansel and colleagues used starch, a naturally-occurring biodegradable polysaccharide, that they modified by etherification to present positive charges, and directly used as a flocculant to harvest *Scenedesmus dimorphus* cells (Hansel *et al.* 2014). In this study, the authors found that this polymer could adsorb at the surface of several cells, thus bridging them together. The patch mechanism was also found to be at play as the adsorption of the polymer to the cell surface created localized areas of positive charges, which consequently attracted neighboring oppositely charged cells. However, it must be noted that in these three last studies, the cationic moiety used to modify guar gum, cassia and starch, CHPTAC ((2-chloro-2-hydroxypropyl)trimethylammonium chloride), presents some safety issues and may not be adapted for all applications. As a last example, in a recent study conducted by Blockx and co-workers, the authors created cellulose nanocrystals (CNCs) by acid hydrolysis of the amorphous region of cellulose, the most abundant natural polymer on earth. They then linked cationic pyridinium- and methylimidazolium-based grafts (for which the potential toxicity under this form has

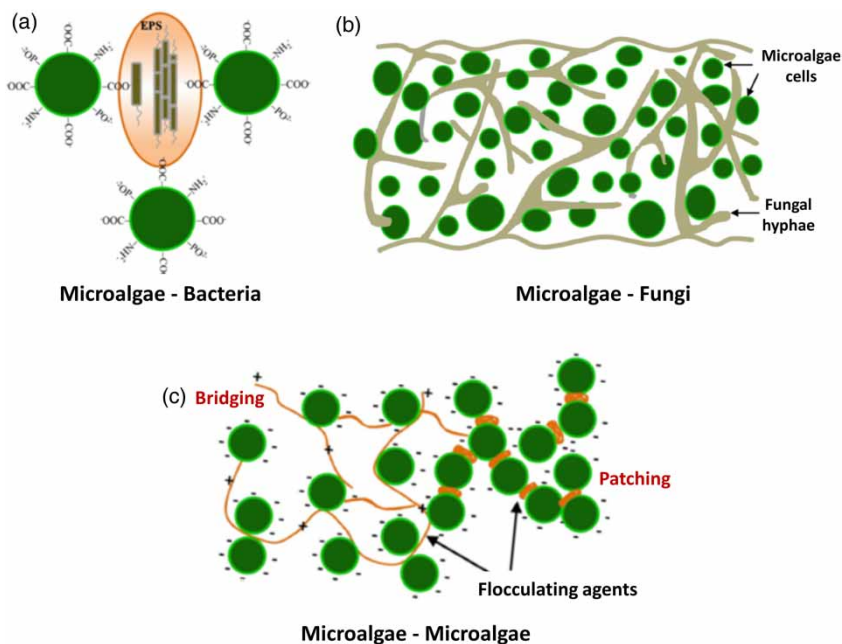
not yet been evaluated) to these CNCs to induce the flocculation of *C. vulgaris*. Their results showed that cationic CNCs could be used as an efficient flocculant and that, in this case, bridging was not involved, which otherwise is often the case with biopolymers. Indeed, CNCs present a rigid backbone that prevent them from coiling and bending to bridge cells together, and carry charges on both sides, which thus led the authors to suggest that the flocculation mechanism in this case was the patch mechanism (Blockx *et al.* 2019).

Flocculation by other microorganisms

But while in all these different examples described so far, the idea is to add a biopolymer, chemically modified or not to flocculate the cells, another strategy to induce natural flocculation in microalgae is to mix them with other microorganisms that will directly flocculate them. In view of this, several works have been performed involving mixed cultures of different microalgae species, or mixed cultures of microalgae with bacterial species or with fungal species. A selection of these studies are reported in Table 2. A first possibility is to mix microalgae cells with a different microorganism, a fungal species or a bacterial species. Flocculation mechanisms of the algal-bacterial and algal-fungal cultures are represented in Figure 2(a) and 2(b), respectively. Microbial flocculation was first suggested as a harvesting technique for microalgae as early as 1996 (Benemann & Oswald 1996). In most cases, the flocculation mechanism relies on the production of extracellular polymers by the bacteria or fungi, which directly flocculate the cells usually through the bridging mechanism. Then two possibilities exist; in the first one, the microorganisms are cultured separately, the bacterial/fungal species produce the bioflocculant over the culture and are then mixed with the microalgae cells to proceed to the flocculation. This is for example the case in a study by Oh *et al.* (2001), where bacterial cells from the strain *Paenibacillus* sp. AM49 were cultivated to produce a bioflocculant efficient at harvesting several species of green microalgae. Wan and co-workers also implemented this strategy in 2013 to produce a bioflocculant using the bacterial strain *Solibacillus silvetris* W01. To flocculate the marine microalgae species *Nannochloropsis oceanica*, the authors then mixed the supernatant of the bacterial culture directly with the microalgae culture and could obtain a flocculation efficiency of 90% (Wan *et al.* 2013). In both cases, there is no detailed information given on the mechanism of flocculation, as the focus of these studies was to identify and use bacteria-produced bioflocculants. Moreover, while we chose to mention these two cases as mixed cultures

Table 2 | Natural flocculation mechanisms induced by other microorganisms

Microalgae species	Micro-organism	Species	Flocculation mechanism	Efficiency	Reference
<i>Chlorella vulgaris</i>	Bacteria	<i>Paenibacillus</i> sp.	Extracellular secreted bioflocculant	93%	Oh et al. (2001)
<i>Nannochloropsis oceanica</i>	Bacteria	<i>Solibacillus silvestris</i>	Extracellularly secreted flocculant	90%	Wan et al. (2013)
<i>Scenedesmus obliquus</i>	Bacteria	<i>Solibacillus silvestris</i>	Extracellular secreted bioflocculant	77%	Wan et al. (2013)
<i>C. vulgaris</i>	Bacteria	<i>Solibacillus silvestris</i>	Extracellular secreted bioflocculant	51%	Wan et al. (2013)
<i>Pleurochrysis carterae</i>	Bacteria	Tap water bacterial inoculum	Increase in floc size	90%	Lee et al. (2009)
<i>C. vulgaris</i>	Fungus	<i>Aspergillus niger</i>	Fungal pelletization	98.1%	Zhang & Hu (2012)
<i>C. vulgaris</i>	Fungus	<i>Aspergillus</i> sp.	Fungal pelletization	89.8%	Zhou et al. (2012)
<i>C. vulgaris</i>	Fungus	<i>Cunninghamella echinulata</i>	Fungal pelletization	99%	Xie et al. (2013)
<i>C. vulgaris</i>	Fungus	<i>Aspergillus oryzae</i>	Fungal pelletization	100%	Zhou et al. (2013)
<i>Chlorella</i> sp.	Fungus	<i>Pleurotus ostreatus</i>	Fungal pelletization	64.8%	Luo et al. (2019)
<i>C. vulgaris</i>	Microalgae	<i>Afrocarpus falcatus</i>	Bridging	22%	Salim et al. (2011)
<i>C. vulgaris</i>	Microalgae	<i>Scenedesmus obliquus</i>	Patch	32%	Salim et al. (2011)
<i>Neochloris oleoabundans</i>	Microalgae	<i>Tetraselmis suecica</i>	Patch	72%	Salim et al. (2011)
<i>Chlorella</i> sp.	Microalgae	<i>Ankistrodesmus</i> sp.	Bridging	82%	Lananan et al. (2016)
<i>Chlorella</i> sp.	Microalgae	<i>T. suecica</i>	Bridging (EPS)	67.3%	Kawaroe et al. (2016)
<i>Nannochloropsis</i> sp.	Microalgae	<i>T. suecica</i>	Bridging (EPS)	42.4%	Kawaroe et al. (2016)

**Figure 2** | Mixed species cultures mechanisms. Proposed mechanism of (a) microalgae–bacteria mixed cultures, (b) microalgae–fungi mixed cultures and (c) microalgae–microalgae mixed cultures. Reprinted and adapted with permission from Alam et al. (2016).

cases, one can argue that the fact that the microorganisms are not cultured together in the same broth, but separately, qualifies them more appropriately as classic bioflocculation cases.

Thus the second possibility consists in growing the different microorganisms in symbiosis, so that the microbial species directly flocculate microalgae cells *in situ*. For instance Lee and co-workers, in 2009, used directly tap water containing microbes: some heterotrophic bacteria present in the water, which therefore did not have the same nutritional requirements as microalgae cells, produced EPS under nutrient deficient conditions allowing the flocculation of the microalgae species *Pleurochrysis carterae* (Lee *et al.* 2009). Moreover, Lee *et al.* (2013) showed that in non-axenic cultures of *C. vulgaris*, the use of flocculants (CaCl_2 , FeCl_3) or pH variations resulted in high flocculation efficiencies while it was not the case in axenic cultures of *C. vulgaris*. These results thus highlighted the important role of microalgae-associated bacterial species, three identified in this study, on the flocculation behavior of the microalgae cells. The suggested mechanism underlying this positive effect was that these bacterial cells and the extracellular substances they produce increased the microalgae floc size, which allowed them to be separated from the water by settling (Lee *et al.* 2013). Other studies have explored the potential of mixed cultures with filamentous fungi. In liquid cultures, filamentous fungi can either grow in filamentous form, featuring homogeneously dispersed hyphae or filaments, or in spherical pellets consisting of compact aggregated hyphal structures (Veiter *et al.* 2018). In some specific cases, these filamentous fungal strains can entrap microalgal cells and form fungi–algae pellets, thus allowing efficient algae harvesting. This technique has notably been proven efficient to harvest different microalgae species in several cases (Zhang & Hu 2012; Zhou *et al.* 2012, 2013; Xie *et al.* 2013; Luo *et al.* 2019). While the mechanism at the origin of the interaction between the fungus and the microalgae cells may be related to several possible reasons, one of these reasons may be related to surface charge. Indeed, for example in the case of co-cultures of the fungus *Aspergillus flavus* and *C. vulgaris*, it has been shown that fungal cells have a positive zeta potential, thus allowing their electrostatic interactions with negatively charged *C. vulgaris* cells (Zhang & Hu 2012). Although it is worth mentioning these examples of mixed cultures to induce flocculation of microalgae, as they represent valuable strategies to harvest cells without the addition of any flocculants or modified biopolymers, it is clear that the mechanisms of flocculation in these cases are very specific, and expand out of the ‘classic’ flocculation mechanisms that were described in the first part of this review.

Finally another possibility is to mix different microalgae species together, so that one will act as a flocculant for the other. This type of mixed cultures presents important advantages compared to mixing them with bacteria or fungi: it does not require different cultivation conditions, which reduces costs, and it prevents contaminations. Another advantage in this case is that both microalgae species can produce the molecule of interest in the process; thus all the biomass can then be used for downstream processes (Salim *et al.* 2011). Flocculation mechanisms of algal-algal culture are represented in Figure 2(c). An example of microalgae mixed cultures is presented in the study by Lananan and colleagues, already described earlier in this review, where *Ankistrodesmus* sp. cells, positively charged at pHs between 6.10 and 7.10, could flocculate negatively charged *C. vulgaris* cells through the bridging mechanism (Lananan *et al.* 2016). In another study performed by Kawaroe and co-workers, the marine species *Tetraselmis suecica* was directly used as a flocculant to harvest cells from the species *Chlorella* sp. and *Nannochloropsis* sp. To do so, the authors mixed *T. suecica* with the two other species, separately, at different ratio, and obtained after only 1 hour harvesting rates of 67.3% for *Chlorella* sp. and of 42.4% for *Nannochloropsis* sp. In both cases, the addition of the flocculant species in larger volume increased the flocculation efficiency. Concerning the flocculation efficiency, the fact that the two species are in competition for the nutrients as the culture goes on induces a stress on the cells, which in the case of *T. suecica* triggers the production of exopolysaccharides. These EPS are then responsible for bridging the cells together and flocculating them (Kawaroe *et al.* 2016). Other examples of successful mixed microalgae cultures can also be found in Salim *et al.* (2011), where different flocculation mechanisms are described depending on the flocculating microalgae species: bridging in the case where long EPS are partly bound to the producing cells, and patch mechanism if these EPS are short and bind completely to the producing cells, therefore creating positive patches at their surface (Salim *et al.* 2011).

Induced natural flocculation but not always so natural ...

It is thus possible to artificially induce natural flocculation mechanisms in microalgae using biopolymers or mixed species cultures. As far as we know, the only biopolymer that has been successfully used to flocculate microalgae cells is chitosan, although its use should be adapted depending on the microalgae species used. Most of the

biopolymer-based strategies involve chemically modifying the natural molecules. First this involves additional costs, but also such strategies can be questionable from the toxicity point of view. So far in the examples described here no evaluation of the toxicity of the molecules was performed; thus there is for the moment no information as to whether these modified biopolymers represent a risk of biomass contamination or not. This is also a problem when using mixed cultures with different microorganisms, as fungi and bacteria also contaminate the biomass. In view of this, the ideal situation would be to be able to induce natural flocculation in microalgae species without having to add any molecules or microorganisms, but by acting directly on the microalgae itself to make it able to flocculate.

ALTERNATIVE DIRECTIONS IN NATURAL FLOCCULATION

In this idea of not to contaminate the biomass by any added molecule, an interesting strategy would be to genetically engineer the microalgae species so that they could flocculate without any modification of their culture medium. Genetic engineering consists in modifying the genome of the cells so that they express the desired molecules, or are able to use certain molecules present in the medium. While genetic engineering is widely used for bacteria, yeasts and plants (Barton & Brill 1983; Dequin 2009; Riglar & Silver 2018), its development for microalgae still remains confined. For the moment, the efforts regarding microalgae have mostly concentrated on increasing or modifying lipids or other energy storage molecules for biofuels applications (Dunahay *et al.* 1996). However, such strategies can also be used to engineer microalgae strains to enhance their flocculation capabilities, and this is what we will describe in the third part of this review. It is possible to think that such strategies could be the future directions to take in flocculation, although the use of genetically modified organisms is always controversial, and could not for instance take place in certain applications such as wastewater treatment. However, in closed photobioreactors, with no release in the environment, using genetically modified microalgae could be a possibility.

In addition to being a barrier against the environment, the algal cell wall is also an obstacle against engineering processes. Moreover, genetic manipulation of microalgae presents several other challenges, which are (i) the lack of suitable promoters and other regulatory sequences, (ii) the low efficiency and instability of transgene expression,

(iii) the fact that microalgae are a highly heterogeneous group of microorganisms and thus procedures have to be adapted in each case, (iv) the insufficient genetic data availability and (v) the lack of a standard toolbox for genetic engineering manipulations (León & Fernández 2007; Daboussi *et al.* 2014). While we will not go over the details of molecular biology strategies that are used to modify microalgae genomes as it is not the scope of the review, we will give and discuss examples where genetically modified microalgae species have been successfully used in flocculation processes. In a first example, Scholz and colleagues have tested the capacity of a mutant strain of *Chlamydomonas reinhardtii*, *cw15*, produced by Davies and Plaskitt in 1971 (Davies & Plaskitt 1971), to flocculate in the presence of the flocculant CaCl_2 , in nitrogen-deprived conditions. The specificity of this mutant is that it lacks a cell wall and flagella, and thus has no mobility. The results obtained showed that the flocculation efficiency of this mutant strain was 83% whereas for the wild-type strain (with no genetic mutations), it was only 24% (Scholz *et al.* 2011). In the discussion the authors mention that other authors obtained similar results with another microalgae species having a cell wall (Sukenik *et al.* 1985); thus they suggest that the flocculation in this case may be due to the lack of flagella, which prevents them from moving and thus makes them more susceptible to the flocculant used. A further study by Fan *et al.* (2017) also used mutant cells of *C. reinhardtii*, deficient in a cell wall and flagella, but for the production of starch, and could also observe differences in the flocculation compared to wild-type strains, depending on the flocculant used, which they suggest can be attributed to the mutations. These examples are a good illustration that using microalgae strains where a simple genetic mutation is introduced can be a promising strategy to enhance the efficiency of flocculation and further flotation. But in this case, still a flocculant added to the culture medium is needed to achieve efficient flocculation, though it is also possible to engineer microalgae strains that self-flocculate with no addition of flocculant.

A first possibility to reach this goal has been presented by Diaz-Santos *et al.* (2016). In this study, the authors developed a strategy to express a gene from the yeast species *Saccharomyces bayanus* responsible for the flocculation, called *SbFLO5*. Flocculation in yeast is also a subject that has been extensively studied. In yeasts, a family of genes called FLO encodes specific cell surface glycoproteins, known as flocculins, which are responsible for the natural flocculating behavior of yeast cells (Stratford 1994). The mechanism by which they bind to other cells is thought to be by interacting with specific carbohydrate residues present

at the surface of adjacent cells (Miki *et al.* 1982). Later, Goossens and co-workers, among others, specified this mechanism by showing that one of these flocculins, Flo1p, could bind to the mannose residues present at the surface of yeast cells, thanks to two mannose carbohydrate binding sites present in the N-terminal region of the protein (Goossens *et al.* 2011). In a previous study in 2015, Díaz-Santos and colleagues used *S. bayanus* to produce these flocculins. The authors then extracted them from the supernatant of the yeast cultures and used them directly as flocculants in *C. reinhardtii* and in *Picochlorum* sp. cultures. Figure 3 shows the difference in the flocculation of *Picochlorum* sp. cells before and after addition of the flocculins isolated from fermentative cultures of *S. bayanus*. Their results showed that they could reach a recovery efficiency of 95% in the case of *C. reinhardtii* and of 75% in the case of *Picochlorum* sp., thus indicating that flocculins from yeasts are also able to bind to glycosidic residues present at the surface of microalgae cells, with a higher specificity in the case of *C. reinhardtii* (Díaz-Santos *et al.* 2015). It is after this study that the authors then suggested that the expression of FLO genes from *S. bayanus* to create self-flocculating *C. reinhardtii* transformants could be a promising method to enhance flocculation efficiency. After inserting the *FLO5* gene from *S. bayanus* into *C. reinhardtii*, they could show that these engineered mutant cells that express FLO

genes exhibited better self-flocculation, resulting in flocculation performance up to 3.5-fold higher compared to wild-type (Díaz-Santos *et al.* 2016). This study thus proves that self-flocculation phenotypes can be generated in microalgae through genetic engineering methods like insertion of the gene that is responsible for adhesive protein production. Then a second possibility to engineer self-flocculated microalgae strains is through the direct analysis of the microalgae genes using DNA sequencing technologies to identify flocculation genes and over-express them or transfer them from a strain to another. It has been reported that several microalgae species, such as *C. vulgaris*, *Ankistrodesmus falcatus*, *Scenedesmus obliquus* and *T. suecica*, have a higher tendency towards natural flocculation (Salim *et al.* 2011, 2012; Zhang *et al.* 2016). Such species could thus represent good candidates for DNA sequencing studies aiming at identifying which genes are responsible for their self-flocculating behavior. While over-expression or duplication of flocculating genes has not yet been performed, genetic studies have already been realized on microalgae. For instance, Blanc and co-workers sequenced the green alga *Coccomyxa subellipsoidea* C-169 genome, which was the first eukaryotic microorganism from a polar environment to have its genome sequenced. This study was conducted to analyze the mechanism of adaptation of life of this species to extreme polar environmental conditions. Their results

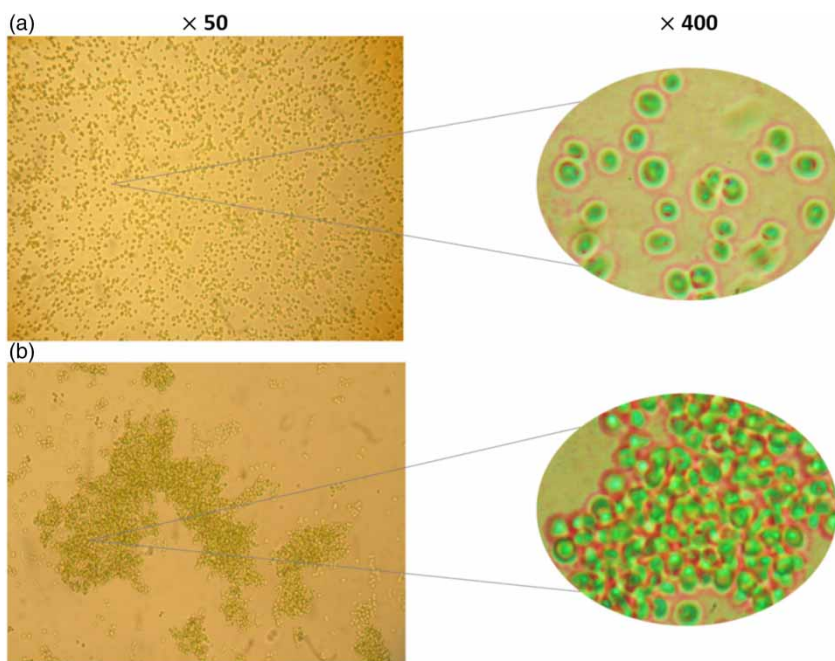


Figure 3 | Example of *S. bayanus* Flo protein induced flocculation. Microscopic analysis of *Picochlorum* sp. HM1 cells before (a) and after (b) addition of proteins isolated from fermentative cultures of *Saccharomyces bayanus* var. *uvarum*. Reprinted with permission from Díaz-Santos *et al.* (2015).

showed that this microalgae species had more enzymes engaged in the biosynthesis and lipid modification than other sequenced microalgae species. This thus implies that *C. subellipsoidea* has adapted to extreme cold conditions by making its lipid metabolism more versatile, enabling it to synthesize a wide range of cell membrane components (Blanc et al. 2012). However, this microalgae species is not the only species that has been sequenced. Another example is *Dunaliella tertiolecta*, whose genome has been sequenced to classify existing genes for enzyme encoding. This way corresponding lipid and starch pathways were reconstructed in order to increase the biofuel production of these species. Such results show the potential of using transcriptomic data from next-generation sequencing to identify pathways of interest and potential targets for microalgae metabolic engineering. These findings can for example be used to genetically engineer *D. tertiolecta* and this way maximize the production of commercial microalgae-based biofuels (Rismani-Yazdi et al. 2011). These examples demonstrate that after DNA sequencing analysis, it is possible to detect the genes that are responsible for a specific phenotype. Thus using this strategy, it could be possible to identify genes responsible for the flocculation in the case of harvesting studies.

CONCLUSIONS

While microalgae harvesting represents for the moment an economic burden slowing down the development of industrial processes to produce molecules of interest, such as biofuels, from microalgae, harvesting techniques, such as flotation, could represent a promising alternative. But flotation, at the moment, and in the specific case of microalgae, needs a flocculation step. Microalgae flocculation can be performed using chemical flocculants that in the end contaminate the harvested biomass and can interfere with downstream processes. This is why the scientific community has focused over the last few years on natural flocculation. From this review several important facts about natural flocculation can be identified. First, natural flocculation in microalgae species represents a sustainable and cost-effective alternative to the use of metal salts and other chemical flocculants. However, while the general mechanisms of flocculation (compression of the double electric layer, charge neutralization, bridging, patch mechanisms and sweeping) are well-known and described, their role in microalgae natural flocculation is specific to the microalgae species considered and to the culture conditions. Thus it is

important for each case to specifically study the mechanism underlying the observed flocculation to be able to control it and to further implement it in large-scale applications. Yet, the quite important numbers of studies produced on the subject have allowed researchers to develop strategies to artificially induce these mechanisms in microalgae, through the use of biopolymers, chemically modified or not, or through the use of mixed cultures. However, still these alternatives present some issues, as both chemically modified biopolymers and added microorganisms can be associated with biomass contamination problems. Thus new strategies need to be developed, and in this context genetic engineering can be an interesting one as it would allow creation of self-flocculating microalgae species that would require no added flocculant. And perhaps it could also be possible to simply eliminate this flocculation step, for instance in the flotation process. In view of this, an original idea is to directly functionalize the bubbles used in flotation with surfactants that would promote their adhesion to microalgae cells, with no flocculation step needed. Studies have been published on this topic, where positively charged bubbles were successfully used to harvest microalgae by flotation (Hanumanth Rao et al. 2018), thus demonstrating the feasibility of such an idea.

ACKNOWLEDGEMENTS

C. F.-D. is a researcher at CNRS. This work has been supported by the ANR JCJC project FLOTALG to C.F.-D. (ANR-18-CE43-0001-01).

REFERENCES

- Ahmad, A. L., Mat Yasin, N. H., Derek, C. J. C. & Lim, J. K. 2011 Optimization of microalgae coagulation process using chitosan. *Chemical Engineering Journal* **173**, 879–882.
- Alam, M. A., Vandamme, D., Chun, W., Zhao, X., Foubert, I., Wang, Z., Muylaert, K. & Yuan, Z. 2016 Bioflocculation as an innovative harvesting strategy for microalgae. *Reviews in Environmental Science and Bio/Technology* **15** (4), 573–583.
- Banerjee, C., Ghosh, S., Sen, G., Mishra, S., Shukla, P. & Bandopadhyay, R. 2013 Study of algal biomass harvesting using cationic guar gum from the natural plant source as flocculant. *Carbohydrate Polymers* **92** (1), 675–681.
- Banerjee, C., Ghosh, S., Sen, G., Mishra, S., Shukla, P. & Bandopadhyay, R. 2014 Study of algal biomass harvesting through cationic cassia gum, a natural plant based biopolymer. *Bioresource Technology* **151**, 6–11.
- Barton, K. A. & Brill, W. J. 1983 Prospects in plant genetic engineering. *Science* **219** (4585), 671–682.

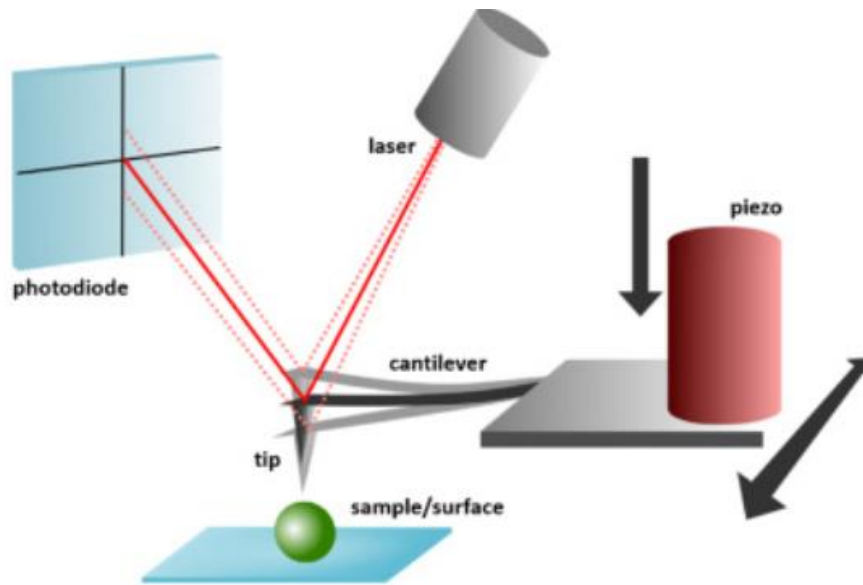
- Benemann, J. R. & Oswald, W. J. 1996 *Systems and Economic Analysis of Microalgae Ponds for Conversion of CO₂ to Biomass*. Final report. California University, Department of Civil Engineering, Berkeley, CA, USA. <https://www.osti.gov/biblio/493389> (accessed 3 December 2019).
- Besson, A. & Guiraud, P. 2013 High-pH-induced flocculation-flotation of the hypersaline microalga *Dunaliella salina*. *Bioresource Technology* **147**, 464–470.
- Besson, A., Formosa-Dague, C. & Guiraud, P. 2019 Flocculation-flotation harvesting mechanism of *Dunaliella salina*: from nanoscale interpretation to industrial optimization. *Water Research* **155**, 352–361.
- Bilanovic, D., Shelef, G. & Sukenik, A. 1988 Flocculation of microalgae with cationic polymers – effects of medium salinity. *Biomass* **17** (1), 65–76.
- Blanc, G., Agarkova, I., Grimwood, J., Kuo, A., Brueggeman, A., Dunigan, D. D., Gurnon, J., Ladunga, I., Lindquist, E., Lucas, S., Pangilinan, J., Pröschold, T., Salamov, A., Schmutz, J., Weeks, D., Yamada, T., Lomsadze, A., Borodovsky, M., Claverie, J.-M., Grigoriev, I. V. & Van Etten, J. L. 2012 The genome of the polar eukaryotic microalga *Coccomyxa subellipsoidea* reveals traits of cold adaptation. *Genome Biology* **13** (5), R39.
- Blockx, J., Verfaillie, A., Thielemans, W. & Muylaert, K. 2018 Unravelling the mechanism of chitosan-driven flocculation of microalgae in seawater as a function of pH. *ACS Sustainable Chemistry & Engineering* **6** (9), 11273–11279.
- Blockx, J., Verfaillie, A., Eyley, S., Deschaume, O., Bartic, C., Muylaert, K. & Thielemans, W. 2019 Cationic cellulose nanocrystals for flocculation of microalgae: effect of degree of substitution and crystallinity. *ACS Applied Nano Materials* **2** (6), 3394–3403.
- Bolto, B. & Gregory, J. 2007 Organic polyelectrolytes in water treatment. *Water Research* **41** (11), 2301–2324.
- Brennan, L. & Owende, P. 2010 Biofuels from microalgae – a review of technologies for production, processing, and extractions of biofuels and co-products. *Renewable and Sustainable Energy Reviews* **14** (2), 557–577.
- Chisti, Y. 2007 Biodiesel from microalgae. *Biotechnology Advances* **25** (3), 294–306.
- Coward, T., Lee, J. G. M. & Caldwell, G. S. 2015 The effect of bubble size on the efficiency and economics of harvesting microalgae by foam flotation. *Journal of Applied Phycology* **27** (2), 733–742.
- Cui, Y., Yuan, W. & Cheng, J. 2014 Understanding pH and ionic strength effects on aluminum sulfate-induced microalgae flocculation. *Applied Biochemistry and Biotechnology* **173** (7), 1692–1702.
- Daboussi, F., Leduc, S., Maréchal, A., Dubois, G., Guyot, V., Perez-Michaut, C., Amato, A., Falcitore, A., Juillerat, A., Beurdeley, M., Voytas, D. F., Cavarec, L. & Duchateau, P. 2014 Genome engineering empowers the diatom *Phaeodactylum tricornutum* for biotechnology. *Nature Communications* **5** (1), 1–7.
- Davies, D. R. & Plaskitt, A. 1971 Genetical and structural analyses of cell-wall formation in *Chlamydomonas reinhardtii*. *Genetics Research* **17** (1), 33–43.
- Dequin, S. 2001 The potential of genetic engineering for improving brewing, wine-making and baking yeasts. *Applied Microbiology and Biotechnology* **56** (5), 577–588.
- Díaz-Santos, E., Vila, M., de la Vega, M., León, R. & Vígara, J. 2015 Study of bioflocculation induced by *Saccharomyces bayanus* var. *uvarum* and flocculating protein factors in microalgae. *Algal Research* **8**, 23–29.
- Díaz-Santos, E., Vila, M., Vígara, J. & León, R. 2016 A new approach to express transgenes in microalgae and its use to increase the flocculation ability of *Chlamydomonas reinhardtii*. *Journal of Applied Phycology* **28** (3), 1611–1621.
- Dismukes, G. C., Carrieri, D., Bennette, N., Ananyev, G. M. & Posewitz, M. C. 2008 Aquatic phototrophs: efficient alternatives to land-based crops for biofuels. *Current Opinion in Biotechnology* **19** (3), 235–240.
- Dunahay, T. G., Jarvis, E. E., Dais, S. S. & Roessler, P. G. 1996 Manipulation of microalgal lipid production using genetic engineering. *Applied Biochemistry and Biotechnology* **57** (1), 223.
- Fan, J., Zheng, L., Bai, Y., Saroussi, S. & Grossman, A. R. 2017 Flocculation of *Chlamydomonas reinhardtii* with different phenotypic traits by metal cations and high pH. *Frontiers in Plant Science* **8**. <https://www.frontiersin.org/articles/10.3389/fpls.2017.01997/full> (accessed 20 November 2019).
- Formosa-Dague, C., Gernigon, V., Castelain, M., Daboussi, F. & Guiraud, P. 2018 Towards a better understanding of the flocculation/flotation mechanism of the marine microalgae *Phaeodactylum tricornutum* under increased pH using atomic force microscopy. *Algal Research* **33**, 369–378.
- Garg, S., Li, Y., Wang, L. & Schenk, P. M. 2012 Flotation of marine microalgae: effect of algal hydrophobicity. *Bioresource Technology* **121**, 471–474.
- Georgianna, D. R. & Mayfield, S. P. 2012 Exploiting diversity and synthetic biology for the production of algal biofuels. *Nature* **488** (7411), 329–335.
- Golueke, C. G. & Oswald, W. J. 1965 Harvesting and processing sewage-grown planktonic algae. *Journal – Water Pollution Control Federation* **37** (4), 471–498.
- Goossens, K. V., Stassen, C., Stals, I., Donohue, D. S., Devreese, B., De Greve, H. & Willaert, R. G. 2011 The N-terminal domain of the Flo1 flocculation protein from *Saccharomyces cerevisiae* binds specifically to mannose carbohydrates. *Eukaryotic Cell* **10** (1), 110–117. <https://ec.asm.org/content/10/1/110.short> (accessed 20 March 2020).
- Hansel, P. A., Guy Riefler, R. & Stuart, B. J. 2014 Efficient flocculation of microalgae for biomass production using cationic starch. *Algal Research* **5**, 133–139.
- Hanumanth Rao, N. R., Yap, R., Whittaker, M., Stuetz, R. M., Jefferson, B., Peirson, W. L., Granville, A. M. & Henderson, R. K. 2018 The role of algal organic matter in the separation of algae and cyanobacteria using the novel ‘Posi’ – dissolved air flotation process. *Water Research* **130**, 20–30.
- Huo, S., Shang, C., Wang, Z., Zhou, W., Cui, F., Zhu, F., Yuan, Z. & Dong, R. 2017 Outdoor growth characterization of an unknown microalga screened from contaminated *Chlorella* culture. *BioMed Research International*.

- <https://www.hindawi.com/journals/bmri/2017/5681617/> (accessed 19 March 2020).
- Jagadevan, S., Banerjee, A., Banerjee, C., Guria, C., Tiwari, R., Baweja, M. & Shukla, P. 2018 Recent developments in synthetic biology and metabolic engineering in microalgae towards biofuel production. *Biotechnology for Biofuels* **11**. <https://www.ncbi.nlm.nih.gov/pmc/articles/PMC6026345/> (accessed 15 October 2018).
- Kawaroe, M., Prartono, T., Sunuddin, A. & Saputra, D. 2016 Marine microalgae *Tetraselmis suecica* as flocculant agent of bio-flocculation method. *HAYATI Journal of Biosciences* **23** (2), 62–66.
- Kurniawati, H. A., Ismadji, S. & Liu, J. C. 2014 Microalgae harvesting by flotation using natural saponin and chitosan. *Bioresource Technology* **166**, 429–434.
- Lam, M. K. & Lee, K. T. 2012 Microalgae biofuels: a critical review of issues, problems and the way forward. *Biotechnology Advances* **30** (3), 673–690.
- † Lam, G. P., Vermuë, M. H., Olivieri, G., van den Broek, L. A. M., Barbosa, M. J., Eppink, M. H. M., Wijffels, R. H. & Kleinegris, D. M. M. 2014 Cationic polymers for successful flocculation of marine microalgae. *Bioresource Technology* **169**, 804–807.
- Lananan, F., Mohd Yunos, F. H., Mohd Nasir, N., Abu Bakar, N. S., Lam, S. S. & Jusoh, A. 2016 Optimization of biomass harvesting of microalgae, *Chlorella* sp. utilizing auto-flocculating microalgae, *Ankistrodesmus* sp. as bio-flocculant. *International Biodeterioration & Biodegradation* **113**, 391–396.
- Lee, A. K., Lewis, D. M. & Ashman, P. J. 2009 Microbial flocculation, a potentially low-cost harvesting technique for marine microalgae for the production of biodiesel. *Journal of Applied Phycology* **21** (5), 559–567.
- Lee, J., Cho, D.-H., Ramanan, R., Kim, B.-H., Oh, H.-M. & Kim, H.-S. 2013 Microalgae-associated bacteria play a key role in the flocculation of *Chlorella vulgaris*. *Bioresource Technology* **131**, 195–201.
- León, R. & Fernández, E. 2007 Nuclear transformation of eukaryotic microalgae. In: *Transgenic Microalgae as Green Cell Factories*. *Advances in Experimental Medicine and Biology* (R. León, A. Galván & E. Fernández, eds). Springer, New York, USA, pp. 1–11. https://doi.org/10.1007/978-0-387-75532-8_1 (accessed 18 March 2020).
- Levy, N., Magdassi, S. & Bar-Or, Y. 1992 Physico-chemical aspects in flocculation of bentonite suspensions by a cyanobacterial bioflocculant. *Water Research* **26** (2), 249–254.
- Liao, J. C., Mi, L., Pontrelli, S. & Luo, S. 2016 Fuelling the future: microbial engineering for the production of sustainable biofuels. *Nature Reviews Microbiology* **14** (5), 288–304.
- Luo, S., Wu, X., Jiang, H., Yu, M., Liu, Y., Min, A., Li, W. & Ruan, R. 2019 Edible fungi-assisted harvesting system for efficient microalgae bio-flocculation. *Bioresource Technology* **282**, 325–330.
- Markou, G. & Nerantzis, E. 2013 Microalgae for high-value compounds and biofuels production: a review with focus on cultivation under stress conditions. *Biotechnology Advances* **31** (8), 1532–1542.
- Miki, B. L., Poon, N. H., James, A. P. & Seligy, V. L. 1982 Possible mechanism for flocculation interactions governed by gene FLO1 in *Saccharomyces cerevisiae*. *Journal of Bacteriology* **150** (2), 878–889.
- Minhas, A. K., Hodgson, P., Barrow, C. J. & Adholeya, A. 2016 A review on the assessment of stress conditions for simultaneous production of microalgal lipids and carotenoids. *Frontiers in Microbiology* **7**. <http://www.ncbi.nlm.nih.gov/pmc/articles/PMC4853371/> (accessed 22 June 2016).
- Molina Grima, E., Belarbi, E.-H., Ación Fernández, F. G., Robles Medina, A. & Chisti, Y. 2003 Recovery of microalgal biomass and metabolites: process options and economics. *Biotechnology Advances* **20** (7–8), 491–515.
- Muylaert, K., Vandamme, D., Foubert, I. & Brady, P. V. 2015 Harvesting of microalgae by means of flocculation. In: *Biomass and Biofuels from Microalgae: Advances in Engineering and Biology*. *Biofuel and Biorefinery Technologies* (N. R. Moheimani, M. P. McHenry, K. de Boer & P. A. Bahri, eds). Springer International Publishing, Cham, Switzerland, pp. 251–273. https://doi.org/10.1007/978-3-319-16640-7_12 (accessed 18 November 2019).
- Ndikubwimana, T., Zeng, X., He, N., Xiao, Z., Xie, Y., Chang, J.-S., Lin, L. & Lu, Y. 2015 Microalgae biomass harvesting by bioflocculation-interpretation by classical DLVO theory. *Biochemical Engineering Journal* **101**, 160–167.
- Ndikubwimana, T., Chang, J., Xiao, Z., Shao, W., Zeng, X., Ng, I.-S. & Lu, Y. 2016 Flotation: a promising microalgae harvesting and dewatering technology for biofuels production. *Biotechnology Journal* **11** (3), 315–326.
- Oh, H. M., Lee, S. J., Park, M. H., Kim, H. S., Kim, H. C., Yoon, J. H., Kwon, G. S. & Yoon, B. D. 2001 Harvesting of *Chlorella vulgaris* using a bioflocculant from *Paenibacillus* sp. AM49. *Biotechnology Letters* **23** (15), 1229–1234.
- Pahl, S. L., Lee, A. K., Kalaitzidis, T., Ashman, P. J., Sathe, S. & Lewis, D. M. 2013 Harvesting, thickening and dewatering microalgae biomass. In: *Algae for Biofuels and Energy*. *Developments in Applied Phycology* (M. A. Borowitzka & N. R. Moheimani, eds). Springer Netherlands, Dordrecht, The Netherlands, pp. 165–185. https://doi.org/10.1007/978-94-007-5479-9_10 (accessed 9 December 2019).
- Pal, S., Mal, D. & Singh, R. P. 2005 Cationic starch: an effective flocculating agent. *Carbohydrate Polymers* **59** (4), 417–425.
- Phoochinda, W. & White, D. A. 2003 Removal of algae using froth flotation. *Environmental Technology* **24** (1), 87–96.
- Pragya, N., Pandey, K. K. & Sahoo, P. K. 2013 A review on harvesting, oil extraction and biofuels production technologies from microalgae. *Renewable and Sustainable Energy Reviews* **24**, 159–171.
- Renault, F., Sancey, B., Badot, P.-M. & Crini, G. 2009 Chitosan for coagulation/flocculation processes – an eco-friendly approach. *European Polymer Journal* **45** (5), 1337–1348.
- Riglar, D. T. & Silver, P. A. 2018 Engineering bacteria for diagnostic and therapeutic applications. *Nature Reviews Microbiology* **16** (4), 214–225.

- Rismani-Yazdi, H., Haznedaroglu, B. Z., Bibby, K. & Peccia, J. 2011 Transcriptome sequencing and annotation of the microalgae *Dunaliella tertiolecta*: pathway description and gene discovery for production of next-generation biofuels. *BMC Genomics* **12** (1), 148.
- Ritthidej, G. C. 2011 Nasal delivery of peptides and proteins with chitosan and related mucoadhesive polymers. In: *Peptide and Protein Delivery* (C. Van Der Walle, ed.). Academic Press, Boston, MA, USA, pp. 47–68. <http://www.sciencedirect.com/science/article/pii/B9780123849359100033> (accessed 22 July 2019).
- Rodolfi, L., Chini Zittelli, G., Bassi, N., Padovani, G., Biondi, N., Bonini, G. & Tredici, M. R. 2009 Microalgae for oil: strain selection, induction of lipid synthesis and outdoor mass cultivation in a low-cost photobioreactor. *Biotechnology and Bioengineering* **102** (1), 100–112.
- Salim, S., Bosma, R., Vermuë, M. H. & Wijffels, R. H. 2011 Harvesting of microalgae by bio-flocculation. *Journal of Applied Phycology* **23** (5), 849–855.
- Salim, S., Vermuë, M. H. & Wijffels, R. H. 2012 Ratio between autoflocculating and target microalgae affects the energy-efficient harvesting by bio-flocculation. *Bioresource Technology* **118**, 49–55.
- Salim, S., Kosterink, N. R., Tchetskoua Wacka, N. D., Vermuë, M. H. & Wijffels, R. H. 2014 Mechanism behind autoflocculation of unicellular green microalgae *Ettlia texensis*. *Journal of Biotechnology* **174**, 34–38.
- Scholz, M., Hoshino, T., Johnson, D., Riley, M. R. & Cuello, J. 2011 Flocculation of wall-deficient cells of *Chlamydomonas reinhardtii* mutant cw15 by calcium and methanol. *Biomass and Bioenergy* **35** (12), 4835–4840.
- Spilling, K., Seppala, J. & Tamminen, T. 2011 Inducing autoflocculation in the diatom *Phaeodactylum tricornutum* through CO₂ regulation. *Journal of Applied Phycology* **23** (6), 959–966.
- Stratford, M. 1994 Genetic aspects of yeast flocculation: in particular, the role of FLO genes in the flocculation of *Saccharomyces cerevisiae*. *Colloids and Surfaces B: Biointerfaces* **2** (1), 151–158.
- Sukenik, A. & Shelef, G. 1984 Algal autoflocculation–verification and proposed mechanism. *Biotechnology and Bioengineering* **26** (2), 142–147.
- Sukenik, A., Schröder, W., Lauer, J., Shelef, G. & Soeder, C. J. 1985 Coprecipitation of microalgal biomass with calcium and phosphate ions. *Water Research* **19** (1), 127–129.
- Uduman, N., Qi, Y., Danquah, M. K., Forde, G. M. & Hoadley, A. 2010 Dewatering of microalgal cultures: a major bottleneck to algae-based fuels. *Journal of Renewable and Sustainable Energy* **2** (1), 012701.
- Vandamme, D., Foubert, I. & Muylaert, K. 2013 Flocculation as a low-cost method for harvesting microalgae for bulk biomass production. *Trends in Biotechnology* **31** (4), 233–239.
- Vandamme, D., Pohl, P. I., Beuckels, A., Foubert, I., Brady, P. V., Hewson, J. C. & Muylaert, K. 2015 Alkaline flocculation of *Phaeodactylum tricornutum* induced by brucite and calcite. *Bioresource Technology* **196**, 656–661.
- Weiter, L., Rajamanickam, V. & Herwig, C. 2018 The filamentous fungal pellet – relationship between morphology and productivity. *Applied Microbiology and Biotechnology* **102** (7), 2997–3006.
- Vergnes, J. B., Gernigon, V., Guiraud, P. & Formosa-Dague, C. 2019 Bicarbonate concentration induces production of exopolysaccharides by *Arthrospira platensis* that mediate bioflocculation and enhance flotation harvesting efficiency. *ACS Sustainable Chemistry & Engineering* **7** (16), 13796–13804.
- Waltz, E. 2009 Biotech's green gold? *Nature Biotechnology* **27** (1), 15–18.
- Wan, C., Zhao, X.-Q., Guo, S.-L., Asrafal Alam, M. & Bai, F.-W. 2013 Bioflocculant production from *Solibacillus silvestris* W01 and its application in cost-effective harvest of marine microalga *Nannochloropsis oceanica* by flocculation. *Bioresource Technology* **135**, 207–212.
- Xie, S., Sun, S., Dai, S. Y. & Yuan, J. 2013 Efficient coagulation of microalgae in cultures with filamentous fungi. *Algal Research* **2** (1), 28–33.
- Xu, Y., Purton, S. & Baganz, F. 2013 Chitosan flocculation to aid the harvesting of the microalga *Chlorella sorokiniana*. *Bioresource Technology* **129**, 296–301.
- Yang, C., Dabros, T., Li, D., Czarnecki, J. & Masliyah, J. H. 2001 Measurement of the zeta potential of gas bubbles in aqueous solutions by microelectrophoresis method. *Journal of Colloid and Interface Science* **243** (1), 128–135.
- Zhang, J. & Hu, B. 2012 A novel method to harvest microalgae via co-culture of filamentous fungi to form cell pellets. *Bioresource Technology* **114**, 529–535.
- Zhang, X., Zhao, X., Wan, C., Chen, B. & Bai, F. 2016 Efficient biosorption of cadmium by the self-flocculating microalga *Scenedesmus obliquus* AS-6-1. *Algal Research* **16**, 427–433.
- Zheng, H., Gao, Z., Yin, J., Tang, X., Ji, X. & Huang, H. 2012 Harvesting of microalgae by flocculation with poly (γ -glutamic acid). *Bioresource Technology* **112**, 212–220.
- Zhou, W., Cheng, Y., Li, Y., Wan, Y., Liu, Y., Lin, X. & Ruan, R. 2012 Novel fungal pelletization-assisted technology for algae harvesting and wastewater treatment. *Applied Biochemistry and Biotechnology* **167** (2), 214–228.
- Zhou, W., Min, M., Hu, B., Ma, X., Liu, Y., Wang, Q., Shi, J., Chen, P. & Ruan, R. 2013 Filamentous fungi assisted bio-flocculation: a novel alternative technique for harvesting heterotrophic and autotrophic microalgal cells. *Separation and Purification Technology* **107**, 158–165.
- Ziolkowska, J. R. 2014 Prospective technologies, feedstocks and market innovations for ethanol and biodiesel production in the US. *Biotechnology Reports* **4**, 94–98.

First received 9 December 2019; accepted in revised form 2 April 2020. Available online 15 April 2020

2.2. The contribution of Atomic Force Microscopy (AFM) in microalgae studies: A review



Irem Demir-Yilmaz, Pascal Guiraud and Cécile Formosa-Dague

Algal research 60 (2021): 102506

Abstract

Background: Atomic Force Microscopy (AFM) has been extensively used these recent years to study biological samples in living conditions. Researchers take advantages of its nanoscale resolution imaging capacities and ability to record piconewton scale forces to gain insights into the topography, nanomechanical properties and molecular interactions of cells with their surroundings.

Scope of the review: Microalgae are unique microorganisms able to convert light, water and inorganic nutrients into a biomass rich in value-added products such as proteins, polysaccharides, or lipids. For this reason, they have attracted a great interest from a biotechnological point of view. Although AFM has shown to be a powerful tool for microbiology research throughout the years, its application to microalgae research is still limited. First in this review, we go through the basics of AFM and the various ways it may be used to characterize cells. The use of AFM in understanding the effects of environmental variables and external stress on microalgae cells is described in the second section. Finally, we illustrate how AFM may be used to investigate how microalgae interact with their environment, and how such fundamental research can be used to improve microalgae production systems.

Major conclusions: These bibliography work shows the potential of this technology in answering fundamental questions about the interfaces of microalgae cells, the impact of environmental or stress conditions on their nanoscale features, and microalgae interacting characteristic with their environment. To fully exploit the potential of microalgae at industrial scales, as well as create and optimize the various steps involved in production systems such as production, harvesting or extraction, such fundamental knowledge must be acquired.



The contribution of Atomic Force Microscopy (AFM) in microalgae studies: A review

Irem Demir-Yilmaz^{a,b}, Pascal Guiraud^a, Cécile Formosa-Dague^{a,*}

^a TBI, Université de Toulouse, CNRS, INRAE, INSA, Toulouse, France

^b LAAS, Université de Toulouse, CNRS, Toulouse, France

ARTICLE INFO

Keywords:

Atomic force microscopy
Microalgae
Cell nanostructure
Nanomechanics
Interactions

ABSTRACT

Atomic force microscopy (AFM) has now become a major technology to study single cells in living conditions. It provides nanoscale resolution imaging capacities and is a sensitive force machine able to record piconewton-scale forces, thereby making it possible to gain insights into the nanomechanical properties and molecular interactions of cells. While an extensive number of studies on microorganisms have demonstrated the potential of AFM to understand complex phenomena at cell's interfaces, its use in microalgae studies remains limited. These recent years, microalgae have been the subject of a significant number of fundamental studies notably because of their capacity to convert light, water and inorganic nutrients into a biomass resource rich in value-added products. The existing literature reporting AFM use to understand microalgae cell morphology, their nanomechanical properties or their interactions with their environment give a large overview of the contribution AFM can bring into microalgae studies. In this review, we will first present the principles of AFM and the different possibilities it offers to characterize cells. Then in a second part, the contribution of AFM to understand the effects of environmental conditions and external stress on microalgae cells will be discussed. Finally, we will show how AFM can be used to probe the interactions of microalgae with their environment and how such fundamental studies can represent a basis to improve microalgae production systems. Overall, this review, the first on this topic, aims to highlight the opportunities that AFM technology can bring to this field of research.

1. Introduction

Microalgae are unique microorganisms able to convert light, water and inorganic nutrients into a biomass rich in value-added products such as proteins, polysaccharides, or lipids [1,2]. For this reason they have a great interest from a biotechnological point of view, and microalgae are nowadays cultivated and exploited in large-scale production systems [3]. But despite the promises of this resource, at the moment, exploiting the potential of microalgae at the industrial scale faces several challenges linked to the different steps of microalgae production (biomass growth, harvesting and down-stream extraction processes), that have made its development for the moment economically unviable [4]. Meeting these challenges has motivated a number of basic research studies aiming at answering fundamental questions on microalgae's cell physiology, on their response to different environments, on how to harvest them, disrupt them, or on how to enhance their potential through genetic engineering. It is indeed through the comprehension of these questions that it will be possible to find solutions to exploit

microalgae at the industrial scale in a cost-effective way.

Basic research on microalgae has started as early as 1960, but it is really at the beginning of the years 2000s that the number of research publications has started to become significant. The graph presented in Fig. 1 shows the number of studies on microalgae referenced by the Scopus database since 1960 (grey curve); each year the number of studies published on the topic increases, up to more than 3500 publications produced in 2020. This increasing number of publications clearly demonstrates the growing interest of scientists for these microorganisms and the need for more basic research on microalgae. Compared to other microorganisms, however these numbers remain quite low; for instance the search "bacteria" retrieves more than 69,000 publications only for the year 2020; the microalgae field can still be considered as an emerging field of research. Traditionally, microalgae are mainly studied using molecular biology and genetic approaches, or chemical engineering approaches. Regarding cell imaging, optical and electron microscopy remain the gold standards techniques [5-7], although, a small, but significant number of studies also use other type

* Corresponding author.

E-mail address: formosa@insa-toulouse.fr (C. Formosa-Dague).

<https://doi.org/10.1016/j.algal.2021.102506>

Received 9 July 2021; Received in revised form 6 September 2021; Accepted 19 September 2021

Available online 28 September 2021

2211-9264/© 2021 Elsevier B.V. All rights reserved.

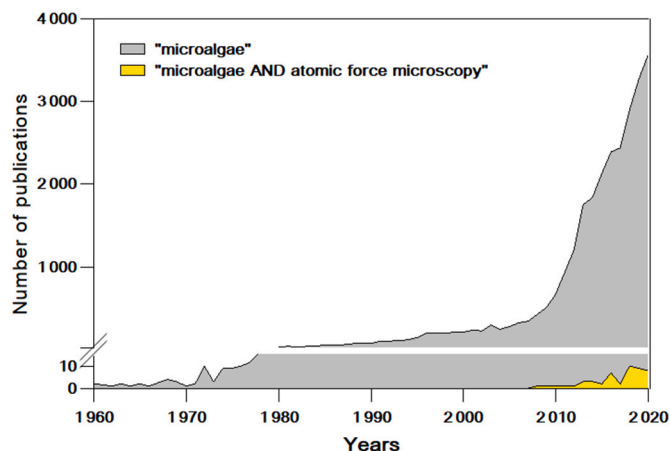


Fig. 1. Microalgae studies published since 1960. Graphic representing the number of publications retrieved by entering the search “microalgae” (grey) or by entering the search “microalgae AND atomic force microscopy” (yellow) in the Scopus database (search within article titles, abstracts and keywords), from 1960 to 2020. (For interpretation of the references to colour in this figure legend, the reader is referred to the web version of this article.)

of microscopies such as atomic force microscopy (AFM).

AFM, first developed in 1986 [8], relies on the control of a force acting between a sharp tip and a surface, while scanning a sample. This method is thus a surface probing method, making it different from other types of microscopies such as electron or optical microscopies. As the tip scans the surface of the sample, the cantilever on which it is fixed gets deflected. This deflection is recorded thanks to a laser reflected on a photodiode, thereby allowing to collect the signal (Fig. 2) [9]. This technology is particularly well suited for the study of microorganisms under living conditions, as it has high-resolution imaging capacities, down to the nanometer scale, and is able to operate in liquid [10]. However, the potential of AFM does not limit to imaging; AFM is also a highly sensitive force machine, able to record forces as small as 20 pN. Indeed, AFM, in force spectroscopy mode, can record force-distance curves, where the force experienced by the probe is plotted as a function of the probe-sample separation distance. These curves can then be interpreted through different physical models, thereby giving access to the nanomechanical and nanoadhesive properties of cell surfaces [10]. An important asset of AFM is that these quantified forces can be simultaneously localized at the surface of cells, which thus allows to

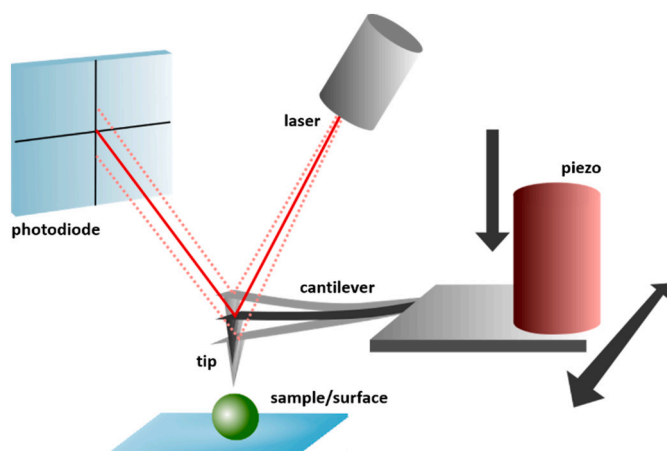


Fig. 2. Atomic force microscopy principle. A sharp tip mounted on a cantilever can move in the x, y and z direction thanks to a piezo-electric ceramic. While scanning the sample, the deflection of the cantilever is recorded thanks to a laser reflected on a photodiode. Adapted from [15,9].

correlate nanomechanics and molecular interactions with cell’s surface ultrastructures [11]. Finally, the tips used for AFM imaging or force spectroscopy can be functionalized with living cells [12], biomolecules [13] or inert particles [14], which opens up new avenues to probe specific interactions between these functionalized tips and cell surfaces.

While AFM has demonstrated over the years to be a powerful tool for microbiology studies [15,16], its use to study microalgae still remains limited; as presented in Fig. 1 (yellow curve), the total number of microalgae studies using AFM is of 49, which represents 0.17% of the total number of microalgae studies. Nevertheless, as for bacteria or yeasts, this technology could bring unique opportunities to understand cells, their morphology, their nanomechanical properties, their interactions with their environment, but also their response to different conditions such as environmental stress. In this work, we review the different studies where AFM was used as a principal tool to study microalgae cells; through these studies, we will describe the different possibilities of this technology, and the significant impact it can have on this field of research.

2. AFM as a tool to characterize microalgae cells

2.1. Imaging of microalgae cells with nanoscale resolution

One of the attractive advantages of AFM over other nanoscale microscopies is its ability to operate in liquid, which makes it possible to monitor live cells in real time. This provides the opportunity for direct visualization of cell surface morphology in physiologically relevant conditions. Different AFM modes can be used to image cell surfaces; contact mode or oscillating mode. In contact mode, the tip is in direct contact with the sample and scans it while maintaining the force constant. Although this allows providing high resolution images, in the case of soft samples, it is possible that the AFM tip deforms the surface during the scan, which may result in topographic images poorly associated with the deviations in height across the sample. In oscillating mode, the tip is oscillated near to its resonance frequency while scanning over the sample; the change in the oscillation amplitude reports on the surface topography. In this mode the tip is not in contact with the sample which reduces significantly the lateral forces that exist in contact mode. However in the case of biological samples with high electrolyte concentrations, interactions of the tip with low-range surface forces can impact the vibrating tip along its trajectory and modify the oscillation amplitude, which can result in sample deformation [17]. In the case of microalgae, contact mode is the principal imaging mode that has been used to characterize the morphology of cells. The first AFM images of diatoms were realized in 2001, where the nanostructure of the silica-based cell wall (valve or frustule) of live *Pinnularia viridis* (Nitzsch) Ehrenberg cells, was investigated [18]. In this study, the authors could show thanks to high-resolution images that the cell wall was coated with a thick mucilaginous material. In addition, imaging of the cell’s valves revealed silica nanostructures composed of conglomerates of packed silica spheres of approximately 45 nm of diameter. Later on in 2002, the same team also imaged the nanostructures present on the valve’s surface of the diatom *Craspedostauros australis*, showing pores and rows in the girdle band region that forms the connecting region where the two valves of the diatom overlap. Then in 2003, the team of Gebeshuber and coworkers imaged the frustules of benthic freshwater diatom species, and could reveal the presence of an organic case enveloping the cells of approximately 10 nm of thickness [19]. Later in 2008, Francius and coworkers also used contact mode to image the three different morphotypes of the diatom *Phaeodactylum tricoratum* (fusiform, triradiate and oval, Fig. 3A) [20]. Notably, the authors extracted quantitative information on the roughness of the cell surfaces thanks to high-resolution images and showed that the cell surface in the oval form is rougher than for the other two morphologies, which can be explained by the presence in this morphotype of excreted polymers on the surface. Finally, another team used contact mode to image the diatom species

Cylindrotheca closterium (Fig. 3B) and *Cylindrotheca fusiform*. The images produced in this case in air could show the morphological details of cells, such as girdle bands, raphe openings (siliceous structures present on the valve, which have slits running the longitudinal axis of the cell) or fibulae (silica arches that connect the raphe strips that border the raphe slit) (Fig. 3B) [21,22]. Diatoms constitute an interesting group of microalgae, notably because of the large diversity of shapes and nanostructures present on the valves of these cells, which have been so far mostly explored using electron microscopy [23]. These studies show that AFM is also a suitable technique to characterize these morphologies, with the advantages of requiring minimum sample preparation compared to electron microscopy, as cells can be directly observed without any treatment. In addition, AFM imaging can also reveal the presence of organic layers around the cells, or polymers or mucilages, which can have important implications in the adhesive behavior of cells or in their mobility. While these studies are focused on diatoms, other microalgae species have also been imaged using AFM, such as *Ventricaria ventricosa* [24], *C. vulgaris* [25], or *Dunaliella tertiolecta* [26].

In addition to whole cells, AFM has also been used to visualize substances produced by microalgae, such as exopolysaccharides (EPS). EPS are complex polymers composed mainly of polysaccharides, that can also contain other components, for example protein moieties [27]. They have attracted a lot of interest because of their potential for industrial applications in food and health [28], and for these reasons they have been the focus of many studies, most of them dedicated to their chemical analysis by chromatography, mass spectrometry or nuclear magnetic resonance (NMR), among other techniques [27]. However, understanding EPS nanostructure thanks to AFM can also bring valuable information to further use them in specific applications. In this view, a study conducted by Cybulska and coworkers used AFM to characterize the EPS produced by the green microalgae *Dictyosphaerium chlorelloides*

[29]. For that, the authors analyzed two different concentrations of the material, and showed that EPS formed a regular and porous matrix at higher concentration (1 mg/mL), whereas at low concentration (10 µg/mL), single molecules created a regular network containing interconnected polymers with numerous side chains and loops. Such findings thus showed that at high concentration, thanks to the porosity of the matrix formed, these EPS could for example be used to selectively immobilize particles [29]. In another study conducted in 2020, the EPS produced by *Arthrospira platensis* (Spirulina) were imaged using a force spectroscopy-based AFM imaging mode. In this mode, images are reconstructed by measuring the height of the contact point on force curves acquired on a matrix of points over the sample [30]. This type imaging has the advantage of reducing the lateral forces exerted by the tip in contact mode, where the tip scans laterally the sample while in contact with it. Moreover, force spectroscopy-based AFM imaging mode also offers the possibility to provide information on the nanomechanical and adhesive properties of the cells simultaneously. Using this mode, Vergnes and co-workers could show that the EPS produced by *A. platensis* formed a soft, adhesive gel in the medium surrounding the cells. Thanks to these information, the authors could conclude on the role of these EPS on cell flocculation and thus on the possibility to harvest them [31].

2.2. Probing the nanomechanical properties of microalgae cells

Besides its imaging capacities, AFM, as mentioned in the introduction, can also record forces in force spectroscopy mode, thereby giving access to the nanomechanical properties of cell surfaces, which can be a key aspect to understand fundamental aspects such as cell morphology, or for further microalgae application, for example to optimize cell disruption steps in production systems. For that, nanoindentation

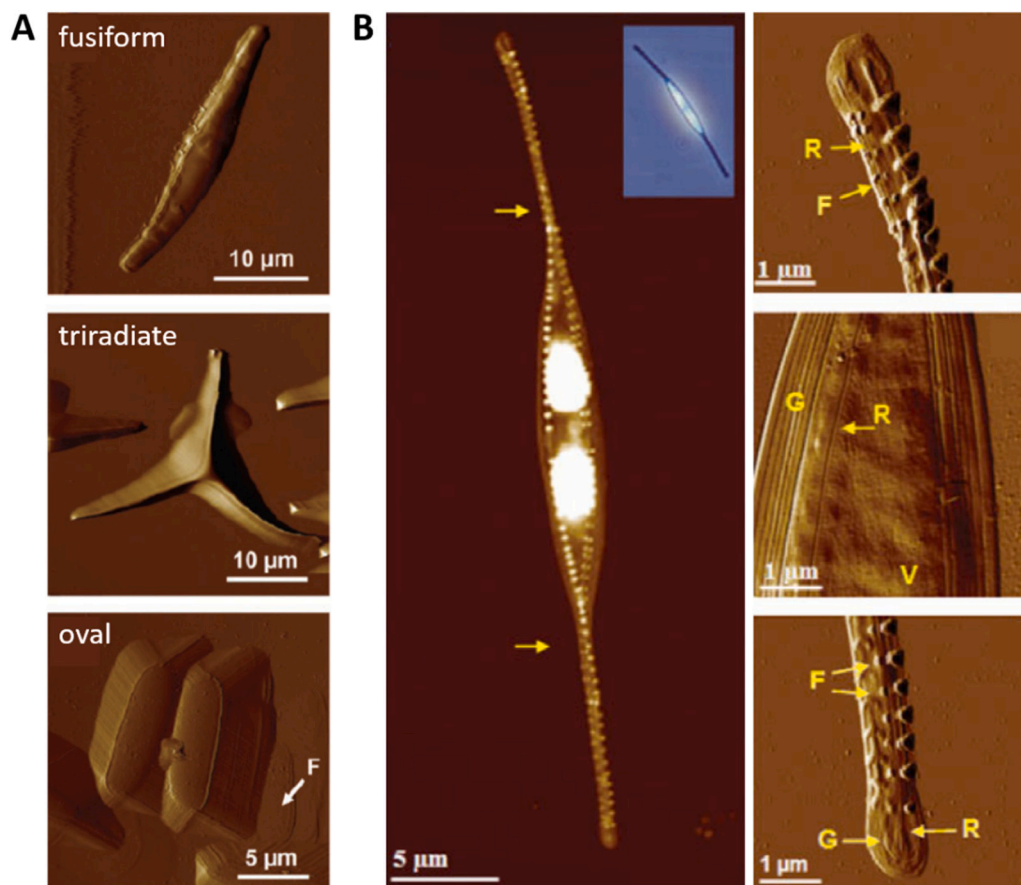


Fig. 3. AFM imaging of diatoms. A) AFM deflection images of the diatom *P. tricorutum* morphotypes; fusiform, triradial and ovoid. B) AFM images of the diatom *C. closterium*. Yellow arrows in the middle image indicate the spiral twist around the longitudinal cell axis. The inset shows a light microscopy image of the live cell. Deflection images (on the right) feature morphological details of cell wall: V, valve; G, girdle band; R, raphe opening; F, fibulae. Reprinted with permission from [20] and [21]. (For interpretation of the references to colour in this figure legend, the reader is referred to the web version of this article.)

measurements are performed, in which a cantilever with known mechanical properties, is pushed against a sample at a defined force. This way, the resistance of the cell wall to the compression can be quantified, by extracting from the force curves obtained the cell wall spring constant (stiffness) or elasticity (Young's modulus, Y_m). These values are obtained by converting the force curves into force vs indentation curves by subtracting the deformation of the cantilever upon compression. Then these curves are analyzed using theoretical models such as the Hooke's law (stiffness), the Hertz model (Y_m), or other appropriate models, depending on the shape of the tip and the type of the sample probed. Such nanomechanical measurements provide important information on the cell wall which is responsible for maintaining cell morphology, and which represents its interface with the surrounding environment. Notably it has been shown in multiple studies on different microorganisms that both the shape of the cells and the external conditions that cells undergo can greatly influence the cell wall nanomechanics [32,33,15]. For instance, in the study conducted by Francius *et al.*, the

authors also explored the nanomechanical properties of the three morphotypes of *P. tricorutum* using AFM force-indentation curves. Their results showed that the young modulus of the cell wall of cells in the oval form is five-fold higher than for the other two morphotypes, which constitute relevant information to gain insight into the mechanism leading to the different *P. tricorutum* morphotypes [20]. With the same species, Formosa-Dague and co-workers in 2018 showed that the elasticity of the cell wall changes depending on the pH of the surrounding medium. Nanoindentation measurements performed in this study showed that the AFM tip was able to indent deeper into the cell wall at pH 8 than at pH 10; indeed, the cell wall Y_m increased sevenfold at pH 10 (Fig. 4A) [14]. The same tendency was also observed in *Chlorella vulgaris* cells, a freshwater green microalgae species, where an increase of the pH from 6 to 8 resulted in a threefold increase of the rigidity of the cell wall of cells (Fig. 4B) [25]. Changes in the nanomechanics of the cell wall often reflect changes in its composition or in its architecture, which can affect both the interactions of cells with their environment, as well

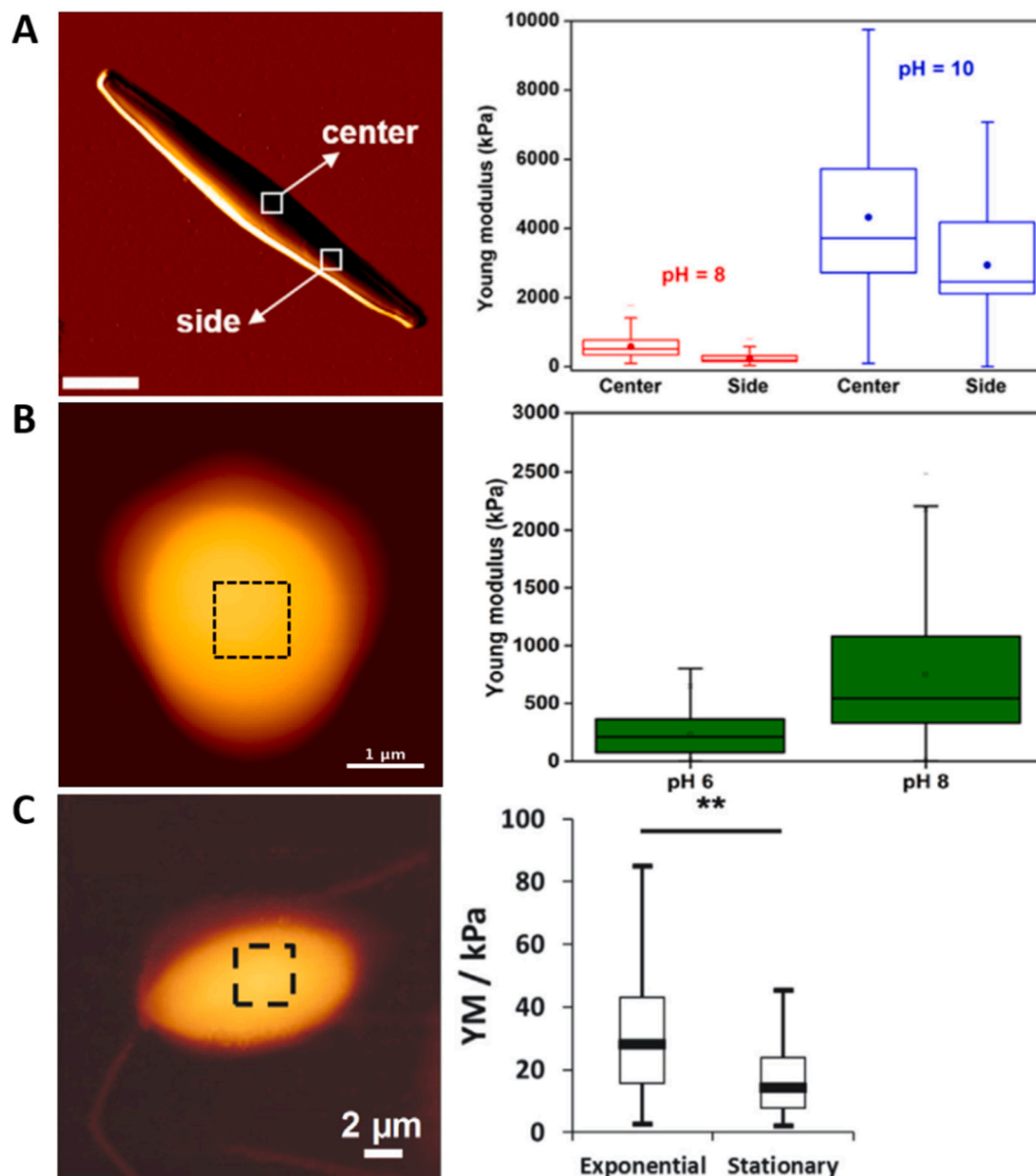


Fig. 4. Nanomechanical properties of microalgae probed by AFM. A) AFM vertical deflection image of a *P. tricorutum* cell and box plot showing the distribution of Y_m values obtained from force curves recorded on the center or on the side of cells at pH 8 or pH 10. B) AFM height image of a *C. vulgaris* cell and box plot showing the distribution of Y_m values measured on top of cells at pH 6 and 8. C) AFM height image of a *D. tertiolecta* cell in stationary phase and box plot showing the distribution of Y_m values recorded on top of cells in exponential phase and stationary phase. Reprinted with permission from [14,25,26].

as their shapes and deformability. For instance in the case of *P. tricorutum*, the important increase of the rigidity of cell's cell wall at pH 10 has been associated with a better separation from water by flotation, possibly due to a better interaction between rigid fusiform cells with bubbles [14]. Another study conducted by Pillet and co-workers investigated the nanomechanical properties of *Dunaliella tertiolecta* in different phases of culture (exponential and stationary) [26]. In this case, the interesting point is that *D. tertiolecta* cells lacks a rigid cell wall and is instead enclosed in a thin plasma membrane covered by a mucous layer. Compared to other microalgae species, the resulting elasticity of cells was quite low, of 25 kPa approximately, compared to *P. tricorutum* cells for which elasticities of 100–500 kPa have been found [20,14]. The authors found that cells in stationary phase were even softer, with a Y_m reduced by 40% compared to exponential phase, suggesting a molecular remodeling of the cell envelope upon aging (Fig. 4C) [26]. Finally, as a last example, in a recent work conducted by Xiao *et al.* force spectroscopy experiments were performed directly on the external layers of different microalgae species. The force curves obtained by the authors led them to develop an analysis method based on a multiscale decomposition of derivative force-distance curves to quantify the elastic responses of these layers upon mechanical deformation. This work is interesting notably because thanks to this analysis method, it provides original information on the external layers protecting microalgae from their environment [34].

2.3. Probing the nanoadhesive properties of microalgae cells

While nanomechanical properties of cells are retrieved by analyzing the approach part of force curves obtained in force spectroscopy, a lot of information can also be extracted from the retract parts, *i. e.* when the AFM tip is retracted from the sample to go back to its initial position. As the tip is retracted, if there is an interaction between the tip and a molecule at the surface of the sample, the molecule will unfold until the pulling force becomes stronger than the force of the interaction recorded. At this point, the interaction breaks, which is reflected on the force curve as a retract peak. The force at which the interaction was ruptured then informs about the strength of the interaction between the tip and the sample; the distance from the contact point at which the interaction breaks gives information on the length of the unfolded molecules and thus on their nature. Examples of such analysis have been provided as early as 2002, mainly by two different groups. The group of Gebeshuber and co-workers first investigated the adhesive properties of the freshwater diatom species *Eunotia sudetica*, and more specifically of the adhesive polymer cells produce at their surface to attach to substrates [35]. The force curves the authors recorded in this case showed multiple adhesion peaks with a sawtooth pattern, which they attributed to the successive unbinding of intra-chain loops from the adhesive, or to the successive release of inter-chain bonds holding a cross-linked multi-chain adhesive matrix together. Interestingly, the authors also suggested that these bonds, unfolded by the tip retracting, can rebond after several seconds, meaning that the adhesive is capable of “self-healing”. In a further study in 2003, the same team also demonstrated that compared to a man-made adhesive (sticky tape), the diatom adhesive is more robust in a wet environment as over a period of several hours, no changes in the shape of the force curves recorded were observed [19]. Such experiments allowed to provide molecular scale information on the nanoadhesive properties of diatoms adhesives, useful for example to develop new and more powerful adhesives. In parallel, the group of Higgins *et al.* performed similar experiments on the adhesive mucilage strands secreted at the raphe region of the diatom *C. australis* [36]. In this case also, the authors could determine that the adhesive was very strong, and forces up to 60 nN were needed to break its interactions with the tip. The next year, this same research group compared the interactions obtained with *C. australis* to those obtained with the adhesive excreted at the raphe region of another diatom species, *Pinnularia viridis* [37]. For both species the authors could observe multiple peaks on the

force curves with a sawtooth pattern suggesting here also the successive unbinding of modular domains from the adhesive. In addition, the experiments revealed that the adhesive strands for both species were highly extensible and accumulated to form tethers. In this case also, such information on the molecular adhesive behavior of the polymers produced by cells could result in the development of new strong adhesive. Additionally, such information also informs on the mechanisms involved in cell attachment to a substrate, which allows cells to colonize habitats in natural environments. From a more general perspective, understanding the adhesive properties of microalgae cells thanks to AFM could also help optimizing processes in production systems, for example to control fouling phenomena taking place in bioreactors or at the surface of membranes used for cell separation.

Altogether these studies highlighted here show the potentialities of AFM to describe: (i) the nanoscale morphology of cells or of the EPS they excrete in the medium, (ii) their nanomechanical properties and so the architecture of their cell wall or membrane in different conditions, and (iii) the adhesive properties of polymers cells produce at their surface. The examples chosen here are rather descriptive of the different microalgae models, but they illustrate the potential AFM can have to understand fundamental processes taking place at their interfaces, for example in response to different conditions they experience in production processes or naturally in their environments. In addition, AFM being a label-free technique allowing to characterize samples in relevant environmental conditions, the data generated could be integrated into correlative approaches in order to provide even more encompassing data on microalgae.

3. AFM as a tool to understand the effects of environmental conditions on microalgae cells

3.1. Effects of stress conditions on cells

As the possibilities to use AFM techniques to characterize microalgae cells and their adhesive properties have emerged, more groups have used this technology to understand the effects of specific conditions on microalgae cell's surfaces. This is of particular interest to design efficient microalgae production systems, as for example stress conditions like culture conditions can greatly influence the production of certain molecules by the cells. In this view Yap and coworkers measured the nanomechanical properties of cells from the species *Chlorococcum* sp. in response to nitrogen deprivation [38]. N-deprivation is a proven strategy for inducing triacylglyceride accumulation in microalgae, lipids that can be used for biofuel production for example. The results obtained in this study showed that the Y_m of N-deprived cells (775 kPa) was approximately 30% higher than for N-replete cells (619 kPa). Thanks to TEM analysis of the thickness of the cell wall of cells, the authors suggested that this increase of the Y_m could be directly correlated to an increase in the cell wall thickness in N-deprived conditions. Although these specific culture conditions had an important impact on the cell wall, they did not affect the susceptibility of cells to mechanical rupture, which is an important aspect for the downstream processing of cells and extraction of the lipids. For instance a study by Lee *et al.* used AFM to determine the force needed to rupture cells, by indenting cells with an AFM tip [39]. This way the authors could show that the disruption energy needed varied depending on the location on the cell surface, and was on average of approximately 670 J/kg of dry microalgae biomass. This value is much lower than the one required in existing mechanical cell disruption processes, such as hydrodynamic cavitation, which suggests that more efficient disruption processes could be developed [39]. Later in 2014, another study conducted by Warren *et al.* reported on the nanomechanical properties of *Scenedesmus dimorphus* in an aqueous and in dried state to provide information useful to develop efficient techniques for mechanical cell disruption [40]. Using nanoindentation measurements, the authors showed that the Y_m of cells increased from approximately 2 to 58 MPa from an aqueous state to a dried state, which

can then orientate choices when designing a cell disruption process. Finally, besides biomass production and cell disruption, AFM has also contributed to understand the effects of flocculants used to harvest microalgae on their cell surface. For instance, Landels and co-workers used AFM to image *Chlorella sorokiniana* cells after harvesting by electro-coagulation flotation with $\text{Al}(\text{OH})_3$ used as a metal flocculant. Their results showed cells that were embedded into the $\text{Al}(\text{OH})_3$ hydrogel, which allows understanding how cells interact with the flocculant [41].

3.2. Effects of changes in natural conditions

But in addition to their potential for producing a wide variety of molecules in production systems, microalgae also play a fundamental role in aquatic ecosystems as they are the basis of aquatic food webs, on which many living organisms rely. Therefore understanding the effects of natural conditions is a key aspect. For example, environmental pollutants on microalgae cells is a subject of interest as this is how pollutants can enter food chains, which can be explored thanks to AFM. A first study in 2012 used AFM to investigate the effects of silver nanoparticles, which have toxic effects on algae cells, on the diatoms *C. closterium* and *Cylindrotheca fusiformis* and on their EPS [22]. AFM high-resolution imaging experiments showed that the nanoparticles could penetrate the cell wall through the valve region of cells, and caused local damages inside the cell, notably in the chloroplasts region, without disintegration of the cell wall. In addition, the authors could also show that EPS production increased with nanoparticle exposure, and that the gel-like structure of EPS contained nanoparticles and aggregates of nanoparticles. This was an important finding of this study as the entrapment of these nanoparticles in the EPS produced by cells allows their persistence and accumulation in the water [22]. Then later in 2017, Nolte and co-workers investigated the effects of another type of nanoparticles that can be found in the environment, plastic nanoparticles (polystyrene), on the cell wall of the green microalgae species *Pseudokirchneriella subcapitata* [42]. In this study, AFM imaging of cells in interaction with plastics revealed that positively charged nanoparticles (bearing $-\text{NH}_2$ functional groups) could adsorb at the cell surface, while negatively charged ones ($-\text{COOH}$) resulted in a low cell coverage. The authors

attributed this to the fact that positive particles could adsorb on the cellulose present in the cell wall of *P. subcapitata*. Finally another type of pollutant, cadmium metal, was also investigated using AFM on different microalgae species; the green microalgae *D. tertiolecta* [43], and the diatoms *P. tricornutum* [44] and *Nitzschia closterium* [45]. Cadmium is recognized as a major pollutant of the marine environment, constituting a hazard to marine organisms. In 2019, the group of Ivosevic DeNardis and co-workers used AFM to probe the nanomechanical properties of *D. tertiolecta* cells in the presence of cadmium. The results showed that cells in the presence of cadmium had an increased stiffness of around 80% compared to control cells, which has consequences on their initial attachment to surfaces and on their deformation. Additional experiments performed in this study suggested that a different protein expression profile may be the cause of these changes in the cell surface properties under cadmium stress [43]. In parallel, another team also worked on cadmium stress, this time on the diatom *N. closterium*, and evaluated the influence of salinity on cadmium adsorption by the cells. Their results showed notably that a decreased salinity increased cell surface roughness, because of the presence at low salinity of silica particles on the cell surface (Fig. 5A). This has for consequence to increase the specific surface area in cells, leading to a better adsorption of cadmium at low salinity [45]. Then in 2021, the same team worked on the effects this time of the cell morphotype of the diatom *P. tricornutum* on the cadmium adsorption on cells. In this study, AFM imaging combined with zeta potential measurements showed that the oval morphotype, which has a rougher and more negative surface compared to the triradiate and fusiform morphotypes, attracts more metal ions onto its surface (Fig. 5B). The authors suggested that these different surface properties of oval cells may be related to their different cell wall composition compared to fusiform and triradiate cells, as determined by XPS analysis [44]. Altogether, in these studies on the effects of stress, AFM brings the opportunity to not only monitor the effects of pollutants on cells, but also to give insights into the mechanisms leading to pollutant adsorption by the cells. This is a major contribution of AFM as such fundamental data can be used to predict and evaluate the effects of various pollution in aquatic ecosystems.

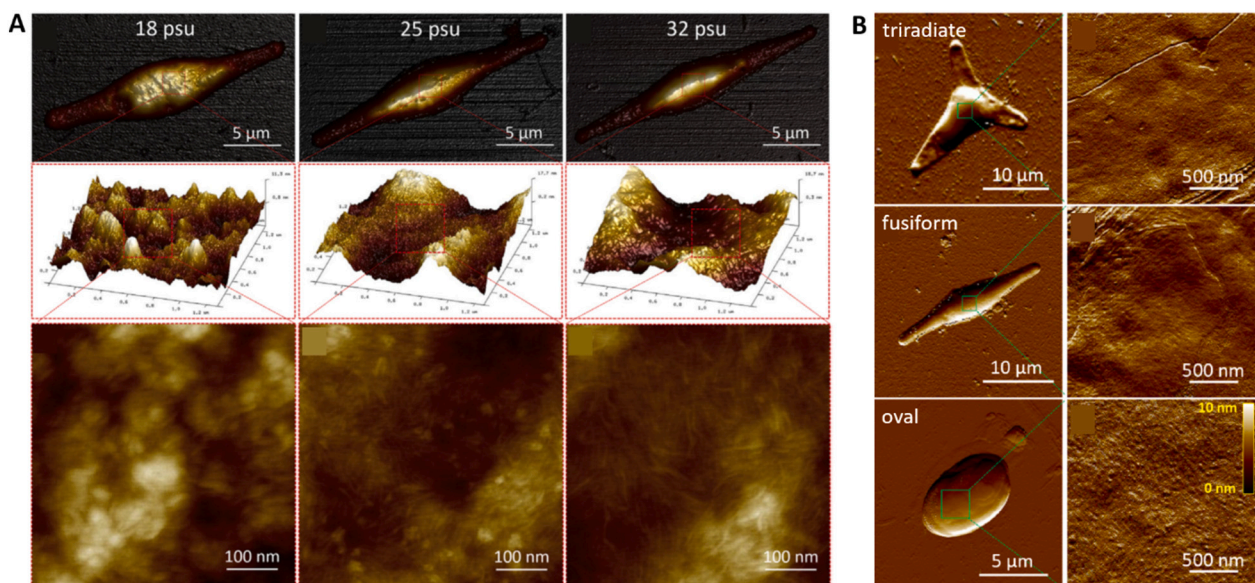


Fig. 5. Influence of salinity or of cell morphotype on cadmium adsorption by cells. A) AFM height images of *N. closterium* cells acclimated at 18, 25, and 32 psu (first line) and amplified 3D morphology of typical difference in roughness on the cell walls of cells cultivated at these different salinities (middle line). AFM height images showing the nanoscale structures on the cell surfaces at the different salinities are presented in the third line. B) AFM vertical deflection images showing the morphology of the triradiate, fusiform, and oval morphotypes and their corresponding nanoscale cell wall topography (right column). Reprinted with permission from [44,45].

4. AFM to probe the interactions between cells and their environment

As discussed earlier, AFM, thanks to its imaging and force probing possibilities, has proven to be a useful tool to probe the effects of environmental conditions on cells, or to understand how environmental conditions modify their responses to pollutants in aquasystems. In this part, we will now discuss how AFM can be used to understand the specific interactions between cells and surfaces or particles present in the environment. In a first study, Kreis and co-workers used a micropipette force spectroscopy technique to measure the adhesion forces between *Chlamydomonas reinhardtii* flagella and silicon substrates [46]. In this case, the authors did not use a standard AFM set-up, but instead, they designed a micropipette force sensor with borosilicate glass capillaries that they used to pick-up single living cells (Fig. 6A) and record forces through force spectroscopy experiments (Fig. 6B). Using this set-up they could orientate cells and determine that only flagella could mediate adhesion to the substrates (Fig. 6B). The force curves obtained showed that interestingly, this flagella-mediated adhesion could be reversibly switched on and off by light, in a timescale of seconds, and that the adhesion forces recorded varied depending on the illumination wavelength. Such findings may be used to control the adhesion properties of photoactive cells such as *C. reinhardtii* cells, and this way enhance culture efficiencies by inhibiting biofilm formation on photobioreactors surfaces [46].

Such strategy to measure the adhesion forces between single cells and substrates has also been used in a recent study conducted by Demir and co-workers [25]. In this study, instead of using a micropipette, the authors directly immobilized cells at the edge of tipless cantilevers, and probed their interactions with chitosan, a bio-sourced flocculant used for microalgae harvesting. So far the literature on chitosan-induced production in microalgae suggested a flocculation mechanism based on electrostatic interactions between negatively charged cells and chitosan, which is positively charged at a pH under its pKa (6.5). Thanks to the force spectroscopy experiments conducted in this study, the authors could show that in fact, the interactions between cells and chitosan did not rely on electrostatic interactions but rather on specific interactions between chitosan and specific polymers at the surface of cells. But interestingly, the authors found that this mechanism was taking place at low pH (6), but not at higher pH. In this case, cells did not interact with chitosan anymore, but were instead flocculated by getting entrapped into the precipitate that chitosan forms at higher pH. Such AFM experiments thus brought important information to generalize the use of chitosan-induced flocculation for microalgae harvesting [25]. With the same objective to understand flocculation mechanisms in microalgae,

two other studies conducted by the same team showed that a same flocculant, magnesium hydroxide, could induce flocculation through different mechanisms in different microalgae species. Magnesium hydroxide results from the precipitation at high pH of magnesium ions present notably in marine waters. To understand the interactions between this flocculant and microalgae cells, the authors developed an original protocol to functionalize the AFM tips directly with magnesium hydroxide particles [14], and with these tips, they then probed the interactions with the surface of *P. tricornutum* [14] and *D. salina* cells [47]. Their results showed that while for *P. tricornutum*, magnesium hydroxide particles could directly interact with the cell surface through electrostatic interactions [14], in the case of *D. salina*, no interactions could be recorded, thereby suggesting another flocculation mechanism. Further experiments showed that indeed cells in this case were flocculated through a sweeping mechanism, *i. e.* by getting entrapped in a massive precipitate [47]. Then in these studies, AFM, by making it possible to access the interactions between cells and particles at the molecular scale, allowed to understand the complexity of flocculation mechanisms. Such knowledge could have an important impact to optimize efficient harvesting processes.

5. Perspectives outlooks and conclusions

This review is a quite exhaustive view of what “conventional” AFM techniques can bring to the field of microalgae. However, other advanced techniques already used in studies focused on other types of microorganisms could also bring valuable information to further understand microalgae. Single-molecule force spectroscopy (SMFS) is one of these techniques. It consists in functionalizing AFM tips with biomolecules in order to study their interactions with specific molecules at the surface of cells. For instance, such tips modifications have been used to detect and locate a specific mannoprotein (Ccw12) at the surface of living yeast cells of *Saccharomyces cerevisiae* [13] or to understand the strength and dynamics of homotypic interactions mediated by a specific protein (SdrC) at the surface of bacterial cells of *Lactococcus lactis* [48]. Used in microalgae studies, SMFS could bring new information useful to understand cell adhesion for example, or to understand cell wall surface composition. Another example of an AFM advanced technique is chemical force microscopy (CFM), where gold coated tips are functionalized with hydrophobic thiols to probe the surface of cells. For instance, such strategy has been used to probe the hydrophobic properties of spores of *Aspergillus fumigatus* [49], or to show the role of glycopeptidolipids in the surface hydrophobicity of the bacteria *Mycobacterium abscessus* [50]. Although this technique has been used in one microalgae study [26], its general use could help researchers gain

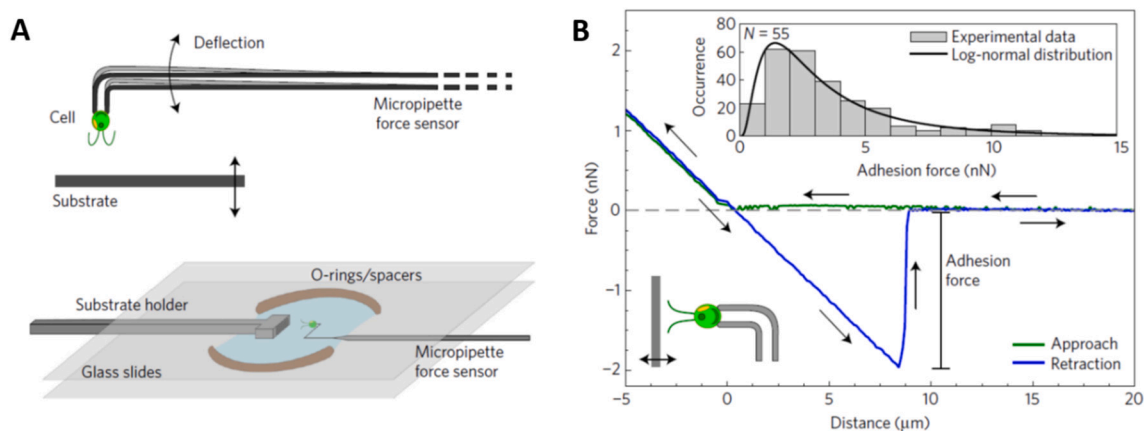


Fig. 6. *In vivo* micropipette force spectroscopy of *Chlamydomonas reinhardtii* microalgae. A) Schematic representation of measurement principle and experimental set-up. B) Force distance curves obtained for cells orientated with their flagella in contact with the substrate. The adhesion force corresponds to the force needed to detach the cell from the substrate. Reprinted with permissions from [46].

insights into the physico-chemical properties of microalgae cells depending on their environmental conditions.

Moreover, these recent years, new developments of original AFM techniques have emerged and offer exciting prospects for microalgae studies. One of these recent developments, FluidFM, combines AFM with microfluidics [51]. With this system, standard AFM cantilevers are replaced by microfluidic ones, which contain a microchannel that can be filled with liquid. A pressure controller connected to these cantilevers then allow to exert a positive or negative pressure inside the cantilever. In different fields, such technology has already been used for example to probe the interactions of single cells aspirated at the aperture of cantilevers [52,53], to aspirate liquids from a cell 's interior for further analysis [54,55] or to create a micro-sized bubble to measure the hydrophobicity of single cells [56]. Such experiments applied to microalgae could help in analyzing the lipid profiles of different strains or in different conditions, which could bring valuable information to optimize culture conditions or microalgae strains. In this view another interesting development of AFM is its combination with a tunable infrared laser source (AFM-IR), which has allowed for *Streptomyces* cells to measure the size and map the distribution of oil inclusions inside cells [57]. Finally, new imaging techniques are emerging, such as high-speed AFM (HS-AFM), which makes it possible to acquire images on the surface of cells at a video rate. Recently, Evans and co-workers developed an immobilization procedure to apply HS-AFM to microalgae cells; this study represents an important basis to further image dynamic processes taking place at the surface of microalgae [58]. These few examples reflect on the recent technological advancements that are continuously made over the years with AFM, and suggest new and original questions that can be answered about microalgae.

Altogether, these AFM studies show the possibilities that such technology offers to answer fundamental questions on microalgae cells interfaces, on the effects of environmental or stress conditions on their nanoscale properties, and on their interacting behavior with their environment. Such fundamental questions need to be answered to exploit the potential of microalgae at industrial scales, and develop and optimize the different steps involved in production systems (production, harvesting, extraction). In addition, as we discussed, it is also a way to understand how microalgae in the environment can be affected by various pollutants that modern society produces. Although imaging is still the most common application of AFM in microalgae studies, force spectroscopy measurements to probe the nanomechanical or adhesive properties of cells have also demonstrated to bring new original information that can be useful to develop cost-effective processes for example for cell harvesting or cell disruption.

CRedit authorship contribution statement

Irem Demir-Yilmaz: Resources, Writing - original draft, Writing - review & editing. **Pascal Guiraud:** Writing - review & editing. **Cécile Formosa-Dague:** Supervision, Resources, Writing - original draft, Writing - review & editing.

Declaration of competing interest

The authors declare that they have no known competing financial interests or personal relationships that could have appeared to influence the work reported in this paper.

Acknowledgements

This work was performed thanks to a funding from Agence Nationale de la Recherche (ANR), JCJC project FLOTALG (ANR-18-CE43-000101). C.F.-D. is a researcher at CNRS.

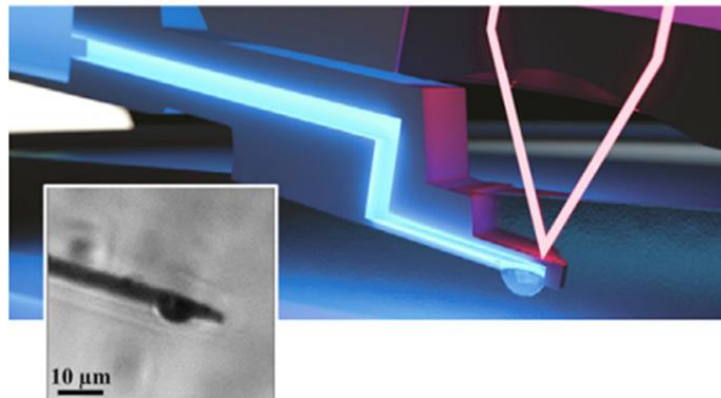
References

- [1] N. Pragma, K.K. Pandey, P.K. Sahoo, A review on harvesting, oil extraction and biofuels production technologies from microalgae, *Renew. Sust. Energ. Rev.* 24 (2013) 159–171, <https://doi.org/10.1016/j.rser.2013.03.034>.
- [2] O. Pulz, W. Gross, Valuable products from biotechnology of microalgae, *Appl. Microbiol. Biotechnol.* 65 (2004) 635–648.
- [3] Y. Torres-Tijji, F.J. Fields, S.P. Mayfield, Microalgae as a future food source, *Biotechnol. Adv.* 41 (2020), 107536, <https://doi.org/10.1016/j.biotechadv.2020.107536>.
- [4] E. Waltz, Biotech's green gold? *Nat. Biotechnol.* 27 (2009) 15–18, <https://doi.org/10.1038/nbt0109-15>.
- [5] T. Ismagulova, A. Shebanova, O. Gorelova, O. Baulina, A. Solovchenko, A new simple method for quantification and locating P and N reserves in microalgal cells based on energy-filtered transmission electron microscopy (EFTEM) elemental maps, *PLoS One* 13 (2018), e0208830, <https://doi.org/10.1371/journal.pone.0208830>.
- [6] C. Uwizeye, J. Decelle, P.-H. Jouveau, B. Gallet, J.-B. Keck, C. Moriscot, F. Chevalier, N. Schieber, R. Templin, G. Curien, Y. Schwab, G. Schoehn, S. Zeeman, D. Falconet, G. Finazzi, In-Cell Quantitative Structural Imaging of Phytoplankton Using 3D electron Microscopy, 2020, <https://doi.org/10.1101/2020.05.19.104166>.
- [7] A.M. Barlow, A.D. Slepokov, A. Ridsdale, P.J. McGinn, A. Stolow, Label-free hyperspectral nonlinear optical microscopy of the biofuel micro-algae *Haematococcus Pluvialis*, *Biomed. Opt. Express*, BOE. 5 (2014) 3391–3402, <https://doi.org/10.1364/BOE.5.003391>.
- [8] G. Binnig, C.F. Quate, C. Gerber, Atomic force microscope, *Phys. Rev. Lett.* 56 (1986) 930–934.
- [9] C. Formosa-Dague, M. Castelain, H. Martin-Yken, K. Dunker, E. Dague, M. Sletmoen, The role of glycans in bacterial adhesion to mucosal surfaces: how can single-molecule techniques advance our understanding? *Microorganisms*. 6 (2018) 39, <https://doi.org/10.3390/microorganisms6020039>.
- [10] C. Formosa-Dague, R.E. Duval, E. Dague, Cell biology of microbes and pharmacology of antimicrobial drugs explored by atomic force microscopy, in: *Seminars in Cell & Developmental Biology*, 2017, <https://doi.org/10.1016/j.semcdb.2017.06.022>.
- [11] Y.F. Dufrene, T. Ando, R. Garcia, D. Alsteens, D. Martinez-Martin, A. Engel, C. Gerber, D.J. Müller, Imaging modes of atomic force microscopy for application in molecular and cell biology, *Nat. Nanotechnol.* 12 (2017) 295–307, <https://doi.org/10.1038/nnano.2017.45>.
- [12] C. Formosa-Dague, P. Speziale, T.J. Foster, J.A. Geoghegan, Y.F. Dufrene, Zinc-dependent mechanical properties of *Staphylococcus aureus* biofilm-forming surface protein SasG, *PNAS*. 113 (2016) 410–415, <https://doi.org/10.1073/pnas.1519265113>.
- [13] C. Formosa, V. Lachaize, C. Galés, M.P. Rols, H. Martin-Yken, J.M. François, R. E. Duval, E. Dague, Mapping HA-tagged protein at the surface of living cells by atomic force microscopy, *J. Mol. Recognit.* 28 (2015) 1–9, <https://doi.org/10.1002/jmr.2407>.
- [14] C. Formosa-Dague, V. Gernigon, M. Castelain, F. Daboussi, P. Guiraud, Towards a better understanding of the flocculation/flotation mechanism of the marine microalgae *Phaeodactylum tricornutum* under increased pH using atomic force microscopy, *Algal Res.* 33 (2018) 369–378, <https://doi.org/10.1016/j.algal.2018.06.010>.
- [15] F. Pillet, L. Chopinet, C. Formosa, É. Dague, Atomic force microscopy and pharmacology: from microbiology to cancerology, *Biochimica et Biophysica Acta (BBA)* 1840 (2014) 1028–1050, <https://doi.org/10.1016/j.bbagen.2013.11.019>, general subjects.
- [16] J. Xiao, Y. Dufrene, Optical and force nanoscopy in microbiology, *Nat. Microbiol.* 1 (2016) 16186.
- [17] L. Chopinet, C. Formosa, M.P. Rols, R.E. Duval, E. Dague, Imaging living cells surface and quantifying its properties at high resolution using AFM in QITM mode, *Micron*. 48 (2013) 26–33, <https://doi.org/10.1016/j.micron.2013.02.003>.
- [18] S.A. Crawford, M.J. Higgins, P. Mulvaney, R. Wetherbee, Nanostructure of the diatom frustule as revealed by atomic force and scanning electron microscopy, *J. Phycol.* 37 (2001) 543–554, <https://doi.org/10.1046/j.1529-8817.2001.037004543.x>.
- [19] I.C. Gebeshuber, J.H. Kindt, J.B. Thompson, Y.D. Amo, H. Stachelberger, M. A. Brzezinski, G.D. Stucky, D.E. Morse, P.K. Hansma, Atomic force microscopy study of living diatoms in ambient conditions, *J. Microsc.* 212 (2003) 292–299, <https://doi.org/10.1111/j.1365-2818.2003.01275.x>.
- [20] G. Francius, B. Tesson, E. Dague, V. Martin-Jézéquel, Y.F. Dufrene, Nanostructure and nanomechanics of live *Phaeodactylum tricornutum* morphotypes, *Environ. Microbiol.* 10 (2008) 1344–1356, <https://doi.org/10.1111/j.1462-2920.2007.01551.x>.
- [21] G. Pletikapić, A. Berquand, T.M. Radić, V. Svetličić, Quantitative Nanomechanical mapping of marine diatom in seawater using peak force tapping atomic force microscopy, *J. Phycol.* 48 (2012) 174–185, <https://doi.org/10.1111/j.1529-8817.2011.01093.x>.
- [22] G. Pletikapić, V. Žutić, I.V. Vrček, V. Svetličić, Atomic force microscopy characterization of silver nanoparticles interactions with marine diatom cells and extracellular polymeric substance, *J. Mol. Recognit.* 25 (2012) 309–317, <https://doi.org/10.1002/jmr.2177>.
- [23] A.I. Salimon, P.V. Sapozhnikov, J. Everaerts, O. Yu Kalinina, C. Besnard, C. Papadaki, J. Cvjetinovic, E.S. Statnik, Y. Kan, P. Aggrey, V. Kalyaev, M. Lukashova, P. Somov, A.M. Korsunsky, A mini-Atlas of diatom frustule electron

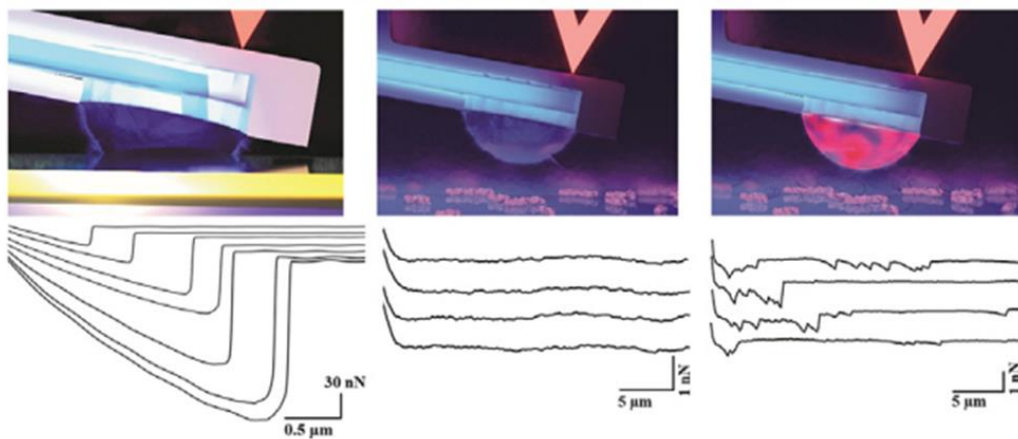
- microscopy images at different magnifications, *Materials Today: Proceedings*. 33 (2020) 1924–1933, <https://doi.org/10.1016/j.matpr.2020.05.602>.
- [24] E.M. Eslick, M.J. Beilby, A.R. Moon, A study of the native cell wall structures of the marine alga *Ventricaria ventricosa* (Siphonocladales, Chlorophyceae) using atomic force microscopy, *Microscopy*. 63 (2014) 131–140, <https://doi.org/10.1093/jmicro/dft083>.
- [25] I. Demir, J. Blockx, E. Dague, P. Guiraud, W. Thielemans, K. Muylaert, C. Formosa-Dague, Nanoscale evidence unravels microalgae flocculation mechanism induced by chitosan, *ACS Appl. Bio Mater.* 3 (2020) 8446–8459, <https://doi.org/10.1021/acscabm.0c00772>.
- [26] F. Pillet, E. Dague, J. Pečar Ilić, I. Ružić, M.-P. Rols, N. Ivošević DeNardis, Changes in nanomechanical properties and adhesion dynamics of algal cells during their growth, *Bioelectrochemistry*. 127 (2019) 154–162 (<https://doi.org/voelcker>).
- [27] C. Delattre, G. Pierre, C. Laroche, P. Michaud, Production, extraction and characterization of microalgal and cyanobacterial exopolysaccharides, *Biotechnol. Adv.* 34 (2016) 1159–1179, <https://doi.org/10.1016/j.biotechadv.2016.08.001>.
- [28] M.F. de J. Raposo, R.M.S.C. de Morais, A.M.M. Bernardo de Morais, Bioactivity and applications of sulphated polysaccharides from marine microalgae, *Mar Drugs*. 11 (2013) 233–252, <https://doi.org/10.3390/md11010233>.
- [29] J. Cybulska, M. Halaj, V. Cepák, J. Lukavský, P. Capek, Nanostructure features of microalgae biopolymer, *Starch - Stärke*. 68 (2016) 629–636, <https://doi.org/10.1002/star.201500159>.
- [30] L. Chopinet, C. Formosa, M.P. Rols, R.E. Duval, E. Dague, Imaging living cells surface and quantifying its properties at high resolution using AFM in QITM mode, *Micron*. 48 (2013) 26–33, <https://doi.org/10.1016/j.micron.2013.02.003>.
- [31] J.B. Vergnes, V. Gernigon, P. Guiraud, C. Formosa-Dague, Bicarbonate concentration induces production of exopolysaccharides by *Arthrospira platensis* that mediate bioflocculation and enhance flotation harvesting efficiency, *ACS Sustain. Chem. Eng.* 7 (2019) 13796–13804, <https://doi.org/10.1021/acsschemeng.9b01591>.
- [32] C. Formosa, M. Grare, R.E. Duval, E. Dague, Nanoscale effects of antibiotics on *P. aeruginosa*, *Nanomedicine* 8 (2012) 12–16, <https://doi.org/10.1016/j.nano.2011.09.009>.
- [33] C. Formosa, M. Schiavone, H. Martin-Yken, J.M. François, R.E. Duval, E. Dague, Nanoscale effects of caspofungin against two yeast species, *Saccharomyces cerevisiae* and *Candida albicans*, *Antimicrob. Agents Chemother.* 57 (2013) 3498–3506, <https://doi.org/10.1128/AAC.00105-13>.
- [34] Y. Xiao, Y. Cheng, P. He, X. Wu, Z. Li, New insights into external layers of cyanobacteria and microalgae based on multiscale analysis of AFM force-distance curves, *Sci. Total Environ.* 774 (2021), 145680, <https://doi.org/10.1016/j.scitotenv.2021.145680>.
- [35] I.C. Gebeshuber, J.B. Thompson, Y.D. Amo, H. Stachelberger, J.H. Kindt, In vivo nanoscale atomic force microscopy investigation of diatom adhesion properties, *Mater. Sci. Technol.* 18 (2002) 763–766, <https://doi.org/10.1179/026708302225003857>.
- [36] M.J. Higgins, S.A. Crawford, P. Mulvaney, R. Wetherbee, Characterization of the adhesive mucilages secreted by live diatom cells using atomic force microscopy, *Protist*. 153 (2002) 25–38, <https://doi.org/10.1078/1434-4610-00080>.
- [37] M.J. Higgins, P. Molino, P. Mulvaney, R. Wetherbee, The structure and nanomechanical properties of the adhesive mucilage that mediates diatom-substratum adhesion and motility, *J. Phycol.* 39 (2003) 1181–1193, <https://doi.org/10.1111/j.0022-3646.2003.03-027.x>.
- [38] B.H.J. Yap, S.A. Crawford, R.R. Dagastine, P.J. Scales, G.J.O. Martin, Nitrogen deprivation of microalgae: effect on cell size, cell wall thickness, cell strength, and resistance to mechanical disruption, *J. Ind. Microbiol. Biotechnol.* 43 (2016) 1671–1680, <https://doi.org/10.1007/s10295-016-1848-1>.
- [39] A.K. Lee, D.M. Lewis, P.J. Ashman, Force and energy requirement for microalgal cell disruption: an atomic force microscope evaluation, *Bioresour. Technol.* 128 (2013) 199–206, <https://doi.org/10.1016/j.biortech.2012.10.032>.
- [40] K.M. Warren, J.N. Mpagazehe, P.R. LeDuc, C.F. Higgs, Probing the elastic response of microalga *Scenedesmus dimorphus* in dry and aqueous environments through atomic force microscopy, *Appl. Phys. Lett.* 105 (2014), 163701, <https://doi.org/10.1063/1.4898636>.
- [41] A. Landels, T.A. Beacham, C.T. Evans, G. Carnovale, S. Raikova, I.S. Cole, P. Goddard, C. Chuck, M.J. Allen, Improving electrocoagulation floatation for harvesting microalgae, *Algal Res.* 39 (2019), 101446, <https://doi.org/10.1016/j.algal.2019.101446>.
- [42] T.M. Nolte, N.B. Hartmann, J.M. Kleijn, J. Garnæs, D. van de Meent, A. Jan Hendriks, A. Baun, The toxicity of plastic nanoparticles to green algae as influenced by surface modification, medium hardness and cellular adsorption, *Aquat. Toxicol.* 183 (2017) 11–20, <https://doi.org/10.1016/j.aquatox.2016.12.005>.
- [43] N. Ivošević DeNardis, J. Pečar Ilić, I. Ružić, N. Novosel, T. Mišić Radić, A. Weber, D. Kasum, Z. Pavlinska, R.K. Balogh, B. Hajdu, A. Marček Chorvátová, B. Gyurcsik, Algal cell response to laboratory-induced cadmium stress: a multimethod approach, *Eur. Biophys. J.* 48 (2019) 231–248, <https://doi.org/10.1007/s00249-019-01347-6>.
- [44] J. Ma, B. Zhou, F. Chen, K. Pan, How marine diatoms cope with metal challenge: insights from the morphotype-dependent metal tolerance in *Phaeodactylum tricornutum*, *Ecotoxicol. Environ. Saf.* 208 (2021), 111715, <https://doi.org/10.1016/j.ecoenv.2020.111715>.
- [45] J. Ma, B. Zhou, D. Duan, K. Pan, Salinity-dependent nanostructures and composition of cell surface and its relation to Cd toxicity in an estuarine diatom, *Chemosphere*. 215 (2019) 807–814, <https://doi.org/10.1016/j.chemosphere.2018.10.128>.
- [46] C.T. Kreis, M. Le Blay, C. Linne, M.M. Makowski, O. Bäumchen, Adhesion of *Chlamydomonas* microalgae to surfaces is switchable by light, *Nat. Phys.* 14 (2018) 45–49, <https://doi.org/10.1038/nphys4258>.
- [47] A. Besson, C. Formosa-Dague, P. Guiraud, Flocculation-flotation harvesting mechanism of *Dunaliella salina*: from nanoscale interpretation to industrial optimization, *Water Res.* 155 (2019) 352–361, <https://doi.org/10.1016/j.watres.2019.02.043>.
- [48] C. Feuillie, C. Formosa-Dague, L.M.C. Hays, O. Vervaeck, S. Derclaye, M. P. Brennan, T.J. Foster, J.A. Geoghegan, Y.F. Dufrière, Molecular interactions and inhibition of the staphylococcal biofilm-forming protein SdrC, *Proc. Natl. Acad. Sci. U. S. A.* 114 (2017) 3738–3743, <https://doi.org/10.1073/pnas.1616805114>.
- [49] E. Dague, D. Alsteens, J.-P. Latgé, C. Verbelen, D. Raze, A.R. Baulard, Y.F. Dufrière, Chemical force microscopy of single live cells, *Nano Lett.* 7 (2007) 3026–3030, <https://doi.org/10.1021/nl071476k>.
- [50] A. Viljoen, F. Viela, L. Kremer, Y.F. Dufrière, Fast chemical force microscopy demonstrates that glycopeptidolipids define nanodomains of varying hydrophobicity on mycobacteria, *Nanoscale Horizons*. 5 (2020) 944–953, <https://doi.org/10.1039/C9NH00736A>.
- [51] A. Meister, M. Gabi, P. Behr, P. Studer, J. Vörös, P. Niedermann, J. Bitterli, J. Polesel-Maris, M. Liley, H. Heinzelmann, T. Zambelli, FluidFM: combining atomic force microscopy and nanofluidics in a universal liquid delivery system for single cell applications and beyond, *Nano Lett.* 9 (2009) 2501–2507, <https://doi.org/10.1021/nl901384x>.
- [52] E. Pothhoff, O. Guillaume-Gentil, D. Ossola, J. Polesel-Maris, S. LeibundGut-Landmann, T. Zambelli, J.A. Vorholt, Rapid and serial quantification of adhesion forces of yeast and mammalian cells, *PLoS One* 7 (2012), e52712, <https://doi.org/10.1371/journal.pone.0052712>.
- [53] E. Pothhoff, D. Ossola, T. Zambelli, J.A. Vorholt, Bacterial adhesion force quantification by fluidic force microscopy, *Nanoscale*. 7 (2015) 4070–4079, <https://doi.org/10.1039/C4NR06495J>.
- [54] O. Guillaume-Gentil, T. Rey, P. Kiefer, A.J. Ibáñez, R. Steinhoff, R. Brönnimann, L. Dorwling-Carter, T. Zambelli, R. Zenobi, J.A. Vorholt, Single-cell mass spectrometry of metabolites extracted from live cells by fluidic force microscopy, *Anal. Chem.* 89 (2017) 5017–5023, <https://doi.org/10.1021/acs.analchem.7b00367>.
- [55] A. Saha-Shah, A.E. Weber, J.A. Karty, S.J. Ray, G.M. Hieftje, L.A. Baker, Nanopipettes: probes for local sample analysis, *Chem. Sci.* 6 (2015) 3334–3341, <https://doi.org/10.1039/C5SC00668F>.
- [56] I. Demir, I. Lichteinfeld, C. Lemen, E. Dague, P. Guiraud, T. Zambelli, C. Formosa-Dague, Probing the interactions between air bubbles and (bio)interfaces at the nanoscale using FluidFM technology, *J. Colloid Interface Sci.* 604 (2021) 785–797, <https://doi.org/10.1016/j.jcis.2021.07.036>.
- [57] A. Deniset-Besseau, C.B. Prater, M.-J. Virolle, A. Dazzi, Monitoring TriAcylglycerols accumulation by atomic force microscopy based infrared spectroscopy in *Streptomyces* species for biodiesel applications, *J. Phys. Chem. Lett.* 5 (2014) 654–658, <https://doi.org/10.1021/jz402393a>.
- [58] C.T. Evans, S.J. Baldock, J.G. Hardy, O. Payton, L. Picco, M.J. Allen, A. Non-Destructive, Tuneable method to isolate live cells for high-speed AFM analysis, *Microorganisms*. 9 (2021) 680, <https://doi.org/10.3390/microorganisms9040680>.

Chapter 3: Probing the interactions between air bubbles and (bio)-interfaces at the nanoscale using FluidFM technology

FluidFM to produce stable microsized bubbles



Interactions between clean or functionalized bubbles and (bio)surfaces



Irem Demir, Ines Lüchtfeld, Claude Lemen, Etienne Dague, Pascal Guiraud, Tomaso Zambelli and Cécile Formosa-Dague

Journal of Colloid and Interface Science 604 (2021): 785-797

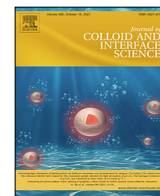
Abstract

Context: This chapter is an international collaborative work with Dr. Tomaso Zambelli from ETH Zurich (Switzerland) allowed the development of the method based on FluidFM to produce bubbles and measure their interactions with cells.

Background: Bubbles play crucial roles in several applications. From agriculture to cell harvesting, including microdynamics of fluids, materials science and engineering, or again in therapeutic applications. In these applications, most of the time bubbles interact with solid particles, and in some cases, they may also interact with living organisms for example to move non adherent microorganism or separate microorganism from their aqueous medium.

Scope of the study: Our aim is to understand the biological and physico-chemical basis of these bubble-microorganism interactions in order to control the processes they are involved in. But first we need to access these interactions at the molecular scale. For that we use FluidFM, which combines AFM with microfluidics. In this study, we used FluidFM in an original manner to produce bubble directly at the aperture of the micro-channeled cantilever. For that, we fill the cantilever with air and immerse it in a liquid environment: by applying a positive pressure inside the cantilever, a bubble can form at the aperture of it, its size depending on the pressure applied. Then by adjusting the flow rate in real time during the experiments, the pressure inside the cantilever stays constant over time, allowing to keep the size of the bubble constant by compensating the gas dissolution due to the Laplace pressure. With this bubble probe we then measure the interactions with both abiotic surfaces and biotic (cells). Then we go one step forward and modulate the interactions in the case of cells by functionalizing the bubble surface using specific amphiphilic molecules.

Major conclusions: In this work we develop a new method to produce stable micro-sized bubble and probe their interactions with both abiotic surfaces and living cells using FluidFM. In addition, we also develop a strategy to functionalize the surface of bubbles produced with biomolecules and we show for the first time that these bubble surface functionalization allows to modulate their interactions with cells.



Probing the interactions between air bubbles and (bio)interfaces at the nanoscale using FluidFM technology



Irem Demir^{a,b}, Ines Luchtefeld^c, Claude Lemen^a, Etienne Dague^{b,d}, Pascal Guiraud^{a,d}, Tomaso Zambelli^c, Cécile Formosa-Dague^{a,d,*}

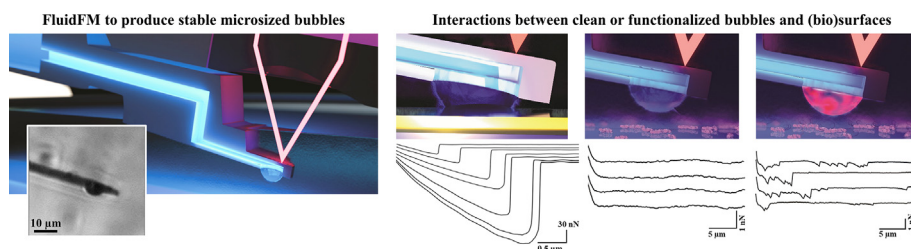
^aTBI, Université de Toulouse, INSA, INRAE, CNRS, Toulouse, France

^bLAAS-CNRS, Université de Toulouse, CNRS, Toulouse, France

^cLaboratory of Biosensors and Bioelectronics, Institute for Biomedical Engineering, ETH Zurich, Zurich, Switzerland

^dFédération de Recherche Fermat, CNRS, Toulouse, France

GRAPHICAL ABSTRACT



ARTICLE INFO

Article history:

Received 19 May 2021

Revised 23 June 2021

Accepted 6 July 2021

Available online 13 July 2021

Keywords:

Air bubbles

Interactions

Fluidic force microscopy

Atomic force microscopy

Hydrophobicity

Microorganisms

ABSTRACT

Understanding the molecular mechanisms underlying bubble-(bio)surfaces interactions is currently a challenge that if overcome, would allow to understand and control the various processes in which they are involved. Atomic force microscopy is a useful technique to measure such interactions, but it is limited by the large size and instability of the bubbles that it can use, attached either on cantilevers or on surfaces. We here present new developments where micro-sized and stable bubbles are produced using FluidFM technology, which combines AFM and microfluidics. The air bubbles produced were used to probe the interactions with hydrophobic samples, showing that bubbles in water behave like hydrophobic surfaces. They thus could be used to measure the hydrophobic properties of microorganisms' surfaces, but in this case the interactions are also influenced by electrostatic forces. Finally a strategy was developed to functionalize their surface, thereby modulating their interactions with microorganism interfaces. This new method provides a valuable tool to understand bubble-(bio)surfaces interactions but also to engineer them.

© 2021 Elsevier Inc. All rights reserved.

1. Introduction

Over the past decades, air bubbles have attracted much attention because of their remarkable characteristics. In liquid,

air bubbles feature (i) a great stability [1], (ii) an affinity for hydrophobic surfaces [2], (iii) a high interface area per unit of volume [3], (iv) an ability to interact with organic molecules (proteins, lipids, and polymers), or surfactants [4], and (v) a capacity to adhere to solid surfaces [5]. Because of these properties, bubbles play crucial roles in several application fields such as agriculture [6], microdynamics of fluids [7], material science [8] or (bio)chemical engineering [9]. For example in chemical engineering, bubbles

* Corresponding author at: Toulouse Biotechnology Institute, INSA de Toulouse, 135 avenue de Rangueil, 31077 Toulouse Cedex 4, France.

E-mail address: formosa@insa-toulouse.fr (C. Formosa-Dague).

can be used to separate cells from their liquid culture medium [10], or when combined with membrane filtration, they can prevent or reduce membrane fouling [11]. Bubbles have also been used in health-related clinical applications in recent years, where they act as efficient carriers for genes and drugs [12–14]. A common point in all these applications is that bubbles interact either with an abiotic surface or with living cells. Thus understanding the physico-chemical basis of these bubble-(bio)surfaces interactions becomes an important aspect, as this comprehension would allow to understand and control the processes they are involved in.

While fluid dynamics aspects of bubbles-(bio)surfaces interactions are to some extent understood [15,16], the underlying molecular mechanisms have not been fully deciphered. One possibility to access these interactions is to use atomic force microscopy (AFM) [17]. AFM, first developed in 1986 [18], has demonstrated over the years to be a powerful tool for surface characterization and force detection at the nanoscale. It was first used to measure the interactions between air bubbles and particle(s)/surface(s) in 1994 [19]. For that the authors attached silica particles on cantilevers [20] and used these colloidal probes to measure the interactions with bubbles of several hundreds of μm in diameter, stabilized on hydrophobic surfaces [19]. By analyzing the force curves obtained with hydrophilic and hydrophobic silica spheres, they could determine that gas bubbles in water behave like hydrophobic surfaces. To access the interactions between bubbles and different surface samples, Vakarelski et al. developed in 2008 another strategy where single bubbles of 90–120 μm in diameter, are picked up on hydrophobized V-shaped cantilevers [21]; this method was used to probe the interactions with other bubbles and provided details on how bubbles interact in natural conditions. This strategy has also been used to probe the interactions between bubbles and microorganisms [22,23]. In a first study by Ditscherlein et al., the interactions between air bubbles of 20–150 μm in diameter and layers of yeast cells were probed [22]; the results obtained indicated that these interactions are hydrophobic, but can be affected by pH, salt concentration or ionic strength. Later on, Yumiyama et al., using the same technique, measured the interactions between air bubbles of 50 μm in diameter, and single yeast cells instead of layers [23]. Their results also showed that hydrophobic interactions were involved; however, in this case, bubbles were ten times bigger than yeast cells, thus depending on the force applied, bubbles could also interact with the surface on which cells were immobilized.

In all these examples, even though experimental parameters such as pH or ionic strength, as well as system parameters such as applied force, approach velocity or contact time are adjustable, issues related to the bubble size remain, as it cannot be controlled over time because of the Laplace pressure [24,25]. Laplace pressure is the differential pressure across inside and outside of a curved interface that forms a boundary between gas and liquid regions [26]. Over time the gases inside the bubble dissolve in the water which modifies their size, and thus the contact area between the bubble and the sample. In the case of interactions with cells, the change in the contact area could modify the number of molecules from the cell surface involved in the interaction, which can have an impact on the final adhesion force recorded [27,28]. This aspect is also related to a second issue that is the variability in size of the bubbles used to probe the interactions. Indeed, using these methods, the size of a bubble is not controllable from one bubble to another, thus for each bubble the contact area is different, thereby possibly leading to differences in the adhesion forces. Finally, in the case where interactions with single microorganisms are probed, the size of the bubbles is too large compared to the size of cells, which can also lead to the introduction of a bias in the results.

To overcome these challenges, we here develop a new method to probe the interactions between bubbles and (bio)interfaces

using fluidic force microscopy technology (FluidFM) that combines AFM with microfluidics. In this system, a micro-sized channel is integrated into an AFM cantilever and connected to a pressure controller, thus creating a continuous and closed fluidic conduit that can be filled with a solution, while the tool can be immersed in a liquid environment [29]. An aperture at the end of the cantilever allows liquids to be dispensed locally. In this configuration, FluidFM technology has been used in various types of studies in material science, for example to functionalize surfaces with polymer layers [30], or in life sciences for example to perform single-cell force spectroscopy experiments [31,32]. In this study, we use FluidFM in an original manner, and develop a method to produce stable micro-sized bubbles at the aperture of FluidFM cantilevers. We first describe this method; after the characterization of the bubbles produced, we probed their interactions with hydrophobic surfaces and living cells. Finally, we also demonstrate the possibility to functionalize the surface of these bubbles in order to modify their interactions with microorganisms.

2. Material and methods

2.1. Microalgae strain and culture

The green freshwater microalgae *Chlorella vulgaris* strain CCAP 211/11B (Culture Collection of Algae and Protozoa) was cultivated in Wright's cryptophyte (WC) medium prepared with deionized water [33], at 20 °C, under 120 rpm agitation, in an incubator equipped with white neon light tubes providing illumination of approximately 40 $\mu\text{mol photons m}^{-2} \text{s}^{-1}$ with a photoperiod of 18 h light: 6 h dark. All experiments were carried out with 7 days exponential phase batch cultures. Before experiments, cells were first harvested by centrifugation (3000 rpm, 3 min), washed two times in PBS at pH 7.8, and immobilized on polyethylenimine (PEI, Sigma-Aldrich P3143) coated glass slides prepared as previously described [34]. Briefly, freshly oxygen activated glass slides were covered by a 0.2% PEI solution in deionized water and left for incubation overnight. Then the glass slides were rinsed with deionized water and dried under nitrogen. A total of 1 mL of the cell suspension was then deposited on the PEI slides, allowed to stand for at least 30 min at room temperature, and rinsed with PBS.

2.2. Yeast strain and culture

Candida albicans (from ABC Platform[®] Bugs Bank, Nancy, France) was stocked at –80 °C, revived on a standard rich YPD (Yeast extract Peptone Dextrose) agar (Difco; 242720) and grown in YPD broth (Difco; 242820) for 20 h at 30 °C under 230 rpm agitation. Yeast cells were then harvested by centrifugation (4500 rpm, 3 min), washed two times in acetate buffer (18 mM CH_3COONa , 1 mM CaCl_2 , 1 mM MnCl_2 , pH 5.2), and immobilized on Concanavalin A (ConA) coated surfaces. For that, 200 μL of ConA (10 $\mu\text{g/mL}$) were deposited on polystyrene Tissue Culture dish (Sterilized by radiation, TPP Switzerland) and incubated overnight. Then the Petri dishes were rinsed with deionized water and dried under nitrogen. A total of 1 mL of the cell suspension was then deposited on the ConA coated Petri dishes, allowed to stand for at least 30 min at room temperature, and rinsed with acetate buffer.

2.3. Bacterial strain and culture

Pseudomonas aeruginosa cells (ATCC 27853) were stocked at –80 °C, revived on Mueller Hinton Agar (Difco, 225250) and grown in Mueller Hinton Broth (Difco, 275730) for 18 h (stationary phase) at 35 °C under static conditions. Cells were harvested by

centrifugation (3000 rpm, 3 min) and washed two times in PBS at pH 7.8. Before experiments cells were immobilized on PEI coated glass slides.

2.4. Preparation of hydrophobic surfaces

Monolayers of CH₃- (1-dodecanethiol, Sigma-Aldrich, 471364) and OH-terminated (11-mercapto-1-undecanol, Sigma-Aldrich, 447528) alkanethiols, mixed in different proportions were self-assembled on gold surfaces to obtain different contact angles, as described in Dague et al. 2007. For that, silicon wafers (Siltronix, France) were first coated by electron beam thermal evaporation with a 5-nm-thick Cr layer followed by a 30-nm-thick Au layer. These gold-coated surfaces were then cleaned by oxygen plasma (3 min), rinsed with ethanol and dried under nitrogen. They were finally immersed for 14 h in ethanol solutions containing 1 mM 1-dodecanethiol (CH₃-) and 11-mercapto-1-undecanol (OH-) in different proportions depending on the degree of hydrophobicity wanted, and rinsed with ethanol before use.

2.5. Water-contact angle measurement

Water contact angles were measured at a 0.1° resolution with a white light source (Digidrop GBX, France). Sesile drop method has been used to measure the water contact angle. Shortly, a water droplet (approx. 4 µL volume) is first released on top of the sample. Then, an edge-detection method is applied to find the drop contour in the image and thus measure the contact angle. For each surface three measurements were performed prior to each experiment.

2.6. Bubble formation using FluidFM

First, tipless FluidFM probes with an aperture of 8 µm of diameter (Cytosurge AG, Switzerland) were made hydrophobic by coating them with self-assembled monolayers (SAMs) of silanes via SAMs vapor deposition technique. FluidFM cantilevers were functionalized with 1H,1H,2H,2H-Perfluorodecyltrichlorosilane (FDTS) using an Orbis-1000 equipment (Memsstar, Livingston, UK) to make their external surface and inside microchannel hydrophobic. The deposition was realized under vacuum at 40 torrs and -40 °C, for 5 min [36]. Then the microchannel of these silanized cantilevers was filled with air and the probe was immersed in a liquid environment (buffer used to perform the experiments). To eliminate any particle or dust contamination or to prevent clogging of the FluidFM cantilever, a slight over pressure of 20 mbar is applied. Then to produce a bubble at the aperture of the cantilever, a positive pressure from 100 to 200 mbar was applied inside the microfluidic cantilever in buffer. The silanized probes were calibrated using the thermal noise method [37] before each measurement.

2.7. Side images

Side images of the microbubbles were recorded using a 0.50 mm right angle reflective prism (Al coated hypotenuse, Edmund Optics, USA). Prism is illuminated with manual lateral light source. This reflective prism and side light source made it possible to image the cantilever and bubble from the side, and measure its perpendicular size depending on the pressure applied. Fig. 2a shows a scheme of the experimental procedure used to obtain these side images.

2.8. Force spectroscopy experiments

Force spectroscopy experiments were conducted using a NanoWizard III AFM (Bruker, USA), equipped with FluidFM technology

(Cytosurge AG, Switzerland). In each case, experiments were performed in either Phosphate Buffer Saline (PBS) or acetate buffer, using micropipette probes with an aperture of 8 µm (spring constant of 0.3, 2, and 4 N/m) (Cytosurge AG, Switzerland). Interactions between the formed bubbles and hydrophobic surfaces were recorded with probes with a spring constant of 2 and 4 N/m at a constant applied force of 1 nN, while interactions with cells were measured using probes with a spring constant of 0.3 and 2 N/m, at a constant applied force of 1 nN. Force curves were recorded with a retraction z-length of up to 20 µm and a constant retraction speed of 4.0 µm/s to 20 µm/s. High z-lengths of 20 µm were reached using the CellHesion module on the NanoWizard III AFM (Bruker). CellHesion Module has a vertical range of movement of 100 µm due to the piezo-driven movement of the sample holder. Data were analyzed using the Data Processing software from Bruker. Adhesion forces were obtained by calculating the maximum adhesion force for each curve. For the interactions with surfaces, experiments were repeated at least five times with one surface in each case. For the interactions with microorganisms, experiments were repeated three times with ten different cells coming from at least three different cultures.

2.9. AFM imaging

AFM images were recorded on cells immobilized on PEI-coated glass slides (for *P. aeruginosa* and *C. vulgaris* cells) or on ConA coated petri dishes (for *C. albicans*). For *C. albicans* and *C. vulgaris*, images were recorded in acetate buffer at pH 5.2 and in PBS at pH 7.4 respectively, using the Quantitative Imaging mode available on the Nanowizard III AFM (Bruker), with MSCT cantilevers (Bruker, nominal spring constant of 0.01 N/m). Images were recorded at 128 pixels × 128 pixels with an applied force kept at 1.5 nN for all conditions and a constant approach/retract speed of 90 µm/s (z-range of 3 µm). For *P. aeruginosa*, images were recorded in contact mode, using a set point inferior to 1 nN. In all cases the cantilevers spring constants were determined by the thermal noise method prior to imaging [37].

2.10. AFM cantilever functionalization

Tips functionalized with phosphorus dendrimers, so-called “dendritips”, were prepared as previously described [38]. Briefly, MLCT AUWH cantilevers (Bruker, USA, spring constant of 0.01 N/m) were first cleaned using oxygen plasma (3 min, 0.5 mbar), placed in a 5.52 M ethanolamine solution (3.3 mL of ethanolamine hydrochloride were dissolved in 6.6 mL Dimethyl sulfoxide (DMSO)) and incubated overnight at room temperature. The tips were then washed with DMSO and ethanol, and dried under nitrogen. These amino tips were next incubated for 5–6 h in the dendrimer solution (58 µM in Tetrahydrofuran (THF)), rinsed in THF and ethanol, and dried under nitrogen. Such “dendritips” were finally functionalized with colistin. For that, they were incubated in a drop of 100 µL of colistin sulfate salt (0.1 mg/L, Sigma Aldrich, C4461) for 1 h at room temperature. Then 10 µL of NaCNBH₃ (20 mM final concentration) were added in the colistin drop for 15 min to let the reduction take place. Finally, tips were washed in PBS and used to probe the interactions with cells.

2.11. Bubble functionalization

A zwitterionic head group labeled with 1,2-dipalmitoyl-sn-glycero-3-phosphoethanolamine-N- (lissamine rhodamine B sulfonyl) (ammonium salt) was used as a fluorescent surfactant. First, the FluidFM cantilever was immersed in a solution of 0.01 g/L of the fluorescent surfactant. This solution was aspirated inside the cantilever by gradually decreasing the pressure from 0 mbar to

–200 mbar. After that the FluidFM cantilever containing the surfactant solution was immersed in PBS buffer without surfactants. By increasing the pressure to 200 mbar, the surfactant solution was then locally dispersed in the buffer and a bubble was formed: the surfactant then assembled at the surface of the produced bubble. To functionalize the bubble surface with colistin, a solution of 20 mg/L of colistin sulfate salt ($\geq 19,000$ IU/mg, Sigma-Aldrich) was used; the same procedure was applied.

2.12. Side image analysis

Images were first calibrated to calculate the size of one pixel. The optical focus was kept constant throughout the calibration procedure and the cantilever was retracted with a $10\ \mu\text{m}$ -step increment. This allowed to calculate the pixel scale size. Sub ROI extraction method was then used to calculate the bubble sizes with color channel separation of red (R) green (G) and blue (B).

3. Results and discussion

3.1. FluidFM allows to produce stable microbubbles at the aperture of microfluidic cantilevers

To produce micro-sized bubbles at the aperture of FluidFM cantilevers (Fig. 1A), we first functionalized FluidFM cantilevers with self-assembled monolayers (SAMs) of silanes (FDTS) to make them hydrophobic. Then, as depicted in Fig. 1A, the microfluidic channel inside the cantilever is filled with air, and immersed in liquid. By applying a positive pressure (200 mbar) inside the can-

tilever, bubbles were formed directly at the aperture. Because the pressure is maintained constant in the cantilever during experiments, the gas dissolution from the bubble is compensated, which allows keeping its size constant over time. Moreover, the hydrophobic coating allows maintaining the bubble produced at the aperture of the cantilever, otherwise it could rise up in the suspension. In our case, buffers were used (PBS or acetate buffers depending later on the type of cells probed) as we observed bubbles in pure water collapse upon touching the surface. Tipless cantilevers with a circular aperture of $8\ \mu\text{m}$ of diameter were used; with smaller apertures, the Laplace pressure was so important that the pressure needed to form the bubble was beyond the maximum value achievable with our system (800 mbar). Fig. 1B and C shows optical images of the microfluidic cantilever from a bottom view (Fig. 1B) and from a side-view (Fig. 1C). While the bubble on the bottom view is not clearly visible, the side image of the cantilever shows the presence of the bubble at the aperture of the cantilever so that we could follow the bubble formation *in situ*, and afterwards fully characterize its shape and size.

To obtain such side images, we used a 45° prism with a reflective side (0.5 mm) manually positioned next to the FluidFM probe and laterally illuminated with an external light source. This set-up is described in Fig. 2A; it is inspired by recent approaches described in the literature where side-view imaging paths were developed for AFM integration [39,40]. The side-view images presented in Fig. 2B–E show bubble formation depending on the applied pressure in the cantilever. Since these images are not direct images, but images upon reflection from the prism, there are several factors affecting the size observed on the images, *i.e.*, the position of

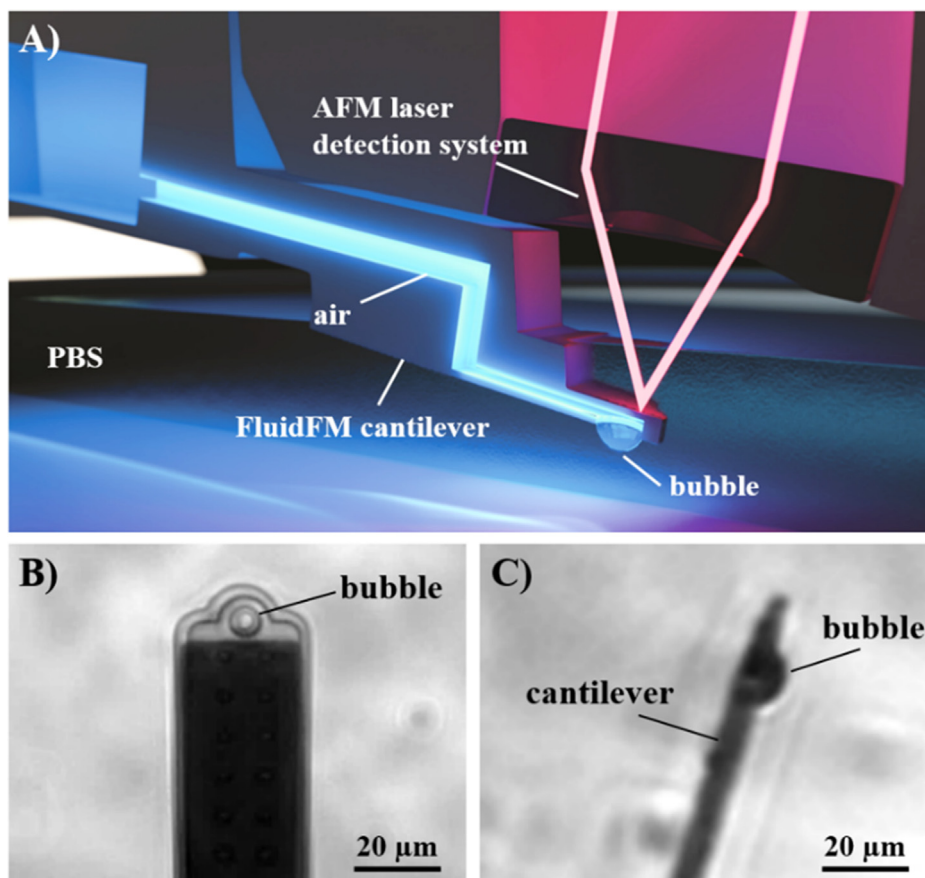


Fig. 1. Schematic representation of the method to produce bubbles using FluidFM technology. (A) A FluidFM microchanneled cantilever with a circular aperture of $8\ \mu\text{m}$ diameter, connected to a pressure controller, is filled with air and immersed in liquid. By applying a positive pressure, an air bubble can be formed at the aperture of the cantilever. (B) Bottom image of a FluidFM probe with a bubble formed at its aperture (200 mbar) and (C) corresponding side image.

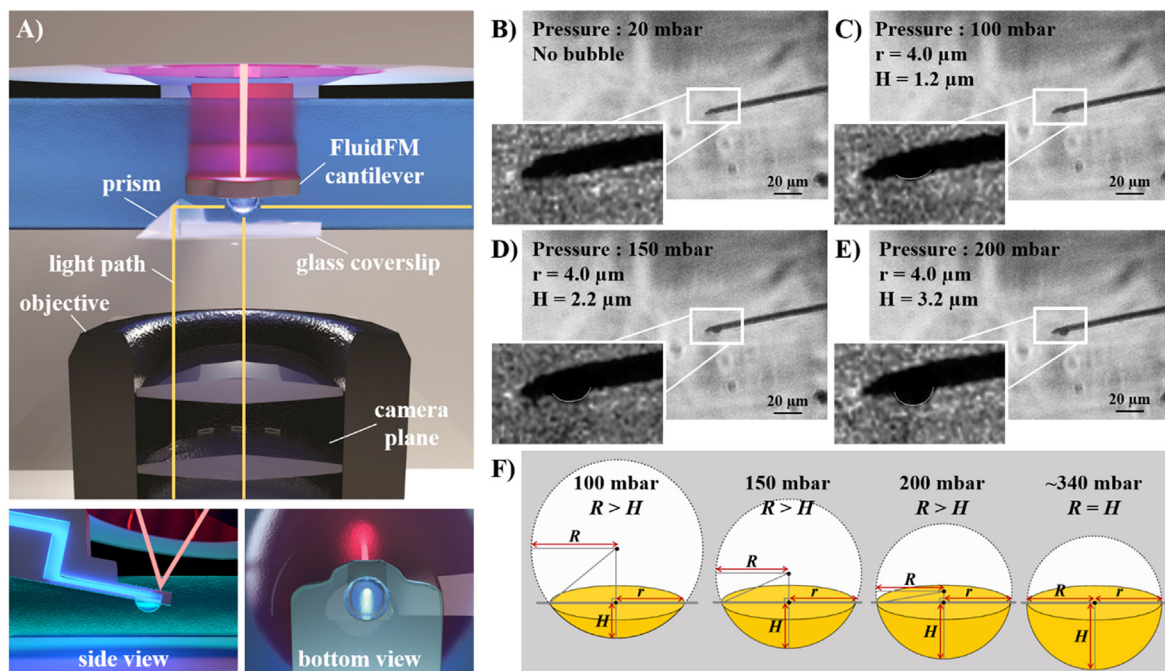


Fig. 2. Characterization of the bubbles produced at the FluidFM cantilever aperture. (A) Schematic representation of the experimental set-up used to obtain side images of the cantilever. A reflective prism is placed next to the FluidFM probe; by illuminating it from the side, it is possible to visualize the cantilever from the side. Side images of the FluidFM cantilever at (B) 20 mbar, (C) 100 mbar, (D) 150 mbar and (E) 200 mbar. In each case, the spherical cap radius r and perpendicular size H are measured. (F) Schematic representation of the spherical cap bubble depending on the pressure applied.

the FluidFM cantilever, the position of the reflective prism, the angle between the reflective prism and the cantilever (if it is fully perpendicular to the cantilever or not) and finally the angle of the side light source. Thus, the first step is to calibrate the images obtained to accurately determine the size of one pixel. For that, the FluidFM cantilever was moved in the Z-direction with known distances (from position $x = 0 \mu\text{m}$ to $x = 70 \mu\text{m}$) using an increment of $10 \mu\text{m}$. By measuring the distance on the images it was possible to determine the size of each pixel, and thus to measure the dimensions of the bubbles produced (see [Supplementary Fig. S1](#)). Knowing the pixel size on the side-images obtained, we thus measured the sizes of bubbles as a function of the pressure p , $100 < p < 200$ mbar. For $p < 100$ mbar, no bubbles were observed ([Fig. 2B](#)). On the contrary, for $p > 100$ mbar, a bubble appears at the aperture of the probe: optically we inferred a radius (r) of $4 \mu\text{m}$ and a perpendicular size (H) of $1.2 \mu\text{m}$ ([Fig. 2C](#)). When the pressure is further increased, r remains constant ($4 \mu\text{m}$), matching the aperture size, whereas H increases from 2.2 to $3.2 \mu\text{m}$. At 200 mbar, the bubbles produced are stable, meaning that their size is constant over time, as showed by time course side images recorded during 1 h ([Supplementary Fig. S2](#)). Finally, above a pressure of 200 mbar, bubbles are not stable anymore, *i.e.* they detach from the cantilever and rise up in the suspension. When we consider the Laplace law, which gives the Laplace pressure as a ratio between the surface tension and the interface radius, as the pressure increases, the bubble radius should decrease. What we see is that when the pressure increases, the bubble radius r stays constant while its perpendicular size H increases. To understand what is happening when a bubble is formed, we need to consider that the bubble produced is actually a spherical cap as described in [Fig. 2F](#), where only the part depicted in yellow is visible at the aperture of the cantilever. When a low pressure is applied, the perpendicular size H of the produced spherical cap is low, but in fact its surface radius, R , in this case is large (for a flat interface, the radius is infinite). As we increase the pressure inside the cantilever,

the perpendicular size H increases, in turn meaning that the surface radius R of the spherical cap decreases. Thus indeed as the pressure increases, its surface radius decreases. With this in mind, it is then possible to calculate the critical pressure to apply to keep the bubble stable, using the Laplace law given by the following equation:

$$\Delta P = \frac{2\gamma}{R} \tag{1}$$

where ΔP is the difference of pressure inside and outside the bubble, γ is the surface tension of the surrounding liquid, and R the surface radius of the spherical cap. We can then apply the Pythagoras theorem to determine the length of its radius:

$$R^2 = r^2 + (R^2 - H^2) \tag{2}$$

$$R = \frac{r^2 + H^2}{2H} \tag{3}$$

where R is the spherical cap surface radius which corresponds to the hypotenuse, H is the perpendicular size of the spherical cap, which corresponds to its height, and r is the bubble radius at the cantilever aperture ([Fig. 2F](#)). Both r and H are measured on the side images. Equation (3) can be used during the first step of the inflation process where $H < r$ and $R > r$, until $H = r$ where the Laplace pressure is maximum because the surface radius R of the spherical cap is minimal. During this first inflation step, the combination of equation (1) and (3) results in the following formula for the Laplace pressure:

$$\Delta P = \frac{4\gamma H}{r^2 + H^2} \tag{4}$$

This means that the applied pressure needed to increase the bubble size, also needs to increase to overcome the Laplace pressure, corresponding to what was observed in the experiments. It shows that the maximum spherical cap height H that can be

reached is of 4 μm , which corresponds to the value of the spherical cap radius r on the cantilever, and thus to the radius of its aperture, for a theoretical applied pressure of 340 mbar. If the applied pressure keeps increasing, the spherical cap surface radius R increases again so that the internal Laplace pressure decreases. The applied pressure suddenly becomes larger than the internal pressure, leading to a rapid increase of the gas flow towards the bubble, which inflates in an unstable process as the Laplace internal pressure continues to decrease. The consequence is that the bubble rapidly becomes too large to stay attached to the cantilever and rises up in the solution due to the Archimedes force. This fully explains the experimental behaviors observed, even if the observed maximum pressure that can be applied is closer to 250 mbar.

The method we propose here allows to produce small bubbles, which have a constant size over time. This is possible because the FluidFM system (controller, tubing and FluidFM chip) in our operating conditions contains a large volume of air (of several mL) at a defined pressure. Given the small size of the bubbles produced, it means that the volume of gas dissolving from the bubble is negligible compared to this overall gas volume, which thus ensures that the bubble diameter stays constant. In addition, the microfluidic controller of the FluidFM regulates the applied pressure inside the system; this regulation system this way refills any lost air. Thanks to this steady supply of air, the diameter of the bubble produced is determined by the active pressure and surface tension, and is not limited by the available volume of air, even if in our case, it should be large enough to maintain the bubble constant over a very long period of time. Another important aspect is that the bubbles produced are small, thus their interface is rigid, which means that they should not deform during force spectroscopy experiments. Bubble deformation has already been the subject of several studies in the literature [22,27,41]. In a recent study, Ditscherlein et al. calculated the bubble deformation using the Johnson-Kendall-Roberts (JKR) theory. Their findings showed that the deformation of the bubble depends on the applied force and for low applied forces (below 50 nN), the deformation fits well with the theoretical model especially for bubbles with smaller radii (below 60 μm) [22]. In our case, the bubbles produced have a maximum radius R of 4 μm . Using the Laplace equation, we can calculate the internal pressure of these bubbles which is over 400 mbar, meaning that to deform the bubble, the pressure applied on it needs to be more important than this value. We can convert this pressure into a force applied, as the force corresponds to the pressure multiplied by the surface area. Considering a sphere of 4 μm of radius, we find that the force applied needed to deform the bubble would be of 2000 nN. Because the bubbles produced by FluidFM are small, stable and non-deformable, in force spectroscopy studies the contact area between the bubble and the sample surface will be the same at a given applied force, thereby allowing to accurately measure interaction forces.

3.2. Bubbles produced behave like hydrophobic surfaces

Once the protocol for the formation of stable bubble validated, we considered force spectroscopy experiments to investigate the interactions between bubbles and surfaces (Fig. 3A). We focused on hydrophobic surfaces because, when measuring the interactions between bubbles and hydrophobic or hydrophilic silica particles, Ducker and co-authors concluded that an air bubble in water is likely to behave like a hydrophobic surface [19]. To verify this finding, we first produced surfaces with different water contact angles (WCA) by functionalizing flat gold coated surfaces with CH_3 - or OH- terminated alkanethiols, as described in [35,42]. By mixing the two different thiols in different proportions, it was possible to obtain hydrophobic surfaces with a WCA ranging from 42.5 to 79.8°, as measured using the sessile drop method. The retract force

curves obtained on the different surfaces are shown in Fig. 3B. The peaks observed are typical of non-specific interactions such as hydrophobic interactions, and the adhesion force recorded increases with the WCA of the surface. The quantification of these adhesion forces is presented in Fig. 3C (adhesion forces values obtained for each surfaces can be found in Supplementary Table S1), where it is clear that increasing the WCA of the surfaces results in an increase in the adhesion forces, from 36.4 ± 9.0 nN for a surface with a WCA of 42.5°, to 268.3 ± 31.9 nN for a surface with a WCA of 79.8°. We can also see on this histogram that small differences in the WCAs measured resulted in important differences in the adhesion forces recorded.

Ducker and co-workers in 1994, concluded from their experiments that an air bubble in water interacts like a hydrophobic surface [19] because of the presence of long-ranged attractive forces visible on the force curves obtained between bubbles and hydrophobic surfaces, which are longer ranged than expected from the Derjaguin-Landau-Verwey-Overbeek (DLVO) theory. After that several studies followed [2,43–45], notably the study of Fielden et al., who also showed that when a bubble interacts with a hydrophobic surface, a hydrophobic force is operating in addition to DLVO forces [43]. Indeed, at close separation distances between bubbles and surfaces, forces resulting from the electrical double-layers (EDL) and van der Waals (VDW) interactions are expected to be repulsive, thus if an attractive force between bubbles and surfaces is measured, it means that hydrophobic forces are significant and that their range is longer compared to EDL forces and VDW. What happens is that when the bubble approaches a hydrophobic surface, an aqueous film will separate the two. While EDL and VDW interactions are likely to stabilize this film, the strong attraction resulting from the hydrophobic interaction will lead to the film breakage and the further bubble attachment to the surface by the formation of a three-phase contact line (TPC, three phases are surface, water, air) [46,47]. In our case, bubbles are negatively charged [48], the gold surfaces produced are neutral at the pH considered (7.4 [49]), thus the electrostatic interactions are not attractive. Regarding the VDW forces, although not known for our system, the Hamaker constant of the interactions air-water-hydrocarbon is negative [50]. Considering that hydrocarbons are hydrophobic as well as our surfaces, and because most studies involving bubble attachment to hydrophobic surfaces consider a negative Hamaker constant [51–54], then we can assume that the VDW interaction is repulsive as well. On our approach force curves, we do not observe any repulsive forces, on the contrary, as the bubble approaches the surface, we observe a “jump-in” reflecting the fact that the bubble gets suddenly attached to the surface (Supplementary Fig. S3A). This jump-in, as in the previous studies on bubble-hydrophobic surface interaction show, is most likely due to a long-range hydrophobic force that causes the disruption of the water film and the formation of the TPC line, as illustrated in Supplementary Fig. S3B.

Considering this, we thus chose to confront our data to the JKR theory [55], which allows to link the adhesion force to the work of adhesion, which is, according to the Young equation, related to the wettability of the surfaces, and thus to their WCA. More specifically, the JKR model describes the adhesion mechanism between a spherical or curved particle (the bubble in our case) and a flat surface (the hydrophobic samples in our case) in a medium (PBS in our case) [56]. It predicts that:

$$F_{adh} = 1.5\pi ReW_{adh} \quad (5)$$

where F_{adh} is the adhesion force recorded, W_{adh} the work of adhesion, and Re is the effective radius of curvature of the bubble area in contact with the sample surface (Inset in Fig. 3A). By simplifying the equation and substituting the W_{adh} , the following linear equa-

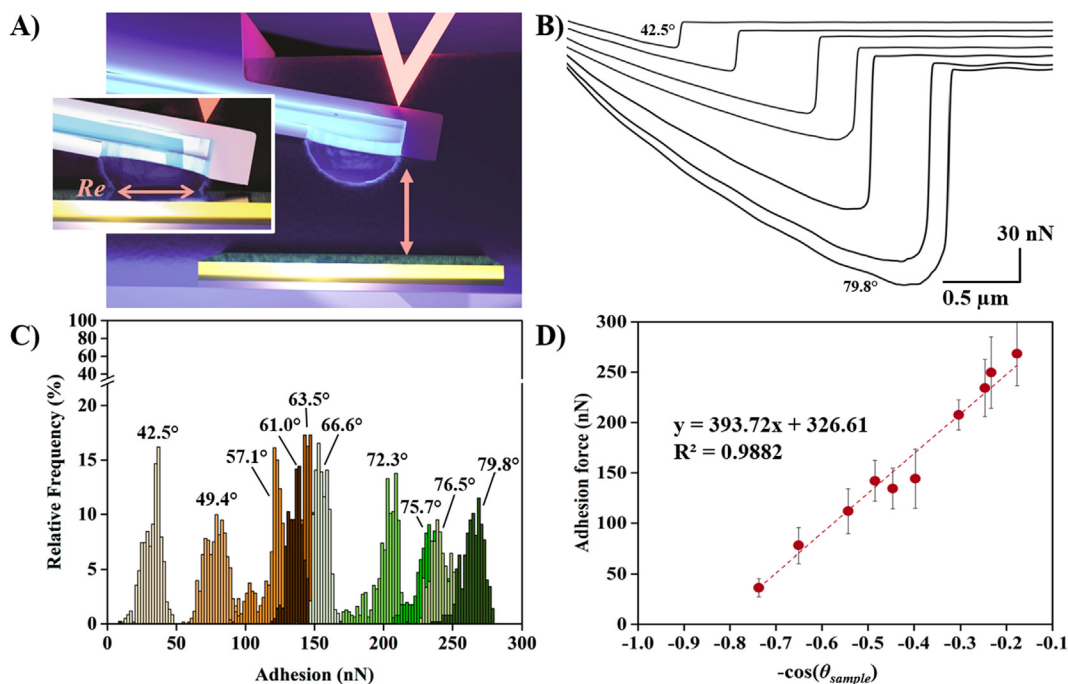


Fig. 3. Probing the interactions between bubbles and hydrophobic surfaces. (A) Schematic representation of the interaction between bubbles and hydrophobic surfaces. The inset shows the bubble attachment on the hydrophobic surface and what the effective bubble radius corresponds to. (B) Representative force curves obtained for hydrophobic surfaces with an increasing WCA. (C) Adhesion force histogram obtained for the interactions between bubbles and the different hydrophobic surfaces. For each surfaces, one representative area on the surface is presented. (D) Graphic showing the variation of the adhesion force as a function of the cosine of the WCA.

tion was obtained (detailed calculations can be found in Supplementary text 1):

$$F_{adh} = 330.1 - 401.3 \cos \theta_{sample} \quad (6)$$

Thus to verify the JKR theory in our case, we plotted the adhesion force as a function of the cosine of the WCA of the samples, $-\cos \theta_{sample}$, as showed in Fig. 3D. Adhesion forces increase linearly with $-\cos \theta$, and the regression equation obtained is the following:

$$F_{adh} = 326.6 - 393.7 \cos \theta_{sample} \quad (7)$$

Equation (6) agrees well with the regression equation (7) of Fig. 3D. Thus our results show a good agreement between experimental and theoretical adhesion forces, proving that indeed the bubble probe behaves like a hydrophobic surface. This supports and confirms the hypothesis that the attractive forces observed between bubbles and hydrophobic surfaces are due to a hydrophobic interactions. To further argument on this point, we can compare our work to the one of Alsteens and co-authors who used in 2007 hydrophobic tips to probe the local hydrophobic forces on hydrophobic surfaces, by assembling SAMs of alkanethiols on both tips and surfaces [42]. Their results also showed a linear relation between the adhesion force and the WCA, which also led them to conclude that the forces probed were indeed hydrophobic forces. Note that the forces ranges in the Alsteens study are smaller than it is the case here, which is due to the difference in the contact area between tips (tip radius is of ~ 20 nm) and bubbles (contact area radius assumed to be of $1.2 \mu\text{m}$). Overall, from our results obtained on hydrophobic surfaces, we can conclude that the microbubble probe that we produce using FluidFM is highly sensitive to differentiate small changes in hydrophobicity, and represents a new and easy method to sensitively and accurately measure the hydrophobicity of complex systems such as cell surfaces where WCA measurements are tricky or can give misleading results.

3.3. The bubble probe is a valuable tool to measure the hydrophobicity of cell surfaces

In the next steps we assessed the interactions between bubbles and microorganisms in order to corroborate whether a bubble probe can indeed be utilized to measure and differentiate the hydrophobicity of living microorganisms' surfaces, which compared to the hydrophobic samples we produced, present a higher complexity. To this end, we selected three different microorganisms' species relevant for their bio-medical or industrial implications *i.e.*, a bacterial species (*Pseudomonas aeruginosa*), a yeast species (*Candida albicans*) and a microalgae species (*Chlorella vulgaris*) with different cell wall compositions and thus most probably different hydrophobic properties. Cells were immobilized on glass-slides coated with ConA or PEI depending on the species and the interactions with bubbles formed by FluidFM were measured in buffer at pH 7.4 (Fig. 4A, B and C). Based on the cell's respective sizes as well as on the size ratio between cells and bubbles, the interactions were measured between bubbles and single *C. albicans* (Fig. 4E) and *C. vulgaris* (Fig. 4F) cells, whereas they were measured with a layer of cells in the case of *P. aeruginosa* (Fig. 4D). Indeed, while for *C. albicans* ($5\text{--}7 \mu\text{m}$ in diameter) and *C. vulgaris* ($3\text{--}5 \mu\text{m}$ in diameter) the cell size is in the same range as the bubble size, in the case of *P. aeruginosa*, cells are relatively small compared to the bubble (approximately $1 \mu\text{m}$ in width) and the bubble could interact with the surface as well. For each species, the results were acquired on 10 different cells for each microorganism coming from at least three independent cultures. In the case of *P. aeruginosa* cell layers, the retract force curves ($n = 6250$ force curves obtained from 10 cells, inset in Fig. 4G) show no retract peaks, which means that bubbles do not interact at all with *P. aeruginosa* cell surface. In the case of *C. albicans* (Fig. 4H) a single peak occurring at the contact point is visible on the force curves with an average adhesion force of 0.4 ± 0.2 nN ($n = 5800$ force curves obtained from 10 cells, all adhesion values can be found in Supplementary

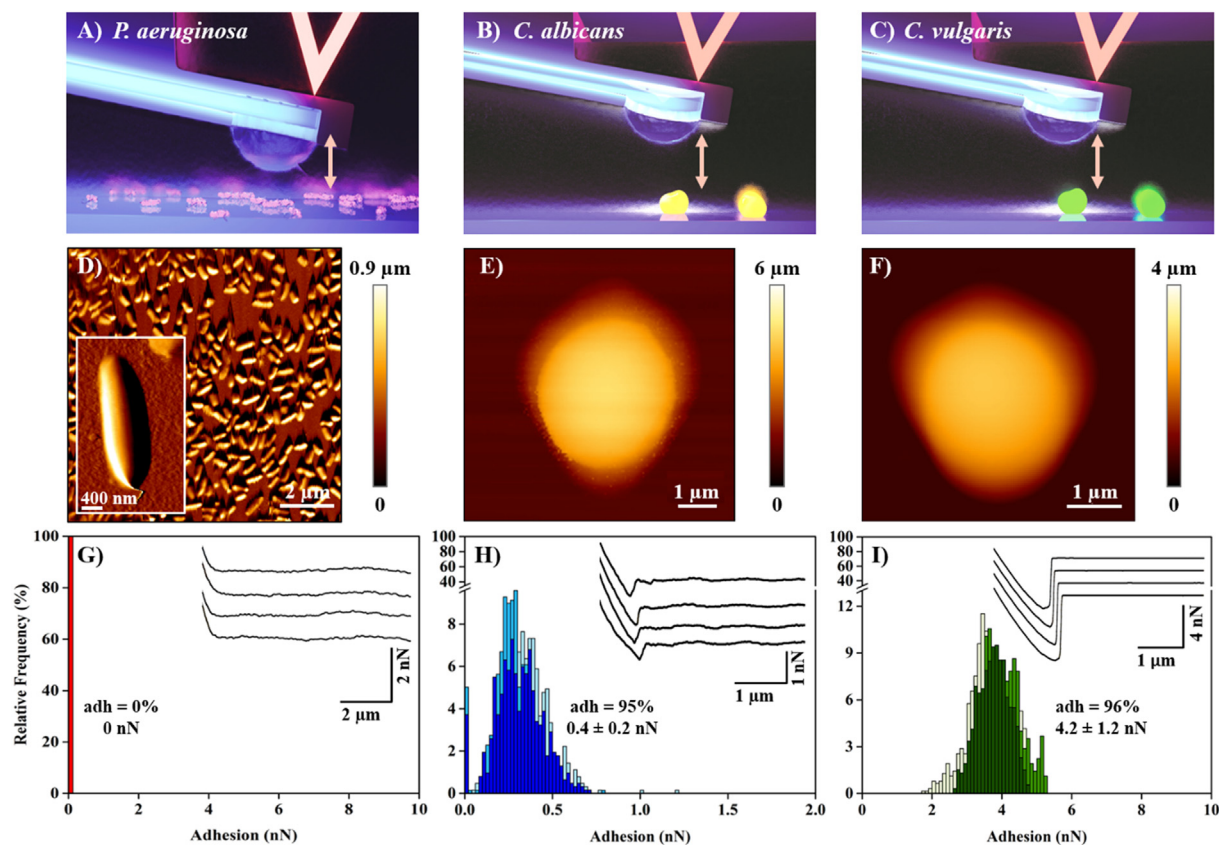


Fig. 4. Probing the interactions between bubbles and microorganism. Schematic representation of (A) bubble – *P. aeruginosa* interaction, (B) bubble – *C. albicans* single cells interactions and (C) bubble – *C. vulgaris* interactions. (D) Standard AFM vertical deflection image of *P. aeruginosa* cell layers, the inset is a zoom-in of one single cell. AFM height images (E) of a single *C. albicans* cell and (F) of a single *C. vulgaris* cell. Adhesion force histograms obtained for (G) bubble – *P. aeruginosa* interactions, (H) bubble – *C. albicans* single cells interactions and (I) bubble – *C. vulgaris* single cells interactions. In each case, 3 different cells are presented. Insets in panels (C), (F) and (I) show representative force curves obtained in each case.

Table S2). A similar type of interaction was obtained for *C. vulgaris*-microbubble interactions (Fig. 4I); however, in this case the average adhesion force recorded was of 4.2 ± 1.2 nN ($n = 5800$ force curves obtained from 10 cells, all adhesion values can be found in Supplementary Table S3), thus 10 times higher than for *C. albicans*. Giving the shape of the retract peaks obtained on the force curves (inset in Fig. 4H and 4I) for both *C. albicans* and *C. vulgaris*, our results suggest that non-specific physico-chemical interactions are involved, most probably reflecting the hydrophobic properties of the cell surfaces. An interesting point to note is that the bubble probe is able to detect forces as low as 0.4 nN, thus showing its sensitivity. These experiments thus tend to prove that the bubble probe produced using our method is indeed a valuable tool to measure the hydrophobicity of cell surfaces. In the case of *C. vulgaris* and *C. albicans*, to confirm that the forces recorded are due to only interactions with cells, we probed the interactions between bubbles and the surfaces they are immobilized on, i.e. PEI coated glass slides for *C. vulgaris* and ConA coated glass slides for *C. albicans*. The results presented in Supplementary Fig. S4 show that the average adhesion force recorded between bubbles and ConA surfaces is of 212.4 ± 21.7 nN (Supplementary Fig. S4A, $n = 2500$ force curves) whereas it is of 91.7 ± 39.7 nN (Supplementary Fig. S4B, $n = 1416$ force curves) for PEI surfaces. These adhesion forces are much higher than the ones we attribute to cells (maximum 10 nN), thus meaning that the bubbles produced with FluidFM have a diameter small enough to probe single cells. This is an important advantage of the FluidFM method we develop here, as understanding these interactions with single cells is key to understand the complex

interplay of physico-chemical forces involved in their interactions with bubbles [57].

As it was previously shown in the literature, the adhesion between cells and bubbles may be hydrophobic but can further be affected by pH, salt concentration or ionic strength [22]. To verify if this is also the case with bubbles produced by FluidFM, additional experiments were carried out with *C. albicans* to probe the interactions between single bubbles and single cells at two different pH (Fig. 5A and B) and at different salt concentrations (Fig. 5C). These results are presented in Fig. 5. They show that when the pH is decreased from 7.4 to 5.2, similar non-specific interactions are visible on the force curves but the adhesion forces recorded are higher: while they are of 0.4 ± 0.2 nN at pH 7.4 (Fig. 5D), they increase to 6.2 ± 2.5 nN at pH 5.2 (Fig. 5E, $n = 6249$ force curves, adhesion values obtained for 10 cells can be found in Supplementary Table S4). When we increase the salt concentration by adding 500 mM NaCl in the buffer at pH 5.2, the charges present on the cells and bubbles are shielded, which results in the decrease of the adhesion forces recorded, from 6.2 ± 2.5 nN to 0.4 ± 0.2 nN in the presence of salts (Fig. 5F, $n = 1875$ force curves, adhesion values obtained for 5 cells can be found in Supplementary Table S5). These results are in line with the previous literature on the interactions of bubbles with yeast cells [22,23], as the interactions are also in our case influenced by pH or ionic strength. This suggests that in addition to hydrophobic forces, potentially other types of non-specific interactions are involved, such as electrostatic interactions.

It is interesting to see that the interactions between bubbles and the different microorganisms result in different adhesion

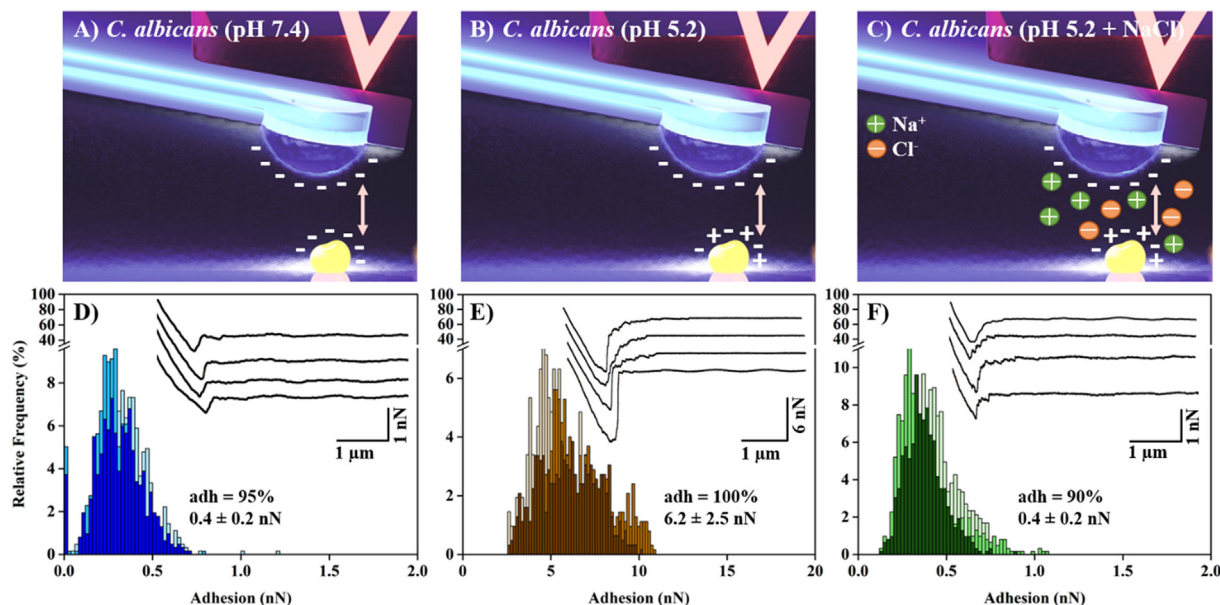


Fig. 5. Characterization of the interactions between bubbles and *C. albicans* cells. Schematic representation of (A) bubble – *C. albicans* interactions at pH 7.4, (B) bubble – *C. albicans* interactions at pH 5.2 and (C) bubble – *C. albicans* interactions at pH 5.2 after addition of 500 mM of NaCl. Adhesion force histograms obtained for (D) bubble – *C. albicans* interaction at pH 7.4, (E) bubble – *C. albicans* interaction at pH 5.2 and (F) bubble – *C. albicans* interaction at pH 5.2 after addition of 500 mM of NaCl. In each case, 3 different cells are presented. Insets in panels (D), (E) and (F) show representative force curves.

forces. In the case of *P. aeruginosa*, it is surprising that our experiments show no interactions at all with bubbles, as based on the literature, our strain of *P. aeruginosa* (ATCC 27853) is supposed to have a hydrophobic surface [58]. To find an answer to this, we looked at the cell's surface charge, which is negative [59]. The bubbles being also negatively charged in water, it is thus possible that in this case, the electrostatic repulsion between bubbles and cells may be dominant compared to the hydrophobic force. To evaluate this, we looked at the approach curves obtained when the bubble interacts with *P. aeruginosa* cells, presented in Supplementary Fig. S5. Compared to the curves obtained on *C. vulgaris* or *C. albicans*, we observe continuously increasing repulsive forces during the approach with the bubble to the bacterial surface. These repulsive forces were recorded at a distance of more than 100 nm, thus at longer range than the hydrophobic jump-in that we can see in the case of *C. vulgaris*, and could very well be attributed to the repulsion between the two negatively charged surfaces. What happens then is that the bubble can go to close contact with the cells but the water film between the bubble and the cell is never ruptured and the TPC line never forms. Thus in the specific case of *P. aeruginosa*, the fact that bubbles do not interact with cell surfaces seem not to reflect its hydrophobic properties, but rather its electronegativity. Regarding the interactions with *C. albicans*, the approach curves show no repulsive forces. *C. albicans* is known to present a cell surface hydrophobicity [60,61]. Thus the adhesion peaks visible on the retract force curves can be at first attributed to hydrophobic interactions between cells and bubbles. However, when the pH of the PBS buffer is decreased from 7.4 to 5.2, the adhesion forces recorded are increased by a factor of 15. This can be due to the fact that changes in the pH can have an impact on the tertiary structure of surface proteins by denaturation, which can lead to a change in the hydrophobicity of the cell surface [22]. However, here also the surface charge of the cells should be taken into consideration. Indeed, a study by Chen and co-workers showed that *C. albicans* cells have a more negative global charge at pH 7.4, of -26 mV, than at pH 5.2 (-15 mV) [62]. In our case, it can thus mean that the decreased adhesion forces recorded at pH 7.4 are due to the increased electrostatic repulsion with the

negatively charged bubbles. The role of electrostatic interactions in the total force recorded is also confirmed by the experiments we performed in the presence of 500 mM of salts, where the charges present on the surfaces are screened, which resulted in the decrease of the adhesion forces recorded. Thus in the case of *C. albicans*, compared to *P. aeruginosa*, the electrostatic repulsion does not dominate the hydrophobic force, but influences it in an important manner. Thus the forces recorded between bubbles and microorganisms result from a balance between electrostatic repulsion and hydrophobic interaction. It is then probably also the case for *C. vulgaris*, for which the approach force curves show a jump-in that can be attributed to the hydrophobic force between bubbles and cells, which is dominant compared to the electrostatic repulsion. While the cell wall composition of *C. vulgaris* is not fully known, studies have shown that *C. vulgaris* cells are hydrophobic (hydrophobic proteins available on the cell wall) and negatively charged at the pH considered (7.4) [63,64].

Altogether, if we compare the bubble probe to a hydrophobic AFM tip like it was developed by Alsteens et al., the bubble probe goes a step further towards the understanding of the interactions between hydrophobic interfaces and cells, by taking into account not only the hydrophobicity of the cell surfaces but also their charge. This new method will thus be of great importance to design or engineer processes in which such interactions take place. Let's give a concrete example; in cell separation processes by flotation [65–67,9], using this method will allow to predict the efficiency by determining if cells and bubbles will attach in large-scale processes.

3.4. Interactions of cells with bubbles can be modulated

In 1994 Ducker and co-workers used sodium dodecylsulfate (SDS), a surfactant that adsorbs at the bubble surface to render it hydrophilic. When probing the interactions with a silica sphere, their results showed the removal of the hydrophobic force that was taking place with clean bubbles [19]. These experiments were the first to demonstrate that it is possible to modify the interaction of bubbles by modifying their surface physico-chemical properties.

Thus in order to modulate the interactions between bubbles and cells, we decided to work on the possibility to functionalize the surface of bubbles produced using FluidFM with molecules expected to specifically interact with the cell wall. As a model experiment, we first used a fluorescent surfactant for direct visualization of the functionalization of the bubble interface. The strategy that we developed to functionalize bubbles consists first in filling the microchannel of the FluidFM probe with air and dipping it in a surfactant solution (Fig. 6A), followed by aspirating the amphiphilic surfactant (fluorescent surfactant or colistin) inside the front of the microchannel, by applying a negative pressure (Fig. 6B). The filled cantilever is then immersed in a petri dish where the cells are immobilized in buffer. The surfactant solution is locally released by applying a positive pressure (Fig. 6C), leading to the formation of a bubble when all the surfactant solution is out (Fig. 6D). Because of the close proximity of the surfactants to the bubble, they directly assemble at bubble surface. Moreover, the silanization process we use to hydrophobize the cantilevers, under vacuum, allows also the hydrophobization of the inside of the cantilever, thus the liquid inside the cantilever can easily be ejected. The corresponding fluorescence microscopy images are presented in Fig. 6E–G. Fig. 6E shows a bottom-view of the cantilever filled with the fluorescent surfactant at a pressure of 0 mbar with no bubble at the aperture of the cantilever. When a pressure of 200 mbar is applied, the surfactants are ejected from the cantilever and a bubble forms at its aperture. As it can be visualized in Fig. 6F the bubble produced is fluorescent, which means that the fluorescent surfactants are present at its surface. To verify the stability of the surfactant on the gas/liquid interphase, time course images were taken using fluorescence microscopy for 15 min. The resulting image (Fig. 6G) shows that the surfactant do not diffuse from the microbubble to its surroundings, proving that the functionalized bubble is stable over time and can be used in force spectroscopy.

While this model experiment demonstrates the possibility and applicability of the microbubble functionalization process, we then used this method to functionalize the bubbles with a molecule allowing to modulate its interactions with cells. As in the case of *P. aeruginosa*, bubbles do not interact with the cell wall, we thus looked for an amphiphilic molecule able to bind specifically the cell wall of this bacterial species. Colistin, also known as polymyxin E, is a natural polycyclic antibacterial peptide which specifically interacts with lipopolysaccharide (LPS) [68], the main component of *P. aeruginosa* outer cell membrane. Moreover, colistin contains both hydrophilic and hydrophobic moieties that gives it amphiphilic properties. As a first step, we probed the interactions between colistin functionalized directly on an AFM cantilever (concentration of 100 $\mu\text{g/L}$) and *P. aeruginosa* cells in single-molecule force spectroscopy experiments (Fig. 7A). In this case the retract force curves obtained show multiple retract adhesions on rather long distances, with a maximum adhesion force of 332.1 ± 207.2 pN (Fig. 7D and G $n = 2346$ force curves, adhesion values obtained for 10 cell areas can be found in Supplementary Table S6). These unfoldings can be attributed to the unfolding of surface polymers, notably LPS, which interacts specifically with colistin at the surface of tips. We then used colistin to functionalize the surface of bubbles (concentration of 20 mg/L, Fig. 7B); the interactions obtained show a similar pattern as in the case of the functionalized AFM tips, with similar unfoldings (Fig. 7E) and a maximum average adhesion force of 590.0 ± 317.5 pN (Fig. 7H, $n = 4560$ force curves, adhesion values obtained for 10 cell areas can be found in Supplementary Table S7). While this force is in the same range as the one obtained with functionalized tips, it is still almost two times higher. Moreover, in this case, the unfoldings events were recorded at longer distances, up to 20 μm . Note that in this case, a 100 μm -long piezo (CellHesion module) was used to reveal the full length of these unfoldings. The fact that the unfolding pattern is similar on the

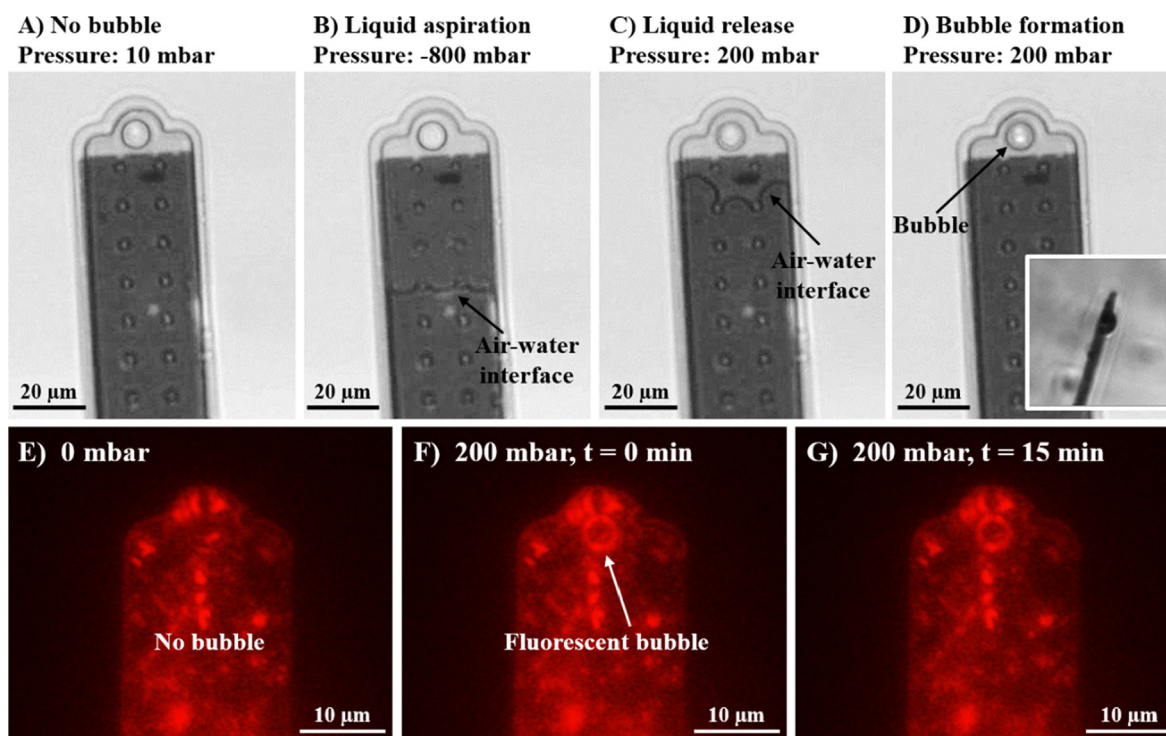


Fig. 6. Functionalizing bubbles using a fluorescent surfactant. Bottom view of a FluidFM probe (A) at an applied pressure of 10 mbar, (B) at an applied pressure of -800 mbar to aspirate the liquid, (C) at an applied pressure of 200 mbar to locally dispense the liquid outside of the cantilever and (D) at an applied pressure of 200 mbar pressure when a bubble forms after releasing all the liquid inside the cantilever. Fluorescence images of the bottom view of (E) a FluidFM probe containing surfactants at 0 mbar, (F) the same FluidFM probe at 200 mbar with a bubble formed at its aperture and (D) after 15 min.

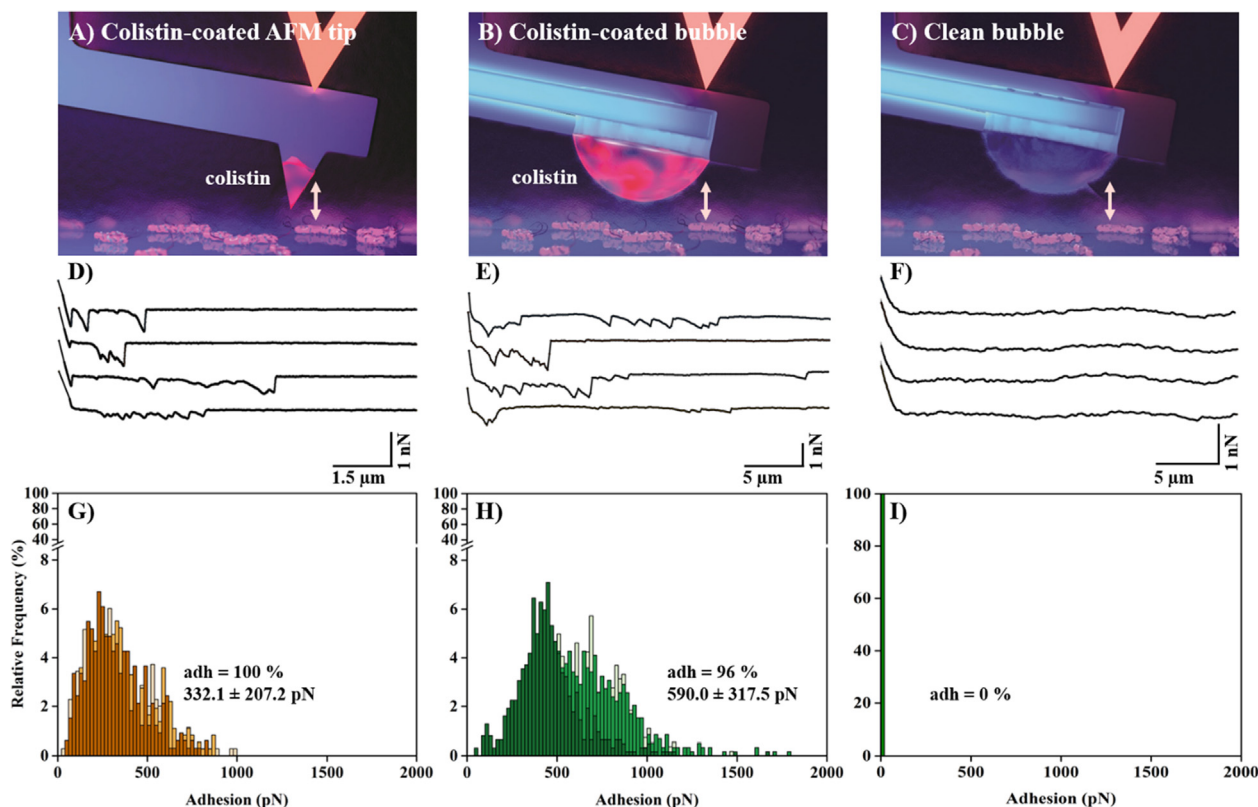


Fig. 7. Modulation of the interactions between bubbles and *P. aeruginosa* cells by colistin. Schematic representation of (A) colistin-coated AFM tips – *P. aeruginosa* cell layers interactions, (B) colistin-coated bubbles – *P. aeruginosa* cell layers interactions and (C) clean bubbles – *P. aeruginosa* cell layers interactions. Representative force curves obtained for (D) colistin-coated AFM tips – *P. aeruginosa* cell layers interactions, (E) colistin-coated bubbles – *P. aeruginosa* cell layers interactions using a 100- μm long piezo and (F) clean bubbles – *P. aeruginosa* cell layers interactions using a 100- μm long piezo. Adhesion force histograms obtained for (G) colistin-coated AFM tips – *P. aeruginosa* cell layers interactions, (H) colistin-coated bubbles – *P. aeruginosa* cell layers interactions using a 100- μm long piezo and (I) clean bubbles – *P. aeruginosa* cell layers interactions using a 100- μm long piezo. In each case, 3 different cells are presented.

force curves obtained with tips or with bubbles proves that colistin molecules are present at the surface of the bubble and interact with the bacterial surface. The difference in the adhesion force and unfolding length between the tip and the bubble is attributed to the difference in the contact area between the two systems. AFM tips have an apex curvature radius smaller than 50 nm, thus the contact area between colistin molecules and cells is smaller compared to the bubble which has a much larger degree of curvature. Thus in the case of bubbles, more LPS molecules are involved in the interaction with more colistin, resulting in higher adhesion forces and unfolding lengths. Finally the same 100 μm -long piezo was used to probe the interactions between bubbles without colistin; as it was already the case in the previous experiment with a classic 15 μm -long piezo (Fig. 4G), no interactions with the cells were observed (Fig. 7C), as force curves shows no retract adhesion peaks (Fig. 7F and I). Moreover in this case, the repulsive electrostatic force that was visible on the force curves with clean bubbles were not visible anymore. This is due to the fact that the presence colistin on the bubble surface changes its charge. In addition, as the hydrophobic part of colistin most probably remains inside the bubble, the hydrophilic part of it is exposed on the surface interacting with the cells, thus, like in the case of SDS in Ducker's work, rendering the bubble hydrophilic. This is the reason why no hydrophobic peak is visible on the force curves in this case; the positive colistin molecules on the bubble interacts electrostatically with the LPS, which is then unfolded from the cell surface upon retraction, as proved by the long unfoldings visible on the retract force curves. These results thus demonstrate that by functionalizing the bubble produced using FluidFM, it is possible to modulate their interactions with cells.

To further prove the good functionalization of bubbles with colistin in these experiments, we characterized the functionalized bubbles produced and found that at 200 mbar of pressure applied in the cantilever, their perpendicular size H is of 2.3 μm instead of 3.2 μm as it is observed from the clean bubbles (Supplementary Fig. S6). This change in the bubble size thus means that with colistin, the surface tension was modified. Using the Laplace equation, it is easy, knowing the bubble dimension, to find the surface tension, which we estimate in this case at 47 mN/m. Knowing that the surface tension of PBS is of 71 mN/m, this proves that the bubble surface was indeed functionalized. However when we measure the surface tension of a colistin solution at the concentration used (20 mg/L), the surface tension is unchanged compared to PBS only. This means that when using our procedure, all the colistin molecules present in the solution aspirated in the cantilever concentrate locally at the bubble surface, changing the surface tension and thus its dimensions for the same pressure applied. Note that at colistin concentrations higher than 20 mg/L, no bubbles could be formed, thus probably because of the too high local concentration of colistin. What happens is that as we increase the pressure, the liquid gets ejected from the cantilever but not the colistin molecules, which stay stuck at the gas/liquid interphase. This ensures that no colistin molecules are free in the medium and contaminate the cell surface. Even if it was the case, given the small volume of the colistin solution aspirated (approximately up to 400 fL), and because this is performed far away from the surface (in the z -direction), the probability that we may measure the interaction between the bubble and colistin attached to the cell surface is very low. This final step in our study is in fact a very important step as here we provide the possibility to (i) modify easily the sur-

face of the bubbles produced using FluidFM, and (ii) to show in what way the modification of the bubble surface influences the nature and strength of the interaction with cells. This has many implications in the different fields where bubble-microorganisms interactions take place.

4. Conclusions

Compared to existing AFM approaches, these new developments based on FluidFM allow to produce stable, micro-sized bubbles and to probe their interactions with abiotic surfaces and cell's interfaces. The fact that it is now possible to maintain the size of bubbles constant over time is the main advantage of this new method. Indeed, this ensures that the contact areas between bubbles and samples stay constant at a given applied force during force spectroscopy experiments, allowing to record adhesion forces with accuracy and reliability. While on hydrophobic samples, the results show that bubbles behave like hydrophobic surfaces, the results obtained on cells show that in addition to hydrophobic forces, interactions are also influenced by electrostatic forces. This makes this new method an ideal tool to apprehend all the complexity of bubble-microorganisms interactions. Finally, we develop a strategy to functionalize the surface of bubbles produced using FluidFM with biomolecules and we show for the first time that these modifications modify their interactions with cells. This is a major advancement as it will open the possibility to engineer bubbles and this way exploit their full potential in various application fields. For instance, our team is at the moment using this strategy to engineer a new flotation process to harvest microalgae cells, by functionalizing the bubble surface with amphiphilic chitosan, a molecule that we have already shown to promote microalgae aggregation [32]. In future projects, this strategy could also be used to specifically separate cell populations from each other; for example to separate bacterial cells from human blood cells in the case of sepsis, but many other applications can now be envisioned.

CRediT authorship contribution statement

Irem Demir: Methodology, Investigation, Writing - original draft, Writing - review & editing. **Ines Luchtefeld:** Methodology, Investigation, Writing - review & editing. **Claude Lemen:** Methodology, Investigation, Writing - review & editing. **Etienne Dague:** Methodology, Conceptualization, Supervision, Writing - review & editing. **Pascal Guiraud:** Methodology, Conceptualization, Supervision, Writing - review & editing. **Tomaso Zambelli:** Methodology, Conceptualization, Supervision, Writing - review & editing. **Cécile Formosa-Dague:** Methodology, Conceptualization, Supervision, Writing - original draft, Writing - review & editing.

Declaration of Competing Interest

The authors declare that they have no known competing financial interests or personal relationships that could have appeared to influence the work reported in this paper.

Acknowledgment

This work was performed thanks to a funding from Agence Nationale de la Recherche (ANR), JCJC project FLOTALG (ANR-18-CE43-000101). C.F.-D. and E.D are researchers at CNRS. The authors would like to thank Dr. Pablo Döerig for fruitful discussions on the FluidFM. This work was partly supported by LAAS-CNRS micro- and nano- technologies platform, member of the French RENA-TECH network. Finally we thank Yannick Carbonnaux (makitbe.com) for the artwork and illustrations.

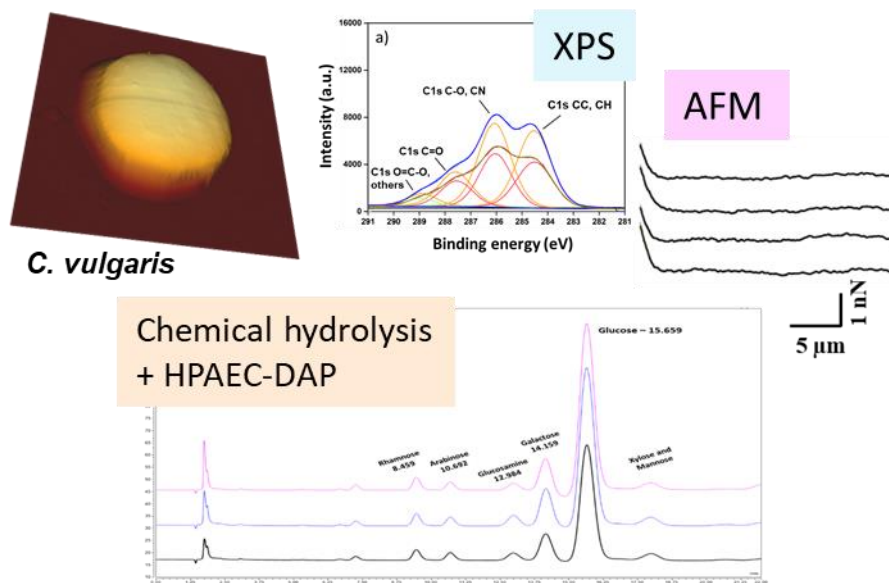
Appendix A. Supplementary material

Supplementary data to this article can be found online at <https://doi.org/10.1016/j.jcis.2021.07.036>.

References

- [1] D. Lohse, X. Zhang, Surface nanobubbles and nanodroplets, *Rev. Mod. Phys.* 87 (2015) 981–1035, <https://doi.org/10.1103/RevModPhys.87.981>.
- [2] J. Israelachvili, R. Pashley, The hydrophobic interaction is long range, decaying exponentially with distance, *Nature* 300 (1982) 341–342, <https://doi.org/10.1038/300341a0>.
- [3] J. Wen, Q. Sun, Z. Sun, H. Gu, An improved image processing technique for determination of volume and surface area of rising bubble, *Int. J. Multiph. Flow* 104 (2018) 294–306, <https://doi.org/10.1016/j.ijmultiphaseflow.2018.02.004>.
- [4] S.R. Sirsi, M.A. Borden, Microbubble compositions, properties and biomedical applications, *Bubble Science, Engineering & Technology*, 2016, <https://www.tandfonline.com/doi/abs/10.1179/175889709X446507> (accessed February 10, 2021).
- [5] J.E. George, S. Chidangil, S.D. George, Recent progress in fabricating superaerophobic and superaerophilic surfaces, *Adv. Mater. Interfaces* 4 (2017), <https://doi.org/10.1002/admi.201601088> 1601088.
- [6] K. Minamikawa, M. Takahashi, T. Makino, K. Tago, M. Hayatsu, Irrigation with oxygen-nanobubble water can reduce methane emission and arsenic dissolution in a flooded rice paddy, *Environ. Res. Lett.* 10 (2015), <https://doi.org/10.1088/1748-9326/10/8/084012> 084012.
- [7] A. Ushida, T. Hasegawa, T. Nakajima, H. Uchiyama, T. Narumi, Drag reduction effect of nanobubble mixture flows through micro-orifices and capillaries, *Exp. Therm. Fluid Sci.* 39 (2012) 54–59, <https://doi.org/10.1016/j.expthermflusci.2012.01.008>.
- [8] R. Lavrijsen, D.M.F. Hartmann, A. van den Brink, Y. Yin, B. Barcones, R.A. Duine, M.A. Verheijen, H.J.M. Swagten, B. Koopmans, Asymmetric magnetic bubble expansion under in-plane field in Pt/Co/Pt: effect of interface engineering, *Phys. Rev. B* 91 (2015), <https://doi.org/10.1103/PhysRevB.91.104414> 104414.
- [9] A. Besson, C. Formosa-Dague, P. Guiraud, Flocculation-flotation harvesting mechanism of *Dunaliella salina*: from nanoscale interpretation to industrial optimization, *Water Res.* 155 (2019) 352–361, <https://doi.org/10.1016/j.watres.2019.02.043>.
- [10] T. Ndikubwimana, J. Chang, Z. Xiao, W. Shao, X. Zeng, I.-S. Ng, Y. Lu, Flotation: a promising microalgae harvesting and dewatering technology for biofuels production, *Biotechnol. Appl. Biochem.* (2016) 315–326, [https://doi.org/10.1002/biot.201500175@10.1002/\(ISSN\)1470-8744\(CAT\)VirtualIssues\(VI\)BiotechnologyinChinacollection](https://doi.org/10.1002/biot.201500175@10.1002/(ISSN)1470-8744(CAT)VirtualIssues(VI)BiotechnologyinChinacollection).
- [11] Z. Wu, H. Chen, Y. Dong, H. Mao, J. Sun, S. Chen, V.S.J. Craig, J. Hu, Cleaning using nanobubbles: defouling by electrochemical generation of bubbles, *J. Colloid Interface Sci.* 328 (2008) 10–14, <https://doi.org/10.1016/j.jcis.2008.08.064>.
- [12] A. Delalande, M. Postema, N. Mignet, P. Midoux, C. Pichon, Ultrasound and microbubble-assisted gene delivery: recent advances and ongoing challenges, *Ther. Delivery* 3 (2012) 1199–1215, <https://doi.org/10.4155/tde.12.100>.
- [13] Z. Gao, A.M. Kennedy, D.A. Christensen, N.Y. Rapoport, Drug-loaded nano/microbubbles for combining ultrasonography and targeted chemotherapy, *Ultrasonics* 48 (2008) 260–270, <https://doi.org/10.1016/j.ultras.2007.11.002>.
- [14] E. Unger, T. Porter, J. Lindner, P. Grayburn, Cardiovascular drug delivery with ultrasound and microbubbles, *Adv. Drug Deliv. Rev.* 72 (2014) 110–126, <https://doi.org/10.1016/j.addr.2014.01.012>.
- [15] S. Poulain, L. Bourouiba, Biosurfactants change the thinning of contaminated bubbles at bacteria-laden water interfaces, *Phys. Rev. Lett.* 121 (2018), <https://doi.org/10.1103/PhysRevLett.121.204502> 204502.
- [16] P.L.L. Walls, J.C. Bird, L. Bourouiba, Moving with bubbles: a review of the interactions between bubbles and the microorganisms that surround them, *Integr. Comp. Biol.* 54 (2014) 1014–1025, <https://doi.org/10.1093/icb/ictu100>.
- [17] Y. Xing, X. Gui, L. Pan, B.-E. Pinchasik, Y. Cao, J. Liu, M. Kappel, H.-J. Butt, Recent experimental advances for understanding bubble-particle attachment in flotation, *Adv. Colloid Interface Sci.* 246 (2017) 105–132, <https://doi.org/10.1016/j.cis.2017.05.019>.
- [18] G. Binnig, C.F. Quate, Ch. Gerber, Atomic force microscope, *Phys. Rev. Lett.* 56 (1986) 930–933, <https://doi.org/10.1103/PhysRevLett.56.930>.
- [19] W.A. Ducker, Z. Xu, J.N. Israelachvili, Measurements of hydrophobic and DLVO forces in bubble-surface interactions in aqueous solutions, *Langmuir* 10 (1994) 3279–3289, <https://doi.org/10.1021/la00021a061>.
- [20] W.A. Ducker, T.J. Senden, R.M. Pashley, Direct measurement of colloidal forces using an atomic force microscope, *Nature* 353 (1991) 239–241, <https://doi.org/10.1038/353239a0>.
- [21] I.U. Vakarelski, J. Lee, R.R. Dagastine, D.Y.C. Chan, G.W. Stevens, F. Grieser, Bubble colloidal AFM probes formed from ultrasonically generated bubbles, *Langmuir* 24 (2008) 603–605, <https://doi.org/10.1021/la7032059>.
- [22] L. Ditscherlein, S. Jolan Gulden, S. Müller, R.-P. Baumann, U.A. Peuker, H. Nirschl, Measuring interactions between yeast cells and a micro-sized air bubble via atomic force microscopy, *J. Colloid Interface Sci.* 532 (2018) 689–699, <https://doi.org/10.1016/j.jcis.2018.08.031>.
- [23] S. Yumiyama, S. Kato, Y. Konishi, T. Nomura, Direct measurement of interaction forces between a yeast cell and a microbubble using atomic force

Chapter 4: Combining AFM, XPS and chemical hydrolysis to understand the complexity and dynamics of *C. vulgaris* cell wall composition and architecture



Irem Demir-Yilmaz, Marion Schiavone, Jérôme Esvan, Pascal Guiraud and

Cécile Formosa-Dague

Algal research, Under review

Abstract

Context: This chapter is composed of a national collaborative work with Marion Schiavone from TBI (Toulouse/France) and Jérôme Esvan from Lallemand SAS (Toulouse/France). Marion has expertise on cell wall composition analysis where as Jérôme has expertise on XPS.

Background: Understanding the cell wall of microalgae is critical since the cell wall represents the interface between the cell and its environment. The microalgae cell wall is a complex structure that is rigid and mechanically strong, protecting the cells from predators and harsh environmental conditions. Furthermore, the cell wall maintains the biological and biomechanical stability of the cell, considerably influencing its interaction with its environment. Despite this, in the case of microalgae, it still remains poorly understood due to the diversity in cell wall composition and structure among the multitude of microalgae species, and because of its characteristic of being a dynamic structure that changes with time and depending on environmental factors.

Scope of the study: In this work we study the cell wall composition and dynamics of *C. vulgaris* under three conditions: exponential phase, stationary phase, and salt stress condition, all of which being relevant for industrial applications such as lipid production. The approach we design for this purpose combines three different methods. To begin, AFM is used to image cells, measure the cell wall roughness and investigate their nanomechanical characteristics depending on the conditions. Then XPS analysis provide a global picture of the cell wall composition, by allowing to quantify the relative proportions of the three main cell wall constituents, protein polysaccharides and lipids. Finally, to obtain a more detailed view of the polysaccharidic fraction that is the main one, chemical hydrolysis followed by HPLC was used to determine and quantify the different monosaccharides present in the cell wall.

Major conclusions: The combination of these three techniques not only provides a comprehensive picture of the effects of culture conditions on the composition and dynamics of *C. vulgaris* cell wall, but also helps to understand the relationship between composition and architecture, as well as the effects of composition changes on cell surface biophysical properties.

Combining AFM, XPS and chemical hydrolysis to understand the complexity and dynamics of *C. vulgaris* cell wall composition and architecture

Irem Demir-Yilmaz^{1,2}, Marion Schiavone^{1,3}, Jérôme Esvan⁴, Pascal Guiraud^{1,5} and

Cécile Formosa-Dague^{1,5*}

¹ TBI, Université de Toulouse, CNRS, INRAE, INSA, Toulouse, France

² LAAS, Université de Toulouse, CNRS, Toulouse, France

³ Lallemand SAS, Toulouse-Blagnac, France

⁴ CIRIMAT, Université de Toulouse, CNRS, INPT, UPS, Toulouse, France

⁵ Fédération de Recherche FERMAT, CNRS, Toulouse, France

*Corresponding author: Cécile Formosa-Dague, formosa@insa-toulouse.fr

Address: INSA de Toulouse, Toulouse Biotechnology Institute
135 avenue de Rangeuil,
31400 Toulouse, France

Abstract

The microalgae cell wall represents its interface with its environment and a strong barrier to disrupt in order to extract the cell's products. Understanding its composition and architecture is a challenge that if overcome, could lead to substantial advancements in optimizing microalgae-production systems. However, the cell wall is a dynamic and complex structure that evolves depending on the growth phase or culture conditions. To apprehend this complexity, an experimental approach combining AFM, XPS, and chemical hydrolysis followed by HPAEC-PAD was developed to understand the cell wall of *Chlorella vulgaris*, a biotechnologically-relevant green microalgae species. Exponential and stationary growth stages were investigated, as well as saline stress condition inducing lipid production. Results showed that both the cell wall composition and architecture changes in stationary phase, with an increase of the lipidic fraction at the expense of the proteic fraction, changes in the polysaccharidic composition, and a significant increase of its rigidity. Under saline stress, cell wall architecture seems to be affected as its rigidity decreases importantly. Altogether, this study demonstrates the power of combining these three techniques to give new insights into *C. vulgaris* cell wall, in terms of composition and architecture, and of its dynamics in different conditions.

Keywords: Cell wall, AFM, XPS, chemical hydrolysis, Microalgae

Microalgae are unique microorganisms that convert light energy, water, and inorganic nutrients into a biomass resource rich in value-added products such as carbohydrates, proteins, or pigments [1]. In addition, microalgae are also highlighted as an alternative and renewable source of energy because of their important capacity to produce oil [1] that can be transformed into biofuel [2]. For this reason notably, a lot of attention has been paid to optimize culture conditions where the production of lipids by microalgae is maximized. For example, environmental stresses such as salinity increase, has been described to change the biomass composition and induce lipid accumulation in cells. For this reason, applying this type of stress, in different cultivation systems, has attracted a lot of interest for microalgae-based biofuel production [3]. In fact, high extracellular concentrations of Na⁺ directly influence the ionic balance inside cells and subsequently the cellular activities [4]. In particular, salinity stimulates the synthesis of storage neutral lipids, notably triacylglycerides (TAGs), produced as secondary metabolites and stored as energy reservoirs [5]. Then, in biofuel production systems, after cell harvesting, the lipids produced need to be extracted from cells, which is still a critical challenge that needs to be overcome by the industry and research community. For the moment, existing extraction techniques require a significant amount of chemicals or energy because of the chemically complex and structurally strong nature of microalgae cell walls [6]. Therefore, a better understanding of the ultrastructure and the composition of microalgae cell walls and their dynamics in different culture conditions, such as saline stress conditions, is needed to develop efficient and targeted extraction procedures of valuable intracellular products such as lipids.

The microalgae cell wall is a sophisticated structure, rigid and mechanically strong, which protects microalgae cells from predators and harsh environments [6]. In addition, the cell wall regulates the biological and biomechanical stability of the cell, influencing significantly its interaction with its surroundings [7]. But because of the diversity existing in cell wall composition and structure depending on microalgae strains, and because of its dynamics depending on culture conditions, the microalgae cell wall remains poorly understood. Yet, several studies have showed the development of methods to isolate microalgae cell walls and determine their composition. Most of these studies focus on determining the polysaccharidic composition of the cell wall, using a combination of mechanical disruption with chemical and/or enzymatic hydrolysis. For example, some studies applied mechanical disruption of cells to extract the cell walls, which were then treated using chemical treatments, with LiCl [8] or with strong acids [9], or/and using enzymatic hydrolysis [10]. This way the authors hydrolyze the polysaccharides present in the cell wall, and can then identify the saccharidic monomers released using high performance liquid chromatography (HPLC) [9,10]. Using these methods, Canelli *et al.* reported differences in the cell wall saccharidic composition of cells in exponential phase and in stationary phase for *C. vulgaris* [9], meaning that the amount and profile of sugars of the cell wall of microalgae depend on the growth stage, thus highlighting the dynamics of microalgae cell wall composition. To determine the total and relative composition of microalgae cell walls (proteic, polysaccharidic, and lipidic fractions), other studies use surface characterization techniques such as Fourier-transform Infrared spectroscopy (FTIR) [11] or cryo-X-ray Photoelectron Spectroscopy (cryo-XPS) [12,13]. For instance, a recent study by Shchukarev *et al.* could determine the surface composition in terms of polysaccharides, lipids and proteins of three different microalgae species, *C. vulgaris*, *Coelastrella sp.* and *S. obliquus* [13]. This study showed that the relative amounts of the different fractions were different for the three species considered, showing thus the diversity but most importantly the complexity of microalgae cell walls.

However, while these techniques, HPLC-based polysaccharidic determination and XPS, have been used separately so far to study microalgae cell walls, their combination could result in a more complete understanding of the composition and dynamic characterization of microalgae cell walls. In addition, other surface characterization techniques could be used to probe microalgae cell walls, such as atomic force microscopy (AFM). AFM, first developed in 1986 [14], is a powerful tool to image cells with nanometer-scale resolution and probe their nanomechanical properties under liquid conditions. For cell wall characterization, such technique has been used notably with yeast cells to measure both the roughness and the rigidity of the cell wall; such measurements brought valuable information to understand the architecture of cell walls [15]. In the microalgae field, AFM has also proven to be an efficient technique to understand microalgae cells, their morphology, their nanomechanical properties, and their response to different conditions such as environmental stress [16].

Among the wide variety of microalgae species, several have been considered for biofuel production, including *Chlorella vulgaris*. *C. vulgaris*, first discovered in 1890 by a Dutch researcher [17], is one of the most studied microalgae species mainly because of its biotechnological importance for the production of proteins used in nutrition and for biofuel production [18]. Indeed, *C. vulgaris* is a unicellular freshwater microalgae species able to accumulate significant amounts of lipids under specific culture conditions, with a fatty acid profile adapted for biofuel production [19,20]. In this study, we investigated the cell wall composition and dynamics of *C. vulgaris* in three different conditions: in exponential phase, stationary phase, and salinity stress condition (0.1 M NaCl). For that, the approach that we developed combined three types of analysis. First, AFM was used to image the cells and probe the cell wall roughness and nanomechanical properties. Then, XPS analysis was used to give a global view of the cell wall composition and determine this way the relative amounts of the three fractions, proteic, saccharidic, and lipidic. Finally, to give a complete view of the cell wall composition, chemical hydrolysis followed by HPLC was performed to determine the saccharidic composition of the cell wall. In the end, the combination of these three techniques allow to get a complete picture of the effects of culture condition on the cell wall composition and dynamics of *C. vulgaris* cell wall, but also to understand the link between composition and architecture and the effects of composition changes on cell surface biophysical properties. These results provide important information that can be further used to develop more efficient and targeted lipid extraction methods for industrial applications, but also to better apprehend the microalgae cell wall and its interaction with its environment.

MATERIALS AND METHODS

Microalgae strain and culture. The green freshwater microalgae *Chlorella vulgaris* strain CCAP 211/11B (Culture Collection of Algae and Protozoa, Scotland, UK) was cultivated in sterile conditions in Wright's cryptophyte (WC) medium prepared with deionized water, as previously described [21]. Cells were cultivated at 20°C, under 120 rpm agitation, in an incubator equipped with white neon light tubes providing illumination of approximately 40 $\mu\text{mol photons m}^{-2} \text{s}^{-1}$ with a photoperiod of 18h light: 6h dark. Exponential phase experiments were carried out with 7 days batch cultures, whereas stationary phase and salinity stress condition (0.1M NaCl) experiments were carried out with 21 days batch cultures. Cell growth was monitored (cell abundance) for three different cultures in each condition.

AFM imaging. Before experiments, cells were first harvested by centrifugation (3000 g, 3 min), washed two times in PBS at pH 7.4, and immobilized on polyethylenimine (PEI, Sigma-Aldrich P3143) coated

glass slides prepared as previously described [22]. AFM images of *C. vulgaris* cells were then recorded in PBS at pH 7.4, using the Quantitative Imaging mode available on the Nanowizard III AFM (Bruker, USA), with MSCT cantilevers (Bruker, nominal spring constant of 0.01 N/m). Images were recorded with a resolution of 150 pixels × 150 pixels, at an applied force of <1.0 nN and a constant approach/retract speed of 90 μm/s (z-range of 3 μm). In all cases the cantilevers spring constants were determined by the thermal noise method prior to imaging [23]. In each case, 3 cells were imaged.

Roughness analyses. Roughness analyses were performed on *C. vulgaris* cells immobilized on positively charged glass slides (Superfrost™ Plus adhesion, Eprelia, USA). High resolution images of the cell walls were recorded in PBS using QI advanced imaging mode available on the Nanowizard III AFM (Bruker, USA), using MSCT cantilevers (Bruker, nominal spring constant of 0.01 N/m). In each case, 13 cells coming from at least 2 independent culture were imaged and images were recorded with a resolution of 150 x 150 pixels using an applied force < 1 nN. In all cases the cantilevers spring constants were determined by the thermal noise method prior to imaging [23]. The height images obtained were then analyzed using the Data Processing software (Bruker, USA) to determine the arithmetic average roughness (Ra)..

Nanomechanical Analyses. For nanoindentation experiments, the AFM was used in force spectroscopy mode using an applied force comprised between 0.5 and 2 nN depending on the condition, with MSCT cantilevers (Bruker, nominal spring constant of 0.1 N/m). In each case, 12 cells coming from at least 3 independent culture were analyzed (approximately 600 force curve for each cells, details are given in the Results and Discussion section). Young's moduli were then calculated from the indentation curves obtained (50 nm long indentation segments were used) using the Hertz model in which the force F , indentation (δ), and Young's modulus (Y_m) follow equation 1, where α is the tip opening angle (17.5°), and ν the Poisson ratio (arbitrarily assumed to be 0.5). The cantilevers spring constants were determined by the thermal noise method [23].

$$F = \frac{2 \times Y_m \times \tan \alpha}{\pi \times (1 - \nu^2) \times \delta^2} \quad (1)$$

Isolation of microalgae cell walls. The isolation process is based on the study by Schiavone *et al.* [24]. Briefly, cells coming from at least 3 independent culture in each case were harvested by centrifugation (4700 g, 10 min) and washed 2 times with sterile deionized water. Then the pellets were resuspended in 10 mL of sterile water and transferred to a 15 mL falcon tube containing 2 g of acid washed glass beads (0.5 mm of diameter, Thermofisher, G8772-100G). Cells were then disrupted using a Fastprep system (MP Biomedicals): 10 cycles of 20 s with intervals of 1 min were performed while keeping the pellets on ice. The cell suspension was directly collected, and the glass beads in the pellet were extensively washed with cold deionized water. The supernatant and washings were pooled and centrifuged at 4700 g for 15 min at 4 °C. The cell wall-containing pellet was again washed two times with cold deionized water. Then, pellets were frozen at -80°C and lyophilized in a freeze dryer until complete dryness.

Acid hydrolysis of microalgae cell walls and quantification of carbohydrates by HPAEC-PAD. Sulphuric acid (72 %) hydrolysis of the cell wall was carried out as described previously [24,25]. Briefly the freeze-dried biomass (10 mg) was suspended in 75 μL of 72% H₂SO₄ and vortexed to dissolved the powder. After 3 hours of incubation of the suspension at room temperature (20-25 °C) (vortex every 30 min) sample were diluted to reach 2N H₂SO₄ and incubated in a sand bath for 4 hours at 100°C (vortex every

1h). This was followed by a neutralization step with 40 g/L Ba(OH)₂, then, samples were filled with water until 25 mL volume is reached. Finally the suspensions were centrifuged (10 min 3000 g) and supernatants were collected. The supernatant was filtered on a 0.2 µm Amicon and then was analyzed by high-performance anion exchange chromatography (HPAEC) on ICS 3000 system (ThermoFisher Scientific, France). Separation of the released monosaccharides (glucose, galactose, rhamnose, arabinose, glucosamine, xylose, mannose) were performed on a CarboPac PA1 analytical column (250 x 4 mm) with a guard column CarboPac PA1 using an isocratic elution at 18 mM NaOH (200 mM) for 20 min at 1 mL/min and 25°C. After a washing step was performed with 200 mM NaOH for 5 min and 300 mM sodium acetate in 200 mM NaOH for 10 min, following a cycle of equilibration of the column with 18 mM NaOH for 20 min. Sugar residues were detected on a pulsed amperometric system equipped with a gold electrode and a reference electrode (Ag/AgCl) using the method “Carbohydrate standard quadruple potential”.

XPS analysis. The photoelectron emission spectra were recorded using a monochromatised Al K α (hv = 1486.6 eV) source on a ThermoScientific K-Alpha system. The X-ray Spot size was about 400 µm. The Pass energy was fixed at 30 eV with a step of 0.1 eV for core levels and 160 eV for surveys (step 1 eV) The spectrometer energy calibration was done using the Au 4f_{7/2} (83.9 ± 0.1 eV) and Cu 2p_{3/2} (932.8 ± 0.1 eV) photoelectron lines. XPS spectra were recorded in direct mode N (Ec) and the background signal was removed using the Shirley method. The flood Gun was used to neutralize charge effects on the top surface. For each condition, experiments were performed in triplicate on cell walls isolated from cells coming from at least 2 independent cultures were conducted.

Protein quantification. Protein quantifications were performed with cells coming from at least 3 independent cultures in each case using a bicinchoninic acid (BCA) protein assay kit (ThermoScientific, 23225) according to Smith *et al.* [26]. Bovine serum albumin (BSA) was used as a standard and the protocol was followed at 60 °C for 30 minutes following the manufacturer guidelines.

Hydrophobicity measurements. Hydrophobicity measurements were conducted using AFM and FluidFM as described in Demir *et al.* [27] Briefly, an air-bubble was produced using a Nanowizard III AFM (Bruker, USA), equipped with FluidFM technology (Cytosurge AG, Switzerland). Experiments were performed in PBS, using microfluidic micropipette probes with an aperture of 8 µm (spring constant of 0.3, and 2 N/m, Cytosurge AG, Switzerland). The probes were calibrated using the thermal noise method prior to measurement.[23] *C. vulgaris* cells were first harvested by centrifugation (3000 g, 3 min), washed two times in PBS at pH 7.4 and immobilized on positively charged glass slides (Superfrost™ Plus adhesion, Eprelia, USA). Interactions between the formed bubbles at the aperture of the microfluidic micropipette probes and 8 cells coming from at least 2 independent culture were measured in force spectroscopy mode using a constant applied force of 1 nN. Force curves (approximately 625 force curve for each cell) were recorded with a retraction z-length of up to 3 µm and a constant retraction speed of 3.0-6.0 µm/s. The adhesion force between bubble and *C. vulgaris* cell wall corresponds to the height of the adhesion peak.

Statistical analysis. Experimental results represent the mean ± standard deviation (SD) of at least three replicates. For each experiments, the number of replicates is indicated both in the Material and Methods section in the corresponding paragraphs, and in the Results and Discussion section. For large samples (n>20 values) unpaired student t-test was used to evaluate if the differences between the conditions are significant. For small samples (n<20 values) non-parametric Mann and Whitney test was used to assess the differences. The differences were considered significant at p <0.05.

RESULTS AND DISCUSSION

Influence of salinity stress on growth of *C. vulgaris*

A first step in the study was to evaluate the effects of the culture conditions used on cell growth over time. For that, *C. vulgaris* cells were cultured during 30 days in normal conditions or under salinity stress; the optical density (OD) of the suspensions was measured every day to monitor cell growth. The results are presented in Figure 1. A first information from these growth curves is that both in control and in salinity stress condition, they do not show a lag phase, meaning that cells did not need time to adapt to the presence of salt in the medium. *C. vulgaris* cells cultured in standard conditions were in an exponential growth phase during 21 days, before reaching the stationary phase. However, when cells were cultivated under salinity stress, the exponential growth phase was significantly reduced to 15 days. Then cells stayed in stationary phase during 10 more days, after that cell concentration decreased by 15%, indicating partial cell death. This decline phase is not observed for cells cultivated in standard conditions. Studies in the literature have determined that the NaCl present in the medium, at a certain concentration, becomes toxic and reduces the growth, explaining the decline in saline stress condition. For instance Singh and coworkers reported similar growth curves patterns with a decline for *C. vulgaris* cells cultivated in saline stress conditions using, different salt concentrations [28]. These measurements thus show that culture conditions have an important impact on cell growth, and thus most likely on cell wall structure and composition. In addition, it has been showed that cells in stationary phase undergo a pH increase that modifies cell wall properties, such as composition [29] and architecture [22,30]. Thus in the next part of this work, we used AFM, XPS and chemical hydrolysis followed by HPLC to analyze the cell wall of cells grown in standard conditions in both exponential (7 days of culture) and stationary phase (21 days of culture), and of cells grown in saline stress (0.1 M of NaCl) during 21 days. Analysis of *C. vulgaris* cultivated with 0.1M NaCl (salinity stress condition) were performed at 21 days with stationary phase cells, where the highest difference in growth is observed compared to cells in cultured in normal conditions.

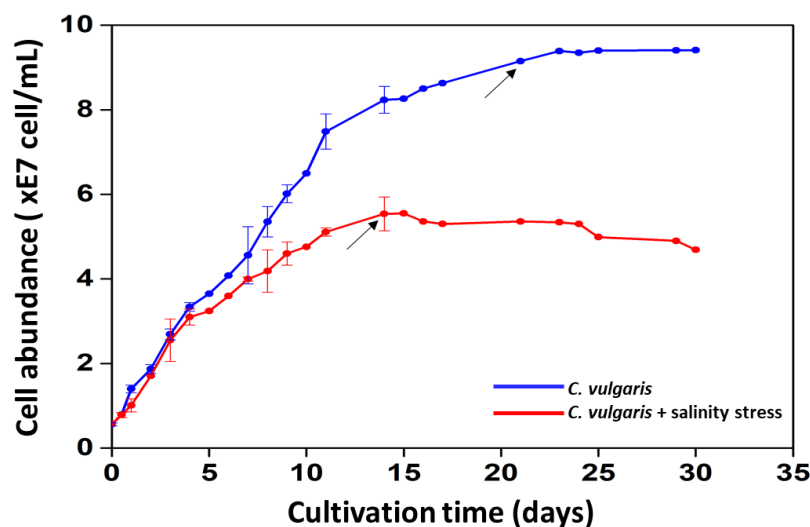


Figure 1. *C. vulgaris* growth. Variation in cell abundance (cell/mL) measured over time for batch cultures of *C. vulgaris* in standard conditions (WC culture medium, blue curve) and in salinity stress condition (WC culture medium supplemented with 0.1 M NaCl, red curve). The black arrows indicate in each case the end of exponential phase and the beginning of stationary phase.

Probing the biophysical properties of cell surfaces in the different culture conditions using AFM

Then in a next step, *C. vulgaris* cells grown in the different conditions described above were analyzed using AFM. For that, first, height images of the whole cells were obtained using a force spectroscopy-based imaging mode (Quantitative Imaging mode, QI [31]) with a resolution of 150 x 150 pixels. Images are shown in Figure 2a, b and c for exponential phase, stationary phase and salinity stress condition respectively. For cells grown in standard conditions, no significant morphological changes could be observed between the two different growth stages (exponential phase and stationary phase). However, under saline stress, defects at the cell surface can be observed; the cell wall appears to rougher compared to cells grown in standard conditions. To quantify this, we then made zoom-in high resolution images on small areas on top of cells (300 nm x 300 nm) using QI imaging mode, as shown in Figure 2d, e and f for exponential phase, stationary phase and salinity stress condition respectively. The cross-sections (Figure 2g-i) taken along the white lines on these images show that surface morphology is modified both for stationary phase cells and saline stress cells compared to exponential phase cells. In the case of the salinity stress, even larger patterns are visible on the cross-section indicating a larger deformation of the cell surface. To quantify these deformations, the average roughness R_a of the surface was measured directly from the height images presented in Figure 2d-f. In each condition, roughness measurements were performed on 13 different *C. vulgaris* cells coming from at least two independent culture; the results are shown in the box plot in Figure 2j. This quantitative analysis shows that in exponential phase, cells have an average roughness of 1.1 ± 0.4 nm which increases to 1.5 ± 0.7 nm in stationary phase and to 1.7 ± 1.2 nm in salinity stress condition. A statistical analysis (Mann-Whitney test) shows that these differences are not significant. This is in line with the existing literature; for instance, similar roughness values were also recorded for *Dunaliella tertiolecta* cells grown in exponential and stationary phase [32]. These results prove that the growth stage of cells does not have a significant effect on the cell surface roughness. However, when we compare the distribution of the roughness values measured in each case, in salinity stress condition the standard deviation is higher (1.2 nm) compared to stationary phase (0.7 nm) or exponential phase cells (0.4 nm). Thus even though the differences between conditions are not significant, still, applying a stress seem to increase the heterogeneity of the surface roughness values measured on different cells. A modification of cell surface roughness for cells under stress condition has already been showed for other types of microorganisms. For example, Schiavone *et al.* studied the effects of ethanol stress on the yeast *Saccharomyces cerevisiae* and reported a 50% increase in cell surface roughness when cells were submitted to this stress [33]. In our case, the increase in the heterogeneity of the roughness values that we observe in salinity stress condition could indicate that more molecules protrude from the cell surface, as it was hypothesized in a previous AFM study on *C. vulgaris* [21] or that charged surface molecules get coiled because of the salt present in the medium which could also result in a change in surface roughness [34].

Other properties that we can measure using AFM to get information on the structure or architecture of the cell wall are the nanomechanical properties. To obtain quantitative information on the nanomechanical properties of *C. vulgaris* cell wall, we determined the Young's modulus (Y_m) using nanoindentation measurements (Figure 2 k and l). In this type of measurement, a cantilever with known mechanical properties, is pressed against the cell surface at a specific force. This allows extracting the Y_m of the cell wall, in other words its compression resistance. The Y_m is thus a value that reflects the cell wall rigidity; the higher the Y_m value, the more rigid the cell wall. In this study, nanoindentation measurements, which provide access to force *versus* distance curves, were

performed on areas of 300 nm × 300 nm on top of cells, on 12 cells coming from at least three independent cultures. Ym values were then obtained first by converting the force curves into force versus indentation curves as shown in Figure 2k, and then by fitting them with a theoretical model, in our case, the Hertz model [35] (black circles on the curves in Figure 2k). Nanoindentation curves, obtained on cells in the different conditions, show a different slope, meaning that the AFM probe does not indent the same way in each case. For instance, it is able to indent deeper in exponential phase cells compared to stationary phase, meaning that this change in the growth phase increases the rigidity of the cell wall. The indentation is even deeper for cells cultured in salinity stress condition (21-days of culture) compared to stationary phase cells, showing that addition of salts have a direct impact on cell wall rigidity. Quantitative analysis of the Ym extracted from thousands of force curves recorded on 12 cells in each condition confirm these findings and show that exponential phase cells have an average Ym of 981.6 ± 554.5 kPa ($n = 6011$ force curves), which increases to 2.1 ± 1.3 MPa for stationary phase cells ($n = 6580$ force curves, the difference is significant at a p-value of 0.05, unpaired t-test). These values are comparable with previous nanomechanical measurements performed on *C. vulgaris* [21]. Moreover, a difference in the rigidity of cells in the two growth phases has already been observed for another microalgae species: for instance Pillet and co-workers investigated the nanomechanical properties of *D. tertiolecta* in exponential and stationary phase and found that cells in stationary phase are softer [32]. These modifications of rigidity over time can be explained by the fact that the pH of microalgae cultures changes with time. Indeed, several studies have showed that pH changes have a direct effect on microalgae cell wall nanomechanical properties [21,30]. For instance in our case, in normal conditions, the initial pH of *C. vulgaris* cultures is of 7.8, and then increases to 9.0 at the end of exponential phase (7 days) and to 8.5 in stationary phase (21 days). For cells submitted to saline stress, the Ym value this time drops to 433.2 ± 415.9 kPa ($n = 7005$ force curves, the difference is significant at a p-value of 0.05, unpaired t-test). This difference in the Ym value in this case can be explained by the direct impact of the environmental stress on the cell wall, as other studies have showed. For example, Yap *et al.* found that *Chlorococcum sp.* cells submitted to a N-deprivation had a Ym approximately 30% higher than for N-replete cells [36]. However, it could also be due to the osmotic pressure; in this saline condition, water may flow out of the cell, thereby changing its turgor pressure and thus the Ym of the cell wall [37]. To verify this point, we measured the diameter of different cells in all three conditions; no significant difference in the diameters measured were observed (Supplementary Figure S1). To understand if the changes observed in the roughness or in the rigidity of cells in stationary phase can be linked to the cell wall architecture, we need to determine the biochemical cell wall composition. Such correlation between cell surface biophysical properties and cell wall composition has been made already for different microorganisms such as yeasts [15], and might also be true in the case of this study.

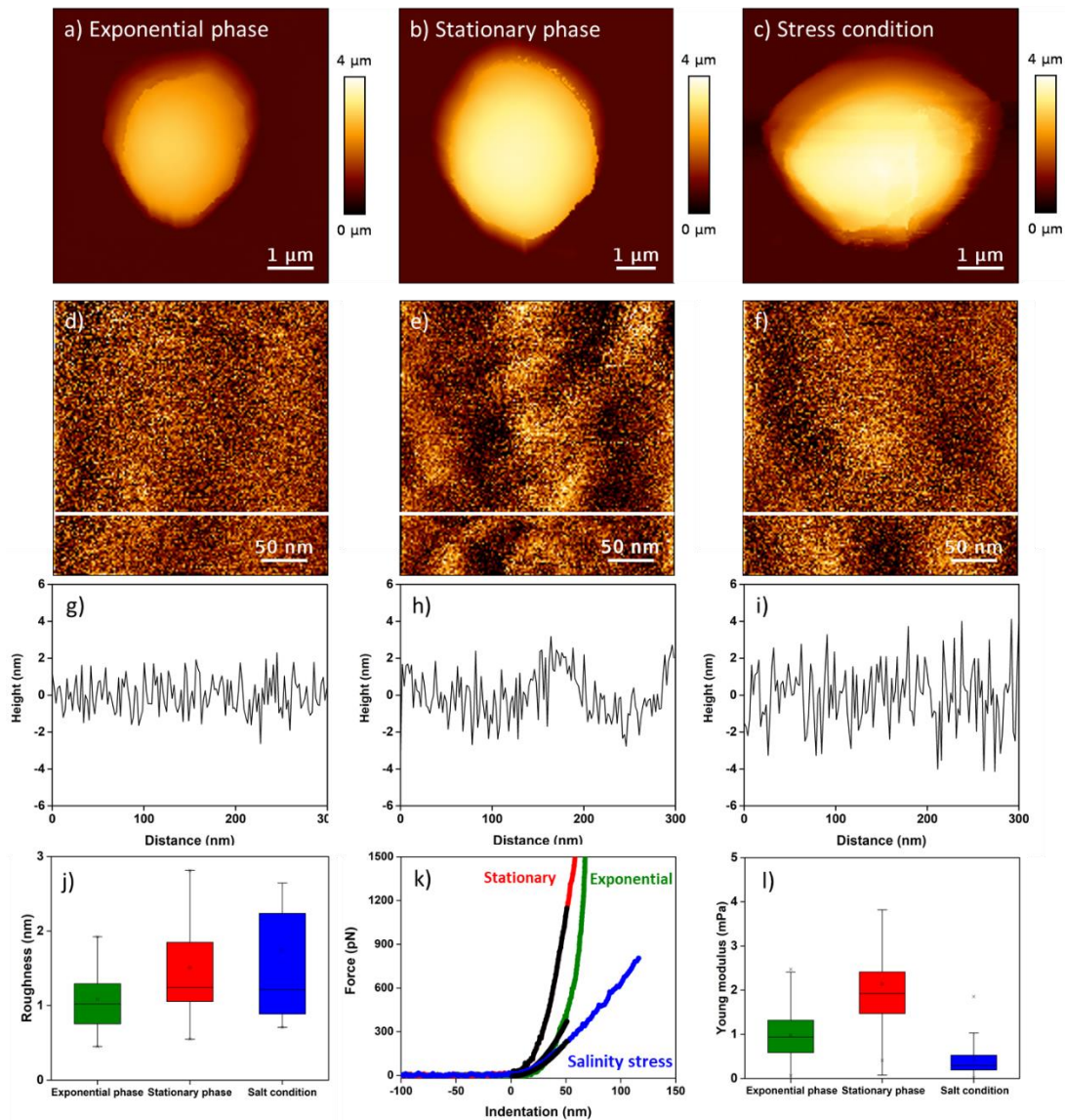


Figure 2. Roughness and nanomechanics of *C. vulgaris* cell wall. AFM images of single *C. vulgaris* cell in a) exponential phase b) stationary phase and c) salinity stress condition. AFM height images recorded on an area of 300 nm x 300 nm on top of cells in d) exponential phase e) stationary phase and f) salinity stress condition. g), h) and i) are cross-section taken along the white lines in d), e) and f) respectively. j) is a box plot showing the distribution of *C. vulgaris* surface roughness in exponential phase (green box), stationary phase (red box) and salinity stress conditions (blue box). k) Indentation curves (green, red and blue lines) fitted with the Hertz model on a 50 nm indentation segment (black lines) recorded on top of *C. vulgaris* cells in exponential phase (green curve), stationary phase (red curve) and salinity stress conditions (blue curve). l) Boxplot showing the distribution of Young's modulus values measured on top of *C. vulgaris* cells in exponential phase (green box), stationary phase (red box) and salinity stress conditions (blue box).

Biochemical composition of microalgae *C. vulgaris* cells based on XPS

Thus to explore the biochemical composition of *C. vulgaris* cell wall depending on the different culture conditions used in this study, we used XPS. XPS technique quantitatively measures the elemental composition of a surface, biotic or abiotic, including the chemical functionalities in which the elements are involved [38]. XPS has proven to be a powerful technique to determine the cell wall

composition of yeast and bacteria; in the case of microalgae, the few available studies use cryo-XPS, whose difference with conventional XPS relies in the sample preparation procedure.¹⁸ In the case of our study, the XPS analysis were performed on isolated freeze-dried cell walls. Because of XPS probing depth of less than 10 nm, and the thickness of *C. vulgaris* cell wall being of approximately 60 nm [6], using whole cells would provide information only on the near-surface region of cell wall. This is why we chose to work with isolated cell walls: by performing several measurements for each conditions we can this way have a more global information on the composition of the whole cell wall as they are mixed and not only its surface. On XPS spectra, the position of the XPS peak is known to be dependent on the chemical environment of the element, the binding energy having a tendency to decrease as the electron density on the atom increases [39]. XPS overall spectra to identify the elements are shown in supplementary Figure S2. Moreover, carbon, nitrogen and oxygen spectra and elemental atomic percentages obtained for cells in exponential phase, stationary phase and salinity stress conditions are presented in Supplementary Figures S3, S4 and S5 as well as Tables S1, S2 and S3 respectively. Figure 3 presents the XPS carbon 1s spectra recorded on *C. vulgaris* cells in exponential phase, in stationary phase and in salinity stress condition. The positions, relative intensities and average atomic percentages (out of three replicates) of the carbon peaks are presented in the spectra.

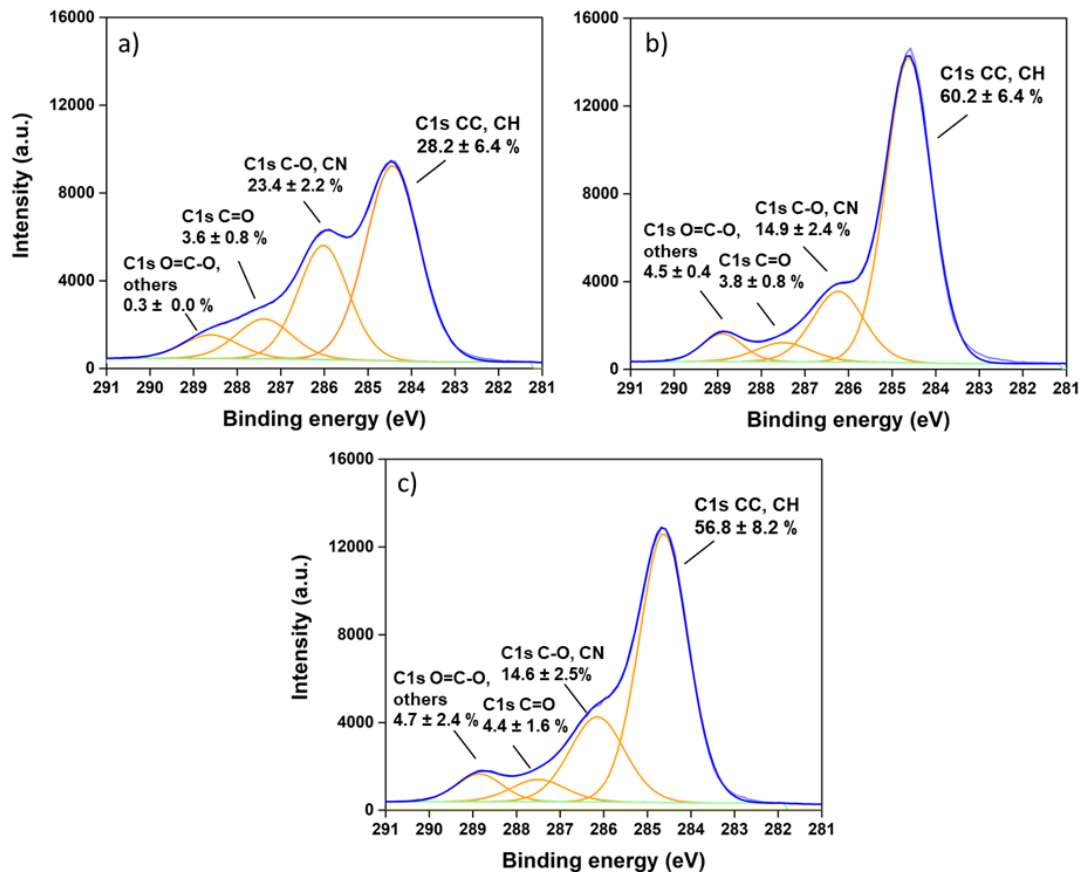


Figure 3. XPS analysis of *C. vulgaris* cell wall. Carbon 1s peaks recorded on *C. vulgaris* cell walls isolated from cells grown in standard condition in a) exponential phase, b) stationary phase and c) salinity stress condition. Average atomic percentages and standard deviations were calculated from triplicates ($n=3$)

In each case, one spectra representative of all the measurements performed is presented; the mean atomic percentages obtained for the three different measurements performed in each conditions are indicated. Exponential phase, stationary phase and salinity stress condition showed reproducible surface composition between the different cultures; the standard deviations obtained

for the atomic percentages reflect the normal heterogeneity found between different biological cultures. The average atomic percentage of C–C components increases by a factor of 2 from exponential phase (28.2 ± 6.4) to stationary phase (60.2 ± 6.4), and then slightly decreases from stationary phase to salinity stress condition (56.8 ± 8.2). Regarding C–O components, their average atomic percentage decreases by a factor of 1.6 from exponential phase (23.4 ± 2.2) to both stationary phase (14.9 ± 2.4) and salinity stress condition (14.6 ± 2.5). C=O components stay relatively constant between the three conditions, while the atomic percentage of O–C=O components is 15 times higher in exponential phase (0.3 ± 0.0) compared to stationary phase (4.5 ± 0.4), and slightly further increases when cells are exposed to salinity stress condition (4.7 ± 2.4). To understand the implications of these changes in terms of cell wall composition, we analyzed the XPS data using theoretical models developed by Rouxhet and coworkers [39]. For many biological systems, including the microalgae cell wall, three main classes of model compounds can be considered: proteins (Pr), polysaccharides (Po), and lipids (HC). The authors proposed a set of equations that allows to evaluate the proportion of carbon associated with these three model compounds, based on the three main components of the carbon peak. This model predicts that:

$$[C = O/C]_{obs} = 0.279 [Pr] + 0.167 [Po] \quad (2)$$

$$[C - (O, N)/C]_{obs} = 0.293[Pr] + 0.833[Po] \quad (3)$$

$$[C - (C, H)]_{obs} = 0.428[Pr] + [HC] \quad (4)$$

Simultaneously solving these carbon base equations gives the proportion of proteins, polysaccharides and lipids present in the cell wall of *C. vulgaris* in exponential phase, stationary phase and salinity stress condition; the results obtained are presented in Figure 4 and summarized in Supplementary Table 4.

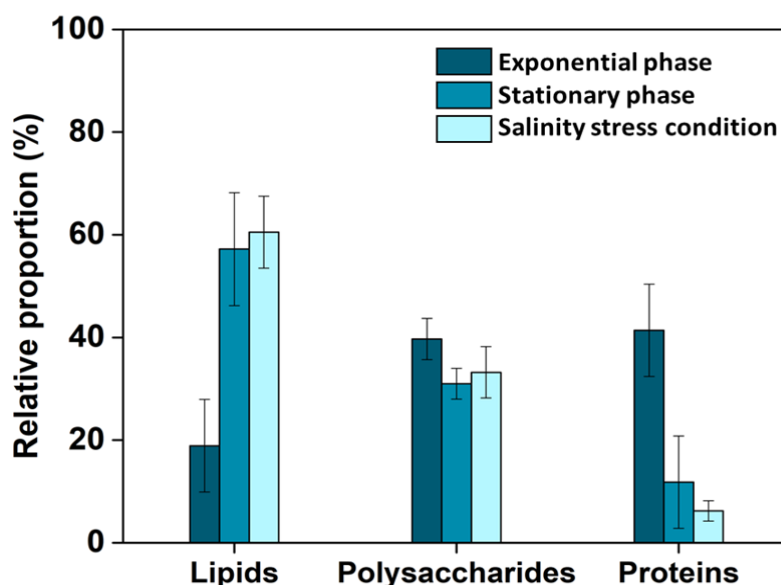


Figure 4. Biochemical composition of *C. vulgaris* cell wall. This histogram shows the relative proportions of carbon associated with lipids, polysaccharides and proteins in the cell wall of cells in exponential phase, stationary phase and salinity stress condition (0.1M NaCl). The XPS values are here normalized to 100% using a calculation based on the carbon concentration in each type of constituent (mmol of carbon/g of constituent) [39] and represent the relative proportion of the corresponding compounds. The error bars indicate the deviation from the average of the triplicates ($n=3$).

In exponential phase, the dominant constituents in the cell wall of *C. vulgaris* are proteins ($41.4 \pm 9.2\%$) and polysaccharides ($39.7 \pm 3.5\%$). This is in line with the study by Shchukarev *et al.*, where the authors also found that these compounds were predominant in the cell wall of *C. vulgaris* using cryo-XPS [13]. With aging from exponential phase to stationary phase, the difference in the cell wall composition is pronounced. The lipid content increases by a 3.0-fold at the expense of a 3.5-fold decrease in the protein content. The polysaccharide proportion decreases as well but in a non-significant manner. This increase in the lipid content is even more pronounced with cells exposed to the saline stress, in this case also at the expense of a decrease in the protein content. The proportion of polysaccharides, as for it, remains approximately the same compared to stationary phase cells. To make sure these analysis are correct, we also determined the protein concentration in the cell walls from cells in the three conditions using an assay kit. The results obtained (Supplementary Figure S6) showed that the highest protein concentration is observed for exponential phase cells and decreases importantly, in the same proportions than observed using XPS, for stationary phase and salinity stress condition. This additional experiment thus gives confidence in the validity of the XPS measurements performed.

These results are quite interesting. Indeed, it has been showed by multiple studies that salt stress induces the accumulation of lipids in *C. vulgaris*, more specifically of storage neutral lipids (TAG) [40,41]. These neutral lipids are present in the cells as droplets in the chloroplast matrix and in the cytoplasm [42]. Thus by definition, they should not be present in the cell wall. The lipids that have a structural role and that are located on the cell wall are polar lipids, which are mainly phospholipids and glycolipids. But while the effects of salinity stress on storage lipid accumulation has been investigated before, its effects on the production of polar lipids composing the cell wall has never been studied, as far as we know. The XPS data obtained here seem to indicate that their production is also increased in stationary phase or under salinity stress. To prove this, a way is to evaluate the hydrophobic properties of the cell wall, as lipids are the only components that can provide hydrophobic properties to cells. Indeed, polysaccharides are hydrophilic, and while proteins could also have hydrophobic properties, their relative fraction in the cell wall in stationary phase and in salinity stress condition is small, making it unlikely that they could participate in a significant manner to the hydrophobicity of the cell wall. Hydrophobic organic material are mostly composed of large fractions of aliphatic or aromatic substances. Thus the ratio of aliphatic carbon components to the total carbon in the C1 spectra can be directly linked to the hydrophobicity of the surface [39,43,13]. This method to determine hydrophobicity has already been applied in different studies, for example, to compare the hydrophobicity of bacteria between aqueous phase and organic phase [43], or to compare the relative hydrophobicities of different microalgae species [13]. In the case of our study, the aliphatic content in *C. vulgaris* in exponential phase corresponds to $42.9 \pm 7.0\%$ of the total carbon, which is lower than for the other two conditions, where the ratios are of $71.9 \pm 5.1\%$ in stationary phase and of $70.3 \pm 7.2\%$ in salinity stress condition. This means that cells are more hydrophobic in stationary phase and salinity stress condition compared to exponential phase, most likely because of the increased amount of lipids present in the cell wall in these conditions.

To confirm the XPS data and further prove that the amount of structural lipids in the cell wall is increased in stationary phase and salinity stress conditions, we performed another type of experiments to evidence their presence in the cell wall. For that, we probed the hydrophobic properties of the surface of living cells in the different conditions using a method recently developed in our team based on FluidFM [44], which combines AFM and microfluidics. It consists in producing a

bubble at the aperture of a FluidFM cantilever, and probing its interactions with cells in force spectroscopy experiments [27]. As bubbles in water behave like hydrophobic surfaces, the interactions recorded directly reflect the hydrophobic properties of cells. The higher the adhesion force, the more hydrophobic the surface is. The results are presented in Figure 5, a schematic representation of the experiment's principle is shown in Figure 5a. For cells in exponential phase, force curves show a single retract peak at the contact point, typical of hydrophobic interactions [45], (inset in Figure 5b) with an average force of 3.7 ± 0.7 nN (Figure 5b, $n = 4950$ force curves obtained from 8 cells coming from 2 independent cultures). The same type of adhesion peak is observed in stationary phase and in saline stress conditions, but in these cases, the adhesion force is increased to 4.9 ± 0.8 nN for cells in exponential phase (Figure 5c, $n = 4938$ force curves obtained from 8 cells coming from 2 independent cultures), and to 5.6 ± 1.1 nN in saline stress conditions. (Figure 5d, $n = 4774$ force curves obtained from 8 cells coming from 2 independent cultures). These values are all significantly different at a p -value < 0.05 (unpaired student test). These results are important; they were performed on live cells cultivated in the different conditions used in this study, and also show that cells are more hydrophobic and thus that more lipids are present in stationary phase and in saline stress conditions. Thus they confirm the XPS data obtained and indeed, in these conditions, not only the production of storage lipids by the cells is increased, but also the production of structural lipids present in the cell wall.

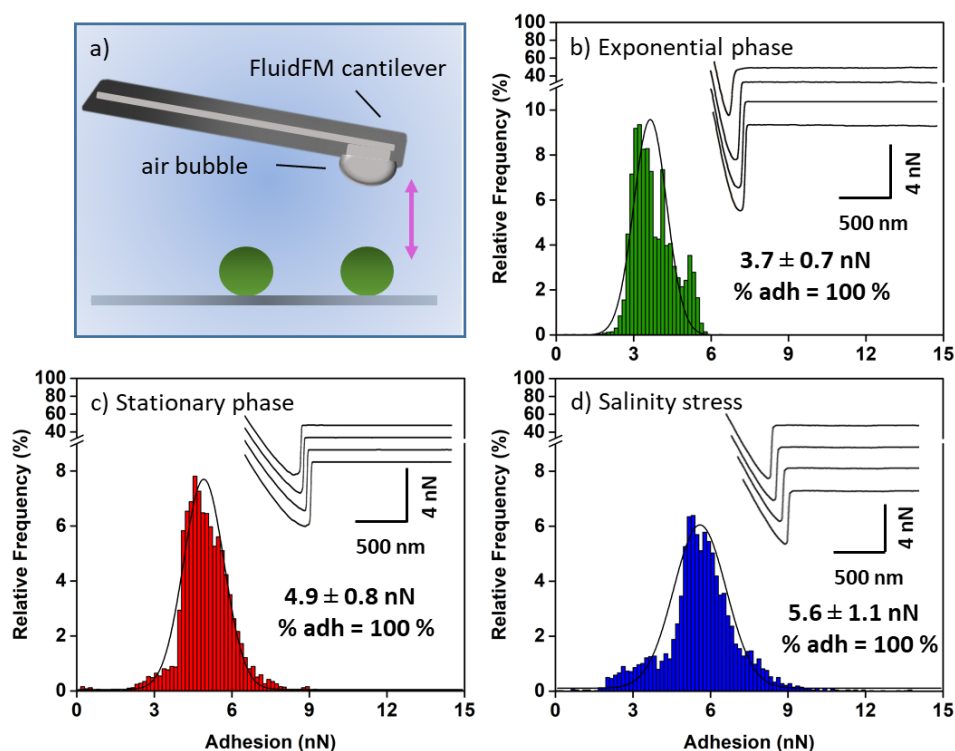


Figure 5. Probing the hydrophobic properties of *C. vulgaris* cell wall. a) Schematic representation of the experiment's principle: the interactions between bubbles produced at the aperture of FluidFM cantilevers and *C. vulgaris* cells immobilized on a surface are probed in force spectroscopy mode. Adhesion force histogram obtained between bubble and *C. vulgaris* cells in b) exponential phase c) stationary phase and d) salinity stress condition. Insets in b), c) and d) show representative force curves obtained in each case.

Regarding the variations observed in the proteic content in the cell wall, the decrease of this fraction can be explained by the fact that in stationary phase or under salt stress condition, the photosynthesis is inhibited [46]. This has for consequence to decrease the chlorophyll content in cells

which results in cell growth inhibition, as we could observe on the growth curves (Figure 1), but also in the decrease of the proteic content of cells. This has already been showed for *C. vulgaris* cells submitted to the same saline stress (0.1 M) as in this study [28]. In addition, a genomic study has showed that under saline stress conditions, the expression of a large number of genes was down-regulated, in particular genes involved in the photosystem light-harvesting pathways as well as genes involved in protein synthesis and stability [47].

Altogether collecting these information on the cell wall composition allows understanding better the biophysical observations made with AFM in terms of cell wall roughness and rigidity. For instance, XPS results show that the proportion of polysaccharides does not vary much; polysaccharides are long polymers that can be exposed at the outer surface of cells, and thus which can be responsible for the cell wall roughness [48,49]. Our AFM data showed no significant difference in the roughness between the three conditions; this could perhaps be due to the fact that the proportion of this fraction remains similar in the different conditions tested. Also the rigidity of cells in stationary phase is significantly more important than for cells in exponential phase; in this case the change in the rigidity can be attributed to the different cell wall composition between these two conditions. This is an interesting point because it shows that the cell wall is a dynamic and complex structure able to rearrange during the growth of cells. Cells in stationary phase and in saline conditions have a similar cell wall composition, but a very different rigidity. In saline condition, the decrease in the rigidity of the cells can probably be mainly attributed to a decrease of turgor pressure. However, another hypothesis could also be that in this case, because of the environmental stress applied, the cell wall rearranges with a different architecture than for cells in stationary phase. This different architecture, for a same composition, could also contribute to the variation in the rigidity observed. Thus taken together, the combination of XPS data with AFM analysis of the cell wall enlightens its complexity and dynamics. These are important information for example to optimize disruption procedures to extract the lipid content of cells. For instance, if mechanical disruption is used, using a saline stress on cells to produce lipids might be a better alternative; cells are less rigid in this condition and can be more easily ruptured. In addition, different disruption procedures using enzymatic degradations, or a combination of enzymatic degradation and mechanical rupturing can be used; to optimize such procedures and select adapted enzymes, more information is needed on the polysaccharides present in the cell wall.

The saccharidic composition of *C. vulgaris* cell wall is influenced by the growth phase and culture conditions

Thus to determine the polysaccharidic composition of the cell wall of *C. vulgaris* in the different conditions, isolated cell walls were used for acid hydrolysis using the well-known concentrated sulfuric acid method. The monosaccharide composition of microalgae cell walls is reported in Figure 6 (HPAEC-PAD spectra are presented in Supplementary Figure S3); in this figure the monomer concentrations are expressed as (w/w) mg of monomer per gram of dry cell wall (DCW). Our results show that *C. vulgaris* cell wall is composed predominantly of glucose followed by galactose, rhamnose, arabinose and glucosamine. Other monosaccharides are also present but in smaller amounts; xylose and mannose, although for those, the peaks on the spectra overlap (see HPAEC-PAD spectra in Supplementary Figure S3), meaning that their quantification is not feasible. Glucose and galactose represent the main components of *C. vulgaris* carbohydrates biomass in all three conditions, and account for 78% of the total amount of cell wall carbohydrates in stationary phase and in salinity stress conditions, and for 86% in exponential phase. Therefore, the main composition changes taking place in the different

conditions thus concern these two sugars. Indeed, glucose concentration drops from 96.0 mg/g in exponential phase to 55.3 mg/g in stationary phase and 40.1 mg/g in saline stress condition. While the relative quantities are less important for galactose, the same tendency is observed, the concentration decreases from 18.4 mg/g for exponential phase cells to 12.8 mg/g and 9.8 mg/g for stationary phase and salinity stress conditions cells respectively. The concentrations of the other monosaccharides present, rhamnose, arabinose and glucosamine remain almost the same in the different conditions. Regarding xylose and mannose, while no concentration values can be given in this case, the comparison of the total peak area (combination of xylose and mannose) shows an increase of almost 80% in the total concentration of these sugar from exponential to stationary phase and then shows a decrease of almost 50% from stationary phase to salinity stress condition. As already mentioned the protein concentration was determined using the bicinchoninic acid method (Supplementary Figure S6), thus the proportion of lipids can be deduced. These proportions obtained based on these results are presented in Supplementary Figure S8; they follow the same pattern than what was obtained using XPS data, thus confirming the validity of our observations. Note that the percentages obtained for each fractions are different in the two cases because of the two different modes of calculation used, but the relative differences between the two techniques are similar showing the robustness of our analysis.

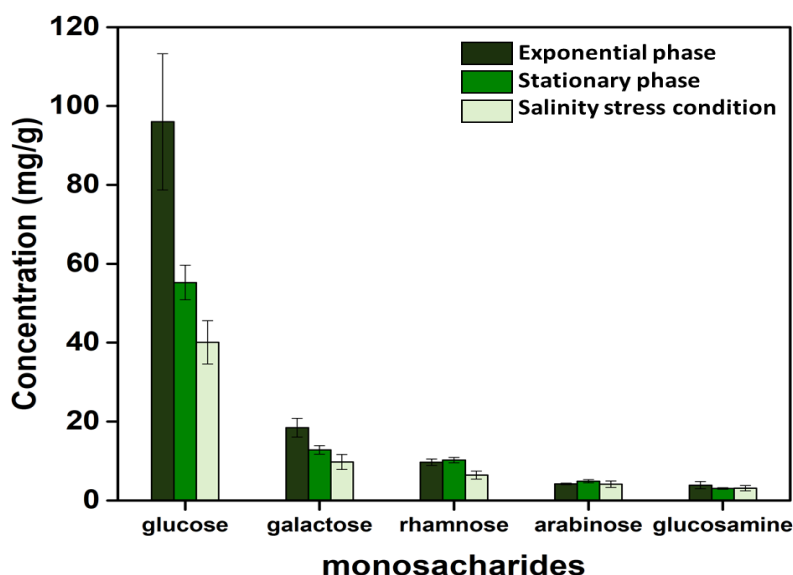


Figure 6: Monosaccharide composition of *C. vulgaris* cell wall in exponential phase, stationary phase and salinity stress condition (0.1M NaCl). The composition is expressed as milligram of monomer per gram of dry cell wall. The error bars indicate the deviation of the triplicates (n=3) from the average.

Different studies in the literature have analyzed the monosaccharidic composition of microalgae cell walls using similar experimental approaches. For example, in line with our findings, high glucose and galactose concentrations have also been reported by other authors in the case of *C. vulgaris* [9,50]. However, on the same microalgae species *C. vulgaris*, a study by Canelli *et al.* shows that the growth stage has no major effect on the monosaccharide composition [9]. This is different to what we observe here, however, in this study, a different strain of *C. vulgaris* was used, in different culture conditions. In the case of yeast microorganisms, it has been showed that the strains used, as well as their harvesting time play a critical role in the composition of the cell wall [51], thus the differences between our results and the study by Canelli *et al.* might be only due to these two parameters. This hypothesis is further comforted by a study performed on another microalgae species that shows that strain and culture conditions have an effect on the full biomass composition [52]. In

addition, for different microalgae species, different compositions were reported at different growth phase. For example, major changes were observed in *Thalassiosira pseudonana*, where an increase in ribose, galactose, and mannose and a significant decrease of glucose [53] were reported for stationary phase cells. Additionally, in our case, cells in stationary phase and in saline stress conditions may have started consuming intercellular carbohydrate depositories, which could decrease the glucose fraction in the cell wall [9].

In these experiments, the polysaccharides present in the cell wall are hydrolyzed into monosaccharides. Identifying them however does not allow determining the polysaccharides they come from, which could be an interesting information to obtain if further cell wall degradations processes are developed to extract the cell's contents. One way to identify the polysaccharides that could be present in the cell wall is to hydrolyze them with specific enzymes; if the substrate of the enzyme is present, the enzyme will release monosaccharides that can be detected by further HPLC analysis. So far, such studies have not been performed on microalgae cells walls, however, one study by Gerken *et al.* in 2013 consisted in treating cells on agar plates with specific enzymes; in this case an inhibition of cell growth was linked to the presence or not of their substrates in the cell wall [6]. Their work included the strain of *C. vulgaris* used in this study (strain CCAP211/11B); the main enzymes the authors identified as inhibiting cell growth for this strain are listed in Table 2. The polysaccharides that these enzymes hydrolyze and their corresponding monomers are also listed in this table. Hydrolysis with chitinase, chitosanase and lysozyme results in the release of the same monomer called glucosamine, which was identified in our experiments. This means that either chitin or chitosan (acetylated form of chitin) can be present in the cell wall of our strain. However, in Gerken's study, chitosanase, which is specific to chitosan, only partially inhibited cell growth which could mean that perhaps chitin is the main form present in the cell wall of our cells. This could also mean that another type of glucosamine-based polymer is present: for instance, Canelli *et al.* stated that in stationary phase, a microfibrillar chitosan-like layer composed of glucosamine is present in *C. vulgaris* cell wall [9]. Lysozyme can hydrolyze various substrates among which chitin and chitosan, but as stated in Gerken's study, chitinase and lysozyme have different activities towards *C. vulgaris* cell wall, and the activity of lysozyme is required to expose other polymers in stationary phase cells. This thus may be in line with the findings of Canelli *et al.* and the glucosamine present in our cells, in stationary phase at least, could rather indicate the presence of another chitosan-like polymer. According to Gerken's study, another enzyme that completely inhibited *C. vulgaris* cell growth is β -glucuronidase, however, we did not detect its corresponding monomer (glucuronic acid) in the cell wall. Either its concentration is lower than the limit of detection of our HPLC system, or the polysaccharides it hydrolyzes, glucuronides, are not present in our cells perhaps because of different culture conditions between Gerken's and our study. Further, laminarinase, which can hydrolyze β -glucans into glucose monomers, has also been showed to completely inhibit *C. vulgaris* cell growth. Glucose is the most abundant monomer that we find in our experiments in all conditions. Thus this could mean that β -glucans form a large part of the polysaccharidic fraction of the cell wall, and the slight decrease in polysaccharides that we observe in stationary phase and in saline stress conditions compared to exponential phase (XPS data) may be due to the decrease in these conditions of these types of polysaccharides. Glucose is also the monomer constituting cellulose, however, Gerken *et al.* found that cellulase enzyme had no activity on *C. vulgaris* cells, meaning that this strain most likely does not contain cellulose, in contrast with other microalgae species [9,54]. Finally, the activity of pectinase and sulphatase enzymes found by Gerken *et al.*, could explain the presence of rhamnose, arabinose and galactose in our analysis,

which could be part of pectic substances (rhamnose and arabinose) and of proteoglycans or glycosaminoglycans (galactose). Concerning the mannose and xylose that we found in our HPLC analysis, they could be coming from the degradation of mannoproteins or of hemicellulose. Despite the fact that some authors note the presence of hemicelluloses in cell wall of *Chlorella sp.*, there is no consensus on the type of hemicelluloses present in these cells [55].

Altogether, determining the saccharidic composition of the cell wall in this study allows to enhance our understanding of the cell wall. By comparing our data to the existing literature, we can make strong hypothesis on the polysaccharides present in the cell wall, which is an important point to understand the cell wall and develop strategies to disrupt it, for example through enzymatic degradations. Indeed, these disruption methods have been shown to consume less energy than mechanical or thermal treatments, and have already been successfully used for different types of microalgae [56]. In addition, as polysaccharides are often present directly at the cell surface, these hypothesis can also be important to understand the interacting behavior of cells, which can be determinant for example in harvesting processes using flocculation [21].

Table 1: Hypothesis on the polysaccharides present in *C. vulgaris* cell wall, formulated based on the enzymes that have been shown to inhibit cell growth by Gerken et al. [6]. The last column refers to references where it was found that the degradation of the corresponding polysaccharides led to the release of the monomers indicated.

Enzyme [6]	Polysaccharide	Monomer	Reference
Chitinase (+++)	chitin	N-acetyl-D-glucosamine (GlcNAc)	[57]
Chitosanase (++)	chitosan oligosaccharides	β -(1,4)-D glucosamine	[58]
Lysozyme (+++)	Peptidoglycan lipoproteins, lipopolysaccharides (LPS), and some hydrophobic peptides	N-acetylglucosamine N- acetyl muramic acid	[59,60]
B-Glucuronidase (+++)	Glucuronide/ β - glucuronides	Glucuronic Acid	[61]
Laminarinase (+++)	β -glucans	Glucose	[62]
Pectinase (+++)	Pectic substances; pectin, protopectin and pectic acids	Rhamnose arabinan, galactan or arabinogalactan	[63]
Sulphatase (+++)	Proteoglycans, glycosaminoglycans	galactose	[64,65]

CONCLUSIONS

In this work, three different techniques, AFM, XPS and chemical hydrolysis followed by HPAEC-PAD, were used to analyze *C. vulgaris* cell wall in different conditions relevant for the production of lipids used for biofuel production. The combination of these methods is original and has provided different information, which, taken together, has allowed to get new insights into the complexity of *C. vulgaris* cell wall and its dynamics depending on growth phase and culture conditions. For instance, we

could show that in exponential phase, the cell wall is composed in similar proportions (approximately 40%) of polysaccharides (mainly glucose and galactose-based polysaccharides) and proteins and also contained around 20% of lipids. These proportions change with the growth phase; the cell wall evolves during growth and its composition changes with a large increase of lipids at the expense of proteins. While the polysaccharidic fraction stays constant, the composition of this fraction also changes, with a decrease of glucose and galactose-based polymers. This composition variation is accompanied by an architectural changes that could be determined by probing the nanomechanical properties of the cell wall, which becomes significantly more rigid in stationary phase compared to exponential phase. Finally, when cells are submitted to a saline stress, their cell wall has a similar composition than for stationary phase cells but interestingly, it seems that the architecture of the cell wall is affected by the stress as they become a lot softer. Although in this case, the loss of turgor pressure induced by the osmotic stress may also partly explain the decrease in the rigidity observed. These new fundamental data, provided thanks to the original experimental approach developed in this study combining AFM, XPS and chemical hydrolysis, can be of great use to optimize important steps in microalgae-based biofuel production processes, such as harvesting or cell disruption. We believe these information will concretely contribute to the advancement of this field of research.

ACKNOWLEDGMENTS

C. F.-D. is a researcher at CNRS. C. F.-D. acknowledges financial support for this work from the Agence Nationale de la Recherche, JCJC project FLOTALG (ANR-18-CE43-0001-01). The authors would like to thank Pauline Herviou for her help with HPLC measurements, and Malak Souad Ftouhi for help with microalgae cultures.

CONFLICT OF INTEREST

The authors declare no conflicts of interest.

REFERENCES

- [1] N. Pragma, K.K. Pandey, P.K. Sahoo, A review on harvesting, oil extraction and biofuels production technologies from microalgae, *Renewable and Sustainable Energy Reviews*. 24 (2013) 159–171. <https://doi.org/10.1016/j.rser.2013.03.034>.
- [2] S. Fon Sing, A. Isdepsky, M.A. Borowitzka, N.R. Moheimani, Production of biofuels from microalgae, *Mitig Adapt Strateg Glob Change*. 18 (2013) 47–72. <https://doi.org/10.1007/s11027-011-9294-x>.
- [3] B.-H. Kim, R. Ramanan, Z. Kang, D.-H. Cho, H.-M. Oh, H.-S. Kim, *Chlorella sorokiniana* HS1, a novel freshwater green algal strain, grows and hyperaccumulates lipid droplets in seawater salinity, *Biomass and Bioenergy*. 85 (2016) 300–305. <https://doi.org/10.1016/j.biombioe.2015.12.026>.
- [4] T. Atikij, Y. Syaputri, H. Iwahashi, T. Praneenararat, S. Sirisattha, H. Kageyama, R. Waditee-Sirisattha, Enhanced Lipid Production and Molecular Dynamics under Salinity Stress in Green Microalga *Chlamydomonas reinhardtii* (137C), *Marine Drugs*. 17 (2019) 484. <https://doi.org/10.3390/md17080484>.
- [5] Q. Hu, M. Sommerfeld, E. Jarvis, M. Ghirardi, M. Posewitz, M. Seibert, A. Darzins, Microalgal triacylglycerols as feedstocks for biofuel production: perspectives and advances, *The Plant Journal*. 54 (2008) 621–639. <https://doi.org/10.1111/j.1365-3113X.2008.03492.x>.
- [6] H.G. Gerken, B. Donohoe, E.P. Knoshaug, Enzymatic cell wall degradation of *Chlorella vulgaris* and other microalgae for biofuels production, *Planta*. 237 (2013) 239–253. <https://doi.org/10.1007/s00425-012-1765-0>.

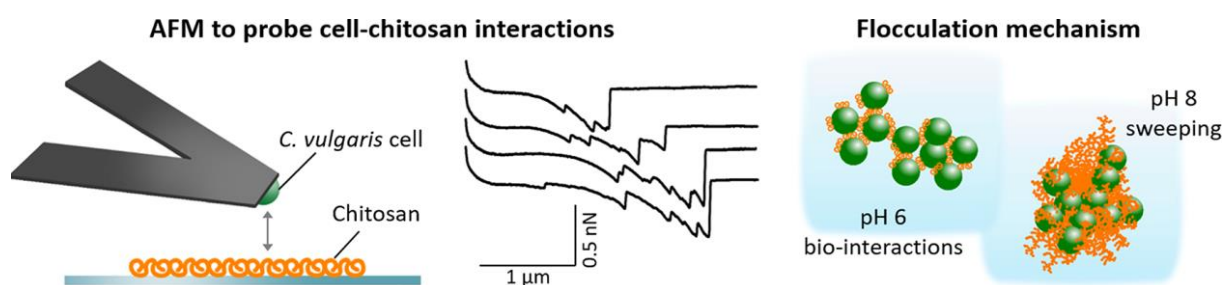
- [7] Z.A. Popper, G. Michel, C. Hervé, D.S. Domozych, W.G.T. Willats, M.G. Tuohy, B. Kloareg, D.B. Stengel, Evolution and Diversity of Plant Cell Walls: From Algae to Flowering Plants, *Annual Review of Plant Biology*. 62 (2011) 567–590. <https://doi.org/10.1146/annurev-arplant-042110-103809>.
- [8] J. Voigt, A. Stolarczyk, M. Zych, P. Malec, J. Burczyk, The cell-wall glycoproteins of the green alga *Scenedesmus obliquus*. The predominant cell-wall polypeptide of *Scenedesmus obliquus* is related to the cell-wall glycoprotein gp3 of *Chlamydomonas reinhardtii*, *Plant Science*. 215–216 (2014) 39–47. <https://doi.org/10.1016/j.plantsci.2013.10.011>.
- [9] G. Canelli, P. Murciano Martínez, S. Austin, M.E. Ambühl, F. Dionisi, C.J. Bolten, R. Carpine, L. Neutsch, A. Mathys, Biochemical and Morphological Characterization of Heterotrophic *Cryptothecodinium cohnii* and *Chlorella vulgaris* Cell Walls, *J. Agric. Food Chem.* 69 (2021) 2226–2235. <https://doi.org/10.1021/acs.jafc.0c05032>.
- [10] R.S. Alavijeh, K. Karimi, R.H. Wijffels, C. van den Berg, M. Eppink, Combined bead milling and enzymatic hydrolysis for efficient fractionation of lipids, proteins, and carbohydrates of *Chlorella vulgaris* microalgae, *Bioresource Technology*. 309 (2020) 123321. <https://doi.org/10.1016/j.biortech.2020.123321>.
- [11] A. Robic, D. Bertrand, J.-F. Sassi, Y. Lerat, M. Lahaye, Determination of the chemical composition of ulvan, a cell wall polysaccharide from *Ulva* spp. (Ulvales, Chlorophyta) by FT-IR and chemometrics, *J Appl Phycol*. 21 (2009) 451–456. <https://doi.org/10.1007/s10811-008-9390-9>.
- [12] Z. Gojkovic, A. Shchukarev, M. Ramstedt, C. Funk, Cryogenic X-ray photoelectron spectroscopy determines surface composition of algal cells and gives insights into their spontaneous sedimentation, *Algal Research*. 47 (2020) 101836. <https://doi.org/10.1016/j.algal.2020.101836>.
- [13] A. Shchukarev, Z. Gojkovic, C. Funk, M. Ramstedt, Cryo-XPS analysis reveals surface composition of microalgae, *Applied Surface Science*. 526 (2020) 146538. <https://doi.org/10.1016/j.apsusc.2020.146538>.
- [14] G. Binnig, C.F. Quate, Ch. Gerber, Atomic Force Microscope, *Phys. Rev. Lett.* 56 (1986) 930–933. <https://doi.org/10.1103/PhysRevLett.56.930>.
- [15] C. Formosa, M. Schiavone, H. Martin-Yken, J.M. François, R.E. Duval, E. Dague, Nanoscale Effects of Caspofungin against Two Yeast Species, *Saccharomyces cerevisiae* and *Candida albicans*, *Antimicrobial Agents and Chemotherapy*. 57 (2013) 3498–3506. <https://doi.org/10.1128/AAC.00105-13>.
- [16] I. Demir-Yilmaz, P. Guiraud, C. Formosa-Dague, The contribution of Atomic Force Microscopy (AFM) in microalgae studies: A review, *Algal Research*. 60 (2021) 102506. <https://doi.org/10.1016/j.algal.2021.102506>.
- [17] M.W.I. Beijerinck, Kulturversuche mit Zoochlorellen, Lichenengonidien und anderen niederen algen, *Botanische Zeitung*. 48 (1890) 729.
- [18] R. Halim, M.K. Danquah, P.A. Webley, Extraction of oil from microalgae for biodiesel production: A review, *Biotechnology Advances*. 30 (2012) 709–732. <https://doi.org/10.1016/j.biotechadv.2012.01.001>.
- [19] C. Safi, B. Zebib, O. Merah, P.-Y. Pontalier, C. Vaca-Garcia, Morphology, composition, production, processing and applications of *Chlorella vulgaris*: A review, *Renewable and Sustainable Energy Reviews*. 35 (2014) 265–278. <https://doi.org/10.1016/j.rser.2014.04.007>.
- [20] X.-F. Shen, Q.-W. Qin, S.-K. Yan, J.-L. Huang, K. Liu, S.-B. Zhou, Biodiesel production from *Chlorella vulgaris* under nitrogen starvation in autotrophic, heterotrophic, and mixotrophic cultures, *J Appl Phycol*. 31 (2019) 1589–1596. <https://doi.org/10.1007/s10811-019-01765-1>.
- [21] I. Demir, J. Blockx, E. Dague, P. Guiraud, W. Thielemans, K. Muylaert, C. Formosa-Dague, Nanoscale Evidence Unravels Microalgae Flocculation Mechanism Induced by Chitosan, *ACS Appl. Bio Mater.* 3 (2020) 8446–8459. <https://doi.org/10.1021/acsabm.0c00772>.
- [22] G. Francius, B. Tesson, E. Dague, V. Martin-Jézéquel, Y.F. Dufrêne, Nanostructure and nanomechanics of live *Phaeodactylum tricornerutum* morphotypes, *Environmental Microbiology*. 10 (2008) 1344–1356. <https://doi.org/10.1111/j.1462-2920.2007.01551.x>.

- [23] J.L. Hutter, J. Bechhoefer, Calibration of atomic-force microscope tips, *Review of Scientific Instruments*. 64 (1993) 1868–1873. <https://doi.org/10.1063/1.1143970>.
- [24] M. Schiavone, A. Vax, C. Formosa, H. Martin-Yken, E. Dague, J.M. François, A combined chemical and enzymatic method to determine quantitatively the polysaccharide components in the cell wall of yeasts, *FEMS Yeast Research*. 14 (2014) 933–947. <https://doi.org/10.1111/1567-1364.12182>.
- [25] N. Dallies, J. François, V. Paquet, A new method for quantitative determination of polysaccharides in the yeast cell wall. Application to the cell wall defective mutants of *Saccharomyces cerevisiae*, *Yeast*. 14 (1998) 1297–1306. [https://doi.org/10.1002/\(SICI\)1097-0061\(1998100\)14:14<1297::AID-YEA310>3.0.CO;2-L](https://doi.org/10.1002/(SICI)1097-0061(1998100)14:14<1297::AID-YEA310>3.0.CO;2-L).
- [26] P.K. Smith, R.I. Krohn, G.T. Hermanson, A.K. Mallia, F.H. Gartner, M.D. Provenzano, E.K. Fujimoto, N.M. Goetze, B.J. Olson, D.C. Klenk, Measurement of protein using bicinchoninic acid, *Analytical Biochemistry*. 150 (1985) 76–85. [https://doi.org/10.1016/0003-2697\(85\)90442-7](https://doi.org/10.1016/0003-2697(85)90442-7).
- [27] I. Demir, I. Lüchtfeld, C. Lemen, E. Dague, P. Guiraud, T. Zambelli, C. Formosa-Dague, Probing the interactions between air bubbles and (bio)interfaces at the nanoscale using FluidFM technology, *Journal of Colloid and Interface Science*. 604 (2021) 785–797. <https://doi.org/10.1016/j.jcis.2021.07.036>.
- [28] R. Singh, A.K. Upadhyay, P. Chandra, D.P. Singh, Sodium chloride incites reactive oxygen species in green algae *Chlorococcum humicola* and *Chlorella vulgaris*: Implication on lipid synthesis, mineral nutrients and antioxidant system, *Bioresource Technology*. 270 (2018) 489–497. <https://doi.org/10.1016/j.biortech.2018.09.065>.
- [29] B. Tesson, M.J. Genet, V. Fernandez, S. Degand, P.G. Rouxhet, V. Martin-Jézéquel, Surface Chemical Composition of Diatoms, *ChemBioChem*. 10 (2009) 2011–2024. <https://doi.org/10.1002/cbic.200800811>.
- [30] C. Formosa-Dague, V. Gernigon, M. Castelain, F. Daboussi, P. Guiraud, Towards a better understanding of the flocculation/flotation mechanism of the marine microalgae *Phaeodactylum tricornutum* under increased pH using atomic force microscopy, *Algal Research*. 33 (2018) 369–378. <https://doi.org/10.1016/j.algal.2018.06.010>.
- [31] L. Chopinet, C. Formosa, M.P. Rols, R.E. Duval, E. Dague, Imaging living cells surface and quantifying its properties at high resolution using AFM in QI™ mode, *Micron*. 48 (2013) 26–33. <https://doi.org/10.1016/j.micron.2013.02.003>.
- [32] F. Pillet, E. Dague, J. Pečar Ilić, I. Ružić, M.-P. Rols, N. Ivošević DeNardis, Changes in nanomechanical properties and adhesion dynamics of algal cells during their growth, *Bioelectrochemistry*. 127 (2019) 154–162. <https://doi.org/voelcker>.
- [33] M. Schiavone, C. Formosa-Dague, C. Elsztein, M.-A. Teste, H. Martin-Yken, M.A. De Morais, E. Dague, J.M. François, Evidence for a Role for the Plasma Membrane in the Nanomechanical Properties of the Cell Wall as Revealed by an Atomic Force Microscopy Study of the Response of *Saccharomyces cerevisiae* to Ethanol Stress, *Applied and Environmental Microbiology*. 82 (2016) 4789–4801. <https://doi.org/10.1128/AEM.01213-16>.
- [34] G.P. 't Lam, J.B. Giraldo, M.H. Vermuë, G. Olivieri, M.H.M. Eppink, R.H. Wijffels, Understanding the salinity effect on cationic polymers in inducing flocculation of the microalga *Neochloris oleoabundans*, *Journal of Biotechnology*. 225 (2016) 10–17. <https://doi.org/10.1016/j.jbiotec.2016.03.009>.
- [35] H. Hertz, Über die Berührung fester elastischer Körper, *Journal Für Die Reine Und Angewandte Mathematik*. 92 (1882) 22.
- [36] B.H.J. Yap, S.A. Crawford, R.R. Dagastine, P.J. Scales, G.J.O. Martin, Nitrogen deprivation of microalgae: effect on cell size, cell wall thickness, cell strength, and resistance to mechanical disruption, *Journal of Industrial Microbiology and Biotechnology*. 43 (2016) 1671–1680. <https://doi.org/10.1007/s10295-016-1848-1>.
- [37] D. Chang, S. Sakuma, K. Kera, N. Uozumi, F. Arai, Measurement of the mechanical properties of single *Synechocystis* sp. strain PCC6803 cells in different osmotic concentrations using a robot-

- integrated microfluidic chip, *Lab on a Chip*. 18 (2018) 1241–1249.
<https://doi.org/10.1039/C7LC01245D>.
- [38] H. Wei, X.-Y. Yang, H.C. van der Mei, H.J. Busscher, X-Ray Photoelectron Spectroscopy on Microbial Cell Surfaces: A Forgotten Method for the Characterization of Microorganisms Encapsulated With Surface-Engineered Shells, *Front Chem*. 9 (2021) 666159.
<https://doi.org/10.3389/fchem.2021.666159>.
- [39] P.G. Rouxhet, M.J. Genet, XPS analysis of bio-organic systems, *Surface and Interface Analysis*. 43 (2011) 1453–1470. <https://doi.org/10.1002/sia.3831>.
- [40] S. White, A. Anandraj, F. Bux, PAM fluorometry as a tool to assess microalgal nutrient stress and monitor cellular neutral lipids, *Bioresource Technology*. 102 (2011) 1675–1682.
<https://doi.org/10.1016/j.biortech.2010.09.097>.
- [41] N. Nordin, N. Yusof, T. Maeda, N.A. Mustapha, M.Z. Mohd Yusoff, R.F. Raja Khairuddin, Mechanism of carbon partitioning towards starch and triacylglycerol in *Chlorella vulgaris* under nitrogen stress through whole-transcriptome analysis, *Biomass and Bioenergy*. 138 (2020) 105600. <https://doi.org/10.1016/j.biombioe.2020.105600>.
- [42] S. Obeid, N. Beauvils, S. Camy, H. Takache, A. Ismail, P.-Y. Pontalier, Supercritical carbon dioxide extraction and fractionation of lipids from freeze-dried microalgae *Nannochloropsis oculata* and *Chlorella vulgaris*, *Algal Research*. 34 (2018) 49–56.
<https://doi.org/10.1016/j.algal.2018.07.003>.
- [43] R. Nakao, M. Ramstedt, S.N. Wai, B.E. Uhlin, Enhanced Biofilm Formation by *Escherichia coli* LPS Mutants Defective in Hep Biosynthesis, *PLOS ONE*. 7 (2012) e51241.
<https://doi.org/10.1371/journal.pone.0051241>.
- [44] A. Meister, M. Gabi, P. Behr, P. Studer, J. Vörös, P. Niedermann, J. Bitterli, J. Polesel-Maris, M. Liley, H. Heinzelmann, T. Zambelli, FluidFM: Combining Atomic Force Microscopy and Nanofluidics in a Universal Liquid Delivery System for Single Cell Applications and Beyond, *Nano Lett*. 9 (2009) 2501–2507. <https://doi.org/10.1021/nl901384x>.
- [45] E. Dague, D. Alsteens, J.-P. Latgé, C. Verbelen, D. Raze, A.R. Baulard, Y.F. Dufrêne, Chemical Force Microscopy of Single Live Cells, *Nano Lett*. 7 (2007) 3026–3030.
<https://doi.org/10.1021/nl071476k>.
- [46] A.J. Martínez-Roldán, H.V. Perales-Vela, R.O. Cañizares-Villanueva, G. Torzillo, Physiological response of *Nannochloropsis* sp. to saline stress in laboratory batch cultures, *J Appl Phycol*. 26 (2014) 115–121. <https://doi.org/10.1007/s10811-013-0060-1>.
- [47] N. Abdellaoui, M.J. Kim, T.J. Choi, Transcriptome analysis of gene expression in *Chlorella vulgaris* under salt stress, *World J Microbiol Biotechnol*. 35 (2019) 141.
<https://doi.org/10.1007/s11274-019-2718-6>.
- [48] M. Schiavone, N. Sieczkowski, M. Castex, E. Dague, J. Marie François, Effects of the strain background and autolysis process on the composition and biophysical properties of the cell wall from two different industrial yeasts, *FEMS Yeast Research*. 15 (2015).
<https://doi.org/10.1093/femsyr/fou012>.
- [49] E. Dague, R. Bitar, H. Ranchon, F. Durand, H.M. Yken, J.M. François, An atomic force microscopy analysis of yeast mutants defective in cell wall architecture, *Yeast*. 27 (2010) 673–684.
<https://doi.org/10.1002/yea.1801>.
- [50] K.H. Kim, I.S. Choi, H.M. Kim, S.G. Wi, H.-J. Bae, Bioethanol production from the nutrient stress-induced microalga *Chlorella vulgaris* by enzymatic hydrolysis and immobilized yeast fermentation, *Bioresource Technology*. 153 (2014) 47–54.
<https://doi.org/10.1016/j.biortech.2013.11.059>.
- [51] B. Aguilar-Uscanga, J. m. François, A study of the yeast cell wall composition and structure in response to growth conditions and mode of cultivation, *Letters in Applied Microbiology*. 37 (2003) 268–274. <https://doi.org/10.1046/j.1472-765X.2003.01394.x>.
- [52] L.M.L. Laurens, S. Van Wychen, J.P. McAllister, S. Arrowsmith, T.A. Dempster, J. McGowen, P.T. Pienkos, Strain, biochemistry, and cultivation-dependent measurement variability of algal

- biomass composition, *Analytical Biochemistry*. 452 (2014) 86–95.
<https://doi.org/10.1016/j.ab.2014.02.009>.
- [53] J.N.C. Whyte, Biochemical composition and energy content of six species of phytoplankton used in mariculture of bivalves, *Aquaculture*. 60 (1987) 231–241. [https://doi.org/10.1016/0044-8486\(87\)90290-0](https://doi.org/10.1016/0044-8486(87)90290-0).
- [54] A.C.M. Kwok, J.T.Y. Wong, Cellulose Synthesis Is Coupled to Cell Cycle Progression at G1 in the Dinoflagellate *Cryptocodinium cohnii*, *Plant Physiology*. 131 (2003) 1681–1691.
<https://doi.org/10.1104/pp.102.018945>.
- [55] T.M.M. Bernaerts, L. Gheysen, C. Kyomugasho, Z. Jamsazzadeh Kermani, S. Vandionant, I. Foubert, M.E. Hendrickx, A.M. Van Loey, Comparison of microalgal biomasses as functional food ingredients: Focus on the composition of cell wall related polysaccharides, *Algal Research*. 32 (2018) 150–161. <https://doi.org/10.1016/j.algal.2018.03.017>.
- [56] M. Demuez, A. Mahdy, E. Tomás-Pejó, C. González-Fernández, M. Ballesteros, Enzymatic cell disruption of microalgae biomass in biorefinery processes, *Biotechnology and Bioengineering*. 112 (2015) 1955–1966. <https://doi.org/10.1002/bit.25644>.
- [57] S. Haran, H. Schickler, I.Y. 1996 Chet, Molecular mechanisms of lytic enzymes involved in the biocontrol activity of *Trichoderma harzianum*, *Microbiology*. 142 (n.d.) 2321–2331.
<https://doi.org/10.1099/00221287-142-9-2321>.
- [58] R.L. Monaghan, D.E. Eveleigh, R.P. Tewari, E.T. Reese, Chitosanase, a Novel Enzyme, *Nature New Biology*. 245 (1973) 78–80. <https://doi.org/10.1038/newbio245078a0>.
- [59] G. Lesnierowski, J. Kijowski, Lysozyme, in: R. Huopalahti, R. López-Fandiño, M. Anton, R. Schade (Eds.), *Bioactive Egg Compounds*, Springer, Berlin, Heidelberg, 2007: pp. 33–42.
https://doi.org/10.1007/978-3-540-37885-3_6.
- [60] E. Li-Chan, S. Nakai, Enzymic dephosphorylation of bovine casein to improve acid clotting properties and digestibility for infant formula, *Journal of Dairy Research*. 56 (1989) 381–390.
<https://doi.org/10.1017/S0022029900028843>.
- [61] W.H. Fishman, β -Glucuronidase, in: H.U. Bergmeyer (Ed.), *Methods of Enzymatic Analysis* (Second Edition), Academic Press, 1974: pp. 929–943. <https://doi.org/10.1016/B978-0-12-091302-2.50082-7>.
- [62] M.V. Liberato, E.T. Prates, T.A. Gonçalves, A. Bernardes, N. Vilela, J. Fattori, G.C. Ematsu, M. Chinaglia, E.R.M. Gomes, A.C.M. Figueira, A. Damasio, I. Polikarpov, M.S. Skaf, F.M. Squina, Insights into the dual cleavage activity of the GH16 laminarinase enzyme class on β -1,3 and β -1,4 glycosidic bonds, *Journal of Biological Chemistry*. 296 (2021).
<https://doi.org/10.1016/j.jbc.2021.100385>.
- [63] S.N. Gummadi, T. Panda, Purification and biochemical properties of microbial pectinases—a review, *Process Biochemistry*. 38 (2003) 987–996. [https://doi.org/10.1016/S0032-9592\(02\)00203-0](https://doi.org/10.1016/S0032-9592(02)00203-0).
- [64] K. Nakazawa, K. Kagabe, Galactose-6-sulfatase from *Actinobacillus* sp. IFO-13310 and its action on sulfated oligosaccharides from keratan sulfate, *Biochimica et Biophysica Acta (BBA) - Enzymology*. 527 (1978) 391–402. [https://doi.org/10.1016/0005-2744\(78\)90353-4](https://doi.org/10.1016/0005-2744(78)90353-4).
- [65] S. Bhattacharyya, J.K. Tobacman, Steroid sulfatase, arylsulfatases A and B, galactose-6-sulfatase, and iduronate sulfatase in mammary cells and effects of sulfated and non-sulfated estrogens on sulfatase activity, *The Journal of Steroid Biochemistry and Molecular Biology*. 103 (2007) 20–34. <https://doi.org/10.1016/j.jsbmb.2006.08.002>.

Chapter 5: Nanoscale Evidence Unravels Microalgae Flocculation Mechanism Induced by Chitosan



Irem Demir, Jonas Blockx, Etienne Dague, Pascal Guiraud, Wim Thielemans, Koenraad Muylaert, and Cécile Formosa-Dague

ACS Applied Bio Materials 3.12 (2020): 8446-8459

Abstract

Context: This chapter is a work of the collaborative study with Prof. Dr. Koenraad Muylaert from the Katholieke Universiteit Leuven (KU-Leuven, Belgium) helped in understanding the interactions at the molecular level between chitosan and cells.

Background: Chitosan is a bio-based nontoxic polymer that has been effectively used to harvest both fresh-water and marine microalgae species. While the reported flocculation mechanism is said to rely on electrostatic interactions between chitosan and the negative cell surface, no molecular evidence has yet confirmed this mechanism. In addition, mixed results have been reported in the literature regarding its efficiency depending on the microalgae species used. For example, in the case of marine microalgae species where the high ionic strength of salts screens all the charges present on chitosan and cells, flocculation still takes place, suggesting that perhaps a different mechanism is at play.

Scope of the study: In this work we perform force spectroscopy atomic force microscopy (AFM) experiments to probe the interactions between *C. vulgaris* cells and chitosan at the molecular scale and decipher its flocculation mechanism. The results obtained show that chitosan interacts with *C. vulgaris* cell wall dominantly through specific interactions between chitosan and polymers at the surface of cells that are being unfolded during the experiments. We also show that at higher pH, a different mechanism is involved, based on chitosan precipitation. Indeed at pH 8, chitosan forms a precipitate in which cells get entrapped and thus are flocculated through a sweeping mechanism.

Major conclusions: This study demonstrates the interest of using AFM to probe molecular-scale interactions and this way understand flocculation mechanisms. These experiments allowed to reveal the complexity of chitosan-induced flocculation, which is not based on the same mechanism depending on the pH. They also give some elements of answers concerning species-dependency of its efficiency reported in the literature.

Nanoscale Evidence Unravels Microalgae Flocculation Mechanism Induced by Chitosan

Irem Demir,[#] Jonas Blockx,[#] Etienne Dague, Pascal Guiraud, Wim Thielemans, Koenraad Muylaert, and Cécile Formosa-Dague*



Cite This: <https://dx.doi.org/10.1021/acsabm.0c00772>



Read Online

ACCESS |



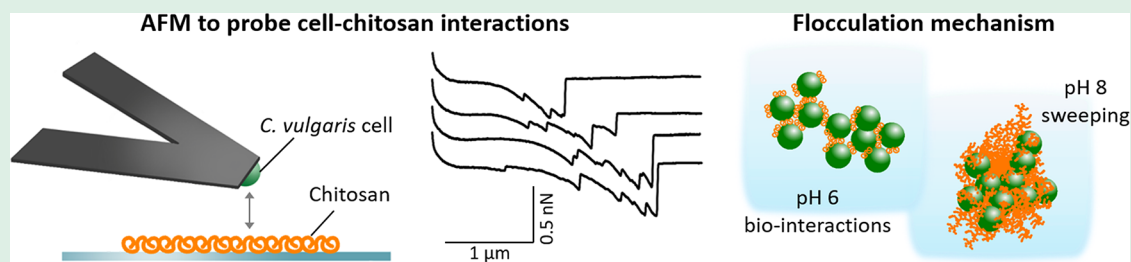
Metrics & More



Article Recommendations



Supporting Information



ABSTRACT: Microalgae are a promising resource for biofuel production, although their industrial use is limited by the lack of effective harvesting techniques. Flocculation consists in the aggregation and adhesion of cells into flocs that can be more easily removed from water than individual cells. Although it is an efficient harvesting technique, contamination is a major issue as chemical flocculants are often used. An alternative is to use natural biopolymers flocculants such as chitosan. Chitosan is a biobased nontoxic polymer that has been effectively used to harvest *Chlorella vulgaris* cells at a pH lower than its pK_a (6.5). While the reported flocculation mechanism is said to rely on electrostatic interactions between chitosan and the negative cell surface, no molecular evidence has yet confirmed this mechanism. In this study, we performed force spectroscopy atomic force microscopy (AFM) experiments to probe the interactions between *C. vulgaris* cells and chitosan at the molecular scale to decipher its flocculation mechanism. Our results showed that at pH 6, chitosan interacts with *C. vulgaris* cell wall through biological interactions rather than electrostatic interactions. These observations were confirmed by comparing the data with cationically modified cellulose nanocrystals, for which the flocculation mechanism, relying on an electrostatic patch mechanism, has already been described for *C. vulgaris*. Further AFM experiments also showed that a different mechanism was at play at higher pH, based on chitosan precipitation. Thus, this AFM-based approach highlights the complexity of chitosan-induced flocculation mechanisms for *C. vulgaris*.

KEYWORDS: atomic force microscopy, force spectroscopy, microalgae, flocculation, chitosan, cellulose nanocrystals

INTRODUCTION

These last two decades, the global interest in microalgae has increased, notably because of their oil production capacity that makes them an interesting alternative resource for biofuel production.¹ Indeed, several studies have estimated that microalgae could produce between 40 000 and 90 000 L of biofuel per Ha, depending on the sunlight and the biomass oil content of the species considered.^{2–4} This represents up to 200-times more liters than soybean and 25-times more liters than oil palm.⁵ Among the wide variety of microalgae species, several have been considered for biofuel production including *Chlorella vulgaris*. *C. vulgaris* is a unicellular freshwater microalgae species first discovered in 1890 by a Dutch researcher.⁶ This species first attracted attention in the 1950s for its nutritional value, as its protein content represents up to 55% of its dry mass.⁷ Nowadays, *C. vulgaris* is mainly used for nutraceutical purposes; studies have shown for example that it has immune-modulating and anticancer properties,^{8,9} but it has also received interest for biofuel production.⁴ Indeed, *C.*

vulgaris has the capacity to accumulate important amounts of lipids under certain culture conditions, with a fatty acid profile adapted for biofuel production.^{7,10,11}

At present, the commercialization of microalgae-based biofuels is hindered by the lack of economically competitive harvesting techniques, as this step is generally estimated to represent 20–30% of the total microalgal biomass production cost.^{12,13} In the case where the harvesting step is combined with lipid extraction, as needed in biofuel production processes, this cost can increase up to 90%, resulting in a negative energy balance for the production of microalgae-based

Received: June 23, 2020

Accepted: October 28, 2020

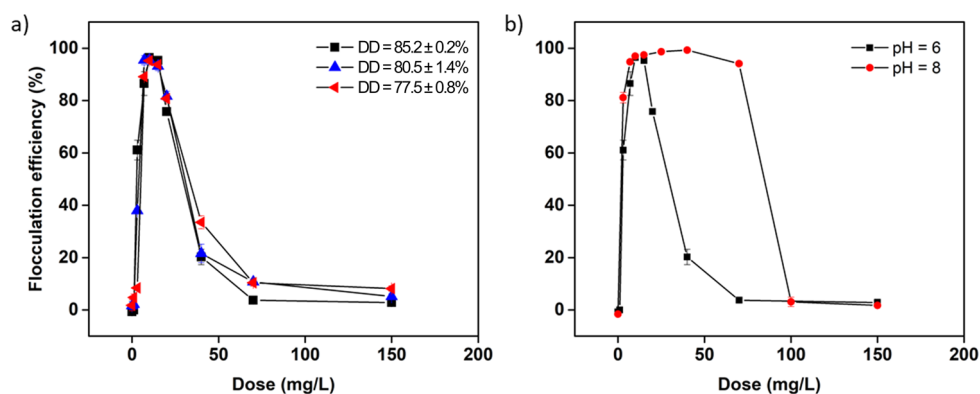


Figure 1. Flocculation experiments of *C. vulgaris* with chitosan. Flocculation efficiency of (a) different chitosan molecules with different deacetylation degree (DD) at pH 6 and (b) chitosan molecules with DD = 77.5 ± 0.8% at pH 6 and 8.

biofuels at large scale.^{14–16} The parameters that make harvesting microalgae such a challenging task are their low concentration in water, their small cell size, their negatively charged surface, and their low density. So far, different harvesting techniques have been proposed including centrifugation, filtration, flotation, flocculation, and electrical-based processes. A recent review compared and described the advantages and disadvantages of each of these techniques.¹³ Among them, flocculation stands out as it is inexpensive, making it an option for large-scale harvesting for a wide variety of microalgae species.¹⁷ Flocculation consists in the aggregation of cells to facilitate their separation from water by sedimentation or flotation for example. While this technique presents many advantages, a major issue in flocculation is contamination, as it often requires the use of chemical flocculants to induce flocculation, which end up in the harvested biomass, and can interfere with downstream processes or with its final application.¹⁸ In this context, an interesting alternative is to use biopolymers to induce flocculation,¹⁹ the most popular in microalgae harvesting being chitosan.

Chitosan is a cationic polyelectrolyte obtained by deacetylation of chitin, an abundant natural polymer. Chitosan presents many advantages compared to traditional inorganic flocculants as it is nontoxic, biodegradable, biocompatible, and renewable.^{20,21} Moreover, chitosan does not contaminate the harvested biomass as chitin-like polysaccharides are naturally present in the cell wall of many microalgae species, including *C. vulgaris*, and thus, harvested cells can then be directly exploited.²² Chitosan-induced flocculation has so far been used to harvest successfully both fresh-water and marine microalgae species. For fresh-water species such as *C. vulgaris*, its efficiency is mostly attributed to the amino groups present in chitosan. These groups have a pK_a value of about 6.5,²³ and thus, below this pH these groups are mostly protonated and confer a positive charge to chitosan, which supposedly allows for electrostatic interaction with the negatively charged surface of microalgae cells.²⁴ As a result, cells are believed to be flocculated through a charge neutralization mechanism.^{25–27} In the case of marine microalgae species, mixed results on chitosan efficiency have been reported. Indeed, at the high ionic strengths of marine waters, it is believed that the positive charges of chitosan are shielded, preventing further flocculation through charge neutralization. However, some studies reported successful flocculation of certain marine species by chitosan,^{28–31} which may suggest that chitosan-induced flocculation

may rely on different interactions between chitosan and cells than only electrostatic interactions. In this view, an interesting paper from 2011 focused on the influence of the cell wall carbohydrate composition of *C. vulgaris* on the efficiency of chitosan-induced flocculation.³² The results obtained in this study showed that a higher polysaccharide content (including neutral sugars, uronic acids, and amino sugars) in the cell wall is associated with a better efficiency of flocculation with chitosan at pH 8.5, suggesting that non-electrostatic absorption of chitosan on cells may be more important than electrostatic neutralization in *C. vulgaris*. However, in all the reported cases of flocculation of *C. vulgaris* using chitosan as a flocculant, no molecular evidence has been provided so that the mechanism(s) underlying the flocculation remain(s) unclear.

In this study, we investigated the interactions between chitosan and *C. vulgaris* cells using an advanced technique: atomic force microscopy (AFM). AFM, first developed in 1986,³³ is a highly sensitive force machine able to record forces as small as 20 pN, making it possible to gain insights into the molecular interactions between single living cells and their environment. Our team recently used AFM to understand the flocculation mechanism involved for three different microalgae species, demonstrating the interest of using this technology to answer such questions.^{34–36} Thanks to AFM force spectroscopy experiments, we show for the first time that at pH 6 below its pK_a , chitosan interacts with *C. vulgaris* cell wall through non-electrostatic interactions, that is, through specific interactions between chitosan and polymers at the surface of cells that are being unfolded upon retraction. These observations were confirmed by comparing the data obtained with cationically modified cellulose nanocrystals (CNCs), for which the flocculation mechanism, relying on an electrostatic patch mechanism, has been suggested in a previous study from our team on *C. vulgaris*.³⁷ Further AFM experiments, including force spectroscopy but also roughness analysis, however, showed that at higher pH, the mechanism at play is different, as chitosan is not able to interact electrostatically with cells at such high pH. Thus, our AFM-based approach allows this study to highlight the complexity of chitosan-induced flocculation in the case of *C. vulgaris*, and enables to identify, at pH 6, a new flocculation mechanism based on the biological binding of chitosan with the cell wall of cells. Given the wide use of chitosan in microalgae harvesting processes, these new data provide important information to optimize microalgae-based biofuel production.

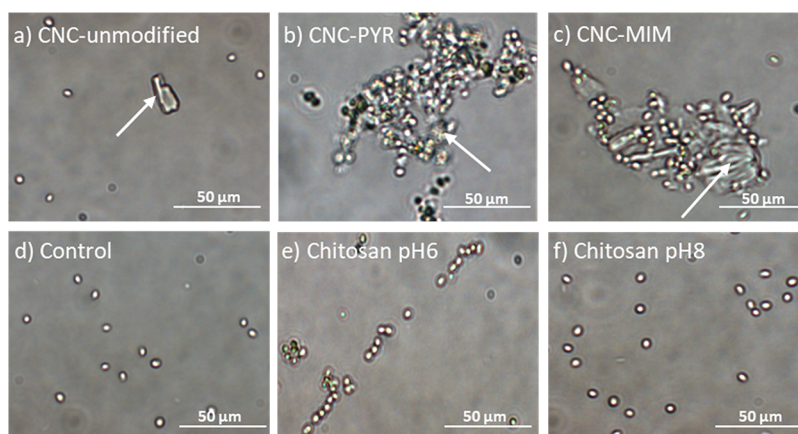


Figure 2. Optical imaging of *C. vulgaris* flocculation. Optical image of *C. vulgaris* cells after resuspension in PBS containing (a) 100 mg/L of CNC-unmodified at pH 8, (b) 100 mg/L of CNC-PYR at pH 8, (c) 100 mg/L of CNC-MIM at pH 8, (d) nothing at pH 6, (e) 10 mg/L of chitosan at pH 6, and (f) 10 mg/L of chitosan at pH 8. The arrows in panels a, b, and c indicate the CNC particles.

RESULTS AND DISCUSSION

Macroscopic Observations Show That Chitosan Does Not Interact Electrostatically with Cells. In a previous work where we evaluated the efficiency of cationically modified CNCs to flocculate *C. vulgaris* cells, we showed that the number of positive charges present on the CNCs was directly correlated with the flocculation efficiency.³⁷ Indeed, CNCs bearing more positive charges enabled a more efficient flocculation compared to CNCs with less positive charges. This was explained by the fact that positive CNCs interact with cells through electrostatic interactions, and thus, the more positive charges present, the more interactions can occur with cells, resulting in a higher flocculation efficiency. On the basis of the literature, this situation should be similar for chitosan at a pH of 6, so below the pK_a value of the amine groups of chitosan. To test this hypothesis, we performed flocculation experiments using chitosan molecules with different degrees of deacetylation (DD), thus bearing more or less positive charges. The DD of each chitosan was determined using conductometric titration and established to be of $77.5 \pm 0.8\%$, $80.5 \pm 1.4\%$, and $85.2 \pm 0.2\%$ (see Supporting Figure S1 and Supporting Table S1). The dynamic viscosity of the chitosan stock solutions (5 g/L in 0.04 M HCl) was measured under different shear stress (see Supporting Table S2). Chitosan in solution acts as a non-Newtonian liquid: increasing shear stress reduces the dynamic viscosity. The results obtained for the flocculation experiments are presented in Figure 1a. They show that surprisingly, the flocculation efficiency is similar for each chitosan tested, with a maximum efficiency reached for a dose of 10 mg/L, thus showing that there is no influence of the DD of chitosan and thus of its number of positive charges on the flocculation of cells. This is in line with the work of Chen et al., who also showed that the DD of chitosan had indeed a limited impact on the flocculation of bentonite.³⁸ Moreover, this study also showed that the molecular weight of chitosan had a dominant influence on the flocculation efficiency, with high molecular weights allowing them to reach higher flocculation efficiencies. In our case, the MW of the chitosan that was used is of 345.2 kDa, thus high, which explains perhaps the high efficiencies reached in our flocculation experiments (>95%). To verify this observation, we compared the flocculation efficiencies with the ones obtained at a pH of 8 where chitosan does not present positive charges. In this case, if the

flocculation efficiency of chitosan is based on electrostatic interactions, then no flocculation should be observed at this higher pH environment. However, the results obtained, presented in Figure 1b, show that a maximum flocculation efficiency can be reached for the same chitosan dose at pH 6 and at pH 8. While this efficiency drops at higher doses for a pH of 6, it remains maximum for doses up to 80 mg/L for a pH of 8. This result can be correlated to previous data obtained in our team for the marine species *Nannochloropsis oculata* where it was shown that chitosan was effective even when used under higher pH conditions.³¹ It was shown that at higher pH, the uncharged chitosan precipitates causing the flocculation of the cells through a sweeping mechanism where cells are mechanically trapped in the interconnected percolated network of the precipitate,³⁹ instead of charge neutralization as it is supposed to be the case at pH 6. Overall, the flocculation results presented here seem not to be in accordance with the literature, and support the idea, previously raised in 2011 for *C. vulgaris*,³² that the interactions between cells and chitosan may not rely on electrostatic interactions.

To understand this phenomena further, we performed an optical microscopy assay with cells incubated with CNCs and chitosan used at concentrations for which the best flocculation efficiency was obtained (10 mg/mL for chitosan and 100 mg/L for CNCs³⁷). For chitosan, we chose to work with the chitosan with a degree of deacetylation of $77.5 \pm 0.8\%$ (4.2 mmol charges/g). Three types of CNCs were used in this study: unmodified CNCs, CNCs modified with pyridinium grafts (CNC-PYR, DS = 0.20, 0.92 mmol charges/g), and CNCs modified with methylimidazolium grafts (CNC-MIM, DS = 0.23, 0.99 mmol charges/g). The used CNCs were fully characterized in a previous study by the authors.³⁷ Both CNC-PYR and CNC-MIM have quaternary ammonium groups, which carry a permanent positive charge independent of pH, unlike chitosan, for which the charge carried by its primary amines are only charged after protonation at low pH.^{37,40} The results are presented in Figure 2. When CNCs were used, CNC particles could directly be observed in the images (indicated by arrows): in the case of unmodified CNCs (Figure 2a), no cells are attached to the particles, while for CNC-PYR and CNC-MIM, cells aggregated around the particles could be observed (Figure 2b,c). This is then coherent with the patch mechanism already described for *C. vulgaris* in our previous work where cells interact electrostatically

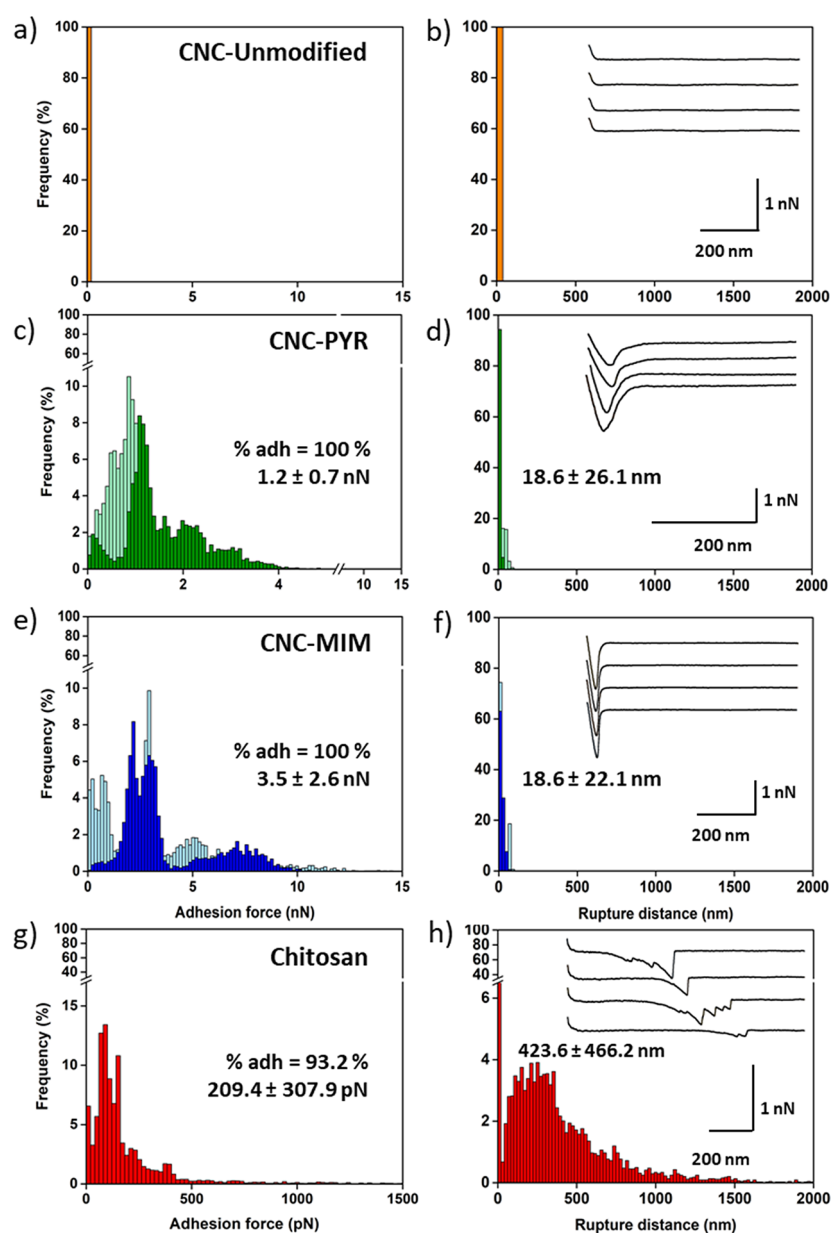


Figure 3. Interactions between CNCs or chitosan and single *C. vulgaris* cells. (a) Adhesion force histogram between *C. vulgaris* cells and CNCs-unmodified at pH 8 and (b) corresponding rupture distance histogram. (c) Adhesion force histogram between *C. vulgaris* cells and CNCs-MIM at pH 8 and (d) corresponding rupture distance histogram. The light green distributions correspond to values obtained with method 1, and the dark green distributions correspond to values obtained with method 2. (e) Adhesion force histogram between *C. vulgaris* cells and CNCs-MIM at pH 8 and (f) corresponding rupture distance histogram. The light blue distributions correspond to values obtained with method 1, and the dark blue distributions correspond to values obtained with method 2. (g) Adhesion force histogram between *C. vulgaris* cells and chitosan spin-coated on a glass slide at pH 6 and (h) corresponding rupture distance histogram. Insets in panels b, d, f, and h show representative force curves obtained. Data were recorded using a set-point of 0.25 nN.

cally with cationic CNC particles. Thus, in the case of unmodified CNCs that do not have positive charges, no interactions with cells could be observed. However, for chitosan, the situation is different: at pH 6, small aggregates of cells were observed, with smaller size than the CNC aggregates (Figure 2e), suggesting that chitosan does interact with cells, but that perhaps the nature of the bond is different, not as strong as for CNCs. At pH 8, cells do not seem to be aggregated (Figure 2f). If we follow the hypothesis formulated in our previous work on *N. occulata*,³¹ then this results could be explained by the fact that at higher pH, the flocculation mechanism is based on sweeping, and thus, there are no direct

interactions between chitosan and cells. This is also in line with what was already demonstrated for another microalgae species, *Dunaliella salina*; when sweeping mechanism is involved, there are no interactions between the flocculant and the cells.³⁵ Thus, at this stage, our macroscopic analysis seems to show that in contrast to the literature, chitosan-induced flocculation in *C. vulgaris* may not rely on electrostatic interactions, even at pH 6 where chitosan is positively charged. However, what is then the mechanism involved?

AFM Nanoscale Experiments Reveal the Role of Biological Interactions between Cells and Chitosan during Flocculation. To answer this question, we used

atomic force microscopy (AFM) to directly probe the interactions between the flocculants and cells and to get a better insight into the flocculation mechanisms involved in each case. We first performed force spectroscopy experiments to probe the interactions between CNCs and single *C. vulgaris* cells. For that, a first method (method 1 described in the [Methods](#) section, [Supporting Figure S2a](#)) consisted of using tips directly modified with CNCs ([Supporting Figure S3](#)) to probe the interactions with cells immobilized on a positive glass surface at a pH of 8. In the case of CNCs, the charge present on the particles is not dependent on the pH because the modified CNCs carry a quaternary ammonium group that is permanently positively charged. However, because this first method was difficult to implement for modified CNCs, as the forces recorded between the CNCs particles and cells were stronger than the electrostatic forces between the cells and the surface on which they were immobilized, only a small number of cells could be probed. Indeed, during force spectroscopy, the cells would detach from the surface to adhere to the CNC particle on the probe, therefore making the measurements impossible. To overcome this challenge, we also recorded data using FluidFM technology (method 2 in the [Methods](#) section, [Supporting Figure S2b](#)). In this case, single cells were aspirated at the aperture of microfluidic probes by exerting a negative pressure inside the cantilever microchannel. This negative pressure was sufficient to keep the cells attached to the cantilever, and thus, more measurements could be performed. The data presented in [Figure 3](#) combine data obtained with these two methods for modified CNCs (details of these data can be found in [Supporting Table S3](#)); in the case of unmodified CNCs, only the first method was used. In this figure, the adhesion forces, rupture distances, and representative force curves recorded in PBS buffer are presented. The adhesion force corresponds to the strongest adhesion event in each force curve, while the rupture length is the distance of the last adhesion event recorded. The percentage of adhesion indicated corresponds to the percentage of the force curves presenting retract adhesions. In each case, the results presented correspond to the interactions recorded with 10 cells coming from at least two independent cultures. In the case of unmodified CNCs ([Figure 3a,b](#)), and in line with our previous work, no interactions with cells can be observed, as retract force curves show no retract peaks. In the case of CNC-PYR ([Figure 3c,d](#)), a single retract peak happening at the contact point can be observed, with in this case an average force of 1.2 ± 0.7 nN ($n = 9801$ force curves). This force signature is typical of non-specific interactions, most likely reflecting electrostatic interactions between the negative surface of the cells and the positive surface of PYR-modified CNCs.³⁴ Similar force curves were obtained for CNCs-MIM ([Figure 3e,f](#)); however, in this case, the average adhesion force recorded was of 3.5 ± 2.6 nN ($n = 8845$ force curves), so almost 3-times higher than for CNCs-MIM. The adhesion force difference between CNC-MIM and PYR is significant at a p-value of 0.001 (unpaired *t* test). This is an interesting point; indeed, CNC-MIM have a higher number of positive charges compared to CNC-PYR, and our results indicate that this difference influences the adhesion force recorded. Thus, the more positive charges on the CNCs are present, the stronger is the electrostatic bond with the cell's surface. However, the difference in DS between both cationic CNCs is small (CNCs-PYR, DS = 0.20 and CNCs-MIM, DS = 0.23), not fully explaining the big differences in adhesion forces. An

explanation for these differences might reside in the chemical structure of the cationic grafts on the CNCs. In the CNC-PYR sample, the cationic charge is distributed over a 6-membered ring, while only over a 5-membered ring in the CNC-MIM sample, causing different charge densities at the atomic level. Moreover, methylimidazolium has two nitrogen atoms in its ring structure, while pyridinium only contains one; this could also contribute to the difference recorded in the adhesion forces. Regarding the rupture distances recorded, they were on average of 18.6 ± 26.1 nm for CNC-PYR, and of 18.6 ± 22.1 nm for CNC-MIM, indicating that no molecules were pulled away from the surface of the cells. Thus, these results confirm that the interactions between cationic CNCs and cells are non-specific and electrostatic. Hence, this molecular data confirm that in the case of CNCs-induced flocculation, a charge neutralization mechanism is involved, and it explains why better flocculation efficiencies are obtained using CNCs bearing a higher number of positive charges. To further prove this point, and exclude possible contributions of other types of interactions between CNCs and cells, additional experiments were carried out to measure the interactions between beads bearing COOH functionalities, thus negatively charged at a pH of 8, and CNCs immobilized on mica surfaces. These beads have a similar size to the cells and thus are here used as artificial non-living analogues of microalgae cells bearing only negative charges and no surface polymers. The results ([Supporting Figure S4](#)) show the same tendency, that is, single peak retract force curves and lower adhesion values obtained with CNCs-PYR (5.3 ± 1.4 nN, $n = 800$ force curves obtained with 2 different beads), when compared to CNCs-MIM (49.6 ± 10.6 nN, $n = 800$ force curves obtained with 2 different beads). In this case, the adhesion values are higher than those obtained with cells; this can be explained by the fact that the beads were more negatively charged than cells. Indeed, zeta potential measurements have shown that at a pH of 8, cells have a surface potential of -21.9 mV, whereas the zeta potential of beads is of -43.2 mV. Finally, to confirm the electrostatic nature of the interactions between CNCs and cells, the interactions between CNCs-MIM and cells were probed in the presence of salts that screen the charges present on cells and CNC particles. The results obtained ([Supporting Figure S5](#)) show a drastic decrease of the adhesion force recorded, from 3.5 ± 2.6 nN without salts to 147.4 ± 86.4 pN with salts, thus confirming that the interactions observed are indeed due to the charges present on CNCs particles and cells.

However, the interesting result from these force spectroscopy analyses concerns chitosan ([Figure 3g,h](#)). In this case, the interactions between a single living *C. vulgaris* cell immobilized at the edge of a tipless cantilever⁴¹ and a chitosan-functionalized surface by spin-coating^{42,43} were probed at a pH of 6 (method 3 in the [Methods](#) section, [Supporting Figure S2c](#)). In this case, retraction force profiles showed multiple binding events with an average adhesion force of 209.4 ± 307.9 pN ($n = 5698$ force curves), that is, much lower than the forces recorded for cationic CNCs. In contrast, the average rupture length for chitosan was of 423.3 ± 466.2 nm, whereas in the case of cell interactions with CNCs, it was close to zero. Note that the large standard deviations come from the wide distributions of the values visible on the histograms, caused by the heterogeneity inherent to living cells. The extended ruptures, the low adhesion forces recorded, as well as the lack of defined force patterns are consistent with the stretching of long molecules from the cell wall of cells.^{44–46} Given the

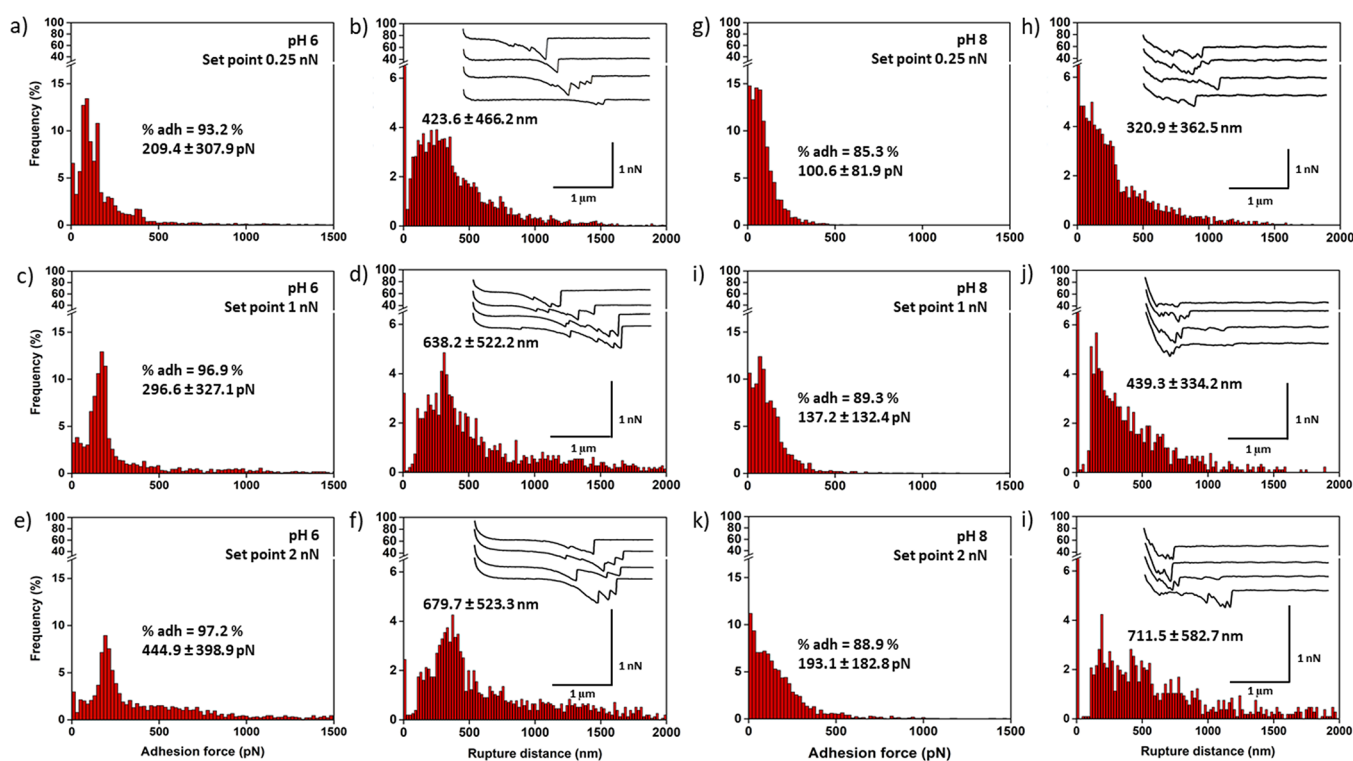


Figure 4. Interaction between chitosan and single *C. vulgaris* cells at pH 6 and 8 at varying applied forces. (a) Adhesion force histogram and (b) corresponding rupture distance histogram between a *C. vulgaris* cell-functionalized cantilever and chitosan spin-coated on a glass slide at pH 6 using a set-point of 0.25 nN, (c, d) using a set-point of 1 nN, (e, f) using a set-point of 2 nN. (g) Adhesion force histogram and (h) rupture distance histogram between a *C. vulgaris* cell-functionalized cantilever and chitosan spin-coated on a glass slide at pH 8 using a set-point of 0.25 nN, (i, j) using a set-point of 1 nN, (k, l) using a set-point of 2 nN. Insets in panels b, d, f, h, j, and l show representative force curves obtained.

difference in the force signatures obtained, our results suggest that in the case of chitosan, even when positively charged, no electrostatic interactions are involved in the bonding with cells, or at least if electrostatic interactions are involved, they are not predominant in the interactions and are masked by the biological interactions. This inherently implies that chitosan is able to interact specifically with polymers present at the surface of cells that are then unfolded upon retraction in our force spectroscopy experiments, resulting in the long rupture distances observed. To confirm that these multiple binding events are not due to the detachment of chitosan from the surface over consecutive measurements, but indeed to the unfolding of cell surface polymers, we verified that the adhesion force recorded was constant over the area probed. If chitosan would detach from the surface and stick on the cell, then the adhesion forces recorded would decrease as the functionalized cantilever moves on the chitosan surface. This analysis (Supporting Figure S6) shows that this is not the case, the adhesion force recorded stays constant, thus proving that only cell surface polymers unfold in our experimental conditions. Taking into account the work of Cheng and co-workers, who showed that the carbohydrate composition of the cell wall of *C. vulgaris* has a direct influence on the efficiency of flocculation obtained with chitosan,³² we may suggest that chitosan is able to specifically interact with these polysaccharides. Moreover, similar force patterns were already observed for microalgae by Higgins and co-workers who extended mucilage (composed of polysaccharides) from the cell wall of *Craspedostauros australis*, a marine diatom, and of *Pinnularia viridis*, a freshwater diatom.⁴⁷ This further supports that the unfolding observed in our case may be due to the

unfolding of polysaccharides from the *C. vulgaris* cell wall. For the moment, such specific structural interactions between chitosan and polysaccharides, not dependent on electrostatic interactions, have been described only in a few cases, for example, with cellulose⁴⁸ or with alginate,⁴⁹ for which interactions with chitosan have been observed at high or low pH, where either the polysaccharides or the chitosan are uncharged. Moreover, previous studies have also reported the possible interaction between chitosan and glycoproteins in the case of microorganism flocculation: for example Barany et al. showed that *Escherichia coli* flocculation by chitosan relied on chitosan adsorption to polymers from the cells, rather than on electrostatic factors.⁵⁰ Thus, at this stage, the data obtained indicate that at pH 6 chitosan flocculation of *C. vulgaris* does not occur through electrostatic interactions but rather through biological interactions, meaning that chitosan interacts with biomolecules at the cell surface that are then unfolded from it. These biomolecules might be polysaccharides present at the surface of cells. More questions can now be raised: can further data prove this? Is this mechanism also at play at pH 8?

Chitosan Induced-Flocculation of *C. vulgaris* at Higher pH Does Not Occur through the Same Mechanism. To further investigate the flocculation mechanism of chitosan, we decided to compare the interactions between chitosan and cells at pH 6 and 8 at varying applied forces. When the applied force is increased during force spectroscopy experiments, because the chitosan layers are deformable (Y_m of 15.6 ± 30.5 kPa at pH 6, $n = 1554$ force curves, and of 19.2 ± 23.2 kPa at pH 8, $n = 1349$ force curves, values extracted from force curves at an indentation segment of 100 nm, data not showed), the contact area between the cells

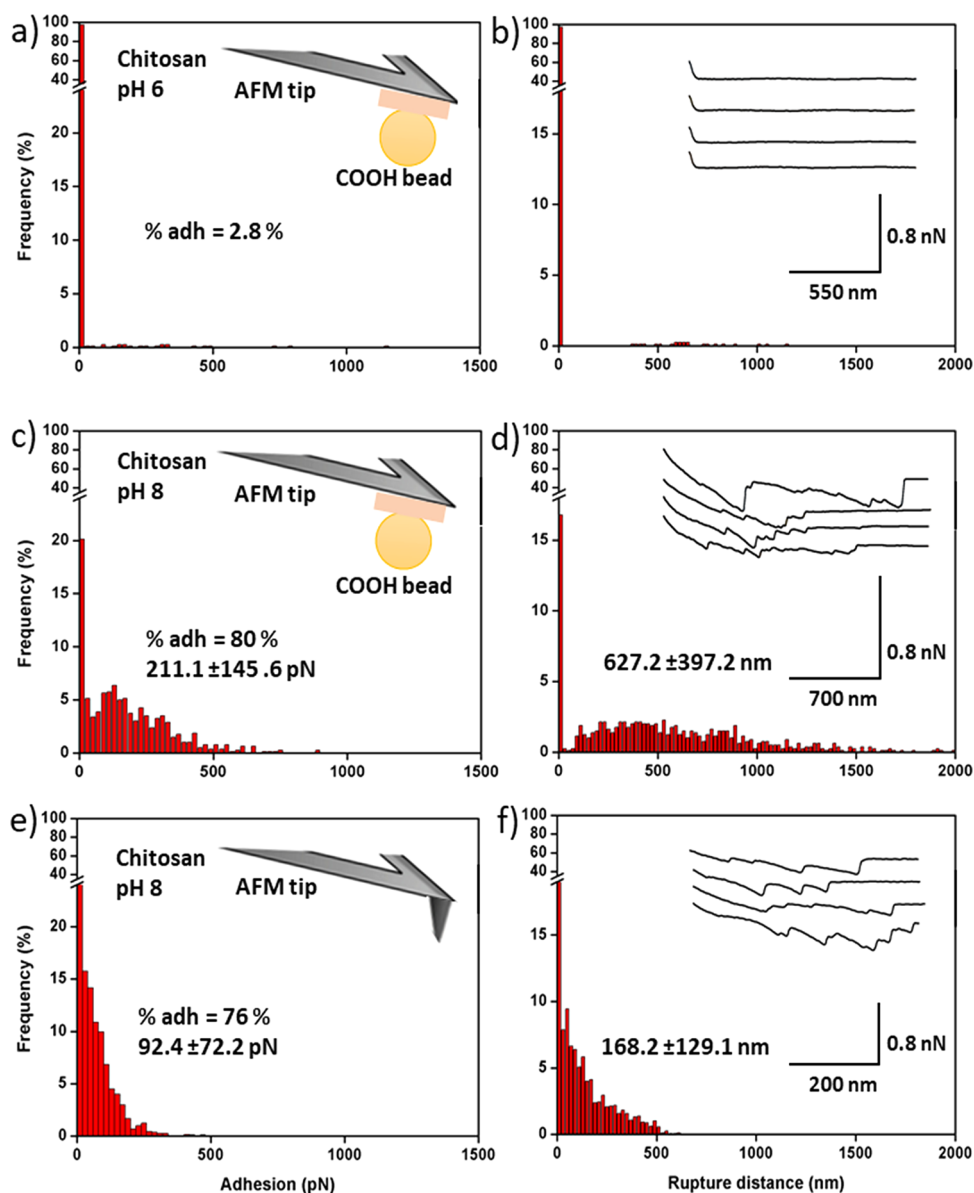


Figure 5. Interaction between bare tips and negative beads-functionalized cantilevers with chitosan surfaces. (a) Adhesion force histogram between a COOH bead-functionalized cantilever and chitosan spin-coated on a glass slide at pH 6 and (b) corresponding rupture distance histogram. (c) Adhesion force histogram between a COOH bead-functionalized cantilever and chitosan spin-coated on a glass slide at pH 8 and (d) corresponding rupture distance histogram. (e) Adhesion force histogram between a bare AFM tip chitosan spin-coated on a glass slide at pH 8 and (f) corresponding rupture distance histogram. Insets in panels b, d, and f show representative force curves obtained. Data were recorded using a set-point of 0.25 nN.

and the chitosan surface increases as well. This increase should lead to higher adhesion forces as more molecules from the cell wall are able to interact with the chitosan surface; rupture lengths will also provide useful information on the nature of the molecules unfolded. The results of these experiments are presented in Figure 4; they were obtained in the case of a set point of 0.25 nN with 10 different cells, and in the cases of higher set points with 4 different cells coming from at least 2 independent cultures (details of the data can be found in Supporting Tables S3–S5). In each case, the differences between the adhesion forces recorded at pH 6 and pH 8, for the different set-points, are significantly different with a *p*-value of 0.001 (unpaired *t* test). At pH 6, we can observe that the more the applied force was increased, the more the average adhesion force increased, from 209.4 ± 307.9 pN at an applied

force of 0.25 nN (Figure 4a, *n* = 5698 force curves), to 296.6 ± 327.1 pN at 1 nN (Figure 4c, *n* = 2050 force curves) and 444.9 ± 398.9 pN at 2 nN (Figure 4e, *n* = 2050 force curves), thus two-times higher. As for the rupture distances, they also increased with the applied force, from an average of 423.6 ± 466.2 nm at 0.25 nN (Figure 4b) to 679.7 ± 523.3 nm at 2 nN (Figure 4f). This thus indicates that as the contact surface area increases between the cell and the chitosan surface, the more molecules, probably polysaccharides, from the cell wall involved in the interactions with chitosan were extended, resulting in higher adhesion forces and rupture distances. When these experiments were performed at a pH of 8, a similar trend was observed, with an increase in both the maximum adhesion force and rupture length when the applied force is higher. However, an interesting point to note in this case is the

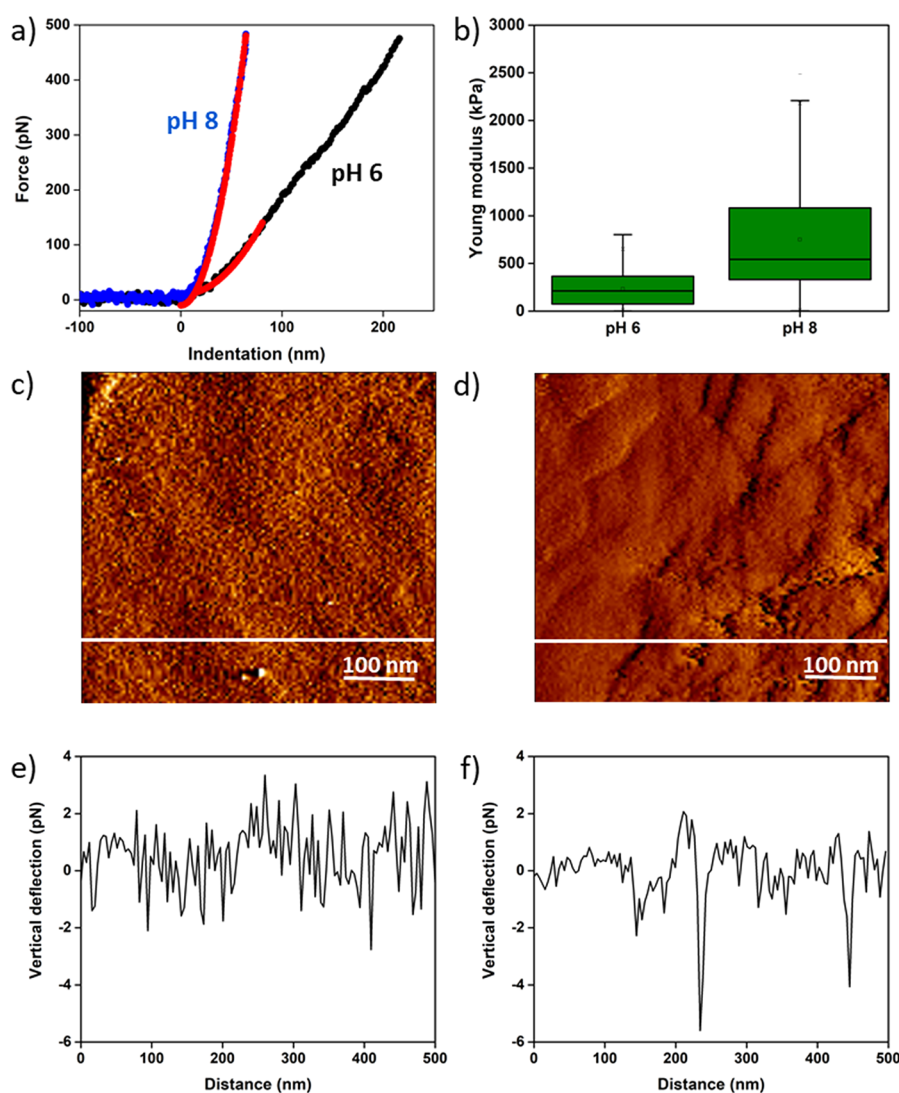


Figure 6. Nanomechanics and cell wall roughness of the *C. vulgaris* cell wall. (a) Indentation curves (blue and black lines) fitted with the Hertz model at 80 nm of indentation (red lines) recorded on top of *C. vulgaris* cells at pH 6 and 8. (b) Boxplot of the Young's modulus values measured on top of *C. vulgaris* cells at pH 6 and 8. (c) Vertical deflection AFM image of an area (500 nm × 500 nm) of the cell surface at pH 6 and (d) vertical deflection AFM image of an area (500 nm × 500 nm) of the cell surface at pH 8. (e) Cross-section taken along the white line in panel c and (f) cross-section taken along the white line in panel d.

difference in values between the measurements performed at pH 6 and pH 8. Indeed, in the case of pH 8, the average adhesion force recorded was of 193.1 ± 182.8 pN at an applied force of 2 nN (Figure 4k, $n = 2050$ force curves), thus almost equivalent to the adhesion force recorded at pH 6 for the smallest applied force (0.25 nN). Regarding rupture lengths, although the average distances recorded were similar at a high applied force, their difference is important at a low applied force (423.6 ± 466.2 nm at pH 6 and 320.9 ± 362.5 nm at pH 8). The differences in these values are surprising as one would expect that if the interaction mechanism is indeed based on biological interactions, the same molecules would unfold from the cell surface irrespective of the pH, resulting in similar unfoldings with similar rupture distances. It is however also possible that the changes in the pH affect the solvated state of the surface-bound molecules, thereby directly affecting the measured forces.

To understand this behavior, we performed experiments with negatively charged beads, and probed the interactions with chitosan surfaces at pH 6 and 8. The results are presented

in Figure 5. At pH 6, few interactions were recorded between the beads and the chitosan surface (2.8% of the force curves), as most retract force curves present no retract peaks (Figure 5a,b). This thus proves our first hypothesis that chitosan interactions with cells do not rely dominantly on electrostatic interactions but on biological interactions. Indeed, COOH beads enable the cell surface to be mimicked by bearing negative charges but have the advantage to exclude the molecules that are present on the cell walls. In this case, it is clear that the biological polymers that are present on the microalgal cell surface are essential for the interaction of chitosan with the cells and that the charge of chitosan is not dominant in the interaction with cells under our experimental conditions. Moreover, as for experiments where the interactions between cells and chitosan were probed at pH 6 (Figure 4), no electrostatic interactions were recorded. This further indicates that these interactions either do not take place or are smaller than the limit of detection of AFM (20 pN) and thus cannot be captured. This is an interesting point because at pH 6 chitosan is positively charged and should in theory

interact with negatively charged surfaces; thus, perhaps these interactions are too weak to be detected. The poor strength of electrostatic interactions between positively charged chitosan at low pH and negative surfaces has already been described in other research fields. For example, chitosan has been used to bind with negatively charged drugs to form drug loaded chitosan nano- and microparticles.⁵¹ However, it is shown in several studies that the release of the drugs from chitosan particles is rapid, indicating that the binding properties of chitosan through electrostatic interactions may be poor.⁵¹

When the same experiments were performed at a pH of 8 (Figure 5c,d), force curves showed multiple peaks with a similar profile to the ones obtained using cells instead of beads, with average adhesion forces and rupture lengths recorded values of 211.1 ± 145.6 pN and 627.2 ± 397.2 nm ($n = 800$ force curves, with 2 different beads), respectively. Using bare tips instead of beads (Figure 5e,f), the same unfolding events were recorded, with similar adhesion and rupture distances values as in the case of cells. This result is unexpected: indeed, the bare tips used, as for the beads, carried no polymers, that is, the multi-peaks observed on the force curves must correspond to the unfolding of chitosan picked up directly from the surface upon retraction by the tips or the beads. This indicates that at this pH, the structure of chitosan must be different than at pH 6 where bare tips do not allow the unfolding of chitosan. Moreover, this gives the explanation for the results obtained using living cells at pH 8 (Figure 4g–l): in this case also, the chitosan must be unfolded from the surface, which explains why the adhesion forces and rupture lengths values obtained are different from those obtained at pH 6. Given the fact that the same chitosan unfoldings were obtained with cells, negative beads or bare tips, we can thus conclude that at pH 8 there is no biological nor electrostatic interaction between the cells and chitosan, in agreement with the optical images obtained (Figure 2e) where no cell aggregation could be visualized. The fact that higher adhesion and rupture length values were recorded with beads compared to with cells or with bare AFM tips is explained by the fact that the surface contact with beads is larger (6–7 μm of diameter compared to 3–4 μm of diameter for cells), thus allowing to pull more chitosan from the surface. The flocculation mechanism of cells at pH 8 is thus based on a different mechanism than at pH 6; our hypothesis is that at this pH, the chitosan precipitates and flocculates the cells by sweeping, as we have demonstrated in our previous study.³¹ We now need to verify this hypothesis.

Sweeping Mechanism Is Involved in Flocculation of *C. vulgaris* at pH 8. The previous results have demonstrated that cells do not interact through biological or electrostatic interactions with chitosan at pH 8. However, the question is now to understand if this is due to changes in the cell wall properties of the cells, to changes in the chitosan structure, or to both? It has been shown previously with the marine species *Phaeodactylum tricornutum* that the cell wall rigidity changes with pH, which impacted on the deformability of the cells and thus on their interactions with their environment.³⁴ Moreover, AFM studies on microorganisms have shown that under some conditions, the architecture and network of molecules at the surface of cells can change depending on external conditions, which thus impact the availability of molecules to interact with their environment.⁴⁵ To verify these two points in our study, we performed nanomechanical analysis of the cell wall of cells as well as surface roughness analysis. These results are presented in Figure 6. To obtain quantitative information on

the nanomechanical properties of the cells, we determined the Young's modulus (Y_m) of the microalgae cells through nanoindentation measurements, in PBS at pH 6 and pH 8 (Figure 6a,b). In this type of measurement, the cantilever, for which the mechanical properties are known, is pressed against the cells with a given force. This enables us to extract the Y_m of the cell wall, a parameter that reflects its resistance to compression (the higher the Young modulus value, the more rigid the cell wall). Nanoindentation measurements, which give access to force versus distance curves, were performed on areas of $500 \text{ nm} \times 500 \text{ nm}$ on top of cells, on 8 cells coming from at least 2 independent cultures. Y_m values were then obtained first by converting the force curves obtained into force versus indentation curves, shown in Figure 6a, and then by fitting them with a theoretical model, in our case, the Hertz model⁵² (black empty circles on the curves in Figure 6a). The results show that the indentation curves obtained on cells at pH 6 and 8 are different; indeed, the AFM probe is able to indent deeper into cells at pH 6 than at pH 8, meaning that increasing the pH also increases the rigidity of the cell wall. Quantitative analysis of the Y_m extracted from thousands of these curves on 8 cells in each case confirmed this finding, and showed that at pH 6, cells have an average Y_m of 232.9 ± 175.6 kPa ($n = 8192$ force curves), whereas cells at pH 8 have a Y_m of 750.2 ± 589.0 kPa ($n = 8182$ curves, differences are significant at a p-value of 0.001, unpaired t test, details can be found in Supporting Table S6). While the nanomechanical properties of *C. vulgaris* have never been determined using AFM before, these values are in the range of Y_m values obtained on other microorganisms such as yeasts, which have a cell wall composition comparable to microalgae.⁵³ Moreover, this increase in the rigidity, due to the increase of pH, has already been shown for *P. tricornutum*.³⁴ Hence, increasing the pH changes the nanomechanical properties of the cell wall and thus its architecture, perhaps explaining in part the fact that cells are not able to interact with chitosan at pH 8. Indeed, it could mean that the molecules involved in the interaction with chitosan are not available anymore for interaction or that their conformation at elevated pH prevents the interaction with chitosan. Regarding the cell wall roughness, this parameter was directly extracted from contact images of $500 \text{ nm} \times 500 \text{ nm}$ obtained on top of 8 cells coming from at least 2 independent cultures. The results obtained (Figure 6c–f) show that the surface morphology is slightly modified by the increase in pH, as shown by the vertical deflection images recorded on top of the cells in Figure 6c and d. Cross-sections taken along the white lines in Figure 6c and d show this difference, as the profile of this cross-section at pH 8 presents larger patterns. The quantitative analysis of the roughness measured on several cells showed that at pH 6, cells have an average roughness of 0.9 ± 0.5 nm, which increased to 1.7 ± 0.9 nm at pH 8. While this difference is significant, it remains low and indicates that at pH 8, more molecules protrude from the surface of the cell, which might mask the molecules involved in the interaction with chitosan, or perhaps might indicate that these molecules are coiled and not able to interact anymore.⁴⁵ Overall, this biophysical analysis of the cell wall of *C. vulgaris* indicates that a pH increase from 6 to 8 clearly affects its rigidity and its roughness. These changes, as discussed, may explain why cells do not interact with chitosan anymore at pH 8.

To determine if this lack of interactions is also due to the chitosan itself, we also performed roughness measurements on the chitosan functionalized surfaces used in all the experiments.

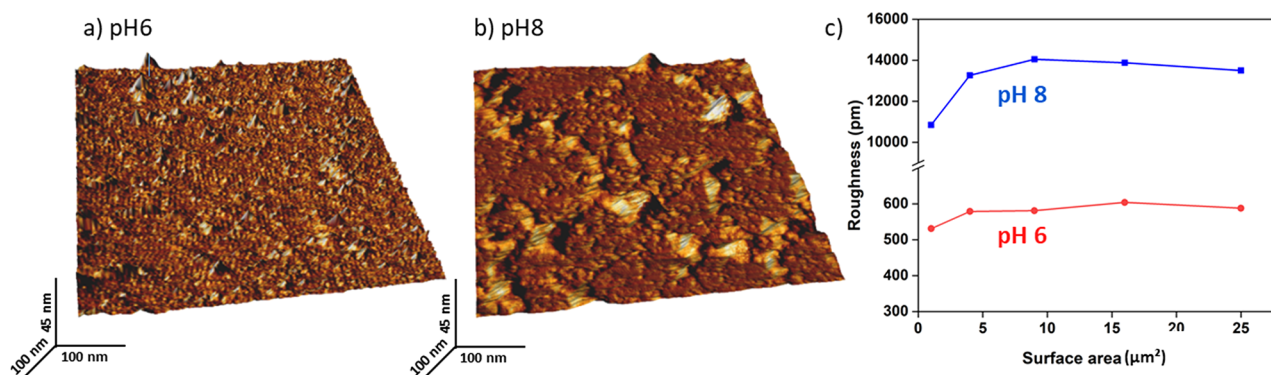


Figure 7. Characterization of chitosan surfaces at two different pH. (a) 3D AFM height image of chitosan surface at pH 6. (b) 3D AFM height image of chitosan surface at pH 8. (c) Quantification of chitosan surface roughness at pH 6 and 8.

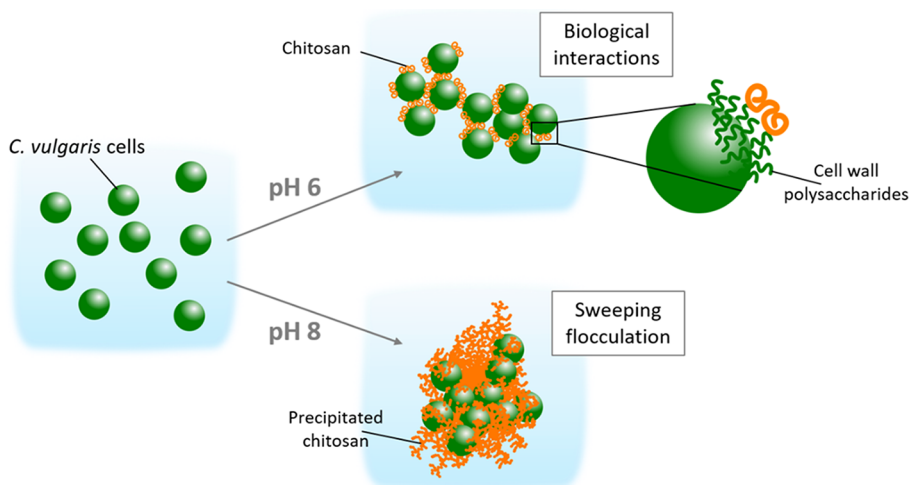


Figure 8. Schematic representation of the flocculation mechanisms induced by chitosan at pH 6 and 8 for *C. vulgaris*.

The results, presented in Figure 7, showed an average roughness of chitosan of 0.6 ± 0.1 nm at pH 6, which increased dramatically, to 13 ± 5 nm at pH 8. This result indicates that the pH has an important effect on the structure of chitosan, which precipitates and gets detached from the surface. This detachment from the surface creates aggregates of chitosan, as it can be seen on the height image recorded (Figure 7b), leading to important roughness developments. This explains why chitosan can be pulled away from the surface in force spectroscopy experiments, whatever the probe used (cell, negatively charged bead, or bare AFM tip). This precipitation might lead to a decrease of its specific surface available for interaction, which can also be a rational explanation for the fact that cells do not interact with chitosan at pH 8. Thus, from these experiments, we can conclude that the fact that chitosan does not interact with the cell wall of *C. vulgaris* at pH 8 results from the combination of changes associated directly with the structure of the cell wall with changes in the structure of chitosan itself caused by its precipitation.

CONCLUSION

Chitosan, given its many advantages, has been widely used as a flocculant to efficiently harvest diverse species of microalgae. Since understanding the flocculation mechanisms is key to control them and use them in larger-scale processes, the case of chitosan has generated a lot of debate in the scientific

community. Indeed, while for freshwater species that grow at a pH below 6.5, chitosan-induced flocculation is believed to rely on a charge neutralization mechanism, and some studies also showed that it becomes more efficient at higher pH, in marine waters where the salt present screens the charges of chitosan, chitosan can still flocculate microalgae. It is therefore of great importance to provide new data, using original techniques, to finally shed light on the flocculation mechanism at play. For that we have chosen the freshwater green species, *C. vulgaris*, and studied at the nanoscale its interactions with chitosan using atomic force microscopy. Our results demonstrate that depending on the pH, the interaction mechanism is different, which reveals the complexity of chitosan flocculation. Indeed, preliminary macroscopic observations suggest that the charge of chitosan is not involved in the interaction with cells, as different degrees of deacetylation result in the same flocculation efficiency at pH 6. At increased pH, for the same degree of deacetylation, the flocculation behavior is different as high doses of chitosan still allow an efficient separation, which is not the case at pH 6. On the basis of these observations, our force spectroscopy experiments show that at pH 6, chitosan interacts in a specific way with most probably polysaccharides present on the surface of cells and that the chitosan charge is not significantly involved in these interactions. This was confirmed by comparing these data with those obtained for cationically modified CNCs, for which a previous study has demonstrated the contribution only of

charge neutralization in the flocculation mechanism.³⁷ However, such biological interactions between chitosan and the surface of cells could not be detected at pH 8. Indeed, biophysical analysis of the cell wall of *C. vulgaris* cells, as well as roughness analysis of the chitosan used in this study, suggests that at this pH, both the architecture of the cell wall and the structure of chitosan are modified, resulting in an absence of interactions with the cells. On the basis of a previous work published last year where we had found that a sweeping mechanism is involved in the chitosan-induced flocculation of *N. oculata* at high pH, we thus suggest that this mechanism is also at play for the flocculation of *C. vulgaris* at high pH. These different mechanisms of flocculation are depicted in Figure 8. This study thus represents an original contribution to the field of microalgae harvesting as molecular-scale data allow to understand the flocculation mechanisms and to show the important influence of the culture medium pH on these mechanisms. Therefore, this work brings important information that will help to implement chitosan-induced flocculation in the harvest of microalgae at a large scale. Further work is now needed to identify the polymers from the cell surface that interact specifically with chitosan below its pK_a (pH 6). Because a large amount of microalgae species share the same surface characteristics, in particular the composition, this knowledge would make it then possible to perform efficient chitosan flocculation with a wide range of microalgae species.

METHODS

Microalgae Cultivation. The green freshwater microalgae *Chlorella vulgaris* strain CCAP 211/11B (Culture Collection of Algae and Protozoa) was cultivated in sterile conditions in Wright's cryptophyte (WC) medium prepared in deionized water, adjusted to a pH of 7.8.⁵⁴ Cells were cultivated at 20 °C, under agitation (120 rpm), in 1 L Erlenmeyer (300 mL of culture) flasks. The incubator was equipped with white neon light tubes providing illumination of approximately 40 $\mu\text{mol photons m}^{-2} \text{s}^{-1}$ with a photoperiod of 18 h light:6 h dark. All experiments were carried out with exponential phase batch cultures (day 7).

Cationically Modified Cellulose Nanocrystals (CNCs) Synthesis. N-Benzylmethylimidazolium grafted CNCs ([Br][BnIm]-g-CNCs, referred in the text as CNCs-MIM) and benzylpyridinium grafted CNCs ([Br][BnPy]-g-CNCs, referred in the text as CNCs-PYR), were synthesized and characterized in a previous study and described in Blockx et al.³⁷ For the CNCs-MIM, the sample with a degree of substitution (DS) of 0.23 was used, whereas for the CNCs-PYR, the sample with a DS of 0.20 was used.

Chitosan. Three different types of chitosan were used in this study. Commercial chitosan was purchased from Sigma-Aldrich (from shrimp, practical grade, $\geq 75\%$ degree of deacetylation (DD)). In an earlier study, it was determined that this chitosan has a M_n and M_w of 151.3 and 345.2 kDa, respectively, and a polydispersity of 2.28.³¹ This chitosan was used throughout the paper for the flocculation experiments and all AFM experiments. For flocculation experiments, two chitosan samples with different DD (labeled as 70–75% and 80–85%) were prepared from shrimp shells and kindly provided by Nha trang University, Vietnam. Chitosan stock solutions were produced by dissolving 5 g/L of the three types of chitosan in 0.04 M of HCl, while stirring (1000 rpm) at ambient conditions for 2 h. A more exact degree of deacetylation was determined for the three chitosan samples via conductometric titrations (Metrohm 856 Conductivity Module and 801 Stirrer with Tiamo™ software). For that, 2 mL of stock solution was diluted 50-fold in MiliQ water and titrated with 5.75 mM NaOH under constant stirring. The results are shown in Supporting Figure S1 and Supporting Table S1. The DD was determined from the volume of NaOH required to neutralize the chitosan (plateau area of the curves), where each chitosan sample was measured three times. The DD of the commercial Sigma-Aldrich chitosan is of $77.5 \pm 0.8\%$,

and for the chitosan samples provided by the Nha trang University of $80.5 \pm 1.4\%$ and $85.2 \pm 0.2\%$. The dynamic viscosity of the three chitosan samples was measured on a AR-G2 rheometer (TA Instruments) equipped with a steel double wall Couette cell. The experiment consisted of four steps. Step 1: 60 s at a shear rate of 100.0/s to allow the sample to set in the sample holder; step 2: 180 s at a shear rate of 1.0/s; step 3: 180 s at a shear rate of 10.0/s; and step 4: 180 s at a shear rate of 100.0/s. All experiments were carried out at 25 °C, and 1 data point was collected per second. All samples were measured in triplicate. Data analysis was performed with TA Instrument Trios Version 3.3.1.4364. The results are shown in Supporting Table S2.

Flocculation Experiments. Flocculation of *C. vulgaris* was performed using standardized jar tests experiments. The microalgae suspension was adjusted to a pH of 6, and the initial optical density ($OD_{i, 750 \text{ nm}}$) was set at 0.7 (corresponding to 0.28 g/L). The 50 mL tests samples were taken and intensively stirred at 550 rpm to mix the suspension. Different concentrations of chitosan were then added (0, 1, 3, 7, 10, 15, 20, 40, 70, 150 mg/L) from the 5 g/L stock solutions, and the suspensions were stirred at 200 rpm for 20 min to induce flocculation. The suspensions were subsequently decanted in falcon tubes and allowed to settle for 30 min before the optical density was measured after settling (OD_f) of the supernatant (at approximately 3 cm below the surface). The flocculation efficiency (η_a) was calculated according to the following eq 1. For experiments at pH 8, the microalgae suspension was adjusted to a pH of 8 prior to flocculation experiments, and the chitosan concentrations used were 0, 3, 7, 10, 15, 25, 40, 70, 100, 150 mg/L:

$$\eta_a = \frac{OD_i - OD_f}{OD_i} \quad (1)$$

Optical Imaging Experiments. Flocculation was directly observed after resuspension of the cells in Phosphate Buffer Saline (PBS) at a pH of 6 or 8 containing chitosan at a concentration of 10 mg/L or CNCs-PYR or CNCs-MIM, both at a concentration of 100 mg/L. Flocculation levels were observed using an Axio Observer Z1 microscope (Zeiss, Germany) at a magnification of 50 \times .

Zeta Potential Experiments. The global electrical properties of *C. vulgaris* cell surface as well as of negative beads (COOH functionalized polystyrene beads diameter of 6.83 μm , Spherotech, USA) were assessed by measuring the electrophoretic mobility with an automated laser zetameter (Zetasizer NanoZS, Malvern Instruments). To this end, microalgae were harvested by centrifugation (3000 rpm, 3 min), washed two times in PBS at a pH of 6 or 8, and resuspended in the same solution at a final concentration of 1.5×10^6 cell/mL. In the case of beads, they were first centrifuged (3 min, 13 000 rpm) and washed two times in deionized water. For each condition, analysis was performed in triplicate.

AFM Cantilever Functionalization. All AFM cantilever functionalizations were performed using a Nanowizard III AFM (Bruker, USA), with triangular tipless NP-O10 probes (Bruker, USA, nominal spring constant of 0.06 N/m and of 0.2 N/m).

Functionalization with CNCs. Colloidal probes were functionalized with cationic CNC particles. Colloidal probes were obtained by attaching a single silica microsphere (5 μm of diameter, Bangs Laboratories) with a thin layer of UV-curable glue (NOA 63, Norland Edmund Optics). These colloidal probes were then put under UV-light for 10 min to allow the glue to cure. They were further dipped into a thin layer of UV-curable glue, then into a thin layer of CNCs particles deposited on a glass slide. Functionalized cantilevers were then put under UV-light for 10 min to allow the glue to cure and further characterized using scanning electron microscopy (Supporting Figure S3). The spring constant of the colloidal probe was determined after attachment of the CNC particles using the thermal noise method.⁵⁵

Functionalization with Single *C. vulgaris* Cells. AFM cantilevers were also functionalized with single *C. vulgaris* cells grown during 7 days in the conditions described previously. For that, cantilevers were first activated using oxygen plasma (3 min, 0.5 mbar) and then

incubated in a 0.2% polyethylenimine solution (PEI, Sigma-Aldrich) overnight. The AFM cantilevers were then rinsed in PBS at a pH of 6 or 8, brought into contact with an isolated cell, and retracted to attach it. Proper attachment of the cell on the colloidal probe was checked using optical microscopy. The spring constant of the AFM cantilever was determined prior to cell immobilization using the thermal noise method.⁵⁵

Functionalization with Negatively Charged Beads. AFM cantilevers were functionalized using COOH polystyrene beads (negatively charged at pH 6 and 8, diameter of 6.83 μm , Spherotech, USA). Beads were first centrifuged (3 min, 13 000 rpm) and washed two times in deionized water. A drop from this solution was then deposited on a glass slide and allowed to dry at 37 $^{\circ}\text{C}$ during 2 h. Cantilevers were first dipped into a thin layer of UV-curable glue (NOA 63, Norland Edmund Optics) and then brought into contact a single isolated bead on the glass slide and retracted to attach it. Functionalized cantilevers were then put under UV-light for 10 min to allow the glue to cure; proper attachment of the COOH bead on the colloidal probe was checked using optical microscopy. The spring constant of the COOH probe was determined after attachment of the COOH bead using the thermal noise method.⁵⁵

Force Spectroscopy Experiments. Force spectroscopy experiments were conducted either by functionalizing the cantilever with CNCs and probing the interactions with immobilized cells on a surface (method 1), using FluidFM technology to aspirate a single *C. vulgaris* cell at the aperture of a microfluidic AFM probe to probe interactions with cationic CNCs functionalized on a surface (method 2), or by functionalizing the AFM cantilever with a single *C. vulgaris* cell and probing the interactions with chitosan immobilized on a surface (method 3). In each case, experiments were performed in PBS at a pH of 6 or 8, using a NanoWizard III AFM (Bruker, USA). These 3 methods are also depicted in Supporting Figure S2.

Method 1. This method was used to probe the interactions between CNCs or negatively charged beads, and single *C. vulgaris* cells. In this case, CNCs (unmodified, PYR and MIM) or negatively charged beads functionalized cantilevers were directly used to probe the interactions with *C. vulgaris* cells immobilized on polyethylenimine (PEI Sigma P3143) coated glass slides prepared as previously described.⁵⁶ For that, cells were first harvested by centrifugation (3000 rpm, 3 min) and washed two times in PBS at pH 6 or 8. Freshly oxygen activated glass slides were covered by a 0.2% PEI solution in deionized water and left for incubation overnight. Then the glass slides were rinsed with deionized water and dried under nitrogen. A total of 1 mL of the cell suspension was then deposited on the PEI slides, allowed to stand for 30 min at room temperature, and rinsed with PBS at pH 6 or 8.

Method 2. This method was also used to probe the interactions between CNCs and single *C. vulgaris* cells. As the forces recorded between CNCs and cells were stronger than the electrostatic forces between PEI coated glass-slides and cells, this method was alternatively used to complete the data sets. In this case, FluidFM technology was used (Cytosurge AG, Switzerland): this system connects the AFM to a pressure pump unit and a pressure controller through a microfluidic tubing system. Micropipette probes with an aperture of 4 μm (spring constant of 0.3 N/m) were used (Cytosurge AG, Switzerland). First, PBS at a pH 8 was filled in the probe reservoir and was pressed through the cantilever by applying an overpressure (100 mbar). The probe was then immersed in PBS and calibrated using the thermal noise method prior to measurement. A single *C. vulgaris* cell was then picked up from the surface of the Petri dish by approaching the FluidFM probe and applying a negative pressure (-80 mbar). The transfer of the cell on the probe was verified by optical microscopy. The cell probe was then used to probe the interactions with CNCs-functionalized mica surfaces. For that, CNCs solutions at a concentration of 5 g/L were first sonicated for at least 5 min, then deposited on mica surfaces and left for incubation overnight. After that, the mica surfaces were rinsed using PBS at pH 8 and taped at the bottom of the Petri dish used for the AFM experiment.

Method 3. This method was used to probe the interactions between chitosan and single *C. vulgaris* cells. In this case, AFM cantilevers functionalized with a single *C. vulgaris* cell were used to probe the interactions with chitosan-functionalized surfaces, in PBS pH 6 or 8. Chitosan was functionalized at the surface of glass-slide using spin-coating method, according to procedures described in refs 42 and 43. Briefly, 50 mg of chitosan was first dissolved in 10 mL of deionized water containing 30–50 μL of hydrochloric acid (HCl). This solution was then deposited on a clean glass slide and spin-coated at 1000 rpm for 3 min. The glass slides were then dried in an incubator at 50 $^{\circ}\text{C}$ overnight before use.

Roughness Analyses. Roughness analyses were performed on cells immobilized on PEI-coated glass slides and on chitosan-functionalized glass slides. In both cases, images were recorded in PBS at pH 6 or 8 using contact mode on a Nanowizard III AFM (Bruker, USA), with MSCT cantilevers (Bruker, nominal spring constant of 0.01 N/m). Images were recorded using an applied force <0.5 nN. The cantilevers spring constants were determined by the thermal noise method.⁵⁵

Nanomechanical Analyses. For nanoindentation experiments, the applied force was comprised between 0.5 and 2 nN depending on the condition with MSCT cantilevers (Bruker, nominal spring constant of 0.01 N/m). Young's moduli were then calculated from 80 nm indentation curves using the Hertz model⁵² in which the force F , indentation (δ), and Young's modulus (Y_m) follow eq 2, where α is the tip opening angle (17.5°), and ν the Poisson ratio (arbitrarily assumed to be 0.5). The cantilevers spring constants were determined by the thermal noise method:⁵⁵

$$F = \frac{2 \times Y_m \times \tan \alpha}{\pi \times (1 - \nu^2) \times \delta^2} \quad (2)$$

Scanning Electron Microscopy Imaging of AFM Cantilevers.

AFM cantilevers functionalized or not with CNCs or chitosan were first carbonated and then imaged using a Jeol 6400 electron microscope (Jeol, Tokyo, Japan) equipped with an EDS Bruker SDD detector at an acceleration voltage of 20 kV.

■ ASSOCIATED CONTENT

Supporting Information

The Supporting Information is available free of charge at <https://pubs.acs.org/doi/10.1021/acsabm.0c00772>.

Conductometric titration results; dynamic viscosity at different shear rates; adhesion force values recorded between single *C. vulgaris* cells and CNCs/chitosan coated surfaces; adhesion force values and percentage of adhesions recorded between single *C. vulgaris* cells and chitosan coated surface at pH 6 and 8 with increasing set point; Young's modulus values recorded on *C. vulgaris* cells at pH 6 and pH 8; conductometric titration curve of chitosan; schematic representation of the three force spectroscopy methods used; SEM imaging of AFM cantilevers; interactions between negative beads and CNC surfaces; screening electrostatic interactions between CNC-MIM and *C. vulgaris* cells; adhesion force over consecutive measurements (PDF)

■ AUTHOR INFORMATION

Corresponding Author

Cécile Formosa-Dague – TBI, Université de Toulouse, INSA, INRAE, CNRS, 31400 Toulouse, France; Fédération de Recherche FERMAT, CNRS, 31000 Toulouse, France;
✉ orcid.org/0000-0002-8627-3784; Email: formosa@insa-toulouse.fr

Authors

Irem Demir – TBI, Université de Toulouse, INSA, INRAE, CNRS, 31400 Toulouse, France; LAAS, Université de Toulouse, CNRS, 31400 Toulouse, France

Jonas Blockx – Sustainable Materials Lab, Department of Chemical Engineering and Laboratory for Aquatic Biology, KU Leuven, Campus Kulak Kortrijk, 8500 Kortrijk, Belgium; orcid.org/0000-0002-7991-7676

Etienne Dague – LAAS, Université de Toulouse, CNRS, 31400 Toulouse, France; Fédération de Recherche FERMAT, CNRS, 31000 Toulouse, France; orcid.org/0000-0003-3290-9166

Pascal Guiraud – TBI, Université de Toulouse, INSA, INRAE, CNRS, 31400 Toulouse, France; Fédération de Recherche FERMAT, CNRS, 31000 Toulouse, France

Wim Thielemans – Sustainable Materials Lab, Department of Chemical Engineering, KU Leuven, Campus Kulak Kortrijk, 8500 Kortrijk, Belgium; orcid.org/0000-0003-4451-1964

Koenraad Muylaert – Laboratory for Aquatic Biology, KU Leuven, Campus Kulak Kortrijk, 8500 Kortrijk, Belgium; orcid.org/0000-0001-9645-4063

Complete contact information is available at:
<https://pubs.acs.org/10.1021/acsabm.0c00772>

Author Contributions

[#]I.D. and J.B. contributed equally to the work.

Notes

The authors declare no competing financial interest.

ACKNOWLEDGMENTS

C.F.-D. is a researcher at CNRS. C.F.-D. acknowledges financial support for this work from the Agence Nationale de la Recherche, JCJC project FLOTALG (ANR-18-CE43-0001-01). J.B., W.T., and K.M. acknowledge financial support for this work from Research Foundation Flanders (Grant No. G.0608.16N) and from the EU Interreg France-Wallonie-Vlaanderen program through the ALPO project. W.T. further acknowledges the Provincie West-Vlaanderen for the Chair in Advanced Materials, Research Foundation Flanders for his Odysseus fellowship (Grant No. G.0C60.13N), and the European Union's European Fund for Regional Development, Flanders Innovation & Entrepreneurship and the Province of West-Flanders for financial support in the Accelerate³ project (Interreg Vlaanderen-Nederland program). The authors would like to thank Prof. Dries Vandamme for the contribution in the flocculation experiments.

REFERENCES

- (1) Pragma, N.; Pandey, K. K.; Sahoo, P. K. A Review on Harvesting, Oil Extraction and Biofuels Production Technologies from Microalgae. *Renewable Sustainable Energy Rev.* **2013**, *24*, 159–171.
- (2) *Nature* **2007** *447* (7144), 520–521.
- (3) Wijffels, R. H.; Barbosa, M. J. An Outlook on Microalgal Biofuels. *Science* **2010**, *329* (5993), 796–799.
- (4) Mallick, N.; Mandal, S.; Singh, A. K.; Bishai, M.; Dash, A. Green Microalga *Chlorella Vulgaris* as a Potential Feedstock for Biodiesel. *J. Chem. Technol. Biotechnol.* **2012**, *87* (1), 137–145.
- (5) Ziolkowska, J. R. Prospective Technologies, Feedstocks and Market Innovations for Ethanol and Biodiesel Production in the US. *Biotechnology Reports* **2014**, *4*, 94–98.

(6) Beijerinck, M. W. I. Kulturversuche Mit Zoochlorellen, Lichenengonidien Und Anderen Niederen Algen. *Botanische Zeitung* **1890**, *48*, 729.

(7) Safi, C.; Zebib, B.; Merah, O.; Pontalier, P.-Y.; Vaca-Garcia, C. Morphology, Composition, Production, Processing and Applications of *Chlorella Vulgaris*: A Review. *Renewable Sustainable Energy Rev.* **2014**, *35*, 265–278.

(8) Morimoto, T.; Nagatsu, A.; Murakami, N.; Sakakibara, J.; Tokuda, H.; Nishino, H.; Iwashima, A. Anti-Tumour-Promoting Glyceroglycolipids from the Green Alga, *Chlorella Vulgaris*. *Phytochemistry* **1995**, *40* (5), 1433–1437.

(9) Justo, G. Z.; Silva, M. R.; Queiroz, M. L. S. Effects of the Green Algae *Chlorella Vulgaris* on the Response of the Host Hematopoietic System to Intraperitoneal Ehrlich Ascites Tumor Transplantation in Mice. *Immunopharmacol. Immunotoxicol.* **2001**, *23* (1), 119–132.

(10) Shen, X.-F.; Liu, J.-J.; Chauhan, A. S.; Hu, H.; Ma, L.-L.; Lam, P. K. S.; Zeng, R. J. Combining Nitrogen Starvation with Sufficient Phosphorus Supply for Enhanced Biodiesel Productivity of *Chlorella Vulgaris* Fed on Acetate. *Algal Res.* **2016**, *17*, 261–267.

(11) Shen, X.-F.; Qin, Q.-W.; Yan, S.-K.; Huang, J.-L.; Liu, K.; Zhou, S.-B. Biodiesel Production from *Chlorella Vulgaris* under Nitrogen Starvation in Autotrophic, Heterotrophic, and Mixotrophic Cultures. *J. Appl. Phycol.* **2019**, *31* (3), 1589–1596.

(12) Molina Grima, E.; Belarbi, E.-H.; Acien Fernández, F. G.; Robles Medina, A.; Chisti, Y. Recovery of Microalgal Biomass and Metabolites: Process Options and Economics. *Biotechnol. Adv.* **2003**, *20* (7), 491–515.

(13) Singh, G.; Patidar, S. K. Microalgae Harvesting Techniques: A Review. *J. Environ. Manage.* **2018**, *217*, 499–508.

(14) Lardon, L.; Hélias, A.; Sialve, B.; Steyer, J.-P.; Bernard, O. Life-Cycle Assessment of Biodiesel Production from Microalgae. *Environ. Sci. Technol.* **2009**, *43* (17), 6475–6481.

(15) Shimako, A. H.; Tiruta-Barna, L.; Pigné, Y.; Benetto, E.; Navarrete Gutiérrez, T.; Guiraud, P.; Ahmadi, A. Environmental Assessment of Bioenergy Production from Microalgae Based Systems. *J. Cleaner Prod.* **2016**, *139*, 51–60.

(16) Kadir, W. N. A.; Lam, M. K.; Uemura, Y.; Lim, J. W.; Lee, K. T. Harvesting and Pre-Treatment of Microalgae Cultivated in Wastewater for Biodiesel Production: A Review. *Energy Convers. Manage.* **2018**, *171*, 1416–1429.

(17) Vandamme, D.; Foubert, I.; Muylaert, K. Flocculation as a Low-Cost Method for Harvesting Microalgae for Bulk Biomass Production. *Trends Biotechnol.* **2013**, *31* (4), 233–239.

(18) Vandamme, D.; Foubert, I.; Muylaert, K. Flocculation as a Low-Cost Method for Harvesting Microalgae for Bulk Biomass Production. *Trends Biotechnol.* **2013**, *31* (4), 233–239.

(19) Pugazhendhi, A.; Shobana, S.; Bakonyi, P.; Nemestóthy, N.; Xia, A.; Banu, J. R.; Kumar, G. A Review on Chemical Mechanism of Microalgae Flocculation via Polymers. *Biotechnology Reports* **2019**, *21*, No. e00302.

(20) Renault, F.; Sancey, B.; Badot, P.-M.; Crini, G. Chitosan for Coagulation/Flocculation Processes - An Eco-Friendly Approach. *Eur. Polym. J.* **2009**, *45* (5), 1337–1348.

(21) Chen, G.; Zhao, L.; Qi, Y.; Cui, Y.-L. Chitosan and Its Derivatives Applied in Harvesting Microalgae for Biodiesel Production: An Outlook. *J. Nanomater.* **2020**, *2014*, 217537 DOI: [10.1155/2014/217537](https://doi.org/10.1155/2014/217537).

(22) Ahmad, A. L.; Mat Yasin, N. H.; Derek, C. J. C.; Lim, J. K. Optimization of Microalgae Coagulation Process Using Chitosan. *Chem. Eng. J.* **2011**, *173* (3), 879–882.

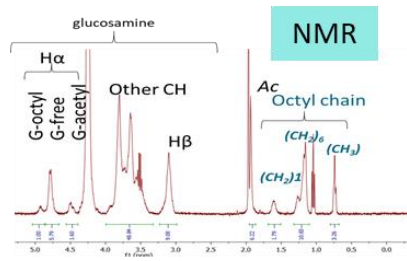
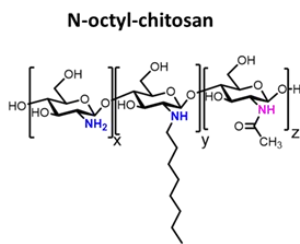
(23) Ritthidej, G. C. Chapter 3 - Nasal Delivery of Peptides and Proteins with Chitosan and Related Mucoadhesive Polymers. In *Peptide and Protein Delivery*; Van Der Walle, C., Ed.; Academic Press: Boston, 2011; pp 47–68. DOI: [10.1016/B978-0-12-384935-9.10003-3](https://doi.org/10.1016/B978-0-12-384935-9.10003-3).

(24) Bilanovic, D.; Shelef, G.; Sukenik, A. Flocculation of Microalgae with Cationic Polymers — Effects of Medium Salinity. *Biomass* **1988**, *17* (1), 65–76.

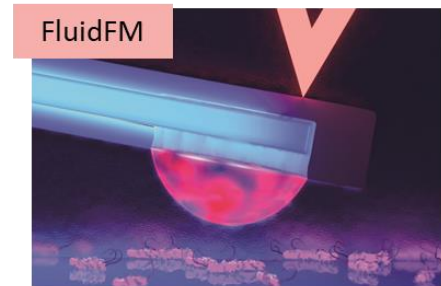
- (25) Rashid, N.; Rehman, S. U.; Han, J.-I. Rapid Harvesting of Freshwater Microalgae Using Chitosan. *Process Biochem.* **2013**, *48* (7), 1107–1110.
- (26) Low, Y. J.; Lau, S. W. Effective Flocculation of *Chlorella Vulgaris* Using Chitosan with Zeta Potential Measurement. *IOP Conf. Ser.: Mater. Sci. Eng.* **2017**, *206*, 012073.
- (27) Matho, C.; Schwarzenberger, K.; Eckert, K.; Keshavarzi, B.; Walther, T.; Steingroewer, J.; Krujatz, F. Bio-Compatible Flotation of *Chlorella Vulgaris*: Study of Zeta Potential and Flotation Efficiency. *Algal Res.* **2019**, *44*, 101705.
- (28) Garzon-Sanabria, A. J.; Ramirez-Caballero, S. S.; Moss, F. E. P.; Nikolov, Z. L. Effect of Algogenic Organic Matter (AOM) and Sodium Chloride on Nannochloropsis Salina Flocculation Efficiency. *Bioresour. Technol.* **2013**, *143*, 231–237.
- (29) Farid, M. S.; Shariati, A.; Badakhshan, A.; Anvaripour, B. Using Nano-Chitosan for Harvesting Microalga Nannochloropsis Sp. *Bioresour. Technol.* **2013**, *131*, 555–559.
- (30) Faridi, M. A.; Ramachandriah, H.; Banerjee, I.; Ardabili, S.; Zelenin, S.; Russom, A. Elasto-Inertial Microfluidics for Bacteria Separation from Whole Blood for Sepsis Diagnostics. *J. Nanobiotechnol.* **2017**, *15* (1), 3 DOI: 10.1186/s12951-016-0235-4.
- (31) Blockx, J.; Verfaillie, A.; Thielemans, W.; Muylaert, K. Unravelling the Mechanism of Chitosan-Driven Flocculation of Microalgae in Seawater as a Function of PH. *ACS Sustainable Chem. Eng.* **2018**, *6* (9), 11273–11279.
- (32) Cheng, Y.-S.; Zheng, Y.; Labavitch, J. M.; VanderGheynst, J. S. The Impact of Cell Wall Carbohydrate Composition on the Chitosan Flocculation of *Chlorella*. *Process Biochem.* **2011**, *46* (10), 1927–1933.
- (33) Binnig, G.; Quate, C. F.; Gerber, C. Atomic Force Microscope. *Phys. Rev. Lett.* **1986**, *56* (9), 930–934.
- (34) Formosa-Dague, C.; Gernigon, V.; Castelain, M.; Daboussi, F.; Guiraud, P. Towards a Better Understanding of the Flocculation/Flotation Mechanism of the Marine Microalgae *Phaeodactylum Tricornutum* under Increased PH Using Atomic Force Microscopy. *Algal Res.* **2018**, *33*, 369–378.
- (35) Besson, A.; Formosa-Dague, C.; Guiraud, P. Flocculation-Flotation Harvesting Mechanism of *Dunaliella Salina*: From Nano-scale Interpretation to Industrial Optimization. *Water Res.* **2019**, *155*, 352–361.
- (36) Vergnes, J. B.; Gernigon, V.; Guiraud, P.; Formosa-Dague, C. Bicarbonate Concentration Induces Production of Exopolysaccharides by *Arthrospira Platensis* That Mediate Bioflocculation and Enhance Flotation Harvesting Efficiency. *ACS Sustainable Chem. Eng.* **2019**, *7* (16), 13796–13804.
- (37) Blockx, J.; Verfaillie, A.; Eyley, S.; Deschaume, O.; Bartic, C.; Muylaert, K.; Thielemans, W. Cationic Cellulose Nanocrystals for Flocculation of Microalgae: Effect of Degree of Substitution and Crystallinity. *ACS Appl. Nano Mater.* **2019**, *2* (6), 3394–3403.
- (38) Chen, L.; Chen, D.; Wu, C. A New Approach for the Flocculation Mechanism of Chitosan. *J. Polym. Environ.* **2003**, *11* (3), 87–92.
- (39) Demir, I.; Besson, A.; Guiraud, P.; Formosa-Dague, C. Towards a Better Understanding of Microalgae Natural Flocculation Mechanisms to Enhance Flotation Harvesting Efficiency. *Water Sci. Technol.* **2020**, *82*, 1009.
- (40) Verfaillie, A.; Blockx, J.; Praveenkumar, R.; Thielemans, W.; Muylaert, K. Harvesting of Marine Microalgae Using Cationic Cellulose Nanocrystals. *Carbohydr. Polym.* **2020**, *240*, 116165.
- (41) Alsteens, D.; Beaussart, A.; Derclaye, S.; El-Kirat-Chatel, S.; Park, H. R.; Lipke, P. N.; Dufrene, Y. F. Single-Cell Force Spectroscopy of Als-Mediated Fungal Adhesion. *Anal. Methods* **2013**, *5* (15), 3657–3662.
- (42) Yao, H.-B.; Fang, H.-Y.; Tan, Z.-H.; Wu, L.-H.; Yu, S.-H. Biologically Inspired, Strong, Transparent, and Functional Layered Organic-Inorganic Hybrid Films. *Angew. Chem., Int. Ed.* **2010**, *49* (12), 2140–2145.
- (43) Carapeto, A. P.; Ferrara, A. M.; Botelho do Rego, A. M. Chitosan Thin Films on Glass and Silicon Substrates. *Microsc. Microanal.* **2015**, *21* (S5), 13–14.
- (44) Formosa, C.; Grare, M.; Jauvert, E.; Coutable, A.; Regnouf-Devains, J. B.; Mourer, M.; Duval, R. E.; Dague, E. Nanoscale Analysis of the Effects of Antibiotics and CX1 on a *Pseudomonas Aeruginosa* Multidrug-Resistant Strain. *Sci. Rep.* **2012**, *2*, 575 DOI: 10.1038/srep00575.
- (45) Formosa-Dague, C.; Speziale, P.; Foster, T. J.; Geoghegan, J. A.; Dufrene, Y. F. Zinc-Dependent Mechanical Properties of *Staphylococcus Aureus* Biofilm-Forming Surface Protein SasG. *Proc. Natl. Acad. Sci. U. S. A.* **2016**, *113* (2), 410–415.
- (46) Formosa-Dague, C.; Feuillie, C.; Beaussart, A.; Derclaye, S.; Kuchariková, S.; Lasa, I.; Van Dijck, P.; Dufrene, Y. F. Sticky Matrix: Adhesion Mechanism of the Staphylococcal Polysaccharide Intercellular Adhesin. *ACS Nano* **2016**, *10* (3), 3443–3452.
- (47) Higgins, M. J.; Molino, P.; Mulvaney, P.; Wetherbee, R. The Structure and Nanomechanical Properties of the Adhesive Mucilage That Mediates Diatom-Substratum Adhesion and Motility1. *J. Phycol.* **2003**, *39* (6), 1181–1193.
- (48) Myllytie, P.; Salmi, J.; Laine, J. the Influence of pH on the Adsorption and Interaction of Chitosan with Cellulose. *Bio Resources* **2009**, *4* (4), 1647–1662.
- (49) Simsek-Ege, F. A.; Bond, G. M.; Stringer, J. Polyelectrolyte Complex Formation between Alginate and Chitosan as a Function of PH. *J. Appl. Polym. Sci.* **2003**, *88* (2), 346–351.
- (50) Barany, S.; Szepesszentgyörgyi, A. Flocculation of Cellular Suspensions by Polyelectrolytes. *Adv. Colloid Interface Sci.* **2004**, *111* (1), 117–129.
- (51) Boonsongrit, Y.; Mitrevej, A.; Mueller, B. W. Chitosan Drug Binding by Ionic Interaction. *Eur. J. Pharm. Biopharm.* **2006**, *62* (3), 267–274.
- (52) Hertz, H. Ueber Die Berührung Fester Elastischer Körper. *Journal für die reine und angewandte mathematik* **1881**, 156–171.
- (53) Formosa, C.; Schiavone, M.; Martin-Yken, H.; François, J. M.; Duval, R. E.; Dague, E. Nanoscale Effects of Caspofungin against Two Yeast Species, *Saccharomyces Cerevisiae* and *Candida Albicans*. *Antimicrob. Agents Chemother.* **2013**, *57* (8), 3498–3506.
- (54) Guillard, R. R. L.; Lorenzen, C. J. Yellow-Green Algae with Chlorophyllide C2. *J. Phycol.* **1972**, *8* (1), 10–14.
- (55) Hutter, J. L.; Bechhoefer, J. Calibration of Atomic-Force Microscope Tips. *Rev. Sci. Instrum.* **1993**, *64* (7), 1868–1873.
- (56) Francius, G.; Tesson, B.; Dague, E.; Martin-Jézéquel, V.; Dufrene, Y. F. Nanostructure and Nanomechanics of Live *Phaeodactylum Tricornutum* Morphotypes. *Environ. Microbiol.* **2008**, *10* (5), 1344–1356.

Chapter 6: Bubble functionalization in flotation process improve microalgae harvesting

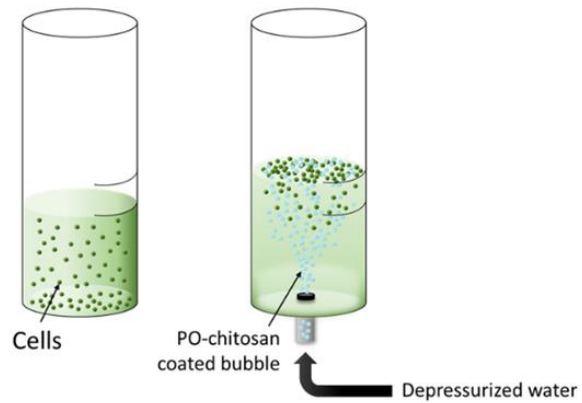
Modifying the target molecule



Functionalize the bubble



Optimizing process at population-scale



Irem Demir-Yilmaz, Malak Souad Ftouhi, Stephane Balayssac, Pascal Guiraud, Christophe Coudret, and Cécile Formosa-Dague

Chemical engineering Journal 452 (2023):139349

Abstract

Context: In this part of the work Christophe Coudret from the Laboratoire Interactions Moléculaires et Réactivités Chimiques et Photochimiques (IMRCP, Toulouse) provided valuable assistance in modifying chitosan and making it amphiphilic.

Background: Microalgae is a promising resource for biofuel production, although the lack of effective harvesting techniques limits their industrial use. In this context, flotation is an interesting separation technique that could drastically reduce harvesting costs and make biofuel-production systems economically viable. But flotation can be challenging in the case of microalgae, because of the repulsive interaction between cells and bubbles.

Scope of the review: We propose here an original strategy to improve the efficiency of flotation for microalgae harvesting, which is based on bubble functionalization. For that, we chose to build on our previous results and modify the bubble surface using chitosan as we now have a complete understanding of its interactions with cells. For that, in a first part, we modify chitosan and add hydrophobic groups on its backbone to obtain an amphiphilic molecule, PO-chitosan, which can assemble on the bubble surface. Then, using the FluidFM method previously developed to probe the interactions between bubbles and cells, we could probe the interactions between PO-chitosan coated bubbles and cells at the molecular scale. The results obtained show an enhanced adhesion of functionalized bubbles to cells compared to clean cells, which is pH-dependent. In addition, flotation experiments performed at the population-scale show a significant increase of the separation efficiency with functionalized bubbles compared to clean bubbles, also pH-dependent.

Major conclusions: This new flotation strategy allows to eliminate the need of a prior flocculation step and thus shortens the time needed for microalgae harvesting. The functionalization of bubbles allows increasing in a significant manner their interactions with cells, in a pH-dependent manner. Further flotation experiments showed that flotation efficiency is directly correlated to the interaction between cells and functionalized bubbles, as flotation efficiency also changes with the pH.



Bubble functionalization in flotation process improve microalgae harvesting

Irem Demir-Yilmaz^{a,b}, Malak Souad Ftouhi^a, Stéphane Balayssac^c, Pascal Guiraud^{a,d},
Christophe Coudret^{c,d}, Cécile Formosa-Dague^{a,d,*}

^a TBI, Université de Toulouse, INSA, INRAE, CNRS, Toulouse, France

^b LAAS, Université de Toulouse, CNRS, Toulouse, France

^c UMR 5623 IMRCP, CNRS, Toulouse, France

^d Fédération de Recherche Fermat, CNRS, Toulouse, France

ARTICLE INFO

Keywords:

Flotation
Flocculation
Functionalized bubbles
Chitosan
Atomic force microscopy
Microalgae

ABSTRACT

Microalgae are a promising resource for biofuel production, although the lack of effective harvesting techniques limits their industrial use. In this context, flotation, and in particular dissolved air flotation (DAF), is an interesting separation technique that could drastically reduce harvesting costs and make biofuel-production systems more economically viable. But because of the repulsive interaction between cells and bubbles in water, the efficiency of this technique can be limited. To solve this problem, we propose here an original DAF process where bubbles are functionalized with a bio-sourced polymer able to specifically bind to the surface of cells, chitosan. In a first part, we modify chitosan by adding hydrophobic groups on its backbone to obtain an amphiphilic molecule, PO-chitosan, able to assemble at the surface of bubbles. Then, using a recently developed technique based on atomic force microscopy (AFM) combined with microfluidics, we probe the interactions between PO-chitosan coated bubbles and cells at the molecular scale; results show an enhanced adhesion of functionalized bubbles to cells (from 3.5 to 12.8 nN) that is pH-dependent. Separation efficiencies obtained in flotation experiments with functionalized bubbles are in line with AFM data, and a microalgae separation efficiency of approximately 60% could be reached in a single step. In addition, we also found that PO-chitosan could be used efficiently as a flocculant (nearly 100% of cells removed), and in this case AFM experiments revealed that the flocculation mechanism is based on hydrophobic interactions between cells and PO-chitosan. Altogether, this comprehensive study shows the interest of PO-chitosan to harvest cells in flotation or flocculation/flotation processes.

1. Introduction

Microalgae are photosynthetic microorganisms capable of capturing sunlight and converting carbon dioxide into value-added products such as biofuels, dietary products and animal feed [1]. For biofuel production, microalgae are currently considered the most promising biomass due to their many advantages over terrestrial plants, such as rapid growth, high capacity to accumulate lipids under certain conditions and the possibility of growing them on non-arable land [2]. Despite these advantages, broad commercialization of microalgae-sourced biodiesel has been restrained due to the high costs involved in production processes. Basically, biofuel production from microalgae can be divided into the following major steps: cultivation, harvesting, extraction and down-

stream processes [3]. The most expensive of these steps is the harvesting of microalgae; as they grow at low concentration (0.3–3 g/L), large volumes of water need to be treated to recover small quantities of biomass [4]. Although the choice of microalgae harvesting technique depends largely on the microalgae species and the desired end product, the most commonly used techniques are centrifugation, filtration and sedimentation [5]. These methods however are generally associated with a low efficiency, high capital costs and important energy and/or chemicals consumptions. For example, centrifugation requires a high energy input (up to 8 kWh/m³ of microalgae, [6]) which represents a huge cost for largescale processing, and may also damage cells due to the high shear forces, resulting in a significant loss of the products of interest [1]. Likewise permeable membranes used for filtration are easily

* Corresponding author at: TBI, INSA de Toulouse, 135 avenue de Rangueil, 31400 Toulouse, France.

E-mail address: formosa@insa-toulouse.fr (C. Formosa-Dague).

<https://doi.org/10.1016/j.cej.2022.139349>

Received 26 July 2022; Received in revised form 13 September 2022; Accepted 17 September 2022

Available online 22 September 2022

1385-8947/© 2022 Elsevier B.V. All rights reserved.

clogged by small microalgae [7], which also leads to important processing costs and material costs.

In this context, flotation could be an interesting alternative harvesting technique as it is a proven technology to efficiently capture small particles in an aqueous solution using air bubbles. In this way, it takes advantage of the natural characteristics of microalgae, namely a relatively low density and a tendency to self-flotation [8]. In addition, because it is a relatively rapid operation, with low space requirements, high flexibility and moderate operational costs, flotation technique has the potential to overcome the bottleneck of feasible microalgal biofuel production [9]. Indeed, when combined to a flocculation step, the energy demand reported can be as low as 1.5 kWh/m³ [10]. However, its efficient use for microalgae harvesting is still challenging as cells are usually negatively charged. The surface of air bubbles being also negatively charged in water, [11] they repeal each other preventing adhesion and thus capture and flotation. To improve flotation efficiency, adding a flocculation step prior to flotation can be a good solution. Synthetic flocculants added to the microalgal suspension aggregate cells into large flocs that can be easily captured by the bubbles [12]. However, contamination is a major issue in this technique as flocculants at the end of the process end up in the harvested biomass and can have an important impact on the final quality of the products [9]. To avoid this problem, natural flocculation is a preferred alternative. So far, two types of natural flocculation mechanisms have been identified: auto-flocculation, where flocculation is triggered by a molecule or precipitate that forms naturally in the culture medium, and bio-flocculation, where a molecule produced by cells is directly responsible for flocculation [13]. But because natural flocculation can be difficult to control or trigger in industrial processes, many studies have showed the interest of using bio-flocculants like biopolymers either directly extracted from other organisms like natural polysaccharides, or modified by various means to control the functional chemical groups they present and induce natural flocculation [14–17]. The most popular biopolymer used for microalgae harvesting is with no doubt chitosan. Chitosan is a cationic polyelectrolyte at pH lower than its pKa (6.5) obtained by deacetylation of chitin. After cellulose, it is the second most abundant natural polymer on earth [18,19]. Moreover as chitin-like polysaccharides are naturally present in the cell wall of several microalgae species [20], chitosan does not contaminate the harvested biomass. To understand its flocculation mechanism, our team recently performed atomic force microscopy (AFM) experiments to probe the interactions between chitosan and cells. AFM, first developed in 1986, is a powerful tool that can be used to study microalgae cells at the nanoscale and characterize their interactions with their environment [21]. The results obtained in this study showed that at low pH, chitosan is able to form specific interactions with polymers present at the surface of cells, in this case, cells of *Chlorella vulgaris*, while at higher pH, chitosan forms a precipitate in which cells get entrapped [17].

Another possibility to improve the efficiency of flotation for microalgae harvesting that has been explored is to modify the surface of the bubbles. The principal example of such a strategy was provided by Henderson's team, who modified the surface of the bubbles with positively charged polymers, thereby changing the charge of the bubbles and making interaction with the cells attractive. Using this strategy named Posi-DAF (positive dissolved air flotation), the authors could obtain a maximum separation efficiency of 97 %, 54 % and 89 % in the case of *Melosira aeruginosa*, *C. vulgaris* and *Asterionella formosa* cells respectively. Here in this work, we also propose a bubble-modification strategy, based on the recent findings that we generated on the mechanism of interaction of chitosan with cells [17]. The hypothesis is that since chitosan is able to bind specifically to microalgae cells at low pH, if we functionalize it at the surface of bubbles, then flotation separation could be efficient without the need of a flocculation step. Removing this step in a large-scale production system could result in reduced costs, reduced harvesting time, and could represent an important step forward for the use of microalgae for biofuel production. This is what is presented in this

study, and for that we worked with a biotechnologically-relevant freshwater microalgae species, *C. vulgaris*. The first step of this work was to modify chitosan so it could be functionalized at the surface of bubbles, by adding hydrophobic groups on its hydrophilic backbone. Then, using a recently developed approach based on FluidFM technology, which combines AFM and microfluidics, we could probe the interactions between functionalized bubbles and cells at the molecular scale, and this way understand the mechanism involved in this interaction [22]. Finally, the effectiveness of this original flotation process in different experimental conditions was determined. But as we were investigating the interacting behavior of this chitosan-based molecule, we also found that it could be successfully used as a flocculant; AFM experiments in this case allow understanding how the modifications made on chitosan affected the physico-chemical basis of its interactions with cells. Altogether, this work has led to the development of an original flotation process based on functionalized bubbles with a modified chitosan molecule, which can also serve as a flocculant depending on the application and needs. Finally the AFM experiments performed at the molecular scale could highlight the mechanisms at play, thereby giving a full understanding of the interaction mechanisms involved in both cases.

2. Materials and methods

2.1. Chemicals

Chemicals for the synthesis of alkyl-chitosan derivatives were the following: chitosan (from shrimp, practical grade, ≥ 75 % degree of deacetylation, C3646), octanal (O5608), sodium hydroxide (S0899), sodium cyanoborohydride reagent grade 95 % (156159), Deuterium chloride solution (543047) were purchased from Sigma-Aldrich as well as glacial acetic acid 99.5 % (W200611) and ethanol 96 % (1.59010) and used as received.

2.2. Synthesis and characterization of polyoctyl chitosan (PO-chitosan)

The *N*-octyl-chitosan derivatives were obtained by reductive amination following a procedure previously described in the literature [23–26]. In brief, 6 g of chitosan were dissolved in 450 mL of 0.2 M acetic acid (AcOH) to which was added 180 mL of ethanol after complete dissolution. The pH was adjusted to 6 with 4 M of NaOH to prevent macromolecule precipitation. A solution of octanal (target alkylation level of 10 %) in 40 % of ethanol was added using a 1:3 ratio prior to adding an excess of sodium cyanoborohydride (NaBH₃CN) (3:1 mol ratio per glucosamine monomer). After stirring for 24 h at room temperature, the pH of the reaction mixture was adjusted to 7–8 using a solution of 4 M of NaOH. The precipitate was collected by centrifugation for 5 min at 6000 rpm at 4 °C and was then thoroughly washed with ethanol/water mixture at least 5 times with increasing ethanol concentration from 40 % (v/v) to 100 % (v/v) before drying until constant weight. NMR spectroscopy was used to characterize both chitosan and *N*-octyl-chitosan derivatives produced to determine the degree of substitution (DS). The NMR spectra were performed on a Bruker Advance spectrometer (Bruker, Switzerland) in D₂O-DCl (pH around 4) at a resonance frequency of 400.13 MHz and 70 °C on the starting material and on the final product. The degree of substitution was calculated from NMR spectra as previously described elsewhere [23]. Integration of the anomeric protons and acetyl groups were obtained using the TOPSPIN 4.0.8 software (Bruker, Switzerland) and gave an acetylation degree of 20 % (consistent with the starting material), 12 % of octylated monomers, and 68 % of free amine monomers.

2.3. Microalgae strain and culture

The green freshwater microalgae *Chlorella vulgaris* strain CCAP 211/11B (Culture Collection of Algae and Protozoa, Scotland, UK) was

cultivated in sterile conditions in Wright's cryptophyte (WC) medium prepared with deionized water, as previously described [17]. Cells were cultivated at 20 °C, under 120 rpm agitation, in an incubator equipped with white neon light tubes providing illumination of approximately 40 $\mu\text{mol photons m}^{-2} \text{s}^{-1}$, with a photoperiod of 18 h light: 6 h dark. Exponential phase experiments were performed with 7-day batch cultures, while stationary phase experiments were performed with 21-day batch cultures.

2.4. Roughness analyses

Roughness analyses were performed on PO-chitosan immobilized on glass slides. PO-chitosan was functionalized at the surface of glass slides using spin-coating, according to a procedure described in Demir *et al.* 2020 [17]. Briefly, 2.5 g/L PO-chitosan (pH around 2 adjusted with HCl) solution was deposited on a clean glass slide and spin-coated at 1000 rpm for 3 min. The glass slides were then dried in an incubator at 37 °C overnight before use. Height images of the PO-chitosan surfaces were recorded in PBS at pH 6, 7.4 and 9 using contact mode available on the Nanowizard III AFM (Bruker, USA), and MSCT cantilevers (Bruker, nominal spring constant of 0.01 N/m). Images were recorded with a resolution of 256 × 256 pixels using an applied force < 1 nN. In all cases the cantilevers spring constants were determined by the thermal noise method prior to imaging [27]. The height images obtained were then analyzed using the Data Processing software (Bruker, USA) to determine the arithmetic average roughness (Ra) of 6 different areas of 25 μm^2 (5 $\mu\text{m} \times 5 \mu\text{m}$) for each sample.

2.5. Flocculation and flotation experiments

Flocculation and flotation separation of *C. vulgaris* was performed in a dissolved air flotation (DAF) homebuilt flotation device, described elsewhere [28]. Briefly, the depressurization at atmospheric pressure of water saturated by air at 6 bars induced the formation of bubbles. Water free of algae was pressurized for 30 min before injection into the jars. The injection was controlled by solenoid valves and a volume of pressurized water was added to each beaker sample. Two types of experiments were conducted, repeated 3 times for each condition with cells coming from 2 independent cultures:

- **Flocculation:** *C. vulgaris* cells were cultured during 7 days until they reached mid-exponential phase. Then 100 mL of cell suspension was directly poured into the test-jars with an initial optical density (OD) at 750 nm of 0.8. Flocculants, chitosan and PO-chitosan, were directly added (final concentration of 10, 15 and 20 mg/L for chitosan and of 12, 17, 22, 25, 30, 40 and 60 mg/L for PO-chitosan) to the suspension, which was stirred at 100 rpm for 20 min to homogenize and left to settle for 30 min. OD at 750 nm of the suspension was measured afterwards to calculate flocculation efficiency.
- **Flotation:** *C. vulgaris* cells were cultured during 7 days until they reached mid-exponential phase. Then, 100 mL of cell suspension was directly poured into the test-jars with an initial OD₇₅₀ of 0.8. PO-chitosan mixed with water was directly added to the pressurization tank (final concentration of 30, 25 and 20 mg/L); the mix was then pressurized during 30 min at 6 bars. Following this, depressurization at atmospheric pressure of the water-PO-chitosan mix saturated by air was performed to inject functionalized microbubbles into each flotation beaker (bubble volume of 20, 50, 80 and 100 mL). The algal suspension was retrieved from the bottom of the test-jars: 30 mL were used for measuring OD at 750 nm and further quantify flotation efficiency.

For both types of experiments, the optical density of the withdrawn microalgae suspension (OD_f) was measured and compared to the optical density of the microalgae suspension measured before the experiments

(OD_i), taking the initial and final volumes into account (V_i and V_f). The flotation efficiency (E) was calculated according to the following Eq. (1).

$$E = \frac{OD_i \cdot V_i - OD_f \cdot V_f}{OD_i \cdot V_i} \quad (1)$$

2.6. Zeta potential experiments

The global electrical properties of *C. vulgaris* cell surface at pH 6, 7.4 and 9 were assessed by measuring the electrophoretic mobility with an automated laser zetameter (Zetasizer NanoZS, Malvern Instruments). To this end, microalgae were harvested by centrifugation (3000 rpm, 3 min), washed two times in PBS at a pH of 6, 7.4 or 9, and resuspended in the same solution at a final concentration of 1.5×10^6 cell/mL. For each condition, analysis were performed in triplicate.

2.7. Granulometry analysis

Particle size distributions of both chitosan and PO-chitosan were determined using a Mastersizer (Malvern Instruments, UK). For that, PO-chitosan was dissolved in water with a pH around 2 (with HCl) and stirred for 1 week at final concentrations of 2.5 g/L, 1 g/L and 0.5 g/L. The refractive index used for micelles was of 1.350. The results are presented as an average number obtained from 3 measurements.

2.8. Force spectroscopy experiments using FluidFM technology

Force spectroscopy experiments were conducted using a Nanowizard III AFM (Bruker, USA), equipped with FluidFM technology (Cytosurge AG, Switzerland). In each case, experiments were performed in PBS at pH 6, using micropipette probes with an aperture of 2 μm (spring constant of 0.3, and 4 N/m, Cytosurge AG, Switzerland). First, PBS at a pH of 6 was used to fill the probe reservoir (5 μL); by applying an overpressure (100 mBar) the PBS then filled the entire cantilever microchannel. The probe was then immersed in PBS and calibrated using the thermal noise method prior to measurement [27]. A single *C. vulgaris* cell was then aspirated from the surface of the Petri dish by approaching the FluidFM probe and applying a negative pressure (−200 mBar). The presence of the cell on the probe was verified by optical microscopy. The cell probe was then used to measure the interactions with PO-chitosan immobilized on glass slides. Interactions between single *C. vulgaris* cells aspirated at the aperture of FluidFM cantilevers and PO-chitosan were recorded at pH 6, 7.4 and 9 at a constant applied force of 1 nN, force curves were recorded with a z-range of up to 2 μm and a constant retraction speed of 2.0 $\mu\text{m/s}$ to 4 $\mu\text{m/s}$. Data were analyzed using the Data Processing software from Bruker. Adhesion forces were obtained by calculating the maximum adhesion force for each retract curves. Results were recorded on ten different cells coming from at least two independent cultures.

2.9. Bubble formation and functionalization using FluidFM

Air-bubbles were formed using FluidFM as described in Demir *et al.* [22], using a Nanowizard III AFM (Bruker, USA), equipped with FluidFM technology (Cytosurge AG, Switzerland). Experiments were performed in PBS, using microfluidic micropipette probes (FluidFM cantilevers) with an aperture of 8 μm (spring constant of 0.3 and 2 N/m, Cytosurge AG, Switzerland). Briefly, hydrophobized FluidFM cantilevers were first filled with air and immersed in PBS. A single bubble was then formed at the aperture of the cantilevers by applying a positive pressure (200 mbar) inside the cantilever thanks to the pressure controller to which it is connected. To produce functionalized bubbles, the FluidFM cantilever was immersed in a solution of 2 mg/L of PO-chitosan. This solution was aspirated inside the cantilever by gradually decreasing the pressure from 0 mbar to −200 mbar. After that the FluidFM cantilever containing the surfactant solution was immersed in PBS buffer without

surfactants. By increasing the pressure to 150 mbar, the surfactant solution was then locally dispersed in the buffer and a bubble was formed: the surfactant then assembled at the surface of the produced bubble. Interactions between PO-chitosan coated bubble produced at the aperture of FluidFM and single *C. vulgaris* cells were recorded at pH 6, 7.4 and 9 at a constant applied force of 1 nN, force curves were recorded with a z-range of up to 2 μm and a constant retraction speed up to 4 $\mu\text{m/s}$.

2.10. Statistical analysis

Experimental results represent the mean \pm standard deviation (SD) of at least three replicates. For each experiments, the number of replicates is indicated in the results and discussion section. For large samples, student *t*-test was used to assess the difference observed in the results. For small samples (<20) Mann and Whitney test was used to assess the difference. The differences were considered significantly at $p < 0.05$.

3. Results and discussion

3.1. Synthesis of PO-chitosan

The first step of this study consisted in the synthesis of PO-chitosan using the reductive amination reaction illustrated in Fig. 1a. Such reaction preserves the number of basic nitrogens and can be performed under mild conditions that do not modify the chitosan molecule itself (degree of acetylation and/or polymerization degree) as described elsewhere [24]. Octanal was chosen as a precursor of the hydrophobic alkyl groups, this way the amphiphilic character of the target molecule PO-chitosan can be reached without the complete alkylation of all glucosamine monomers and indeed a 10 % stoichiometric ratio is sufficient. Thus, some of the primary amino groups of chitosan undergo a Schiff reaction with octanal to yield the corresponding aldimines, which are then converted to alkyl derivatives by reduction with NaBH_3CN . ^1H NMR spectroscopy in $\text{D}_2\text{O}/\text{DCl}$ (pH ~ 4) at 70 $^\circ\text{C}$ was used to characterize both chitosan and PO-chitosan and determine the degree of substitution (DS) of the amine functions by the octyl chains. The ^1H NMR spectra of initial chitosan and PO-chitosan are presented in Fig. 1b and c respectively. The octyl chain in PO-chitosan can be easily identified by the signals in the 0.7 – 1.7 ppm region. Thus, the signal at 0.7 ppm was attributed to the terminal $-\text{CH}_3$ while those at 1.6 ppm and the multiplet at 1.1–1.3 ppm, to respectively the $-\text{CH}_2$ group linked to the N atom and

the core CH_2 of the octyl chain.

The degree of substitution was calculated as previously described [23], by examining the relative integration of the anomeric protons H_α , using the assignation previously reported [23–25].

- * at 4.54 ppm, the acetylglucosamine unit,
- * at 4.80 ppm, the unsubstituted glucosamine unit.
- * at 4.94 ppm, the monosubstituted glucosamine unit.

It was found to be of 12 % (Fig. 1c), meaning that 12 % of the amine functions of chitosan have been modified with octanal molecules. This number is close to the targeted degree of substitution (10 %) and to what was found by Mati-Baouche *et al.* who described the reaction in these specific conditions [24]. The relative number of *N*-acetylated glucosamine remained unchanged compared to the starting chitosan and confirms the mildness of the reaction conditions used.

3.2. Characterization of PO-Chitosan using atomic force microscopy

PO-chitosan has already been characterized on the basis of its water resistance, rheological characteristic and bonding properties to wood and aluminum surfaces [24,25]. Here we characterized PO-chitosan on the basis of its surfactant properties, particle size, roughness and hydrophobicity, which are parameters important to then optimize the next experiments of this study (AFM, flocculation and flotation experiments). PO-chitosan has both hydrophilic ($-\text{NH}_2$ or $-\text{OH}$) and hydrophobic sites (alkyl chains, octanal), and thus possess amphiphilic properties, making it a surfactant. As for any surfactants, it should be able to decrease the surface tension of water with increasing concentration. Surface tension experiments were then performed, the results are presented in Supplementary Fig. 1. They show that with increasing concentration of PO-chitosan, the surface tension of water decreases from approximately 72 to 62 mN/m for a PO-chitosan concentration of 2.5 g/L. This decrease is not as important as it can be with other types of surfactants, but this can be explained by the degree of substitution of the molecule, which is of 12 %. This means that only 12 % of the amine functions of chitosan have been modified with hydrophobic octanal molecules, thus the hydrophobic part of the molecule may not be large enough to change in an important manner the surface tension of water. However, in order to be able to dissolve the molecule in water, there needs to be a balance between the hydrophobic and hydrophilic groups. For instance, for low molecular weight chitosan, even with a substitution degree of 10 %, the resulting molecule is water insoluble. Whereas, for high molecular weight chitosan we are limited with low alkylation level (10–15 %)

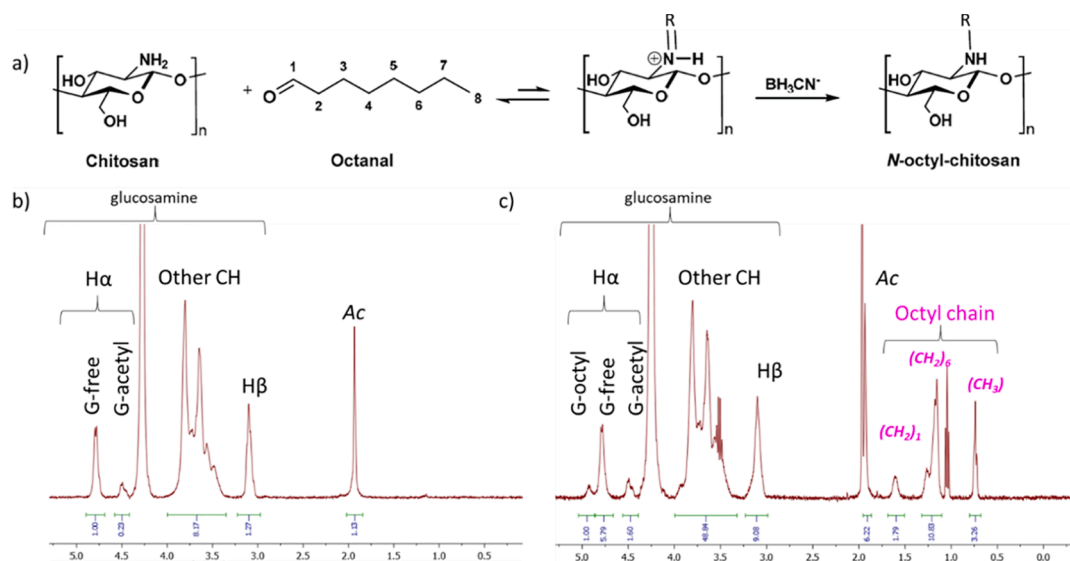


Fig. 1. Synthesis of PO-chitosan. a) Synthesis of PO-chitosan by alkylation, b) ^1H NMR spectra obtained for initial chitosan, c) ^1H NMR spectra obtained for PO-chitosan. The DS obtained for PO-chitosan is of 12 %.

because as the alkylation level increases, water solubility of PO-chitosan decreases, and we need water soluble compounds to use for the next experiments. To verify we can completely dissolve PO-chitosan in water, we measured the particle size of both initial chitosan and PO-chitosan in water using granulometry. The size distribution graphs obtained are shown in [Supplementary Fig. 1b](#) and [c](#) respectively (concentration of

2.5 g/L). They both show a similar pattern which means that the addition of octanal does not modify the size of chitosan significantly (high molecular weight).

Moreover, we also measured the turbidity of chitosan and PO-chitosan solutions at different concentrations (2.5, 1 and 0.5 g/L): the obtained turbidities are of 4.3, 3.2 and 3.5 NTU respectively. This means

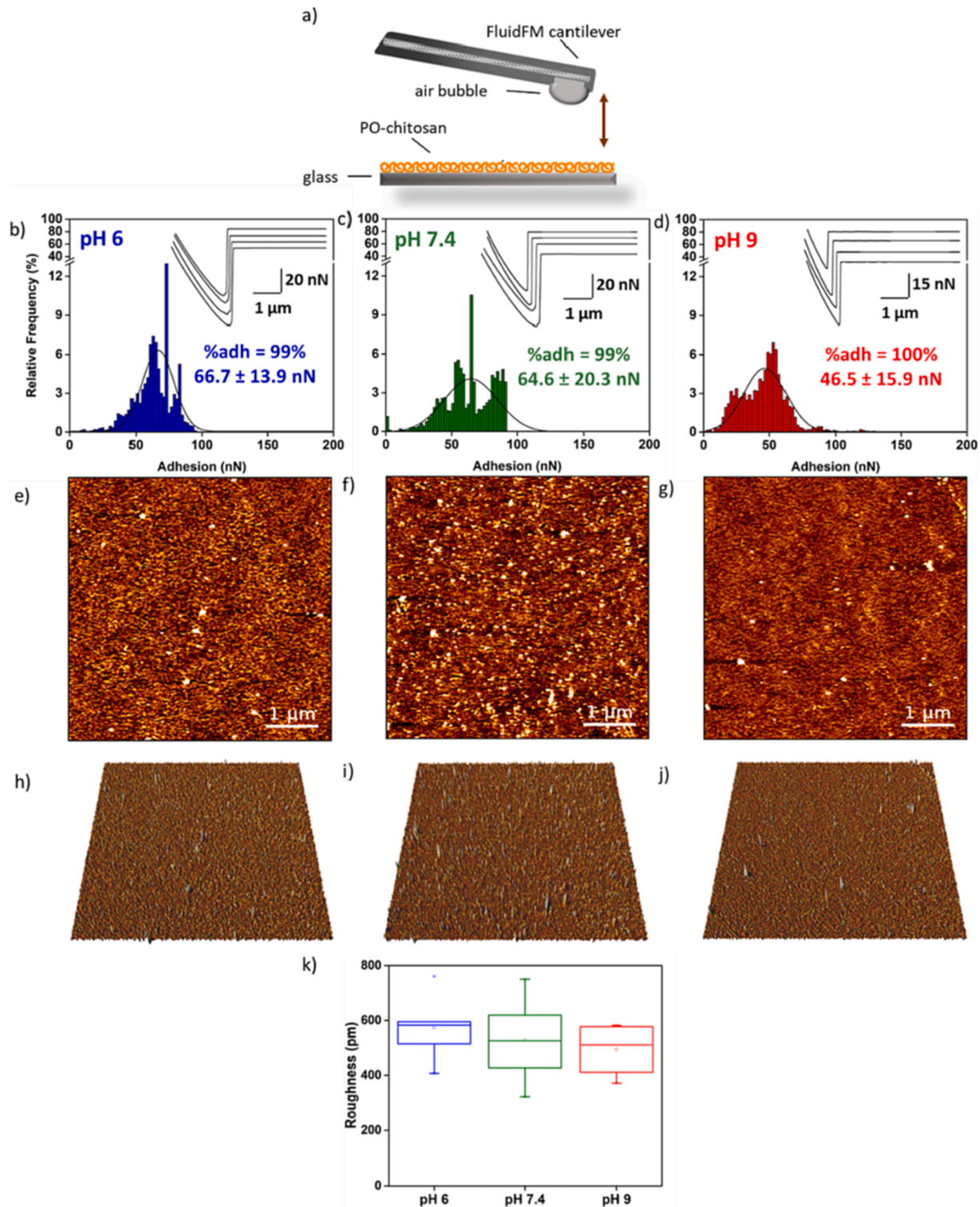


Fig. 2. Characterization of PO-chitosan surface at different pH. a) Schematic representation of bubble and PO-chitosan surface interaction. Adhesion force histogram obtained between bubble and PO-chitosan surface at b) pH 6 c) pH 7.4 and d) pH 9. AFM height images of PO-Chitosan surface at e) pH 6 (color scale = 4 nm) f) pH 7.4 (color scale = 4 nm) and g) pH 9 (color scale = 4 nm) and their corresponding 3D AFM vertical deflection images at h) pH 6, i) pH 7.4 and j) pH 9. k) Quantification of PO-chitosan surface roughness at different pH.

that solutions are clear ($\text{NTU} < 5$ corresponds to clear water). Thus both size measurements and turbidity experiments prove that we are able to dissolve PO-chitosan in water. Moreover, based on the literature, we know that chitosan and PO-chitosan behave differently. For example, rheological analysis show that alkyl-chitosan solutions are non-Newtonian fluids, since the viscosity decreases with increasing shear rate whereas initial chitosan shows a Newtonian behavior [23–25]. Further, Desbrieres *et al.* highlighted that addition of octanal or increase in the DS, is linked with the increase in viscosity of PO-chitosan since the intermolecular hydrophobic interaction is a key element in physico-chemical (rheological) properties of the modified chitosan. The higher the hydrophobic properties (the length of the alkyl chain or degree of substitution) of macromolecular chain the larger the gap to the Newtonian behavior [25]. Thus, more analysis needs to be performed on PO-chitosan to understand the differences with chitosan, such as roughness and hydrophobicity measurements.

Regarding the hydrophobic properties of PO-chitosan, it has been found that pH has an influence on the hydrophilic and hydrophobic balance of the molecule due to the ability of $-\text{NH}_2$ functions (hydrophilic part) to be ionized in acidic conditions [23]. We thus measured the hydrophobicity of PO-chitosan at different pH (pH 6, 7.4 and 9) relevant for flocculation or flotation processes for *C. vulgaris* cells, using a method recently developed in our team based on the interactions between bubbles produced by FluidFM and samples [22,29]. Air bubbles in water behaving like hydrophobic surfaces, by measuring their direct interactions with surfaces it is possible to determine the hydrophobic properties of the samples in terms of adhesion force, and further convert these forces into water contact angles (WCA) [22]. Using WCAs values we can then compare our data directly to the ones available in the literature. To perform these experiments, PO-chitosan was immobilized on glass slides by spin coating and their interaction with bubble were measured in PBS buffer at pH 6, the pH generally used for chitosan induced flocculation, pH 7.4, the optimum pH for *C. vulgaris* growth, or pH 9 which corresponds to the pH *C. vulgaris* cultures reach after 7 days. A schematic representation of these measurements is presented in Fig. 2a. The adhesion force histograms obtained at pH 6, 7.4 and 9 are presented in Fig. 2b, c and d respectively. In each case the force curves obtained show a single peak occurring at the contact point (inset in Fig. 2b, c and d), which is characteristic of non-specific interactions such as hydrophobic interactions [30]. On each force curve obtained, the adhesion force is then quantified by measuring the height of this adhesion peak, which corresponds to the force needed to break the interaction between the bubble and the sample. This force reflects the degree of hydrophobicity of the sample, the stronger the adhesion, the higher the hydrophobicity. In the case of pH 6, the average adhesion force is of 66.7 ± 13.9 nN (Fig. 2b, $n = 3125$ force curves obtained on 5 different measurements). While this value stays similar at a pH of 7.4 (64.6 ± 20.3 nN, Fig. 2c, $n = 1977$ force curves obtained on 5 different measurements), it decreases to 46.5 ± 15.9 nN at pH 9 (Fig. 2d, $n = 1454$ force curves obtained on 5 different measurements). Even though the average adhesion values at pH 6 (66.7 ± 13.9 nN) and 7.4 (64.6 ± 20.3 nN) are close to each other, statistical analysis shows that they are significantly different (p -value of 0.05, unpaired student test). The conversion of these adhesion values into WCAs gives the results presented in Table 1, which show that indeed, pH has an effect on the hydrophobicity of the molecule, as the WCA decreases with increasing pH values. The important point to note as well in this case is that initial chitosan is completely hydrophilic (WCA of 0) and does not interact with bubbles (Supplementary Fig. 2) whatever the pH considered; it is the modifications made on the molecule and the addition of octanal that confers amphiphilic properties to PO-chitosan.

Previous studies have showed that chitosan, at elevated pH, precipitates into the medium [16,17]. This precipitation was visible when we imaged in a previous study chitosan coated surfaces using AFM, where aggregates of chitosan formed on the surface, resulting in an increased roughness (13 ± 5 nm) compared to low pH (0.6 ± 0.1 nm)

Table 1

Hydrophobic properties of chitosan and PO-chitosan at different pH. Adhesion values obtained by FluidFM and corresponding water contact angle (WCA) of chitosan and of PO-chitosan surfaces at pH 6, 7.4 and 9.

Sample	pH	Adhesion value (nN)	WCA (°)
Chitosan	6	0	~ 0
	7.4	0	~ 0
	9	0	~ 0
PO-chitosan	6	66.7 ± 13.9	48.7
	7.4	64.6 ± 20.3	48.3
	9	46.5 ± 15.9	44.6

[17]. To check whether PO-chitosan behaves like chitosan at high pH, we further characterized it by imaging PO-chitosan surfaces at pH 6, 7.4 and 9 using AFM in contact mode. The height images obtained are presented in Fig. 2e, f and g respectively, they show a similar topography in all cases, with no aggregates present on the surface. The quantification of the surface roughness in each case gave similar values (box plot in Fig. 2k), with a roughness of 574.0 ± 105.7 pm at pH 6, of 528.1 ± 144.8 pm at pH 7.4 and of 494.1 ± 82.2 pm at pH 9. Non-parametric statistical tests (Mann and Whitney test) showed that these values indeed are not significantly different. These results confirm the observations from the height images; whatever the pH, PO-chitosan surfaces are homogeneous with no aggregates formed, meaning that PO-chitosan does not precipitate at high pH like chitosan does.

Thus, in summary, the modification of chitosan by addition of hydrophobic octanal molecules on its backbone, with a DS of 12 %, made it amphiphilic as confirmed by surface tension experiments that showed a decrease in the surface tension. The new molecule PO-chitosan can also be completely dissolved in water, as confirmed by particle size and turbidity measurements. Then, using FluidFM experiments, we showed that the modifications made indeed changed the hydrophobic properties of the molecule, which are dependent on the pH, as described in the literature. Finally AFM measurements showed that PO-chitosan, unlike chitosan, does not precipitate at elevated pH. Now the next step of this study is to functionalize it at the surface of bubbles and determine if this functionalization allows a better adhesion of bubbles with cells.

3.3. PO-chitosan functionalized bubbles improve flotation efficiency

The characterization of PO-chitosan has showed that the molecule is indeed amphiphilic, able to act like a surfactant, thus we can use it to coat the surface of bubbles. The question is now to know if the presence of PO-chitosan on the surface of bubbles improves its adhesion to cells, and by which mechanism. To verify this point, we modified the surface of bubbles produced with FluidFM with PO-chitosan (concentration of 2 mg/L) using a protocol previously developed in our team [22]. Briefly, for that, a solution containing PO-chitosan is first aspirated inside a FluidFM cantilever. The cantilever is then immersed in the petri dish containing cells: by applying a positive pressure, the PO-chitosan solution is released, a bubble is formed, and because PO-chitosan molecules are in close proximity of the bubble, they directly assemble at its surface. PO-chitosan coated bubbles can then be used to probe the direct interactions with *C. vulgaris* cells. The results are presented in Fig. 3. Fig. 3a is a schematic representation of the experimental set-up. In this case the retract force curves obtained showed a single retract peak at the contact point (red curve in Fig. 3b) with an average adhesion force of 12.8 ± 1.5 nN at pH 6 (Fig. 3c in dark blue, $n = 3603$ force curves from 7 different cells coming from 2 independent cultures). This interaction is 3.6 times higher than the one obtained between clean bubbles and cells (Fig. 3c in light blue), meaning that indeed, the functionalization of the bubble surface with PO-chitosan enhances the direct interaction with *C. vulgaris* cells. Moreover, the approach force curve also shows a “jump-in” peak reflecting the fact that the PO-chitosan coated bubble gets

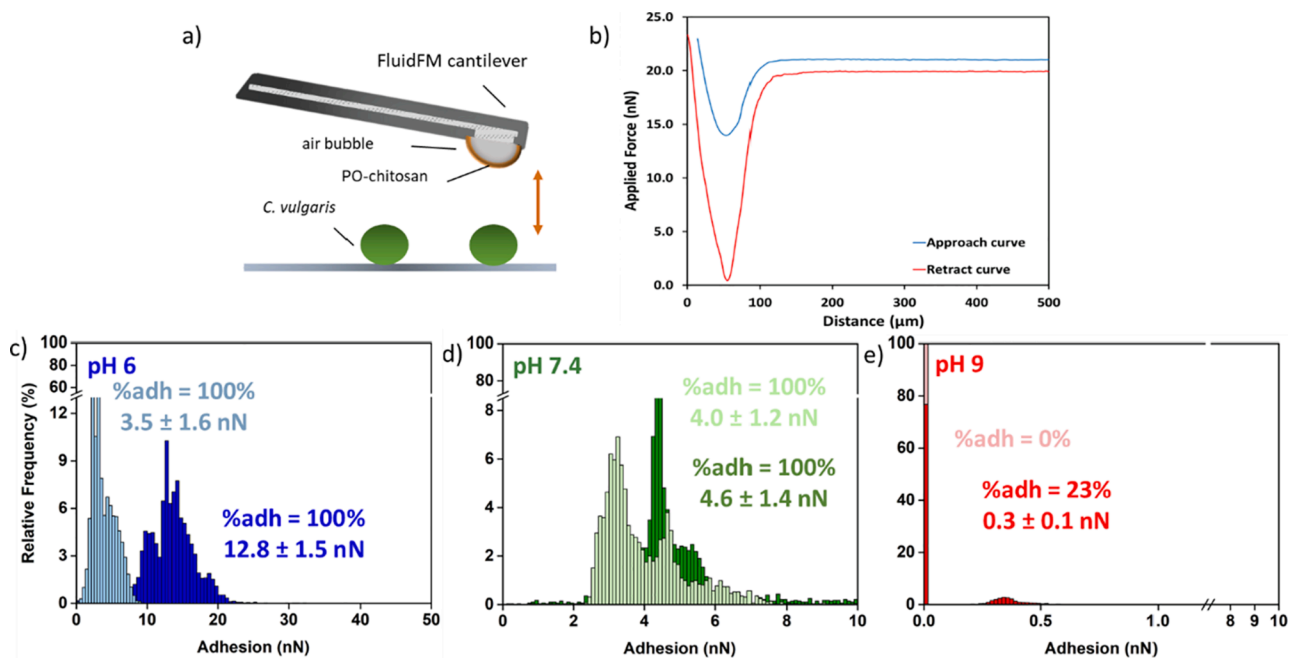


Fig. 3. Modulation of the interactions between bubbles and *C. vulgaris* cells by PO-chitosan. a) Schematic representation of PO-chitosan coated bubble and single *C. vulgaris* cell interaction. b) Representative force curves obtained for PO-chitosan coated bubble and *C. vulgaris* cell at pH 6. Adhesion force histogram obtained for the interactions between PO-chitosan coated bubbles and *C. vulgaris* cell at c) pH 6, d) pH 7.4 and e) pH 9. Lighter colors histograms in c, d and e show clean bubble – *C. vulgaris* cell interactions at the corresponding pH values.

suddenly attached to the *C. vulgaris* cell (Fig. 3b, blue curve). This jump-in, as previous studies on bubble-hydrophobic surface interaction show [22], is most likely due to the long-range hydrophobic force that causes the disruption of the water film and the formation of the three phase contact (TPC) line. This is an important point. Indeed, when we characterized the interactions between chitosan and *C. vulgaris* cells in our previous study, the force curves obtained showed multiple peaks taking place away from the contact point, materializing the unfolding of polymers from the surface of cells upon retraction [17]. In theory, the hydrophobic parts of PO-chitosan should be inside the air bubble, while the rest of the chitosan molecule, which is hydrophilic, should be outside the bubble, available for interaction. Thus, we expected to obtain the same interactions with PO-chitosan coated bubbles as we had with chitosan alone. This is clearly not the case, and our hypothesis to explain this is that when the coated bubble contacts the cell, the specific interaction between the hydrophilic backbone of the chitosan and the cell can take place, but because this interaction is effective, the water film between the bubble and the cell breaks down, resulting in the formation of the TPC line. At this point, when the bubble probe is retracted from the cell, the hydrophobic interaction becomes dominant over the specific interaction, and this is what we see on the force curve. The fact that this hydrophobic force is much higher in the case of PO-chitosan coated bubbles compared to clean bubbles can be explained by the first attractive specific interaction of the cells with the hydrophilic backbone of the chitosan present on the bubble surface. In addition, the formation of the TPC line increases the contact area between the bubble and the *C. vulgaris* cells, which increases the adhesion forces obtained. For example, in our previous study we already prove that there is a direct relationship between effective radius (thus the contact area) and hydrophobic forces. Meaning that increase in hydrophobicity enhances the effective radius between hydrophobic surfaces and bubbles due to the TPC line formation thereby leading to higher adhesion forces [22].

We further repeated these experiments at pH 7.4 and 9 (Fig. 3d and e). At pH 7.4, cells interact more with clean bubbles with an average adhesion force of 4.0 ± 1.2 nN (Fig. 3d, light green histogram, $n = 2814$ force curves from 5 cells) compared to pH 6, which can be explained by some changes perhaps in the hydrophobicity of *C. vulgaris* cells surface at

this pH. When bubbles are functionalized with PO-chitosan, the average force obtained is of 4.6 ± 1.4 nN (Fig. 3d, dark green $n = 2814$ force curves from 5 cells), thus almost 3 times less than at pH 6. In addition in this case, the “jump-in” peak on the approach curves was not visible anymore. This important decrease in the adhesion is most probably due to the decrease in the hydrophobicity of PO-chitosan molecule. Although this decrease is low, it has important consequences on the interactions with cells. At pH 9 (Fig. 3e), cells do not interact with clean bubbles (0 % of adhesion, light red bar in Fig. 3e) at all, while when bubbles are coated with PO-chitosan, the percentage of force curves showing retract adhesions is of 23 %, with an average force of 0.3 ± 0.1 nN (dark red histogram in Fig. 3e, $n = 4419$ from 7 cells coming from 2 independent cultures). In the case of chitosan, there was no interaction with cells at higher pH, but this was explained by the fact that chitosan precipitated at such pH values. The roughness measurements performed in the first part of this work showed that PO-chitosan does not precipitate like chitosan does at higher pH. Therefore, this lack of interaction is probably not related to PO-chitosan, but to the cell surface itself. Indeed, in this case, clean bubbles do not interact with cells, which means that at pH 9, the cell surface is completely hydrophilic. This can be explained by a change in the cell wall composition at higher pH [20], or by a change in the cell surface architecture where hydrophobic molecules at the surface of cells may be masked by other components [17]. Thus, the initial interaction between the hydrophilic chitosan backbone at the surface of bubbles still takes place, as proven by the low adhesions recorded. However, because the cell surface is hydrophilic, the liquid film between the bubbles and the cells cannot be broken, resulting in a weak adhesion force. These results are important because they provide insight into the molecular mechanism underlying the interactions of PO-chitosan bubbles with cells. While the interaction with PO-chitosan bubbles probably starts with a specific interaction between the chitosan molecules present at the surface of bubbles and cell surface polymers, hydrophobicity remains the main factor allowing then the contact between bubbles and cells.

In a next step, to see how these interactions between cells and PO-chitosan bubbles influence cell capture and subsequent separation by the bubbles, we performed flotation experiments. To produce

functionalized bubbles, water containing PO-chitosan was pressurized to 6 bar for 30 min. Then, by introducing the white waters into the flotation jars, the bubbles and surfactants are released into the medium at the same time; since the surfactants are in close proximity to the bubbles, they can assemble on their surface. Fig. 4a is a schematic representation of the flotation process with bubble functionalization, performed in only one step then with no prior flocculation. Unless otherwise indicated all the experiments were performed at pH 6. For that, in a first set of experiments, 50 mL of PO-chitosan white waters were injected from the pressurization tank to each beaker *via* the solenoid valves. Different PO-chitosan concentrations were tested in a range from 12.5 to 100 mg/L, and allowed to determine the best conditions, using 25 mg/L of PO-chitosan, where the highest separation efficiency was obtained (Supplementary Fig. 3). Indeed, at low concentrations, for the volume of bubbles used, there is not enough PO-chitosan to coat the surface of bubbles resulting in poor flotation efficiency. On the contrary, when higher concentrations are used, there is too much PO-chitosan compared to bubbles, thus PO-chitosan molecules may end up in the suspension and saturate it, preventing bubbles to interact with cells.

To confirm this, we then used the best concentration obtained, 25 mg/mL of PO-chitosan, and varied the ratio of bubbles to cells. For that, we decreased or increased the volume of white waters injected in the microalgae suspensions; this results in a lower or higher number of bubbles and thus in a decreased or increased bubble surface area compared to cells. Four different injected white waters volumes were tested (20, 50, 80 and 100 mL); the results obtained are presented in Fig. 4c. On this graph, the light blue bars correspond to the control conditions (clean bubbles) and the dark blue bars correspond to PO-chitosan coated bubbles. The highest separation efficiency was of 55.1

± 13.1 %, obtained with a white water volume of 50 mL, which is 1.6 times higher than the efficiency obtained with clean bubbles (34.6 ± 3.8 %). The fact that using clean bubbles, approximately 30 % of the cells could be separated from the culture medium can result from the capture of cells by clean bubbles or from a natural flocculation of cells in these conditions followed by their capture by bubbles. Lower separation efficiencies, close the ones obtained in control conditions with clean bubbles, were found when using both lower volume (33.2 ± 2.8 % for 20 mL of bubbles) and higher volumes of bubbles (13.7 ± 1.9 % and 12.6 ± 1.6 % respectively for 80 and 100 mL of bubbles). The results obtained using 20 mL can be explained by the fact that in this case the surface area of the bubbles is not large enough compared to the amount of PO-chitosan available, which saturates the suspension and prevents the bubbles from interacting with cells. On the contrary, the poor results obtained using larger volumes may be due to too low a concentration of PO-chitosan relative to the bubbles, which are therefore not all functionalized with the surfactant, resulting in poor interaction with the cells. Furthermore, at these large volumes, the efficiencies obtained with clean bubbles also decrease, suggesting that injecting such volumes of bubbles dilutes the solution, resulting in a low probability of collision between bubbles and cells. Finally, as we found that cells' interactions with PO-chitosan coated bubble are dependent on the pH, we then investigated the influence of pH variation of the separation efficiency using 25 mg/L of PO-chitosan with an injected volume of white waters of 50 mL. The results presented in Fig. 4c show that the highest separation efficiency of 55.1 ± 13.1 % is obtained for pH 6, and decreases gradually to 38.6 ± 0.8 % at pH 7.4 and to 27.3 ± 5.9 % at pH 9. This is in line with the FluidFM experiments which showed higher interactions at pH 6, with average adhesion values decreasing then at pH 7.4 and pH 9. These

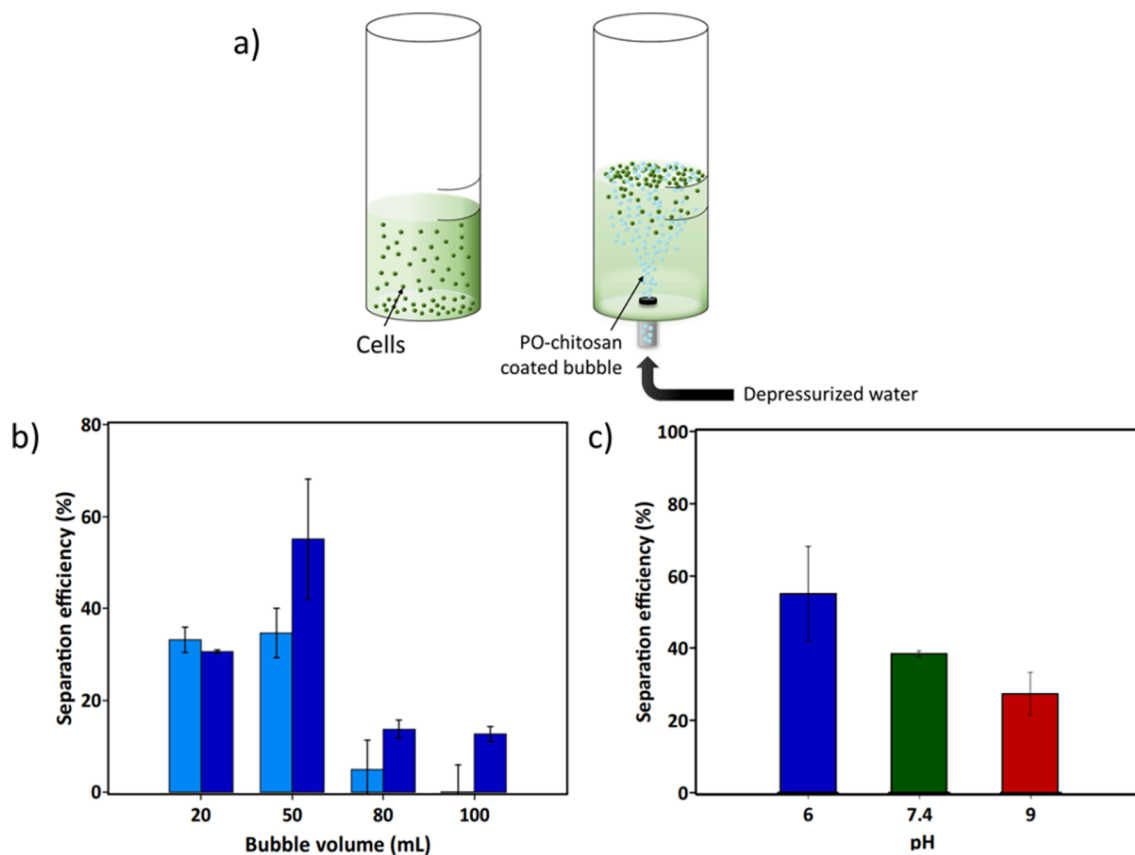


Fig. 4. Flotation experiments of *C. vulgaris* with PO-chitosan coated bubble. a) Schematic representation of one-step flotation experiments. b) Flotation efficiency of *C. vulgaris* with 25 mg/L PO-chitosan coated bubble with varying bubble volumes at pH 6. Light blue bars correspond to the control condition with clean bubbles, and dark blue bars correspond to the test conditions with bubbles coated with PO-chitosan. c) Flotation efficiency of *C. vulgaris* with 25 mg/L and 50 mL PO-chitosan coated bubble at varying pH.

experiments then prove that flotation efficiency using functionalized bubbles is dependent on the interaction that bubbles have with cells; the higher it is, the more efficient the separation process.

The team of Henderson was the first to use functionalized bubbles to improve microalgae harvesting by flotation [31,32]. Their first studies on this topic showed that mixing cationic polymers with water in the saturator of a DAF unit allowed the production of positively-charged bubbles, which could then interact with negatively-charged microalgae cell surfaces and separate them without the need for prior flocculation. They then analyzed the effect of different polymers (different zeta potential and hydrophobic modifications with different groups) on the PosiDAF process and showed that while a change in the zeta potential had an influence on the interaction between polymers and bubbles, a change in the hydrophobic moieties incorporated in the different polymers affected the absorption conformation of polymers on the bubble surface [33]. They then tested these polymers in DAF experiments and showed that depending on the polymer used, the maximum removal efficiency stays more or less constant for the same species. However, depending on the species used, the removal efficiency varies; maximum removal efficiency was around 69 % for *C. vulgaris*, while it was of 38 % for a first strain of *Microcystis aeruginosa* and 93 % for another strain of *M. aeruginosa* [33]. Then later they made the hypothesis that the separation efficiencies obtained were dependent on the algal organic matter (AOM) that cell produce, which differ depending on the species [34]. To test this hypothesis, they removed the AOM from cells and repeated the flotation experiment with positive bubbles: their results showed a decrease of the separation efficiencies for all species. Moreover, by substituting the AOM of one strain of *M. aeruginosa* CS-564/01 (the one for which the highest separation efficiency was obtained) with the second species of *M. aeruginosa*, the separation efficiency increased to 90 %. This thus proved that AOM is indeed an important factor promoting the attachment of cells to the bubble surfaces [34]. In our case, the interactions between the PO-chitosan functionalized bubbles and the cells are not based on an electrostatic interaction, as discussed previously, but rather on a specific interaction between the chitosan backbone of the molecule, present on the surface of the bubbles, and the polymers on the surface of the cells. Thus, the very concept of the bubble functionalization strategy is different from the Posi-DAF process, but similar results could be obtained regarding cell separation. To also test the hypothesis that AOM could be involved in the interaction with PO-chitosan functionalized bubbles, we also performed the experiments with cells in stationary phase, under the conditions for which the best separation efficiency was obtained (pH 6 and 50 mL of injected bubbles). Cells in stationary phase have grown for a longer period of time (21 days instead of 7 for *C. vulgaris*), and have produced more AOM in the culture medium. In this case, the separation efficiency obtained was of 46.1 ± 9.2 %, thus in the same range as for 7-day old cells. This means that in our case, AOM is most likely not involved in the interaction, unlike in the case of Posi-DAF and, as discussed earlier, relies on the specific interaction between chitosan and the cell wall of cells.

Another point that needs to be discussed here is the difference between the bubble functionalization strategy that we develop in this study and another flotation separation process called foam flotation. Foam flotation is a type of DiAF (Dispersed Air Flotation) where surfactants are mixed in the suspension to reduce the surface tension of water. Then bubbles are injected, allowing to create a stable foam where hydrophobic particles are adsorbed [35]. This process, which originates from the mineral industry [36], is also used for industrial waste water treatment [37] or plastic recycling [38]. For microalgae harvesting applications, foam flotation uses cationic surfactants (most often chemical surfactants) that not only stabilize the foam in the system but also enhance microalgae hydrophobicity, which is generally weak [39]. In both cases, cationic surfactants attach either to bubbles or cells which are both negatively-charged through electrostatic interactions, making the bubble surface positively-charged or the cell surface hydrophobic,

allowing the interaction between the two entities. Thus the process we develop in this study is different from foam flotation, first because of the bubble generation procedure, different between DAF and DiAF [40]. Second because no foam is generated in our process as PO-chitosan is not dispersed into the medium but mixed with water directly in the pressurization tank to produce functionalized bubbles. And third because the interaction between functionalized bubbles and cells is based on a specific interaction between the chitosan backbone at the surface of bubbles and polymers at the surface of cells and not on an electrostatic one. While the microalgae recovery rates can be higher in foam flotation than what is obtained here (up to 95 % depending on the type of cationic surfactant used), such processes are usually performed using chemical flocculants (such as CTAB, DAH or DN2) which contaminate the biomass [41]. Bio-surfactants can also be used, such as rhamnolipid or saponin, but very few studies have reported on their efficient use for microalgae harvesting in foam flotation [41,42]. The advantage of the strategy we develop here is that chitosan is a bio-sourced molecule with no impact on cells, for which the mechanism of interaction with cells is known, making it possible to optimize the conditions for flotation. But when considering the concept of foam flotation, a question that can be asked is to know whether PO-chitosan mixed in the suspension could bind to cells, and act as an effective collector molecule that could enhance the hydrophobic properties of cells and promote their interactions with bubbles.

3.4. PO-chitosan is an efficient flocculant for *C. vulgaris* at different pH

To find some answers to this question, we next investigated the interactions of PO-chitosan directly with cells using AFM. For that, we used FluidFM technology, where single *C. vulgaris* cells were aspirated at the aperture of FluidFM probes by exerting a negative pressure inside the microfluidic cantilever, and further used as cell probes to measure the interactions with PO-chitosan surfaces. This FluidFM method, compared to classic single-cell force spectroscopy methods using AFM [43], has the advantage of keeping the cells stable on the cantilever even when in contact with a strongly adhesive surface [17]. In this case also the experiments were performed at different pH (6, 7.4 and 9), given the influence it has on PO-chitosan molecule. The schematic representation of these experiments is shown in Fig. 5a, while the results obtained are presented in Fig. 5b-d. At pH 6 (Fig. 5b), the retract force curves obtained show a single retract peak happening close to the contact point, similar to what was observed with bubbles, this time with a smaller average force of 3.7 ± 1.3 nN ($n = 2851$ force curves with 6 cells coming from 2 independent cultures). As for the interactions with bubbles, this force signature is typical of non-specific interactions such as hydrophobic interactions. This first information is important. Indeed, previous results obtained by performing the same experiments with chitosan surfaces showed force curves with unfolding taking place far from the contact point, reflecting a specific interaction between chitosan and cell wall polymers [17]. This means that for PO-chitosan, the interaction is not based on the same mechanism: instead of a specific interaction with the chitosan backbone of PO-chitosan, it seems here that a hydrophobic interaction between the hydrophobic octanal groups added to the molecule and the cell surface is dominant. Thus by changing the molecule, we also changed the physico-chemical nature of its interactions with cells, and enhanced it as with PO-chitosan the interaction force is 10 times higher than for chitosan. Similar force curves were obtained at pH 7.4, with an average adhesion force of 3.2 ± 1.6 nN ($n = 3194$ force curves with 6 cells coming from 2 independent cultures, Fig. 5c). Once we further increase the pH to 9 (Fig. 5d), *C. vulgaris* interacts with PO-chitosan through the same mechanism (force curves present the same single retract peak at the contact point), but this time with a much lower adhesion force of 0.8 ± 0.6 nN ($n = 2954$ force curves with 6 cells coming from 2 independent cultures). Statistical analysis revealed that all differences are significant (unpaired *t*-test, *p*-value of 0.05) meaning that hydrophobic interactions are progressively suppressed with

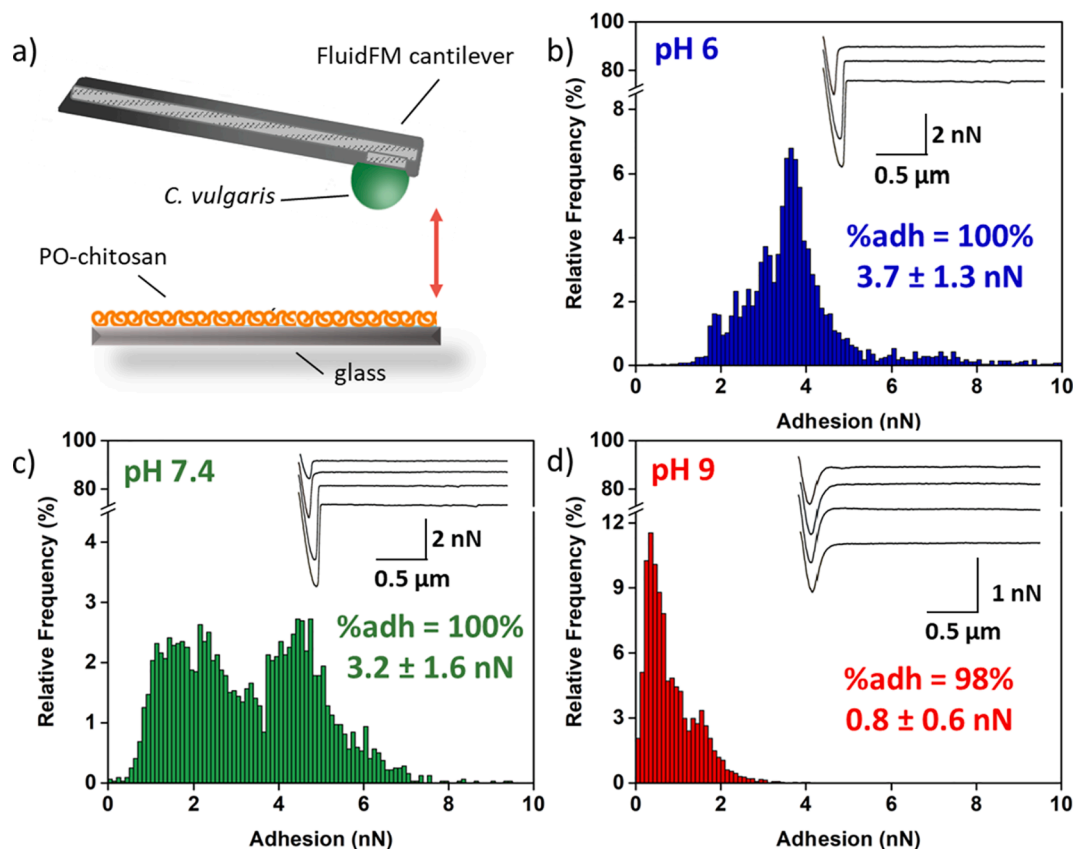


Fig. 5. Interaction between PO-chitosan and single *C. vulgaris* cells at varying pH. a) Schematic representation of *C. vulgaris* and PO-chitosan coated surface interaction with FluidFM. Adhesion force histogram between *C. vulgaris* cells and PO-chitosan coated surface at b) pH 6, c) pH 7.4 and d) pH 9. Insets in panels show representative force curves obtained.

increasing pH. Now that we know that PO-chitosan interactions with cells are dominantly hydrophobic, these difference observed at different pH can be easily explained. Indeed, at pH 9 for instance, both PO-chitosan and cells experience changes in their hydrophobic properties. While the WCA of PO-chitosan decreases to 44.6° , the surface of *C. vulgaris* cells becomes hydrophilic (no interactions with clean bubbles), and thus interacts less with PO-chitosan. These results are important because this means that PO-chitosan could not be used as a collector to enhance the hydrophobic properties of cells. Indeed, it interacts dominantly with cells *via* its hydrophobic groups, thus the chitosan backbone of the molecule is most likely present on the cell surface, making it probably even more hydrophilic. However, given the important adhesion forces obtained especially at pH 6 and 7.4, PO-chitosan could perhaps be efficiently used as a flocculant, which could also be an interesting aspect for harvesting.

To test this hypothesis, we next conducted flocculation experiments with *C. vulgaris* cells at different pH with different PO-chitosan concentrations (Fig. 6a). In these experiments, no bubbles are injected in the solution, cells are mixed with PO-chitosan and then left to settle for 30 min. The effect of PO-chitosan concentration on flocculation efficiency was first studied at pH 6 where the highest flotation efficiencies were reached; the results obtained are presented in Fig. 6b. They show that for low concentrations of PO-chitosan, until 30 mg/L, flocculation efficiency increases with the dose of PO-chitosan used. The maximum flocculation efficiency was of $90.7 \pm 0.5\%$, obtained at a concentration of 30 mg/L. However, for concentrations higher than 30 mg/L, flocculation efficiency decreases dramatically and then reaches a plateau at 48 mg/L where the efficiency is close to 5%. This means that there is a concentration threshold at which the trend is reversed. Such tendency has already been observed in the case of chitosan, where for small concentrations (up to 10 mg/L) flocculation efficiency increases with

increasing chitosan concentrations whereas for higher chitosan concentrations (greater than 20 mg/L) flocculation efficiency declines drastically [17,19]. This may be due to the fact that at high concentrations, the solution is saturated by the large quantity of molecules present in the microalgal suspension, interfering with their encounter with *C. vulgaris* cells and probably interacting with themselves rather than with cells. However in the case of chitosan, only low concentrations (10 mg/L) are needed to achieve high flocculation efficiencies [17]. The fact that PO-chitosan needs a higher dose to reach nearly 100% of flocculated cells is most probably due to the fact that PO-chitosan interacts with cells through its hydrophobic groups, which could substitute only 12% of the amine groups present in chitosan. Thus less groups are available for interactions, meaning that more molecules are needed to flocculate all cells. For the next experiments, we then chose to compare results obtained with 10 mg/L of chitosan and with 30 mg/L of PO-chitosan as these concentrations result in the highest flocculation efficiencies.

As for PO-chitosan coated bubbles, we then evaluated the effects of pH variations on flocculation efficiencies. The results obtained at pH 6, 7.4 and 9 are presented in Fig. 6c. At pH 6 (dark bars), both chitosan (orange bars) and PO-chitosan (blue bars) resulted in high flocculation efficiencies: $95.2 \pm 1.3\%$ and $90.7 \pm 0.5\%$, respectively. While flocculation efficiency decreases at pH 7.4 to $76.6 \pm 2.4\%$ when using chitosan, it remains constant at $91.1 \pm 2.6\%$ for PO-chitosan (middle bars). However, once pH is further increased to 9 (light bars), flocculation efficiencies drop drastically to $11.1 \pm 2.2\%$ and to $10.0 \pm 1.3\%$ for both chitosan and PO-chitosan, respectively. In the case of chitosan, the situation can be easily explained by the fact that at higher pH, chitosan precipitates and does not interact with cells anymore. While there, a high flocculation can still be achieved as cells can get entrapped in the precipitate and flocculated by sweeping, this requires much higher

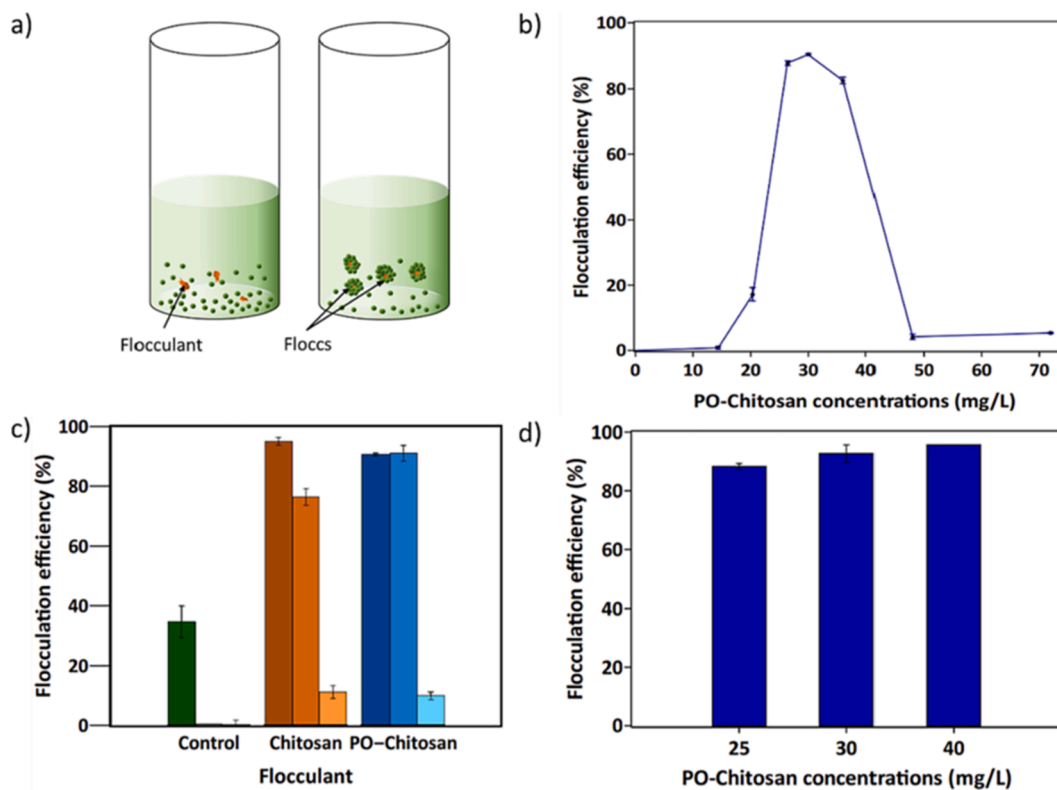


Fig. 6. Flocculation experiments of *C. vulgaris* with PO-chitosan. a) Schematic representation of flocculation experiments. b) Flocculation efficiency of *C. vulgaris* with varying PO-chitosan concentrations. c) Flocculation efficiency of *C. vulgaris* with 10 mg/L chitosan and 30 mg/L PO-chitosan with varying pH. Shades of the color indicates different pH. Darkest color represents pH 6, medium color represents pH 7.4 and lightest color represents pH 9. d) Flocculation efficiency of *C. vulgaris* obtained with 25, 30 and 40 mg/L of PO-chitosan with 0.2 M of NaCl at pH 6.

concentrations of chitosan [16,17]. In the case of PO-chitosan, the situation is different since this molecule does not precipitate at high pH. But this decrease in flocculation efficiency can be easily explained by considering the results obtained by AFM, which showed that indeed at pH 9, the adhesion force between PO-chitosan and cells decreases significantly compared to pH 6 and 7.4. Another interesting part of these results concerns the control conditions (Fig. 5c, green bars). Indeed, at pH 6, when no flocculant are used, cells are still able to flocculate with an efficiency of $33.2 \pm 2.8\%$. This explains why in flotation experiments using clean bubbles, approximately 30 % of the biomass can be separated. While cells can interact directly with clean bubbles through hydrophobic interactions (Fig. 3c, light blue bars), the fact that they are able to flocculate naturally at this pH facilitate their collision with bubbles thereby making it possible to float them. However when the pH is increased to 7.4 and 9, no flocculation at all could be observed, meaning that cells cannot flocculate anymore naturally. Natural flocculation is often due to the production of EPS by cells: perhaps at elevated pH, the charge of these EPS changes, as it is the case for microbial EPS [44] thereby changing their interactions with cells.

Thus these results show that indeed PO-chitosan is an efficient flocculant for *C. vulgaris* cells at pH of 6 and 7.4, and that, as AFM results showed, PO-chitosan is able to interact through hydrophobic interactions with cells. However, at these pH values, PO-chitosan molecule could still be positively charged (pKa of chitosan is of 6.5). Thus to confirm that the flocculation efficiencies observed at low pH are only due to hydrophobic interactions and not to electrostatic interactions between PO-chitosan and cells, we performed more experiments. First we measured the zeta potential of cells at pH 6, 7.4 and 9. The results obtained showed that *C. vulgaris* cells have an average zeta potential of -27.1 , -26.9 and -26.9 mV respectively. Thus, the global charge of *C. vulgaris* cells is negative and does not change depending on the pH. This is a first element, as a change in the charge of cells may have

explained the decreased flocculation efficiency obtained at pH 9, although PO-chitosan should not be positively charged at this pH. Second, we repeated the flocculation experiments and added 0.2 M of NaCl in the suspension at pH 6 to screen the charges present on cells and PO-chitosan molecules. The results obtained are presented at Fig. 6d, they show similar flocculation efficiencies of $88.3 \pm 1.1\%$, $92.7 \pm 2.9\%$ and $95.7 \pm 0.1\%$ using PO-chitosan concentrations of 25, 30 and 40 mg/L. These results at the different concentrations are similar to what was obtained with no salts added (Fig. 6b), showing that indeed, electrostatic interactions are not involved at pH 6. Finally we also performed flocculation experiments with stationary phase cells at pH 6, which we showed in another study are more hydrophobic than exponential phase cells because of the increase of the lipidic fraction in their cell wall upon aging [20]. The results obtained showed flocculation efficiencies of $44.7 \pm 12.6\%$ using chitosan and of $91.6 \pm 0.9\%$ using PO-chitosan (Supplementary Fig. 4). In this case the reduced efficiency obtained using chitosan can be explained by the fact that the cell wall composition and architecture changes with growth [20]. As chitosan interaction with cells is a specific interaction [17], perhaps the polymers with which it interacts is less present at the surface of cells, resulting in less interactions and a decreased flocculation efficiency. The fact that using PO-chitosan, a similar flocculation efficiency is obtained with old cells further confirms that a different mechanisms is involved with this molecule, based, as AFM experiments showed, on hydrophobic interactions.

These results first show that PO-chitosan is also able to efficiently flocculate cells in a pH-dependent manner, as what was found with functionalized bubbles. Thus the interest of this molecule is in fact double, and depending on the process, it can be used either to harvest only part of the biomass using functionalized bubbles and leave cells to continue the culture, or to harvest the totality of the biomass using flocculation or flocculation/flotation in batch cultures. In flocculation,

while the concentration of PO-chitosan needed is more important than for chitosan, it can however be used efficiently in more conditions compared to chitosan. First it is efficient at higher pH (7.4), which is quite important as *C. vulgaris* cultures usually reach pH values close to this in normal culture conditions. Thus using PO-chitosan, there is no need to first adjust the pH of the microalgae suspension, saving time and money in harvesting process. Second, it also allows flocculating stationary phase cells with high efficiency, which is also an important aspect as stationary cells can yield more of certain products, such as lipids [20]. Finally, another interesting aspect of PO-chitosan induced flocculation is the size of the flocs produced (see pictures in Supplementary Fig. 5). For instance, using chitosan, cells aggregate into large flocs, that can be too heavy for microbubbles to carry them to the surface. Therefore using chitosan as a first step in a flocculation/flotation process may not be very efficient. However, the flocs obtained when using PO-chitosan are much smaller, probably because of the different flocculation mechanism involved, and can be carried up to the surface by the bubbles. Finally the originality of PO-chitosan as a flocculant is the fact that it interacts with cells via hydrophobic interactions. Indeed, most of the used bio-sourced flocculants for freshwater microalgae harvesting, including chitosan, interact with cells through electrostatic interactions, and flocculate cells through different mechanisms such as charge neutralization, bridging and patch mechanisms [13]. Examples of such flocculants are poly γ -glutamic acid (γ -PGA), a biopolymer produced by *Bacillus subtilis* [45], guar gum [14] or starch, a naturally-occurring polysaccharide [15]. Because microalgae cells usually have a weak hydrophobicity, most of the research has focused on these electrostatic interactions and cationic flocculants; hydrophobic interactions were never explored, as far as we know. But in fact, even if the hydrophobic properties of cells are weak, the hydrophobic interaction is a strong interaction (typically in the nN range), much stronger than electrostatic interactions (in the pN range). To give a concrete example of this, hydrophobic interactions can overcome an electrostatic repulsion between two entities, as we showed recently when probing the interactions between *C. vulgaris* cells and negatively-charged microplastic particles [28]. Thus even if the cell surface is slightly hydrophobic, this is enough to promote a strong interaction with a hydrophobic flocculant, which can result in high flocculation efficiencies like this is the case with PO-chitosan. In the end, this study, by revealing the potential of hydrophobic interactions to promote flocculation, shows that microalgae flocculation is not limited to positively charged biopolymers, and opens-up new avenues for finding new efficient flocculants.

4. Conclusions

Because microalgae harvesting is currently the most critical challenge for industry to exploit the full potential of this biomass, e.g. for biofuel production, new cost-effective solutions are needed. We propose here a new flotation harvesting process based on the functionalization of bubbles with a molecule that will improve their interactions with the cells. For this purpose, we based on previous knowledge on the interactions between chitosan and cells and modified this molecule with hydrophobic groups to make it amphiphilic. By characterizing this new molecule, we showed that PO-chitosan could be completely dissolved in water thanks to a low degree of substitution of the amine functions by the octanal groups of 12 %, that indeed the modifications made conferred amphiphilic properties to the molecule, and that it does not precipitate at high pH unlike chitosan. We then used this molecule to functionalize the surface of bubbles and probe their interactions with cells. As intended, the functionalization of bubbles allowed increasing in a significant manner their interactions with cells (from 3.5 to 12.8 nN at pH 6), in a pH-dependent manner. Further flotation experiments showed that flotation efficiency was directly correlated to the interaction between cells and functionalized bubbles, as flotation efficiency also changed with the pH. But in our best optimized conditions (pH of 6, 50

% of injected white waters), the removal rate increased from approximately 30 % with clean bubbles to almost 60 %, demonstrating the efficiency of this new flotation process and its potential for continuous microalgae production systems where it could be used to harvest half of the cells and leave the remaining ones for continuing the culture. Then to see if PO-chitosan could also be used in different types of harvesting process, we also looked at its interactions directly with cells, and found that unlike chitosan, PO-chitosan interacts with cells through hydrophobic interactions, still in a pH-dependent manner. We thus tested its potential as a flocculant, and found that in fact PO-chitosan is an effective flocculant, able to flocculate nearly 100 % of the cells in the suspension, in more conditions than chitosan, showing the interest of relying on hydrophobic interactions for flocculation. Here also, the efficiency was pH-dependent, in line with the results obtained using AFM. Altogether, this study presents an innovative flotation process in which the functionalization of bubbles with an amphiphilic chitosan allows enhancing cell capture and separation efficiency. In addition, we show that this molecule can also be used efficiently as a flocculant, making its interest double for large-scale harvesting applications. In each case, single-molecule level force spectroscopy experiments allow understanding the nature of the interactions, providing a complete view of the mechanisms involved and making it possible this way to optimize their use in large-scale applications.

Declaration of Competing Interest

The authors declare that they have no known competing financial interests or personal relationships that could have appeared to influence the work reported in this paper.

Data availability

Data will be made available on request.

Acknowledgements

C. F.-D. is a researcher at CNRS. C. F.-D. acknowledges financial support for this work from the Agence Nationale de la Recherche, JCJC project FLOTALG (ANR-18-CE43-0001-01). The authors want to thank Emma Regourd for her technical support on flocculation/flotation experiments and Abdali Khalfaoui for constant assistance with the flotation device. In addition, the authors want to thank Dr. Juliette Fittreman from IMRCP laboratory in Toulouse for the loan of their AFM head while the one used for this study was under repair.

Appendix A. Supplementary data

Supplementary data to this article can be found online at <https://doi.org/10.1016/j.cej.2022.139349>.

References

- [1] N. Pragma, K.K. Pandey, P.K. Sahoo, A review on harvesting, oil extraction and biofuels production technologies from microalgae, *Renew. Sustain. Energy Rev.* 24 (2013) 159–171, <https://doi.org/10.1016/j.rser.2013.03.034>.
- [2] M.I. Khan, J.H. Shin, J.D. Kim, The promising future of microalgae: current status, challenges, and optimization of a sustainable and renewable industry for biofuels, feed, and other products, *Microb. Cell Fact.* 17 (2018) 36, <https://doi.org/10.1186/s12934-018-0879-x>.
- [3] L. Christenson, R. Sims, Production and harvesting of microalgae for wastewater treatment, biofuels, and bioproducts, *Biotechnol. Adv.* 29 (2011) 686–702, <https://doi.org/10.1016/j.biotechadv.2011.05.015>.
- [4] M.K. Lam, K.T. Lee, Microalgae biofuels: A critical review of issues, problems and the way forward, *Biotechnol. Adv.* 30 (2012) 673–690, <https://doi.org/10.1016/j.biotechadv.2011.11.008>.
- [5] J.J. Milledge, S. Heaven, A review of the harvesting of micro-algae for biofuel production, *Rev. Environ. Sci. Biotechnol.* 12 (2013) 165–178, <https://doi.org/10.1007/s11157-012-9301-z>.

- [6] Y.S.H. Najjar, A. Abu-Shamleh, Harvesting of microalgae by centrifugation for biodiesel production: A review, *Algal Res.* 51 (2020), 102046, <https://doi.org/10.1016/j.algal.2020.102046>.
- [7] N. Uduman, Y. Qi, M.K. Danquah, G.M. Forde, A. Hoadley, Dewatering of microalgal cultures: A major bottleneck to algae-based fuels, *J. Renew. Sustain. Energy* 2 (1) (2010) 012701.
- [8] S. Garg, Y. Li, L. Wang, P.M. Schenk, Flootation of marine microalgae: Effect of algal hydrophobicity, *Bioresour. Technol.* 121 (2012) 471–474, <https://doi.org/10.1016/j.biortech.2012.06.111>.
- [9] D. Vandamme, I. Foubert, K. Muylaert, Flocculation as a low-cost method for harvesting microalgae for bulk biomass production, *Trends Biotechnol.* 31 (2013) 233–239, <https://doi.org/10.1016/j.tbttech.2012.12.005>.
- [10] H. Zhang, X. Zhang, Microalgal harvesting using foam flotation: A critical review, *Biomass Bioenergy* 120 (2019) 176–188, <https://doi.org/10.1016/j.biombioe.2018.11.018>.
- [11] C. Yang, T. Dabros, D. Li, J. Czarniecki, J.H. Masliyah, Measurement of the Zeta Potential of Gas Bubbles in Aqueous Solutions by Microelectrophoresis Method, *J. Colloid Interface Sci.* 243 (2001) 128–135, <https://doi.org/10.1006/jcis.2001.7842>.
- [12] S. Lama, K. Muylaert, T.B. Karki, I. Foubert, R.K. Henderson, D. Vandamme, Flocculation properties of several microalgae and a cyanobacterium species during ferric chloride, chitosan and alkaline flocculation, *Bioresour. Technol.* 220 (2016) 464–470, <https://doi.org/10.1016/j.biortech.2016.08.080>.
- [13] I. Demir, A. Besson, P. Guiraud, C. Formosa-Dague, Towards a better understanding of microalgae natural flocculation mechanisms to enhance flotation harvesting efficiency, *Water Sci. Technol.* 82 (2020) 1009–1024, <https://doi.org/10.2166/wst.2020.177>.
- [14] C. Banerjee, S. Ghosh, G. Sen, S. Mishra, P. Shukla, R. Bandopadhyay, Study of algal biomass harvesting using cationic guar gum from the natural plant source as flocculant, *Carbohydr. Polym.* 92 (2013) 675–681, <https://doi.org/10.1016/j.carbpol.2012.09.022>.
- [15] P.A. Hansel, R. Guy Riefler, B.J. Stuart, Efficient flocculation of microalgae for biomass production using cationic starch, *Algal Res.* 5 (2014) 133–139, <https://doi.org/10.1016/j.algal.2014.07.002>.
- [16] J. Blockx, A. Verfaillie, W. Thielemans, K. Muylaert, Unravelling the Mechanism of Chitosan-Driven Flocculation of Microalgae in Seawater as a Function of pH, *ACS Sustain. Chem. Eng.* 6 (2018) 11273–11279, <https://doi.org/10.1021/acssuschemeng.7b04802>.
- [17] I. Demir, J. Blockx, E. Dague, P. Guiraud, W. Thielemans, K. Muylaert, C. Formosa-Dague, Nanoscale Evidence Unravels Microalgae Flocculation Mechanism Induced by Chitosan, *ACS Appl. Bio Mater.* 3 (2020) 8446–8459, <https://doi.org/10.1021/acsbam.0c00772>.
- [18] S. Ahmed, M. Ahmad, S. Ikram, Chitosan: a natural antimicrobial agent – a review, (2014) 11.
- [19] A.L. Ahmad, N.H. Mat Yasin, C.J.C. Derek, J.K. Lim, Optimization of microalgae coagulation process using chitosan, *Chem. Eng. J.* 173 (2011) 879–882, <https://doi.org/10.1016/j.cej.2011.07.070>.
- [20] I. Demir-Yilmaz, M. Schiavone, J. Esvan, P. Guiraud, C. Formosa-Dague, Combining AFM, XPS and chemical hydrolysis to understand the complexity and dynamics of *C. vulgaris* cell wall composition and architecture (2022) 2022.07.11.499560. doi:10.1101/2022.07.11.499560.
- [21] I. Demir-Yilmaz, P. Guiraud, C. Formosa-Dague, The contribution of Atomic Force Microscopy (AFM) in microalgae studies: A review, *Algal Res.* 60 (2021), 102506, <https://doi.org/10.1016/j.algal.2021.102506>.
- [22] I. Demir, I. Lüchtfeld, C. Lemen, E. Dague, P. Guiraud, T. Zambelli, C. Formosa-Dague, Probing the interactions between air bubbles and (bio)interfaces at the nanoscale using FluidFM technology, *J. Colloid Interface Sci.* 604 (2021) 785–797, <https://doi.org/10.1016/j.jcis.2021.07.036>.
- [23] J. Desbrières, C. Martinez, M. Rinaudo, Hydrophobic derivatives of chitosan: Characterization and rheological behaviour, *Int. J. Biol. Macromol.* 19 (1996) 21–28, [https://doi.org/10.1016/0141-8130\(96\)01095-1](https://doi.org/10.1016/0141-8130(96)01095-1).
- [24] N. Mati-Baouche, C. Delattre, H. de Baynast, M. Grédiac, J.-D. Mathias, A.V. Ursu, J. Desbrières, P. Michaud, Alkyl-Chitosan-Based Adhesive: Water Resistance Improvement, *Molecules* 24 (2019) 1987, <https://doi.org/10.3390/molecules24101987>.
- [25] J. Desbrières, Autoassociative natural polymer derivatives: the alkylchitosans. Rheological behaviour and temperature stability, *Polymer.* 45 (2004) 3285–3295, <https://doi.org/10.1016/j.polymer.2004.03.032>.
- [26] M. Yalpani, L.D. Hall, Some chemical and analytical aspects of polysaccharide modifications. III. Formation of branched-chain, soluble chitosan derivatives, *Macromolecules* 17 (1984) 272–281, <https://doi.org/10.1021/ma00133a003>.
- [27] J.L. Hutter, J. Bechhoefer, Calibration of atomic-force microscope tips, *Rev. Sci. Instrum.* 64 (1993) 1868–1873, <https://doi.org/10.1063/1.1143970>.
- [28] I. Demir-Yilmaz, N. Yakovenko, C. Roux, P. Guiraud, F. Collin, C. Coudret, A. ter Halle, C. Formosa-Dague, The role of microplastics in microalgae cells aggregation: A study at the molecular scale using atomic force microscopy, *Sci. Total Environ.* 832 (2022), 155036, <https://doi.org/10.1016/j.scitotenv.2022.155036>.
- [29] A. Meister, M. Gabi, P. Behr, P. Studer, J. Vörös, P. Niedermann, J. Bitterli, J. Polesel-Maris, M. Liley, H. Heinzelmann, T. Zambelli, FluidFM: Combining Atomic Force Microscopy and Nanofluidics in a Universal Liquid Delivery System for Single Cell Applications and Beyond, *Nano Lett.* 9 (2009) 2501–2507, <https://doi.org/10.1021/nl901384x>.
- [30] E. Dague, D. Alsteens, J.-P. Latgé, C. Verbelen, D. Raze, A.R. Baulard, Y.F. Dufrene, Chemical Force Microscopy of Single Live Cells, *Nano Lett.* 7 (2007) 3026–3030, <https://doi.org/10.1021/nl071476k>.
- [31] R.K. Henderson, S.A. Parsons, B. Jefferson, Surfactants as Bubble Surface Modifiers in the Flootation of Algae: Dissolved Air Flootation That Utilizes a Chemically Modified Bubble Surface, *Environ. Sci. Technol.* 42 (2008) 4883–4888, <https://doi.org/10.1021/es702649h>.
- [32] R.K. Henderson, S.A. Parsons, B. Jefferson, Polymers as bubble surface modifiers in the flotation of algae, *Environ. Technol.* 31 (2010) 781–790, <https://doi.org/10.1080/09593331003663302>.
- [33] N.R. Hanumanth Rao, A.M. Granville, C.I. Browne, R.R. Dagastine, R. Yap, B. Jefferson, R.K. Henderson, Determining how polymer-bubble interactions impact algal separation using the novel “Posi”-dissolved air flotation process, *Sep. Purif. Technol.* 201 (2018) 139–147. doi:10.1016/j.seppur.2018.03.003.
- [34] N.R. Hanumanth Rao, R. Yap, M. Whittaker, R.M. Stuetz, B. Jefferson, W. L. Peirson, A.M. Granville, R.K. Henderson, The role of algal organic matter in the separation of algae and cyanobacteria using the novel “Posi” - Dissolved air flotation process, *Water Res.* 130 (2018) 20–30, <https://doi.org/10.1016/j.watres.2017.11.049>.
- [35] X. Nie, H. Zhang, S. Cheng, M. Mubashar, C. Xu, Y. Li, D. Tan, X. Zhang, Study on the cell-collector-bubble interfacial interactions during microalgae harvesting using foam flotation, *Sci. Total Environ.* 806 (2022), 150901, <https://doi.org/10.1016/j.scitotenv.2021.150901>.
- [36] M.A.S. Barrozo, F.S. Lobato, Multi-objective optimization of column flotation of an igneous phosphate ore, *Int. J. Miner. Process.* 146 (2016) 82–89, <https://doi.org/10.1016/j.minpro.2015.12.001>.
- [37] D.S. Patil, S.M. Chavan, J.U.K. Oubagaranadin, A review of technologies for manganese removal from wastewaters, *J. Environ. Chem. Eng.* 4 (2016) 468–487, <https://doi.org/10.1016/j.jece.2015.11.028>.
- [38] C. Wang, H. Wang, J. Fu, Y. Liu, Flotation separation of waste plastics for recycling—A review, *Waste Manage.* 41 (2015) 28–38, <https://doi.org/10.1016/j.wasman.2015.03.027>.
- [39] M.A.S. Alkarawi, G.S. Caldwell, J.G.M. Lee, Continuous harvesting of microalgae biomass using foam flotation, *Algal Res.* 36 (2018) 125–138, <https://doi.org/10.1016/j.algal.2018.10.018>.
- [40] J. Rubio, M.L. Souza, R.W. Smith, Overview of flotation as a wastewater treatment technique, *Miner. Eng.* 15 (2002) 139–155, [https://doi.org/10.1016/S0892-6875\(01\)00216-3](https://doi.org/10.1016/S0892-6875(01)00216-3).
- [41] A. Krishnan, R. Devasya, Y. Hu, A. Bassi, Fundamental investigation of bio-surfactants-assisted harvesting strategy for microalgae, *Biomass Bioenergy* 158 (2022), 106364, <https://doi.org/10.1016/j.biombioe.2022.106364>.
- [42] H.A. Kurniawati, S. Ismadji, J.C. Liu, Microalgae harvesting by flotation using natural saponin and chitosan, *Bioresour. Technol.* 166 (2014) 429–434, <https://doi.org/10.1016/j.biortech.2014.05.079>.
- [43] A. Beaussart, S. El-Kirat-Chatel, R.M.A. Sullan, D. Alsteens, P. Herman, S. Derclaye, Y.F. Dufrene, Quantifying the forces guiding microbial cell adhesion using single-cell force spectroscopy, *Nat. Protoc.* 9 (2014) 1049–1055, <https://doi.org/10.1038/nprot.2014.066>.
- [44] L.-L. Wang, L.-F. Wang, X.-M. Ren, X.-D. Ye, W.-W. Li, S.-J. Yuan, M. Sun, G.-P. Sheng, H.-Q. Yu, X.-K. Wang, pH Dependence of Structure and Surface Properties of Microbial EPS, *Environ. Sci. Technol.* 46 (2012) 737–744, <https://doi.org/10.1021/es203540w>.
- [45] H. Zheng, Z. Gao, J. Yin, X. Tang, X. Ji, H. Huang, Harvesting of microalgae by flocculation with poly (γ -glutamic acid), *Bioresour. Technol.* 112 (2012) 212–220, <https://doi.org/10.1016/j.biortech.2012.02.086>.

Chapter 7 : French summary / Résumé Français

Introduction générale

Face à la pénurie de combustibles fossiles et à l'augmentation de la pollution, qui est un moteur du changement climatique lié à la combustion des combustibles fossiles, le besoin de sources d'énergie renouvelables et durables pour remplacer la production d'énergie basée sur les combustibles fossiles à savoir le pétrole, le charbon et le gaz naturel est devenu urgent (Fercoq et al., 2016 ; Markou & Nerantzis, 2013). Différentes sources d'énergie alternatives sont déjà disponibles, notamment les biocarburants dérivés de la biomasse. Compte tenu de leur intérêt pour remplacer les carburants non renouvelables, la recherche dans ce domaine est très active. Plusieurs types de biomasse peuvent être utilisés, notamment les plantes cultivées, les sous-produits agricoles ou les ressources marines telles que les algues et les cyanobactéries. Parmi elles, les microalgues représentent la biomasse la plus attractive, qui a été largement explorée dans ce contexte pour son potentiel à produire d'importantes quantités d'huile pouvant être utilisées pour la production de biocarburants (Pragya et al., 2013). Par ailleurs, le potentiel des microalgues est encore plus important car elles représentent également une source importante de biomasse et de molécules d'intérêt pour les domaines de l'alimentation humaine, animale ou de la santé. De plus, les cultures de microalgues constituent une solution intéressante pour les problèmes de traitement des eaux usées en raison de leur capacité à utiliser le phosphore et l'azote inorganiques pour leur croissance (Yu et al., 2017). Les microalgues sont des micro-organismes uniques qui convertissent l'énergie lumineuse, l'eau et les nutriments inorganiques en une ressource de biomasse riche en produits à valeur ajoutée tels que les lipides, les glucides, les protéines et les pigments (Minhas et al., 2016 ; Pragya et al., 2013). Malgré ces avantages, la commercialisation à grande échelle du biodiesel issu des microalgues a été freinée en raison des coûts élevés des processus de production, qui sont principalement associés à l'étape de récolte, car les microalgues se développent à faible concentration (0,3-3 g/L), générant ainsi de grandes quantités d'eau à traiter (Lam & Lee, 2012). Plusieurs méthodes ont été proposées pour la récolte des microalgues, notamment la centrifugation, la filtration, le processus de séparation par membrane et la sédimentation. Cependant, la plupart de ces méthodes ont de faibles rendements ainsi que des coûts d'exploitation et des consommations d'énergie élevés. Dans ce contexte, la flottation est une bonne alternative, qui consiste à générer des bulles d'air ascendantes dans une suspension de microalgues. Par conséquent, les cellules de microalgues se fixent aux bulles et sont transportées à la surface sans être endommagées. Cependant, l'efficacité de cette méthode est limitée par le fait que l'interaction entre les bulles et les cellules est répulsive, en raison de la charge de surface négative des cellules et

des bulles dans l'eau, et de la faible hydrophobie des cellules de microalgues. Afin de rendre cette technique efficace pour la récolte des microalgues, la stratégie originale proposée dans cette thèse repose sur la fonctionnalisation des bulles utilisées dans le processus de flottation avec des composés adhésifs, qui leur permettront de capturer efficacement les cellules lors de leur montée.

Pour cela, nous devons identifier une molécule qui permettrait l'attachement aux cellules et vérifier que les bulles fonctionnalisées avec cette molécule pourraient effectivement favoriser un meilleur attachement aux cellules. Les différentes étapes qui nous ont permis d'atteindre cet objectif sont présentées dans la Figure 1. Dans un premier temps, nous avons développé une méthode basée sur la microscopie à force atomique combinée à la microfluidique (FluidFM) pour produire des bulles fonctionnalisées (Demir et al., 2021a), que nous utilisons pour mesurer à l'échelle moléculaire les interactions avec les cellules. Ensuite, nous avons analysé la composition de la paroi cellulaire des microalgues en utilisant une combinaison de techniques d'analyse de surface que sont la chromatographie liquide et la spectroscopie photoélectronique à rayons X (XPS). Les informations obtenues par ces analyses ont révélé la présence de polymères de type chitine à la surface des cellules, une molécule qui, en théorie, est capable d'interagir avec une autre molécule similaire et biosourcée, le chitosan. Dans un troisième temps, nous avons analysé au niveau moléculaire les interactions entre le chitosan et la paroi cellulaire en utilisant la microscopie à force atomique. Grâce à ces expériences, nous avons pu montrer que le chitosan pouvait se lier efficacement aux cellules et nous avons pu comprendre la base moléculaire de ces interactions. Nous avons ensuite poursuivi avec cette molécule et, dans une quatrième étape, nous l'avons modifiée pour la rendre amphiphile afin qu'elle puisse être fonctionnalisée à la surface des bulles utilisées dans la flottation. Pour évaluer si les bulles fonctionnalisées avec le chitosan peuvent adhérer aux cellules, nous utilisons dans une cinquième étape la méthode basée sur FluidFM pour fonctionnaliser les bulles avec ce chitosan amphiphile et mesurer leurs interactions avec les cellules de microalgues à l'échelle moléculaire. Cette étape permet de valider la stratégie développée dans ce projet de thèse en montrant que ces bulles adhèrent mieux aux cellules que les bulles propres, et en comprenant pourquoi. Ces informations sont nécessaires pour optimiser dans une dernière étape, le procédé de flottation pour séparer les populations de cellules entières dans les expériences de flottation, et ainsi prouver expérimentalement l'efficacité de notre technique.

Les travaux ont été réalisés jusqu'à présent avec une espèce de microalgue verte utilisée pour la production de biocarburants dans les processus biotechnologiques, la *Chlorella vulgaris*. À l'avenir, nous serons en mesure d'optimiser ce nouveau procédé de séparation pour récolter d'autres espèces de microalgues présentant un intérêt biotechnologique, mais aussi de l'utiliser pour d'autres applications que la production de biomolécules à base de microalgues. Ce nouveau procédé de

séparation pourrait par exemple être utilisé pour séparer spécifiquement des micro-organismes de milieux complexes tels que le sang, ce qui serait utile pour le diagnostic des infections sanguines. L'intérêt des travaux menés au cours de cette thèse s'étend donc bien au-delà de la production de biocarburants par les microalgues, ce qui montre son intérêt.

Le présent document est composé de 6 chapitres. Le premier chapitre est une présentation générale du travail de thèse. Il consistera d'abord en un bref aperçu de la littérature sur les microalgues pour les biocarburants et les molécules à valeur ajoutée, les défis des techniques de récolte, les techniques de récolte classiques et leurs inconvénients et les techniques de récolte alternatives basées sur la flottation. Ensuite, une deuxième partie passera en revue les travaux réalisés au cours de la thèse et enfin une discussion et des conclusions sur les principaux résultats obtenus seront proposées. Dans le chapitre 2, deux revues sont présentées ; l'une se concentre sur les mécanismes naturels de floculation pour séparer les cellules de microalgues de leur milieu aqueux, et la seconde traite de l'utilisation de la microscopie à force atomique dans l'étude des microalgues. Le chapitre 3 présente la nouvelle technique développée pour produire des bulles de taille microscopique à l'aide de FluidFM, mesurer leurs interactions avec les (bio)-surfaces à l'échelle moléculaire et les fonctionnaliser pour moduler leurs interactions avec les cellules. Le chapitre 4 est consacré aux travaux réalisés sur l'analyse de la paroi cellulaire de *C. vulgaris* en combinant AFM, XPS et hydrolyse chimique suivie de HPAEC-PAD. Cette partie du travail a été menée pour identifier les macromolécules qui composent la paroi cellulaire de *C. vulgaris*. Ensuite, dans le chapitre 5, les interactions entre le chitosan, la molécule identifiée pour adhérer à la paroi cellulaire de *C. vulgaris*, et les cellules sont sondées à l'échelle moléculaire en utilisant l'AFM. Enfin, le chapitre 6 décrit les modifications chimiques du chitosan pour fonctionnaliser la surface des bulles, les interactions des bulles fonctionnalisées avec les cellules de *C. vulgaris* et le processus de flottation à l'échelle de la population de microalgues. Les annexes à la fin du document sont composées d'articles de recherche auxquels j'ai participé, mais qui ne sont pas directement liés au sujet de mon doctorat.

Cette thèse a été financée par l'Agence Nationale de la Recherche (ANR). Elle a été supervisée par le Dr Cécile Formosa-Dague, chercheuse CNRS à l'Institut de Biotechnologie de Toulouse (TBI) hébergé à l'INSA Toulouse (Institut National des Sciences Appliquées de Toulouse), et le Prof. Dr Pascal Guiraud, professeur de génie chimique à l'INSA-Toulouse. La plupart des travaux expérimentaux ont été réalisés au TBI et au LAAS-CNRS (Laboratoire d'Analyse et d'Architecture des Systèmes), où mon responsable scientifique était le Dr. Etienne Dague, directeur de recherche CNRS au LAAS-CNRS. Ma thèse s'inscrit dans le cadre de collaborations pluridisciplinaires nationales et internationales qui rassemblent différents domaines d'expertise. Ainsi, au cours de ma thèse, j'ai activement collaboré avec le Dr. Etienne Dague du LAAS pour toutes les expériences réalisées avec la microscopie à force

atomique (AFM). La collaboration avec le Dr. Tomaso Zambelli de l'ETH Zurich (Suisse) a permis le développement de la méthode basée sur FluidFM pour produire des bulles et mesurer leurs interactions avec les cellules. La collaboration avec le Prof. Dr. Koenraad Muylaert de la Katholieke Universiteit Leuven (KU-Leuven, Belgique) a permis de comprendre les interactions au niveau moléculaire entre le chitosan et les cellules. Enfin, le Dr Christophe Coudret du Laboratoire Interactions Moléculaires et Réactivités Chimiques et Photochimiques (IMRCP, Toulouse) a fourni une aide précieuse pour modifier le chitosan et le rendre amphiphile. Des collaborations locales entre le TBI, le LAAS et l'IMRCP ont été développées au sein de la fédération de recherche FERMAT. Collaborer avec ces experts, issus de disciplines différentes et complémentaires à la mienne, m'a permis d'évoluer dans un environnement riche et de travailler à l'interface entre différents domaines dans une approche interdisciplinaire. Enfin, ce travail a été réalisé grâce à l'assistance technique de Fabien Mesnilgrete et Sandrine Assié-Souleille du LAAS-CRNS, et d'Abdlali Khalfaoui, Claude Lemen, et Nathalie Clergerie du TBI, responsables du matériel utilisé.

Discussions et conclusions du travail de thèse

L'objectif global de ce projet était de développer un procédé original pour faire de la flottation une technique de récolte efficace afin de mieux exploiter le potentiel de la bioressource microalgale. La stratégie proposée pour atteindre cet objectif, résumée dans la Figure 19, se situe à la frontière entre la biologie, la physique et la chimie, et est basée sur la fonctionnalisation des bulles avec des composés adhésifs qui se fixent aux cellules et les font remonter à la surface. L'idée était qu'en utilisant des composés bio-sourcés existant à la surface des cellules, il serait possible d'éviter la toxicité et l'interférence avec les processus en aval qui peuvent avoir lieu en utilisant des flocculants synthétiques. Ainsi, pour atteindre notre objectif, la première étape de ce doctorat a été de développer une nouvelle méthode pour sonder les interactions bulles-microorganismes à l'échelle moléculaire. Pour ce faire, une combinaison de microscopie à force atomique et de microfluidique a été utilisée afin de produire des bulles de taille microscopique à l'ouverture des cantilevers FluidFM (Figure 19A), et de sonder leurs interactions avec des cellules individuelles. Ensuite, pour identifier une molécule qui pourrait interagir avec les cellules sans être toxique, nous avons émis l'hypothèse qu'il pourrait s'agir d'un polysaccharide présent dans la paroi cellulaire des cellules, car les polysaccharides sont capables de former des liaisons homotypiques. Afin d'identifier ce polysaccharide, nous avons ensuite déterminé la composition de la paroi cellulaire de notre espèce de microalgue modèle, *C. vulgaris*. Pour cela, nous avons utilisé une combinaison de méthodes, AFM, XPS et chromatographie liquide qui ont permis de générer des connaissances fondamentales manquant dans la littérature sur la composition et la dynamique de la paroi cellulaire des microalgues. En utilisant ces nouvelles données, nous avons pu appréhender la complexité de la structure de la paroi cellulaire et faire des hypothèses sur les éventuels polysaccharides qui pourraient la composer (Figure 19B). En utilisant ces résultats ainsi que les données de la littérature, nous avons identifié un polysaccharide qui avait le potentiel d'adhérer à la surface des cellules de *C. vulgaris*, le chitosan. Par la suite, il a fallu déterminer si cette molécule pouvait effectivement interagir avec les cellules et par quel type de mécanisme (Figure 19C). La compréhension des mécanismes de floculation à l'échelle nanométrique est en effet un point important pour pouvoir ensuite optimiser les processus de séparation à grande échelle. Nos résultats ont montré que le chitosan interagit avec la

surface des cellules de *C. vulgaris* par le biais d'interactions biologiques avec une valeur d'adhésion moyenne d'environ 300 pN. A titre de comparaison, les interactions antigène-anticorps se situent généralement dans la gamme pN autour de 70-200 pN (Dammer et al., 1996 ; Willemsen et al., 1998). Les interactions du chitosan avec les cellules sont plus élevées que cela, ce qui indique que le chitosan est capable de se lier fortement aux cellules, ce qui en fait une bonne molécule candidate pour recouvrir les surfaces des bulles. Ensuite, nous avons modifié cette molécule pour la rendre amphiphile afin qu'elle puisse s'assembler à la surface des bulles (Figure 19D). A ce stade, il était important de comprendre le mécanisme d'adhésion aux cellules des bulles fonctionnalisées avec cette nouvelle molécule, le PO-chitosan, et de voir si la modification apportée au chitosan ne changeait pas son efficacité d'adhésion. Pour vérifier cela, nous avons utilisé la méthode développée dans la première étape, pour sonder l'interaction entre la bulle enduite de PO-chitosan et les cellules de *C. vulgaris* (Figure 19E). Nous avons constaté que le PO-chitosan interagit avec les cellules de *C. vulgaris* principalement par une interaction hydrophobe dominante avec une force d'adhésion moyenne d'environ 3 nN. Cela signifie d'abord que le PO-chitosan est capable de se lier aux cellules avec une force 10 fois supérieure à celle obtenue avec le chitosan. Mais dans ce cas, les interactions entre les cellules et les bulles recouvertes de PO-chitosan sont plus complexes qu'avec le chitosan seul. En effet, le PO-chitosan s'absorbe à la surface de la bulle de telle sorte que les unités hydrophiles du chitosan restent à l'extérieur de la bulle dans la partie liquide, tandis que les queues hydrophobes (groupes octanal) ajoutées à la molécule restent à l'intérieur de la bulle, dans la partie gazeuse (voir Figure 17d). Ainsi, nous devrions être en mesure de voir l'interaction biologique entre les cellules de *C. vulgaris* et le squelette du chitosane, or, nous observons des interactions hydrophobes. Ce phénomène peut s'expliquer comme suit : l'interaction spécifique entre la surface des cellules de *C. vulgaris* et les monomères de chitosane existe probablement encore, et comme elle est efficace, le film d'eau entre la bulle et la cellule se rompt et provoque la formation d'une ligne de contact triphasique (TPC), ce qui entraîne une interaction hydrophobe qui devient dominante et masque l'interaction spécifique. Ces modifications de la surface des bulles montrent qu'en effet, en utilisant de telles stratégies d'ingénierie de surface, il est possible de contrôler et de moduler les interactions directes entre bulles et cellules. Enfin, l'efficacité des bulles fonctionnalisées pour capturer des populations de cellules a été évaluée expérimentalement à l'aide d'un dispositif de flottation à l'échelle du laboratoire (Figure 19F). L'idée est qu'en

utilisant cette stratégie, les étapes de prétraitement nécessaires à la récolte des cellules par flottation, comme la floculation, pourraient être éliminées, d'où un gain de temps et d'argent. En utilisant cette méthode de récolte en une seule étape, nous avons pu séparer environ 55% des cellules de leur milieu de culture aqueux. Ce chiffre n'atteint peut-être pas 100%, mais il est en fait très intéressant lorsqu'on considère des processus en mode continu (applications industrielles principalement utilisées), car la séparation d'une partie seulement des cellules permet aux autres de reprendre la culture.

Contribution des travaux à d'autres domaines de recherche et d'applications

Les résultats de tous les travaux réalisés au cours de cette thèse ont jusqu'à présent été présentés du point de vue de leur intérêt pour l'objectif fixé dans cette thèse, à savoir la fonctionnalisation de la surface des bulles pour améliorer la flottation. Cependant, chaque étape de cette thèse a permis de générer des connaissances qui peuvent également contribuer à d'autres domaines de recherche ou à d'autres applications que la flottation : c'est ce que nous allons aborder maintenant dans cette section.

Comme mentionné au chapitre 1.1.1, dans les procédés de séparation par flottation, la floculation est souvent utilisée comme première étape pour améliorer l'efficacité de la flottation. Mais si nous voulons nous débarrasser de cette étape, il est obligatoire de comprendre le comportement des bulles et leur interaction avec les cellules. Pour comprendre cela, nous avons développé une nouvelle méthode pour produire des bulles et mesurer leur interaction avec les cellules en utilisant la microscopie à force fluidique (FluidFM). La FluidFM a déjà été utilisée dans plusieurs applications. Par exemple, en science des matériaux, elle a été utilisée pour la gravure sub-micrométrique (Meister et al., 2009b), pour la fonctionnalisation locale de couches de polymères (Hirt et al., 2015) ou pour l'impression électrochimique 3D de conducteurs avec une résolution à l'échelle microscopique (van Nisselroy et al., 2022). Pour cela, les cantilevers de nanopipettes à microcanaux utilisés sont capables de délivrer de l'électrolyte par des ouvertures submicroscopiques au bord des cantilevers. Ainsi, les constructions imprimées en 3D sont réalisées couche par couche, ce qui permet de construire des formes géométriques sophistiquées, telles que des anneaux doubles, des hélices et des trépieds (van Nisselroy et al., 2022). En outre, la FluidFM est également utilisée dans les sciences biologiques où elle offre la possibilité de surmonter plusieurs problèmes de spectroscopie unicellulaire. Par exemple, la FluidFM permet d'isoler

des cellules uniques en appliquant une sous-pression dans le microcanal ; de cette façon, les cellules uniques peuvent être fermement immobilisées à l'ouverture du cantilever, et peuvent être utilisées pour sonder les interactions cellule-cellule ou les interactions cellule-surface d'une manière fiable (Demir, Blockx, et al., 2020 ; Demir-Yilmaz, Yakovenko, et al., 2022a), ou pour transférer des cellules dans des zones ciblées pour observer les comportements cellulaires. De plus, une application majeure de la FluidFM dans les sciences de la vie est l'extraction de molécules directement du cytoplasme des cellules pour l'analyse moléculaire, en utilisant les pointes des cantilevers pour perforer la membrane externe ou la paroi cellulaire (Guillaume-Gentil et al., 2013, 2016, 2022 ; Potthoff et al., 2015). Cette stratégie peut également être utilisée pour injecter des biomolécules ou des colorants fluorescents dans les cellules, en appliquant une surpression (Guillaume-Gentil et al., 2016). Ici, dans cette thèse, nous avons utilisé FluidFM d'une manière originale et différente, qui n'avait jamais été décrite auparavant pour produire des bulles directement à l'ouverture des cantilevers. Pour cela, un prérequis était d'appliquer d'abord sur le microcanal FluidFM un revêtement hydrophobe en utilisant des monocouches auto-assemblées (SAMs) de silanes via la technique de dépôt en phase vapeur SAMs. Cette étape était importante pour maintenir les bulles produites sur l'ouverture du cantilever, sinon elles seraient remontées à la surface. Ensuite, pour la première fois, nous avons rempli le cantilever d'air, contrairement à toutes les autres applications de FluidFM qui utilisent des cantilevers remplis de liquides. Le revêtement hydrophobe à l'intérieur du cantilever permet de pousser l'air à l'extérieur du microcanal pour former une bulle à son ouverture. Cette méthode de sonde à bulle est une méthode fiable pour mesurer l'interaction entre la bulle et les surfaces complexes car ce système permet de contrôler la taille de la bulle sur des mesures consécutives et même pendant la même mesure. En fait, le maintien de la taille de la bulle constante dans le temps était le principal goulot d'étranglement des méthodes existantes utilisant l'AFM pour sonder les interactions des bulles, ce qui a pu être surmonté grâce à FluidFM. Cette nouvelle méthode n'est pas seulement intéressante dans le contexte de cette thèse de doctorat, car elle peut être utilisée par la communauté scientifique pour mieux comprendre les interactions entre les bulles et tout type de (bio)-surfaces, qui sont impliquées dans de nombreuses applications différentes. Un premier exemple d'une telle application est l'élimination des microorganismes des surfaces où ils forment des biofilms, ce qui est un problème important dans de nombreux processus industriels (dentisterie, filtration de l'eau, stockage de l'eau et canalisation).

Pour résoudre ce problème, les bulles d'air pourraient être un moyen prometteur de contrôler l'encrassement ; par exemple, une étude récente de Kriegel et de ses collègues a examiné le mécanisme sous-jacent à l'élimination des bactéries (*P. aeruginosa*) des surfaces en polycarbonate (hydrophiles) et en PDMS (hydrophobes) avec des bulles d'air (Kriegel & Ducker, 2019). Dans cette étude, les auteurs montrent que la plupart des bactéries sur la surface solide hydrophobe ont pu être éliminées juste après la première interaction avec la bulle, alors qu'une quantité importante de bactéries reste sur les surfaces hydrophiles. Cela peut signifier que l'interaction entre les surfaces hydrophiles et les bactéries est plus forte que l'interaction entre les bulles et les bactéries. En utilisant la méthode des sondes à bulles développée dans cette thèse, les interactions des bulles avec les bactéries pourraient être quantifiées et ensuite comparées à l'interaction entre les bactéries et les différentes surfaces pour évaluer la possibilité d'éliminer réellement les cellules en utilisant les bulles. En outre, les facteurs influençant ces interactions pourraient également être étudiés, tels que les facteurs environnementaux, le pH, la force ionique, ou d'autres facteurs tels que la taille des bulles et la mouillabilité des surfaces. Un autre exemple d'application où la méthode des sondes à bulles pourrait apporter des informations intéressantes est celui des microbulles qui sont utilisées comme vecteurs de médicaments pour traiter des maladies. En effet, Tinkov, Gao et Klibanov et al. ont étudié la possibilité de charger les bulles avec un médicament ou un vecteur de thérapie génique, puis de délivrer et libérer localement les substances transportées en utilisant des ultrasons (Tinkov et al., 2009 ; Gao et al., 2008 ; Klibanov, 2007). Dans ces systèmes complexes, les microbulles sont recouvertes d'anticorps qui leur permettent d'interagir avec des antigènes spécifiques présents sur les membranes cellulaires. Cela permet leur acheminement vers les cellules ciblées (Delalande et al., 2012 ; Klibanov, 2007). Ensuite, une exposition aux ultrasons est réalisée ; cela provoque une perméabilité temporaire de la membrane des cellules, et fait s'effondrer les bulles pour libérer les médicaments encapsulés. Cela augmente considérablement l'absorption intracellulaire des médicaments par les cellules (Delalande et al., 2012 ; Frenkel, 2008). Cette méthode de transport par bulles a été appliquée avec succès pour délivrer des acides nucléiques *in vitro* et *in vivo*, mais il manque des informations fondamentales sur les interactions des bulles avec les cellules, ce qui pourrait aider à développer davantage cette méthode d'administration ciblée de médicaments. Dans ce contexte, la méthode de sonde à bulles développée dans cette thèse pourrait être utilisée pour comprendre le mécanisme de fixation des bulles ciblées aux membranes cellulaires, ce

qui pourrait aider à mieux contrôler le ciblage des cellules. En outre, grâce à cette méthode, différents revêtements de bulles et leur affinité pour les cellules ciblées ainsi que pour les bulles pourraient être évalués dans différentes conditions environnementales.

Parlons maintenant de la paroi cellulaire des microalgues, qui est responsable de l'interaction complexe entre les cellules et leur environnement. Dans le cadre de ce travail, mieux comprendre cette interaction complexe a permis de comprendre ses interactions avec les flocculants pour des applications de récolte. Si nous avons choisi de travailler avec le chitosan, d'autres types de molécules pourraient également être identifiés comme flocculants bio-sourcés potentiels, et ce en comprenant la composition de la paroi cellulaire. Cela permettrait d'optimiser de nouveaux procédés de floculation avec des polymères naturels directement disponibles sur la paroi cellulaire, donc non-toxiques et biocompatibles. De cette façon, les problèmes liés à l'utilisation de polymères synthétiques pourraient être éliminés, comme la contamination des produits finaux. Cependant, la compréhension des caractéristiques dynamiques et de la composition de la paroi cellulaire des microalgues est également importante pour comprendre et contrôler d'autres aspects que l'adhésion cellulaire. Par exemple, la rupture de la paroi cellulaire est un défi important dans les processus d'extraction, où l'objectif est de briser les cellules afin de libérer et de récolter les produits intracellulaires pour lesquels elles ont été cultivées. Le choix des méthodes appropriées pour ce faire peut être une tâche compliquée et dépend de l'espèce de microalgue utilisée, des conditions envisagées et de l'échelle de production. Les principales méthodes de désintégration cellulaire utilisées sont les méthodes mécaniques et chimiques. Elles sont différentes en termes de consommation d'énergie, d'efficacité et d'utilisation de solvants. Comme la plupart des espèces de microalgues possèdent une paroi cellulaire rigide résistant aux facteurs de stress mécaniques et chimiques, ces méthodes de perturbation peuvent être utilisées indépendamment mais aussi en combinaison afin d'obtenir des rendements élevés (Lee et al., 2017). De plus, les méthodes chimiques et mécaniques consomment une énergie importante et ne peuvent pas être mises à l'échelle facilement (de Boer et al., 2012). Pour ces raisons, il est intéressant de développer ou d'optimiser d'autres types de procédés, par exemple basés sur la digestion enzymatique de la paroi cellulaire des microalgues. Les avantages de ces digestions enzymatiques par rapport aux méthodes de perturbation mécanique ou chimique sont la sélectivité biologique des enzymes utilisées, les

conditions de fonctionnement douces nécessaires et la consommation d'énergie réduite (Günerken et al., 2015). La digestion enzymatique a déjà été utilisée dans certains cas mais pas à grande échelle comme c'est le cas pour les traitements mécaniques et chimiques. Malgré les coûts importants des enzymes, les conditions opérationnelles n'étant pas consommatrices d'énergie, ces techniques peuvent au final être moins coûteuses à mettre en place que les traitements mécaniques ou chimiques (Nagappan et al., 2019). De plus, la mise à l'échelle des traitements enzymatiques est relativement facile par rapport aux méthodes mécaniques (Pragya et al., 2013 ; Demuez et al., 2015). Cependant, pour développer et optimiser un tel procédé enzymatique, il est fondamental de comprendre la composition et la dynamique de la paroi cellulaire, pour pouvoir réellement choisir les bonnes enzymes pour les bonnes espèces de microalgues et les bonnes conditions. Le travail que nous avons effectué pour déterminer la composition et l'architecture de la paroi cellulaire de *C. vulgaris* va dans ce sens mais est pour l'instant limité. En effet, il faut maintenant poursuivre les recherches, en utilisant la digestion enzymatique ou la résonance magnétique nucléaire (RMN) à l'état solide pour identifier principalement les polysaccharides présents sur la paroi cellulaire mais aussi les lipides et les protéines, et ainsi fournir les informations nécessaires à l'optimisation des méthodes de rupture des cellules basées sur les digestions enzymatiques.

Après avoir analysé la composition de la paroi cellulaire, nous avons ensuite choisi le chitosan pour poursuivre le travail et comprendre comment il interagit avec les cellules. Le chitosan est un flocculant largement utilisé pour la récolte des microalgues, mais jusqu'à présent des résultats mitigés ont été rapportés sur les efficacités de floculation en fonction des espèces de microalgues utilisées (espèces d'eau douce ou marines) et des conditions expérimentales (pH). Sans une connaissance précise du fonctionnement des flocculants, il est très difficile de les utiliser de manière fiable pour des applications à grande échelle. C'est pourquoi il est important de comprendre leurs mécanismes de floculation. Cependant, les mécanismes de floculation, qu'ils soient naturellement induits ou induits par des molécules ajoutées, sont difficiles à adapter, même à l'échelle du laboratoire, en raison de leur caractère unique pour chaque condition de culture et chaque espèce de microalgue utilisée (Demir, Besson, et al., 2020). C'est pourquoi un grand nombre d'études dans la littérature sont dédiées à la compréhension de ces mécanismes, notamment les paramètres importants qui influencent leur efficacité. Donnons-en des exemples concrets. Ainsi, pour un même flocculant,

l'hydroxyde de magnésium, les mécanismes de floculation sont différents selon l'espèce de microalgues. Par exemple le mécanisme de neutralisation des charges est en jeu pour *P. tricornutum* alors que le mécanisme de floculation par balayage est observé pour *D. salina*, à pH élevé (Besson et al., 2019 ; Besson & Guiraud, 2013 ; Formosa-Dague, Gernigon, et al., 2018a). Nos travaux sur le chitosane ont également mis en évidence que le mécanisme de floculation peut changer en fonction du pH du milieu de culture (Demir, Blockx, et al., 2020), montrant la complexité que ces mécanismes peuvent détenir. Il est donc essentiel d'identifier ces mécanismes impliqués dans chaque cas afin de pouvoir les contrôler et les employer à plus grande échelle (Xu et al., 2013 ; Zhu et al., 2018). Comme nous l'avons montré dans le travail sur les interactions du chitosane (Demir, Blockx, et al., 2020), l'utilisation de l'AFM est en fait une approche intéressante pour cela, car elle permet de comprendre la base moléculaire des mécanismes en jeu dans les interactions floculant-cellule, ce qui permet donc de déterminer les paramètres importants pour contrôler ces interactions et optimiser davantage les processus de floculation à grande échelle. Cette stratégie expérimentale pourrait devenir un outil de référence afin de résoudre les mystères de la floculation pour différents floculants et différentes espèces de microalgues. Jusqu'à présent dans la littérature, la méthode la plus couramment utilisée pour identifier les mécanismes de floculation est la mesure du potentiel zêta. Le potentiel zêta est déterminé en mesurant la charge superficielle des surfaces cellulaires des microalgues. La plupart des floculants utilisés pour la récolte des microalgues sont des floculants cationiques (chitosan, amidon, ...), le potentiel zêta est donc une méthode bien adaptée pour vérifier que le mécanisme de floculation repose bien sur des interactions électrostatiques. Par exemple, Vandamme et al. ont identifié le mécanisme de floculation de la diatomée *Phaeodactylum tricornutum* avec des sels alcalins en utilisant cette méthode. Dans ce cas, l'augmentation des mesures du potentiel zêta pendant la floculation avec la brucite a suggéré que la précipitation de la brucite a provoqué la floculation par neutralisation de la charge. Cependant, les mesures du potentiel zêta sont restées négatives pour la floculation avec la calcite, suggérant ici que la floculation s'est produite par un mécanisme non électrostatique (Vandamme et al., 2015). Cependant, cette méthode est limitée aux interactions électrostatiques et ne permet pas d'évaluer les interactions biologiques et les interactions hydrophobes. Par exemple, comme nous l'avons vu dans le cas du chitosane, même pour les molécules cationiques, les interactions électrostatiques peuvent ne pas être dominantes dans le mécanisme de floculation, montrant le besoin de techniques autres que

les mesures de potentiel zêta qui peuvent aller au-delà et mesurer d'autres types d'interactions. Ensuite, comme nous l'avons également vu dans les travaux développés dans cette thèse, d'autres types d'interactions peuvent être efficaces pour favoriser les interactions (interactions biologiques spécifiques, interactions hydrophobes). Cela signifie que d'autres types de flocculants pourraient être développés, et pour cela un outil comme l'AFM permettrait de comprendre les mécanismes en jeu et donc d'étendre les caractéristiques à rechercher pour trouver des molécules flocculantes efficaces.

Afin d'optimiser la séparation des microalgues par le procédé de flottation et de réduire de manière significative le coût et le temps du procédé, la fonctionnalisation des bulles est une alternative intéressante. Le premier exemple qui montre que les interactions des bulles peuvent être modulées par la fonctionnalisation des bulles a été réalisé en 1994 par Ducker et ses collègues, qui ont utilisé le dodécylsulfate de sodium (SDS), un tensioactif qui absorbe à la surface des bulles en les rendant hydrophiles. En sondant les interactions avec une sphère de silice, leurs résultats ont montré la suppression de la force hydrophobe qui avait lieu avec des bulles propres (Ducker et al., 1994). Ces expériences ont été les premières à démontrer qu'il est possible de modifier l'interaction des bulles en modifiant les propriétés physico-chimiques de leur surface (Demir et al., 2021a). C'est longtemps après, en 2008, que ce concept a été utilisé pour des applications de récolte de microalgues. En effet, l'équipe de Henderson a été la première à utiliser des bulles fonctionnalisées pour développer un nouveau procédé de flottation et améliorer l'efficacité de la récolte (Henderson et al., 2008a, 2010). Dans la stratégie développée par cette équipe, les bulles sont fonctionnalisées avec des polymères cationiques qui rendent la surface des bulles chargée positivement. Ces surfaces de bulles chargées positivement peuvent alors attirer les cellules de microalgues chargées négativement sans qu'il soit nécessaire de les flocculer. Ils ont appelé cette technique PosiDAF car les bulles utilisées ont été générées à l'aide de la technique DAF. Les deux polymères cationiques PosiDAF les plus prometteurs identifiés étaient un agent de surface cationique, le bromure de cétyltriméthylammonium (CTAB), ainsi qu'un polymère, le chlorure de polydiallyldiméthylammonium (polyDADMAC) (Henderson et al., 2008a, 2010). Dans ce cas, pour produire les bulles fonctionnalisées, ces tensioactifs ont été directement ajoutés au saturateur contenant l'eau. Ce mélange a ensuite été pressurisé et agité jusqu'à stabilisation. La solution pressurisée a ensuite été libérée dans la suspension de microalgues pour laisser la

floculation des cellules se produire avec la bulle fonctionnalisée. Cette technique a démontré qu'en fonctionnalisant la surface des bulles, il est possible d'augmenter l'efficacité de l'élimination des microalgues à des niveaux comparables à ceux du processus conventionnel de floculation/flottation, mais sans qu'une floculation préalable soit nécessaire. Une stratégie similaire avait déjà été décrite dans notre équipe, où des microbulles fonctionnalisées en surface - des aphyrons de gaz colloïdaux (CGAs) -, ont été utilisées pour récolter des nanoparticules de SiO₂ (Zhang & Guiraud, 2017). Dans ce cas, des CGAs chargés négativement et positivement ont été produits avec du bromure de cétyle triméthylammonium (CTAB) et du dodécylsulfate de sodium (SDS), conduisant à une efficacité de séparation de 90-99 %. Ainsi, ces travaux démontrent qu'en utilisant des bulles fonctionnalisées, nous pouvons réaliser la flottation en une seule étape et ainsi réduire le temps nécessaire et donc son coût global. Dans ce travail, le même concept a été utilisé, mais au lieu de changer la charge des bulles, le but était de la rendre spécifique afin qu'elle puisse interagir de manière efficace et contrôlée avec les cellules. En outre, l'utilisation du chitosan peut être bénéfique par rapport aux polymères cationiques utilisés par l'équipe d'Henderson, car il n'est pas toxique et n'interfère pas avec les processus en aval. La récolte est sans aucun doute une étape clé de toute technologie basée sur les microalgues, et elle a été identifiée comme un goulot d'étranglement majeur pour atteindre la durabilité et la rentabilité de ces technologies. De plus, afin de maximiser l'efficacité totale du processus, il faut maintenir un bon équilibre entre la durée du processus et le coût énergétique. Par exemple, ce travail de thèse a montré que 10 mg/L de chitosane est nécessaire pour atteindre une efficacité de séparation maximale (floculation suivie d'une flottation) avec les cellules de *C. vulgaris*. Cependant, lorsque nous utilisons le PO-chitosan pour fonctionnaliser les bulles, 25 mg/L sont nécessaires pour atteindre la meilleure efficacité de séparation, bien que le chitosan et le PO-chitosan soient des molécules différentes, une comparaison directe des concentrations utilisées n'est pas vraiment appropriée. Cependant, au moins à l'échelle du laboratoire, il semble que davantage de molécules soient nécessaires pour la fonctionnalisation des bulles, mais lorsque nous considérons le temps nécessaire à la séparation, dans le premier scénario, nous devons ajouter le flocculant et le mélanger à la suspension pendant 15 minutes. Ensuite, 30 minutes sont nécessaires pour que les floccs se stabilisent avant d'injecter les bulles au fond du bocal et de recueillir les cellules agrégées à la surface. Cependant, avec les bulles fonctionnalisées, les deux étapes de mélange et de stabilisation sont sautées (au total 45 min), le processus commence directement avec

l'injection des bulles (15 min), ce qui réduit le temps du processus à $\frac{1}{4}$ du temps initial. Ces temps sont pour le processus à l'échelle du banc d'essai que nous avons développé, mais nous pouvons imaginer que ces différences de temps auraient également lieu à plus grande échelle. Comme à l'échelle industrielle le temps c'est de l'argent, le fait d'opérer la séparation en une seule étape pourrait peut-être augmenter significativement la rentabilité globale des systèmes de production de microalgues et les rendre économiquement plus viables. En fait, une comparaison économique fiable et une analyse du cycle de vie (ACV) doivent être réalisées afin de comparer correctement les deux systèmes de récolte (Laifa et al., 2021). Cette comparaison doit être effectuée à l'échelle industrielle, en tenant compte des économies d'énergie et d'infrastructure dues à la suppression de l'étape de floculation. Seul ce type d'analyse permettra de décider si la flottation en une étape est plus rentable que la floculation suivie de la flottation.

Perspectives d'avenir des travaux réalisés dans le cadre de cette thèse

Bien que les connaissances et les méthodes développées dans ce travail de thèse puissent avoir des impacts importants dans d'autres domaines, nous souhaitons ici regarder vers l'avenir et décrire dans cette section les perspectives concrètes de travail qui peuvent être construites sur la base des résultats générés dans cette thèse. Fondamentalement, il existe de nombreuses perspectives de travail qui pourraient être envisagées sur la base des résultats obtenus dans cette thèse de doctorat. Une première perspective est liée au travail sur la FluidFM, qui pourrait être utilisée non seulement pour produire des bulles mais aussi pour produire d'autres types d'interfaces fluides comme des gouttelettes de liquide. Le développement de systèmes de gouttelettes liquides progresse actuellement à un rythme rapide. Une variété d'applications de preuve de concept dans les biotechnologies sont décrites, soulignant leur potentiel en tant qu'outils pour effectuer des tâches d'ingénierie rapides, fiables et efficaces en termes d'énergie. En effet, leurs divers avantages, tels que l'adaptabilité, la diversité et le rapport surface/volume élevé, leur permettent de servir une gamme plus large d'applications, allant de l'analyse de cellules uniques, aux essais basés sur les cellules ou à la libération contrôlée de médicaments (Y. Wei et al., 2020). Par exemple, dans le domaine croissant de la microfluidique à base de gouttelettes, différentes approches sont développées pour contrôler, manipuler et surtout fonctionnaliser les gouttelettes (Khojasteh et al., 2019). Dans ce contexte, utiliser FluidFM pour produire des gouttes pourrait

être un moyen efficace d'accroître les connaissances nécessaires à l'optimisation de ces applications, et de mesurer leur interaction les différents types de surfaces avec lesquelles elles peuvent être amenées à interagir. Nous pouvons imaginer que pour produire de telles gouttes, le microcanal cantilever FluidFM pourrait être rempli de liquide au lieu d'air et qu'en appliquant une surpression, des gouttes de liquide pourraient être formées dans un autre liquide de densité différente. Cette forme permet d'évaluer les mécanismes d'interaction des gouttelettes de liquide avec les bio-surfaces.

Comme mentionné précédemment, une autre perspective de ce travail de doctorat pourrait porter sur la digestion enzymatique de la paroi cellulaire de *C. vulgaris*. Dans ce manuscrit, nous avons analysé la composition de la paroi cellulaire de *C. vulgaris* et déterminé les fractions relatives des principaux composants : lipides, protéines et polysaccharides. Puis, en franchissant une étape supplémentaire, nous avons identifié les monosaccharides présents dans la paroi cellulaire, en utilisant une hydrolyse acide suivie d'une chromatographie liquide. Cependant, nous n'avons jamais identifié les polysaccharides dont proviennent ces monosaccharides, ce qui, comme nous l'avons vu précédemment, pourrait apporter des informations importantes pour développer, par exemple, des procédés de désintégration cellulaire à base d'enzymes. Pour cette raison, on peut envisager de réaliser un screening d'enzymes pour dégrader la paroi cellulaire de *C. vulgaris*, puis d'analyser la présence de monomères. Si des monomères sont détectés, cela signifie que le polysaccharide ciblé par l'enzyme était présent dans la paroi cellulaire. Dans le cas contraire, une autre enzyme doit être testée et le même processus doit être répété. Cette procédure est basée sur des essais et des erreurs, ce qui prend du temps et peut être coûteux. Cependant, une fois que c'est fait, cette information peut être vraiment utile dans diverses applications, à l'échelle industrielle pour digérer la paroi cellulaire des microalgues, ou pour identifier de nouveaux composés qui pourraient être valorisés. De plus, la spectroscopie RMN à l'état solide pourrait également être une option pour identifier et quantifier les polysaccharides présents dans la paroi cellulaire. Par exemple, Paulhazan et al. ont récemment examiné la composition, les caractéristiques dynamiques et l'organisation spatiale des glycanes pour l'espèce de microalgue *Parachlorella beijerinckii* (Paulhazan et al., 2021). Leurs résultats, basés sur la spectroscopie de RMN à l'état solide (ssNMR) avec rotation à angle magique (MAS), ont montré que l'amidon est la principale molécule rigide et la plus abondante dans la paroi

cellulaire. Jusqu'à présent, très peu d'études ont utilisé cette méthode pour analyser la paroi cellulaire des microalgues (Arnold et al., 2015 ; Ghassemi et al., 2021 ; Separovic & Sani, 2020), mais elles montrent toutes l'intérêt de la RMN du solide pour acquérir une compréhension précise et complète des polysaccharides présents dans la paroi cellulaire des cellules de microalgues.

Une autre perspective pourrait alors être construite sur le travail effectué sur le chitosan pour le modifier et le rendre amphiphile. Dans ce manuscrit, nous avons utilisé l'octanal (C8) comme groupe hydrophobe pour rendre la molécule finale amphiphile. Mais au lieu de l'octanal, des chaînes hydrophobes plus longues ou plus courtes pourraient également être utilisées, comme le dodécanal (C12) ou l'hexanal (C6). L'extension ou la réduction des groupes hydrophobes de la molécule peut augmenter ou diminuer l'activité tensioactive des chitosanes modifiés, et donc à la fois leurs interactions avec les cellules de *C. vulgaris* et leur affinité pour les bulles hydrophobes. Cela pourrait également avoir un impact sur la solubilité des molécules modifiées, et par la suite sur le degré de substitution qui pourrait être atteint. Par exemple, pour le chitosane à haut poids moléculaire (utilisé dans cette thèse), un niveau d'alkylation de 10-15% est la limite pour pouvoir dissoudre la molécule dans l'eau et l'utiliser dans les expériences de récolte. Nous avons également essayé d'utiliser du chitosane de faible poids moléculaire, et dans ce cas, le degré de substitution qui pouvait être atteint était encore plus faible puisqu'à un niveau d'alkylation de 10%, le produit final ne pouvait plus être dissous dans l'eau. Cela montre qu'il doit y avoir un équilibre entre les longueurs relatives de la chaîne hydrophile et hydrophobe dans la molécule, le but étant d'avoir une molécule ayant peut-être une activité tensioactive plus élevée, mais qui peut encore être dissoute. Par exemple, pour les chaînes hydrophobes plus longues, afin de pouvoir dissoudre la molécule dans l'eau, le degré de substitution peut devoir être réduit, tandis qu'en utilisant des chaînes plus courtes, des niveaux d'alkylation plus élevés peuvent être atteints, ce qui permet d'obtenir un équilibre lipophile/hydrophile différent dans la molécule. Ainsi, pour comprendre cela et affiner en fait les propriétés de ces molécules de chitosan amphiphiles, les groupes hydrophobes à la fois plus longs et plus courts pourraient être utilisés, avec des molécules de chitosan de poids moléculaire différent, en utilisant différents degrés de substitution.

Enfin, une perspective qui peut être envisagée lorsqu'on considère la séparation des cellules de l'eau à l'aide de bulles fonctionnalisées est d'effectuer une séparation sélective. La

séparation sélective par procédé de flottation consiste à séparer les particules fines des particules d'autres composants présents dans une phase dispersée (Mathur et al., 2000). Parce qu'historiquement la flottation a été utilisée dans les industries des minerais et des minéraux, la flottation sélective a déjà été utilisée pour séparer sélectivement différents minéraux tels que la wolframite (Lu et al., 2021), le cuivre (Hassanzadeh et al., 2020), la fluorine (W. Jiang et al., 2018), la calcite et la barytine (Ren et al., 2017). Le concept de base de la séparation sélective repose sur la différence des propriétés de surface des minéraux à séparer (Zanin et al., 2019). Pour séparer un minéral d'un autre, l'un doit être hydrophobe tandis que l'autre est hydrophile, de sorte que les minéraux hydrophobes se fixent aux bulles et sont entraînés à la surface tandis que les hydrophiles restent en suspension. Pour contrôler ce phénomène, différents produits chimiques peuvent être utilisés pour modifier les propriétés de surface des minéraux sélectionnés et changer leurs propriétés hydrophobes : collecteurs, dépresseurs, modificateurs ou moussants. (Bulatovic, 2007). Les collecteurs (souvent appelés surfactants) sont utilisés pour améliorer l'hydrophobie de surface donc l'affinité des particules envers les bulles (Laitinen et al., 2016). Par exemple, les acides hydroxamiques sont une classe omniprésente de collecteurs qui peuvent s'adsorber sélectivement sur des minéraux, tels que la wolframite (Meng et al., 2015) et les minéraux de terres rares (Kumari et al., 2015), pour améliorer leur hydrophobie de surface et faciliter leur séparation des minerais polymétalliques par flottation. Alors que les dépresseurs augmentent la différence de flottabilité entre deux minéraux en supprimant l'hydrophobie d'un des minéraux (X. Wang et al., 2022). Les réactifs modificateurs réagissent soit avec les surfaces des minéraux, soit avec les collecteurs et autres ions dans la pulpe de flottation, ce qui entraîne une réponse modifiée et contrôlée de la flottation. L'utilisation de ces produits chimiques permet d'obtenir une séparation sélective des minéraux. Bien que ces stratégies fonctionnent très bien avec les particules de minéraux et de minerais, il pourrait être intéressant de les adapter aux cellules, et d'utiliser ainsi la flottation comme méthode de tri cellulaire, permettant de séparer une population spécifique de cellules d'une autre dans un milieu complexe. Pour cela, bien sûr, une possibilité serait de modifier les propriétés de la surface des cellules en utilisant des collecteurs ou des dépresseurs comme cela est fait pour les minéraux, mais une autre alternative serait de modifier directement la surface de la bulle pour qu'elle interagisse seulement avec un type de cellule et pas les autres. Les travaux réalisés dans le cadre de cette thèse ayant montré qu'il était possible de fonctionnaliser les

bulles avec n'importe quel type de molécule amphiphile afin de contrôler leurs interactions avec les cellules, cette possibilité semble tout à fait réaliste. Une telle stratégie pourrait par exemple être utilisée pour séparer les cellules bactériennes des cellules sanguines humaines dans le cas d'une septicémie, et ainsi être en mesure de fournir un diagnostic précoce de l'espèce bactérienne impliquée afin de cibler un traitement efficace. Cet exemple a déjà attiré notre attention, et au cours de cette thèse, nous avons exploré le potentiel d'interaction des bulles fonctionnalisées avec de la colistine avec des cellules bactériennes Gram-négatives (Demir et al., 2021a). La colistine est un peptide antibactérien polycyclique naturel dérivé de *Bacillus polymyxa*, qui interagit spécifiquement avec la surface des bactéries en se liant à la partie lipide A du lipopolysaccharide (LPS) (Yahav et al., 2012), un glycolipide présent dans la membrane externe des espèces Gram-négatives (Maldonado et al., 2016). Nos travaux ont montré que la fonctionnalisation des bulles avec de la colistine avait un impact positif sur l'adhésion des cellules aux bulles. La colistine étant très spécifique et ne se liant pas aux cellules non-bactériennes, telles que les cellules de mammifères présentes dans le sang, elle pourrait être un moyen potentiel de séparer les bactéries des autres composants du sang et ceci effectuer une séparation sélective. Il s'agit d'une application de ce procédé, mais de nombreuses autres applications peuvent être envisagées, dans différents domaines, pour différentes applications.

En fin de compte, ce manuscrit de thèse a mis en lumière des problèmes scientifiques que les chercheurs actuels n'ont pas encore abordés. Bien qu'elles soient impliquées dans de nombreux systèmes biologiques différents, les interactions bulles-microorganismes ont été peu explorées en raison de l'absence de méthode ou d'outil capable de les sonder. Ce type d'interactions a lieu lors de la récolte des microalgues par flottation, une technique de séparation prometteuse qui pourrait permettre l'utilisation de la biomasse des microalgues dans des processus industriels à grande échelle. Le travail effectué dans le cadre de cette thèse a permis de répondre à une partie de ces questions, de développer un outil permettant d'accéder aux interactions bulles-microorganismes, et de développer un nouveau procédé original de séparation des microalgues utilisant des bulles fonctionnalisées. Pour cela, nous avons réalisé un certain nombre de développements et généré des données fondamentales sur différents aspects des microalgues, qui peuvent servir de base à la communauté scientifique pour de nouveaux développements, dans d'autres domaines d'application,

montrant au final le large impact du travail produit. En outre, ce travail a jeté les bases de nouveaux projets, de nouvelles améliorations et de nouvelles idées qui, nous l'espérons, seront développés dans les prochaines années.

Appendices

Appendix 1: The role of microplastics in microalgae cells aggregation: a study at the molecular scale using AFM

Appendix 2: Investigation of the role of cell hydrophobicity and EPS production in the aggregation of the marine diatom *Cylindrotheca closterium* under salinity stress

Appendix 3: Algal reconstructed vesicles as a potential delivery system

Appendix 1: The role of microplastics in microalgae cells aggregation: a study at the molecular scale using AFM



The role of microplastics in microalgae cells aggregation: A study at the molecular scale using atomic force microscopy



Irem Demir-Yilmaz^{a,b}, Nadiia Yakovenko^c, Clément Roux^c, Pascal Guiraud^{a,d}, Fabrice Collin^c, Christophe Coudret^{c,d}, Alexandra ter Halle^c, Cécile Formosa-Dague^{a,d,*}

^a TBI, Université de Toulouse, INSA, INRAE, CNRS, Toulouse, France

^b LAAS, Université de Toulouse, CNRS, Toulouse, France

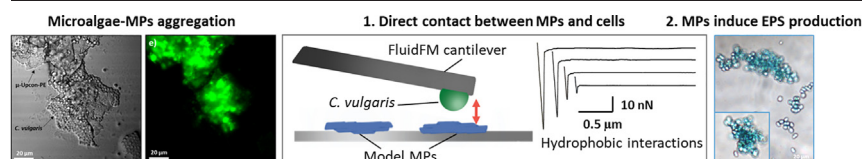
^c UMR 5623 IMRCP, CNRS, Toulouse, France

^d Fédération de Recherche FermaT, CNRS, Toulouse, France

HIGHLIGHTS

- An interdisciplinary approach based on AFM is used to study the interactions between microplastic particles and microalgae
- The model microplastic particles used have a rough, irregular surface with hydrophobic properties
- Microalgae grown with microplastic produce exopolysaccharides responsible for their aggregation
- Cell aggregation can also be induced by direct contact with microplastic particles
- This study allows understanding the consequences of microplastic pollution in aquatic ecosystems

GRAPHICAL ABSTRACT



ARTICLE INFO

Editor: Damia Barcelo

Keywords:

Microplastic
Microalgae
Aggregation
Interaction
Atomic force microscopy

ABSTRACT

Plastic pollution has become a significant concern in aquatic ecosystems, where photosynthetic microorganisms such as microalgae represent a major point of entry in the food chain. For this reason an important challenge is to better understand the consequences of plastic pollution on microalgae and the mechanisms underlying the interaction between plastic particles and cell's interfaces. In this study, to answer such questions, we developed an interdisciplinary approach to investigate the role of plastic microparticles in the aggregation of a freshwater microalgae species, *Chlorella vulgaris*. First, the biophysical characterization, using atomic force microscopy, of the synthetic plastic microparticles used showed that they have in fact similar properties than the ones found in the environment, with a rough, irregular and hydrophobic surface, thereby making them a relevant model. Then a combination of optical imaging and separation experiments showed that the presence of plastic particles in microalgae cultures induced the production of exopolysaccharides (EPS) by the cells, responsible for their aggregation. However, cells that were not cultured with plastic particles could also form aggregates when exposed to the particles after culture. To understand this, advanced single-cell force spectroscopy experiments were performed to probe the interactions between cells and plastic microparticles; the results showed that cells could directly interact with plastic particles through hydrophobic interactions. In conclusion, our experimental approach allowed highlighting the two mechanisms by which plastic microparticles trigger cell aggregation; by direct contact or by inducing the production of EPS by the cells. Because these microalgae aggregates containing plastic are then consumed by bigger animals, these results are important to understand the consequences of plastic pollution on a large scale.

* Corresponding author at: INSA de Toulouse, Toulouse Biotechnology Institute, 135 avenue de Rangueil, 31400 Toulouse, France.
E-mail address: formosa@insa-toulouse.fr (C. Formosa-Dague).

1. Introduction

Plastic is a revolutionary discovery of the early twentieth century that changed our way of life forever. It has become an integral part of all consumer goods such as packaging, clothing, electronic devices, medicine, etc., (Andrady and Neal, 2009). However, high demand, massive production, extensive use, and poor plastic waste management contributes to plastic release and accumulation in the environment, which has become one of the most pressing environmental problems of our time (Geyer et al., 2017). Plastic waste accounts for 60 to 80% of all solid waste present in the aquatic environment (Gregory and Ryan, 1997), most of them being microplastics particles (MPs) (EPA US, 2016). MPs are plastic particles ranging in size from 1 μm to 5 mm (Horton et al., 2017), which are characterized by a variety of physical, chemical, and morphological properties such as different types of polymers and composition, size, shape, density, color, etc. In the environment, MPs represent a group of persistent synthetic pollutants consisting of primary particles, manufactured at the millimetric or sub-millimetric scale under the form of pellets or microbeads, and secondary particles, resulting from the fragmentation of larger plastic debris through thermal, photo-oxidative, mechanical, and biological degradation processes (Cole et al., 2011). Because of their small size and ubiquitous distribution in all environmental compartments (Horton et al., 2017; Peng et al., 2020; Zhang et al., 2020), MPs are of great concern with respect to their bioavailability, toxicity and potential adverse effect on living organisms and ecosystem as a whole. Ingestion of MPs by aquatic living organisms from zooplankton (Cole et al., 2013) to mammals (Zantis et al., 2021), and the wide range of possible negative effects of plastic particles uptake are well documented. (EPA US, 2016; GESAMP, 2016; Peng et al., 2020).

However, there is a gap of knowledge on the interaction and the effects of MPs on the basic organisms of the trophic chain, such as microalgae, which are a major source of food for aquatic animals. Microalgae are photosynthetic microorganisms that are the most numerous primary producers in the entire aquatic ecosystem (Barbosa, 2009; Beardall and Raven, 2004). They are key organisms in a wide range of ecosystem functions, where they have an impact on ocean's carbon sequestration (Singh and Ahluwalia, 2013), oxygen production, nutrient cycling, etc., (Hopes and Mock, 2015). Being ubiquitous, sensitive to environmental disturbances, and easy to cultivate in laboratory, microalgae are an ideal model to study the effects of different pollutants in the environment including MPs (Cid et al., 2012). The interaction between MPs and microalgae is a complex process that can lead to a multitude of effects acting on the further fate and behaviour of both MPs and microalgae, and thus potentially affecting the entire ecosystem (Nava and Leoni, 2021). For instance, in the environment, microalgae tend to colonize and form biofilms on abiotic surfaces (Irving and Allen, 2011), among them plastic surfaces, using them as an abiotic substrate to grow in a biofouling process (Bravo et al., 2011; Carson et al., 2013; Jorissen, 2014; Reisser et al., 2014). While colonizing plastic surfaces or other types of surfaces, microalgae cells secrete extracellular polymeric substances (EPS), which play an important role in biofilm formation. EPS consist of polysaccharides, lipids, nucleic acids, proteins, and other polymeric compounds (Wingender et al., 1999a; Xiao and Zheng, 2016), which favours cells cohesion and future adhesion to the substrate' surface (Wingender et al., 1999b). In addition, biofouling changes the density of plastic particles, affecting their buoyancy (Nava and Leoni, 2021; Oberbeckmann et al., 2015; Rummel et al., 2017) and thus leading to the dissemination of plastic particles through the water column by sinking to the bottom or moving to the surface. This widespread abundance of MPs particles consequently increases their bioavailability for various living organisms. Another effect of biofouling is a decrease in the hydrophobicity of the particle surface (Lobelle and Cunliffe, 2011). As a result, adsorption of toxic pollutants from the aquatic environment to the surface of the plastic particles can be enhanced (Bhagwat et al., 2021; Dong et al., 2017), which can amplify the toxicity of MPs. Moreover, EPS produced by microalgae promote the heteroaggregation of MPs and microalgae. The resulting aggregates become easy food for the aquatic organisms and are also more prone to sediment, thus here also affecting their dissemination through the water

column as mentioned above (Lagarde et al., 2016; Long et al., 2015; Rummel et al., 2017). Then, MPs were also found to have a number of adverse effects on microalgae, including inhibition of growth (Sjollem et al., 2016; Zhang et al., 2017; Liu et al., 2020; Song et al., 2020), decrease in chlorophyll content (Tunali et al., 2020; Wu et al., 2019) and photosynthetic activity (Zhang et al., 2017), physical and morphological damages (Mao et al., 2018), oxydative stress (Xiao et al., 2020). Finally, due to constant movement in the aquatic environment, plastic is a potential vector of geographic transport for the migration of microalgae (Rowenczyk et al., 2021). This phenomenon creates a risk of introducing pathogenic species (e.g. harmful algal blooms) into a new environment where native species are not adapted to defend themselves (Masó et al., 2003; Glibert et al., 2014; Oberbeckmann et al., 2015).

For all these reasons, scientists are making increasing efforts to study the mechanism of MPs and microalgae interaction to better understand its negative impact on a global scale. For instance, a recent review published by Nava et al. reports on the different effects that microplastics can have on microalgae cells. Their study shows that the effects on cell growth, photosynthesis and cell morphology are the most commonly reported effects, although this is highly dependent on both the type of plastic and the microalgae species considered. On the contrary, microalgae, by colonizing microplastics, also alter the plastic polymer, notably their density and sinking behaviour (Nava and Leoni, 2021). However, most of the ecotoxicological studies under laboratory conditions are using commercially manufactured models of MPs, in a vast majority of the studies the model plastic are polystyrene micro- or nano- spheres, which are not representative of plastic particles found in the environment (Gigault et al., 2021; Kokalj et al., 2021; Phuong et al., 2016). Thus, there is a need for research based on the use of an environmentally relevant model of plastic particles. For this purpose, we used a top-down method based on mechanical degradation to prepare more environmentally relevant model of MPs (Yakovenko et al., 2022). Particles were prepared from polyethylene as it is the most produced (Plastics Europe, 2020) and frequently found plastic type in the environment (Peng et al., 2020). The model particles were characterized by polydispersity, irregular shapes, and negative surface charge thereby representing several characteristics in common with the MPs formed in the environment. However, being small in size, these particles are hard to observe in the biotic and abiotic matrices without destructive methods such as density separation or digestion. Thus, to overcome this limitation and make these particles easy to track and image in microalgae, we doped them by Lanthanide-based upconverting nanoparticles (UCNPs) as a luminescent tag. These recently developed phosphors are inorganic materials, very stable and able to convert low energy Near-Infrared photons into visible light (Gu and Zhang, 2018). This allows their detection even in thick samples such as in a tissue or a small animal. The studied model of MPs (Model-MPs) is represented by two types of particles: i) microparticles of PE itself ($\mu\text{-PE}$); and ii) labelled microparticles of PE with UCNPs luminescence tag ($\mu\text{-Upcon-PE}$).

In this study, we investigated the interaction between these Model-MPs and freshwater microalgae cells and their further role in the aggregation of cells using nano- and molecular scale experiments performed with an atomic force microscope (AFM) equipped with fluidic force microscopy (FluidFM). AFM, first developed in 1986 (Binnig et al., 1986), has proven over the years to be a powerful tool for surface characterization at the nano-scale (Pillet et al., 2014; Xiao and Dufrene, 2016). In addition to high-resolution imaging capacities, down to the nanometer scale, AFM is also a sensitive force machine able to record piconewton level forces, thus making it possible to access the nanomechanical and adhesive properties of samples, as well as their interactions with their environment (Formosa-Dague et al., 2018). In the particular context of microalgae, AFM has been used to understand the morphology, nanostructure, nanomechanics and adhesive behaviour of cells (Demir-Yilmaz et al., 2021), but most importantly their interactions with particles or molecules present in their environment (Besson et al., 2019; Demir et al., 2020; Demir-Yilmaz et al., 2021). In FluidFM, a microsized channel is integrated into an AFM cantilever and connected to a pressure controller, thus creating a continuous and closed

fluidic conduit that can be filled with a solution or with air, while the tool can be immersed in a liquid environment (Meister et al., 2009). An aperture at the end of the cantilever allows air or the liquids inside the cantilever to be dispensed locally. In the first part of this study, Model-MPs were first characterized using AFM to visualize the particles and obtain information on their roughness. Then FluidFM was used to probe their hydrophobic properties and probe their interaction with *Chlorella vulgaris* cells, a model green microalgae species. Finally, we describe these interactions by evaluating the possible contribution of EPS in the aggregation of cells.

2. Materials and methods

2.1. Microalgae strain and culture

The green freshwater microalgae *Chlorella vulgaris* strain CCAP 211/11B (Culture Collection of Algae and Protozoa, Scotland, UK) was cultivated in sterile conditions in Wright's cryptophyte (WC) medium prepared with deionized water (Guillard and Lorenzen, 1972). Cells were cultivated at 20 °C, under 120 rpm agitation, in an incubator equipped with white neon light tubes providing illumination of approximately 40 $\mu\text{mol photons m}^{-2} \text{s}^{-1}$, with a photoperiod of 18 h light: 6 h dark. All experiments were carried out with 7 days exponential phase batch cultures. Cells were first harvested by centrifugation (3000 rpm, 3 min at 21 °C), washed two times in phosphate buffered saline (PBS) at pH 7.4 and directly used for the AFM experiments and for some flocculation/flotation experiments (condition 3).

2.2. Microparticles model

The synthesis and full characterization of the high-density polyethylene (HDPE) microparticle model, are described elsewhere (Yakovenko et al., 2022). Briefly, two bulk polymeric materials were prepared, including UCNPs-labelled HDPE (Upcon-PE) and UCNPs-free HDPE (Blank-PE). The oleate-capped NaREF4 (RE = rare earth, 2% Er; 30% Yb; 68% Y) with a diameter of 20 nm were used to provide a green luminescent plastic that can be directly observed by eye under 976 nm irradiation. UCNPs were incorporated into the HDPE (CAS 9002-88-4, Sigma Aldrich, Saint Louis, MO, USA) matrix by dissolving the polymer in boiling o-xylene ($\geq 99.0\%$ (GC grade); Sigma Aldrich, Saint Louis, MO, USA), containing UCNPs in a 10 wt% HDPE:UCNPs ratio. The composite was separated from the reaction mixture by precipitation in the ice bath. The Blank-PE batch of polymer containing only HDPE was prepared following the same protocol. Microparticles model was obtained by exposing each bulk material to a cryogenic grinder (SPEX™ SamplePrep 6775 Freezer/Mill™, Delta Labo, Avignon, France). The resulting polymer particles were dispersed in ethanol and fractionated by subsequent cascade filtration to micro- and nanosized particles. The collected microparticles were named as μ -PE (HDPE microparticles), and μ -Upcon-PE (HDPE labelled with the inclusion of UCNPs as a luminescent tag). The full characterization of the Model-MPs in terms of particle size, shape, crystallinity, chemical composition, surface charge, and luminescence properties, are described elsewhere (Yakovenko et al., 2022).

2.3. Zeta potential measurements

Zeta-potential measurements for Model-MPs were carried out at 25 °C on a Zetasizer Nano-ZS (Malvern Instruments, Ltd., UK) equipped with a He-Ne laser ($\lambda = 633 \text{ nm}$) at an angle of 173°. Samples were prepared by dispersion of particles in 10 mM NaCl solution, to provide minimum level of conductivity in the samples, following ISO and ASTM standard guides (ASTM E2865-12, 2018). Before analysis, pH of every sample was measured. Zeta-potential and standard deviation (SD) were obtained from 5 measurements of 11 runs of 10 s using the Smoluchowski model (Yakovenko et al., 2022).

2.4. Model-MPs size measurements

Size measurements for Model-MPs were carried out by granulometry analysis using a Mastersizer MS3000 (Malvern Panalytical, UK) as described elsewhere (Yakovenko et al., 2022). Briefly, samples were prepared by dispersing the polymer powder in ethanol using HYDRO MV device with stirring at 2500 rpm. The refractive index used for ethanol and MPs were 1.36 and 1.52 respectively with an absorption index for particles of 0.1. Results are expressed as a percentage number. From these results, 90% of particles have a size below $\pm 15 \mu\text{m}$, 50% of particles have size below $\pm 6 \mu\text{m}$, and 10% of particles have a size below $\pm 4 \mu\text{m}$. These are approximate average values obtained from duplicates. The results are summarized in Table 1.

2.5. Flocculation/flotation experiments

To quantify the effects of Model-MPs on cell aggregation, flocculation/flotation separation of *C. vulgaris* was performed in dissolved air flotation (DAF) experiments in a homebuilt flotation device, shown in detail in Supplementary Fig. S1. The depressurization at atmospheric pressure of water saturated by air at 6 bar induced the formation of bubbles. Water free of algae was pressurized for 30 min before injection into the jars. The injection was controlled by a solenoid valve and 20 mL of pressurized water was added to each beaker sample. Prior to bubble injection, cells were left to flocculate during 15 min. Flocculation/flotation tests were conducted in three different conditions, in each case in triplicate, with cells coming from 2 independent cultures.

- **Condition 1:** *C. vulgaris* cells were cultured 7 days together with different concentrations of μ -PE and μ -Upcon-PE (final concentrations of 0, 5, 10 and 40 mg/L for μ -PE and 40 mg/L for μ -Upcon-PE) until they reached mid-exponential phase. Then 100 mL of cell suspension was directly poured into the test-jars with an initial $\text{OD}_{750 \text{ nm}}$ of 1.
- **Condition 2:** *C. vulgaris* cells were grown for 7 days until they reached mid-exponential phase. After that, 100 mL of cell suspension was directly poured into the test-jars with an initial $\text{OD}_{750 \text{ nm}}$ of 1. Then μ -PE and μ -Upcon-PE were separately added (final concentration of 40 mg/L) to the suspension, which was stirred at 100 rpm for 15 min to homogenize it before introduction of the bubbles.
- **Condition 3:** *C. vulgaris* cells were grown for 7 days until they reached mid-exponential phase. After that, cells were harvested by centrifugation at 3000 rpm for 3 min, then washed twice with PBS buffer at pH 7.4. After that, 100 mL of cell suspension was directly poured into the test-jars with an initial $\text{OD}_{750 \text{ nm}}$ of 1. Particles of μ -PE and μ -Upcon-PE were directly added (final concentration of 40 mg/L) to the suspension, which was stirred at 100 rpm for 15 min to homogenize it before introducing bubbles.

For all condition, after bubbles were introduced, the algal suspension was retrieved from the bottom of the test-jars: the first 5 mL of treated phase were discarded, the next 20 mL were used for quantifying flocculation/flotation efficiency. For that, the optical density of the withdrawn microalgae suspension was measured and compared to the optical density

Table 1
Summary of Model-MP characterization.

Sample	Zeta potential (mV)	Size distribution Dn (10) ^a	Size distribution Dn (50) ^b	Size distribution Dn (90) ^c
μ -PE	-71 \pm 7	4.3 \pm 0.0	5.6 \pm 0.1	11.9 \pm 1.1
μ -Upcon-PE	-73 \pm 8	4.12 \pm 0.3	5.7 \pm 0.5	13.25 \pm 0.9

^a 10% of the particles were observed to have sizes below the values given in the table.

^b 50% of the particles were observed to have sizes below the values given in the table.

^c 90% of the particles were observed to have sizes below the values given in the table.

of the microalgae suspension measured before the experiments. The flotation efficiency (E) was calculated according to the following Eq. (1).

$$E = \frac{OD_i \cdot V_i - OD_f \cdot V_f}{OD_i \cdot V_i} \quad (1)$$

2.6. Optical imaging experiments

Flocculation was directly observed after resuspension of the cells in PBS at pH 7.4 containing μ -PE or μ -Upcon-PE at a concentration of 40 mg/L. Flocculation levels were observed using an Axio Observer Z1 microscope (Zeiss, Germany) at high magnification ($\times 50$). To color EPS, an Alcian blue staining was used as described previously (Vergnes et al., 2019). To this end, a solution containing Alcian blue at a final concentration of 0.018% and 0.036% of acetic acid solution was deposited on the glass surfaces where cells were immobilized and allowed to stand for 15 min. Glass surfaces were then immersed in distilled water for 5 min in order to remove the nonfixed staining. Finally, images were recorded at high magnification ($\times 50$) using an Axio Observer Z1 microscope (Zeiss, Germany).

2.7. AFM imaging

For μ -PE and μ -Upcon-PE imaging, particles were immobilized on PDMS substrates. In each case at least 4 different particles were imaged in PBS at pH 7.4, using the Quantitative Imaging mode available on the Nanowizard III AFM (Bruker, USA), with MSCT cantilevers (Bruker, nominal spring constant of 0.01 N/m). Images were recorded with a resolution of 256 pixels \times 256 pixels, at an applied force of <1.0 nN and a constant approach/retract speed of 90 $\mu\text{m/s}$ (z -range of 3 μm). In all cases the cantilevers spring constants were determined by the thermal noise method prior to imaging (Hutter and Bechhoefer, 1993).

2.8. Roughness analyses

Roughness analyses were performed on 9 different μ -PE and μ -Upcon-PE particles immobilized on PDMS and on 10 different *C. vulgaris* cells coming from at least 2 independent cultures after incubation or not with Model-MPs for 7 days, immobilized on positively charged glass slides (Superfrost™ Plus adhesion, Eprexia, USA). Individual μ -PE and μ -Upcon-PE images were recorded in PBS whereas for cells, after incubation with Model-MPs, samples were directly imaged in culture medium using contact mode with a Nanowizard III AFM (Bruker, USA), using MSCT cantilevers (Bruker, nominal spring constant of 0.01 N/m). Images were recorded in contact mode using an applied force of <1 nN for micro-HDPE-(UCNPs) and of <0.5 for cells and the cantilever spring constants were determined by the thermal noise method prior to imaging (Hutter and Bechhoefer, 1993).

2.9. Hydrophobicity measurements

To measure the hydrophobic properties of materials, a recently developed method was used, which consists in measuring using fluidic force microscopy (FluidFM), the interactions between a bubble (hydrophobic surface) and materials (Demir et al., 2021). For that, FluidFM probes with an aperture of 8 μm of diameter (Cytosurge AG, Switzerland) were hydrophobized by coating with self-assembled monolayers (SAMs) of silanes via SAMs vapor deposition technique. FluidFM cantilevers were functionalized with 1H,1H,2H,2H-Perfluorodecyltrichlorosilane (FDTS) using an Orbis-1000 equipment (Memsstar, Livingston, UK) to make their external surface and inside microchannel hydrophobic. The deposition was realized under vacuum at 40 Torr and -40 °C, for 5 min. Then the microchannel of these silanized cantilevers was filled with air and the probe was immersed in PBS $1 \times$. To eliminate any particle or dust contamination or to prevent clogging of the FluidFM cantilever, a slight over

pressure of 20 mbar was applied. Then to produce a bubble at the aperture of the cantilever, a positive pressure of 200 mbar was applied inside the microfluidic cantilever in buffer. The silanized probes were calibrated using the thermal noise method before each measurement (Hutter and Bechhoefer, 1993). The interactions between the bubbles produced and MPs were then recorded in force spectroscopy mode using a maximum applied force of 2 nN, a constant approach/retraction speed of 3 $\mu\text{m/s}$, and a delay time of 1.0 s. For each conditions, areas of $0.5 \times 0.5 \mu\text{m}$ on 5 different MPs were probed. Adhesion forces were obtained by measuring the maximum adhesion force on the retract force curves obtained; data are presented in Supplementary Tables 1–3.

2.10. Force spectroscopy experiments using FluidFM technology

Force spectroscopy experiments were conducted using a NanoWizard III AFM (Bruker, USA), equipped with FluidFM technology (Cytosurge AG, Switzerland). In each case, experiments were performed in PBS, using micropipette probes with an aperture of 2 μm (spring constant of 0.3, and 4 N/m, Cytosurge AG, Switzerland). First, PBS at pH 7.4 was used to fill the probe reservoir (5 μL); by applying an overpressure (100 mBar) the PBS then filled the entire cantilever microchannel. The probe was then immersed in PBS and calibrated using the thermal noise method prior to measurement (Hutter and Bechhoefer, 1993). A single *C. vulgaris* cell was then aspirated from the surface of the Petri dish by approaching the FluidFM probe and applying a negative pressure (-200 mBar). The presence of the cell on the probe was verified by optical microscopy. The cell probe was then used to measure the interactions with Model-MPs. For that, μ -PE and μ -Upcon-PE solutions at a concentration of 40 mg/L were deposited on polydimethylsiloxane (PDMS) surfaces and left for 30 min. After that, the PDMS surfaces were rinsed using PBS and directly used. Interactions between single *C. vulgaris* cells aspirated at the aperture of FluidFM cantilevers and Model-MPs were recorded at a constant applied force of 2 nN, force curves were recorded with a z -range of up to 2 μm and a constant retraction speed of 2.0 $\mu\text{m/s}$ to 20 $\mu\text{m/s}$. In each case, at least 6 cells coming from 2 independent culture were probed. Data were analyzed using the Data Processing software from Bruker; they are presented in Supplementary Tables 4–6. Adhesion forces were obtained by measuring the maximum adhesion force for each retract curves. Experiments were repeated three times with ten different cells coming from at least three different cultures.

2.11. Two-photon microscopy

Samples were imaged on a Zeiss LSM-710 two-photon microscope, equipped with a Ti: Sapphire Chameleon Vision II laser (Coherent, Santa Clara, California), operating at 980 nm (2–3% of max power for UCNPs and 50% for *C. vulgaris* and μ -Upcon-PE samples, 140 f. pulses, 80 MHz repetition rate), and a Zeiss Plan-Apochromat $63 \times /1.40$ oil immersion lens. Upconverted light was collected between 490 and 600 nm for the green band, and 630 and 710 nm for the red band. Emission spectrum of analyzed samples were collected between 418 and 729 nm with a 10 nm step. Images were processed using ImageJ (Fiji) software (Yakovenko et al., 2022).

2.12. Statistical analysis

Experimental results represent the mean \pm standard deviation (SD) of at least three replicates. For each experiments, the number of replicates is indicated both in the Materials and methods section in the corresponding paragraphs, and in the Results and discussion section. For large samples ($n > 20$ values) unpaired student t -test was used to evaluate if the differences between the conditions are significant. For small samples ($n < 20$ values) non-parametric Mann and Whitney test was used to assess the differences. The differences were considered significant at $p < 0.05$.

3. Results and discussion

3.1. Model-MPs are irregular, have a rough surface and hydrophobic properties

The Model-MPs were derived from previous work (Yakovenko et al., 2022), where they were prepared from raw commercially available high-density polyethylene (PE). The top-down method consisted in the cryogenic grinding of the polymer or the nanocomposite (PE loaded with 10% UCNP) by high temperature swelling in xylene). This method is interesting because grinding is achieved at a temperature below the vitreous transition of PE and elastic substances are generally then more easily processed. The grinding at this temperature also prevents the chemical alteration of the PE backbone (this was ensured by infrared measurements) or morphological modification (calorimetric experiments) (Yakovenko et al., 2022). The size distribution of the particles obtained by granulometric analysis showed that around 90% of the particles in number were smaller than 15 μm . These Model-MPs (both $\mu\text{-PE}$ and $\mu\text{-Upcon-PE}$) were first characterized using AFM in contact mode. The images obtained are presented in Fig. 1. The 3D AFM height images (Fig. 1a and b) and vertical deflection (Fig. 1c and d) images recorded show that both types of Model-MPs have an irregular shape and a heterogeneous surface, like microplastics collected in the environment (ter Halle et al., 2016). In addition, they are found mostly aggregated on top of each other, and not present as single isolated particles. This is illustrated by the cross-sections taken along the longer sides of the particles in Fig. 2c and d, which clearly show this irregularity, with height variations over 6 nm in Fig. 1e and f. This tendency of Model-MPs to form aggregates could be explained by their hydrophobicity. Such behaviour is not observed with

model plastic micro- and nanospheres commercially available, which are formulated with different surfactant additives allowing to prevent this aggregation. However, these models are not reliable because their chemical properties and further interactions are different from the plastic particles found in the environment (Phuong et al., 2016).

We then acquired high resolution images on small areas ($5 \mu\text{m} \times 5 \mu\text{m}$) on top of the particles, using advanced quantitative imaging (QI) mode; the resulting images are shown in Fig. 1g–h. In this case, QI mode was used instead of contact mode because of the complexity of Model-MPs surfaces. QI being a force spectroscopy based imaging mode, there is no lateral forces exerted by the tip as occurring in contact mode, which can damage the sample (Chopinnet et al., 2013). This way we could obtain high-resolution images of the particles surface (Fig. 1i and j), and quantify their roughness. Roughness measurements were performed on 9 different particles for both type of Model-MPs (μPE and $\mu\text{-Upcon-PE}$); the results of these analysis are presented in the boxplot Fig. 1k. They show that $\mu\text{-PE}$ have an average roughness of $3.7 \pm 1.1 \text{ nm}$, which increases to $7.6 \pm 5.4 \text{ nm}$ when UCNP are incorporated in the particles ($\mu\text{-Upcon-PE}$). Although there is an important heterogeneity in the measurements in this last case, the difference with the $\mu\text{-PE}$ is not significantly different at 0.05 level (non-parametric Mann and Whitney test). This result thus shows that the incorporation of UCNP may affect the structure of Model-MPs, by modifying their surface morphology; however, the heterogeneity of the measurements performed on $\mu\text{-Upcon-PE}$ reflects the uncontrolled incorporation of the UCNP over the particles present in the sample (Yakovenko et al., 2022). The surface roughness of particles is an important physical characteristic that plays a major role in how they will behave in the environment and interact with

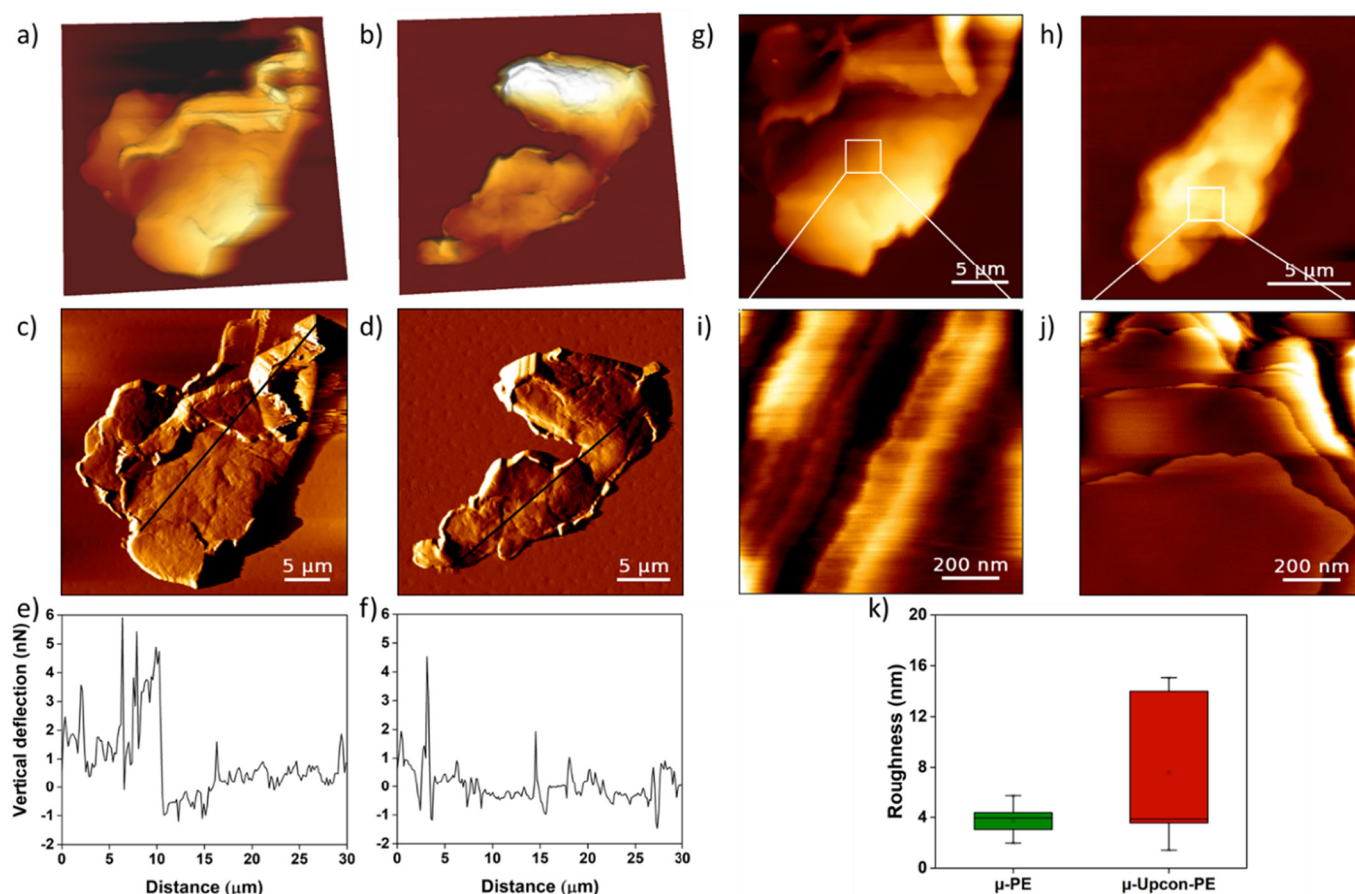


Fig. 1. Imaging and characterization of $\mu\text{-PE}$ surface before and after incorporation of UCNP: a) 3D AFM height image of $\mu\text{-PE}$ (color scale = 7 μm); b) 3D AFM height image of $\mu\text{-Upcon-PE}$ (color scale = 4 μm); c) Vertical deflection images of $\mu\text{-PE}$; d) Vertical deflection images of $\mu\text{-Upcon-PE}$; e) Cross section taken along the larger side in panel c and f) Cross section taken along the larger side in panel d; g) AFM height images of $\mu\text{-PE}$ (color scale = 7 μm) and h) AFM height images of $\mu\text{-Upcon-PE}$ (color scale = 5 μm); i) AFM height images of $\mu\text{-PE}$ surface ($5 \mu\text{m} \times 5 \mu\text{m}$) (color scale = 23 nm) and j) AFM height images of $\mu\text{-Upcon-PE}$ surface ($5 \mu\text{m} \times 5 \mu\text{m}$) (color scale = 19 nm); k) Quantification of $\mu\text{-PE}$ and $\mu\text{-Upcon-PE}$ surface roughness in a box plot.

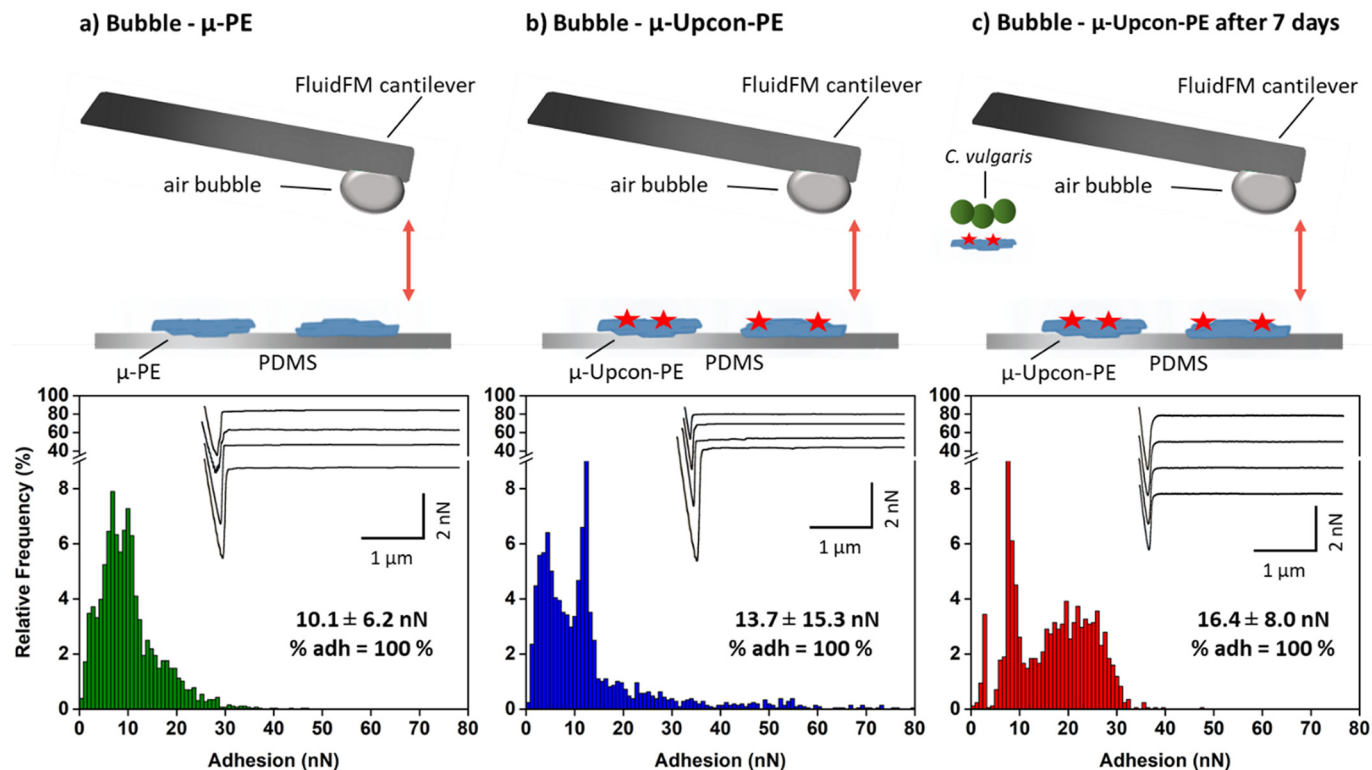


Fig. 2. Probing the interaction between bubble and Model-MPs: Adhesion force histogram obtained for the interaction between bubbles and a) μ -PE, b) μ -Upcon-PE, and c) μ -Upcon-PE after incubation for 7 days with *C. vulgaris* cells. Insets in a, b and c shows the representative force curves obtained during force spectroscopy experiments.

microorganisms. Commercially available models of micro- and nanospheres used for ecotoxicological studies are usually characterized by a very smooth surface (Phuong et al., 2016; Rubin et al., 2021), whereas plastic particles found in the environment are characterized by a rough surface (Roweczyk et al., 2020). Thus, our Model-MPs, which have a high average surface roughness, can be considered as a more reliable model to study the interactions between MPs and microorganisms such as *C. vulgaris*.

In the next step we then assessed the hydrophobic properties of the Model-MPs, which are an important physico-chemical factor that could greatly influence their interactions with microalgae. To this end, we used a recently developed method that consists in probing the interactions of samples with bubbles produced using FluidFM technology (Demir et al., 2021), which combines AFM with microfluidics (Meister et al., 2009). Air bubbles in water behave like hydrophobic surfaces. By producing them using FluidFM, it is then possible to probe their interactions with complex abiotic surfaces such as the MPs, and to measure their hydrophobic properties with accuracy. Such measurements allow avoiding usual issues related to other tests like water contact angle measurement (WCA). To perform these experiments, Model-MPs were immobilized on a PDMS substrate and their interactions with bubbles were measured in PBS buffer at pH 7.4 (Fig. 2a). For both μ -PE and μ -Upcon-PE, 5 different particles were probed. In the case of μ -PE, the retract force curves obtained (inset in Fig. 2a) show a single peak occurring at the contact point, typical of a hydrophobic interaction (Dague et al., 2007), with an average force of 10.1 ± 6.2 nN (Fig. 2a, $n = 2558$ force curves obtained from 5 different particles, adhesion values can be found in Supplementary Table 1). This force corresponds to the height of the adhesion peak, and thus to the force needed to break the interaction between the bubble and the sample. As a hydrophobic interface like bubbles interact with hydrophobic surfaces, then this force reflects the degree of hydrophobicity of the sample, the stronger the adhesion, the higher the hydrophobicity. Similarly, in the case of μ -Upcon-PE, a single peak occurring at the contact point is visible (inset in Fig. 2b); retract adhesion forces in this case were on average of 13.7 ± 15.3 nN (Fig. 2b, $n = 2107$ force curves obtained from 5 different

particles, adhesion values can be found in Supplementary Table 2). The large distribution of the adhesion values obtained in these experiments reflect the irregularities of the Model-MPs used that were visible on the height AFM images in terms of nanostructure. Indeed, in each case these irregularities change the contact area between the bubble and the particle, which can have an impact on the adhesion force value recorded. Thus in conclusion the two samples (μ -PE and μ -Upcon-PE) present hydrophobic properties as they are able to interact with bubbles with a relatively important force (for comparison, the interaction between *C. vulgaris* cell surface and bubbles give an average adhesion force of 4.2 nN, Demir et al., 2021). Plastic particles found in the environment probably have more hydrophilic properties, caused by plastic aging and oxidation (Liu et al., 2021). Thus the Model-MPs used in this study are a relevant model of plastic that has just entered the environment, prior to the oxidation process.

The experiments were then repeated with Model-MPs that were incubated with cells during their culture (7 days, Fig. 2c). In this case also, hydrophobic interactions are recorded, with an average adhesion force of 16.4 ± 8.0 nN ($n = 1685$ force curves obtained from 5 different particles, adhesion values can be found in Supplementary Table 3), a value that is significantly different from the two first conditions (p-value of 0.05, unpaired student test). Thus, the incubation of Model-MPs with cells changes their hydrophobic properties. This is an important point because it means that our Model-MPs, after seven days exposed to the cells, have their surface modified; a plausible hypothesis could be that cells produce EPS in the culture medium, which then could coat the particles surface. Finally, in order to confirm that the forces recorded are due only to the interactions between Model-MPs and bubbles, we also probed the interactions between bubbles and the PDMS surfaces used to immobilize the particles. The results presented in Supplementary Fig. S2 show an average adhesion force recorded of 1500 ± 100 nN ($n = 2500$ force curves). This adhesion force is much higher than the ones obtained with Model-MPs (maximum around 50 nN), thus meaning that we could precisely measure the interaction between bubbles and the particles without interfering with the surface on which they are immobilized. In the natural environment, microplastics undergo

alterations, including among multiple factors, oxidation of the polymer that changes its polarity and possibly its hydrophobicity (Andrady et al., 2011). FTIR analysis performed on the synthesized particle did not show any oxidation bands (Yakovenko et al., 2022). However, Model-MPs have a negative zeta potential and FTIR is most likely not sensitive enough to detect these functionalities if they are present in small proportions. Small microplastics and nanoplastics are expected to be negatively charged (Gigault et al., 2021). Because the particles synthesized here are also negatively charged, they have supposedly a similar behaviour than weathered plastic particles. Thus, altogether the biophysical characterization of the Model-MPs produced in this study show that they are aggregated, have a rough surface and present hydrophobic properties. MPs found in the environment have similar characteristics (Phuong et al., 2016), thus confirming the interest of our methodology to obtain particles close to what can be found in the environment. Our Model-MPs are thus a reliable model to understand the interactions that MPs can have with microalgae in the environment.

3.2. Model-MPs do not affect cell growth or morphology but have an effect on their aggregation

In a second part of the study, we evaluated the effects of Model-MPs on cell growth. In the literature, studies state that PS MPs of 100 μm have no toxic effect up to 50 mg/L (Yan et al., 2021), the same was reported for MPs of 1–5 μm , which had no effect on microalgae up to 41.5 mg/L (Prata et al., 2018). To verify whether it is the case for our Model-MPs

and our microalgae strain, we monitored the cell growth of *C. vulgaris*, incubated or not with Model-MPs at a concentration of 40 mg/L, which is the maximum concentration that we will use throughout this study. This concentration is most likely higher than the exposure concentrations encountered in the environment, however it allows us to observe and further characterize the effects on microalgae cells, which could not be detected otherwise. In addition, for small microplastics like the ones used in this study (5 μm), no data on their environmental concentrations are provided in the literature, as most studies report data for particles between 300 μm and 5 mm. It is thus difficult to predict the concentrations of small particles in a natural sample. The growth curves obtained are presented in Fig. 3a; they show that in each case cell growth is similar, thereby showing that neither $\mu\text{-PE}$ nor $\mu\text{-Upcon-PE}$ affect *C. vulgaris* cell growth. This is in good agreement with the data from the literature although the type of plastic used was not the same. In addition, this also shows that UCNPs are not toxic, as $\mu\text{-Upcon-PE}$ do not have an effect on cell growth. Moreover, incubation with Model-MPs do not extend the exponential phase, meaning that *C. vulgaris* cells and Model-MPs do not have a symbiotic relation either, as it was shown for other species. Indeed, Kang et al. observed that organic intermediates resulting from MPs degradation can serve as a carbon source for algae (Kang et al., 2019). Also in some cases, cell growth can be modified resulting from the EPS production (Casabianca et al., 2020; Cunha et al., 2019; Long et al., 2017), but this is not the case here.

We then went down to the nanometer scale to evaluate if the presence of Model-MPs in the culture medium had an effect on cell surface structure. For that, we incubated *C. vulgaris* during 7 days together with $\mu\text{-PE}$, and

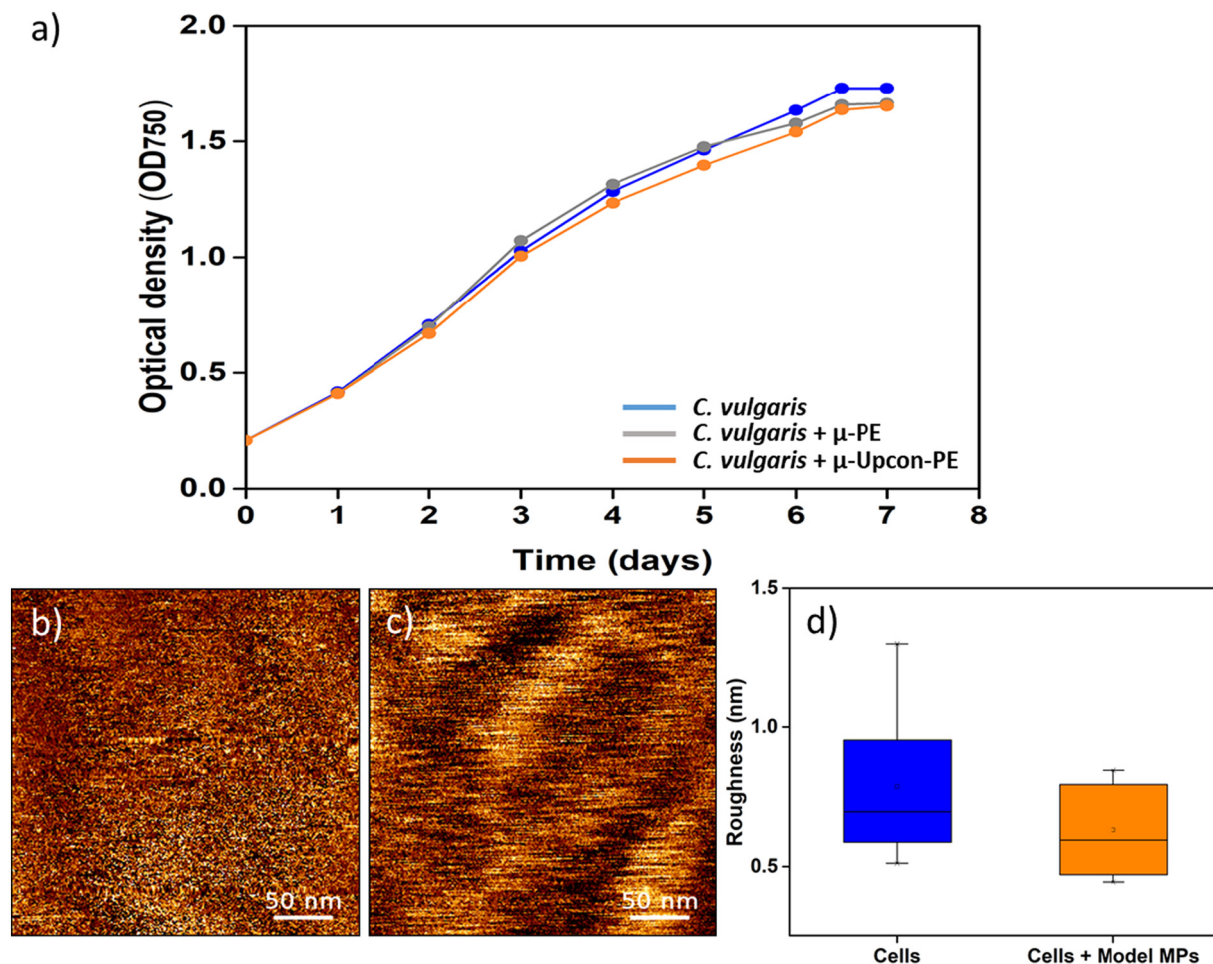


Fig. 3. Characterization of *C. vulgaris* cells in interaction with Model-MPs. a) Variations in optical density of *C. vulgaris* cells before and after incubated with Model-MPs ($\mu\text{-PE}$ and $\mu\text{-Upcon-PE}$); b) AFM height images of *C. vulgaris* cell surface ($0.3 \mu\text{m} \times 0.3 \mu\text{m}$) in contact mode (color scale = 6 nm) and c) AFM height images of *C. vulgaris* cell surface ($0.3 \mu\text{m} \times 0.3 \mu\text{m}$) after incubated 7 days together with Model-MPs in contact mode (color scale = 8 nm); d) Quantification roughness values of *C. vulgaris* cell before and after incubation with Model-MPs for 7 days in a box plot.

took a close look at the cell surface and measured the roughness on small areas ($0.3 \mu\text{m} \times 0.3 \mu\text{m}$) on top of the cells in contact mode, as shown in Fig. 3b and c in normal conditions or incubated with μ -PE for 7 days, respectively. These measurements were repeated on 10 different *C. vulgaris* cells coming from at least 2 independent cultures in each case; the results of these analysis are presented in the boxplot Fig. 3d. They show that *C. vulgaris* cells have an average roughness of $0.8 \pm 0.2 \text{ nm}$, which stays similar, of $0.6 \pm 0.2 \text{ nm}$, when cells are incubated with μ -PE. Cell wall roughness of *C. vulgaris* was determined before at different pH values (6 and 8) using AFM in a study by Demir et al. (Demir et al., 2020) and were in the same range. Overall, these data show that the Model-MPs used at concentrations up to 40 mg/L have no effect on either cell growth or cell nanostructure after 7 days of co-incubation.

Although our Model-MPs do not have an effect on *C. vulgaris* cell growth or cell nanostructure, their addition to the culture medium could have an influence on the cell aggregation. To evaluate this, we performed both optical microscopy imaging (Fig. 4a–c) and two-photon microscopy imaging (Fig. 4d–f). In these experiments, cells were incubated 7 days with μ -PE and μ -Upcon-PE at the concentration of 40 mg/L. In the control condition (Fig. 4a, without Model-MPs), we can see that cells are randomly distributed over the surface and no cell aggregation is observed. In the cases cells were incubated with μ -PE and μ -Upcon-PE (Fig. 4b and c), large aggregates of cells are visible around what seems to be Model-MPs particles, indicated by the arrows on the images.

Thus, these first images suggest that Model-MPs cause the aggregation of cells. However, because of the small size of Model-MPs, it is difficult to identify them with certainty and understand their real implication in cell aggregation. In a next experiment, we thus took advantage of the luminescence properties of μ -Upcon-PE, and made observations of cells incubated with μ -Upcon-PE for 7 days (concentration 40 mg/L) using a two-photon scanning microscope under an excitation at 980 nm (Yakovenko et al., 2022). On the bright field image (Fig. 5a) big aggregates of cells can be observed as well as what we expect to be μ -Upcon-PE particles. The composition of these aggregates was confirmed by the green (Fig. 5b) and red (Fig. 5c) emissions under NIR irradiation. In the case of μ -Upcon-PE, this emission corresponds to strong sharp green (515–575 nm) and red (630–680 nm) emission bands characteristic for Er-based UCNP incorporated into μ -Upcon-PE, as visible on the emission spectra in Fig. 5d. *C. vulgaris* cells are characterized by a weak autofluorescence (Takahashi, 2019; Tang and Dobbs, 2007), also visible on the spectra in Fig. 5d. Upconversion and autofluorescence spectra could be easily unmixed thanks to the limited spectra overlap especially in the green, and the discrepancy in signal intensity (varying from different order of magnitude) between upconversion and 2-photon emission (Fig. 5d). Brightfield as well as bi-photon images of UCNP alone, μ -Upcon-PE alone and *C. vulgaris* cells alone can be found in Supplementary Fig. S3. These results allow us not

only to accurately determine the presence and location of μ -Upcon-PE in cell aggregates, but also to show two different things: i) the μ -Upcon-PE are in fact distributed over a large part of the aggregate, which could not be visible on the standard optical microscopy images, and ii) some cells are not directly bound to the particles (cells in the bottom-left part on the image 5d–f), which suggest that perhaps the aggregation in the presence of Model-MPs can occur through a different mechanism than direct binding.

Because these observations are qualitative, we then looked for a way to quantify the effects of Model-MPs on cell aggregation, and performed flocculation/flotation experiments with different μ -PE concentrations (final concentration of 0, 5, 10 and 40 mg/L) incubated 7 days together with *C. vulgaris* cells. The results are presented in Supplementary Fig. S4. In such experiments, cells can be separated from the water by bubbles only if they are aggregated into flocs that are easily captured by the rising bubbles and carried to the surface. The flotation step allows separating the aggregated cells from the suspension, and thus to quantify the influence of Model-MPs on cell aggregation, which is reflected by the separation efficiency percentage. In this case using bubbles was more efficient than leaving the flocs to settle down because of their small size and low density. In the absence of Model-MPs, the separation efficiency obtained is of $16 \pm 5\%$; this number reflects the natural flocculation taking place in 7 days old-cultures, which is often the result of the natural production of EPS by cells (Vergnes et al., 2019). When adding Model-MPs at a concentration of 5 mg/L and 10 mg/L into the culture medium for the 7 days of the culture, the separation efficiencies are even lower, indicating that in these cases the addition of the MPs do not trigger any flocculation. This is an interesting point because it means that to obtain aggregation, the concentration of MPs must be important in the environment. Finally, as we expected from the optical microscopy experiments, when cells are incubated with Model-MPs at a concentration of 40 mg/L, the separation efficiency increases significantly, to around 50%, indicating that cell aggregation occurs, but does not reach the entire cell suspension. Different hypotheses could explain the fact that at this concentration only, cell aggregation occurs. The principal one could be that the presence of a certain concentration of Model-MPs in the medium during culture triggers the production of EPS, which can flocculate cells, as it has already been showed in the literature (Harrison et al., 2014; Lagarde et al., 2016; Yan et al., 2021).

To test this hypothesis, flocculation/flotation experiments were repeated at 40 mg/L concentration in different conditions (Fig. 6). In the first condition, Model-MPs were incubated for 7 days together with *C. vulgaris* cells before conducting the experiments. In the second condition, the cells in culture were not exposed to the Model-MPs, instead particles were added at the end of the culture, for 15 min before flocculation/flotation experiments. The comparison of the results obtained in these two conditions will help understanding if and how EPS interact with Model-MPs, or

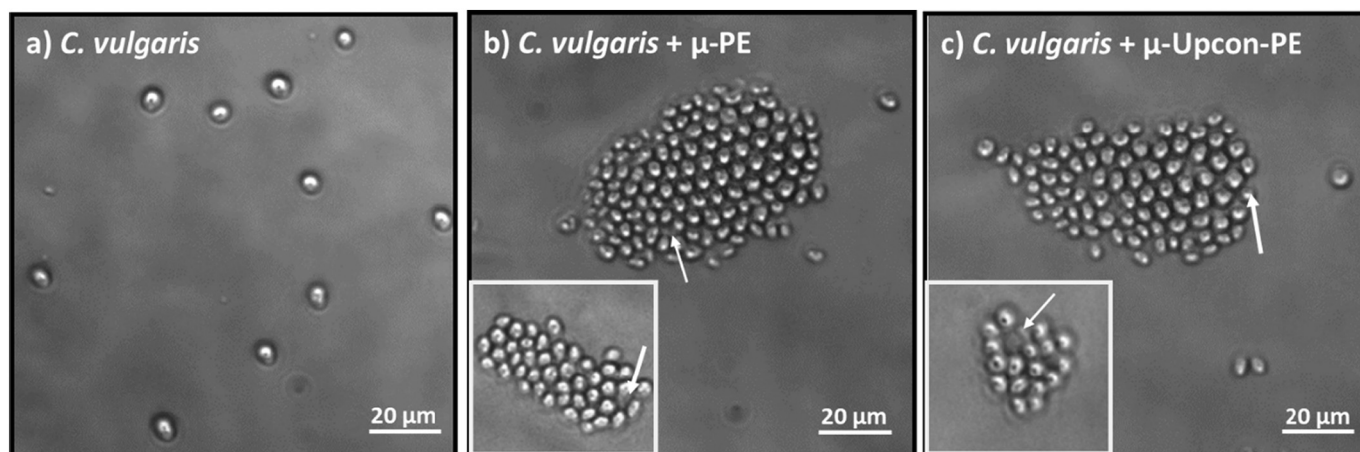


Fig. 4. Images of *C. vulgaris* cells. Bright field images of cells after incubated 7 days with: a) nothing; b) μ -PE; c) μ -Upcon-PE. The arrow indicated the Model-MPs.

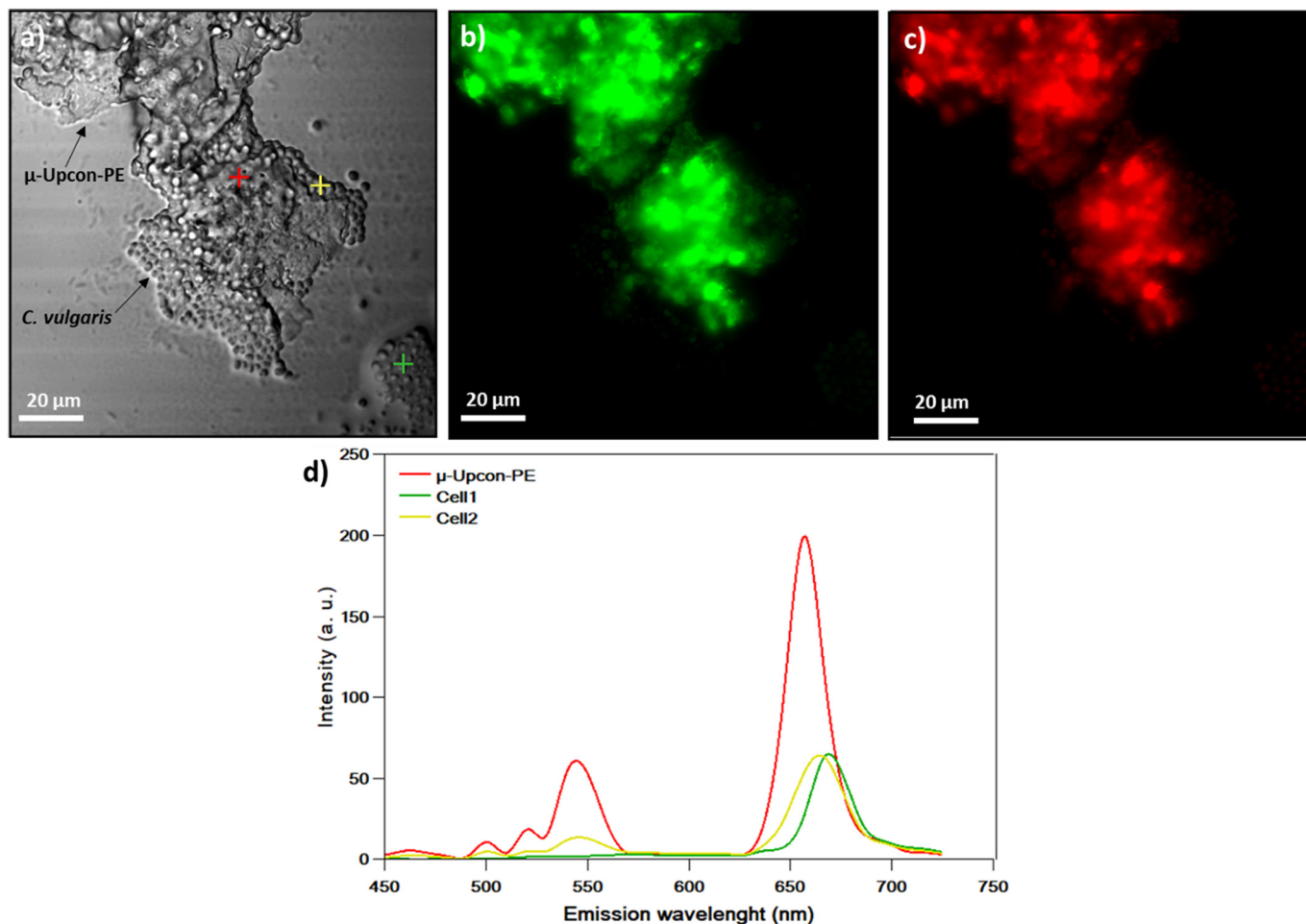


Fig. 5. Two-photon microscopy imaging of μ -Upcon-PE and *C. vulgaris* aggregate after 7 days inoculation together: a) Brightfield image; b) Green emission under NIR irradiation and c) red emission under NIR irradiation observed for μ -Upcon-PE and *C. vulgaris* aggregate. Images show Z-projection in a maximum intensity. d) Upconversion emission spectra of μ -Upcon-PE together with two-photon emission spectra of *C. vulgaris* cells. The positions where the spectra were recorded on the image is indicated by the colored crosses on a). (For interpretation of the references to color in this figure legend, the reader is referred to the web version of this article.)

if cells produce more EPS when they are cultured in the presence of these particles. Finally in the third condition, at the end of the cultures cells were washed in PBS to remove the EPS they may have produced, and then only Model-MPs were added for 15 min before flocculation/flotation experiments. The results obtained in each case are presented in Fig. 6, they show that there is no significant difference between condition 1 (flocculation efficiency of $51 \pm 11\%$ for μ -Upcon-PE) and condition 2 (flocculation efficiency of $61 \pm 4\%$ for μ -Upcon-PE), meaning that even if cells are not grown in the presence of Model-MPs, cell aggregation can still occur, and takes place rapidly as 15 min only are sufficient to obtain a separation efficiency similar to the one obtained in condition 1. An important point to note is that the modification of the Model-MPs used with UCNPs does not have an effect on the flocculation/flotation efficiency, as similar efficiencies are observed with both types of microparticles (μ -PE and μ -Upcon-PE). In condition 3, when EPS are removed from the cells by centrifugation, the separation efficiency stays similar when μ -PE are used (flocculation efficiency of $47 \pm 19\%$ for μ -PE), and decreases to $18 \pm 19\%$ when μ -Upcon-PE are used. Note that in this case, the standard deviations obtained are large; non-parametric statistical test (Mann and Whitney test) showed that the differences with condition 1 and condition 2 are in fact not significant when both samples are used (μ -PE and μ -Upcon-PE). But still, these large standard deviations obtained in conditions 3, even if the differences are not significant, tend to suggest that EPS could be involved in the aggregation of cells, which may interact with MPs when they are added to the culture media.

3.3. Model-MPs induced aggregation can take place through different mechanisms

To understand if the presence of EPS is an important factor or not in the aggregation of cells in the presence of Model-MPs, we performed additional optical microscopy assays using Alcian blue staining. This dye is known to react specifically with acidic polysaccharides (Reddy et al., 1996; Shiraishi, 2015; Vergnes et al., 2019) present in the EPS excreted by microalgae cells, thus we selected this technique to qualitatively evaluate the presence of EPS excreted by cells grown in presence of Model-MPs. The images obtained are presented in Fig. 7. They show that when cells are grown without Model-MPs (Fig. 7a), cells produce EPS in a small amount. In particular, we can see here the presence of small cell aggregates that are entrapped with the EPS visible on the image (Fig. 7a). This is in line with the flocculation/flotation results obtained that shows that cells without MPs can still be separated with an efficiency of 16% (Supplementary Fig. S3). When cells have grown for 7 days in the presence of Model-MPs, large aggregates of cells are visible on the images, on which large amounts of EPS can be observed (Fig. 7b and c). These observations thus suggest that the presence of Model-MPs in the culture medium triggers the production of EPS, as the cells use them as a support to form biofilms around them (Yan et al., 2021), which is in line with the previous literature on this subject (Harrison et al., 2014; Lagarde et al., 2016; Yan et al., 2021). When we put these observations in perspective with the flocculation/flotation tests performed before, it seems that the separation efficiency that we obtain

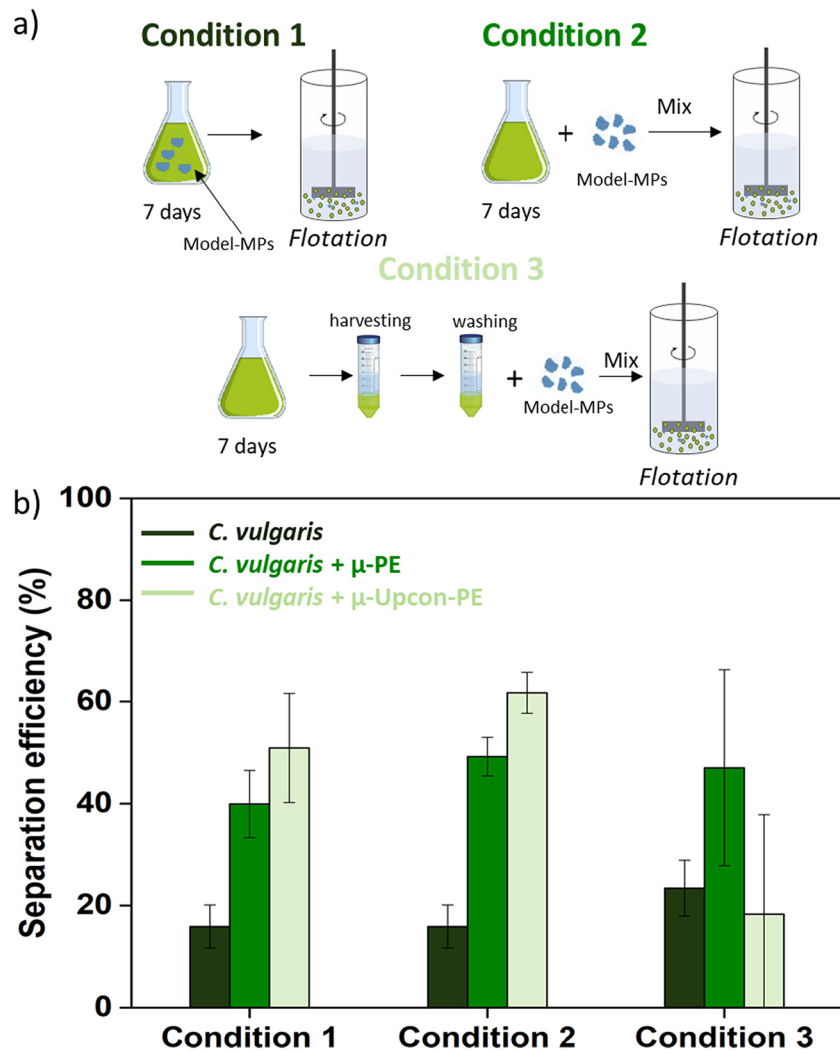


Fig. 6. Flocculation experiments of *C. vulgaris*. a) Schematic representation of the conditions used for flotation/flocculation experiments. Condition 1: Model-MPs + cells after 7 days incubation together (no washing). Condition 2: Model-MPs are directly added to cells (no washing). Condition 3: Model-MPs are directly added to cells (washing PBS). b) *C. vulgaris* cell separation efficiency with Model-MPs (μ -PE and μ -Upcon-PE) at 40 mg/L concentration under the different conditions described in a).

when cells have been grown for 7 days with the MPs is due to the increased production of EPS by the cells in a biofouling process. However, the direct interaction of Model-MPs with cells seem also to induce aggregation (Fig. 6 condition 2); as it can be seen on these images (Fig. 7b and c), cells do produce some EPS even if not grown with MPs, and the decreasing trend of the separation efficiency obtained when cells were washed before flocculation/flocculation experiments (Fig. 6, condition 3) would suggest that MPs can interact directly with these EPS. The fact that the separations efficiencies when cells washed are not significantly different could also suggest that this interaction could also be in part directly with the cell wall of cells. Another interesting point is that when cells have been grown with MPs, a certain concentration is needed to induce cell aggregation: in this case this would mean that both the production of EPS and the aggregation induced by contact between MPs and cells is concentration dependent. When there are not enough MPs in the medium, the surface area of flocculant (MPs) could be too small compared to the surface area of cells to aggregate them.

While these results together bring explanations on the mechanism by which Model-MPs induce the aggregation of cells, a final point needs to be clarified; are the Model-MPs able to directly interact with cells? This would allow understanding why cells that have been in contact with MPs during 15 min only can be aggregated, and also why removing the EPS from cells does not decrease significantly the separation efficiency. To

this end, we performed force-spectroscopy experiments to probe the interactions between single *C. vulgaris* cells and Model-MPs. In these experiments, cells have been washed to remove the EPS from the surface, this way it will be possible to directly probe the interactions between the cell's interface and the Model-MPs. For that, we used FluidFM technology, where single *C. vulgaris* cells are aspirated at the aperture of FluidFM probes by exerting a negative pressure inside the microfluidic cantilever. This negative pressure, compared to classic single-cell force spectroscopy methods using AFM, has the advantage of keeping the cells stable on the cantilever even when in contact with a strongly adhesive surface (Demir et al., 2020). The results of these experiments are presented in Fig. 8. In the case of μ -PE (Fig. 8a), the retract force curves obtained present a single retract peak happening close to the contact point, similar to what was observed with bubbles, with an average force of 14.6 ± 15.3 nN ($n = 2713$ force curves with 8 cells and particles coming from 2 different cultures, adhesion values can be found in Supplementary Table 4). As for the interactions with bubbles, this force signature is typical of non-specific interactions, and most likely reflect hydrophobic interactions, rather strong, between *C. vulgaris* cells and μ -PE. Similar force curves were obtained for μ -Upcon-PE with a similar average adhesion force of 15.4 ± 15.8 nN ($n = 3470$ force curves with 10 cells and particles coming from 2 different cultures, adhesion values can be found in Supplementary Table 5) shown in Fig. 8b. The adhesion forces are not significantly

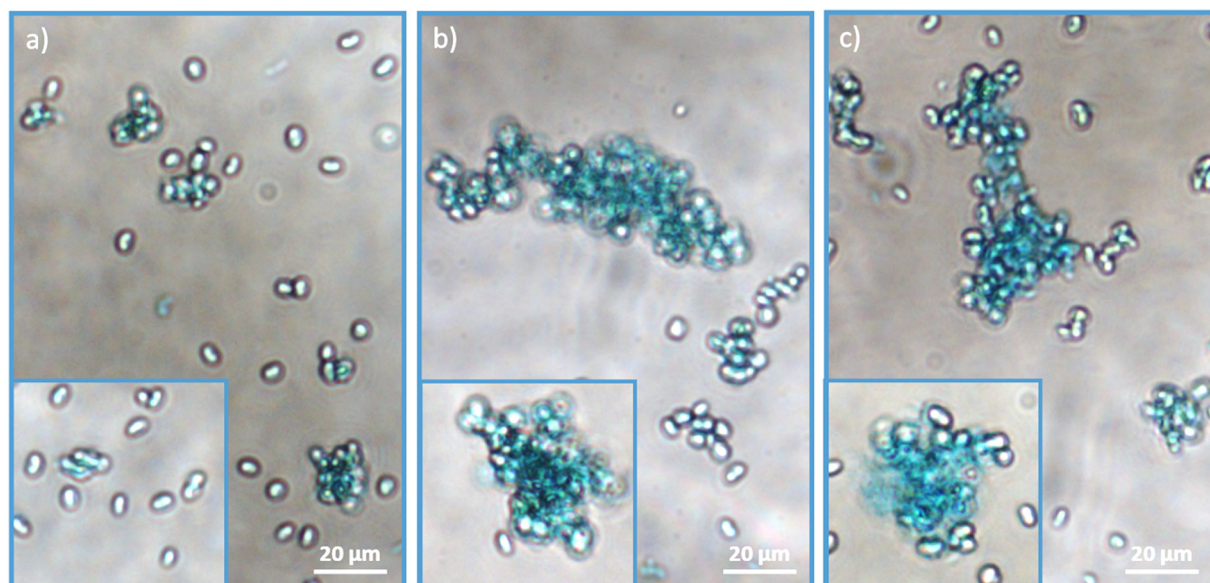


Fig. 7. Staining EPS produced by *C. vulgaris* with Alcian blue. Optical images of cells dyed with Alcian blue, a) grown in normal conditions for 7 days, b) grown in the presence of 40 mg/L of μ -PE during 7 days, and c) grown in the presence of 40 mg/L of μ -Upcon-PE during 7 days. (For interpretation of the references to color in this figure legend, the reader is referred to the web version of this article.)

different at a p-value of 0.05 (unpaired student test). This is in line with the previous flocculation/flotation experiments, incorporating UCNPs to the μ -PE does not affect their interaction with *C. vulgaris* cells. Thus, these results first show that there is indeed an interaction between cells and Model-MPs, and that these interactions are nonspecific and hydrophobic. Recently, we evaluated the hydrophobicity of *C. vulgaris* by measuring the interaction between air bubble and single *C. vulgaris* cells (Demir et al., 2021), and found an average adhesion force of 4.2 nN (Demir et al., 2021), showing that the surface of cells is not completely hydrophilic and has hydrophobic properties. It thus means that Model-MPs can interact with cells directly through a hydrophobic interaction. This is also in line with the bi-photon imaging experiment where microparticles directly in contact with cells can be observed. To verify that no other type of non-specific interactions are involved, like electrostatic interactions, additional force spectroscopy experiments were performed between *C. vulgaris* and μ -Upcon-PE at higher salt concentrations (Fig. 8c). When we increase the salt concentration by adding 500 mM of NaCl in PBS buffer (0.137 M of NaCl) at pH 7.4, the charges present on *C. vulgaris* cells and Model-MPs are shielded. Although the average adhesion force recorded is 11.0 ± 9.0 nN ($n = 1785$ force curves with 6 cells and particles coming from 2 different cultures, adhesion values can be found in Supplementary Table 6), given the wide distribution of the values obtained, it is in the same range as for cells without salt addition. But still the difference is significant (unpaired *t*-test, p-value of 0.05), meaning that electrostatic interactions are involved, but they are not dominant compared to hydrophobic interactions. An interesting point to note concerns the wide distribution of the adhesion values obtained in each case. This heterogeneity can be explained by the fact that in each case we aspirated a different cell. As we have no control over the cell sizes depending on their age, the contact area in each case is different, resulting in different adhesion values. Also, this heterogeneity in the results may be associated with the surface structure of the Model-MPs which is irregular, perhaps modifying the contact area and the adhesion forces recorded. Indeed, when we look at the adhesion forces obtained throughout the surface of the microparticles scanned, we can see that as the cantilever moves on the surface, the Model-MPs adhesion force does not stay constant over consecutive measurements (decreases or increases, Supplementary Fig. S5). Finally, to confirm that the forces recorded are due to only interactions of cells with microparticles, we probed the interactions between *C. vulgaris*

cells and the surfaces which Model-MPs are immobilized on, i.e., PDMS. The results presented in Supplementary Fig. S6a and b show that neither *C. vulgaris* - PDMS nor FluidFM cantilever-Model-MPs interaction occurs, confirming that the interactions described here indeed take place between cells and Model-MPs.

Altogether, these results show that Model-MPs-induced aggregation can take place through different mechanisms. When cells have been grown in the presence of MPs, they use the MPs as a support for forming biofilms which triggers the production of EPS and the further aggregation of cells. However, MPs can also flocculate the cells by directly interacting with them, with their cell surface directly and also with the small amount of EPS they produce at their surface in normal conditions.

4. Conclusions

The ubiquitous presence of plastic in all environmental compartments raises great concern about their potential negative impact on aquatic ecosystems in general. In recent decades, many research efforts have focused on understanding the inclusion, transport, and effects of microplastics on the aquatic trophic chain from zooplankton to mammals. However not much is known about the interaction of MPs with primary producers such as microalgae, which are the base of the trophic chain. This study presents an original interdisciplinary work that allows understanding the interactions between environmentally relevant models of MPs and microalgae cells and the consequences of such interaction. The biophysical characterization of the Model-MPs used in this study showed that these particles are rough and irregular, similar to the ones found in the environment, and also present hydrophobic properties. Then, the combination of optical microscopy imaging assays and population-scale flocculation/flotation experiments allowed us to understand the role of MPs in the aggregation of cells. Our results showed that when cells are grown in the presence of MPs, they produce more EPS responsible for cell aggregation. However, the aggregation can also be induced by the direct contact between MPs and the cell surface or the EPS they produce naturally in normal culture conditions. This was confirmed by single-cell force spectroscopy experiments, which also led us to describe the physico-chemical nature of the interactions between Model-MPs and cells. Altogether, the experimental approach developed in this study has proven powerful to highlight the

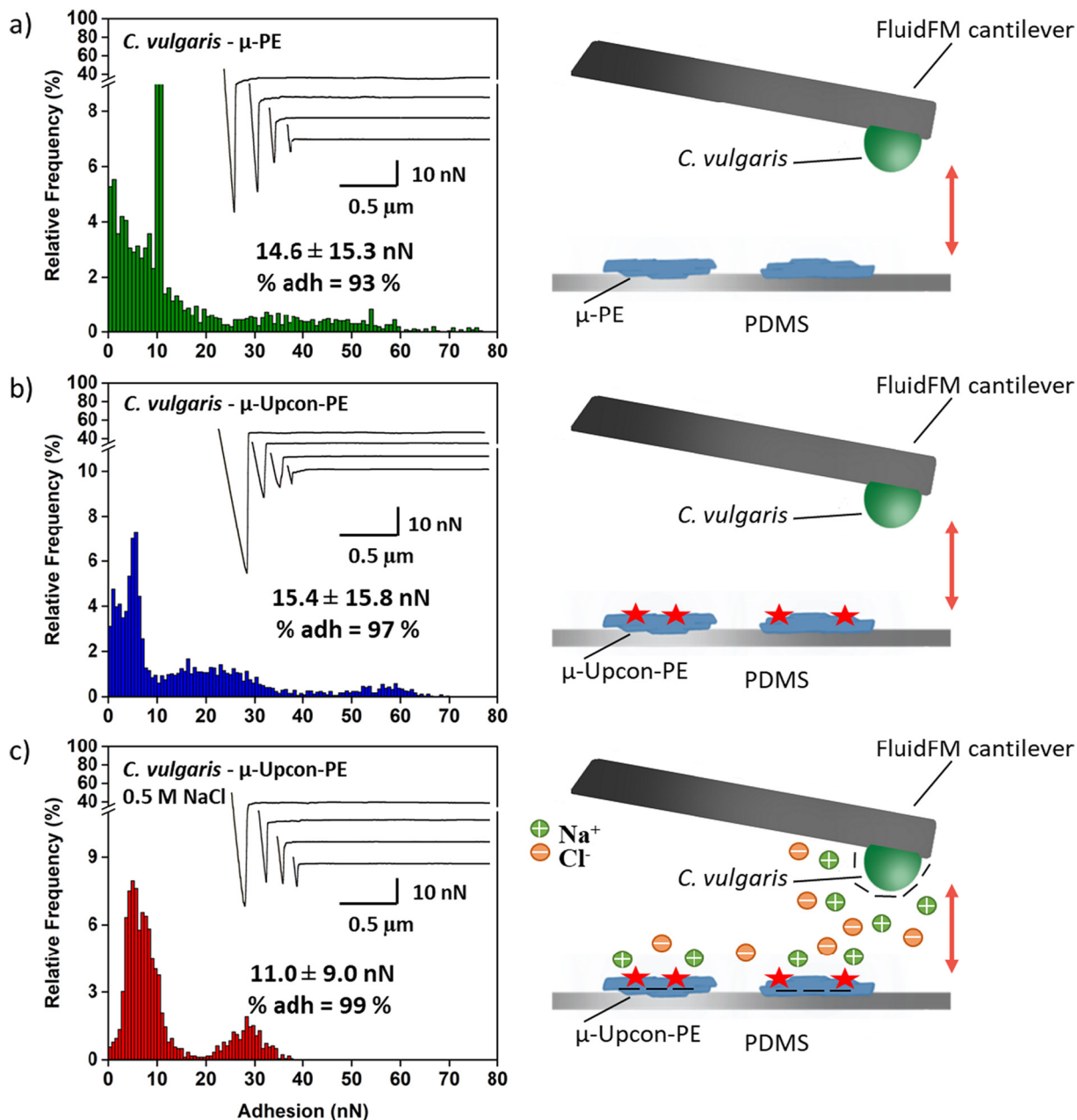


Fig. 8. Probing the interactions between *C. vulgaris* cells and Model-MPs. Histogram showing the distribution of adhesion forces Adhesion force histogram obtained for the interaction between *C. vulgaris* cells and a) μ -PE, b) μ -Upcon-PE, and c) μ -Upcon-PE after 0.5 M NaCl addition. Insets in a, b and c shows the representative force curves obtained during force spectroscopy experiments.

complexity of MPs-microalgae interactions and understand the role of MPs in the formation of cell aggregates. This new information are important to apprehend the impact of plastic pollution on aquatic ecosystems on a large scale.

CRediT authorship contribution statement

Irem Demir-Yilmaz: Methodology, Formal analysis, Investigation, Writing – Original draft.

Nadiia Yakovenko: Methodology, Formal analysis, Investigation, Writing – Original draft.

Clément Roux: Conceptualization, Methodology, Supervision, Writing – Review and Editing, Funding acquisition.

Pascal Guiraud: Conceptualization, Methodology, Supervision, Writing – Review and Editing.

Fabrice Collin: Conceptualization, Methodology, Supervision, Writing – Review and Editing.

Christophe Coudret: Conceptualization, Methodology, Supervision, Writing – Review and Editing, Funding acquisition

Alexandra ter Halle: Conceptualization, Methodology, Supervision, Writing – Review and Editing, Funding acquisition.

Cécile Formosa-Dague: Conceptualization, Methodology, Supervision, Writing – Original draft, Funding acquisition.

Declaration of competing interest

The authors declare that they have no known competing financial interests or personal relationships that could have appeared to influence the work reported in this paper.

- microscopy and nanofluidics in a universal liquid delivery system for single cell applications and beyond. *Nano Lett.* 9, 2501–2507. <https://doi.org/10.1021/nl901384x>.
- Nava, V., Leoni, B., 2021. A critical review of interactions between microplastics, microalgae and aquatic ecosystem function. *Water Res.* 188, 116476. <https://doi.org/10.1016/j.watres.2020.116476>.
- Oberbeckmann, S., Löder, M.G., Labrenz, M., 2015. Marine microplastic-associated biofilms—a review. *Environ. Chem.* 12, 551–562. <https://doi.org/10.1071/EN15069>.
- Peng, L., Fu, D., Qi, H., Lan, C.Q., Yu, H., Ge, C., 2020. Micro- and nano-plastics in marine environment: source, distribution and threats — a review. *Sci. Total Environ.* 698, 134254. <https://doi.org/10.1016/j.scitotenv.2019.134254>.
- Phuong, N.N., Zalouk-Vergnoux, A., Poirier, L., Kamari, A., Châtel, A., Mouneyrac, C., Lagarde, F., 2016. Is there any consistency between the microplastics found in the field and those used in laboratory experiments? *Environ. Pollut.* 211, 111–123. <https://doi.org/10.1016/j.envpol.2015.12.035>.
- Pillet, F., Chopinet, L., Formosa, C., Dague, É., 2014. Atomic Force Microscopy and pharmacology: from microbiology to cancerology. *Biochim. Biophys. Acta Gen. Subj.* 1840, 1028–1050. <https://doi.org/10.1016/j.bbagen.2013.11.019>.
- Plastics Europe, 2020. *Plastics - The Facts 2020*.
- Prata, J.C., Lavorante, B.R.B.O., B.S.M. Montenegro, M.da C., Guilhermino, L., 2018. Influence of microplastics on the toxicity of the pharmaceuticals procainamide and doxycycline on the marine microalgae *Tetraselmis chuii*. *Aquat. Toxicol.* 197, 143–152. <https://doi.org/10.1016/j.aquatox.2018.02.015>.
- Reddy, K.J., Soper, B.W., Tang, J., Bradley, R.L., 1996. Phenotypic variation in exopolysaccharide production in the marine, aerobic nitrogen-fixing unicellular cyanobacterium *Cyanothece* sp. *World J. Microbiol. Biotechnol.* 12, 311–318. <https://doi.org/10.1007/BF00340206>.
- Reisser, J., Shaw, J., Hallegraef, G., Proietti, M., Barnes, D.K.A., Thums, M., Wilcox, C., Hardesty, B.D., Pattiaratchi, C., 2014. Millimeter-sized marine plastics: a new pelagic habitat for microorganisms and invertebrates. *PLOS ONE* 9, e100289. <https://doi.org/10.1371/journal.pone.0100289>.
- Rowenczyk, L., Dazzi, A., Deniset-Besseau, A., Beltran, V., Goudounèche, D., Wong-Wah-Chung, P., Boyron, O., George, M., Fabre, P., Roux, C., Mingotaud, A.F., ter Halle, A., 2020. Microstructure characterization of oceanic polyethylene debris. *Environ. Sci. Technol.* 54, 4102–4109. <https://doi.org/10.1021/acs.est.9b07061>.
- Rowenczyk, L., Leflaive, J., Clergeaud, F., Minet, A., Ferriol, J., Gauthier, L., Gigault, J., Mouchet, F., Ory, D., Pinelli, E., Albignac, M., Roux, C., Mingotaud, A.F., Silvestre, J., Ten-Hage, L., Ter Halle, A., 2021. Heteroaggregates of polystyrene nanospheres and organic matter: preparation, characterization and evaluation of their toxicity to algae in environmentally relevant conditions. *Nanomaterials (Basel)* 11, 482. <https://doi.org/10.3390/nano11020482>.
- Rubin, A.E., Sarkar, A.K., Zucker, I., 2021. Questioning the suitability of available microplastics models for risk assessment – a critical review. *Sci. Total Environ.* 788, 147670. <https://doi.org/10.1016/j.scitotenv.2021.147670>.
- Rummel, C.D., Jahnke, A., Gorokhova, E., Kühnel, D., Schmitt-Jansen, M., 2017. Impacts of biofilm formation on the fate and potential effects of microplastic in the aquatic environment. *Environ. Sci. Technol. Lett.* 4, 258–267. <https://doi.org/10.1021/acs.estlett.7b00164>.
- Shiraishi, H., 2015. Association of heterotrophic bacteria with aggregated *Arthrospira platensis* exopolysaccharides: implications in the induction of axenic cultures. *Biosci. Biotechnol. Biochem.* 79, 331–341. <https://doi.org/10.1080/09168451.2014.972333>.
- Singh, U.B., Ahluwalia, A.S., 2013. Microalgae: a promising tool for carbon sequestration. *Mitig. Adapt. Strateg. Glob. Chang.* 18, 73–95. <https://doi.org/10.1007/s11027-012-9393-3>.
- Sjollema, S.B., Redondo-Hasselerharm, P., Leslie, H.A., Kraak, M.H.S., Vethaak, A.D., 2016. Do plastic particles affect microalgal photosynthesis and growth? *Aquat. Toxicol.* 170, 259–261. <https://doi.org/10.1016/j.aquatox.2015.12.002>.
- Song, C., Liu, Z., Wang, C., Li, S., Kitamura, Y., 2020. Different interaction performance between microplastics and microalgae: the bio-elimination potential of *Chlorella* sp. L38 and *Phaeodactylum tricornutum* MASCC-0025. *Sci. Total Environ.* 723, 138146. <https://doi.org/10.1016/j.scitotenv.2020.138146>.
- Takahashi, T., 2019. Routine management of microalgae using autofluorescence from Chlorophyll. *Molecules* <https://doi.org/10.3390/molecules24244441>.
- Tang, Y.Z., Dobbs, F.C., 2007. Green autofluorescence in dinoflagellates, diatoms, and other microalgae and its implications for vital staining and morphological studies. *Appl. Environ. Microbiol.* <https://doi.org/10.1128/AEM.01741-06>.
- ter Halle, A., Ladirat, L., Gendre, X., Goudouneche, D., Pusineri, C., Routaboul, C., Tenailleau, C., Duployer, B., Perez, E., 2016. Understanding the fragmentation pattern of marine plastic debris. *Environ. Sci. Technol.* 50, 5668–5675. <https://doi.org/10.1021/acs.est.6b00594>.
- Tunali, M., Uzoefuna, E.N., Tunali, M.M., Yenigun, O., 2020. Effect of microplastics and microplastic-metal combinations on growth and chlorophyll a concentration of *Chlorella vulgaris*. *Sci. Total Environ.* 743, 140479. <https://doi.org/10.1016/j.scitotenv.2020.140479>.
- Vergnes, J.B., Gernigon, V., Guiraud, P., Formosa-Dague, C., 2019. Bicarbonate concentration induces production of exopolysaccharides by *Arthrospira platensis* that mediate bioflocculation and enhance flotation harvesting efficiency. *ACS Sustain. Chem. Eng.* 7, 13796–13804. <https://doi.org/10.1021/acssuschemeng.9b01591>.
- Wingender, J., Neu, T.R., Flemming, H.-C. (Eds.), 1999a. *Microbial Extracellular Polymeric Substances: Characterization, Structure And Function*. Springer-Verlag, Berlin Heidelberg <https://doi.org/10.1007/978-3-642-60147-7>.
- Wingender, J., Neu, T.R., Flemming, H.-C., 1999b. What are bacterial extracellular polymeric substances? In: Wingender, J., Neu, T.R., Flemming, H.-C. (Eds.), *Microbial Extracellular Polymeric Substances: Characterization, Structure And Function*. Springer, Berlin, Heidelberg, pp. 1–19. https://doi.org/10.1007/978-3-642-60147-7_1.
- Wu, Y., Guo, P., Zhang, X., Zhang, Y., Xie, S., Deng, J., 2019. Effect of microplastics exposure on the photosynthesis system of freshwater algae. *J. Hazard. Mater.* 374, 219–227. <https://doi.org/10.1016/j.jhazmat.2019.04.039>.
- Xiao, J., Dufrêne, Y.F., 2016. Optical and force nanoscopy in microbiology. *Nat. Microbiol.* 1, 1–13. <https://doi.org/10.1038/nmicrobiol.2016.186>.
- Xiao, R., Zheng, Y., 2016. Overview of microalgal extracellular polymeric substances (EPS) and their applications. *Biotechnol. Adv.* 34, 1225–1244. <https://doi.org/10.1016/j.biotechadv.2016.08.004>.
- Xiao, Y., Jiang, X., Liao, Y., Zhao, W., Zhao, P., Li, M., 2020. Adverse physiological and molecular level effects of polystyrene microplastics on freshwater microalgae. *Chemosphere* 255, 126914. <https://doi.org/10.1016/j.chemosphere.2020.126914>.
- Yakovenko, N., Amouroux, B., Albignac, M., Collin, F., Roux, C., Mingotaud, A.-F., Roblin, P., Coudret, C., Halle, A.T., 2022. Top-down synthesis of luminescent microplastics and nanoplastics by incorporation of upconverting nanoparticles for environmental assessment. <https://doi.org/10.26434/chemrxiv-2022-c5nlv>.
- Yan, Z., Xu, L., Zhang, W., Yang, G., Zhao, Z., Wang, Y., Li, X., 2021. Comparative toxic effects of microplastics and nanoplastics on *Chlamydomonas reinhardtii*: growth inhibition, oxidative stress, and cell morphology. *J. Water Process Eng.* 43, 102291. <https://doi.org/10.1016/j.jwpe.2021.102291>.
- Zantis, L.J., Carroll, E.L., Nelms, S.E., Bosker, T., 2021. Marine mammals and microplastics: a systematic review and call for standardisation. *Environ. Pollut.* 269, 116142. <https://doi.org/10.1016/j.envpol.2020.116142>.
- Zhang, C., Chen, X., Wang, J., Tan, L., 2017. Toxic effects of microplastic on marine microalgae *Skeletonema costatum*: interactions between microplastic and algae. *Environ. Pollut.* 220, 1282–1288. <https://doi.org/10.1016/j.envpol.2016.11.005>.
- Zhang, Y., Kang, S., Allen, S., Allen, D., Gao, T., Sillanpää, M., 2020. Atmospheric microplastics: a review on current status and perspectives. *Earth Sci. Rev.* 203, 103118. <https://doi.org/10.1016/j.earscirev.2020.103118>.

Appendix 2: Investigation of the role of cell hydrophobicity and EPS production in the aggregation of the marine diatom *Cylindrotheca closterium* under salinity stress

Investigation of the role of cell hydrophobicity and EPS production in the aggregation of the marine diatom *Cylindrotheca closterium* under salinity stress

Irem Demir-Yilmaz^{1,2,‡}, Nives Novosel^{3,‡}, Maja Levak Zorinc³, Tea Mišić Radić³, Malak Souad Ftouhi¹,
Pascal Guiraud^{1,4}, Nadica Ivošević DeNardis^{3*} and Cécile Formosa-Dague^{1,4*}

¹ TBI, Université de Toulouse, INSA, INRAE, CNRS, Toulouse, France

² LAAS, Université de Toulouse, CNRS, Toulouse, France

³ Division for Marine and Environmental Research, Ruđer Bošković Institute, Zagreb, Croatia

⁴ Fédération de Recherche Fermat, CNRS, Toulouse, France

‡ These two authors equally contributed to the work

Corresponding authors:

Cécile Formosa-Dague, formosa@insa-toulouse.fr, Nadica Ivošević DeNardis, ivosevic@irb.hr

Abstract

Aggregation of diatoms is of global importance to understand settling of particulate organic carbon in aquatic systems. In this study, we investigate the aggregation of the marine diatom *Cylindrotheca closterium* during the exponential growth phase under hypo-saline conditions. The results of the flocculation/flotation experiments show that the aggregation of the diatom depends on the salinity. At a salinity of 35, which is considered to be favorable growth conditions for diatoms, the highest aggregation is achieved. To explain these observations, we used a surface approach combining atomic force microscopy (AFM) and electrochemical methods to characterize both the cell surface properties and the structure of the extracellular polymeric substances (EPS) cell produce, and to quantify the amount of surface-active organic matter released. At a salinity of 35, the results showed that diatoms are soft, hydrophobic and release only small amounts of EPS organized into individual short fibrils. In contrast, diatoms adapt to a salinity of 5 by becoming much stiffer and more hydrophilic, producing larger amounts of EPS that structurally form an EPS network. Both adaptation responses of diatoms, the hydrophobic properties of diatoms and the release of EPS, appear to play an important role in diatom aggregation and explain the behavior observed at different salinities. This biophysical study provides important evidence allowing to get a deep insight into diatom interactions at the nanoscale, which may contribute to a better understanding of large-scale aggregation phenomena in aquatic systems.

Keywords: aggregation, atomic force microscopy, cell hydrophobicity, *Cylindrotheca closterium*, extracellular polymeric substances, hypo-saline stress

Introduction

Diatoms is the most important group of eukaryotic phytoplankton with a large diversity (100,000 species), thought to be responsible for 20% of the total production on Earth and 40% of the total marine primary production (Scala & Bowler, 2001). In particular, *Cylindrotheca closterium* (*C. closterium*) is a widespread marine diatom in coastal and estuarine environments that can develop in both planktonic and benthic states. On the mudflats found in these regions, this species forms biofilms on the surface of sediments, increasing their stability and promoting the deposition of sediment particles (de Brouwer et al., 2005). When these biofilms are then disturbed, cells become resuspended in the water and continue to live in the planktonic state (Thornton, 2002). In both the benthic and planktonic states, this species can produce large amounts of extracellular polymeric substances (EPS), which it requires for locomotion or to promote its adhesion to the substrate and subsequent biofilm formation (Staats et al., 2000). In the planktonic state, these EPS can be involved in the aggregation (*i.e.*, flocculation) of cells that can then form marine snow, *i.e.*, aggregates of detritus, inorganic material, and living organisms greater than 0.5 mm in diameter (Iversen & Ploug, 2013). Macroaggregates can even reach meter or kilometer scales, as demonstrated by the phenomenon of macroscopic gel formation in the northern Adriatic Sea, which has been shown to be related to the production of extracellular polymers by the dominant diatom species *C. closterium* (Alcoverro et al., 2000; Kovač et al., 2005; Najdek et al., 2005; Pletikapić et al., 2011; Radić et al., 2011; Svetličić et al., 2011; Žutić & Svetličić, 2000). Moreover, these aggregates then sediment and export organic matter such as carbon from the surface to the deep sea, a phenomenon referred to as the biological carbon pump (Piontek et al., 2009; Tréguer et al., 2018).

In coastal and estuarine environments where diatoms such as *C. closterium* occur, salinity is usually a local environmental factor that can vary widely (Glaser & Karsten, 2020). In open oceans, salinity is relatively constant due to intense mixing, but in nearshore or estuarine waters where riverine freshwater mixes with marine water, the degree of salinity dilution is highly variable (Karsten, 2012). In addition, future climate change scenarios foresee less precipitation and more evaporation in these zones, which will lead to further changes in salinity (Glaser & Karsten, 2020). For these reasons, the effects of salinity stress (hypo- or hyper-saline) on diatoms such as *C. closterium* have been the subject of several studies. For

example, authors have shown that changes in salinity can have effects on cell motility (Apoya-Horton et al., 2006; Araújo et al., 2013), cell length (De Miranda et al., 2005), cell growth (Araújo et al., 2013; Glaser & Karsten, 2020; Rijstenbil, 2005; Van Bergeijk et al., 2003), EPS production (Najdek et al., 2005; Steele et al., 2014) or oxidative stress (Roncarati et al., 2008). In particular, a recent study from our group investigated the effects of salinity-induced stress on the surface properties and EPS production of *C. closterium* cells in the stationary phase, which determines their functional behavior in aquatic systems (Novosel et al., 2022). For that, cell adhesive and nanomechanical properties were probed using atomic force microscopy (AFM), which is a powerful technique to study microalgae at the nanoscale and probe their biophysical properties (Demir-Yilmaz et al., 2021b). Moreover, AFM has also been used before to elucidate the molecular mechanisms underlying microalgae cell aggregation for different types of microalgae species showing, its interest in such studies (Besson et al., 2019; Demir, Blockx, et al., 2020; Demir-Yilmaz, Yakovenko, et al., 2022; Formosa-Dague, Gernigon, et al., 2018b; Vergnes et al., 2019).

To date, no studies have examined the effects of salinity on diatom aggregation during the exponential growth phase. In this work, we investigate how hypo-saline conditions affect the aggregation of *C. closterium* cells in the exponential growth phase. We use a flocculation/flotation experiment to investigate the aggregation behavior of *C. closterium* cells at three selected salinities (35, 15, and 5). In addition, AFM was used to determine nanomechanical and hydrophobic properties of diatoms and the structural organization of EPS, while an electrochemical approach allowed quantification of released surface-active organic matter. Overall, this original data set contributes to the understanding of the mechanism underlying cell aggregation of *C. closterium* under hypo-saline conditions. Such data are important for understanding globally important processes that occur in marine waters, such as the formation of marine snow.

Material and Methods

Microalgae strain and culture conditions

The diatom *Cylindrotheca closterium* (Bacillariophyceae, CCMP 1554, Culture Collection Bigelow Laboratory for Ocean Sciences, Bigelow, MN, USA) was cultured under sterile conditions in natural seawater (salinity of 35) and enriched with f/2 medium (Guillard, 1975).

Diatom monocultures were grown in both laboratories (at the RBI and TBI) using seawater from the southern Adriatic Sea and the Mediterranean Sea. In both cases, the culture medium was sterilized before use. Cells were cultured either in flasks at 19°C and 120 rpm in an incubator with white neon tubes providing an illumination of 40 $\mu\text{mol photons m}^{-2} \text{s}^{-1}$ with a photoperiod of 18 hours light:6 hours dark, or in a water bath at 20 rpm and a photoperiod of 12 hours light:12 hours light with an irradiance of 32 $\mu\text{mol photons m}^{-2} \text{s}^{-1}$. Both types of cultivation resulted in similar growth rates under the different conditions tested in this study. To induce salinity stress, natural seawater was diluted with sterile MilliQ water to obtain selected salinities of 15 and 5, and cells were cultured under the same conditions for 7 days. To monitor cell growth, the average cell abundance in duplicate samples was determined using a Fuchs-Rosenthal hemocytometer (Fein-Optik Jena, Germany, depth 0.2 mm) and a light microscope (Olympus BX51, Olympus Corporation, Japan). Growth rate and doubling time were determined in the early exponential growth phase of diatoms (S.-K. Kim, 2015).

Electrochemical method

The electrochemical method of polarography at the dropping mercury electrode allows characterization of released surface-active organic matter from cell culture (Pletikapić & Ivošević DeNardis, 2017; Svetličić et al., 2006). Here, adsorption of organic matter and submicron particles on the dropping mercury electrode leads to a decrease in the surface tension gradient at the mercury interface, which causes the suppression of convective flow proportional to the surfactant concentration in the sample and is referred to as surfactant activity. The surfactant activity of seawater can be expressed as the equivalent amount of the nonionic synthetic surfactant used, Triton-X-100 (polyethylene glycol tert-octylphenyl ether), in milligrams per liter.

Electrochemical measurements

Electrochemical measurements were performed in an air-permeable and thermostatic Metrohm vessel with a three-electrode system. The dropping mercury electrode served as the working electrode and had the following characteristics: dropping time: 2.0 s, flow rate: 6.0 mg s^{-1} , maximum surface area: 4.57 mm^2 . All potentials were referenced to a potential measured at a reference electrode, i.e., Ag/AgCl (0.1 M NaCl) separated from the measured dispersion by a ceramic frit. A platinum wire was used as a counter electrode. Electrochemical measurements were performed using a 174A Polarographic Analyzer (Princeton Applied

Research, Oak Ridge, TN, USA) connected to a computer. Analogue data acquisition was performed using a DAQ card-AI-16-XE-50 (National Instruments, Austin, TX, USA). Data analysis was performed using the application developed in LabView 6.1 software (National Instruments, Austin, TX, USA). Electrochemical measurements of the surfactant activity of the sample were performed by recording polarograms of Hg(II) reduction (current-potential curves) at a scan rate of 10 mV/s. The nonionic surfactant Triton-X-100 (polyethylene glycol tert-octylphenyl ether, Sigma) was used as a standard. Stock solutions of Triton-X-100 (10 g/L) were prepared in artificial seawater with the corresponding salinities. The polarographic maximum Hg(II) was measured for a range of Triton-X-100 concentrations, and surfactant activities were determined at -350 mV, which was used to construct calibration curves. Surfactant activity of *C. closterium* cell cultures in the exponential growth phase was measured by adding 0.5 mL of 0.1 M HgCl₂ to the sample and recording the polarographic maximum of Hg(II).

AFM imaging of living cell

Before AFM imaging experiments, cells were harvested by centrifugation (2000 *g*, 3 min) and washed twice in PBS buffer at pH 7.4. AFM images of *C. closterium* cells were acquired with cells immobilized on positively charged glass slides (Superfrost™ Plus Adhesion, Eprelia, USA) in PBS at pH 7.4. The quantitative imaging mode of Nanowizard III AFM (Bruker, USA) with MSCT cantilevers (Bruker, nominal spring constant of 0.01 N/m) was used. Images were acquired at a resolution of 80 pixels, with an applied force of < 1.5 nN and a constant approach/retract speed ranging from 180 to 200 μm/s (z-range of 1.5 μm). For roughness measurements, images were acquired on areas of 0.5 × 0.5 μm in contact mode with MSCT cantilevers at an applied force < 0.5 nN. In all cases, the spring constants of the cantilevers were determined using the thermal noise method prior to imaging (Hutter & Bechhoefer, 1993).

AFM imaging of EPS

Atomic force microscopy images of EPS were acquired using a Multimode Scanning Probe Microscope with Nanoscope IIIa controller (Bruker, Billerica, MA, USA) equipped with a 125 μm vertical engagement (JV) scanner. *C. closterium* diatoms cultured at salinities of 5, 15, and 35 were separated from the growth medium by gentle centrifugation (2000 *g*, 3 min) on day

7 of growth. The loose pellet was washed twice with filtered seawater of the corresponding salinity, diluted to a final volume of 1 mL with filtered seawater, and used to prepare samples for AFM measurements. A 5 μ L aliquot of the cell suspension was pipetted onto freshly cleaved mica and placed in a closed Petri dish for 1 hour to allow the cells to settle and attach to the surface. The mica discs were then immersed in ultrapure water three times for 30 seconds and dried. After the drying step, the discs were taped to a metal sample pack with double-sided tape and imaged with the AFM. Imaging was performed in contact mode in air with silicon nitride cantilevers (DNP, Bruker, nominal frequency 18 kHz, nominal spring constant 0.06 N m⁻¹). The linear scan rate was between 1.5 and 2 Hz and the scan resolution was 512 samples per line. To minimize the interaction forces between the tip and the surface, the set point was kept at the lowest possible value. Image processing and analysis was performed using NanoScopeTM software (Bruker, Billerica, MA, USA).

Force spectroscopy measurements

For nanoindentation measurements, cells were harvested by centrifugation (2000 *g*, 3 min), washed twice in PBS buffer at pH 7.4, and immobilized on positively charged glass slides (SuperfrostTM Plus Adhesion, Eprelia, USA). In these experiments, a cantilever with known mechanical properties is pressed against the cell surface with a specific force. In this way, the Y_m value of the cell can be determined, a value that reflects its resistance to compression and thus its rigidity. In this study, nanoindentation measurements were performed on 10 cells from 2 independent cultures under all conditions, and 400 force curves were recorded for each cell on areas of 500 \times 500 nm on the cell surface. Force spectroscopy experiments were performed with an applied force between 1 and 3 nN depending on the condition using MLCT AUWH cantilevers with nominal spring constants of 0.1 N/m. Young's moduli were calculated from 40 nm indentation curves using the Hertz model (Hertz, 1881) in which the force F , indentation (δ), and Young's modulus (Y_m) follow equation (1):

$$F = \frac{2 \times Y_m \times \tan\alpha}{\pi \times (1 - \nu^2) \times \delta^2} \quad (1)$$

Here α is the opening angle of the tip (17.5°) and ν is the Poisson's ratio (which is arbitrarily assumed to be 0.5). The spring constants of the cantilevers were determined before each experiment using the thermal noise method (Hutter & Bechhoefer, 1993).

Hydrophobicity measurements

To measure the hydrophobic properties of cells, a recently developed method was used, which consists of using fluidic force microscopy (FluidFM) to measure the interactions between a bubble (hydrophobic surface) and cell surfaces (Demir et al., 2021). For this purpose, FluidFM probes with an aperture of 8 μm in diameter (Cytosurge AG, Switzerland) were hydrophobized by coating with self-assembled monolayers (SAMs) of silanes using SAMs vapor deposition technique. The FluidFM cantilevers were functionalized with 1H,1H,2H,2H-perfluorodecyltrichlorosilane (FDTs) using an Orbis-1000 equipment (Memstar, Livingston, UK) to make their outer surface and the inner surface of the microchannel hydrophobic. The deposition was carried out under vacuum at 40 Torr and -40°C for 5 minutes. Then, the microchannel of these silanized cantilevers was filled with air and the probe was immersed in PBS 1X. A slight overpressure of 20 mbar was applied to remove any particulate or dust contamination or to prevent clogging of the FluidFM cantilever. To create a bubble at the opening of the cantilever, a positive pressure of 200 mbar was then applied inside the microfluidic cantilever in buffer. The silanized probes were calibrated using the thermal noise method before each measurement (Hutter & Bechhoefer, 1993). The interactions between the generated bubbles and *C. closterium* cells under the selected salinities were then recorded in force spectroscopy mode, applying a maximum force of 1 nN and a constant retraction speed of 2 $\mu\text{m}/\text{s}$. For each condition, areas of $0.5 \times 0.5 \mu\text{m}$ were examined on 5 different cells. Adhesion forces were determined by calculating the maximum adhesion force from the obtained retraction force curves.

Flocculation/flotation separation experiments

Flocculation/flotation separation of *C. closterium* was performed in dissolved air flotation (DAF) experiments in a homemade flotation system as described elsewhere (Besson & Guiraud, 2013a; Demir-Yilmaz, Yakovenko, et al., 2022, p.). For this purpose, algal suspensions with an optical density (750 nm) of 0.6 at salinities of 35 and 15 and with an optical density (750 nm) of 0.3 at salinity of 5 were used directly after 7 days of culture. For some experiments, cells were washed (2000 g, 3 min) and resuspended in PBS to remove EPS present in the culture medium. In these cases, the separation experiments were performed in PBS at a pH equal to that of the cells at the end of the cultures (9.4), eliminating the possible effects of pH fluctuations on cell flocculation. The cell suspensions were then added to the

flocculation/flotation jars, and shaken (100 rpm) for 15 min to initiate flocculation. Depressurization at atmospheric pressure of deionized water saturated with air at 6 bar resulted in the formation of bubbles. Algae-free water was pressurized for 30 minutes before injection into the jars. Injection was controlled by a solenoid valve and 20 mL of pressurized water was added to each beaker sample. For all conditions, the algal suspension was removed from the bottom of the test-jars after 15 minutes: The first 5 mL of the treated phase was discarded, and the next 20 mL was used to quantify the flocculation/flotation efficiency. For this purpose, the optical density of the extracted microalgal suspension was measured and compared to the optical density of the microalgal suspension measured before the experiments. The flotation efficiency (E) was calculated according to the following equation 2:

$$E = \frac{OD_i \cdot V_i - OD_f \cdot V_f}{OD_i \cdot V_i} \quad (2)$$

Where OD_i and OD_f are the initial and final optical densities (750 nm), respectively, and V_i and V_f are the initial and final volumes after addition of the bubbles.

Results

Salinity stress affects growth dynamics of *C. closterium* cells

The growth curves obtained for *C. closterium* at the three selected salinities 5, 15, and 35 are shown in Figure 1. The initial abundance of cells in the growth medium was approximately 4.0×10^4 cells/ml. The highest cell number on the day 7 of growth was recorded in cultures with salinity 35, while the cell number was 7 times lower with salinity 5. Diatom growth is salinity dependent, such that the fastest growth rate of 0.40 day^{-1} and the shortest doubling time of 1.71 days were obtained at a salinity of 35, while the growth rate of 0.11 day^{-1} and the longest doubling time of 6.11 days were obtained at a salinity of 5.

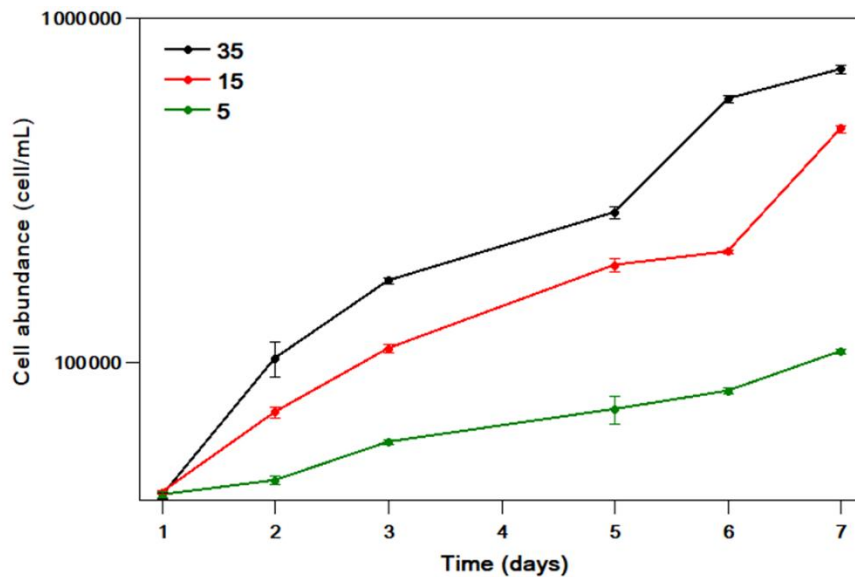


Figure 1. Growth curves of *C. closterium* at the selected salinities (5, 15 and 35). The y-scale is logarithmic.

Salinity stress affects the aggregation behavior of *C. closterium* cells

In this type of experiment, cells are allowed to aggregate under gentle agitation after culture. Then, small bubbles generated by dissolved air flotation (DAF) are introduced at the bottom of the suspension; as they rise, they capture the aggregates formed and bring them to the surface. This separation is only possible if the cells are already aggregated. Thus, the separation efficiency obtained directly reflects the aggregation of the cells. These experiments were performed with cells directly after culture or with cells previously washed by centrifugation in buffer. The centrifugation process probably mainly removes EPS from the cells, as shown in Figure S1. Since EPS are a known factor promoting cell aggregation (Vergnes et al., 2019), including in the case of diatoms (Steele et al., 2014), it is important to evaluate their potential involvement in cell aggregate formation. The results are shown in the histogram in Figure 2; the dark bars show the separation efficiency without washing the cells and the light bars with a washing step. When the cell cultures are used directly for the flocculation experiments (dark bars in Figure 3), the measured separation efficiency for cells cultured at a salinity of 35 is $64.6 \pm 9.4\%$, which is quite high considering that no external flocculants were used. When the salinity is decreased, this efficiency drops to $53.7 \pm 5.0\%$ at a salinity of 15 and even further to $37.4 \pm 6.0\%$ at a salinity of 5. Statistical analysis showed that these differences between salinities 35 and 5 and between salinities 5 and 15 were significant (p-value of 0.01, Mann and Whitney test). When the experiments are repeated with

cells separated and washed from the growth medium prior to the flocculation experiments and from which the EPS were mainly removed, we can see that all separation efficiencies decrease by the same factor of approximately 3. Under these conditions, the separation efficiency is $21.7 \pm 13.5\%$ at a salinity of 35 and decreases to $19.0 \pm 9.9\%$ at a salinity of 15 and to $11.5 \pm 3.1\%$ at a salinity of 5. Thus, the removal of EPS from cells has a significant effect on their aggregation behavior, but nevertheless, cells at a salinity of 35 are able to form more aggregates than cells at lower salinities. Hypo-saline stress thus has a negative effect on cell aggregation.

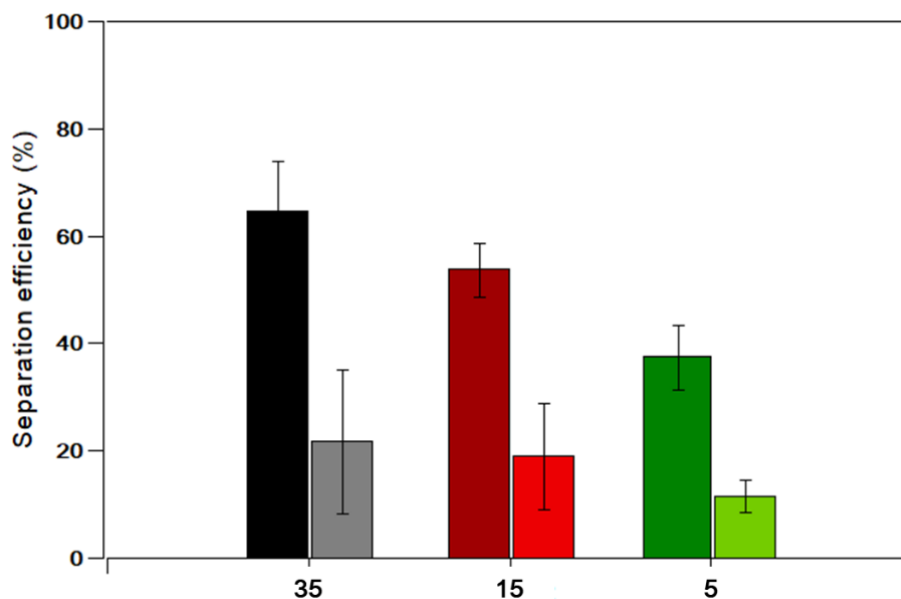


Figure 2. Flocculation/flotation of *C. closterium* cells cultures at selected salinities. The histogram shows the separation efficiency of *C. closterium* cells grown at salinities of 35, 15, and 5. The dark bars were obtained with direct cell cultures and the light bars with cells previously washed in phosphate buffer. In each case, the tests were repeated at least 7 times with independent cultures.

Salinity stress affects the surface properties of cells

To understand the decrease in the ability of cells to aggregate under hypo-saline conditions, we examine the effects of selected salinities on cell surface roughness, nanomechanical properties, and hydrophobicity. Figure 3a-c show AFM height images of *C. closterium* cells at salinities studied. From these images, the reduction in salinity does not seem to affect the morphology of the cells, as they have similar shapes and dimensions. Then, to evaluate

whether the salinity conditions tested in our study could have an effect on the nanostructure of the cell wall, we performed roughness measurements. For this purpose, high-resolution images of small areas (500×500 nm) were acquired and used to measure the average roughness R_a . Under each condition, the measurements were performed on 10 cells from 2 independent cultures (Table S1). Figure 3d shows the distribution of these values. First, we note that the cell wall of *C. closterium* is quite smooth; at salinity of 35 (control), the roughness averages 0.8 ± 0.2 nm. As salinity decreases, the roughness of *C. closterium* cells also appears to decrease. However, statistical analysis (Mann and Whitney test) showed that the observed differences were not significant. Another important property of the cell surface that may change as a function of conditions is the rigidity of the cell wall. To obtain quantitative information about these properties, the elastic modulus (Y_m) of the cell wall was determined by analyzing the force curves obtained during the nanoindentation measurements. The distribution of Y_m values obtained ($n = 4000$ under each condition) is shown in Figure 3e (Table S2). Cells grown at a salinity of 35 have an average Y_m value of 2.7 ± 1.1 MPa. *C. closterium* contains silica in its cell wall, which explains the high rigidity obtained here. As salinity decreases, the Y_m value increases to 3.0 ± 0.7 MPa at a salinity of 15 and to 3.9 ± 1.9 MPa at a salinity of 5. Statistical analysis showed that the differences in this case were significant (two-sample t-test). Thus, when cells are subjected to hypo-saline stress, cell rigidity increases, probably due to molecular changes in the cell wall under these conditions.

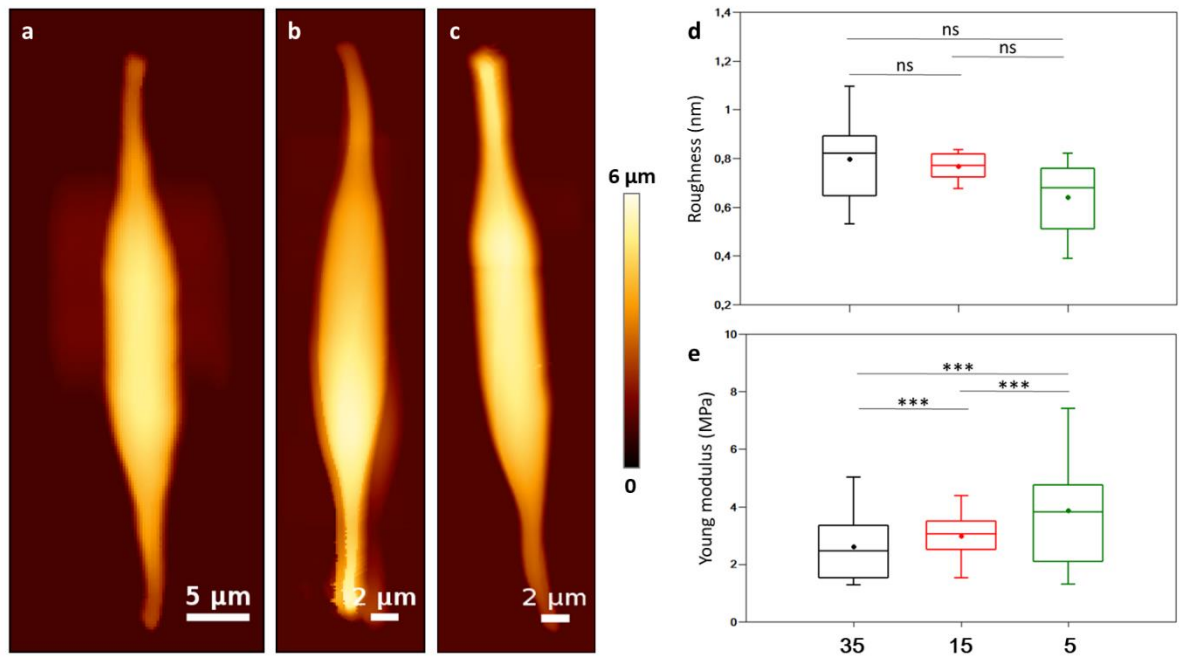


Figure 3. Nanostructural and nanomechanical characterizations of *C. closterium* cells at selected salinities. AFM height images of single *C. closterium* cells cultured for 7 days in medium with salinity of (a) 35, (b) 15, and (c) 5. (d) Box plot showing the distribution of roughness values, each measured on 10 different cells from 2 independent cultures (Table S1). (e) Box plot showing the distribution of Y_m values, each measured on 10 different cells from 2 independent cultures (Table S2).

We therefore investigated hydrophobic properties, using a recently developed technique in our team that consists in probing the interactions between cells and air bubbles produced using FluidFM technology (Demir et al., 2021), which combines AFM with microfluidics (Meister et al., 2009a). This technique provides an accurate way to study the hydrophobic properties of complex surfaces such as microalgal cells, where measuring water contact angle (WCA) can be difficult. Since air bubbles in water behave like hydrophobic surfaces, the stronger the interaction with the bubbles, the more hydrophobic the surface. The results of these experiments are shown in Figure 4. In each case, 5 cells from 2 independent cultures were examined (Table S3). They show that cells grown at a salinity of 35 interact with bubbles with an adhesion force of 367.6 ± 87.0 pN (Figure 4a). The adhesion force decreases for cells grown at a salinity of 15 (Figure 4b), with an average value of 108.5 ± 69.8 pN. At a salinity of 5, the cells no longer interact with the bubbles (no interactions recorded, Figure 3c).

Therefore, the reduction in salinity affects the hydrophobic properties of the cells, as the cells become more hydrophilic under hypo-saline stress.

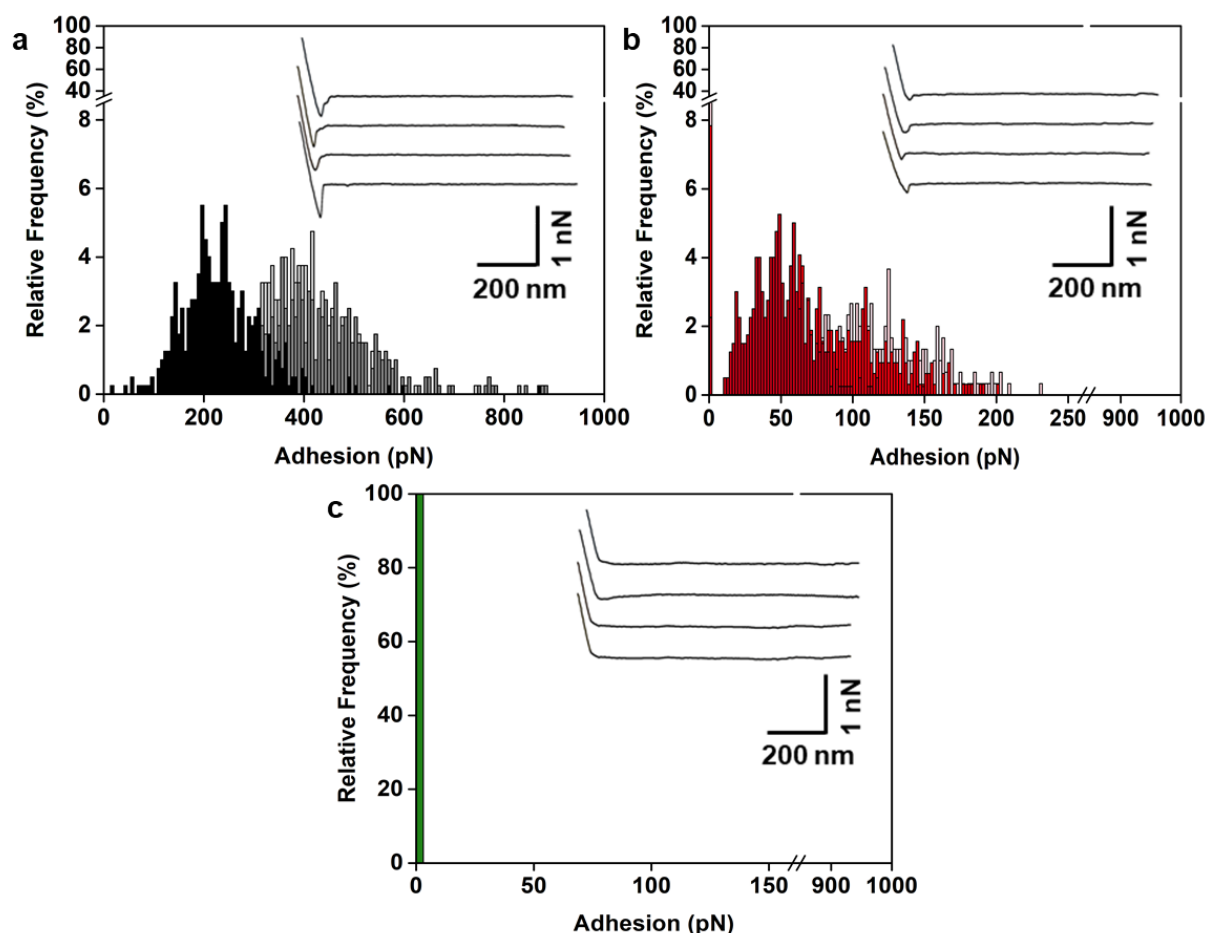


Figure 4. Probing the interactions between air bubbles and *C. closterium* cells cultured at the selected salinities. Adhesion force histogram obtained for the interaction of air bubbles with *C. closterium* cells cultured at salinities of (a) 35, (b) 15 and (c) 5. The insets in the histograms show the representative force curves obtained during the force spectroscopy experiments.

Salinity stress affects the production and nanostructural organization of released EPS

We determined the amount of released surface-active organic matter at the selected salinities, and characterized its nanostructural organization using the electrochemical method of polarography at the dropping mercury electrode and AFM, respectively. For this purpose, diatom cultures grown at the selected salinities were characterized in terms of surfactant activity per cell, which reflects the physiological activity of the cells. The results show that the surfactant activity is highest for the *C. closterium* culture grown at a salinity of 5 (13.9 pg T-X-

100/L), while the lowest surfactant activity was determined for the cells grown at a salinity of 35 (0.9 pg T-X-100/L), as shown in Figure 5.

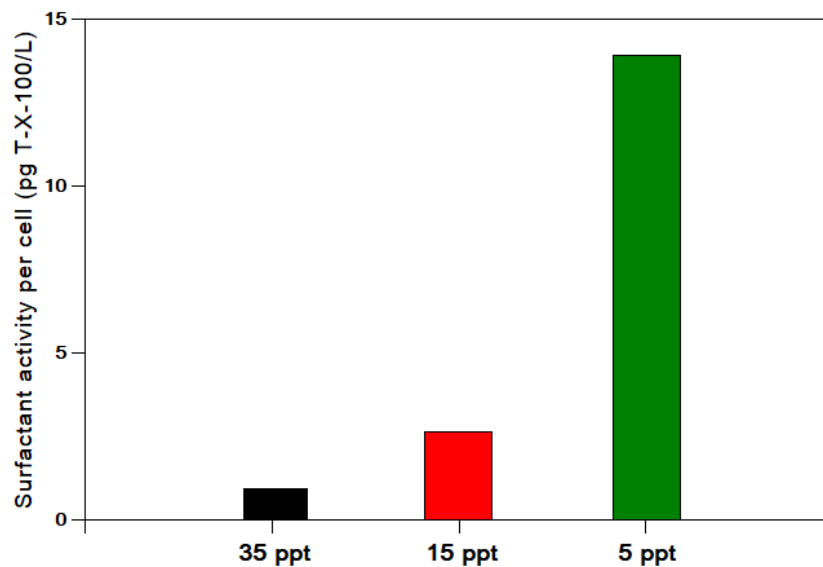


Figure 5. Surfactant activity of *C. closterium* cell cultures at selected salinities.

In addition, high-resolution AFM imaging was used to characterize the supramolecular organization of EPS at selected salinities, as presented in Figure 6). In each case, 10 diatoms were characterized. The results showed that at all salinities studied, the diatoms were surrounded by a dense layer (Figure 6a, d, g) that could extend up to 10 μm beyond the cell and was only a few nm thick. The difference in EPS organization as a function of salinity is very striking in these images. In cells grown at salinity of 35, only short individual fibrils can be seen (1-2 nm high, Figure 6 b and c), whereas in cells grown at salinities of 15 and 5, the EPS form a fibrillar network.

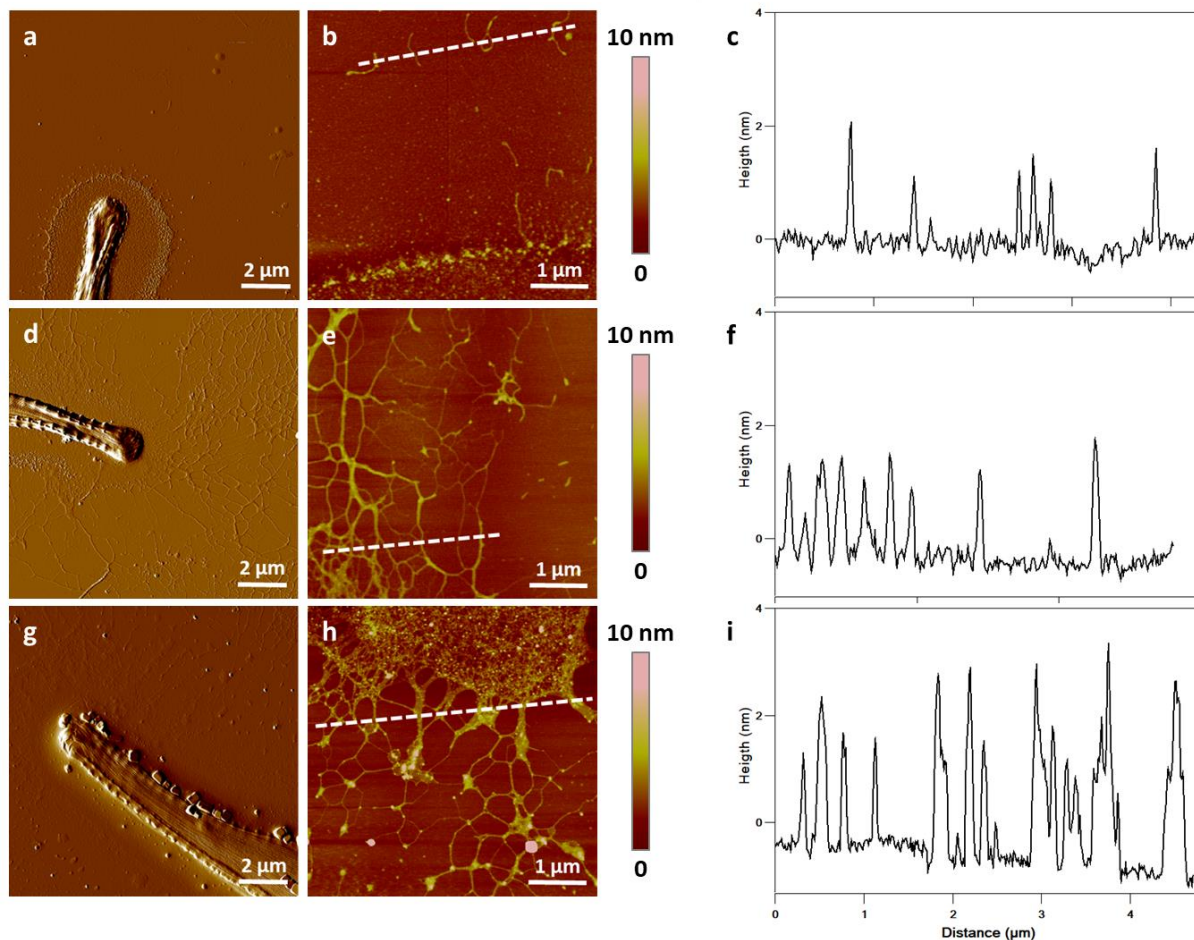


Figure 6. AFM characterization of the EPS produced by *C. closterium* cells at selected salinities. AFM vertical deflection obtained in contact mode in air of *C. closterium* cell rostra at salinities of (a) 35, (d) 15 and (g) 5. (b), (e) and (h) are AFM height images recorded on closed-up 5 x 5 μm areas, respectively. (c), (f) and (i) are cross-sections taken along the white lines in (b), (e) and (h) respectively.

Discussion

Diatom aggregates that form in natural environments contribute significantly to marine snow. Their sedimentation has several effects, the most important being the export of organic material from the surface to the deep sea (Iversen & Ploug, 2013; Thornton, 2002). Because salinity is one of the most important fluctuating parameters in coastal and estuarine regions where *C. closterium* is common, it is important to evaluate the effects of hypo-saline stress on cell aggregation. While the effects of hyper- or hypo-saline conditions on diatoms have been studied, the aggregation mechanism in diatoms during the exponential growth phase is poorly understood. In this study, we investigated the effects of hypo-saline conditions on the

aggregation behaviour of *C. closterium* cells, and nanoscale characterization of cells and released EPS helped to elucidate the corresponding aggregation mechanism.

An initial aspect of the study was to determine the effects of hypo-saline stress on cell growth dynamics. Several studies in the literature have examined the effects of altering salinity on *C. closterium* growth. Rijstenbil *et al.* found that high salinity had a significant negative effect on the photosynthetic activities of cells (Rijstenbil, 2005), whereas Van Bergeijk *et al.* reported that lower salinity levels (11 and 22 psu) had little effect on the growth rate of *C. closterium* cells or on the cell yield of long-term cultures (14 days) (Van Bergeijk *et al.*, 2003). Our results are not consistent with these findings; however, in our case, the effects of reduced salinity on cells in the exponential growth phase were examined, which could explain the differences observed. However, the results are consistent with our recent study that showed that favourable growth conditions for *C. closterium* are at salinities of 27 and 38 (Novosel *et al.*, 2022). Another study conducted with different strains of *C. closterium* isolated from brackish and marine habitats also found that reduced salinity stopped or slowed cell growth in 7-day cultures, confirming our findings (Glaser & Karsten, 2020). Finally, this effect of reduced salinity was also reported by Araujo and coworkers on 72-hour cultures of *C. closterium* (Araújo *et al.*, 2013).

In a second step, the aggregation of cells under hypo-saline conditions was then quantified using flocculation/flotation experiments. The results showed a statistically significant decrease in cell aggregation under hypo-saline conditions. Because EPS has been reported to be an important factor promoting flocculation for several microalgal species (Steele *et al.*, 2014; Vergnes *et al.*, 2019), the experiments were additionally repeated with washed cells, where the majority of EPS was likely removed. The results highlight the important contribution of EPS to cell aggregation behaviour. However, even when most of the EPS was removed, the cells formed aggregates, but significantly less under hypo-saline conditions. This suggests that the EPS present in the culture medium are not the only factor affecting aggregation. To understand this, several hypotheses can be made: (i) salinity affects cell surface properties, (ii) salinity affects released EPS, and (iii) the combination of both factors, cell surface properties and released EPS, affects cell aggregation. To answer these questions, we examine the surface roughness and surface properties of *C. closterium* at the selected salinities. The surface of *C. closterium* in the exponential growth phase is very smooth, as revealed by

roughness measurements in liquid, with an average roughness of 0.8 ± 0.2 nm. In a previous study, roughness measurements on *C. closterium* cells in the stationary growth phase gave roughness values in the range of 2 - 5 nm for salinities of 9, 19, 27, and 38 (Novosel et al., 2022). Higher cell roughness values could be related to roughness measurements in air. In addition, cell roughness depends on the species and stressor. Some microalgal species had a smooth surface, such as *Chlorella vulgaris* (0.9 nm at pH 6, (Demir, Blockx, et al., 2020)), while the diatom *Phaeodactylum tricornutum* had a much rougher surface with values ranging from 5 to 10 nm (J. Ma et al., 2021). Finally, another study investigated the roughness of the diatom *Nitzschia closterium* under selected salinity conditions. Their results showed that the cell surface was rougher at a salinity of 18 (9.9 nm compared to 6.3 nm at a salinity of 32) due to the presence of silica particles on the cell surface, which is therefore not the case here (J. Ma et al., 2019).

As for the nanomechanical measurements performed, our results show that a decrease in salinity leads to an increase in cell rigidity. Several studies have shown that a stress or a change in environmental conditions can have an important impact on the composition or remodeling of the cell wall, changing its nanomechanical properties (Demir, Blockx, et al., 2020; Formosa-Dague, Gernigon, et al., 2018b; Francius et al., 2008; J. Ma et al., 2019). In particular, our previous study of *C. closterium* cells in stationary phase has shown that hypo-saline stress leads to a marked increase in the production of membrane sterols, which make the cells significantly stiffer and more hydrophobic (Novosel et al., 2022). Perhaps a similar mechanism takes place here in the exponential phase. Moreover, changes in nanomechanical properties upon stress have also been reported in other microalgal species; for example, *P. tricornutum* and *C. vulgaris* cells exhibit increased stiffness at elevated pH (Demir, Blockx, et al., 2020; Formosa-Dague, Gernigon, et al., 2018b). In contrast, Ma and co-authors reported no effects on cell rigidity when *N. closterium* cells were exposed to hypo-saline conditions (J. Ma et al., 2019). However, in this case, Y_m values obtained with a different model than that of this study were much higher (about 30 MPa), reflecting the higher content of silica in the cell wall of *N. closterium* compared to *C. closterium* and perhaps explaining the difference with our results.

Hydrophobicity of microalgal cells is also an important factor in aggregation efficiency (Garg et al. 2012; Ozkan and Berberoglu 2013, Novosel et al. 2021). We investigated the hydrophobicity of *C. closterium* cells in the exponential growth phase at selected salinities.

Results showed that diatoms grown under favorable conditions (salinity of 35) behaved more hydrophobically than cells grown under hypo-saline stress, possibly promoting efficient aggregation compared to cells grown at lower salinities. These changes in cell hydrophobicity at different salinity variation suggest a chemical change in lipid metabolism (Novosel et al., 2022). In addition, cell surface properties have been shown to vary with cell age. For example, *D. tertiolecta* cells behave hydrophobic and stiff in exponential phase and under favorable growth conditions, while they are hydrophilic and soft in stationary phase, also suggesting a molecular change in their cell barrier (Pillet et al., 2019). The same trend was observed in *C. closterium* (Novosel et al., 2022).

Regarding the release of EPS, an electrochemical approach allows quantification of the released surface-active organic matter, while AFM imaging provides insights into their nanostructural organisation. The results showed that the production of EPS was about 14 times higher in cells grown under hypo-saline conditions. Overproduction of EPS as an adaptation response of cells was reported when *C. closterium* was exposed to the heavy metal cadmium (Mišić Radić et al., 2021). Such behavior was also observed by Staats et al. who found that cultures of *C. closterium* depleted of nitrogen also produced more EPS (Staats et al., 2000). For example, under hyper-saline stress, it has been shown for *P. tricornutum* cells that increased salinity increases the production of EPS with higher levels of uronic acids and sulphates, possibly allowing EPS to retain more water (Abdullahi et al., 2006). Thus, the higher amount of EPS at salinity 5 (as an unfavorable condition) corresponds to an adaptation of cells to protect themselves against osmotic stress. Regarding the EPS nanostructure, the AFM results showed that the EPS are structured differently depending on the salinity: At salinity 35, the EPS form short single fibrils around the cells, while at salinity 15 and 5, the EPS form a fibrillar network. For *C. closterium* cells in stationary phase, our recent study showed a similar trend, with denser fibrils around the diatoms at lower salinities (9 and 19) with a higher degree of cross-linking (Novosel et al., 2022). As the flocculation/flotation results showed, the EPS play an important role in flocculation, as for all conditions the separation efficiency and thus aggregation decreases by a factor of 3 when the EPS are removed from the cells. It is important to note that the cells aggregate independently of EPS production, implying that the EPS are not the only parameter that triggers cell aggregation at the selected salinities. As mentioned

earlier, cell aggregation independent of the presence of EPS also appears to be driven by the hydrophobic properties of the cells, which allow diatom aggregates to form at salinity 35.

Conclusions

We investigate the effects of hypo-saline stress on the aggregation behavior of the diatom *C. closterium* during the exponential growth phase. Our results show that hypo-saline stress reduces the ability of diatoms to form flocs. To explain this behavior, we characterized both the surface properties of the cells and the EPS released. The AFM results show that the cells are significantly softer and more hydrophobic at a salinity of 35 than under hypo-saline conditions. The amount of EPS released and nanostructural organization were also found to be salinity dependent. At salinity of 35, diatoms released a small amount of EPS organized in short fibrils and still formed diatom aggregates. This can be explained by the fact that cells grown under favorable conditions are more hydrophobic than cells under hypo-saline stress, as hydrophobicity is an important factor promoting cell flocculation. This comprehensive study revealed the complex interplay between cell surface properties and physiological activity on the mechanism of diatom aggregation, which could lead to a fundamental understanding of their survival strategy under hypo-saline stress conditions in aquatic systems and also serve for biotechnological applications. Furthermore, because diatom aggregations in marine environments can have important impacts on ecosystems and the export of organic matter to the water column, these results provide fundamental data needed to understand these phenomena on a large scale.

Acknowledgements

C. F.-D. is a researcher at CNRS. The authors want to thank Emma Regourd for her technical support on flocculation/flotation experiments. In addition, the authors want to thank Dr. Etienne Dague for withdrawing the seawater used in part of this study during his scuba-diving trip with Ecole de Plongée Toulsaine (EPT) in Ile du Levant, France.

Funding

This work was supported by the Croatian-French program "Cogito" partner Hubert Curien (Campus France n°46656ZC), by the Agence Nationale de la Recherche, JCJC project FLOTALG

(ANR-18-CE43-0001-01) and by the Croatian Science Foundation project "From algal cell surface properties to stress markers for aquatic ecosystems" (IP-2018-01-5840).

Author contributions

I. Demir-Yilmaz: Data acquisition, analysis, and interpretation, Writing- review and editing. **N. Novosel:** Data acquisition, analysis, and interpretation, Writing- review and editing. **M. Levak Zorinc:** Data acquisition, analysis, and interpretation, Writing- review and editing. **T. Mišić Radić:** Data acquisition, analysis, and interpretation, Writing- review and editing. **M. Souad Ftouhi:** Data acquisition, analysis, and interpretation, writing- review and editing. **P. Guiraud:** conception of the work, data interpretation, writing – review and editing. **N. Ivošević DeNardis:** Funding acquisition, conception of the work, data interpretation, writing – original draft. **C. Formosa-Dague:** Funding acquisition, conception of the work, data acquisition, analysis and interpretation, writing – original draft.

Declarations

The authors have no competing interests to declare that are relevant to the content of this article.

Data availability statement

The datasets generated during and/or analyzed during the current study are available from the corresponding author on reasonable request.

References

- Abdullahi, A. S., Underwood, G. J. C., & Gretz, M. R. (2006). Extracellular Matrix Assembly in Diatoms (bacillariophyceae). V. Environmental Effects on Polysaccharide Synthesis in the Model Diatom, *Phaeodactylum Tricornutum*1. *Journal of Phycology*, 42(2), 363–378. <https://doi.org/10.1111/j.1529-8817.2006.00193.x>
- Acién, F. G., Molina, E., Fernández-Sevilla, J. M., Barbosa, M., Gouveia, L., Sepúlveda, C., Bazaes, J., & Arbib, Z. (2017). 20—Economics of microalgae production. In C. Gonzalez-Fernandez & R. Muñoz (Eds.), *Microalgae-Based Biofuels and Bioproducts* (pp. 485–503). Woodhead Publishing. <https://doi.org/10.1016/B978-0-08-101023-5.00020-0>
- Ahmad, A. L., Mat Yasin, N. H., Derek, C. J. C., & Lim, J. K. (2011). Optimization of microalgae coagulation process using chitosan. *Chemical Engineering Journal*, 173(3), 879–882. <https://doi.org/10.1016/j.cej.2011.07.070>
- Alam, F., Date, A., Rasjidin, R., Mobin, S., Moria, H., & Baqui, A. (2012). Biofuel from Algae- Is It a Viable Alternative? *Procedia Engineering*, 49, 221–227. <https://doi.org/10.1016/j.proeng.2012.10.131>
- Alcoverro, T., Conte, E., & Mazzella, L. (2000). Production of Mucilage by the Adriatic Epipellic Diatom *Cylindrotheca Closterium* (bacillariophyceae) Under Nutrient Limitation. *Journal of Phycology*, 36(6), 1087–1095. <https://doi.org/10.1046/j.1529-8817.2000.99193.x>
- Apoya-Horton, M. D., Yin, L., Underwood, G. J. C., & Gretz, M. R. (2006). Movement Modalities and Responses to Environmental Changes of the Mudflat Diatom *Cylindrotheca Closterium* (bacillariophyceae)1. *Journal of Phycology*, 42(2), 379–390. <https://doi.org/10.1111/j.1529-8817.2006.00194.x>

- Araújo, C. V. M., Romero-Romero, S., Lourençato, L. F., Moreno-Garrido, I., Blasco, J., Gretz, M. R., Moreira-Santos, M., & Ribeiro, R. (2013). Going with the Flow: Detection of Drift in Response to Hypo-Saline Stress by the Estuarine Benthic Diatom *Cylindrotheca closterium*. *PLOS ONE*, *8*(11), e81073.
<https://doi.org/10.1371/journal.pone.0081073>
- Arnold, A. A., Genard, B., Zito, F., Tremblay, R., Warschawski, D. E., & Marcotte, I. (2015). Identification of lipid and saccharide constituents of whole microalgal cells by ¹³C solid-state NMR. *Biochimica et Biophysica Acta (BBA) - Biomembranes*, *1848*(1), 369–377. <https://doi.org/10.1016/j.bbamem.2014.07.017>
- Aslam, A., Thomas-Hall, S. R., Manzoor, M., Jabeen, F., Iqbal, M., uz Zaman, Q., Schenk, P. M., & Asif Tahir, M. (2018). Mixed microalgae consortia growth under higher concentration of CO₂ from unfiltered coal fired flue gas: Fatty acid profiling and biodiesel production. *Journal of Photochemistry and Photobiology B: Biology*, *179*, 126–133. <https://doi.org/10.1016/j.jphotobiol.2018.01.003>
- Bazaes, J., Sepulveda, C., Acién, F. G., Morales, J., Gonzales, L., Rivas, M., & Riquelme, C. (2012). Outdoor pilot-scale production of *Botryococcus braunii* in panel reactors. *Journal of Applied Phycology*, *24*(6), 1353–1360. <https://doi.org/10.1007/s10811-012-9787-3>
- Benemann, J. (2013). Microalgae for Biofuels and Animal Feeds. *Energies*, *6*(11), Article 11.
<https://doi.org/10.3390/en6115869>
- Besson, A., Formosa-Dague, C., & Guiraud, P. (2019). Flocculation-flotation harvesting mechanism of *Dunaliella salina*: From nanoscale interpretation to industrial optimization. *Water Research*, *155*, 352–361.
<https://doi.org/10.1016/j.watres.2019.02.043>

- Besson, A., & Guiraud, P. (2013a). High-pH-induced flocculation-flotation of the hypersaline microalga *Dunaliella salina*. *Bioresource Technology*, *147*, 464–470.
<https://doi.org/10.1016/j.biortech.2013.08.053>
- Besson, A., & Guiraud, P. (2013b). High-pH-induced flocculation–flotation of the hypersaline microalga *Dunaliella salina*. *Bioresource Technology*, *147*, 464–470.
<https://doi.org/10.1016/j.biortech.2013.08.053>
- Binnig, G., Quate, C. F., & Gerber, Ch. (1986). Atomic Force Microscope. *Physical Review Letters*, *56*(9), 930–933. <https://doi.org/10.1103/PhysRevLett.56.930>
- Blockx, J., Verfaillie, A., Thielemans, W., & Muylaert, K. (2018). Unravelling the Mechanism of Chitosan-Driven Flocculation of Microalgae in Seawater as a Function of pH. *ACS Sustainable Chemistry & Engineering*, *6*(9), 11273–11279.
<https://doi.org/10.1021/acssuschemeng.7b04802>
- Brennan, L., & Owende, P. (2010). Biofuels from microalgae—A review of technologies for production, processing, and extractions of biofuels and co-products. *Renewable and Sustainable Energy Reviews*, *14*(2), 557–577.
<https://doi.org/10.1016/j.rser.2009.10.009>
- Butt, H.-J., Farshchi-Tabrizi, M., & Kappl, M. (2006). Using capillary forces to determine the geometry of nanocontacts. *Journal of Applied Physics*, *100*(2), 024312.
<https://doi.org/10.1063/1.2210188>
- Canelli, G., Murciano Martínez, P., Austin, S., Ambühl, M. E., Dionisi, F., Bolten, C. J., Carpine, R., Neutsch, L., & Mathys, A. (2021). Biochemical and Morphological Characterization of Heterotrophic *Cryptocodinium cohnii* and *Chlorella vulgaris* Cell Walls. *Journal of Agricultural and Food Chemistry*, *69*(7), 2226–2235.
<https://doi.org/10.1021/acs.jafc.0c05032>

- Cheng, Y.-S., Zheng, Y., Labavitch, J. M., & VanderGheynst, J. S. (2011). The impact of cell wall carbohydrate composition on the chitosan flocculation of *Chlorella*. *Process Biochemistry*, *46*(10), 1927–1933. <https://doi.org/10.1016/j.procbio.2011.06.021>
- Chew, K. W., Chia, S. R., Show, P. L., Yap, Y. J., Ling, T. C., & Chang, J.-S. (2018). Effects of water culture medium, cultivation systems and growth modes for microalgae cultivation: A review. *Journal of the Taiwan Institute of Chemical Engineers*, *91*, 332–344. <https://doi.org/10.1016/j.jtice.2018.05.039>
- Chisti, Y. (2008). Biodiesel from microalgae beats bioethanol. *Trends in Biotechnology*, *26*(3), 126–131. <https://doi.org/10.1016/j.tibtech.2007.12.002>
- Chua, E. T., Eltanahy, E., Jung, H., Uy, M., Thomas-Hall, S. R., & Schenk, P. M. (2019). Efficient Harvesting of *Nannochloropsis* Microalgae via Optimized Chitosan-Mediated Flocculation. *Global Challenges*, *3*(1), 1800038. <https://doi.org/10.1002/gch2.201800038>
- Colling Klein, B., Bonomi, A., & Maciel Filho, R. (2018). Integration of microalgae production with industrial biofuel facilities: A critical review. *Renewable and Sustainable Energy Reviews*, *82*, 1376–1392. <https://doi.org/10.1016/j.rser.2017.04.063>
- Converti, A., Casazza, A. A., Ortiz, E. Y., Perego, P., & Del Borghi, M. (2009). Effect of temperature and nitrogen concentration on the growth and lipid content of *Nannochloropsis oculata* and *Chlorella vulgaris* for biodiesel production. *Chemical Engineering and Processing: Process Intensification*, *48*(6), 1146–1151. <https://doi.org/10.1016/j.cep.2009.03.006>
- Coward, T., Lee, J. G. M., & Caldwell, G. S. (2015). The effect of bubble size on the efficiency and economics of harvesting microalgae by foam flotation. *Journal of Applied Phycology*, *27*(2), 733–742. <https://doi.org/10.1007/s10811-014-0384-5>

- Dague, E., Alsteens, D., Latgé, J.-P., Verbelen, C., Raze, D., Baulard, A. R., & Dufrêne, Y. F. (2007). Chemical Force Microscopy of Single Live Cells. *Nano Letters*, 7(10), 3026–3030. <https://doi.org/10.1021/nl071476k>
- Dammer, U., Hegner, M., Anselmetti, D., Wagner, P., Dreier, M., Huber, W., & Güntherodt, H. J. (1996). Specific antigen/antibody interactions measured by force microscopy. *Biophysical Journal*, 70(5), 2437–2441. [https://doi.org/10.1016/S0006-3495\(96\)79814-4](https://doi.org/10.1016/S0006-3495(96)79814-4)
- de Boer, K., Moheimani, N. R., Borowitzka, M. A., & Bahri, P. A. (2012). Extraction and conversion pathways for microalgae to biodiesel: A review focused on energy consumption. *Journal of Applied Phycology*, 24(6), 1681–1698. <https://doi.org/10.1007/s10811-012-9835-z>
- de Brouwer, J. F. C., Wolfstein, K., Ruddy, G. K., Jones, T. E. R., & Stal, L. J. (2005). Biogenic Stabilization of Intertidal Sediments: The Importance of Extracellular Polymeric Substances Produced by Benthic Diatoms. *Microbial Ecology*, 49(4), 501–512. <https://doi.org/10.1007/s00248-004-0020-z>
- De Miranda, M., Gaviano, M., & Serra, E. (2005). Changes in the cell size of the diatom *Cylindrotheca closterium* in a hyperhaline pond. *Chemistry and Ecology*, 21(1), 77–81. <https://doi.org/10.1080/02757540512331323962>
- Delalande, A., Postema, M., Mignet, N., Midoux, P., & Pichon, C. (2012). Ultrasound and microbubble-assisted gene delivery: Recent advances and ongoing challenges. *Therapeutic Delivery*, 3(10), 1199–1215. <https://doi.org/10.4155/tde.12.100>
- Demir, I., Besson, A., Guiraud, P., & Formosa-Dague, C. (2020). Towards a better understanding of microalgae natural flocculation mechanisms to enhance flotation

- harvesting efficiency. *Water Science and Technology*, 82(6), 1009–1024.
<https://doi.org/10.2166/wst.2020.177>
- Demir, I., Blockx, J., Dague, E., Guiraud, P., Thielemans, W., Muylaert, K., & Formosa-Dague, C. (2020). Nanoscale Evidence Unravels Microalgae Flocculation Mechanism Induced by Chitosan. *ACS Applied Bio Materials*, 3(12), 8446–8459.
<https://doi.org/10.1021/acsabm.0c00772>
- Demir, I., Lüchtfeld, I., Lemen, C., Dague, E., Guiraud, P., Zambelli, T., & Formosa-Dague, C. (2021). Probing the interactions between air bubbles and (bio)interfaces at the nanoscale using FluidFM technology. *Journal of Colloid and Interface Science*, 604, 785–797. <https://doi.org/10.1016/j.jcis.2021.07.036>
- Demirbas, A. (Ed.). (2009). Introduction. In *Biohydrogen: For Future Engine Fuel Demands* (pp. 1–42). Springer. https://doi.org/10.1007/978-1-84882-511-6_1
- Demir-Yilmaz, I., Guiraud, P., & Formosa-Dague, C. (2021a). The contribution of Atomic Force Microscopy (AFM) in microalgae studies: A review. *Algal Research*, 60, 102506.
<https://doi.org/10.1016/j.algal.2021.102506>
- Demir-Yilmaz, I., Guiraud, P., & Formosa-Dague, C. (2021b). The contribution of Atomic Force Microscopy (AFM) in microalgae studies: A review. *Algal Research*, 60, 102506.
<https://doi.org/10.1016/j.algal.2021.102506>
- Demir-Yilmaz, I., Schiavone, M., Esvan, J., Guiraud, P., & Formosa-Dague, C. (2022). *Combining AFM, XPS and chemical hydrolysis to understand the complexity and dynamics of C. vulgaris cell wall composition and architecture* (p. 2022.07.11.499560). bioRxiv. <https://doi.org/10.1101/2022.07.11.499560>
- Demir-Yilmaz, I., Yakovenko, N., Roux, C., Guiraud, P., Collin, F., Coudret, C., ter Halle, A., & Formosa-Dague, C. (2022). The role of microplastics in microalgae cells aggregation: A

- study at the molecular scale using atomic force microscopy. *Science of The Total Environment*, 832, 155036. <https://doi.org/10.1016/j.scitotenv.2022.155036>
- Demuez, M., Mahdy, A., Tomás-Pejó, E., González-Fernández, C., & Ballesteros, M. (2015). Enzymatic cell disruption of microalgae biomass in biorefinery processes. *Biotechnology and Bioengineering*, 112(10), 1955–1966. <https://doi.org/10.1002/bit.25644>
- Desbrieres, J. (2004). Autoassociative natural polymer derivatives: The alkylchitosans. Rheological behaviour and temperature stability. *Polymer*, 45(10), 3285–3295. <https://doi.org/10.1016/j.polymer.2004.03.032>
- Desbrières, J., Martinez, C., & Rinaudo, M. (1996). Hydrophobic derivatives of chitosan: Characterization and rheological behaviour. *International Journal of Biological Macromolecules*, 19(1), 21–28. [https://doi.org/10.1016/0141-8130\(96\)01095-1](https://doi.org/10.1016/0141-8130(96)01095-1)
- Dismukes, G. C., Carrieri, D., Bennette, N., Ananyev, G. M., & Posewitz, M. C. (2008). Aquatic phototrophs: Efficient alternatives to land-based crops for biofuels. *Current Opinion in Biotechnology*, 19(3), 235–240. <https://doi.org/10.1016/j.copbio.2008.05.007>
- Ditscherlein, L., Jolan Gulden, S., Müller, S., Baumann, R.-P., Peuker, U. A., & Nirschl, H. (2018). Measuring interactions between yeast cells and a micro-sized air bubble via atomic force microscopy. *Journal of Colloid and Interface Science*, 532, 689–699. <https://doi.org/10.1016/j.jcis.2018.08.031>
- Dong, T., Knoshaug, E. P., Pienkos, P. T., & Laurens, L. M. L. (2016). Lipid recovery from wet oleaginous microbial biomass for biofuel production: A critical review. *Applied Energy*, 177, 879–895. <https://doi.org/10.1016/j.apenergy.2016.06.002>

Ducker, W. A., Senden, T. J., & Pashley, R. M. (1991). Direct measurement of colloidal forces using an atomic force microscope. *Nature*, *353*(6341), Article 6341.

<https://doi.org/10.1038/353239a0>

Ducker, W. A., Xu, Z., & Israelachvili, J. N. (1994). Measurements of Hydrophobic and DLVO Forces in Bubble-Surface Interactions in Aqueous Solutions. *Langmuir*, *10*(9), 3279–3289. <https://doi.org/10.1021/la00021a061>

Erdawati, Kanza, M., Saefurahman, G., Hidayatuloh, S., & Kawaroe, M. (2020). Effect of pH culture and dosage of chitosan nanoemulsion on the effectiveness of bioflocculation in harvesting *Chlorella* sp. Biomass. *IOP Conference Series: Earth and Environmental Science*, *460*(1), 012005. <https://doi.org/10.1088/1755-1315/460/1/012005>

Eriksson, J. C., & Ljunggren, S. (1999). On the mechanically unstable free energy minimum of a gas bubble which is submerged in water and adheres to a hydrophobic wall.

Colloids and Surfaces A: Physicochemical and Engineering Aspects, *159*(1), 159–163.

[https://doi.org/10.1016/S0927-7757\(99\)00171-5](https://doi.org/10.1016/S0927-7757(99)00171-5)

Farid, M. S., Shariati, A., Badakhshan, A., & Anvaripour, B. (2013). Using nano-chitosan for harvesting microalga *Nannochloropsis* sp. *Bioresource Technology*, *131*, 555–559.

<https://doi.org/10.1016/j.biortech.2013.01.058>

Fercoq, A., Lamouri, S., & Carbone, V. (2016). Lean/Green integration focused on waste reduction techniques. *Journal of Cleaner Production*, *137*, 567–578.

<https://doi.org/10.1016/j.jclepro.2016.07.107>

Formosa-Dague, C., Castelain, M., Martin-Yken, H., Dunker, K., Dague, E., & Sletmoen, M. (2018). The Role of Glycans in Bacterial Adhesion to Mucosal Surfaces: How Can Single-Molecule Techniques Advance Our Understanding? *Microorganisms*, *6*(2),

Article 2. <https://doi.org/10.3390/microorganisms6020039>

Formosa-Dague, C., Gernigon, V., Castelain, M., Daboussi, F., & Guiraud, P. (2018a). Towards a better understanding of the flocculation/flotation mechanism of the marine microalgae *Phaeodactylum tricornutum* under increased pH using atomic force microscopy. *Algal Research*, *33*, 369–378.

<https://doi.org/10.1016/j.algal.2018.06.010>

Formosa-Dague, C., Gernigon, V., Castelain, M., Daboussi, F., & Guiraud, P. (2018b). Towards a better understanding of the flocculation/flotation mechanism of the marine microalgae *Phaeodactylum tricornutum* under increased pH using atomic force microscopy. *Algal Research*, *33*, 369–378.

<https://doi.org/10.1016/j.algal.2018.06.010>

Francius, G., Tesson, B., Dague, E., Martin-Jézéquel, V., & Dufrêne, Y. F. (2008).

Nanostructure and nanomechanics of live *Phaeodactylum tricornutum* morphotypes.

Environmental Microbiology, *10*(5), 1344–1356. [https://doi.org/10.1111/j.1462-](https://doi.org/10.1111/j.1462-2920.2007.01551.x)

[2920.2007.01551.x](https://doi.org/10.1111/j.1462-2920.2007.01551.x)

Frenkel, V. (2008). Ultrasound mediated delivery of drugs and genes to solid tumors.

Advanced Drug Delivery Reviews, *60*(10), 1193–1208.

<https://doi.org/10.1016/j.addr.2008.03.007>

Gao, Z., Kennedy, A. M., Christensen, D. A., & Rapoport, N. Y. (2008). Drug-loaded

nano/microbubbles for combining ultrasonography and targeted chemotherapy.

Ultrasonics, *48*(4), 260–270. <https://doi.org/10.1016/j.ultras.2007.11.002>

Garg, S., Li, Y., Wang, L., & Schenk, P. M. (2012a). Flotation of marine microalgae: Effect of algal hydrophobicity. *Bioresource Technology*, *121*, 471–474.

<https://doi.org/10.1016/j.biortech.2012.06.111>

- Garg, S., Li, Y., Wang, L., & Schenk, P. M. (2012b). Flotation of marine microalgae: Effect of algal hydrophobicity. *Bioresource Technology*, *121*, 471–474.
<https://doi.org/10.1016/j.biortech.2012.06.111>
- Gerardo, M. L., Van Den Hende, S., Vervaeren, H., Coward, T., & Skill, S. C. (2015). Harvesting of microalgae within a biorefinery approach: A review of the developments and case studies from pilot-plants. *Algal Research*, *11*, 248–262.
<https://doi.org/10.1016/j.algal.2015.06.019>
- Gerken, H. G., Donohoe, B., & Knoshaug, E. P. (2013). Enzymatic cell wall degradation of *Chlorella vulgaris* and other microalgae for biofuels production. *Planta*, *237*(1), 239–253. <https://doi.org/10.1007/s00425-012-1765-0>
- Ghassemi, N., Poulhazan, A., Deligey, F., Mentink-Vigier, F., Marcotte, I., & Wang, T. (2021). Solid-State NMR Investigations of Extracellular Matrixes and Cell Walls of Algae, Bacteria, Fungi, and Plants. *Chemical Reviews*.
<https://doi.org/10.1021/acs.chemrev.1c00669>
- Glaser, K., & Karsten, U. (2020). Salinity tolerance in biogeographically different strains of the marine benthic diatom *Cylindrotheca closterium* (Bacillariophyceae). *Journal of Applied Phycology*, *32*(6), 3809–3816. <https://doi.org/10.1007/s10811-020-02238-6>
- Grüter, R. R., Vörös, J., & Zambelli, T. (2013). FluidFM as a lithography tool in liquid: Spatially controlled deposition of fluorescent nanoparticles. *Nanoscale*, *5*(3), 1097–1104.
<https://doi.org/10.1039/C2NR33214K>
- Guillard, R. R. L. (1975). Culture of Phytoplankton for Feeding Marine Invertebrates. In W. L. Smith & M. H. Chanley (Eds.), *Culture of Marine Invertebrate Animals: Proceedings—1st Conference on Culture of Marine Invertebrate Animals Greenport* (pp. 29–60). Springer US. https://doi.org/10.1007/978-1-4615-8714-9_3

- Guillaume-Gentil, O., Gäbelein, C. G., Schmieder, S., Martinez, V., Zambelli, T., Künzler, M., & Vorholt, J. A. (2022). Injection into and extraction from single fungal cells. *Communications Biology*, 5(1), 180. <https://doi.org/10.1038/s42003-022-03127-z>
- Guillaume-Gentil, O., Grindberg, R. V., Kooger, R., Dorwling-Carter, L., Martinez, V., Ossola, D., Pilhofer, M., Zambelli, T., & Vorholt, J. A. (2016). Tunable Single-Cell Extraction for Molecular Analyses. *Cell*, 166(2), 506–516. <https://doi.org/10.1016/j.cell.2016.06.025>
- Guillaume-Gentil, O., Zambelli, T., & Vorholt, J. A. (2013). Isolation of single mammalian cells from adherent cultures by fluidic force microscopy. *Lab on a Chip*, 14(2), 402–414. <https://doi.org/10.1039/C3LC51174J>
- Günerken, E., D'Hondt, E., Eppink, M. H. M., Garcia-Gonzalez, L., Elst, K., & Wijffels, R. H. (2015). Cell disruption for microalgae biorefineries. *Biotechnology Advances*, 33(2), 243–260. <https://doi.org/10.1016/j.biotechadv.2015.01.008>
- Gupta, P. L., Lee, S.-M., & Choi, H.-J. (2016). Integration of microalgal cultivation system for wastewater remediation and sustainable biomass production. *World Journal of Microbiology and Biotechnology*, 32(8), 139. <https://doi.org/10.1007/s11274-016-2090-8>
- Hassanzadeh, A., Sajjady, S. A., Gholami, H., Amini, S., & Özkan, S. G. (2020). An Improvement on Selective Separation by Applying Ultrasound to Rougher and Re-Cleaner Stages of Copper Flotation. *Minerals*, 10(7), Article 7. <https://doi.org/10.3390/min10070619>
- Henderson, R. K., Parsons, S. A., & Jefferson, B. (2008a). Successful Removal of Algae through the Control of Zeta Potential. *Separation Science and Technology*, 43(7), 1653–1666. <https://doi.org/10.1080/01496390801973771>

- Henderson, R. K., Parsons, S. A., & Jefferson, B. (2008b). Surfactants as Bubble Surface Modifiers in the Flotation of Algae: Dissolved Air Flotation That Utilizes a Chemically Modified Bubble Surface. *Environmental Science & Technology*, 42(13), 4883–4888. <https://doi.org/10.1021/es702649h>
- Henderson, R. K., Parsons, S. A., & Jefferson, B. (2010). Polymers as bubble surface modifiers in the flotation of algae. *Environmental Technology*, 31(7), 781–790. <https://doi.org/10.1080/09593331003663302>
- Hertz, H. (1881). Ueber die berührung fester elastischer körper. *Journal Fur Die Reine Und Angewandte Mathematik*, 156–171.
- Hirt, L., Grüter, R. R., Berthelot, T., Cornut, R., Vörös, J., & Zambelli, T. (2015). Local surface modification via confined electrochemical deposition with FluidFM. *RSC Advances*, 5(103), 84517–84522. <https://doi.org/10.1039/C5RA07239E>
- Houot, R. (1982). Beneficiation of phosphatic ores through flotation: Review of industrial applications and potential developments. *International Journal of Mineral Processing*, 9(4), 353–384. [https://doi.org/10.1016/0301-7516\(82\)90041-2](https://doi.org/10.1016/0301-7516(82)90041-2)
- Huang, Z., Legendre, D., & Guiraud, P. (2012). Effect of interface contamination on particle–bubble collision. *Chemical Engineering Science*, 68(1), 1–18. <https://doi.org/10.1016/j.ces.2011.07.045>
- Hutter, J. L., & Bechhoefer, J. (1993). Calibration of atomic-force microscope tips. *Review of Scientific Instruments*, 64(7), 1868–1873. <https://doi.org/10.1063/1.1143970>
- Hwang, T., Park, S.-J., Oh, Y.-K., Rashid, N., & Han, J.-I. (2013). Harvesting of *Chlorella* sp. KR-1 using a cross-flow membrane filtration system equipped with an anti-fouling membrane. *Bioresource Technology*, 139, 379–382. <https://doi.org/10.1016/j.biortech.2013.03.149>

- Iversen, M. H., & Ploug, H. (2013). Temperature effects on carbon-specific respiration rate and sinking velocity of diatom aggregates – potential implications for deep ocean export processes. *Biogeosciences*, *10*(6), 4073–4085.
<https://doi.org/10.5194/bg-10-4073-2013>
- Jiang, L., Pei, H., Hu, W., Hou, Q., Han, F., & Nie, C. (2016). Biomass production and nutrient assimilation by a novel microalga, *Monoraphidium* spp. SDEC-17, cultivated in a high-ammonia wastewater. *Energy Conversion and Management*, *123*, 423–430.
<https://doi.org/10.1016/j.enconman.2016.06.060>
- Jiang, W., Gao, Z., Khoso, S. A., Gao, J., Sun, W., Pu, W., & Hu, Y. (2018). Selective adsorption of benzhydroxamic acid on fluorite rendering selective separation of fluorite/calcite. *Applied Surface Science*, *435*, 752–758. <https://doi.org/10.1016/j.apsusc.2017.11.093>
- Jiang, Y., Yoshida, T., & Quigg, A. (2012). Photosynthetic performance, lipid production and biomass composition in response to nitrogen limitation in marine microalgae. *Plant Physiology and Biochemistry*, *54*, 70–77.
<https://doi.org/10.1016/j.plaphy.2012.02.012>
- Karsten, U. (2012). Seaweed Acclimation to Salinity and Desiccation Stress. In C. Wiencke & K. Bischof (Eds.), *Seaweed Biology: Novel Insights into Ecophysiology, Ecology and Utilization* (pp. 87–107). Springer. https://doi.org/10.1007/978-3-642-28451-9_5
- Khojasteh, D., Kazerooni, N. M., & Marengo, M. (2019). A review of liquid droplet impacting onto solid spherical particles: A physical pathway to encapsulation mechanisms. *Journal of Industrial and Engineering Chemistry*, *71*, 50–64.
<https://doi.org/10.1016/j.jiec.2018.11.030>
- Kim, K. H., Choi, I. S., Kim, H. M., Wi, S. G., & Bae, H.-J. (2014). Bioethanol production from the nutrient stress-induced microalga *Chlorella vulgaris* by enzymatic hydrolysis and

- immobilized yeast fermentation. *Bioresource Technology*, 153, 47–54.
<https://doi.org/10.1016/j.biortech.2013.11.059>
- Kim, S.-K. (2015). *Handbook of Marine Microalgae: Biotechnology Advances* (Academic Press).
- Klibanov, A. L. (2007). Ultrasound molecular imaging with targeted microbubble contrast agents. *Journal of Nuclear Cardiology*, 14(6), 876.
<https://doi.org/10.1016/j.nuclcard.2007.09.008>
- Kovač, N., Mozetič, P., Trichet, J., & Défarge, C. (2005). Phytoplankton composition and organic matter organization of mucous aggregates by means of light and cryo-scanning electron microscopy. *Marine Biology*, 147(1), 261–271.
<https://doi.org/10.1007/s00227-004-1531-3>
- Kriegel, A. T., & Ducker, W. A. (2019). Removal of Bacteria from Solids by Bubbles: Effect of Solid Wettability, Interaction Geometry, and Liquid–Vapor Interface Velocity. *Langmuir*. <https://doi.org/10.1021/acs.langmuir.9b01941>
- Laamanen, C. A., Ross, G. M., & Scott, J. A. (2016). Flotation harvesting of microalgae. *Renewable and Sustainable Energy Reviews*, 58, 75–86.
<https://doi.org/10.1016/j.rser.2015.12.293>
- Laifa, R., Morchain, J., Barna, L., & Guiraud, P. (2021). A numerical framework to predict the performances of a tubular photobioreactor from operating and sunlight conditions. *Algal Research*, 60, 102550. <https://doi.org/10.1016/j.algal.2021.102550>
- Lam, M. K., & Lee, K. T. (2012). Microalgae biofuels: A critical review of issues, problems and the way forward. *Biotechnology Advances*, 30(3), 673–690.
<https://doi.org/10.1016/j.biotechadv.2011.11.008>

- Lama, S., Muylaert, K., Karki, T. B., Foubert, I., Henderson, R. K., & Vandamme, D. (2016). Flocculation properties of several microalgae and a cyanobacterium species during ferric chloride, chitosan and alkaline flocculation. *Bioresource Technology*, *220*, 464–470. <https://doi.org/10.1016/j.biortech.2016.08.080>
- Lee, S. Y., Cho, J. M., Chang, Y. K., & Oh, Y.-K. (2017). Cell disruption and lipid extraction for microalgal biorefineries: A review. *Bioresource Technology*, *244*, 1317–1328. <https://doi.org/10.1016/j.biortech.2017.06.038>
- Legendre, D., Sarrot, V., & Guiraud, P. (2009). On the particle inertia-free collision with a partially contaminated spherical bubble. *International Journal of Multiphase Flow*, *35*(2), 163–170. <https://doi.org/10.1016/j.ijmultiphaseflow.2008.10.002>
- Ljunggren, S., & Eriksson, J. C. (1997). The lifetime of a colloid-sized gas bubble in water and the cause of the hydrophobic attraction. *Colloids and Surfaces A: Physicochemical and Engineering Aspects*, *129–130*, 151–155. [https://doi.org/10.1016/S0927-7757\(97\)00033-2](https://doi.org/10.1016/S0927-7757(97)00033-2)
- Lu, Y., Wang, S., & Zhong, H. (2021). Study on the role of a hydroxamic acid derivative in wolframite flotation: Selective separation and adsorption mechanism. *Applied Surface Science*, *550*, 149223. <https://doi.org/10.1016/j.apsusc.2021.149223>
- Ma, J., Zhou, B., Chen, F., & Pan, K. (2021). How marine diatoms cope with metal challenge: Insights from the morphotype-dependent metal tolerance in *Phaeodactylum tricornutum*. *Ecotoxicology and Environmental Safety*, *208*, 111715. <https://doi.org/10.1016/j.ecoenv.2020.111715>
- Ma, J., Zhou, B., Duan, D., & Pan, K. (2019). Salinity-dependent nanostructures and composition of cell surface and its relation to Cd toxicity in an estuarine diatom. *Chemosphere*, *215*, 807–814. <https://doi.org/10.1016/j.chemosphere.2018.10.128>

- Ma, M. (2012). Froth Flotation of Iron Ores. *International Journal of Mining Engineering and Mineral Processing*, 1(2), 56–61. <https://doi.org/10.5923/j.mining.20120102.06>
- Maddah, H., & Chogle, A. (2017). Biofouling in reverse osmosis: Phenomena, monitoring, controlling and remediation. *Applied Water Science*, 7(6), 2637–2651. <https://doi.org/10.1007/s13201-016-0493-1>
- Maldonado, R. F., Sá-Correia, I., & Valvano, M. A. (2016). Lipopolysaccharide modification in Gram-negative bacteria during chronic infection. *FEMS Microbiology Reviews*, 40(4), 480–493. <https://doi.org/10.1093/femsre/fuw007>
- Markou, G., & Nerantzis, E. (2013). Microalgae for high-value compounds and biofuels production: A review with focus on cultivation under stress conditions. *Biotechnology Advances*, 31(8), 1532–1542. <https://doi.org/10.1016/j.biotechadv.2013.07.011>
- Matho, C., Schwarzenberger, K., Eckert, K., Keshavarzi, B., Walther, T., Steingroewer, J., & Krujatz, F. (2019). Bio-compatible flotation of *Chlorella vulgaris*: Study of zeta potential and flotation efficiency. *Algal Research*, 44, 101705. <https://doi.org/10.1016/j.algal.2019.101705>
- Mathur, S., Singh, P., & Moudgil, B. M. (2000). Advances in selective flocculation technology for solid-solid separations. *International Journal of Mineral Processing*, 58(1), 201–222. [https://doi.org/10.1016/S0301-7516\(99\)00072-1](https://doi.org/10.1016/S0301-7516(99)00072-1)
- Mati-Baouche, N., Delattre, C., de Baynast, H., Grédiac, M., Mathias, J.-D., Ursu, A. V., Desbrières, J., & Michaud, P. (2019). Alkyl-Chitosan-Based Adhesive: Water Resistance Improvement. *Molecules*, 24(10), Article 10. <https://doi.org/10.3390/molecules24101987>

- Matis, K. A., & Lazaridis, N. K. (2002). Flotation techniques in water technology for metals recovery: Dispersed-air vs. dissolved-air flotation. *Journal of Mining and Metallurgy A: Mining*, 38(1–4), 1–27.
- Meister, A., Gabi, M., Behr, P., Studer, P., Vörös, J., Niedermann, P., Bitterli, J., Polesel-Maris, J., Liley, M., Heinzelmann, H., & Zambelli, T. (2009a). FluidFM: Combining atomic force microscopy and nanofluidics in a universal liquid delivery system for single cell applications and beyond. *Nano Letters*, 9(6), 2501–2507.
<https://doi.org/10.1021/nl901384x>
- Meister, A., Gabi, M., Behr, P., Studer, P., Vörös, J., Niedermann, P., Bitterli, J., Polesel-Maris, J., Liley, M., Heinzelmann, H., & Zambelli, T. (2009b). FluidFM: Combining Atomic Force Microscopy and Nanofluidics in a Universal Liquid Delivery System for Single Cell Applications and Beyond. *Nano Letters*, 9(6), 2501–2507.
<https://doi.org/10.1021/nl901384x>
- Miettinen, T., Ralston, J., & Fornasiero, D. (2010). The limits of fine particle flotation. *Minerals Engineering*, 23(5), 420–437. <https://doi.org/10.1016/j.mineng.2009.12.006>
- Minhas, A. K., Hodgson, P., Barrow, C. J., & Adholeya, A. (2016). A Review on the Assessment of Stress Conditions for Simultaneous Production of Microalgal Lipids and Carotenoids. *Frontiers in Microbiology*, 7. <https://doi.org/10.3389/fmicb.2016.00546>
- Mishchuk, N., Ralston, J., & Fornasiero, D. (2006). Influence of very small bubbles on particle/bubble heterocoagulation. *Journal of Colloid and Interface Science*, 301(1), 168–175. <https://doi.org/10.1016/j.jcis.2006.04.071>
- Mišić Radić, T., Čačković, A., Penezić, A., Dautović, J., Lončar, J., Omanović, D., Juraić, K., & Ljubešić, Z. (2021). Physiological and morphological response of marine diatom

- Cylindrotheca closterium* (Bacillariophyceae) exposed to Cadmium. *European Journal of Phycology*, 56(1), 24–36. <https://doi.org/10.1080/09670262.2020.1758347>
- Molina Grima, E., Belarbi, E.-H., Acién Fernández, F. G., Robles Medina, A., & Chisti, Y. (2003). Recovery of microalgal biomass and metabolites: Process options and economics. *Biotechnology Advances*, 20(7), 491–515. [https://doi.org/10.1016/S0734-9750\(02\)00050-2](https://doi.org/10.1016/S0734-9750(02)00050-2)
- Nagappan, S., Devendran, S., Tsai, P.-C., Dinakaran, S., Dahms, H.-U., & Ponnusamy, V. K. (2019). Passive cell disruption lipid extraction methods of microalgae for biofuel production – A review. *Fuel*, 252, 699–709. <https://doi.org/10.1016/j.fuel.2019.04.092>
- Najdek, M., Blažina, M., Djakovac, T., & Kraus, R. (2005). The role of the diatom *Cylindrotheca closterium* in a mucilage event in the northern Adriatic Sea: Coupling with high salinity water intrusions. *Journal of Plankton Research*, 27(9), 851–862. <https://doi.org/10.1093/plankt/fbi057>
- Nguyen, A. V., George, P., & Jameson, G. J. (2006). Demonstration of a minimum in the recovery of nanoparticles by flotation: Theory and experiment. *Chemical Engineering Science*, 61(8), 2494–2509. <https://doi.org/10.1016/j.ces.2005.11.025>
- Norsker, N.-H., Barbosa, M. J., Vermuë, M. H., & Wijffels, R. H. (2011). Microalgal production—A close look at the economics. *Biotechnology Advances*, 29(1), 24–27. <https://doi.org/10.1016/j.biotechadv.2010.08.005>
- Novosel, N., Mišić Radić, T., Levak Zorinc, M., Zemla, J., Lekka, M., Vrana, I., Gašparović, B., Horvat, L., Kasum, D., Legović, T., Žutinić, P., Gligora Udovič, M., & Ivošević DeNardis, N. (2022). Salinity-induced chemical, mechanical, and behavioral changes in marine

- microalgae. *Journal of Applied Phycology*. <https://doi.org/10.1007/s10811-022-02734-x>
- Olaizola, M. (2003). Commercial development of microalgal biotechnology: From the test tube to the marketplace. *Biomolecular Engineering*, *20*(4), 459–466.
[https://doi.org/10.1016/S1389-0344\(03\)00076-5](https://doi.org/10.1016/S1389-0344(03)00076-5)
- Ossola, D., Amarouch, M.-Y., Behr, P., Vörös, J., Abriel, H., & Zambelli, T. (2015). Force-Controlled Patch Clamp of Beating Cardiac Cells. *Nano Letters*, *15*(3), 1743–1750.
<https://doi.org/10.1021/nl504438z>
- Ozkan, A., & Berberoglu, H. (2013a). Physico-chemical surface properties of microalgae. *Colloids and Surfaces B: Biointerfaces*, *112*, 287–293.
<https://doi.org/10.1016/j.colsurfb.2013.08.001>
- Ozkan, A., & Berberoglu, H. (2013b). Physico-chemical surface properties of microalgae. *Colloids and Surfaces B: Biointerfaces*, *112*, 287–293.
<https://doi.org/10.1016/j.colsurfb.2013.08.001>
- Pal, S., Mal, D., & Singh, R. P. (2005). Cationic starch: An effective flocculating agent. *Carbohydrate Polymers*, *59*(4), 417–423.
<https://doi.org/10.1016/j.carbpol.2004.06.047>
- Pan, Y.-Y., Wang, S.-T., Chuang, L.-T., Chang, Y.-W., & Chen, C.-N. N. (2011). Isolation of thermo-tolerant and high lipid content green microalgae: Oil accumulation is predominantly controlled by photosystem efficiency during stress treatments in *Desmodesmus*. *Bioresource Technology*, *102*(22), 10510–10517.
<https://doi.org/10.1016/j.biortech.2011.08.091>

- Pillet, F., Dague, E., Pečar Ilić, J., Ružić, I., Rols, M.-P., & Ivošević DeNardis, N. (2019). Changes in nanomechanical properties and adhesion dynamics of algal cells during their growth. *Bioelectrochemistry*, *127*, 154–162. <https://doi.org/voelcker>
- Piontek, J., Händel, N., Langer, G., Wohlers, J., Riebesell, U., & Engel, A. (2009). Effects of rising temperature on the formation and microbial degradation of marine diatom aggregates. *Aquatic Microbial Ecology*, *54*(3), 305–318. <https://doi.org/10.3354/ame01273>
- Pita, F., & Castilho, A. (2017). Separation of plastics by froth flotation. The role of size, shape and density of the particles. *Waste Management*, *60*, 91–99. <https://doi.org/10.1016/j.wasman.2016.07.041>
- Pletikapić, G., & Ivošević DeNardis, N. (2017). Application of surface analytical methods for hazardous situation in the Adriatic Sea: Monitoring of organic matter dynamics and oil pollution. *Natural Hazards and Earth System Sciences*, *17*(1), 31–44. <https://doi.org/10.5194/nhess-17-31-2017>
- Pletikapić, G., Radić, T. M., Zimmermann, A. H., Svetličić, V., Pfannkuchen, M., Marić, D., Godrijan, J., & Žutić, V. (2011). AFM imaging of extracellular polymer release by marine diatom *Cylindrotheca closterium* (Ehrenberg) Reiman & J.C. Lewin. *Journal of Molecular Recognition*, *24*(3), 436–445. <https://doi.org/10.1002/jmr.1114>
- Potthoff, E., Guillaume-Gentil, O., Ossola, D., Polesel-Maris, J., LeibundGut-Landmann, S., Zambelli, T., & Vorholt, J. A. (2012). Rapid and Serial Quantification of Adhesion Forces of Yeast and Mammalian Cells. *PLOS ONE*, *7*(12), e52712. <https://doi.org/10.1371/journal.pone.0052712>

- Potthoff, E., Ossola, D., Zambelli, T., & Vorholt, J. A. (2015). Bacterial adhesion force quantification by fluidic force microscopy. *Nanoscale*, 7(9), 4070–4079.
<https://doi.org/10.1039/C4NR06495J>
- Poulhazan, A., Dickwella Widanage, M. C., Muszyński, A., Arnold, A. A., Warschawski, D. E., Azadi, P., Marcotte, I., & Wang, T. (2021). Identification and Quantification of Glycans in Whole Cells: Architecture of Microalgal Polysaccharides Described by Solid-State Nuclear Magnetic Resonance. *Journal of the American Chemical Society*, 143(46), 19374–19388. <https://doi.org/10.1021/jacs.1c07429>
- Pragya, N., Pandey, K. K., & Sahoo, P. K. (2013). A review on harvesting, oil extraction and biofuels production technologies from microalgae. *Renewable and Sustainable Energy Reviews*, 24, 159–171. <https://doi.org/10.1016/j.rser.2013.03.034>
- Radić, T. M., Svetličić, V., Žutić, V., & Boulgaropoulos, B. (2011). Seawater at the nanoscale: Marine gel imaged by atomic force microscopy. *Journal of Molecular Recognition*, 24(3), 397–405. <https://doi.org/10.1002/jmr.1072>
- Rashid, N., Park, W.-K., & Selvaratnam, T. (2018). Binary culture of microalgae as an integrated approach for enhanced biomass and metabolites productivity, wastewater treatment, and bioflocculation. *Chemosphere*, 194, 67–75.
<https://doi.org/10.1016/j.chemosphere.2017.11.108>
- Rashid, N., Rehman, S. U., & Han, J.-I. (2013). Rapid harvesting of freshwater microalgae using chitosan. *Process Biochemistry*, 48(7), 1107–1110.
<https://doi.org/10.1016/j.procbio.2013.04.018>
- Reifarth, M., Hoepfner, S., & Schubert, U. S. (2018). Uptake and Intracellular Fate of Engineered Nanoparticles in Mammalian Cells: Capabilities and Limitations of

- Transmission Electron Microscopy—Polymer-Based Nanoparticles. *Advanced Materials*, 30(9), 1703704. <https://doi.org/10.1002/adma.201703704>
- Ren, Z., Yu, F., Gao, H., Chen, Z., Peng, Y., & Liu, L. (2017). Selective Separation of Fluorite, Barite and Calcite with Valonea Extract and Sodium Fluosilicate as Depressants. *Minerals*, 7(2), Article 2. <https://doi.org/10.3390/min7020024>
- Renault, F., Sancey, B., Badot, P.-M., & Crini, G. (2009). Chitosan for coagulation/flocculation processes – An eco-friendly approach. *European Polymer Journal*, 45(5), 1337–1348. <https://doi.org/10.1016/j.eurpolymj.2008.12.027>
- Richardson, J. W., & Johnson, M. D. (2014). Economic viability of a reverse engineered algae farm (REAF). *Algal Research*, 3, 66–70. <https://doi.org/10.1016/j.algal.2013.10.002>
- Rijstenbil, J. W. (2005). UV- and salinity-induced oxidative effects in the marine diatom *Cylindrotheca closterium* during simulated emersion. *Marine Biology*, 147(5), 1063–1073. <https://doi.org/10.1007/s00227-005-0015-4>
- Rodolfi, L., Zittelli, G. C., Bassi, N., Padovani, G., Biondi, N., Bonini, G., & Tredici, M. R. (2009). Microalgae for oil: Strain selection, induction of lipid synthesis and outdoor mass cultivation in a low-cost photobioreactor. *Biotechnology and Bioengineering*, 102(1), 100–112. <https://doi.org/10.1002/bit.22033>
- Roncarati, F., Rijstenbil, J. W., & Pistocchi, R. (2008). Photosynthetic performance, oxidative damage and antioxidants in *Cylindrotheca closterium* in response to high irradiance, UVB radiation and salinity. *Marine Biology*, 153(5), 965–973. <https://doi.org/10.1007/s00227-007-0868-9>
- Rouxhet, P. G., & Genet, M. J. (2011). XPS analysis of bio-organic systems. *Surface and Interface Analysis*, 43(12), 1453–1470. <https://doi.org/10.1002/sia.3831>

- Sarrot, V., Guiraud, P., & Legendre, D. (2005). Determination of the collision frequency between bubbles and particles in flotation. *Chemical Engineering Science*, *60*(22), 6107–6117. <https://doi.org/10.1016/j.ces.2005.02.018>
- Sarrot, V., Huang, Z., Legendre, D., & Guiraud, P. (2007). Experimental determination of particles capture efficiency in flotation. *Chemical Engineering Science*, *62*(24), 7359–7369. <https://doi.org/10.1016/j.ces.2007.08.028>
- Scala, S., & Bowler, C. (2001). Molecular insights into the novel aspects of diatom biology. *Cellular and Molecular Life Sciences: CMLS*, *58*(11), 1666–1673. <https://doi.org/10.1007/PL00000804>
- Schenk, P. M., Thomas-Hall, S. R., Stephens, E., Marx, U. C., Mussgnug, J. H., Posten, C., Kruse, O., & Hankamer, B. (2008). Second Generation Biofuels: High-Efficiency Microalgae for Biodiesel Production. *BioEnergy Research*, *1*(1), 20–43. <https://doi.org/10.1007/s12155-008-9008-8>
- Schiavone, M., Vax, A., Formosa, C., Martin-Yken, H., Dague, E., & François, J. M. (2014). A combined chemical and enzymatic method to determine quantitatively the polysaccharide components in the cell wall of yeasts. *FEMS Yeast Research*, *14*(6), 933–947. <https://doi.org/10.1111/1567-1364.12182>
- Scragg, A. H., Illman, A. M., Carden, A., & Shales, S. W. (2002). Growth of microalgae with increased calorific values in a tubular bioreactor. *Biomass and Bioenergy*, *23*(1), 67–73. [https://doi.org/10.1016/S0961-9534\(02\)00028-4](https://doi.org/10.1016/S0961-9534(02)00028-4)
- Separovic, F., & Sani, M.-A. (Eds.). (2020). *Solid-State NMR: Applications in biomembrane structure*. IOP Publishing. <https://doi.org/10.1088/978-0-7503-2532-5>

- Shchukarev, A., Gojkovic, Z., Funk, C., & Ramstedt, M. (2020). Cryo-XPS analysis reveals surface composition of microalgae. *Applied Surface Science*, 526, 146538. <https://doi.org/10.1016/j.apsusc.2020.146538>
- Sheehan, J., Dunahay, T., Benemann, J., & Roessler, P. (1998). *Look Back at the U.S. Department of Energy's Aquatic Species Program: Biodiesel from Algae; Close-Out Report*. https://www.academia.edu/3090889/A_look_back_at_the_US_department_of_ener_gys_aquatic_species_program_biodiesel_from_algae
- Staats, N., Stal, L. J., & Mur, L. R. (2000). Exopolysaccharide production by the epipellic diatom *Cylindrotheca closterium*: Effects of nutrient conditions. *Journal of Experimental Marine Biology and Ecology*, 249(1), 13–27. [https://doi.org/10.1016/S0022-0981\(00\)00166-0](https://doi.org/10.1016/S0022-0981(00)00166-0)
- Steele, D. J., Franklin, D. J., & Underwood, G. J. C. (2014). Protection of cells from salinity stress by extracellular polymeric substances in diatom biofilms. *Biofouling*, 30(8), 987–998. <https://doi.org/10.1080/08927014.2014.960859>
- Stiefel, P., Schmidt, F. I., Dörig, P., Behr, P., Zambelli, T., Vorholt, J. A., & Mercer, J. (2012). Cooperative Vaccinia Infection Demonstrated at the Single-Cell Level Using FluidFM. *Nano Letters*, 12(8), 4219–4227. <https://doi.org/10.1021/nl3018109>
- Svetličić, V., Balnois, E., Žutić, V., Chevalet, J., Hozić Zimmermann, A., Kovač, S., & Vdović, N. (2006). Electrochemical Detection of Gel Microparticles in Seawater. *Croatica Chemica Acta*, 79(1), 107–113.
- Svetličić, V., Žutić, V., Radić, T. M., Pletikapić, G., Zimmermann, A. H., & Urbani, R. (2011). Polymer Networks Produced by Marine Diatoms in the Northern Adriatic Sea. *Marine Drugs*, 9(4), Article 4. <https://doi.org/10.3390/md9040666>

- Taleb, A., Kandilian, R., Touchard, R., Montalescot, V., Rinaldi, T., Taha, S., Takache, H., Marchal, L., Legrand, J., & Pruvost, J. (2016). Screening of freshwater and seawater microalgae strains in fully controlled photobioreactors for biodiesel production. *Bioresource Technology*, *218*, 480–490.
<https://doi.org/10.1016/j.biortech.2016.06.086>
- Tasić, M. B., Pinto, L. F. R., Klein, B. C., Veljković, V. B., & Filho, R. M. (2016). Botryococcus braunii for biodiesel production. *Renewable and Sustainable Energy Reviews*, *64*, 260–270. <https://doi.org/10.1016/j.rser.2016.06.009>
- Thornton, D. C. O. (2002). Diatom aggregation in the sea: Mechanisms and ecological implications. *European Journal of Phycology*, *37*(2), 149–161.
<https://doi.org/10.1017/S0967026202003657>
- Tinkov, S., Bekeredjian, R., Winter, G., & Coester, C. (2009). Microbubbles as ultrasound triggered drug carriers. *Journal of Pharmaceutical Sciences*, *98*(6), 1935–1961.
<https://doi.org/10.1002/jps.21571>
- Tiron, O., Bumbac, C., Manea, E., Stefanescu, M., & Nita Lazar, M. (2017). Overcoming Microalgae Harvesting Barrier by Activated Algae Granules. *Scientific Reports*, *7*(1), Article 1. <https://doi.org/10.1038/s41598-017-05027-3>
- Tréguer, P., Bowler, C., Moriceau, B., Dutkiewicz, S., Gehlen, M., Aumont, O., Bittner, L., Dugdale, R., Finkel, Z., Iudicone, D., Jahn, O., Guidi, L., Lasbleiz, M., Leblanc, K., Levy, M., & Pondaven, P. (2018). Influence of diatom diversity on the ocean biological carbon pump. *Nature Geoscience*, *11*(1), Article 1. <https://doi.org/10.1038/s41561-017-0028-x>

- Uduman, N., Qi, Y., Danquah, M. K., Forde, G. M., & Hoadley, A. (2010). Dewatering of microalgal cultures: A major bottleneck to algae-based fuels. *Journal of Renewable and Sustainable Energy*, 2(1), 012701. <https://doi.org/10.1063/1.3294480>
- Uduman, N., Qi, Y., Danquah, M. K., & Hoadley, A. F. A. (2010). Marine microalgae flocculation and focused beam reflectance measurement. *Chemical Engineering Journal*, 162(3), 935–940. <https://doi.org/10.1016/j.cej.2010.06.046>
- Van Bergeijk, S. A., Van der Zee, C., & Stal, L. J. (2003). Uptake and excretion of dimethylsulphoniopropionate is driven by salinity changes in the marine benthic diatom *Cylindrotheca closterium*. *European Journal of Phycology*, 38(4), 341–349. <https://doi.org/10.1080/09670260310001612600>
- van Nisselroy, C., Shen, C., Zambelli, T., & Momotenko, D. (2022). Electrochemical 3D printing of silver and nickel microstructures with FluidFM. *Additive Manufacturing*, 53, 102718. <https://doi.org/10.1016/j.addma.2022.102718>
- Vandamme, D., Foubert, I., & Muylaert, K. (2013). Flocculation as a low-cost method for harvesting microalgae for bulk biomass production. *Trends in Biotechnology*, 31(4), 233–239. <https://doi.org/10.1016/j.tibtech.2012.12.005>
- Vandamme, D., Pohl, P. I., Beuckels, A., Foubert, I., Brady, P. V., Hewson, J. C., & Muylaert, K. (2015). Alkaline flocculation of *Phaeodactylum tricornutum* induced by brucite and calcite. *Bioresource Technology*, 196, 656–661. <https://doi.org/10.1016/j.biortech.2015.08.042>
- Vergnes, J. B., Gernigon, V., Guiraud, P., & Formosa-Dague, C. (2019). Bicarbonate Concentration Induces Production of Exopolysaccharides by *Arthrospira platensis* That Mediate Bioflocculation and Enhance Flotation Harvesting Efficiency. *ACS*

Sustainable Chemistry & Engineering, 7(16), 13796–13804.

<https://doi.org/10.1021/acssuschemeng.9b01591>

Voigtländer, B. (2015). *Scanning Probe Microscopy: Atomic Force Microscopy and Scanning Tunneling Microscopy*. Springer.

Walls, P. L. L., Bird, J. C., & Bourouiba, L. (2014). Moving with Bubbles: A Review of the Interactions between Bubbles and the Microorganisms that Surround them.

Integrative and Comparative Biology, 54(6), 1014–1025.

<https://doi.org/10.1093/icb/icu100>

Wei, Y., Cheng, G., Ho, H.-P., Ho, Y.-P., & Yong, K.-T. (2020). Thermodynamic perspectives on liquid–liquid droplet reactors for biochemical applications. *Chemical Society Reviews*, 49(18), 6555–6567. <https://doi.org/10.1039/C9CS00541B>

Willemsen, O. H., Snel, M. M. E., van der Werf, K. O., de Grooth, B. G., Greve, J., Hinterdorfer, P., Gruber, H. J., Schindler, H., van Kooyk, Y., & Figdor, C. G. (1998). Simultaneous Height and Adhesion Imaging of Antibody-Antigen Interactions by Atomic Force Microscopy. *Biophysical Journal*, 75(5), 2220–2228.

[https://doi.org/10.1016/S0006-3495\(98\)77666-0](https://doi.org/10.1016/S0006-3495(98)77666-0)

Xu, Y., Purton, S., & Baganz, F. (2013). Chitosan flocculation to aid the harvesting of the microalga *Chlorella sorokiniana*. *Bioresource Technology*, 129, 296–301.

<https://doi.org/10.1016/j.biortech.2012.11.068>

Yahav, D., Farbman, L., Leibovici, L., & Paul, M. (2012). Colistin: New lessons on an old antibiotic. *Clinical Microbiology and Infection: The Official Publication of the European Society of Clinical Microbiology and Infectious Diseases*, 18(1), 18–29.

<https://doi.org/10.1111/j.1469-0691.2011.03734.x>

- Yan, X., Shi, R., Xu, Y., Wang, A., Liu, Y., Wang, L., & Cao, Y. (2016). Bubble behaviors in a lab-scale cyclonic-static micro-bubble flotation column. *Asia-Pacific Journal of Chemical Engineering*, 11(6), 939–948. <https://doi.org/10.1002/apj.2028>
- Yang, C., Dabros, T., Li, D., Czarnecki, J., & Masliyah, J. H. (2001). Measurement of the Zeta Potential of Gas Bubbles in Aqueous Solutions by Microelectrophoresis Method. *Journal of Colloid and Interface Science*, 243(1), 128–135. <https://doi.org/10.1006/jcis.2001.7842>
- Yu, K. L., Show, P. L., Ong, H. C., Ling, T. C., Chi-Wei Lan, J., Chen, W.-H., & Chang, J.-S. (2017). Microalgae from wastewater treatment to biochar – Feedstock preparation and conversion technologies. *Energy Conversion and Management*, 150, 1–13. <https://doi.org/10.1016/j.enconman.2017.07.060>
- Yumiyama, S., Kato, S., Konishi, Y., & Nomura, T. (2019). Direct measurement of interaction forces between a yeast cell and a microbubble using atomic force microscopy. *Colloids and Surfaces A: Physicochemical and Engineering Aspects*, 123963. <https://doi.org/10.1016/j.colsurfa.2019.123963>
- Zhang, M., & Guiraud, P. (2017). Surface-modified microbubbles (colloidal gas aphrons) for nanoparticle removal in a continuous bubble generation-flotation separation system. *Water Research*, 126, 399–410. <https://doi.org/10.1016/j.watres.2017.09.051>
- Zhu, L., Li, Z., & Hiltunen, E. (2018). Microalgae *Chlorella vulgaris* biomass harvesting by natural flocculant: Effects on biomass sedimentation, spent medium recycling and lipid extraction. *Biotechnology for Biofuels*, 11(1), 183. <https://doi.org/10.1186/s13068-018-1183-z>

Ziolkowska, J. R. (2014). Prospective technologies, feedstocks and market innovations for ethanol and biodiesel production in the US. *Biotechnology Reports*, 4, 94–98.

<https://doi.org/10.1016/j.btre.2014.09.001>

Žutić, V., & Svetličić, S. (2000). Interfacial processes. In P. Wangersky (Ed.), *The Handbook of environmental chemistry*1 (pp. 149–165). Springer Verlag.

Appendix 3: Reconstructed membrane vesicles from the microalga *Dunaliella* as a potential drug delivery system

Reconstructed membrane vesicles from the microalga *Dunaliella* as a potential drug delivery system

Maja Levak Zorinc^a, Irem Demir-Yilmaz^{b,c}, Cecile Formosa-Dague^b, Ivna Vrana^a, Blaženka Gašparović^a, Lucija Horvat^a, Ana Butorac^d, Ruža Frkanec^e, Nadica Ivošević DeNardis^{a*}

a Ruđer Bošković Institute, Zagreb, Croatia

b TBI, Université de Toulouse, INSA, INRAE, CNRS, Toulouse, France

c LAAS, Université de Toulouse, CNRS, Toulouse, France

d Biocentre Ltd., Zagreb, Croatia

e Centre for Research and Knowledge Transfer in Biotechnology, University of Zagreb, Croatia

*Corresponding author:

Tel: +385 1 4561-128

Fax: +385 1 4680-242

E-mail address: ivosevic@irb.hr (N. Ivošević DeNardis)

ABSTRACT

The aim of this biophysical study is to characterize reconstructed membrane vesicles obtained from microalgae in terms of their morphology, properties, composition, and ability to encapsulate a model drug. The reconstructed vesicles were either emptied or non-emptied and exhibited a non-uniform distribution of spherical surface structures that could be associated with surface coat proteins, while in between there were pore-like structures of up to 10 nm that could contribute to permeability. The reconstructed vesicles were very soft and hydrophilic, which could be attributed to their composition. The vesicles were rich in proteins and were mostly derived from the cytoplasm and chloroplasts. The lipid classes and their ratio identified in the reconstructed membrane vesicles were conserved as in the mother cell. The vesicles appeared to be permeable to calcein, impermeable to FITC-ovalbumin, and semipermeable to FITC-concanavalin A, which may be due to a specific surface interaction with glucose/mannose units that could serve as a basis for the development of drug carriers. Finally, the reconstructed membrane vesicles could pave a new way as sustainable and environmentally friendly marine bioinspired carriers and serve for studies on microtransport of materials and membrane-related processes contributing to advances in life sciences and biotechnology.

Keywords: drug delivery, membrane vesicle, microalgae, nanomechanics, permeability

Introduction

The development of drug delivery systems has been extensively researched [1-4]. Traditionally, lipid-based drug delivery systems have been the most prominent, followed by inorganic and polymer-based drug delivery systems [5-8]. Since none of these delivery systems mimic the complexity of natural biological membranes, interest in cellular or cell-derived counterparts using human (red blood cells, stem cells, immune cells), animal, and plant cells has increased dramatically over the past decade [4,9-14]. Although these cells have great advantages as drug carriers, mainly because of the recognition of the cells by the target tissue, there are some disadvantages related to the survival, migration and function of the carrier cells that limit the exposure to the drug [15,16]. In addition, there is a risk of tumorigenicity, especially in stem cells [10]. Because of these problems, cell-derived drug delivery systems such as extracellular vesicles and cell membrane-coated particles are now being investigated. Extracellular vesicles are typically released by most types of eukaryotic and some prokaryotic cells [17,18]. Although there are several types of extracellular vesicles, the focus is on exosomes-vesicles with a diameter of 100 to 200 nm that can be isolated from the cell type to be treated with a drug. Because of their good biocompatibility with target tissues, many human-derived exosomal therapies are currently under investigation [4], but the cost of obtaining highly concentrated fractions is high [19]. In the last decade, the development of drug delivery systems based on microalgae has attracted considerable interest [19-22]. For example, diatoms and their biosilicified envelope can be engineered to carry genes, and nucleic acids [20,23] and can also be functionalized to deliver drugs to cancer cells [9]. In addition, various types of green microalgae have been used as a source of algal exosomes (nanoalgosomes), which are also a promising type of carrier, but the disadvantage at present is also the low yield of this type of vesicle [21,22]. Recently, we reported a protocol for the preparation of autofluorescent micrometre-sized reconstructed membrane vesicles from microalgal cells [24]. The aim of this study is to characterize the reconstructed membrane vesicles in terms of their morphology, properties, and composition as well as their ability to encapsulate selected fluorescent dyes. Such reconstructed membrane vesicles could serve as a basis for the development of marine bioinspired carriers for advanced biotechnological applications.

2. Materials and methods

2.1. Cell suspensions

The unicellular marine alga *Dunaliella tertiolecta* Butcher (Chlorophyceae) [Culture Collection, Bigelow Laboratory for Ocean Sciences, length: 6-12 μm] was grown in natural seawater (filtered through 0.2 μm) of salinity 38 enriched with F-2 medium [25] under ambient conditions (25 °C, 12 h light:12 h dark, shaking (20 rpm)). The cell density was 6×10^6 cells/mL after 10 days of growth. Cells were separated from the growth medium by gentle centrifugation (1500 \times g, 5 min). The loose pellet was washed several times with filtered seawater by centrifugation and used to prepare vesicles.

2.2. Preparation of the reconstructed membrane vesicles

The reconstructed membrane vesicles, called ghost vesicles, were prepared by osmotic shock of the photosynthetic marine microalga *Dunaliella tertiolecta* in early stationary phase. The protocol for producing the reconstituted vesicles was recently described in detail [24]. Briefly, the loose algal cell pellet was isolated from 500 mL of cell growth medium by gentle centrifugation (1500 \times g for 5 min) and rinsing with filtered seawater (0.22 μm). The supernatant was completely removed, and 4 mL of the loose algal cell pellet was diluted 40 times with ultrapure water, shaken vigorously, and then allowed to stand at room temperature. After 30 minutes, the samples were centrifuged at 1500 \times g for 4 minutes. Pellet 1 contained released intracellular material, non-empty vesicles, and empty vesicles. Supernatant 1, containing empty vesicles, vesicles with some adherent material, and a small amount of free debris, was centrifuged at 10 000 \times g for 10 minutes, at 10 °C. The resulting Pellet 3 contains mainly debris and some vesicles, whereas Supernatant 3 contains mainly empty reconstructed vesicles and vesicles with some adherent material concentrated in a thin viscous layer near the Pellet 3. The fraction of concentrated vesicles is stabilized with Tris-HCl buffer and MgCl_2 (both final concentrations were 10 mM, pH 8.0). The concentration of reconstructed membrane vesicles in suspension is generally between 10^4 and 10^6 vesicles/mL and in size up to 30 μm .

2.3. Epifluorescence and confocal laser scanning microscopy

An Olympus BX 51 fluorescence microscope was used for preparation of reconstructed vesicles and determination of cell and vesicle density. Confocal measurements were

performed with a Leica TCS SP8 laser scanning confocal microscope equipped with a white light laser and a 63× (N.A. = 1.4) oil immersion objective. The excitation and emission spectra generated by the microscope were used to optimize the emission windows.

Lipophilic membrane stain Dil (Sigma, excitation maximum 552 nm, detection range 570-600 nm) was used to improve visualization of the vesicles. A stock solution of Dil at a concentration of 200 μ M was prepared in anhydrous DMSO. Calcein, FITC-concanavalin A, and FITC-ovalbumin were used to test loading of the vesicles. Calcein (Sigma, excitation maximum 488 nm, detection range 500-540 nm) was prepared as a stock solution (20 mM in ultrapure water). FITC-concanavalin A (Sigma) and FITC-ovalbumin (Invitrogen, Life technologies, USA; excitation maximum 488 nm, detection range 500-540 nm) were prepared in ultrapure water at a concentration of 1 mg/mL. FITC-dextran with different molecular weights (Sigma, 3-5 kDa, 10 kDa, 20 kDa, and 70 kDa) were used for permeability assay. All FITC-dextran were prepared in ultrapure water at 1 mg/mL.

SPY555-tubulin (Tebu-bio SAS, excitation maximum 555 nm, detection range 570-620 nm) was used as a probe for imaging of microtubules. The content of the SPY probe tube was prepared in 50 μ L DMSO solution and diluted 100-fold before imaging. Autofluorescence of the reconstructed membrane vesicles was also recorded (excitation 555 nm, detection range 660-720 nm).

2.4. Sample preparation for confocal imaging

Before use, the slides were washed with ethanol and rinsed several times with water. After drying with a stream of nitrogen, 50 μ L of polyethylenimine (PEI, 0.2% w/v) was added to the slide for 30 minutes. The PEI droplet was then removed and rinsed three times with ultrapure water. Finally, 20 μ L of an aliquot of the vesicles was added to the modified slide and allowed to stand for 30 minutes. Prior to imaging, the fluorescent dye Dil was added at a final concentration of 2 μ M, followed by the addition of FITC-dextran or selected fluorescent dyes. Calcein was added at a final concentration of 5 μ M. FITC-concanavalin A, FITC-ovalbumin and FITC-dextran were added to the sample in aliquots between 1 and 4 μ L, to achieve final concentrations between 50 and 200 μ g/mL.

2.4.1. Analysis of vesicle permeability with Image J software

Fluorescence intensity analysis for vesicle permeability study was performed using Image J (software version 1.53k, National Institute of Health, USA). The measured fluorescence intensities inside the vesicles were compared with the fluorescence intensity outside the vesicles on the confocal images. For each dextran molecular weight, at least 10 vesicles were analyzed on an 8×8 μm image and, in parallel, the vesicle population was analyzed on 25×25 μm images. Measurements were always performed on clear background segments and at a distance of at least 20% from the membrane to exclude possible interference with membrane luminescence. The relative fluorescence intensity within the vesicles was expressed as a percentage of the fluorescence intensity of the background.

2.5. Sample preparation for AFM measurements

For AFM imaging in air, a volume of 5 μL of the suspension containing the reconstructed membrane vesicles was pipetted directly onto freshly cleaved mica and dried in a closed Petri dish for 1 hour before imaging. AFM imaging of the vesicles was performed using a MultiMode Scanning Probe Microscope with Nanoscope IIIa controller (Bruker, Billerica USA) and a 125 μm Vertical Engagement (JV) scanner. Images were acquired in contact mode using a standard silicon nitride tip (DNP-10, Bruker, nominal frequency 18 kHz, nominal spring constant of 0.06 N/m) with a scan resolution of 512 samples per line. Sampling rates were typically optimized to 1-2 Hz. Images were processed and analyzed using NanoScope™ software (Digital Instruments, version V614r1). The force was kept at the lowest possible value to minimize interaction forces between the tip and the surface. Measurements were performed in air, at room temperature and 50-60% relative humidity, so that the samples have a small hydration layer that helps to preserve the structure [26]. All images are presented as raw data, except for the two-dimensional first-order flattening.

For AFM imaging in liquid, vesicles were first immobilized on glass slides coated with PEI. For this purpose, freshly activated slides were coated with a 0.2 % PEI solution in deionized water and incubated overnight. The slides were then rinsed with deionized water and dried with nitrogen. A total of 1 mL of the vesicle suspension was then applied to the PEI-coated slide, allowed to stand for 30 minutes, and rinsed with Tris-HCl buffer and MgCl₂ (both final concentrations were 10 mM, pH 8.0) to remove nonsticky vesicles. Height images of the

reconstructed membrane vesicles were acquired with the quantitative imaging (QI) mode of Nanowizard III AFM (Bruker, USA) using MSCT cantilevers (Bruker, nominal spring constant of 0.01 N/m), in 10 mM Tris-HCL with addition of 10 mM MgCl₂ buffer. Images were acquired at a resolution of 150x150 pixels, applying a force of < 1 nN. In all cases, the spring constants of the cantilevers were determined using the thermal noise method prior to imaging [27]. The obtained height images were then analyzed using Data Processing Software (Bruker, USA).

2.6. AFM Force Spectroscopy

AFM in force spectroscopy mode was used to measure the nanomechanical properties of vesicles. A maximum force of 0.5 nN was applied using MSCT cantilevers (Bruker, nominal spring constant of 0.1 N/m). In each case, 18 reconstructed vesicles immobilized on PEI-coated glass slides were analyzed from 2 independent series (400 force curves were recorded for each algal vesicle). Young's moduli were then calculated from the 300-nm indentation curves using the Hertz model [28], in which the force F , indentation (δ), and Young's modulus (Y_m) follow equation 1, where α is the tip aperture angle (17.5°) and ν is the Poisson's ratio (arbitrarily assumed to be 0.5). The spring constants of the cantilevers were determined before each experiment using the thermal noise method [27].

$$F = \frac{2 \times Y_m \times \tan \alpha}{\pi \times (1 - \nu^2) \times \delta^2} \quad (1)$$

For the hydrophobicity experiments, AFM was used in combination with FluidFM as described in [29]. Briefly, an air bubble was generated using a Nanowizard III AFM (Bruker, USA) equipped with FluidFM technology (Cytosurge AG, Switzerland). Experiments were performed in PBS at pH 7.4 using microfluidic micropipette probes with an aperture of 8 μm (spring constant of 0.3 N/m, Cytosurge AG, Switzerland). The probes were calibrated using the thermal noise method [27] before the measurements. Then, the interactions between the bubbles formed at the aperture of the microfluidic micropipette probes and 7 algal vesicles were measured in force spectroscopy mode with a constant applied force of 0.5 nN. Force curves (400 force curves for each vesicle) were recorded with a retraction z-length of up to 2 μm and a constant retraction speed of 1.0-2.0 $\mu\text{m/s}$. The adhesion force between the bubble

and the algal vesicle was calculated by measuring the height of the adhesion peak using Bruker data processing software (Bruker, USA).

2.7. Lipid extraction and analysis

Lipid extractions were performed from 50 mL of an algal cell monoculture in the early stationary growth phase and 15 mL of an algal-derived vesicle suspension. Samples were filtered through a pre-combusted (450 °C/5 h) 0.7 µm Whatman GF/F filter. Extraction was performed using a modified one-phase solvent mixture of dichloromethane-methanol-water [30]: 10 mL of one-phase solvent mixture dichloromethane/methanol/deionized water (1:2:0.8 v/v/v) and 5 µg of standard methyl stearate (to estimate recoveries in subsequent steps of sample analysis) were added to the cut filters. They were then ultrasonicated for 3 min, stored overnight in the refrigerator, filtered through a sinter funnel into a separatory funnel, washed again with 10 mL of the one-phase solvent mixture and then washed once with 10 mL of dichloromethane/0.73 % NaCl solution (1:1 v/v) and finally with 10 mL of dichloromethane. Lipid extracts collected in dichloromethane were evaporated to dryness under nitrogen flow and dissolved in 34 to 54 µL dichloromethane before analysis. All solvents were purchased from Merck Corporation (USA).

Lipid classes were determined by thin-layer chromatography with flame ionization detection (TLC-FID; Iatroscan MK-VI, Iatron, Japan). Lipids were separated on Chromarods SIII. Quantification was determined by external calibration of lipid classes. Analysis was performed using a hydrogen flow of 160 mL/min and an airflow of 2000 mL/min. We determined representative membrane lipid classes: three glycolipids (monogalactosyldiacylglycerols (MGDG), digalactosyldiacylglycerols (DGDG), and sulfoquinovosyldiacylglycerols (SQDG)), three phospholipids (phosphatidylglycerols (PG), phosphatidylethanolamines (PE), and phosphatidylcholines (PC)) and sterols (ST), and lipid degradation indices (DI) which include free fatty acids, fatty alcohols, 1,3-diacylglycerols, 1,2-diacylglycerols and monoacylglycerols. The total lipid concentration is the sum of the individual lipid classes. The standard deviation determined from duplicate runs was 0-15%. The detailed procedure is described in [31,32].

2.8. Protein analysis

The concentration of total proteins was determined by the Bradford method [35] in duplicate samples. For protein analysis, 200 µL of the vesicle sample was mixed with 20 µL 10% SDS

(pH=7.2) and boiled in a water bath for 1 minute; 5 volumes of ice-cold acetone were added to the sample, and the proteins were precipitated overnight at -20 °C. The precipitated proteins were pelleted by centrifugation (10 000 × g, 4 °C, 10 min). The pellet was dissolved in 25 µl 25 mM ammonium bicarbonate buffer (pH=7.8). Digestion was performed with trypsin (Promega, SAD) overnight at 37 °C. The peptides obtained after digestion were separated according to the method described in [34]. NanoLC system Dionex Ultimate 3000 RSLCnano (Thermo Fisher Scientific, Germany) coupled to Proteiner fcll (Bruker, Germany) was used for separation and peptide collection. Mass spectrometry (MS) was performed using an Autoflex speed MALDI-TOF /TOF analyzer (Bruker, Germany). Mass spectra were obtained according to the method described in [34]. Protein identification was performed using ProteinScape software version 3.0 (Bruker, Germany) with the search engine MASCOT. An in-house database of protein sequence data of *D. tertiolecta* was used. Protein sequence data were downloaded from the UniProt database (accessed March 19, 2022, no. of entry 12 786). Search parameters were set as follows: a missing trypsin cleavage, oxidation on methionine as a variable modification, precursor ion mass tolerance 50 ppm, and fragment ion mass tolerance 0.6 Da. The protein-protein interaction network (PPI) of the identified proteins was generated using STRING version 11.0 with a minimum confidence level of 0.4. A multiple sequence search was used.

2.9. Carbohydrate analysis

The standard stock solution of glucose (1 mg/mL) was diluted to a concentration of 0 to 0.1 mg/mL and used to construct the calibration curve. The anthrone reagent was prepared as follows: 200 mg of anthrone (ACS reagents, Sigma-Aldrich) was added to a 100 mL volumetric flask, and the volume was adjusted to 100 mL with 96 % sulfuric acid (Biochem). The vesicle suspension sample was diluted 1:10 with deionized water. 1 mL of the diluted glucose standards or sample was added to the tube along with 4 mL of anthrone reagent, vortexed, and incubated at 80 °C in a water bath (Lauda, Alpha RA8) for 10 minutes. After cooling on ice to room temperature, absorbance was determined at 630 nm in duplicate samples (UV/VIS spectrophotometer, Cary 100, Agilent Technologies). Total carbohydrate content is expressed as glucose equivalent in mg per mL of sample.

3. Results

3.1. Nanomorphological characterization of the reconstructed membrane vesicles

Figure 1 shows reconstructed membrane vesicles deposited on mica and imaged by AFM in air.

Here Fig.1.

The topographic image shows densely packed vesicles, many of which overlap on the outside (Fig. 1a). The vesicles are nearly round, although some elongation may be due to the drying step and less than optimal adhesion to the mica surface. Cross-sectional analysis of 21 vesicles shows that the diameter and height of the vesicles were $13.5 \pm 2.1 \mu\text{m}$ and $87.9 \pm 6.8 \text{ nm}$, respectively. Thus, the vesicles were not deflated but contained a thick membrane and some embedded intracellular material. Topographic and 3-D views show round reconstructed membrane vesicle (Figs. 1d, 1f). Cross-sectional analysis shows that the diameter and height of the vesicle correspond to $10.2 \mu\text{m}$ and 62.8 nm , respectively, indicating embedded intracellular material and particles adhering to the membrane surface (Fig. 1e). Topographic and 3-D views show individual reconstructed membrane vesicles that can be considered nearly depleted (Figs. 1g, 1i). Cross-sectional analysis shows that the diameter and height of the vesicle correspond to $3.0 \mu\text{m}$ and 20.2 nm , respectively, while the internal height of the vesicle ranges from 2 to 4 nm. Insights into the surface structure of the reconstructed membrane obtained from the AFM deflection image and 3D view are provided in Fig. S1. The heterogeneously distributed spherical surface structures were predominantly about 100 nm in diameter and 5 to 10 nm in height, with pits in between. The roughness of the vesicles in air was determined on the areas of $8 \times 8 \mu\text{m}$ on the surface of 21 vesicles and corresponded to $11.5 \pm 1.4 \text{ nm}$. The reconstructed membrane vesicles were also imaged by AFM in liquid. The height image and the corresponding 3D view of a vesicle are shown in Fig. 2a and 2b, respectively.

Here Fig. 2

The cross-section (Fig. 2c) taken along the white line in Fig. 2b shows the morphology of the surface. The reconstructed membrane vesicle has a round shape with a height of more than $2 \mu\text{m}$. The average maximum height of the vesicles measured on 6 different vesicles was $2.92 \pm 0.50 \mu\text{m}$, which was much higher than under near-dry conditions. This difference is probably

due to the hydration of the vesicles, which increases their size. Finally, the roughness of the vesicles was also measured under liquid conditions. For this purpose, high-resolution images were taken on areas of $1.5 \times 1.5 \mu\text{m}$ on the surface of six vesicles. An example of such an image is shown in Figs. 2d and 2e along with the cross-section. The average roughness found was $9.29 \pm 5.36 \text{ nm}$. The large standard deviation in this case illustrates the heterogeneity of the vesicle surfaces.

3.2. Determination of pore size on reconstructed membrane vesicles

Figure 3 shows representative confocal images of reconstructed membrane vesicles after addition of FITC-dextran with selected molecular weights of 3-5 kDa, 10 kDa, 20 kDa, and 70 kDa.

Here Fig.3.

The fluorescence intensity inside and outside the vesicle is completely balanced, i.e., the relative fluorescence intensity inside the vesicle is 95 % of the fluorescence intensity outside the vesicle. Therefore, it is assumed that the vesicles are fully permeable to 3-5 kDa dextran. After addition of 10 kDa FITC-dextran, the fluorescence intensity inside the vesicles is 84 % of the background fluorescence intensity, so the reconstructed membrane vesicles are also predominantly permeable to 10 kDa dextran (Fig. 3a). Figure 3b shows reconstructed membrane vesicles in contact with 20 kDa FITC-dextran. Quantitative analysis shows that the fluorescence intensity inside the vesicles drops to 37 % of the background fluorescence intensity. Thus, the reconstructed membrane vesicles are predominantly impermeable to dextran of this size. Finally, after the addition of 70 kDa dextran, the highest fluorescence intensity is outside the vesicles, indicating that the majority of the reconstructed membrane vesicles are also predominantly impermeable to dextran of this molecular weight (Fig. 3c). The fluorescence intensity within the vesicles in contact with 70 kDa dextran is 17 % of the background fluorescence intensity. Overall, the permeability of reconstructed membrane vesicles decreased with an increase in the molecular weight of dextran from 3 to 70 kDa (Fig. S2). Between 10 and 20 kDa, a significant decrease in the accumulation of dextran in the vesicles was observed. Although the pores of the reconstructed membrane vesicles varied in size, 20 kDa could be considered as the threshold.

3.3. Nanomechanical and chemical characterization of the reconstructed membrane vesicles

Nanoindentation experiments were performed to obtain quantitative information on the nanomechanical properties of the reconstructed vesicles in terms of Young's modulus (Y_m) (Figs. 4a and 4b).

Here Fig.4.

In these experiments, a cantilever with known mechanical properties is pressed against the vesicle surface with a certain force. In this way, the Y_m value of the sample can be determined, a parameter that reflects its resistance to compression. Thus, Y_m is a value related to the rigidity; the higher the Y_m value, the more rigid the sample. In this study, nanoindentation measurements were performed on areas of $1.5 \times 1.5 \mu\text{m}$ on the surface of 17 reconstructed membrane vesicles obtained from two independent batches of samples. Nanoindentation measurements provide access to force-displacement curves. From these curves, Y_m values can be determined by converting the force curves into force versus indentation curves (black line in the inset of Fig. 4a) and then fitting them with the Hertz model [28] (orange line in Fig. 4a). Quantitative analysis of all Y_m values extracted from the force curves yielded an average Y_m value of $0.37 \pm 0.31 \text{ kPa}$ ($n = 5959$ force curves).

The hydrophobic properties of the reconstructed membrane vesicles were also determined. For this purpose, we used a recently developed method consisting in studying the interactions between samples and air bubbles prepared with FluidFM technology [29], which combines AFM with microfluidics [35]. Air bubbles in water behave like hydrophobic surfaces. Therefore, if interactions between bubbles and vesicles are recorded, it means that the vesicles have hydrophobic properties. This method has been used to measure the hydrophobic properties of complex surfaces such as cells [29] or microplastic particles [36] and is a more accurate method for measuring hydrophobicity than measuring water contact angle (WCA), which can be difficult for biological samples. Moreover, compared to classical measurements using hydrophobic AFM tips, this method has the advantage of providing access to the global hydrophobic properties of the samples, since the radius of the bubble in contact with the sample is about $1.2 \mu\text{m}$ [29], which is 60 times higher than a regular AFM tip (20 nm) [37,38]. The results of these experiments are shown in Fig. 4b. The force curves obtained in this case show no adhesion peaks on the retraction force curves (inset in Fig. 4b), which means that the

reconstructed membrane vesicles do not interact with the bubbles. Thus, they are completely hydrophilic.

3.4. Composition of the reconstructed membrane vesicles

3.4.1. Lipids

The concentrations of total lipids in the *D. tertiolecta* cells and the reconstructed membrane vesicles were $9265 \pm 2229 \mu\text{g/L}$ and $8957 \pm 563 \mu\text{g/L}$, respectively. The difference between *D. tertiolecta* and the reconstructed membrane vesicles is that there are approximately 1.5 times more lipids in the *D. tertiolecta* mother cell than in the reconstructed membrane vesicles. The concentration of total lipids per *D. tertiolecta* is $4.03 \pm 0.98 \text{ pg/cell}$, whereas the concentration of total lipids per vesicle is $2.63 \pm 0.17 \text{ pg/vesicle}$. The composition of lipid classes in the *D. tertiolecta* cells and the reconstructed membrane vesicles is shown in Figs 5a and 5b, respectively. All lipid classes detected in the *D. tertiolecta* cells are also embedded in vesicles. During the process of membrane reconstruction, there are no major changes in the ratios of lipid classes. Polar lipids dominated in both *D. tertiolecta* cells and reconstructed membrane vesicles ($76.7 \pm 0.5\%$ and $80.8 \pm 0.7\%$, respectively), with glycolipids MGDG and phospholipids PG being the dominant classes. MGDG contributed $30.50 \pm 0.06\%$ and $26.76 \pm 0.85\%$, while PG contributed $16.76 \pm 1.70\%$ and $21.46 \pm 0.11\%$ in *D. tertiolecta* and reconstructed membrane vesicles, respectively.

3.4.2. Proteins

The determined concentration of total proteins in the reconstructed membrane vesicle suspension corresponds to 0.1 mg/mL . Further protein analysis was performed to identify the proteins incorporated into the vesicles. In addition, STRING analysis was used to investigate the PPI network between the identified proteins. The results are shown in Fig. 6 and Table S1. The results indicate that the proteins incorporated into the vesicles are biologically connected as a group (the calculated PPI enrichment P value is $< 1.0 \times 10^{-16}$, indicating that the nodes are not random and that the observed number of edges is significant). According to the gene ontology (GO), most of the identified proteins are involved in the carbohydrate metabolic process (GO:0005975), cellular amino acid biosynthetic process (GO:0008652), photosynthesis (GO:0015979), oxidoreductase activity (GO:0016491) and microtubule-based

process (GO:0007017). Judging from the subcellular location, most proteins originate from the cytoplasm and chloroplasts.

3.4.3. Carbohydrate content

The determined total carbohydrate concentration in the reconstructed membrane vesicle suspension corresponds to 0.087 mg/mL based on UV/VIS spectrophotometric analysis. In the HPLC-RID analysis of glucose in the sample, the glucose concentration is below the detection limit (less than 0.15 mg/mL).

3.5. Loading of the fluorescent dyes into the reconstructed membrane vesicles

Figure 7b shows that the fluorescence of calcein is evenly distributed inside and outside the reconstructed membrane vesicles, i.e., the vesicles behave permeably to calcein. On the other hand, the fluorescence intensity of FITC-ovalbumin is highest outside the vesicles, whereas no fluorescence occurs inside the vesicles, i.e., the vesicles are impermeable to the corresponding dye, as shown in Fig. 7e. Fig. 7h shows that the fluorescence intensity in the case of FITC-concanavalin is higher at the membrane edge than in the surrounding medium. Since the fluorescence intensity inside the vesicles is close to zero, the vesicles could either be semipermeable or a small part of the luminescence is due to the out-of-focus membrane luminescence.

4. Discussion

The major limitations in drug carrier manufacturing are protocol inefficiency, bioincompatibility and high cost. There is a great need to overcome these limitations and meet the requirements of sustainability and environmental friendliness. This can be achieved by using the microalgae presented here, which can be easily cultivated. They are widely used as a food source, dietary supplement, pharmacological agent, and energy source. On the other hand, the potential of microalgae to produce reconstructed membrane vesicles for drug encapsulation has not been adequately explored. To address this gap, this study focuses on a comprehensive screening of reconstructed membrane vesicles by investigating the relationship between morphology, properties, and composition and testing their ability to

encapsulate a model drug to serve as an alternative carrier for advanced biotechnological applications.

We are interested in marine microalgae, in particular the widely distributed species *D. tertiolecta*, as a natural biomaterial for the preparation of reconstructed membrane vesicles based on a recently published protocol [24]. The main feature for the use of the microalga *D. tertiolecta* is that it has no cell wall, but only a glycocalyx-type cell envelope, which makes it very soft. Another advantage is its semipermeable membrane, which is why *Dunaliella* is used for osmoregulation studies. When the algae are subjected to hypoosmotic shock, the volume of the cells increases, pores form, the cells burst, intracellular material is released, and the remaining membrane fragments fuse to form reconstructed algal vesicles with high yield.

Nanomorphological characterization revealed a mixed population of micrometer-sized, nearly round, deflated and nondeflated membrane vesicles with embedded intracellular material and some adherent particles. When the vesicles are nearly deflated, the membrane thickness corresponds to 20 nm, indicating that each membrane bilayer has a thickness of 10 nm (Fig. 1h). This is consistent with the cell envelope thickness of 9 nm determined by electron microscopy [39]. This relatively high membrane thickness is likely due to the presence of water residues, other cellular components entrapped in the vesicle membrane, and the high glycoprotein content in the cell envelope. The "envelope" of *Dunaliella* cells appears to be composed of glycoproteins of 150 kDa present in the outer layer surrounding the cells [40]. AFM images (in air and in liquid) also showed that the vesicle surface is uneven and contains irregularly distributed spherical surface structures and pits (Figs. 1, S1, 3). Based on their height, these could be surface coat proteins with different functions [41,42]. A similar surface roughness was imaged by AFM in ghosts of red blood cells [43-45]. This revealed the structure of the cytoskeleton, which consists of spectrin dimers connected by actin filaments and proteins to form a two-dimensional network [43]. Actin filaments were also observed in our system of reconstructed membrane vesicles, but only within the membrane [24]. The spherical surface structures on the reconstructed membrane vesicles are assembled in a specific way to form pore-like structures, which could be responsible for the permeability of the vesicles to hydrophilic molecules. A permeability assay with labeled dextrans of different molecular weights showed that the reconstructed membrane vesicles were predominantly impermeable to FITC-dextran of 20 kDa and above (Figs. 3, S2). The variations in permeability

are related to a small fraction of vesicles with larger pores that did not close after osmotic shock and to dextran molecules, which are known to be deformable and therefore have non-uniform molecular size [46]. The hydrodynamic radius of the dextran 20 kDa corresponds to 5.2 ± 0.5 nm [47]. The pore sizes of the reconstructed membrane vesicles should be predominantly smaller than dextran of this size. Therefore, the diameter of pores in reconstructed membrane vesicles could be as small as 10 nm. In addition, pore properties (lipophilicity/hydrophilicity) may also affect membrane permeability and leakage of encapsulated molecules of different sizes [48]. Membrane permeability and pores formed in the reconstructed membrane vesicle are a major advantage in the potential application of such vesicles for drug delivery, as there is considerable effort to develop self-assembling nanovesicles and artificial cells containing membranes that can be easily manipulated to transport cargo into and out of internal compartments [49]. Skinkle et al. (2020) investigated the distribution of pore size in a population of giant plasma membrane vesicles derived from rat basophilic leukemia cells [50]. They also found heterogeneity in pore size, likely due to the shear stress that occurs during vesicle formation. In particular, the vesicles were impermeable to dextrans with a molecular weight of 40 kDa and above.

The results showed that the surface properties of the reconstructed vesicles were similar to those of the mother cells in terms of rigidity and hydrophilicity (Fig. 4). The average rigidity of *D. tertiolecta* grown at a salinity of 38 corresponds to 3.5 kPa [51], while the rigidity of the reconstructed vesicles is about ten times lower due to the lack of cytoskeletal network within the vesicle. In addition, cells and vesicles behave hydrophilically [51], which is consistent with the identified lipid classes and their ratio. The most important observed feature is that the ratio of lipid classes of the mother cell and the reconstructed membrane vesicles is not significantly perturbed (Fig. 5). All lipid classes of *D. tertiolecta* are involved in the formation of the reconstructed membrane vesicles, suggesting high utilization. Moreover, the ratio of proteins : lipids : carbohydrates per reconstructed membrane vesicle corresponds to 28 pg : 2.63 pg : 0.03 pg, so that the protein content predominates, which is consistent with the first study by Jokela [39]. For the first time, 47 proteins were identified and determined to be derived from the cytoplasm and chloroplasts (Fig. 6, Table S1). Although, the reconstructed membrane vesicles show weak autofluorescence (Fig. S3b) at the wavelength of chlorophyll [24], the presence of a corresponding chlorophyll a-b binding protein as found in the mother

cells (unpublished data) was not identified here, probably due to signal suppression by other protein classes. Therefore, we will perform further protein profiling studies. On the other hand, protein analyzes have been performed for mammalian cell-derived extracellular vesicles to predict therapeutic responses of these drug carriers [52,53]. However, little is known about the protein profiles in extracellular vesicles from plants and algae under different culture conditions and how much protein is incorporated into the vesicles. Indeed, extracellular vesicles from plants invaded by pathogens show enrichment of proteins involved in signal transduction in response to biotic and abiotic stresses, proteins responsible for immunity, and enzymes that remodel the cell wall [54]. In addition, cytosolic proteins, metabolic enzymes, chaperones, hydrolases, and membrane channels/transporters have been identified in various plant vesicles. Aquaporins have been reported to play an important role in vesicle stability in plasma membrane vesicles purified from broccoli plants [55]. In the reconstructed membrane vesicles of *D. tertiolecta*, we identified proteins involved in the carbohydrate metabolic process, cellular amino acid biosynthetic process, photosynthesis, oxidoreductase activity, and microtubule-based process. Although further studies are needed, we can assume that proteins involved in microtubule-based processes (tubulin alpha and beta chains) may be responsible for the stability of the reconstructed vesicles [56]. The microtubule networks were only associated with the membrane of the vesicle, as shown in Fig. S3a. Microtubulins have also been reported to be a target for anticancer drugs [57].

The reconstructed membrane vesicles differ in their loading capacity for calcein, FITC-ovalbumin, and FITC-concanavalin A because of the different physicochemical properties of the dye and the structural features of the membrane (Fig. 7). Calcein is a small hydrophilic molecule ($M_w = 0.6$ kDa) with a hydrodynamic radius of 0.74 nm [58], which is much smaller than the determined pore size of the membrane. Therefore, calcein spontaneously permeates the vesicle membrane. FITC-ovalbumin, a globular protein ($M_w=43$ kDa), does not penetrate or interact with the vesicle membrane and therefore cannot be considered a drug cargo (Fig. 7e). FITC-concanavalin A is a carbohydrate-binding protein that consists of 4 subunits and has a molecular weight of 104 kDa. When the dye was added to the immobilized vesicles, a different behavior was observed compared with calcein and ovalbumin (Fig. 7h). As the figure shows, the high fluorescence intensity of FITC-concanavalin A on the membrane itself is probably due to specific interactions with glucose and mannose units and glycoconjugates on

the membrane [59]. This is confirmed by the fact that the mother cell of *D. tertiolecta* contains glycocalyx [40], and glycolipids [51] and carbohydrate content were determined. Moreover, FITC-concanavalin A also showed specific binding to the cell wall of the algal cells of *Evernia prunastri* and *Xanthoria parietina* thalli [59]. Continuing our studies to find an effective targeted delivery vehicle, we have previously reported the study of the interaction of mannosylated liposomes with concanavalin A, where the affinity of concanavalin A for mannose molecules on the surface of the liposome is increased by the presence of a multivalent ligand [60,61]. In addition, the interaction of spin-labeled ovalbumin and lipids in the cationic and anionic liposomes was investigated. The results showed that the total amount of entrapped protein is higher in cationic liposomes when the ionic strength of the buffer is lower, while in anionic liposomes the entrapment efficiency of ovalbumin does not depend on the ionic strength of the buffer. The non-specific interactions between ovalbumin and the liposomal membrane affect the entrapment efficiency of ovalbumin [62,63].

We wondered if we could tailor the surface properties of the reconstructed membrane vesicles? To answer this question, the surface properties of the mother cell used for vesicle preparation must be known. The surface properties of algal cells change when exposed to abiotic stress conditions by varying temperature or salinity [51,64]. The results showed that *Dunaliella* became statistically significantly stiffer at 12 °C and behaved hydrophilically over a wide range of temperatures, while *Dunaliella* behaved almost neutrally under favorable conditions (18 °C, salinity of 38). On the other hand, *Dunaliella* became statistically significantly stiffer when cells were exposed to salinity 9, where they behaved hydrophobically. Thus, by manipulating the cultivation conditions of the mother cells, the desired surface properties and thus the chemical composition of the reconstructed membrane vesicle can be achieved. For example, an increase in the relative content and unsaturation of MGDG, the major class present in both the mother cell and the reconstructed membrane vesicles, can be achieved by reducing the salinity of the *D. tertiolecta* growth medium [65]. Cultivation at temperatures above the optimum and the lack of nitrogen nutrients lead to an accumulation of lipids in the cell of *Chaetoceros pseudocurvisetus*, taking into account that growth and reproduction are slowed down under unfavorable cultivation conditions [66]. Increasing irradiance leads to the accumulation of triglycerides in the cells of *Dunaliella viridis*

[67]. The accumulation of lipids, proteins, and carbohydrates in cultures of *Nannochloropsis* sp. and *Tetraselmis* sp. at pH 7.5 and 8.5 was reported in contrast to cell growth at pH 7 [68].

5. Conclusions

For the first time, reconstructed membrane vesicles from microalgae were characterized in terms of their nanomorphology, surface properties, composition, and encapsulation of model fluorescent dyes. The microalgal cell *Dunaliella tertiolecta*, which has only a glycocalyx-like cell envelope, is a good candidate to achieve high yield in the preparation of micrometer-sized reconstructed membrane vesicles. The vesicles imaged by AFM have a rather round shape and are found in both depleted and non-depleted states. They exhibit a densely packed spherical surface structure, which could indicate surface proteins with different functions. Pits were mapped between the spherical surface structures, which could indicate pore-like structures, as large as 10 nm, as determined by permeability tests. In terms of composition, the reconstructed membrane vesicles contain about 10 times more proteins than membrane lipids. All lipid classes and their ratios in the mother cell are not significantly perturbed in the reconstructed membrane vesicles. The results show that the vesicles are very soft (less than kPa), and hydrophilic, and retain the surface properties of the mother cell. The permeability of the reconstructed membrane vesicles depends on the structural features of the membrane and the physicochemical properties of the model fluorescent dye. The vesicles are permeable to calcein, impermeable to FITC-ovalbumin, and semipermeable to FITC-concanavalin A, probably because of specific surface interactions with the glucose and mannose moieties of the membrane, which could serve as a basis for the development of drug carriers. Finally, reconstructed membrane vesicles could pave a new way as sustainable and environmentally friendly marine bioinspired carriers that can be efficiently fabricated and could serve for studies on microtransport of materials and membrane-related processes that contribute to advances in life sciences and biotechnology.

Declaration of competing interests

The authors declare that they have no known competing financial interests or personal relationships that could influence the work in this article.

Acknowledgments

This work is supported by the Croatian Science Foundation projects "From algal cell surface properties to stress markers for aquatic ecosystems" (IP-2018-01-5840), "Synthesis of Supramolecular Self-assembled Nanostructures for Construction of Advanced Functional Materials" (IP-2018-01-6910), and by the Croatian-French program "Cogito" partner Hubert Curien (Campus France n°46656ZC).

6. References

- [1] A.M. Vargason, A.C. Anselmo, S. Mitragotri, The evolution of commercial drug delivery technologies, *Nat. Biomed* 5 (2021) 951-967. <https://doi.org/10.1038/s41551-021-00698-w>.
- [2] G. Pedrioli, E. Piovesana, E. Vacchi, C. Balbi, 2021. Extracellular vesicles as promising carriers in drug delivery: Considerations from a cell biologist's perspective. *Biology* 10, 376. <https://doi.org/10.3390/biology10050376>.
- [3] Z. Li, Y. Wang, Y. Ding, L. Repp, G.S. Kwon, Q. Hu, 2021. Cell-based delivery systems: Emerging carriers for immunotherapy. *Adv. Funct. Mater.* 31, 2100088. <https://doi.org/10.1002/adfm.202100088>.
- [4] I. K. Herrmann, M.J.A. Wood, G. Fuhrmann, Extracellular vesicles as a next-generation drug delivery platform, *Nat. Nanotechnol.* 16 (2021) 748-759. <https://doi.org/10.1038/s41565-021-00931-2>.
- [5] L. Sercombe, T. Veerati, F. Moheimani, S.Y. Wu, A.K. Sood, S. Hua, 2015. Advances and challenges of liposome assisted drug delivery. *Front. Pharmacol.* 6, 286. <https://doi.org/10.3389/fphar.2015.00286>.
- [6] A. Srivatsava, T. Yadav, S. Sharma, A. Nayak, A.A. Kumari, N. Mishra, Polymers in drug delivery, *J. Biosci. Med.* 4 (2016) 69-84. <http://dx.doi.org/10.4236/jbm.2016.41009>.
- [7] Z. Shi, Y. Zhou, T. Fan, Y. Lin, H. Zhang, L. Mei, Inorganic nano-carriers based smart drug delivery systems for tumor therapy, *Smart Mater. Medic.* 1 (2020) 32-47. <https://doi.org/10.1016/j.smaim.2020.05.002>.

- [8] P. Bhatt, S. Trehan, N. Inamdar, V. K. Mourya, A. Misra, *Polymers in Drug Delivery: An update*, in: A. Misra, A. Shahiwala (Eds), *Applications of Polymers in Drug Delivery*, Elsevier, 2020. <https://doi.org/10.1016/B978-0-12-819659-5.00001-X>.
- [9] J. Delasoie, F. Zobi, 2019. Natural diatom biosilica as microshuttles in drug delivery systems. *Pharmaceutics*. 11, 537. <https://doi.org/10.3390/pharmaceutics11100537>.
- [10] H. Lutz, S. Hu, P.-U. Dinh, K. Cheng, 2019. Cells and cell derivatives as drug carriers for targeted delivery. *Med. Drug Disc.* 3, 100014. <http://dx.doi.org/10.1016/j.medidd.2020.100014>.
- [11] J.S. Brenner, D.C. Pan, J.W. Myerson, O.A. Marcos-Contreras, C.H. Villa, P. Patel, H. Hekierski, S. Chatterjee, J.-Q. Tao, H. Parhiz, K. Bhamidipati, T.G. Uhler, E.D. Hood, R. Yu Kiseleva, V.S. Shuvaev, T. Shuvaveva, M. Khoshnejad, I. Johnston, J.V. Gregory, J. Lahann, T. Wang, E. Cantu, W.M. Armstead, S. Mitragotri, V. Muzykantov, 2018. Red blood cell-hitchhiking boosts delivery of nanocarriers to chosen organs by orders of magnitude. *Nat. Comm.* 9, 2684. <https://doi.org/10.1038/s41467-018-05079-7>.
- [12] X. Wan, S. Zhang, F. Wang, W. Fan, C. Wu, K. Mao, H. Wang, Z. Hu, Y.-G. Yang, T. Sun, Red blood cell-derived nanovesicles for safe and efficient macrophage-targeted drug deliver in vivo, *Biomater. Sci.* 7 (2019) 187-195. <https://doi.org/10.1039/C8BM01258J>.
- [13] F. Combes, E. Meyer, N.N. Sanders, Immune cells as tumor drug delivery vehicles, *J. Control. Release* 327 (2020) 70-87. <https://doi.org/10.1016/j.jconrel.2020.07.043>.
- [14] K. Kuruvinashetti, S. Pakkiriswami, M. Packirisamy, Algal extracellular vesicles for therapeutic applications, 2020 IEEE 20th International Conference on Nanotechnology (IEEE-NANO), 2020, pp. 354-357. <https://doi.org/10.1109/NANO47656.2020.9183452>.
- [15] W. Zhang, M. Wang, W. Tang, R. Wen, S. Zhou, C. Lee, H. Wang, W. Jiang, I.M. Delahunty, Z. Zhen, H. Chen, M. Chapman, Z. Wu, E.W. Howerth, H. Cai, Z. Li, J. Xie, 2018. Nanoparticle-laden macrophages for tumor-tropic drug delivery. *Adv. Mater.* 30, 1805557 <https://doi.org/10.1002/adma.201805557>.
- [16] N. L. Klyachko, R. Polak, M.J. Haney, Y. Zhao, R.J. Gomes Neto, M.C. Hill, A.V. Kabanov, R.E. Cohen, M.F. Rubner, E.V. Batrakova, Macrophages with cellular backpacks for targeted

drug delivery to the brain, *Biomaterials* 140 (2017) 79-87.
<https://doi.org/10.1016/j.biomaterials.2017.06.017>.

[17] D. Vorselen, S. M. van Dommelen, R. Sorkin, M. C. Piontek, J. Schiller, S. T. Döpp¹, S. A.A. Kooijmans, B. A. van Oirschot, B. A. Versluijs, M. B. Bierings, R. van Wijk, R. M. Schiffelers, G. J.L. Wuite, W. H. Roos, 2018. The fluid membrane determines mechanics of erythrocyte extracellular vesicles and is softened in hereditary spherocytosis. *Nat. Commun.* 9, 4960.
<https://doi.org/10.1038/s41467-018-07445-x>

[18] S. Gill, R. Catchpole, P. Forterre, Extracellular membrane vesicles in the three domains of life and beyond, *FEMS Microbiol. Rev.* 43 (2019) 273-303.
<https://doi.org/10.1093/femsre/fuy042>.

[19] F. Bayat, A. Afshar, N. Baghban, 2021. Algal cells-derived extracellular vesicles: a review with special emphasis on their microbial effects. *Front. Microbiol.* 12, 785716.
<https://doi.org/10.3389/fmicb.2021.785716>.

[20] C. Tramontano, G. Chianese, M. Terracciano, L. de Stefano, I. Rea, 2020. Nanostructured biosilica of diatoms: from water world to biomedical applications. *Appl. Sci.* 10, 6811.
<https://doi.org/10.3390/app10196811>.

[21] G. Adamo, D. Fierli, D.P. Romancino, S. Picciotto, M.E. Barone, A. Aranyos, D. Božič, S. Morsbach, S. Raccosta, C. Stanly, C. Paganini, M. Gai, A. Cusimano, V. Martorana, R. Noto, R. Carrotta, F. Librizzi, L. Randazzo, R. Parkes, U.C. Palmiero, E. Rao, A. Paterna, P. Santanicola, A. Iglič, L. Corcuera, A. Kisslinger, E. Di Schiavi, G.L. Liguori, K. Landfester, V. Kralj-Iglič, P. Arosio, G. Pocsfalvi, N. Touzet, M. Manno, A. Bongiovanni, 2021. Nanoalgosomes: Introducing extracellular vesicles produced by microalgae. *J. Extracell. Vesicles* 10, e12081.
<https://doi.org/10.1002/jev2.12081>.

[22] S. Picciotto, M.E. Barone, D. Fierli, A. Aranyos, G. Adamo, D. Božič, D.P. Romancino, C. Stanly, R. Parkes, S. Morsbach, S. Raccosta, C. Paganini, A. Cusimano, V. Martorana, R. Noto, R. Carrotta, F. Librizzi, U.C. Palmiero, P. Santanicola, A. Iglič, M. Gai, L. Corcuera, A. Kisslinger, E. Di Schiavi, K. Lanfester, G.L. Liguori, V. Kralj-Iglič, P. Arosio, G. Pocsfalvi, M. Manno, N. Touzet, A. Bongiovanni, Isolation of extracellular vesicles from microalgae: towards the

production of sustainable and natural nanocarriers of bioactive compounds, *Biomater. Sci.* 9 (2021), 2917-2930. <https://doi.org/10.1039/d0bm01696a>.

[23] S. Jin, K. Ye, Nanoparticle-mediated drug delivery and gene therapy, *Biotechnol. Prog.* 23 (2007) 32-41. <https://doi.org/10.1021/bp060348j>.

[24] N. Ivošević DeNardis, G. Pletikapić, R. Frkanec, L. Horvat, P.T. Vernier, 2020. From algal cells to autofluorescent ghost plasma membrane vesicles. *Bioelectrochemistry* 134, 107524. <https://doi.org/10.1016/j.bioelechem.2020.107524>.

[25] R. R. L. Guillard, Culture of phytoplankton for feeding marine invertebrates, in: W.L. Smith, M.H. Chanley (Eds.), *Culture of Marine Invertebrate Animals*, Springer, Boston, MA, USA, 1975, pp. 29–60. https://doi.org/10.1007/978-1-4615-8714-9_3.

[26] G. Pletikapić, T. Mišić Radić, A. Hozić Zimmermann, V. Svetličić, M. Pfannkuchen, D. Marić, J. Godrijan, V. Žutić, AFM imaging of extracellular polymer release by marine diatom *Cylindrotheca closterium* (Ehrenberg) Reiman & J. C. Lewin, *J. Mol. Recognit.* 24 (2011) 436-445. <https://doi.org/10.1002/jmr.1114>.

[27] J.L. Hutter, J. Bechhoefer, Calibration of atomic-force microscope tips, *Rev. Sci. Instrum.* 64 (1993) 1868–1873. <https://doi.org/10.1063/1.1143970>.

[28] H. Hertz, Ueber die Berührung fester elastischer Körper. *J. für die Reine und Angew. Math.* 1981, 156-171. <https://doi.org/10.1515/crll.1882.92.156>.

[29] I. Demir, I. Lüchtfeld, C. Lemen, E. Dague, P. Guiraud, T. Zambelli, C. Formosa-Dague, Probing the interactions between air bubbles and (bio)interfaces at the nanoscale using FluidFM technology, *J. Colloid Interf. Sci.* 604 (2021) 785-797. <https://doi.org/10.1016/j.jcis.2021.07.036>.

[30] E.G. Bligh, W.J. Dyer, A rapid method of total lipid extraction and purification, *Can. J. Biochem. Physiol.* 37 (1959), 911-917. <https://doi.org/10.1139/o59-099>.

[31] B. Gašparović, S.P. Kazazić, A. Cvitešić, A. Penezić, S. Frka, Improved separation and analysis of glycolipids by *latroscan* thin-layer chromatography–flame ionization detection, *J. Chromatog A* 1409 (2015) 259-267. <https://doi.org/10.1016/j.chroma.2015.07.047>.

- [32] B. Gašparović, S.P. Kazazić, A. Cvitešić, A. Penezić, S. Frka, Corrigendum to “Improved separation and analysis of glycolipids by Iatroscan thin-layer chromatography–flame ionization detection” [J Chromatogr A 1409 (2015) 259–267]. J. Chromatog A 1521 (2017) 168-169. <https://doi.org/10.1016/j.chroma.2017.09.038>.
- [33] N. J. Kruger, The Bradford method for protein quantitation, in: J.M. Walker (Ed.) The protein protocols handbook, Humana Press Totowa, NJ, USA, 2009, pp. 17-24. https://doi.org/10.1007/978-1-59745-198-7_4.
- [34] S. Dekić Rozman, A. Butorac, R. Bertoša, J. Hrenović, M. Markeš, Loss of thermotolerance in antibiotic-resistant *Acinetobacter baumannii*, Int. J. Environ. Health Res. 32 (2022) 1581-1593. <https://doi.org/10.1080/09603123.2021.1898550>.
- [35] A. Meister, M. Gabi, P. Behr, P. Studer, J. Vörös, P. Niedermann, J. Bitterli, J. Polesel-Maris, M. Liley, H. Heinzemann, T. Zambelli, FluidFM: Combining atomic force microscopy and nanofluidics in a universal liquid delivery system for single cell applications and beyond, Nano Lett. 9 (2009) 2501-2507. <https://doi.org/10.1021/nl901384x>.
- [36] I. Demir-Yilmaz, N. Yakovenko, C. Roux, P. Guiraud, F. Collin, C. Coudret, A. Ter Halle, C. Formosa-Dague, 2022. The role of microplastics in microalgae cells aggregation: A study at the molecular scale using atomic force microscopy. Sci. Total Environ 832, 155036. <https://doi.org/10.1016/j.scitotenv.2022.155036>.
- [37] D. Alsteens, E. Dague, P.G. Rouxhet, A.R. Baulard, Y.F. Dufrêne, Direct measurement of hydrophobic forces on cell surfaces using AFM, Langmuir 23, (2007) 11977–11979, <https://doi.org/10.1021/la702765c>.
- [38] E. Dague, D. Alsteens, J.-P. Latgé, C. Verbelen, D. Raze, A.R. Baulard, Y.F. Dufrêne, Chemical force microscopy of single live cells, Nano Lett. 7 (2007) 3026–3030. <https://doi.org/10.1021/nl071476k>.
- [39] A.C-C. Tang Jokela, Outer Membrane of *Dunaliella tertiolecta*: Isolation and Properties, PhD Thesis, University of California, 1969.
- [40] M. A. Borowitzka, L. J. Borowitzka, *Dunaliella*, in: M.A. Borowitzka, L. J. Borowitzka (Eds.), Micro-algal biotechnology, Cambridge University Press, Cambridge, UK, 1988, pp. 27.

- [41] A. Katz, P. Waridel, A. Shevchenko, U. Pick, Salt-induced changes in the plasma membrane proteome of the halotolerant alga *Dunaliella salina* as revealed by blue native gel electrophoresis and nano-LC-MS/MS analysis, *Mol. Cell. Proteomics*, 6 (2007) 1459–1472. <https://doi.org/10.1074/mcp.M700002-MCP200>.
- [42] A. Ben Amotz, J.E.W. Polle, D.V. Subba Rao (Eds.), *The alga Dunaliella: Biodiversity, Physiology, Genomics and Biotechnology*, Science Publishers, Enfield, NH, USA, 2009. pp. 555
- [43] M. Takeuchi, H. Miyamoto, Y. Sako, H. Komizu, A. Kusumi, Structure of the erythrocyte membrane skeleton as observed by atomic force microscopy, *Biophys. J.* 74 (1998) 2171-2183. [https://doi.org/10.1016/S0006-3495\(98\)77926-3](https://doi.org/10.1016/S0006-3495(98)77926-3).
- [44] A.H. Swihart, J.M. Mikrut, J.B. Ketterson, R.C. Macdonald, Atomic force microscopy of the erythrocyte membrane skeleton, *J. Microsc.* 204 (2001) 212-225. <https://doi.org/10.1046/j.1365-2818.2001.00960.x>.
- [45] J.-Y. Wang, L.-P. Wang, Q.-S. Ren, Atomic force microscope observation on biomembrane before and after peroxidation, *Biophys. Chem.* 131 (2007) 105-110. <https://doi.org/10.1016/j.bpc.2007.09.010>.
- [46] H. de Balmann, R. Nobrega, The deformation of dextran molecules. Causes and consequences in ultrafiltration, *J. Membrane Sci.* 40 (1989) 311-327. [https://doi.org/10.1016/S0376-7388\(00\)81153-9](https://doi.org/10.1016/S0376-7388(00)81153-9)
- [47] H. Wen, J. Hao, S.K. Li, Characterization of human sclera barrier properties for transscleral delivery of Bevacizumab and Ranibizumab, *J. Pharm. Sci* 102 (2013) 892-903. <https://doi.org/10.1002/jps.23387>.
- [48] H.P. Erickson, Size and shape of protein molecules at the nanometer level determined by sedimentation, gel filtration, and electron microscopy, 2009. *Biol. Proced. Online.* 11, 32. <https://doi.org/10.1007/s12575-009-9008-x>.
- [49] C.E. Hilburger, M.L.Jacobs, K.R. Lewis, J.A. Peruzzi, N.P. Kamat, Controlling secretion in artificial cells with a membrane AND Gate, *ACS Synth. Biol.* 8 (2019) 1224-1230. <https://doi.org/10.1021/acssynbio.8b00435>.

[50] A.D. Skinkle, K.R. Levental, I. Levental, Cell-derived plasma membrane vesicles are permeable to hydrophilic molecules, *Biophys. J.* 118 (2020) 1292-1300.

<https://doi.org/10.1016/j.bpj.2019.12.040>.

[51] N. Novosel, T. Mišić Radić, M. Levak Zorinc, J. Zemla, M. Lekka, I. Vrana, B. Gašparović, L. Horvat, D. Kasum, T. Legović, P. Žutinić, M. Gligora Udovič, N. Ivošević DeNardis, Salinity induced chemical, mechanical and behavioral changes in marine microalgae, *J. Appl. Phycol.* 34 (2022) 1293-1309. <https://doi.org/10.1007/s10811-022-02734-x>.

[52] F. Tian, S. Zhang, C. Liu, Z. Han, Y. Liu, J. Deng, Y. Li, X Wu, L. Cai, L. Qin, Q. Chen, Y. Yuan, Y. Liu, Y. Cong, B. Ding, Z. Jiang, J. Sun, 2021. Protein analysis of extracellular vesicles to monitor and predict therapeutic response in metastatic breast cancer. *Nat. Comm.* 12, 2536. <https://doi.org/10.1038/s41467-021-22913-7>.

[53] C. Charoenviriyakul, Y. Takanashi, M. Nishikawa, Y. Takakura, Preservation of exosomes at room temperature using lyophilization, *Int. J. Pharmac.* 553 (2018) 1-7. <https://doi.org/10.1016/j.ijpharm.2018.10.032>.

[54] E. Woith, G. Guerriero, J.-F. Hausman, J. Renaut, C. C. Leclercq, C. Weise, S. Legay, A. Wang, M.F. Melzig, 2021. Plant extracellular vesicles and nanovesicles: focus on secondary metabolites, proteins and lipids with perspectives on their potential and sources. *Int. J. Mol. Sci.* 22, 3719. <https://doi.org/10.3390/ijms22073719>.

[55] M. Alfieri, A. Leone, A. Ambrosone, 2021. Plant-derived nano and microvesicles for human health and therapeutic potential in nanomedicine. *Pharmaceutics* 13, 498. <https://doi.org/10.3390/pharmaceutics13040498>.

[56] G.M. Cooper, *The Cell: A molecular approach*, Sunderland, MA, USA, 2000. pp. 592.

[57] T. Hashimoto, 2015. Microtubules in Plants. *TAB* 13 (2015). <https://doi.org/10.1199/tab.0179>.

[58] Y. Tamba, H. Ariyama, V. Levadny, M. Yamazaki, Kinetic Pathway of Antimicrobial Peptide Magainin 2-Induced Pore Formation in Lipid Membranes, *J. Phys. Chem. B* 114 (2010) 12018-12026, <https://doi.org/10.1021/jp104527y>.

- [59] B. Fontaniella, A.M. Millanes, C. Vincente, M.-E. Legaz, Concanavalin A binds to a mannose-containing ligand in the cell wall of some lichen phycobionts, *Plant Physiol Biochem.* 42 (2004) 773-779. <https://doi.org/10.1016/j.plaphy.2004.09.003>.
- [60] A. Štimac, J. Trmčić Cvitaš, L. Frkanec, O. Vugrek, R. Frkanec, Design and syntheses of mono and multivalent mannosyl-lipoconjugates for targeted liposomal drug delivery, *Int J Pharmaceutics* 511 (2016) 44–56. <https://doi.org/10.1016/j.ijpharm.2016.06.123>.
- [61] A. Štimac, S. Šegota, M. Dutour Sikirić, R. Ribić, L. Frkanec, V. Svetličić, S. Tomić, B. Vranešić, R. Frkanec, Surface modified liposomes by mannosylated conjugates anchored via the adamantyl moiety in the lipid bilayer, *BBA-Biomembrane* 1818 (2012) 2252-2259. <https://doi.org/10.1016/j.bbamem.2012.04.002>.
- [62] M. Brgles, D. Jurašin, M. Dutour Sikirić, R. Frkanec, J. Tomašić, Entrapment of ovalbumin into liposomes – factors affecting entrapment efficiency, liposome size and zeta potential. *J Liposome Res.* 18 (2008) 235-248. <https://doi.org/10.1080/08982100802312762>.
- [63] M. Brgles, K. Mirosavljević, V. Noethig-Laslo, R. Frkanec, J. Tomašić, Spin-labelling study of interactions of ovalbumin with multilamellar liposomes and specific anti-ovalbumin antibodies. *Int. J. Biol. Macromol.* 40 (2007) 312-318. <https://doi.org/10.1016/j.ijbiomac.2006.08.012>.
- [64] N. Novosel, T. Mišić Radić, J. Zemla, M. Lekka, A. Čačković, D. Kasum, T. Legović, P. Žutinić, M. Gligora Udovič, N. Ivošević DeNardis, Temperature-induced response in algal cell surface properties and behaviour: an experimental approach, *J. Appl. Phycol.* 34 (2021) 243-259. <https://doi.org/10.1007/s10811-021-02591-0>.
- [65] I. Vrana, S. Bakija Alempijević, N. Novosel, N. Ivošević DeNardis, D. Žigon, N. Ogrinc, B. Gašparović, Hyposalinity induces significant polar lipid remodeling in the marine microalga *Dunaliella tertiolecta* (Chlorophyceae), *J. Appl. Phycol.* 34 (2022) 1457-1470. <https://doi.org/10.1007/s10811-022-02745-8>
- [66] L. Flanjak, I. Vrana, A. Cvitešić Kušan, J. Godrijan, T. Novak, A. Penezić, B. Gašparović, Effects of high temperatures and nitrogen availability on the growth and composition of the marine diatom *Chaetoceros pseudocurvisetus*. *J. Exp. Bot.* 73 (2022) 4250-4265. <https://doi.org/10.1093/jxb/erac145>.

[67] F.J.L. Gordillo, M. Goutx, F.L. Figueroa, F.X. Niell, Effects of light intensity, CO₂ and nitrogen supply on lipid class composition of *Dunaliella viridis*. *J. Appl. Phycol.* 10 (1998) 135-144. <https://doi.org/10.1023/A:1008067022973>.

[68] H. Khatoon, N.A. Rahman, S. Banerjee, N. Harun, S.S. Suleiman, N.H. Zakaria, F. Lananan, S.H.A. Hamid, A. Endut, Effects of different salinities and pH on the growth and proximate composition of *Nannochloropsis* sp and *Tetraselmis* sp isolated from South China Sea cultured under control and natural condition, *Int. Biodeterior. Biodegradation* 95 (2014) 11-18. <https://doi.org/10.1016/j.ibiod.2014.06.022>.

Authors' contributions

MLZ cell cultivation, vesicle preparation, AFM imaging, analysis and data interpretation, writing of original manuscript. **ID** and **CFD** nanomechanical characterization, analysis and data interpretation, writing of original manuscript. **IV** and **BG** lipidomic characterization, analysis and data interpretation, writing of original manuscript. **LH** confocal measurements, analysis, writing of manuscript. **AB** proteomic characterization, analysis and data interpretation, writing of manuscript. **RF** participation in planning the experiment, data interpretation, writing of manuscript. **NID** designing the experiments, monitoring the study, data interpretation, writing of original manuscript, obtaining funding. All authors read and approved the final manuscript.

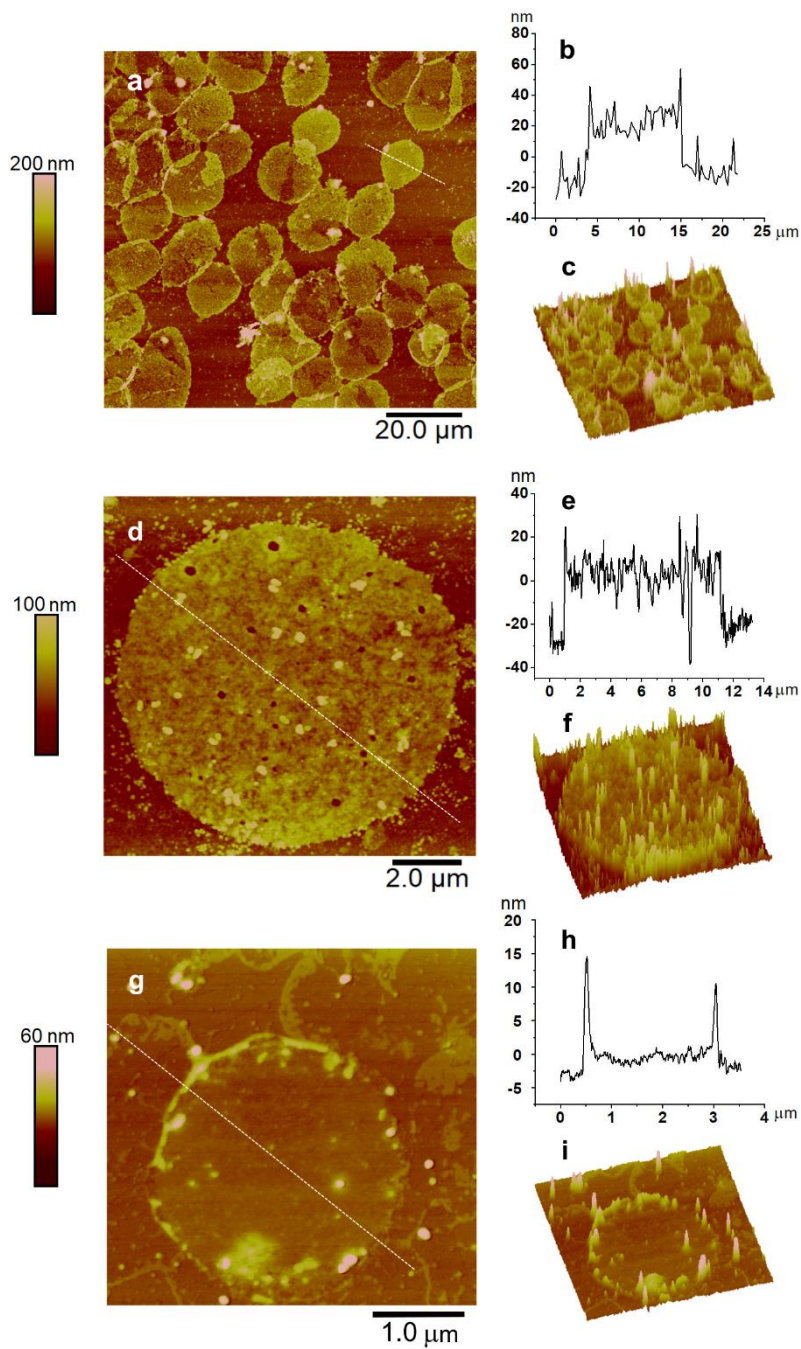


Fig. 1. AFM images of densely packed reconstructed membrane vesicles (a), individual vesicle with embedded material (d), and individual reconstructed nearly empty membrane vesicle (g) with corresponding cross-sections along the indicated lines (b,e,h) and 3D views (c,f,i), respectively. Scan sizes are 100 x 100 μm (a), 11 x 11 μm (d), 4 x 4 μm (g).

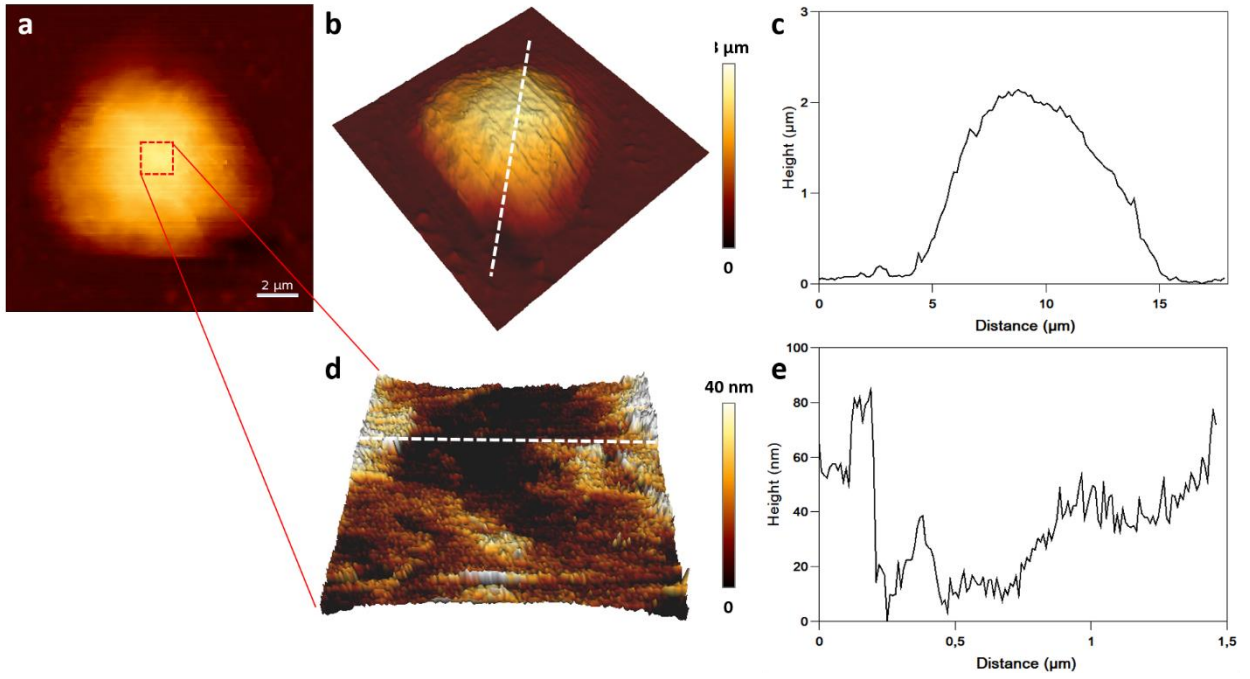


Fig. 2. AFM height image of a reconstructed membrane vesicle recorded in liquid (a) and the corresponding 3D view (b). Cross-sectional data (c) acquired along the white line in (b). High-resolution height image (d) taken in the area indicated by the red square in (a), and cross-sectional data (e) taken along the white line in (d).

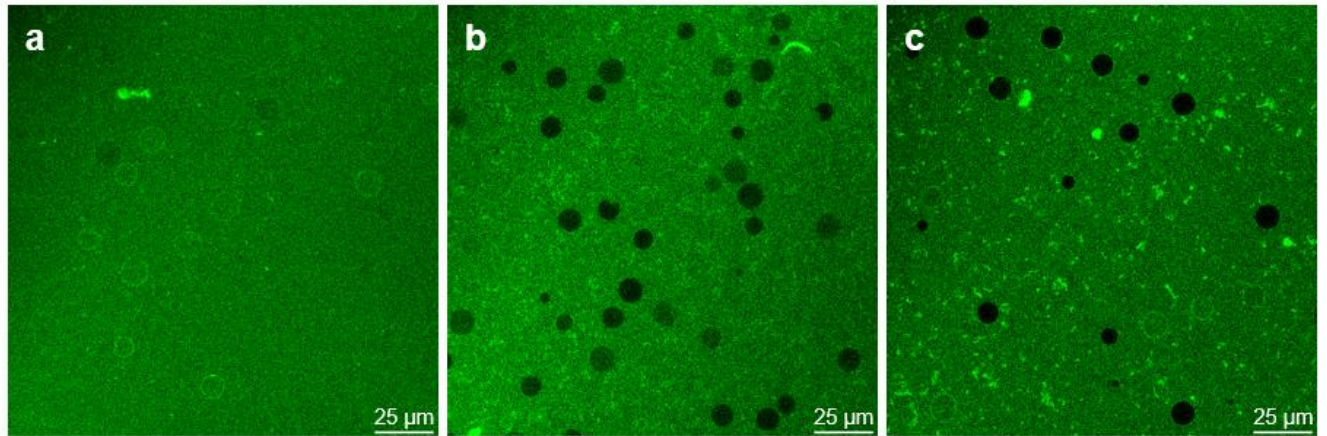


Fig. 3. Representative confocal images of reconstructed membrane vesicles after addition of FITC-dextran with different molecular weights: 10 kDa (a), 20 kDa (b), and 70 kDa (c).

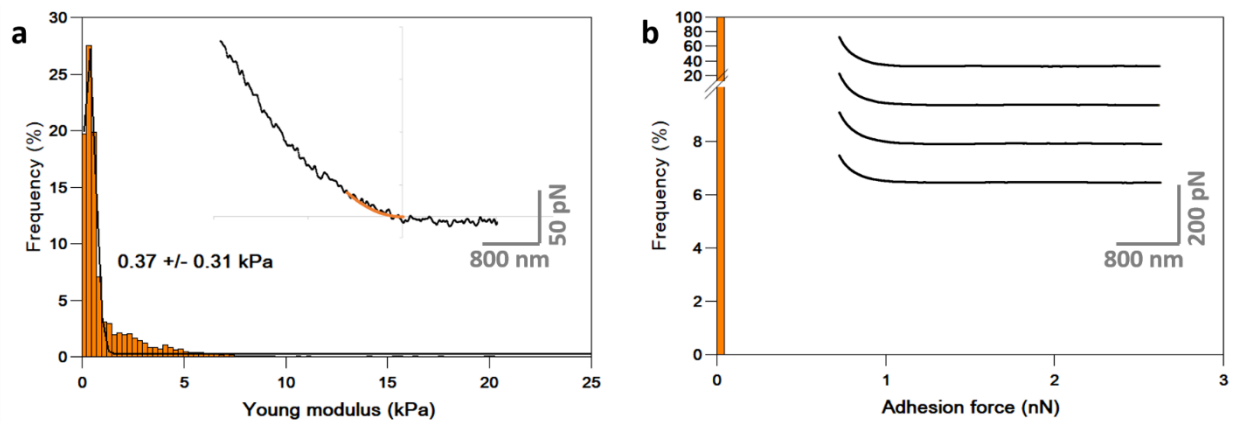


Fig. 4. The histogram shows the distribution of Young's modulus values obtained from nanoindentation measurements on areas of $1.5 \times 1.5 \mu\text{m}$ on the surface of 17 cells from 2 independent batch cultures (a). The inset shows an indentation curve (black line) fitted with the Hertz model (orange line) over 300 nm indentation depth. The histogram shows the distribution of adhesion force values obtained from force spectroscopy experiments between bubbles formed with FluidFM and 7 vesicles from a batch culture (b).

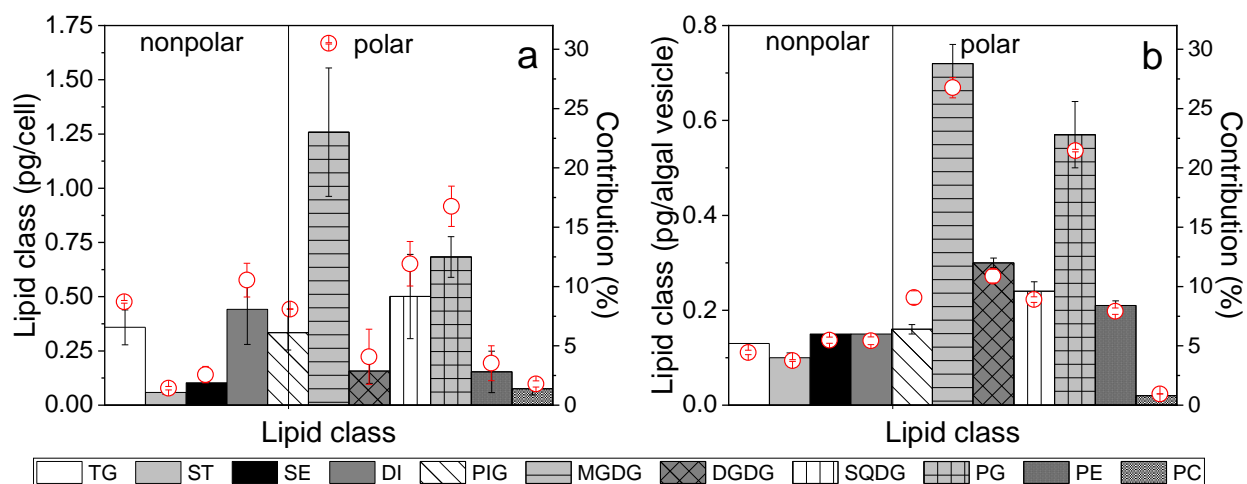


Fig. 5. Lipid class content (left y-axis, columns) and their contribution to total lipids (right y-axis, open red circles) of *D. tertiolecta* cells (a) and the reconstructed membrane vesicles (b).

Data are expressed as mean \pm SD.

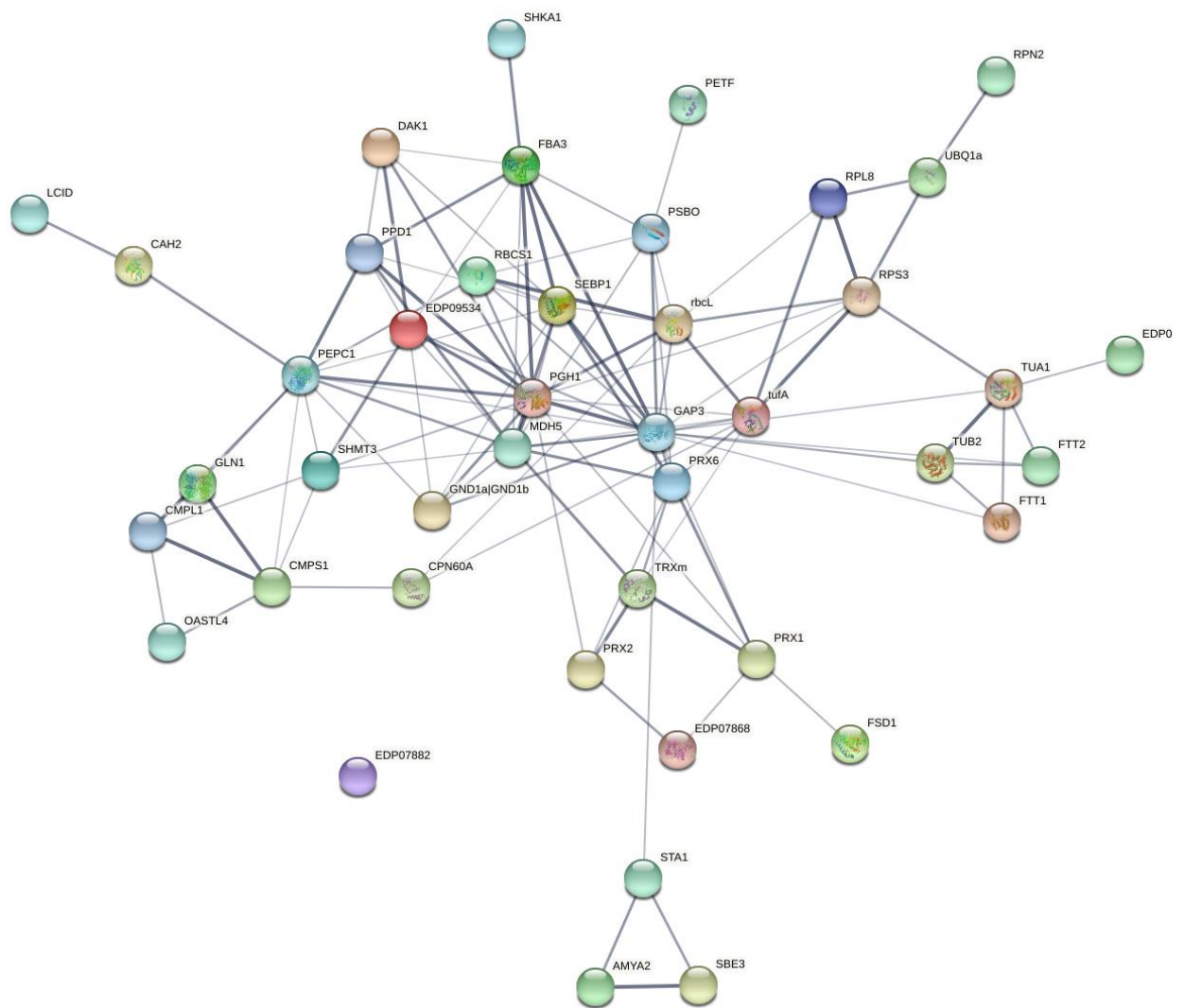


Fig. 6. Interactome shows protein-protein interactions between identified proteins in the reconstructed membrane vesicle. Colored nodes represent the proteins interrogated (Table S1), and color saturation of edges indicates the confidence of functional association.

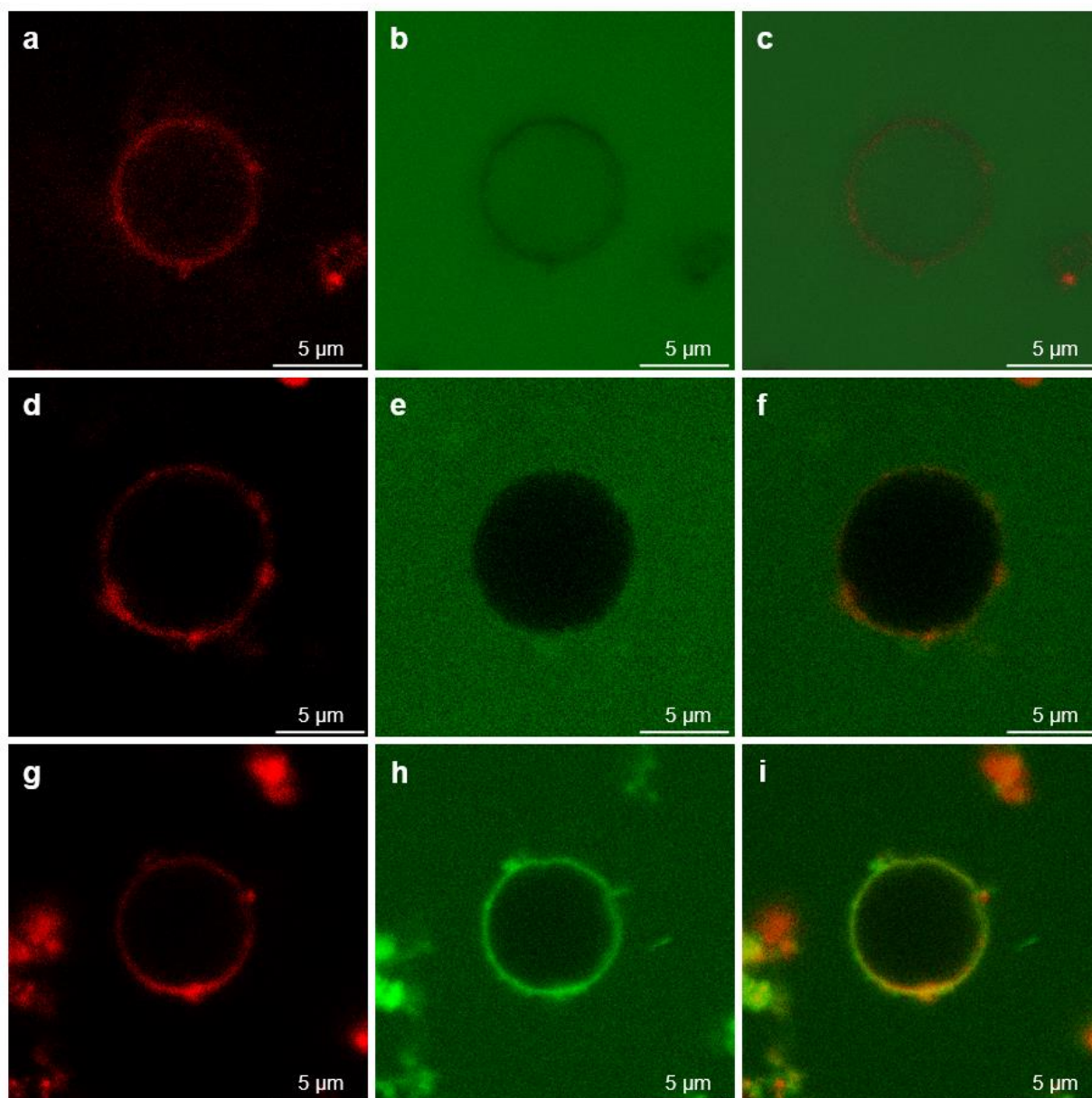


Fig. 7. Representative confocal images of reconstructed membrane vesicles stained with DiI (a,d,g), after addition of calcein (b), overlapping image (c), after addition of FITC-ovalbumin (e) and overlapping image (f), after addition of FITC-concanavalin A (h) and overlapping image (i).

